STRUCTURAL PERFORMANCE OF

POLYESTER RESIN CONCRETE

by

TAHA NASR EL DIN MEGAHED, B.Sc., M.Sc.

A Thesis submitted for the degree of

Doctor of Philosophy

Department of Civil Engineering

University of Glasgow

September, 1985

ProQuest LLC.
789 East Eisenhower Parkway
P.O. Box 1346
Ann Arbor, MI 48106 – 1346

ACKNOWLEDGEMENTS

The work reported in this thesis was carried out in the Department of Civil Engineering at the University of Glasgow under the general direction of Professor A.Coull, whose encouragement is deeply acknowledged.

I would like to express my sense of obligation to my supervisor Dr. I.A. Smith to whom I give full credit for his appreciated involvement in this work and for his matchless supervision as manifested in useful criticisms, sincere efforts, valuable guidance and admirable interests.

I feel an obligation to Professor H.B. Sutherland for his irreplaceable supports throughout this work.

Gratitude is also due to:
Dr. P.V. Arthur for his interest and useful discussions particularly those pertaining to the experimental work.
Dr. D.R. Green for his constructive proposals and positive response in permitting special testing requirements to be carried out.
Mr. T.W. Finlay for useful information.
Members of the teaching staff of Civil Engineering Department, University of Glasgow for their cooperation.
All my post-graduate collegues in the same department for their useful discussions and comments.
The staff of the Structural Laboratory and the Concrete Laboratory, in particular the late Mr. J. Love, Mr. J. Thompson and Mr. J. Colman for their valuable assistance in PC

processing and testing.
Mr. I. Todd for the help he gave in recording various electric and electronic experimental readings.
Mrs. L. Williamson for her efficient typing ot the tables.

Thanks are also reserved for the managements of the following companies for their responsible response in supplying the raw materials needed and the relevant information ;
Scott Bader Polyester Division and Strand Glassfibre, Glasgow Regional Centre.
Cairneyhill Quarry, near Airdrie.
Alexander Russel Plc, Glasgow.
TILCON - Scotland.

I would like to express my indebtedness to the Government of the Arab Republic of Egypt for the full financial support that enabled me to carry out this work.

Finally I pay my heartfelt feelings of acknowledgement to my parents, wife and son for their priceless forbearance and peerless endurance that kept my spirit up all through this research period.

SUMMARY

This work was carried out in an attempt to widen the potential use of polymer concrete in the construction industry. The concept of ultimate strength limit state in design of PC is furnished on the bases of the mechanical properties found experimentally.

Five distinct PC grades of polyester resin concrete that might fairly represent average properties of PC were proportioned after studying the potential optimization techniques of resin mortar mix design for which a mix design chart is developed.

Most of the mechanical properties of the five PC grades were investigated under short term conditions. The stress block shape and parameters of the compression zone in flexure are explored. Empirical and theoretical values for the stress block parameters are developed. These values were used in full scale structural applications, a beam and a column for each PC grade, and were found to be satisfactorily accurate. The concept of specific reinforcement ratio to be used with high tensile steel reinforcement which has no definite yield point is established.

The effects of rate of loading and sustained load were studied. Expressions for long-term ultimate compressive strength, long-term modulus of elasticity, sustained strength, macrocracking strain and creep strains are given for various PC grades.

Ultimate strength design procedures and their design charts for various loading conditions and relevant values of capacity reduction factors are suggested on the basis of the structural performance of PC under short-term and long-term conditions.

CONTENTS

LIST OF ABBEREVIATIONS

PC	Polymer-concrete.
PCC	Portland-cement concrete.
PPCC	Polymer-portland cement concrete.
PIC	Polymer-impregnated concrete.
REC	Resin concrete.
RM	Resin mortar.

LIST OF NOTATIONS

A, B Constants of the steel tension stress-strain curve at any of the three idealized zones.

A',B' Constants of the steel compression stress-strain curve at any of the three idealized zones.

A_s Area of tension steel.

A'_s Area of compression steel.

b Width of rectangular cross-section.

C_c Concrete compression force.

C_s Steel compression force.

C_r Coefficient of relative retained carrying capacity.

c Compression zone depth.

c_u Compression zone depth at ultimate strength.

d Effective depth of the cross-section.

d_1 Distance measured from the extreme compression fibre to the centroid of the outermost tension steel layer.

d_2 Distance measured from the extreme compression fibre to the centroid of the innermost tension steel layer.

d' Distance measured from the centoid of the compression steel layer to the extreme compression fibre.

d'' Distance between the two centroids of the innermost and outermost tension steel layers.

d_{sm} Maximum specific depth.

d_{sn} Minimum specific depth.

E_c Compression modulus of elasticity.

E_f Flexure modulus of elasticity.

e_c Basic creep strain.

e_{cu} Ultimate creep strain.

e_i Instantaneous strain.

e_l Limiting failure strain.

e_{su} Total sustained strain.

e_t Total creep strain.

e Eccentricity of normal force from the centroid of the tension steel.

er Ratio of eccentricity level.

e*r Balanced eccentricity ratio.

Fc Ratio of filler content by weight.

F_{cr} Capacity reduction factor.

F_s Steel tension force.

f_{ba} Anchorage bond strength.

f_{bl} Local bond strength.

f_c Compressive strength.

f_{cf} Compressive stress of the stress block in flexure.

f_{cl} Long-term axial compressive strength.

f_{cu} Ultimate compressive strength.

f_{cy} Axial cylinder compressive strength.

f_f Modulus of rupture.

f_i Induced tensile stress.

f_r Ratio of ultimate strength at any strain rate to ultimate strength at rate [1].

f_s Stress in tension steel.

f'_s Stress in compression steel.

f_{su} Sustained strength.

f_{sy} Yield strength of steel.

f_t Splitting strength.

G Global coefficient of average uniform stress.

h Overall depth of cross-section.

K1 Parameter of average uniform stress distribution.

K2	Parameter of stress block-resultant location.
K2u	Value of K2 at ultimate strength.
K3	Parameter of maximum compressive stress in flexure.
Ko3	Peak value of the parameter K3.
k	Index of mix richness.
k_c	Coefficient of creep.
k_{cu}	Ultimate coefficient of creep.
k_i	Coefficient of instantaneous creep recovery.
k_r	Coefficient of creep recovery.
L	Coefficient of reduced load.
Lu	Coefficient of reduced load at ultimate strength.
Mc	Moisture content of aggregates.
MF	Modulus of fineness.
P	Normal force acting on a cross-section.
R	Ratio of tension reinforcement.
R'	Ratio of compression reinforcement.
R_s	Specific tension reinforcement ratio.
R'_s	Specific compression reinforcement ratio.
r	Rate of loading.
r_c	Creep recovery.
r_i	Instantaneous recovery.
r_t	Total strain recovery.
SA	Nominal surface area.
Sl	Normal distribution significance level.
SSA	Nominal specific surface area.
ST/UP	Ratio of styrene/ unsaturated polyester by weight.
Stc	Styrene content.
T	Coefficient of reduced compression zone depth.
Tg	Gel time.

Ti	Polymerization induction interval.
Tp	Polymerization propagation interval.
T_s	Index of tension reinforcement.
T'_s	Index of compression reinforcement.
Tu	Coefficient of reduced compression depth at ultimate strength.
t_m	Time required for PC to develop its macrocracking.
t_u	Time corresponding to the ultimate creep strain.
W/C	Water/ cement ratio by weight .
Wlb	Binder working life.
Wlc	Polymer concrete working life.
Ws	Ratio of sand content in the mix by weight.
Y	Overall stress block coefficient.
Z	Coefficient of reduced moment.
Zu	Coefficient of reduced moment at ultimate strength.
ε_c	Maximum concrete strain (compressive extreme fibre).
ε_{cl}	Lateral concrete strain.
ε_{cm}	Axial concrete macrocracking strain.
ε_{cu}	Ultimate concrete strain.
ε_{cv}	Volumetric concrete strain.
ε_{ml}	Long-term concrete axial macrocracking strain.
ε_{mr}	Ratio of ε_{cm} at any strain rate to that at rate [1].
ε_{oc}	Concrete strain at maximum stress.
ε_s	Strain in tension steel.
$\varepsilon_{s'}$	Strain in compression steel.
ε_{sy}	Yield strain of steel.

CHAPTER ONE

INTRODUCTION

1.1. Recent attitudes in the construction industry

Progress in the construction industry depends on the greater understanding of and improvement in basic properties of materials. Improved methods of construction and better economics can be achieved by improving existing materials and by the development of new ones. Portland-cement concrete (PCC) will be as indispensible in the future as it is now. Its use is a technology which is well understood.

PCC has been available for more than 150 years and has a good range of mechanical properties. Despite possessing high qualities of short and long-term stability, however, PCC still has poor flexural tensile strength and low tensile cracking and ultimate compressive strains. These limitations must be considered at the design stage. In this respect, probably the most critical inherent weakness of PCC lies in its low limiting strains which may lead to progressive crushing and spalling. These in turn make the material more permeable, less durable and increasingly sensitive to external effects. Consequently restrictions may be imposed in exploring new fields where PCC could be used. Permeability influences concrete vulnerability to frost and corrosion of reinforcement where heads of water and humidity differences exist along and across concrete structures. Permeability can have a decisive effect on performance, particularly when considering chemical resistance, abrasion and erosion-resistance.

New construction materials must have better performance and

economics than existing ones. New materials also require careful and reliable interpretation of laboratory-research results before they can be used efficiently in actual design. This is due to the lack of available accumulated data based on previous experience with these materials. The prevailing attitude in the construction industry is by nature a traditional one, and any new material must challenge it to gain acceptance. This can only be done by providing and proving a better cost-performance efficiency. The cost effectiveness of these materials is one major element in justifying their use, and pilot applications often have to be investigated first if new markets are to be explored.

1.2. Concrete-polymer materials and their definitions

Concrete-polymer materials like other composite materials may generally be defined as a three-dimensional combination of at least two chemically and mechanically distinct phases; namely a polymer matrix or phase and dispersed aggregates. In some cases portland cement may form a third phase. Electron-microscope photographs of the microstructure of these materials are shown in Fig.(1.1) (1). There is a definite interface between the different components.

Although there are many different versions of concrete-polymer materials, they can be specifically categorized into three main types as follows;

(a) Polymer-portland cement concrete or polymer-modified cement concrete, abbreviated as PPCC. This is prepared by using both polymer and portland cement to form the binding

paste or the system matrix. Mixing is carried out in the same way as when mixing conventional concrete.

(b) Polymer-concrete or resin-concrete, abbreviated as PC or REC, which is prepared by mixing resin as the only binder, with selected aggregates without any other cementing agent or water.

(c) Polymer-impregnated concrete, abbreviated as PIC which is prepared by monomer impregnation into hardened precast cement concrete elements with subsequent polymerization.

1.3. Historical development of concrete polymer materials

In the late fifties following the growth of the petrochemical industry, synthetic rubber latexes, resin emulsions and monomers were produced and developed . Their production activated fundamental and practical research on concrete-polymer materials in general. Trials using polymers with concrete were undertaken in different places , and some British patents on the concept of a natural latex-hydraulic cement systems were issued about sixty years ago (2).

1.3.A. Polymer-portland cement concrete (PPCC) The first concrete polymer material was PPCC, for which neither synthetic resins nor advanced techniques were required. Monomers usable with concrete were available. Work was initiated primarily in enhancing cement concrete properties by adding to the mixture, while still in fresh state, water-soluble latexes and emulsions. The first report on this type of material was produced in Japan by M.Itakura in 1953 (3), and concerned polyvinyl acetate-modified concrete. In the

following years extensive work on the development of PPCC and its mortar was undertaken by different institutes and research laboratories. Since that time polymer modified concretes and mortars have often been used in building and construction works such as those needed for the Tokyo Olympics in Japan, 1964. Table (1.1) shows some of the properties of typical polymer-cement mortars used in Japan, where work to standardize quality and testing methods of PPCC was commenced in 1974. A specific standard was established recently (1978) and included in the Japanese Industrial Standards (J.I.S.) (4). Some results of the early research (2) on PPCC made with different polymers are shown in Fig.(1.2). They represent the effect of polymer/cement ratio and polymer type on the compressive, tensile, flexural and shear strength of PPCC.

In Germany since around 1948 PPCC had been under research using various aqueous polymer dispersions, as well as some powder-form dispersions. The work in Germany aimed at improving specific properties of concrete, mortar and slurry for particular applications. The polymers initially used were acrylic-ester based copolymers and vinylproprionate copolymers. The results obtained using these polymers are shown in Fig.(1.3) and Fig.(1.4). In these figures the effects of polymer addition to cement mortars on the mechanical properties are demonstrated. The only gain was the improvement in the adhesive properties of the different formulated mortars or slurries. These mixes are covered by DIN standards (5). Synchronized work was being carried out in Germany for improving flow properties and workability of conventional PCC. Using plasticizers the W/C ratio could be reduced without

reducing workability and higher strengths could be attained. In this work (6) dispersions based on vinylacetate aroused interest initially, but because of some shortcomings regarding water curing, work turned eventually to other polymer types. The influence of water on the performance of the polymers used can be seen by comparing Fig.(1.5) with Fig.(1.6). Generally, satisfactory improvements in flow properties could be obtained by using acrylates, ethylene and many others.

In the U.K. different institutions have been involved in modifying conventional concrete by introducing polymer dispersions. At the beginning of the 1970's a programme was conducted by The Building Research Establishment (7) to investigate all missing data required for reliable evaluation of PPCC properties and its performance in different environments. Many of the polymers originally introduced had been found to perform badly in wet conditions, see Figs.(1.7, 1.8 & 1.9). Acrylic-based polymers gave the best results as shown in Figs.(1.10, 1.11 & 1.12).Numerous polymer dispersions were investigated such as polyvinyl acetate, polyvinylidene dichloride, acrylic methacrylate, vinyl propionate and many others. In this programme various curing and testing methods were used over very long testing periods. Another study was undertaken in the University of Southampton (8) in an attempt to overcome some of the drawbacks of cement mortars and concretes such as poor tensile impact stregth, limited resistance to corrosion and poor adhesion to old concrete. This work formed a part of a study of the interrelationships between mechanical properties and the microstructure of cement paste modified by the addition of a

styrene-butadiene polymer latex to the mixing water. Additional research work was aimed at producing competitively low-cost flooring compounds using special epoxy-water slurries. The concept of a fibre-reinforced polymer cement composite, was introduced tentatively and on a small scale through various universities and companies in the U.K. (9). More recently there has been an upsurge in interest in fibre-reinforced polymer cement composites. It has been recognised that polymer dispersions may have a valuable role to play if used with fibres. By the begining of the 1980's a great deal of information about most properties of PPCC was available. However very little was known about their long-term deformation characteristics under different loading conditions. Since a knowledge of these properties is of great importance in assessing the advantages and applications of PPCC products, some experimental work has been initiated recently cocerning the study of creep properties for different PPCC's (10).

In the U.S.A. latex-modified concrete dates back to the 1950's, but the real impetus for using polymers in concrete developed in the late 1960's with the publication of research performed by the Brookhaven National Laboratory and the Bureau of Reclamation (now the U.S. Water and Power Resources Services) (11) & (12). This research was primarily oriented towards polymer-impregnated concrete. The dramatic increase in strength, stiffness and durability created considerable interest in potential applications of different concrete polymer composites. The American Concrete Institute ACI recognised the importance of these new materials, and in 1971

"Committee 548-Polymers in Concrete" was formed with the intention of gathering, correlating and evaluating information on the effects and properties of polymers in concrete, and different symposia were sponsored by this committee (13) & (14).

Polymer latexes have been used very successfully to make latex-modified concretes, these latexes are mainly copolymers which include acrylic and vinyl acetate, styrene, vinyl chloride, butadieneand other latexes which are commercially available in different formulations. However, PPCC has not received as much attention in the U.S. as PIC or PC, since most of the successful polymers that have been identified for PPCC have been proprietary. In the late 1970's, investigations at Washington State University, made a preliminary evaluation of the feasibility of preparing PPCC with furfuryl alchol. A study was also carried out for the determination of the effects of various proportions of aniline hydrochloride catalyst and calcium chloride on the development of concrete strength. These effects have been reported on in the Soviet Union as increasing strength and durability of concrete. The resultsfor a two mix series are shown inFigs.(1.13 & 1.14) (15). Many other studies concerning PPCC have been carried out in different countries , such as the Soviet Union, France, Australia, Spain, Italy and Canada. Some of the results of these studies will be dealt with later in this chapter.

1.3.B. Polymer-impregnated cocrete (PIC) As mentioned earlier, PPCC and PC materials have been studied since the 1950's. However PIC came to the fore in the development of polymer use in concrete in 1966. At that time research sponsored by the

U.S. Government, was initiated to develop methods for impregnating hardened portland cement concrete (PCC). Various liquid monomers were employed in the impregnation process, based on the known fact that this impregnation treatment provided a material with significant improvements in strength and durability. Initial tests of PIC showed that the structural and durability properties of this new composite could be quite remarkable. The U.S.Government spent several millions of dollars over the next few years to identify suitable monomers for impregnation, to enhance impregnation processes and to study and develop applications for PIC. It should be noted that a patent for PIC had been issued in the Soviet Union in 1954, although work on PIC was not started in that country until after the U.S. work had become available in the literature (16).

The improvements in properties which were being achieved through polymer impregnation of concrete generated considerable interest among investigators in many countries around the world and resulted in numerous other researches. By the early 1970's several applications had been produced. The American Concrete Institute, recognizing the importance of this rapidly developing new family of construction materials, formed the previously mentioned "Committee 548", whose membership includes representatives from countries around the world, and which sponsored two symposia on "Polymers In Concrete" in 1972 and 1973 (16). Two more sessions were held in 1976 on the same subject. Most of these symposia proceedings were published by the ACI in 1978. The committee also prepared a state-of-the-art report on polymers in

concrete which was published in 1977.

As a part of other international activities in this field, a number of symposia and conferences have been held since 1967 by different organizatios. Since then, research on PIC was spread in different directions; one of which, concerned with relating pore-structure with degree of pore-filling in terms of polymer molecular weight, was carried out in Canada (17). Another investigation was carried out in Japan to clarify the relationship between the molecular weight of polymer formed in PIC and the condition of its manufacturing process. In this the monomer used was methyl methacrylate (MMA). Two main relationships were determined; molecular weight as a function of polymerization temperature, and molecular weight as a function of impregnation depth (18). These two relationships are represented in Figs. (1.15 & 1.16).

Further studies showed that, not only does the performance of concrete impregnation depend upon decrease of porosity or increase in degree of pore-filling (which is a function of matrix capillary pore diameter and distribution, viscosity and surface tension of the monomer used), but also it depends upon molecular dimensions and the interaction between cement capillary walls and and organic molecules of monomer. In Italy through research conducted by A.Rio (19), it was found that one must first have very well compacted concreete for it to be structurally fit for impregnation. High quality concrete, fully impregnated with low polymer content, will show higher mechanical strengths than a lower quality concrete, even if the latter was fully impregnated with a larger quantity of

monomer. So the main improvement in PIC performance, can be attributed to the cement matrix prior to impregnation. This matrix should have diffused micro-porosity allowing easy permeation of monomer and also low total porosity to limit the quantity of monomer needed for partial or full impregnation. Similar studies were made in W.Germany by H.Schorn (20), in Canadaby B.B. Hope (21) and in other countries in the early seventies. By the begining of the 1980's, the concept of PIC was well established internationally. Since then, different aspects were dealt with in more detail, such as the effect of polymerization techniques, impregnation depth, monomer types available and high temperatures on the performance of PIC. Other applications were developed ranging from ceramics to containers for the disposal of low and intermediate level radio-active wastes.

1.3.C. Polymer-concrete (PC) Polymer-concrete was used commercially as early as 1958 in the U.S. (22) to produce precast building panels; and "cultured marble" has been in use for many years to produce many items ranging from bath tubes and drain tops to submarine periscopes. Initially most of PC was made with polyester and epoxy resins. In the late 1970's MMA monomer received high attention especially for repairing deteriorated PCC structures. More recently the aim has been to develop multi-functional resins that will ensure polymerization at ambient conditions and within prescribed times of hardening. As far as resin or binder type is concerned, there are in general five types of thermosetting resins which are used with PC. Epoxy, polyester, polyurethane, poly-MMA and furane. Limitations applicable to one alone can

not be applied to another binder or another mix. The low shrinkage and versatility of epoxy resin and its ability to set and to develop excellent adhesion to aggregates of various types in wet air conditions, make it suitable for use in difficult environments; while polyester for example, is preferred for precasting.

One of the earliest studies on PC was conducted by Holifield National Laboratory in the U.S., to determine the effect of different constituent materials on PC properties and to obtain data for evaluating the feasibility of "tailor-made" resin-aggregate mixtures with a wide range of predictable strength, density and stiffness properties (23). The resins used were polyester and epoxy with different chemical and physical properties. Widely varying groups of coarse and fine aggregates were carefully selected for better understanding of the contribution of each constituent in the composite. Some of the relevant findings of this work are quoted as shown in Figs.(1.17, 1.18& 1.19).In the U.S., the deterioration of concrete bridge decks imposed an increasing problem for all state high-way departments ; it has been estimated that approximately 105000 bridges in the U.S. are in need of repair (24). Ideally, the repair should be made quickly, allow the bridge to be opened to traffic in a few hours and be permanent. Those requirements accelerated the development and use of PC in the U.S., made with polyester and MMA-based polymers. Recently the use of PC for major restoration of hydraulic structures and their protection, has increased very rapidly, and both user-formulated and proprietary PC's are now in use.

Most PC formulations will cure in thirty to sixty minutes at 5 C° and higher. Curing time is adjustable as desired at ambient temperatures. Very special resin formulations might be required for particular constructions and restorations where temperature is as low as -5 C° and when time available is very limited. The U.S. Air Force sponsored research for developing certain PC formulations for repairs to airfields that would cure in a very short time at very low temperatures and as D.W.Fowler states, this work has been achieved successfully (25).

In Japan, the first research and development of PC was conducted in the Electrical Communication Laboratory of Nippon Telegraph and Telephone Public Corp. (NTTP) in the late 1950's, and the results were reported in 1961 (26). The practical development of PC was initiated in the Meihan Resin Concrete Industries Corp. and several other boards in Japan. K.Okada et al. carried out exclusive basic studies on PC and its structural applications (27) & (28). Responding to the active practical development of PC, work on standardization of quality and testing methods for polyester PC has been in progress since 1974 (29). In 1978, and with the supervision of K.Okada, six JIS's have been issued describing different methods for manufacturing and testing polyester PC. As far as the practical applications used in Japan are concerned, developed manholes made of PC were designed and installed by NTTP, and the estimated figures of production amounted to 20000 tons of PC annually. Pipes were also produced at the rate of about 30000 tons/year (29). Many other structural applications of PC are now in progress in Japan.

In the U.K. research seems to be involved in PPCC development and its practical applications. Very few studies have been made regarding PC applications, out of which the work of B.W. Staynes and Brighton Polytechnic (30) will be quoted hereafter. However resin mortars have been used for repair work and jointing in the civil and structural engineering fields. In most cases, these applications have been supported by acceptance-testing of the materials employed, without attempting to evaluate their ultimate capabilities, or their behaviour under long-term loadings in particular. A notable exception is the extensive study carried out by Johnson (31) on long-term loading and other effects on epoxy resin-mortar joints. As a logical extension to this work, B.W.Staynes carried out a full investigation for the production of epoxy resin-concrete and the optimization of mix propotions. He also recommended some precautions to be taken in the manufacture of PC dating back to the early 1970's (32).

1.4. Manufacturing techniques and the nature of strength

1.4.A Polymer-portland cement concrete (PPCC) Polymer-portland cement concretes and mortars are made by partial substitution of the portland cement by a polymer. Polymers used should be either aqueous polymer-dispersions (latexes and emulsions) or water-soluable polymers (monomers). As shown in Fig.(1.20), these polymers can be added to the mixing water or to the fresh concrete (or mortar). Curing can be carried out in the same ways as with PCC. Accelerated curing techniques are applicable whether performed under high temperature, high

presuure or both. The amounts of polymers added (the solid content of the disperion) are normally within 5 to 20% of cement weight (solid polymer/ cement by weight). Proper anti-foaming agents are often used to control excessive air entrainment. On curing a polymer film is formed and enhances the cement-aggregate bond, which is reflected in higher mechanical strengths, increased ductility and improved water proofness.

The nature of PPCC strength is mainly attributed to the binder interface influence, and its capability of transferring stress between different components without excessive deformation. The portland cement matrix, which provides the binder for ordinary concrete, is responsible for the final strength of the composite through the precipitation of cement hydrates into interlaced and elongated crystals, with high cohesive or adhesive properties. Another theory (33) accounts for the cement matrix strength through the colloidal effects of the hydrated calcium silicates, which being almost insoluble, form a rigid gel mass. Whatever the exact nature of cement-concrete strength , the randomly-formed crystallates represented by cement hydrates are intrinsically weaker than high molecular weight amorphous polymers. They also are inherently less suited as an interface, particularly for the transfer of tensile stresses. In this respect the salient feature of PPCC technology , as repeatedly confirmed by chemists, is that ionic bonding can be an additional factor contributing to the performance of concrete. It has been shown (34) that all the components of high performance composites are linked by ionic bonds, a feature which is not present in PCC, and it is from

this stand point that the idea of PPCC has initially emerged. Although not all ionic bonds are chemical ones, there is a contribution to performance in actual use provided by ionic associations, i.e., between cement hydrates and the pendant groups on a polymer chain. Comatrix structures of the crystalline skeleton inside an amorphous polymer particularly present a high potential for ionic association (34). The formation of the polymer-cement comatrix can be achieved through different chemical and biochemical reactions. For instance with a polyvinylidiene comatrix, hydration of both cement and polymer is dominant. The condensation process may take place if the polymers used have reactive terminal groups, such as epoxide resins and furfuraldehyde. In the case of acrylic and methacrylic esters reaction is initiated by free radicals using conventional oil-soluble catalysts. In either of the previous cases, it is reported that fairly satisfying achievements in PPCC technology are within reach.

Regarding its processing, PPCC batching is a quite different process from that of PCC, primarily because polymer formation starts when its different components are distributed by mixing with the aggregate. A balance is necessary between the rate of increase in polymer-viscosity (polymerization) and the completion of the whole system reaction (initial cement hydration). For that reason and others, it is recommended (35) that polymer-dispersion should be added up to one hour after the addition of the mixing water to the cement and aggregate. In some studies and practical applications (36), special Super High Early Strength cement was used to overcome this difficulty. The use of this cement resulted in a far better

performance as shown in Figs. (1.21 to 1.24), obtained by Y.Ohama. It is also reported (35) that excessive vibration and steam-heat curing techniques have deleterious effects on PPCC performance.

1.4.B Polymer-impregnated concrete (PIC) PIC is made by impregnating a hardened and dried cement-concrete base with one of a wide variety of polymerizable polymers or monomers. Polymerization is usually carried out by thermal or radioactive techniques. The production of PIC depends chiefly upon the degree of monomer absorption and the consequent degree of pore-filling in the finished product. Processing technology for the production of PIC can be listed as follows: [a] Concrete fabrication : It was noticed that concrete mix variables (W/C, entrained air, aggregate size and type, etc.) do not greatly affect the properties of PIC. Low or high strength concrete gave almost the same improved strength after impregnation. The main effect of concrete quality is reflected in the polymer loading and the consequent cost of unit production. However the question of whether the base concrete should be of high quality with low required polymer loadings, or of lower quality with higher polymer loadings is still a controversial one (20). As shown in Fig.(1.25), the matrix porosity and the degree of polymer-filling strongly affect the strength of PIC.

[b] Dehydration : After conventional curing of the concrete units, they are oven-dried to get rid of the free moisture at temperatures ranging from 100 to 250 C°, according to production requirements. Particular attention should be paid to the dehydration degree which must be sufficient to remove

only free-pore water (evaporable water) and not the combined water (nonevaporable); otherwise concrete destruction will take place. The effect of the degree of dehydration on strength is shown in Figs.(1.26 & 1.27).

[c] Impregnation : Impregnation is performed in two main stages as follows;

(1) Evacuation of fully dried elements by using vacuum pumps to the desired value of pressure, to get rid of the entrained air, partially or totally, and to aid in the polymer absorption process.

(2) Soaking the cured, dried and evacuated base concrete element in pressurized polymer liquid in sealed containers. Soak-pressure may vary from 0.1 to 1.0 N/mm2. depending on different processing parameters. These parameters are the degree of drying performed, the evacuation vacuum applied and, the time of soaking and the required impregnation depth, etc.

[d] Polymerization : This can be achieved by a wide range of techniques, depending in the first place on the type of polymer used. Most commonly, polymerization is carried out thermally, catalytically or by radiation. Different combinations of these three techniques can be used.

If polymerization is to be made without the use of encapsulating techniques, certain precautions should be taken to prevent or help reduce monomer evaporation and drainage losses from concrete units. A specific processing technique for producing PIC is shown in Fig.(1.28), in which polymerization is carried out under water (37).

The high performance of PIC with regard to the mechanical properties or durability can be simply attributed to the decrease of the composite porosity. However this decreased porosity can not account for the differences in performance recorded with different polymers. Additional factors are involved, one of which is the interphase bonding in its broadest sense. As shown in Fig.(1.29), the only fillable pores in the system matrix (cement paste or mortar) are those which are connected to the capillary pore system (free-water pores). Evidently, reducing matrix porosity means reducing microcracks and flaws as well as matrix capillary pores. This implies a reduced probability of microfracture initiation at crack tips, and an enhanced mechanical performance of the system matrix as a whole.

Many studies suggest that the increased linearity of the stress-strain curve for PIC is attributed to the improved paste-aggregate interfacial bond. But more recently investigations show that it is the smaller difference between the improved elastic modulus of the cement-paste phase and that of aggregate phase, which causes this increase in linearity and strength. This reduction in the moduli difference , as shown in Fig.(1.30), produces less cracking at the paste-aggregate interface (21).

Depending on the nature of the polymer itself, there is evidence that chemical interaction between the paste capillary walls and the monomer, introduced during polymerization, interferes with and improves the microstructure of the paste (18).

Recently, progress in PIC processing has been directed towards partial impregnation techniques, since full impregnation proved to be almost impossible, especially for large structural elements. Partial impregnation may be carried out to a specified impregnation depth without resorting to the soaking of concrete units under pressure in huge sealed vessels. It can also be used for restoring deteriorated structures such as platforms, bridge decks and in many other applications for which full impregnation techniques are not practically possible (38).

1.4.C Polymer-concrete (PC) PC consists of aggregates bound with a polymeric material and contains no hydraulic cement or water. This type of material has many of the advantages of PIC, as will be seen later, though its processing techniques are much easier and simpler than those of PIC. PC processing is very similar to that of conventional concrete, provided precautions are taken. Processing techniques depend on the finished product desired and the required performance. One process is shown in Fig.(1.31) and is suggested for some prercast applications (4).

To summarise, PC processing can be classified into four main stages as follows :

[a] Proportioning : In which different constituents are selected according to the desired performance in the fresh and hardened stages. Polymer, catalyst and accelerator, if needed, are selected and mixed uniformly just prior to mixing with aggregate and filler. In certain processing techniques,

formulated polymer is mixed first with filler, then the aggregate is added gradually until the desired consistency is reached. This is done to help provide complete uniformity in the binding polymeric paste (resin and filler). A saving in the mixing time after the addition of the aggregate is also gained.

[b] Mixing : Any type of concrete mixer can be used provided that an effective 'washing-up' solvent is available. There is a wide variety of resin-diluting agents that can be used depending primarily upon the resin type itself and its formulation. Resin should be carefully formulated so that hardening or setting will not be initiated while the materials are still in the mixer. Careful production-supervision should allow complete and uniform mixing while the PC is fresh. For precasting, the mixer should be cleaned periodically, if there is a continuous line of production. Dry-mixing of filler and aggregate before the addition of resin usually produces a better mix uniformity.

[c] Casting : Before placing PC releasing agents should be used to provide easy and sound demoulding. Vibration may be needed with some harsh PC mixes, but generally excessive vibrating times are not recommended.

[d] Curing : This can be carried out in several ways but in principle there are only two; catalytic or thermal. The wide range of catalysts (hardeners) and accelerators (initiators) available are capable of initiating and completing the polymerization of liquid resins in different ways. Curing rates can be enhanced by applying some high temperature during

the hardening time, or even after the initial hardening. The finished product can also be subjected to heated dry-air for a prescribed period and temperature compatible with the resin used.

PC as a composite material can be closely investigated at the macrostructure or microstructure level, as shown in Fig.(1.32). On the macrostructure level, PC can simply be regarded as a continuous phase of polymer containing dispersed inert aggregate with irregular pores. On the microstructure level, the polymeric paste can be described as a combination of filler particles each covered with a film or thin envelope consisting of different polymer-chain layers, as shown in Fig.(1.32). Those layers can be categorised into fully-oriented, semi-oriented and unoriented layers. The continuous polymer matrix is formed mainly through covalent bond reactivities, which result in long chains with high molecular weight compounds. These long chains are crosslinked through their active sites and provide a high-performance matrix, on which the overall PC performance depends. Naturally the strength of PC is strongly dependent on the properties of the resulting polymer matrix, the degree of its crosslinking, the length of the formed chains and consequently their molecular weight.

The chemistry of polyester resin-concrete is briefly described in the following chapter. However it must be emphasized here that at the microstructure level, the polymer matrix is primarily responsible for all rheological properties of PC, including shrinkage strains on hardening, creep and stress relaxation (39). The system matrix also provides the necessary

cohesion and adhesion for the dispersed aggregate phase. On the macrostructure level, PC performance depends on the type of aggregate and filler used, on their gradings and on the way they are compacted. As far as the filler-binder or aggregate-binder interface is concerned, studies carried out in the U.S.S.R. (39) have revealed a clear relationship between the change in the nature of long-chain molecule formation and the associated polymer/filler ratio. A clear dependence of the internal shrinkage stresses on the nature of the polymer and the filler was also found.

Many investigations aimed at reaching a theoretical estimation of PC strength or optimum mix-design, were carried out recently in the U.S.S.R. Theoretical models were developed and helped produce several equations. These equations were derived to predict PC compressive strengths and strength development rates (39) & (40) and were experimentally verified.

1.5. Advantages and disadvantages of polymers in concrete

Different concrete-polymer materials have proved themselves reliable as construction materials over the last decade. As with all new materials, future applications and developments are generally different from those initially anticipated. For example, in the early 1970's PIC appeared to be the most promising of the concrete-polymer materials. At present, PC is attracting much more attention than PIC (22). The initial interest in PC was for the restoration of structures like bridges and airfield runways. But the largest future use now appears to be in the industrial applications such as machine

parts , machine foundations and particularly for precast parts and components made using continuous processing.

Apart from the high cost and other economic aspects of PC, which will be dealt with later, the main disadvantages found with concrete-polymer materials in general are as follows :

(1) Certain physical and mechanical shortcomings : In the initial stages of research, a large range of applications was envisaged. However, as more data became available for the different concrete-polymer types, a number of unacceptable properties were found which restricted the wide potential use of these materials. The main shortcoming being their poor rheological performance. High shrinkage strains with consequent high internal tensile stresses usually cause some setting cracks. The development of shrinkage strains and their relation to strength development, for PC made of polyester (41), are shown in Fig.(1.33 & 1.34). This effect is encountered much more clearly when steel reinforcement is used. Fig.(1.34) represents the effect of reinforcement ratio on the setting-shrinkage strains. Creep behaviour and stress relaxation constitute more restrictions for most structural applications.

Due to the nature of polymers, these materials suffer some deterioration in performance in moist and wet environments when not completely cured. They are sensitive to high temperatures and fire attack. Their performance under dynamic loads is still unsatisfactory especially under repetitive loads which induce internal heat evolution. In one research series conducted in Japan (42), the internal temperature

recorded in fatigue tests with PC specimens, reached well over 80 C° as shown in Fig.(1.35), and caused excessive strength reduction.

(2) Lack of suitable polymers for use with concrete : Due to the lack of cooperation between biochemical and civil engineering on one hand, and to the lack of exchange of experience between polymer manufacturers and concrete-polymer dealers on the other hand, the expected rate of development has not been attained. For example, the absence of structural knowledge in biochemical engineering resulted in a very wide variety of monomers and polymers which unfortunately have no structural value at all. The lack of meaningful performance-data for most polymers and monomers, makes it impossible for a structural engineer or consultant to evaluate them. The manufacturers of polymers usually describe their product in terms of acid-value, non-volatile content and stability in darkness or viscosity gel-time, etc.

No polymers , so far, have been specially developed and produced for use with concrete. The structural engineer will often find it difficult to decide on the best polymer that would result in the most desirable end-use properties. In this context, it seems that changes in attitudes are required generally. As chemical companies turn more attention towards the expanding market of concrete-polymer materials, it is likely that significant development will occur.

When considering the advantages of concrete-polymer materials, it is essential to make a clear distinction between the different types of these materials. As shown in table (1.2),

most concrete mechanical properties are improved with polymer inclusion. PC and PPCC generally have lower moduli of elasticity than conventional cement concrete. The most significant improvements are those related to durability. In certain tests of freeze-thaw resistance, PC had a weight loss of almost zero after 1500 cycles, while the corresponding PCC specimens lost 25% of their weight after only 700 similar cycles. Improvement in erosion and abrasion resistance is remarkable. Chemical resistance for concrete-polymer materials is much better than that of cement concrete.

Several advantages can be mentioned for the PC-type in particular, apart from its high mechanical and durability properties. These are as follows :

[a] Simple production techniques are involved : Processing is adaptable to existing PCC technology. It can be used either for cast in place or precast applications.

[b] Versatility : PC can be tailor-made in an almost unlimited number of different mixes with various properties. Setting time can be very finely controlled, as shown in Fig.(1.36), at all temperatures even those well below zero C°(43). PC can be made with different toughnesses and stiffnesses depending on the incorporated constituents.

[c] Esthetic and decorative uses : Using special colour dyes dissolved in the polymer before or during mixing, can result in a 'terrazzo' effect with a lustrous finished product. This can in some applications be of considerable benefit.

1.6 State of the art of concrete polymer materials

1.6.A Polymer-impregnated concrete (PIC) In the last five years, the rate of PIC development has decreased dramatically. The excellent structural performnace and the enhanced durability could not in themselves justify commercial use on a large scale. At the outset it was thought that this type of construction material would revolutionise the construction industry. But the complicated techniques and industrial hazards involved halted the anticipated progress. Perhaps the most serious factor was and still is, the insistence on having full impregnation. Another factor that has limited the growth of PIC is the progress and the competitiveness of other concrete polymer materials such as PC.

Full impregnation techniques can only be used for precast products, which are relatively small (44). Usually they have an adverse balance between cost and performance. Recently PIC has gained a sudden wider use in outdoor applications, all of which are based on surface impregnation techniques. Several methods have been suggested and carried out, in which applying monomer at atmospheric pressure could result in an impregnation depth varying from 20 to 50 mm (44). Primarily, these methods can be used with horizontal and flat surfaces such as bridge decks and panels, platforms and heavy-duty flooring. Impounding the impregnant over the cured and dried cement concrete base, is the latest technique for partial impregnation. Several bridge deck constructions and repairs have been carried out in the U.S., Japan and other countries using such simple ponding techniques. Specially-formulated monomers are used for better results and deeper penetration.

In certain applications, the time elapsed from the start of impregnant ponding till the completion of polymerization was 30-40 minutes; and the resulting impregnation depths varied from 20-25 mm.(45).

Now it is universally established that PIC can be classified into three different groups. Depending on the techniques used and the consequent impregnation depth, PIC can have full, partial or surface impregnation. The last is being extensively used at the present time, where most of the advantages of full impregnation are retained while most of its processing disadvantages are avoided.

Surface impregnation is used for the protection of many hydraulic structures like outlet walls of dams, spillway and stilling basins. It is also used to improve runway and roadway construction and maintenance. One major field of application is the repair of bridge decks. This technique, despite being a simple one, could be used in very particular ways. For instance, it could be used for consolidating and stiffening soft materials in a zone of loose soil for certain petrographic excavations (44). Ferro-cement products have been enhanced by polymer impregnation. Containers for radio-active wastes, made of PIC, are now under investigation in many countries.

1.6.B Polymer-cement concrete (PPCC) Polymer-cement concretes and mortars have been in use since the early fifties. However, polymer-modified cement mortars and slurries have been used more often than polymer-modified concretes. Those polymer-modified cementitious materials are mainly used for protective

linings and finishing works. Concretes modified by polymers have not obtained a worldwide practical acceptance because their cost can not be justified.

Many new latexes, emulsions and water-dispersable polymers have been developed and have helped widen the potential fields of application for polymer modified mortars. These applications are numerous, but can be simply classified into flooring, waterproofing, decorating and adhesive works. Table (1.3) shows some of these applications (45). Many additives have been developed for the enhancement of polymer modified mortars, such as anti-foaming agents, fire-retardants, anti-corrosive agents and many others which have enlarged the possible fields of application.

Now there are commercially available certain prepacked PPCC's, mortars and slurries which can be used satisfactorily (45). Apart from prepacking, the process of PPCC mixing is similar to that of conventional concrete. It is noteworthy that in Japan, eight Japanese Industrial Standards have been established for the quality control and testing methods of PPCC; where their annual consumption of polymers in PPCC manufacturing amounted to 100000 tons.

1.6.C Polymer-concrete (PC) Polymer-concretes and mortars have recently attracted much more interest than any other type of concrete-polymer material. New resins, techniques and research on PC have brought it into the front line of new construction materials. Generally its use is distributed equally amongst load-carrying elements, aggressive media-protecting elements and decorative or esthetic elements.

Tables (1.4 &1.5) show these possible fields of application (45). These applications are still to be explored and exploited. Load-carrying elements are mostly precast products such as underground components, sea-water structures, supporting systems, housing elements,machine tools and even street furniture.

As a protective coating against aggressive media, PC and mortars are extensively used for industrial flooring and paving. In the U.K., flooring is by far the widest field of application. In one construction project, newly-setting cement concrete (green) was covered by a resin-mortar layer resulting in 15 years of maintenance-free heavy-duty flooring (46). The range of industrial and commercial flooring applications is being progressively extended to include areas not subjected to aggressive media. For instance, the increasing demand for very level, easily maintained and dust-free floors is being met by fine PC finishes which offer direct cost competition with ordinary cement concrete. Coatings to marine pipelines, dam spillways, channel linings and aircraft pavements are now popular in the U.K. Cast-iron for the bed and frame segments in machines is being replaced by PC.

Another interesting field for using PC and its mortar is in grouting. British Telecom used some 8000 tons of polyester mortar for installing or raising manholes in roads. They proved cost-effective and it is reported that no more regrouting is likely to be required. Another example of mass grouting is that made for the heavy-duty crane rails of the giant Goliath Krupp Crane in Belfast, in which 280 tons of

epoxy-mortars were grouted between the rail-soleplates and the supporting beams (47). Many similar applications for structural joints , bedding of bridge-bearings, fixing of street furniture and the like are in wide use in the U.K.

Recently, interests have developed on a wide scale in the U.S. and other countries for producing thermal insulator panels and electrical insulators made of PC. Some major work comprising the installation of thermal insulating panels was carried out in the U.S. These panels protected dykes that contain liquid gas tanks, against explosive spilling by the impounded liquid gas reaching a high temperature. Light-weight polyester mortar and concrete was specially formulated for this project, using certain cellular-structure aggregates (48). Thermal conductivity was reported to be very much lower than that of conventional concrete insulators , that is in addition to the better structural performance and durability that was given by the new PC insulating panels.

A major field of PC use is the rehabilitation and repairing of deteriorated structures, and the restoration of historical structures. Special types of quick-setting resin mortars are now available. They can be used for protecting and replacing spalled concretes caused by steel corrosion. They can be simply trowelled vertically or overhead without any supporting or slipping forms. An example of the size of a similar repair work can be quoted from the latest bridge-repair project carried out in the U.S. In this project, in 1983, two bridges alone have utilized 1800 tons of PC for the repair of their decks (49).

Several continuous-mixing machines are now available on the market for PC processing. Due to the nature of PC, most mixing and casting techniques should be subject to high quality control. For that reason and others, many of the continuous and ordinary mixing machines for PC, are automatically controlled. Different types of these machines are capable of PC-shotcreting up to 20 m and in some cases up to 45 m. (50). One of those PC-shotcreting machines is shown in Fig.(1.37) along with its basic system 'flow-chart'. This and similar machines are now in wide use in Japan, W.Germany and other countries.

New methods in PC processing have evolved such as 'ready-to-cast' PC sacks, and polymer injection to the already compacted and placed aggregates. In Japan, a new construction method for making small-diameter tunnels (up to 1.20 m) has been operated successfully (51). In this method , as shown in Fig.(1.38), automated tunnelling and lining with a 100 mm.-thick PC layer was achieved. The fast curing and high early strength of PC segments cast in place, replaced what would have been conventional 'cut-and-cover' techniques using other materials.

1.7. Objectives of the present work

From the previous review of different concrete polymer materials, one is left with no doubt that these materials could form a useful tool for the construction industry. The number of the practical applications and their relevant research programmes are increasingly expanding. Both PIC and PPCC, with some exceptional applications, could not compete in

cost with PC. With the current progress in the petro-chemical industry, new resins are being developed and produced regularly all over the world. Thus the future should show a greater spread in use of PC.

Most of the research on PC , as reviewed earlier, has been dedicated to its physical and mechanical properties . Mix proportioning and the effect of different constituents on the performance of PC is by far the widest field of ongoing research. In addition, studying the physiochemical parameters of the micro and macrostrcture of PC and their effect on its performance is another active field of research.

So far the majority of PC structural elements are made of mortars or plain PC. Relatively few applicationshave used reinforcement in any form . The number of PC structural members reinforced with steel bars is surprisingly limited. Most of those structures are designed with margins of safety so large as to lose all the structural advantages of PC. The lack of research in the field of structural performance of reinforced PC is mainly responsible for this situation.

Very little is known about the flexural behaviour Of PC when reinforced. Not enough knowledge about how to utilize efficiently the high performance of PC together with steel bars, is available. Structural limits related to different modes of failure do not exist. Some researchers have used high tensile steel with PC members, but no general flexural theory is established yet. The long term structural performance has been completely ignored, and almost no one seems to have been interested in applying the different creep test results or the

vital rheological behaviour findings of PC to real structural elements using reinforced PC. In addition the economic aspects and the feasibility of producing structural elements of PC have been paid very little attention.

Based on these above mentioned conclusions of PC utiliy in the present construction industry, the objectives of this work were chosen to be as follows :

(A) Optimizing mix-proportioning of the available materials to produce five different grades of PC. These grades would serve as the base materials for the coming objectives.

(B) Studying different physical and mechanical properties of those grades, either in short-term or long-term performance.

(C) Studying flexural stress-strain distribution , flexural stress-block parameters and their dependence on mechanical properties and time.

(D) Deriving an 'ultimate-flexure theory' that would help calculate the actual ultimate capacity in both short and long-terms for any reinforced PC member. This would also help establish a ' design code' based on chosen factors of safety within the ultimate structural limits and serviceability limits to be set later.

(E) Applying the findings to full-scale structural members made of reinforced PC using a beam and a column for each grade.

Table 1.1: Properties of Typical Polymer Cement Mortars

Property / Type of Mortar	Flexural strength N/mm^2		Comprehensive Strength N/mm^2		Water absorption (%)	Dry Shrinkage $\times 10^{-4}$	Adhesion in Shearing Compression N/mm^2	Abrasion (Taber Index) mg/100rev.	Shock resistance (Height of fall mm)
	Dry cure	Water cure	Dry cure	Water cure					
Ordinary mortar	3.02	4.06	10.3	20.2	11.4	10.50	0.53	18512	250.0
SBR-1	5.60	4.81	19.9	18.9	1.2	8.29	1.31	454	2100.0
SBR-2	9.42	5.22	28.3	16.1	3.9	8.93	1.89	392	1000.0
CR	7.87	4.32	11.4	20.1	6.6	14.07	1.11	386	1200.0
NBR	6.56	5.08	20.2	18.1	2.4	3.64	1.42	403	1100.0
NR	2.00	2.00	4.5	4.4	3.6	9.57	1.51	622	2350.0
PVAC	6.42	2.47	14.5	10.1	5.5	24.07	0.14	281	700.0
PVDC	8.19	4.41	24.9	23.9	3.0	9.64	1.33	696	500.0

Table 1.2: Typical Properties of Concrete-Polymer Materials

Property	Conventional Portland Cement Concrete	PIC	PC	PPCC
Compressive strength, N/mm^2	28.0 - 35.0	100.0 - 150.0	40.0 - 150.0	28.0 - 56.0
Tensile strength, N/mm^2	2.1 - 2.5	8.5 - 11.5	7.0 - 14.0	4.0 - 6.5
Modulus of Rupture, N/mm^2	-	-	8.5 - 21.0	10.0 - 12.5
Modulus of Elasticity, N/mm^2	20 - 25	35 - 40	7 - 35	10 - 15
Water Absorption, %	5 - 6	0.3 - 0.6	-	-
Freeze-Thaw Resistance, No. of Cycles/% Weight Loss	700/25	2,000-4,000/0-2	1,500/0-1	-
Resistance to Acid, Factor of Improvement Over Control	-	5 - 10	8 - 10	1 - 6
Abrasion Resistance, Factor of Improvement Over Control	-	2 - 5	5 - 10	10

Table 1.3: Typical Applications and Standard Mix Design of Polymer-Modified Mortars

Application	Location of Work	Standard Mix Proportions (By weight)			Thickness of Trowe-ling or Coating (mm)
		Cement	Sand	Polymer Dispersion	
Paving Material Floorings	Floors for general houses, warehouses, offices and shops, toilet floors.	1	3	0.2-0.3	5-10
	Passages, stairs, chemical plants, railway platforms, roads, garages,etc.	1	3	0.3-0.5	10-15
Waterproofing Materials	Concrete roof-deck, mortar and concrete block walls, water tanks, swimming pools, septic tanks, silos.	1	2-3	0.3-0.5	5-20
Adhesives	Adhesives when flooring materials, walling materials, heat insulating materials are bonded to concrete floors and walls.	1	0-3	0.2-0.5	-
	Jointing new concrete to old concrete and new mortar to old mortar.	1	0-1	over 0.2	-
	Repair of cracks.	1	0-3	over 0.2	-
Anti-corrosive Linings	Effluent drains, chemical factory floors, grouting for acid-proof tiles, septic tanks, foundations for machinery plant, floors for chemical laboratories, pharmaceutical warehouse, etc.	1	2-3	0.4-0.6	10-15
Deck coverings	Internal and external ship decks 4 bridge decks, foot bridge decks. Undercoat	1	2-3	0.9-1.0	1-2
	Mid-coat	1	3	0.4-0.6	5-6
	Top-coat	1	3	0.5-0.6	3-4

Table 1.4: Applications of Polymer Mortars

Application	Location of Work
Floorings (including Decorative Finishings)	Floors for general houses, warehouses, offices, schools, hospitals, factories and shops, toilet floors, passages, stairs, garages, railway platforms, train floors, etc.
Pavings	Roads (footways and travelled ways), bridge decks foot-bridge decks, parking lots, runways, etc.
Anti-corrosive Linings	Effluent drains, chemical and machinery floors, grouts for acid-proof tiles, floors for chemical laboratories and pharmaceutical warehouses, septic tanks, electrolytic baths, hot spring baths, offshore structures, e.g., piers and sea berths, etc.
Adhesives	Adhesives for floorings, walling materials and heat-insulating materials, tile adhesives, adhesives for jointing new cement concrete or mortar to old cement concrete or mortar, embedment of anchor bolts, etc.
Repairing Materials	Grouts for repairing cracks and delaminations of concrete structures, patching materials for damaged concrete structures, protective coatings for corroded reinforcing bars, etc.
Integral waterproofings	Concrete roof-decks, mortar walls, concrete blocks, water tanks, swimming pools, septic tanks, silos, etc.
Small-diameter Automatic Tunnelling System	Telecommunication cable lines, etc.
Precast Products	FRP-reinforced mortar pipes for sewerage and irrigation systems, FRP-reinforced mortar panels, vibration isolators, etc.

Table 1.5: Applications of Polyester Concretes

Application	Location of Work
Structural Precast Products	Manholes and handholes for telecommunication cable lines, electric power cable lines and gas pipelines, tunnel liner segments for telephone cables and sewerage systems, piles for port or hot spring construction, machine tool structures, e.g., beds and saddles, FRP-reinforced frame or panels for buildings, etc.
Non-Structural Precast Products	Gutter covers, U-shaped gutters, footpath panels, terrazzo tiles and panels and large-sized or curved decorative panels for buildings, partition wall panels, sinks, prefabricated cellars, counters, washstands, speakes for stereo phonographs, etc.
Cast-In-Place Applications	Spillway coverings in dams, protective linings of stilling basin in hydro-electric power stations, coverings of checkdams, foundations of buildings in hot spring areas, etc.

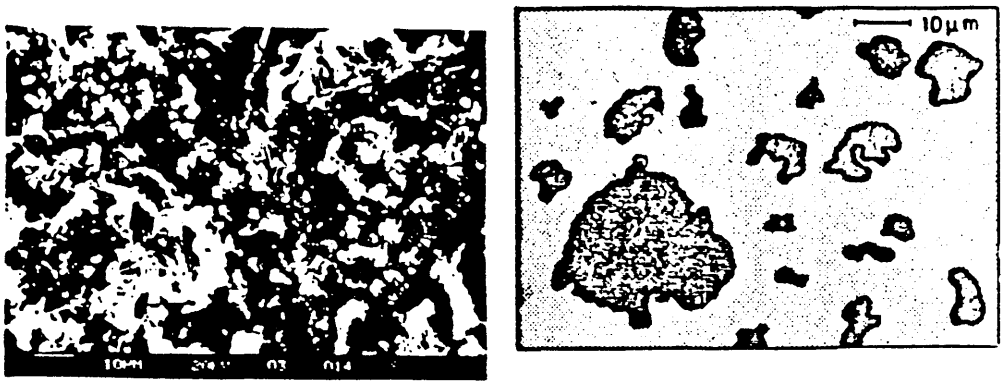

(a) Resin Modified Concrete

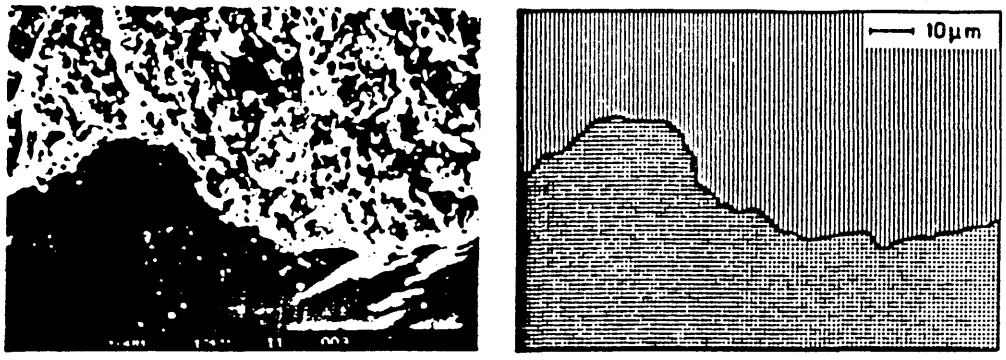

(b) Resin Concrete

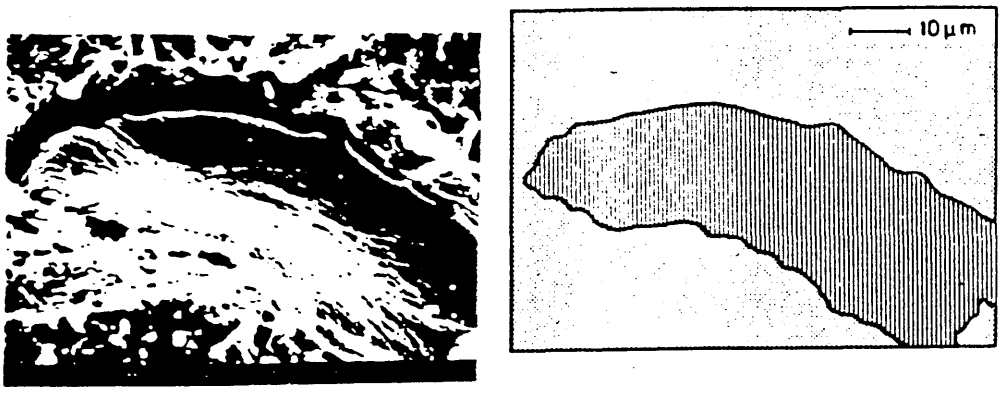

(c) Resin Impregnated Concrete

Cement
Reactive Resin
Aggregates
Predominantly resinous

Fig. (1.1) Microstructure of Concrete Polymer materials.

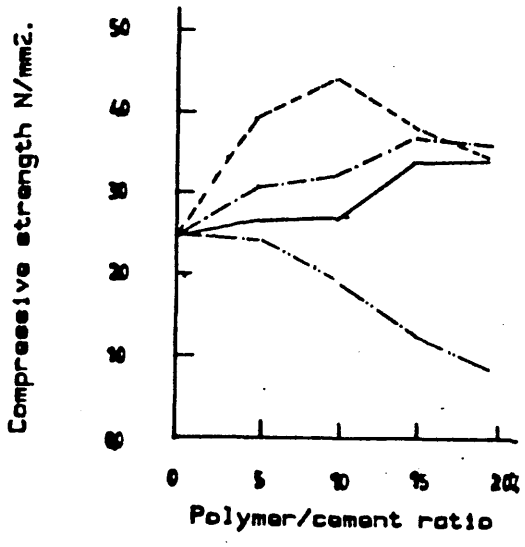

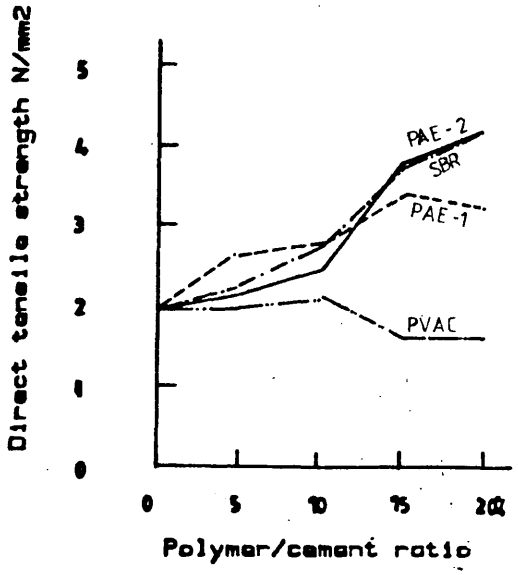

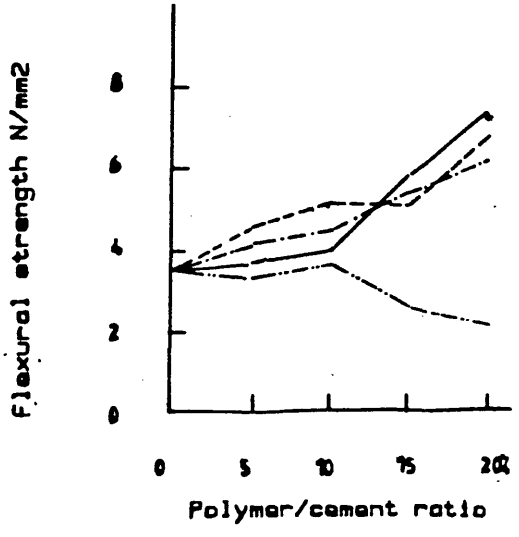

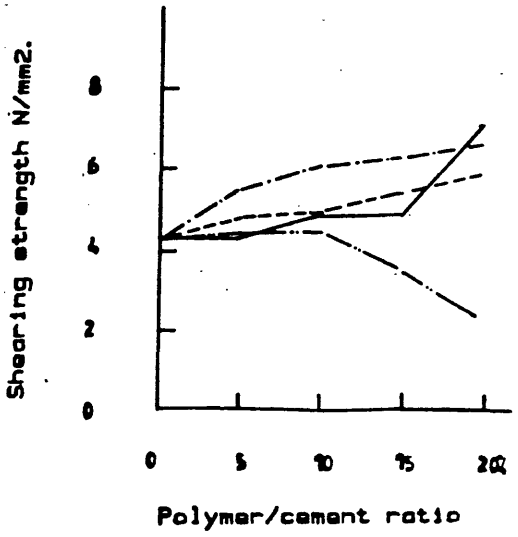

PAE: Polyacrylic ester.

PVAC: Polyvinyl acetate

SBR: styrene butadiene rubber

Fig. 1.2 Strength properties of various PCC.

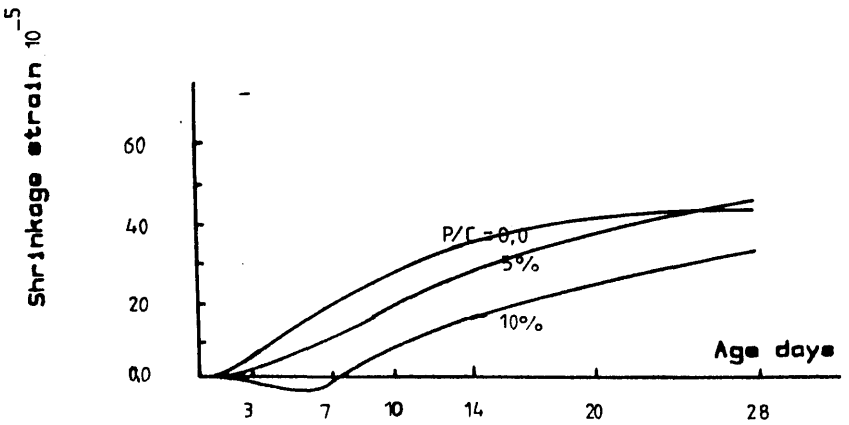

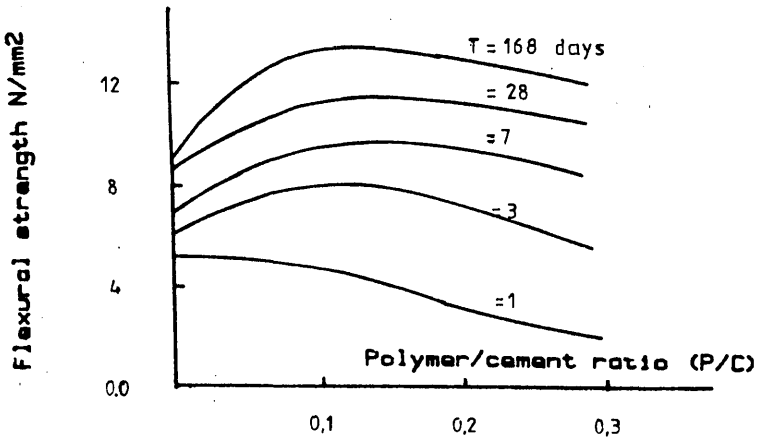

Fig. 1.3 Effect of vinylpropionate on shrinkage and flexural strength of mortar

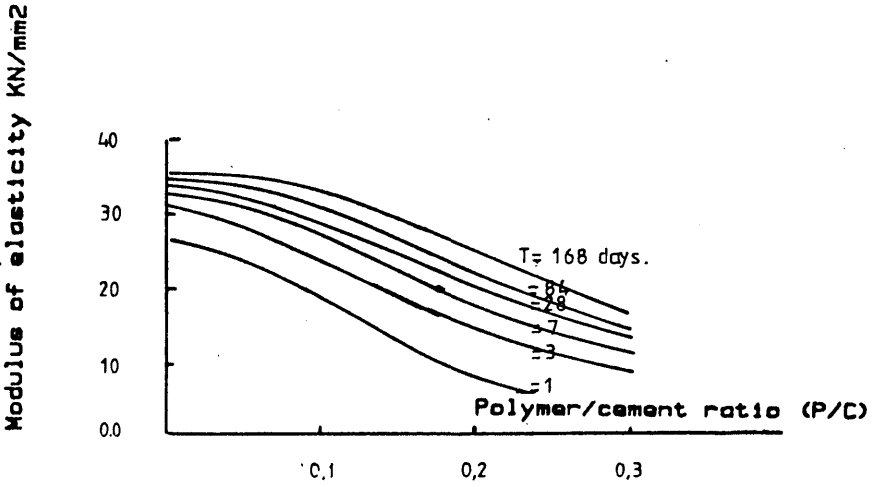

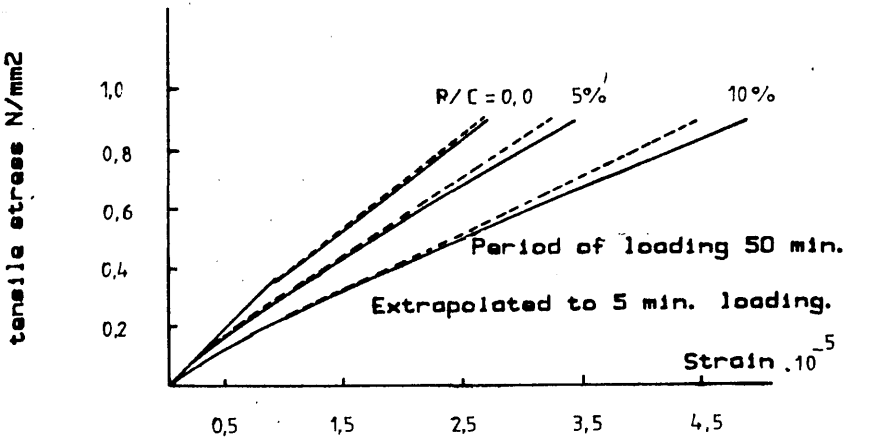

Fig. 1.4 Effect of vinylpropionate on compressive modulus of elasticity and tensile stress-strain relationships of mortar.

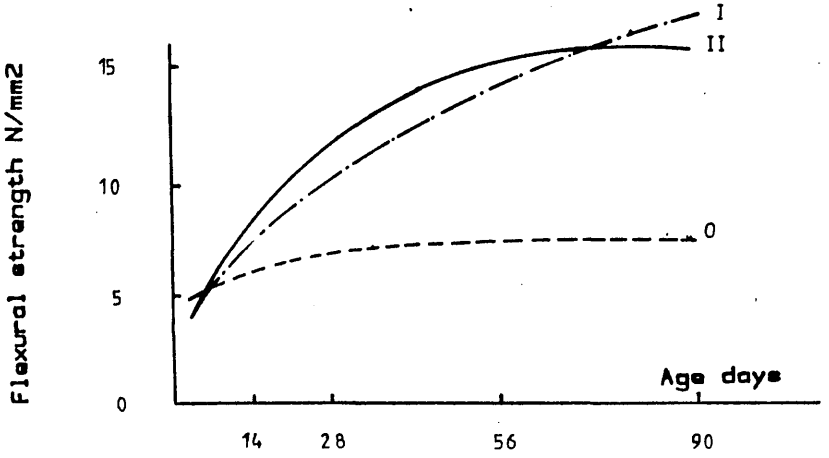

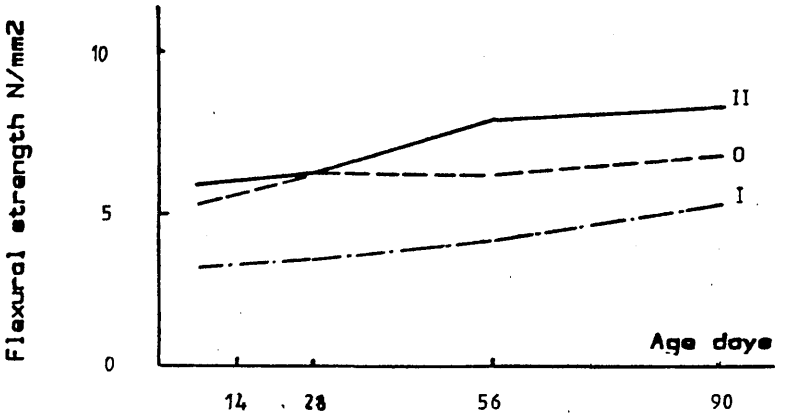

I: Polyvinyl acetate
II: Acrylic ester
0: Non-modified

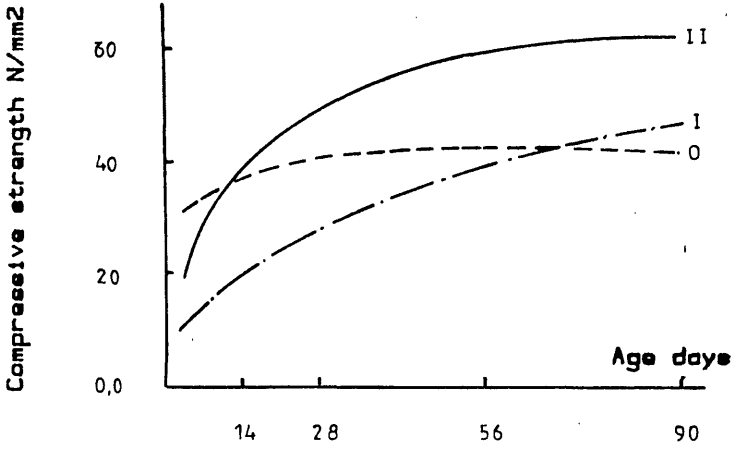

Fig. 1.5 Flexural and compressive strength development in an industrial flooring system, normal climate.

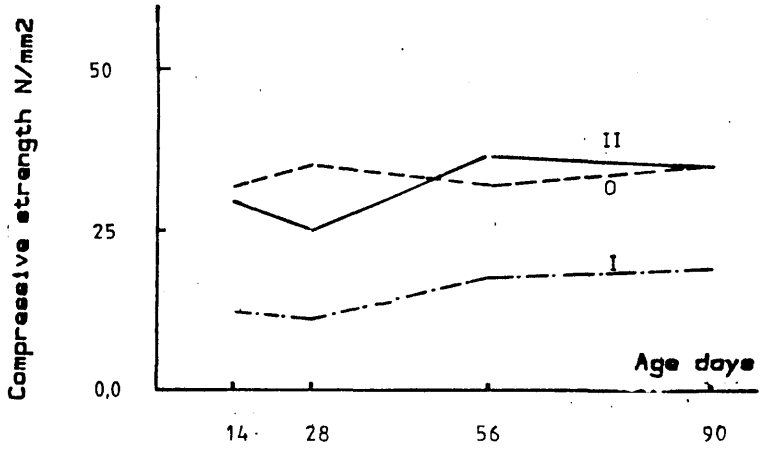

Fig. 1.6 Flexural and compressive strength development in an industrial flooring system, water treatment.

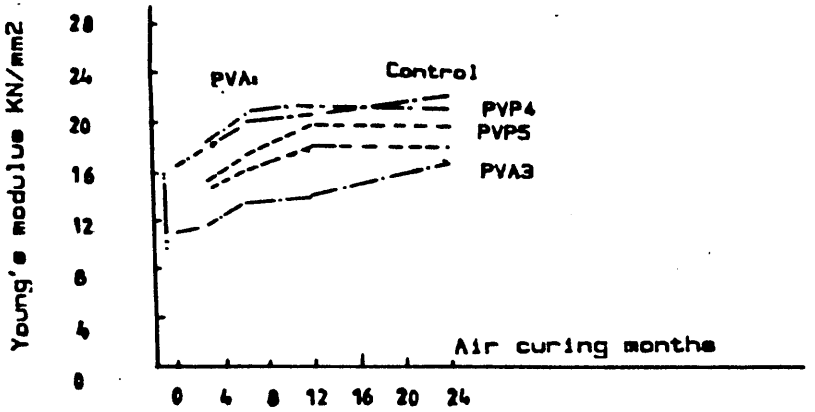

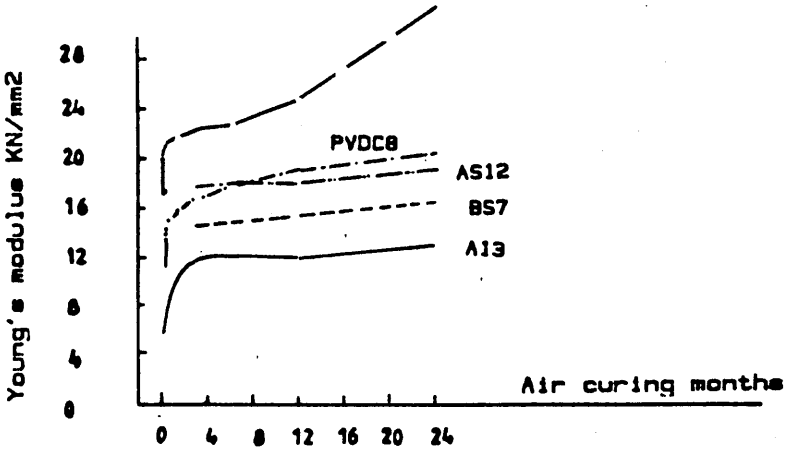

PVDC: Polyvinylidene dichloride
PVP: Polyvinyl propionate
AM: Acrylic methacrylic
BS: Butadiene styrene
PVA: Polyvinyl aceta
AS: Acrylic styrene

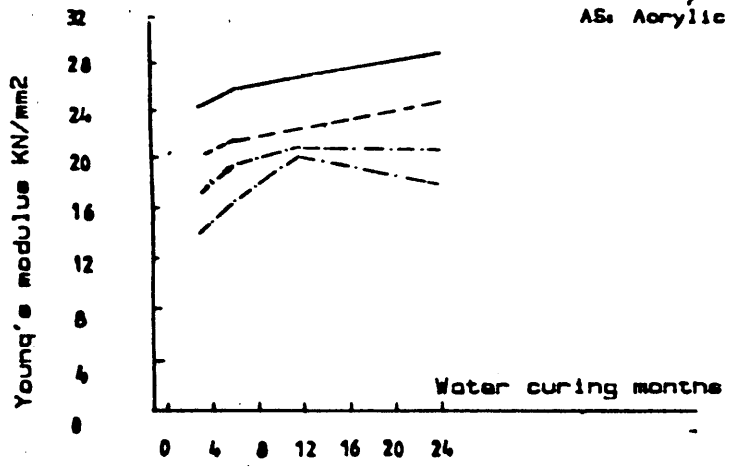

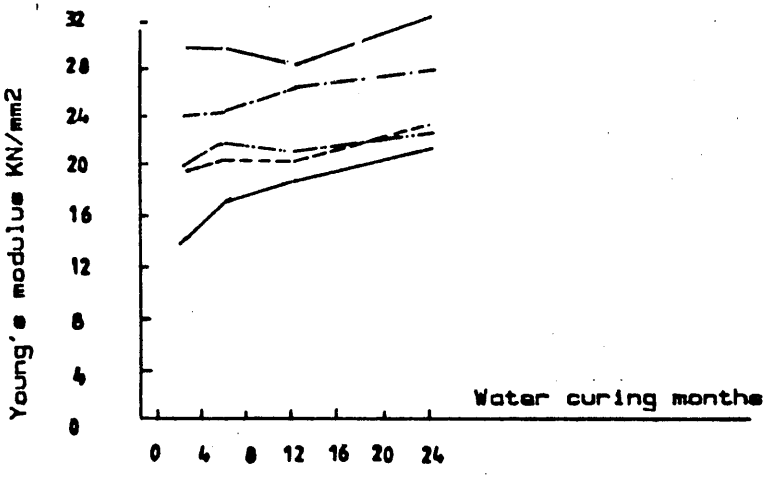

Fig. 1.7 Young's modulus versus storage time for various polymer modified cement mortars , W/C=0.35

Fig. 1.8 Young's modulus versus storage time for various polymer modified cement mortars , W/C=0.3.

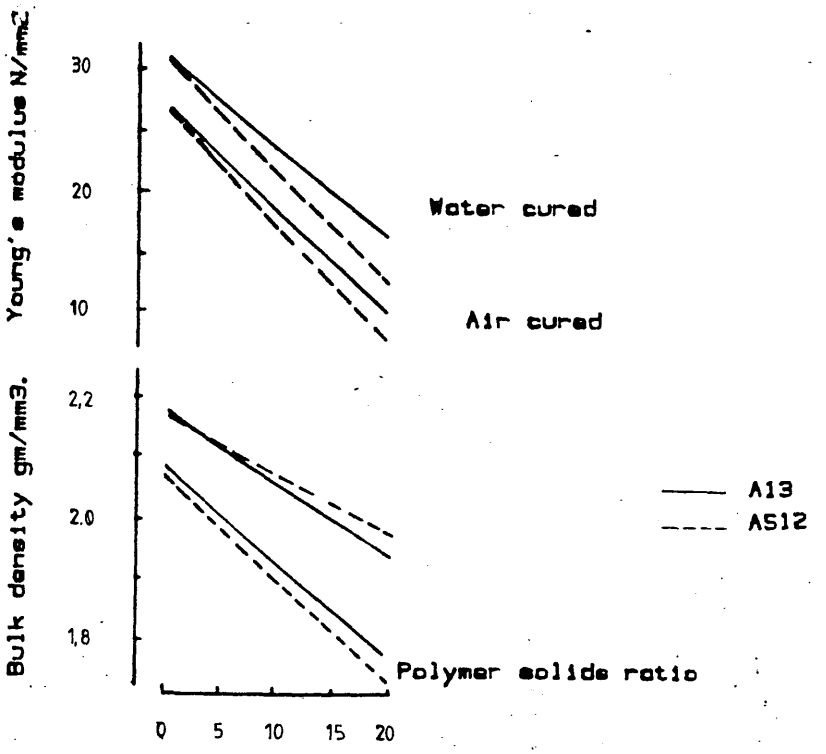

Fig 1.9 Density and Young's modulus versus P/C after 1 year storage

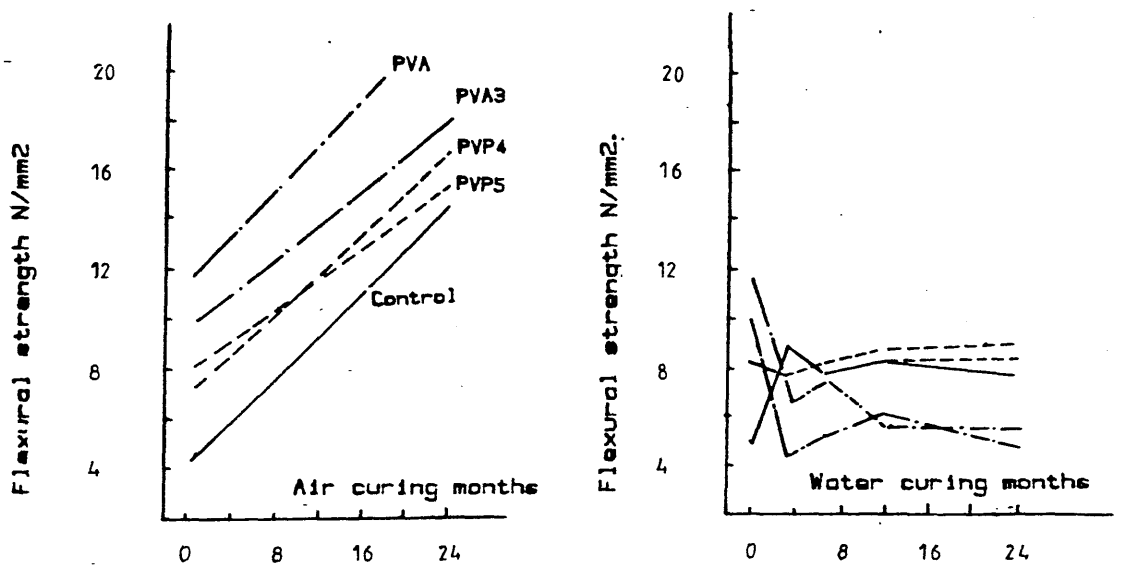

Fig. 1.10 Flexural strength versus storage time for various polymer modified cement mortars . W/C=0.35.

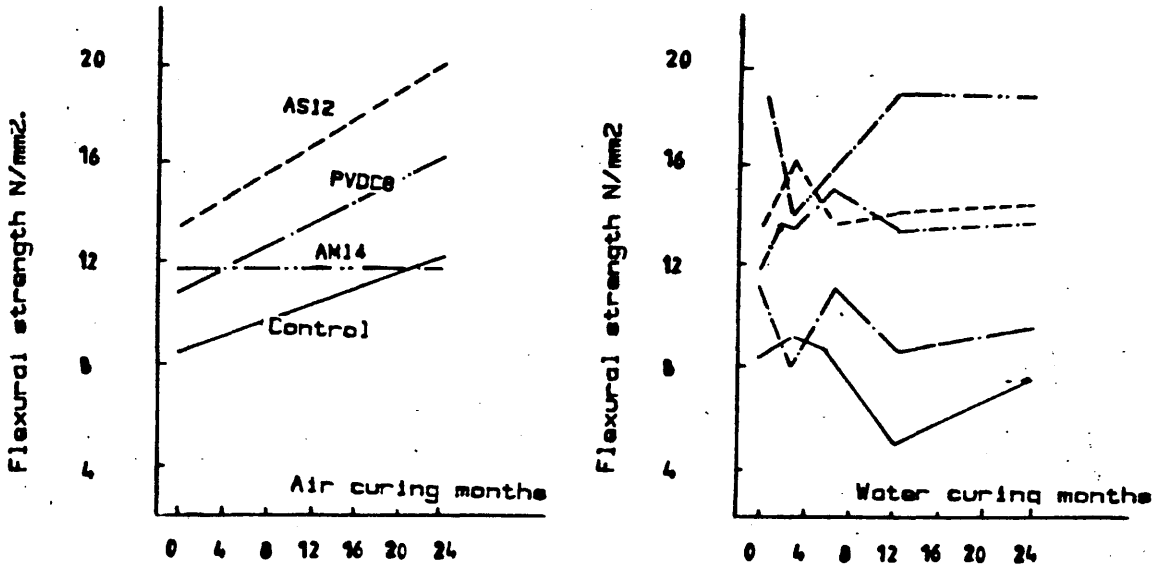

Fig. 1.11 Flexural strength versus storage time for various polymer modified cement mortars. W/C=0.3.

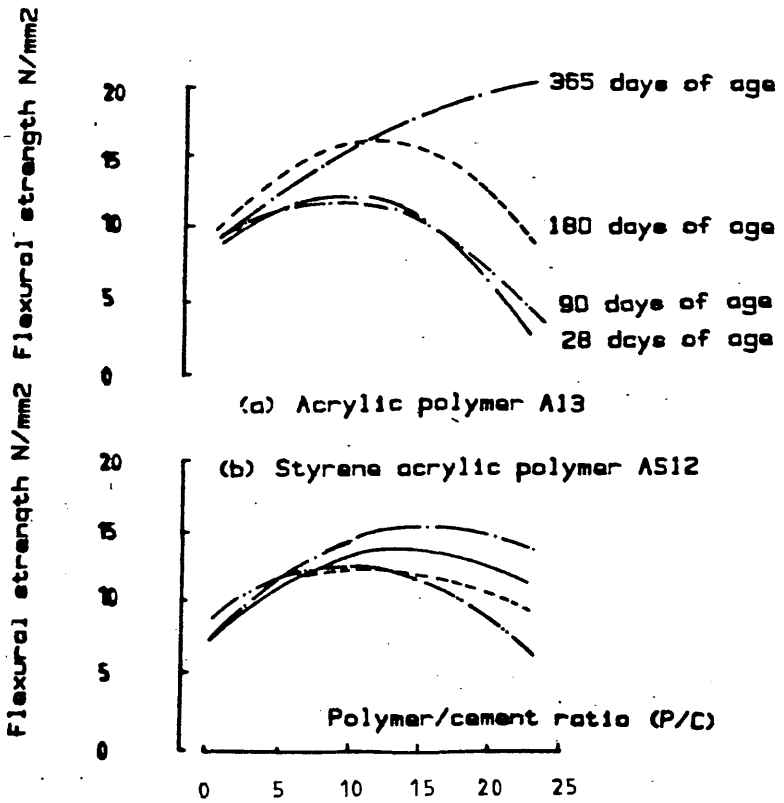

Fig. 1.12 Flexural strength versus P/C at various ages.

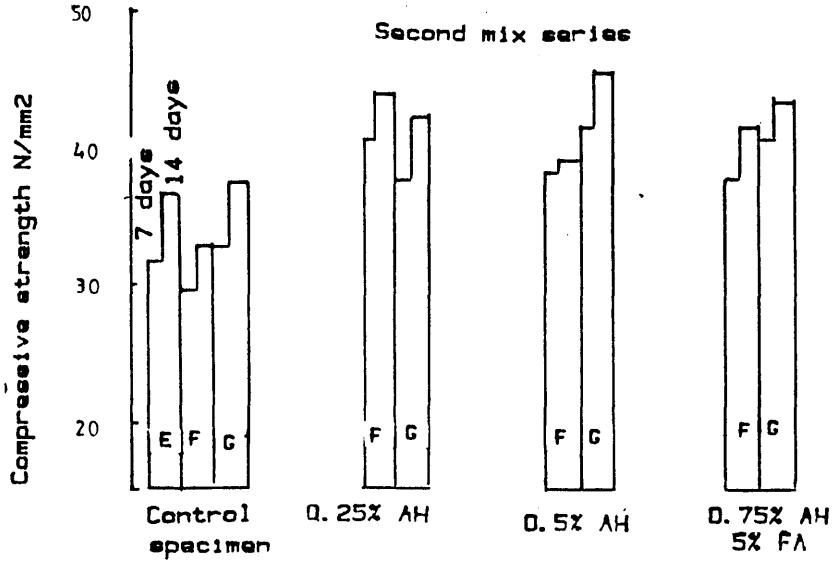

Fig. (1.13) Effect of aniline hydrochloride (AH) addition on compressive strength of cement mortars.

1st mix:
- A Portland cement
- B Shrinkage compensating cement
- C Portland cement + 1% CaCl2
- D Portland cement + fly ash

2nd mix:
- E Portland cement
- F Portland cement + 2% CaCl2
- G Portland cement + 3% CaCl2

FA: Fly ash

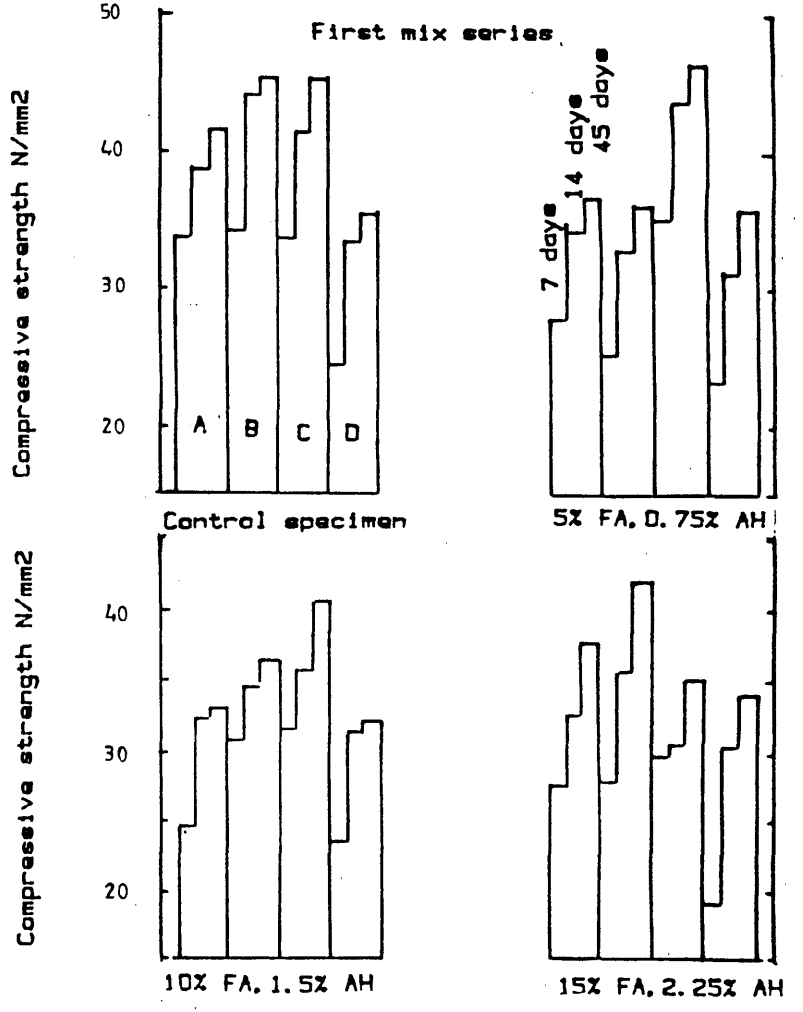

Fig. 1.14. Effect of aniline hydrochloride addition on compressive strength of cement mortar.

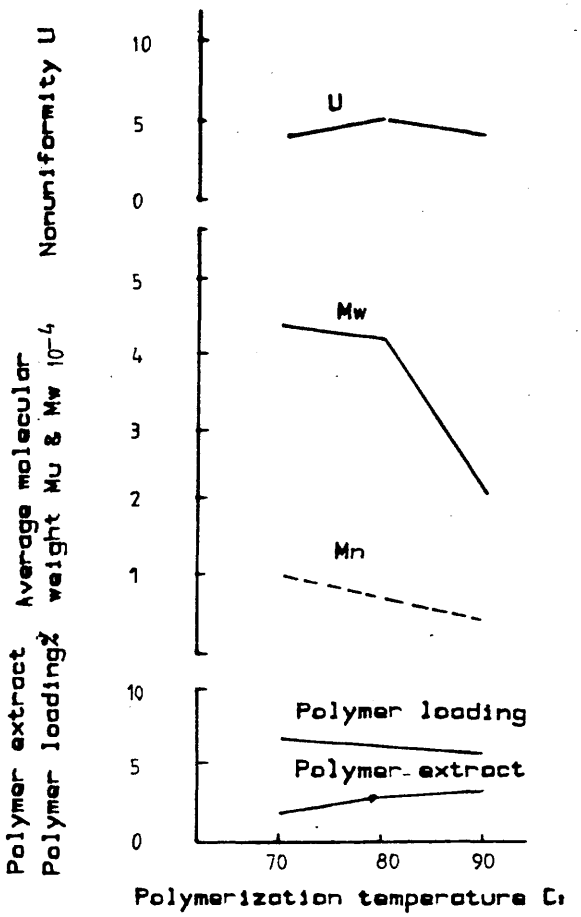

Fig. 1.15 Polymerization temperature versus molecular weight or nonuniformity of polymer formed in PMMA-IC.

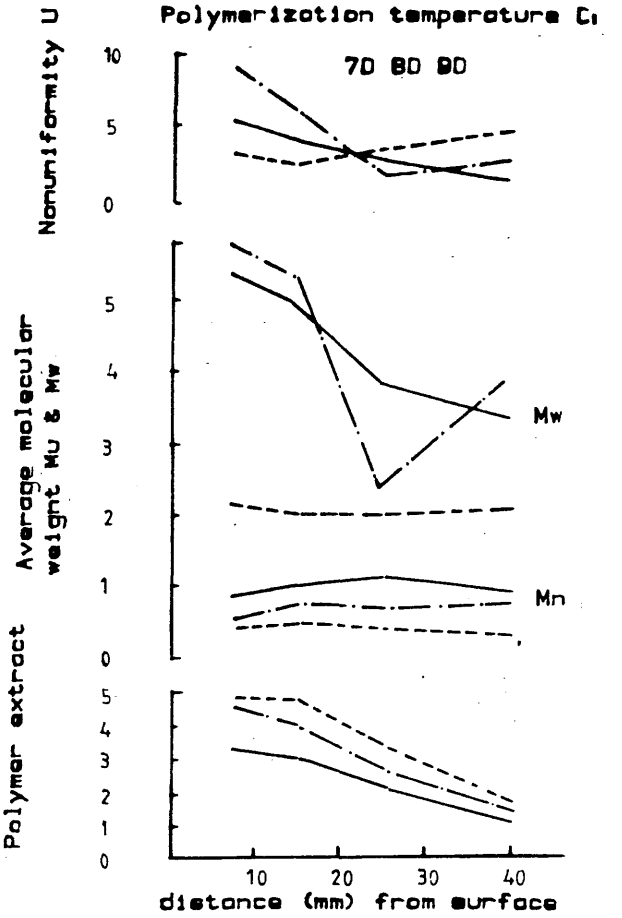

Fig. 1.16 Cross sectional location versus molecular weight or nonuniformity of polymer formed in PMMA-IC.

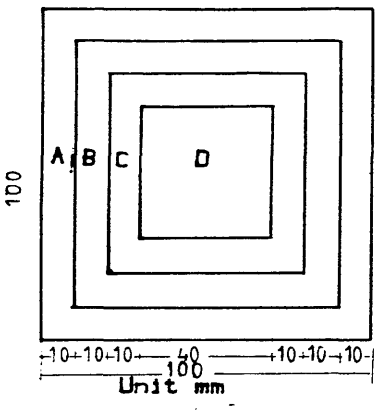

Sampling section in PMMA-IC specimen for molecular weight determination.

PMMA: Polymethyl methacrylate

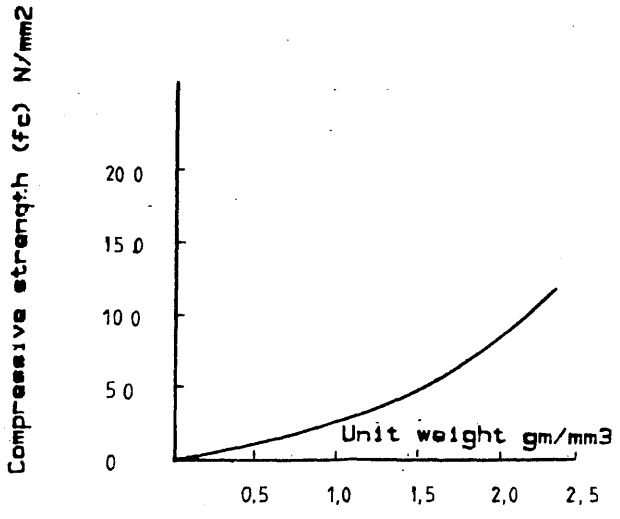

ig. 1.17 Compressive strength versus unit weight for different PC's.

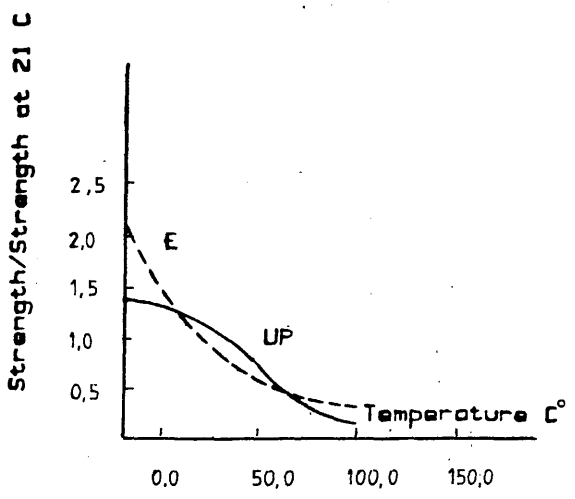

Fig. 1.18 Effect of temperat on compresive strength

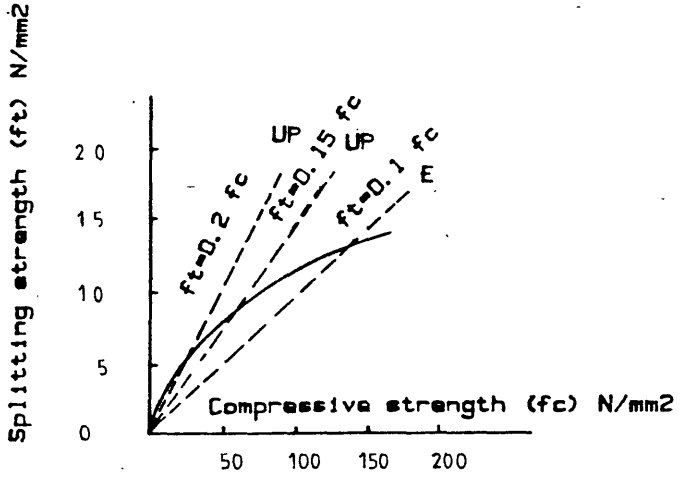

Fig. 1.19 Compressive strength versus splitting strength for various PC's.

UP: Polyester PC
E: Epoxy PC.

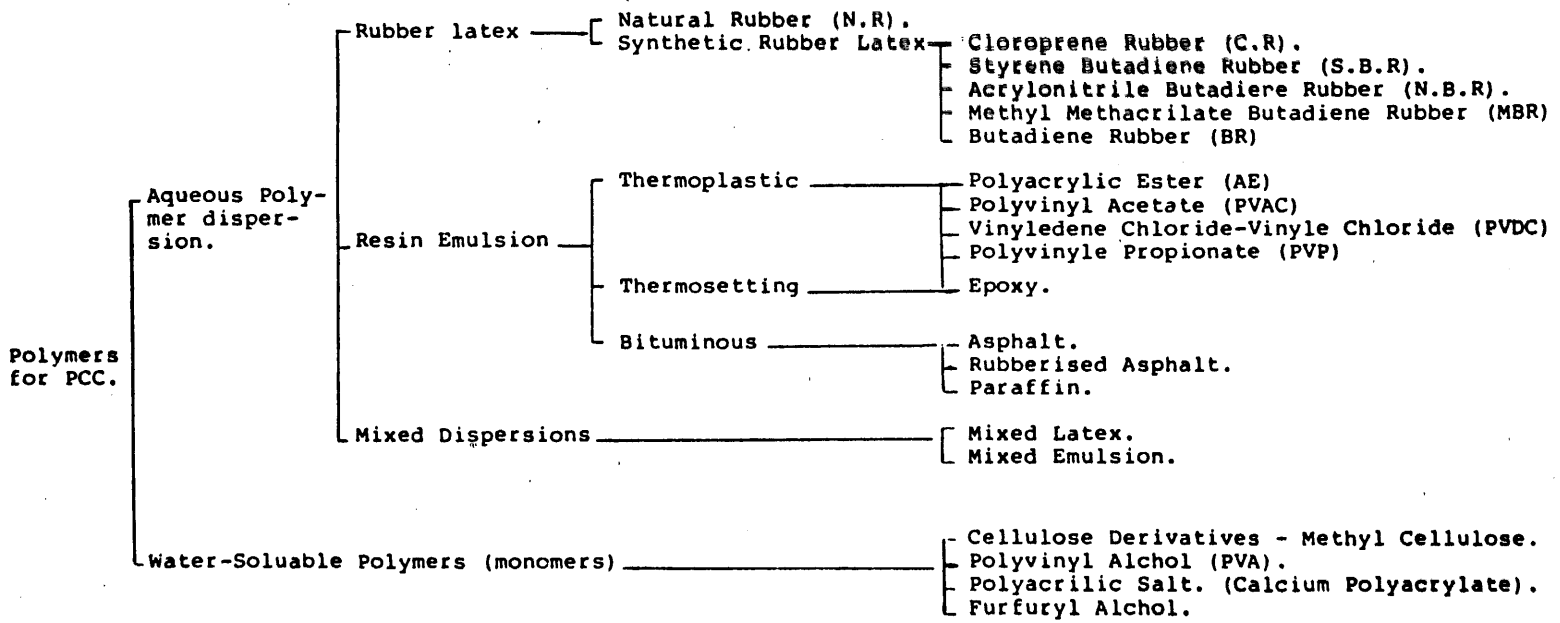

Fig. 1.20 POLYMERS for P.C.C.

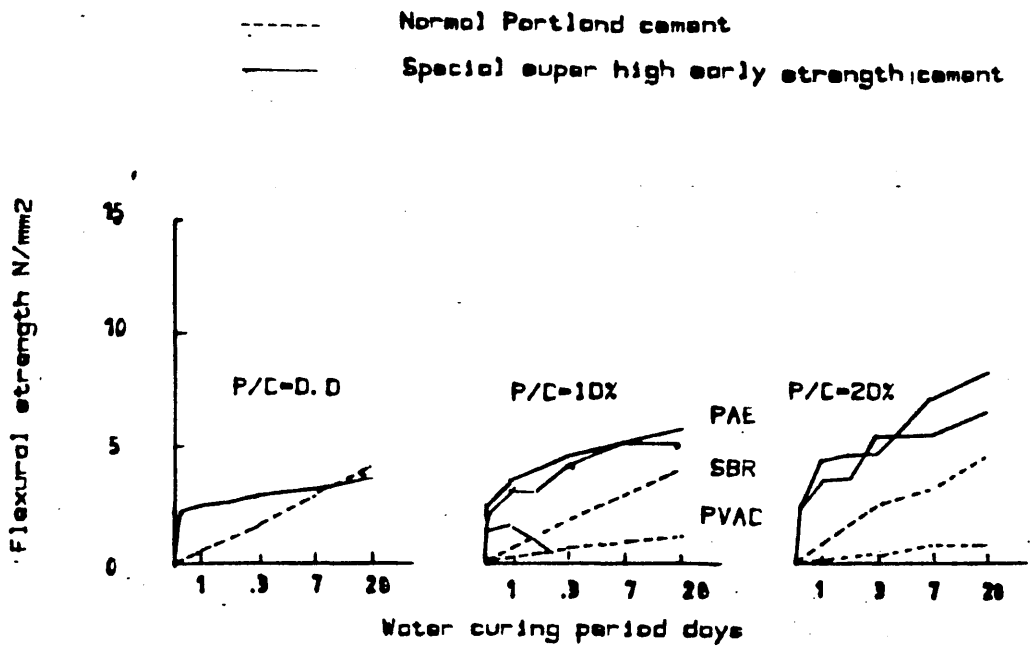

Fig. 1.21 Water curing period versus flexural strength of polymer modified mortar

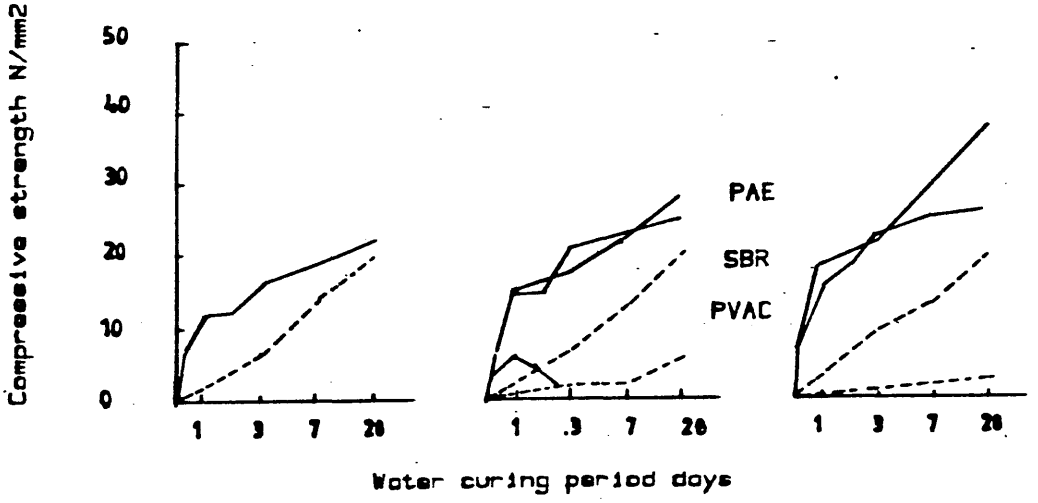

Fig. 1.22 Water curing period versus compressive strength of polymer modified mortar

PAE: Polyacrylic ester
SBR: Styrene butadiene rubber
PVAC: Polyvinyl acetate

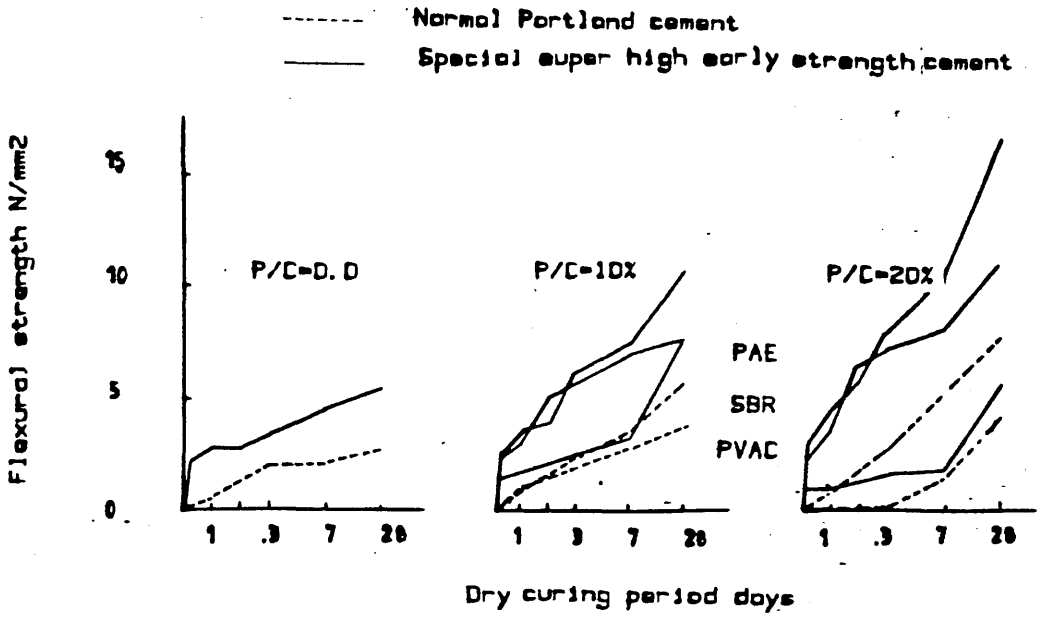

Fig. 1.23 Dry curing period versus flexural strength of polymer modified mortar

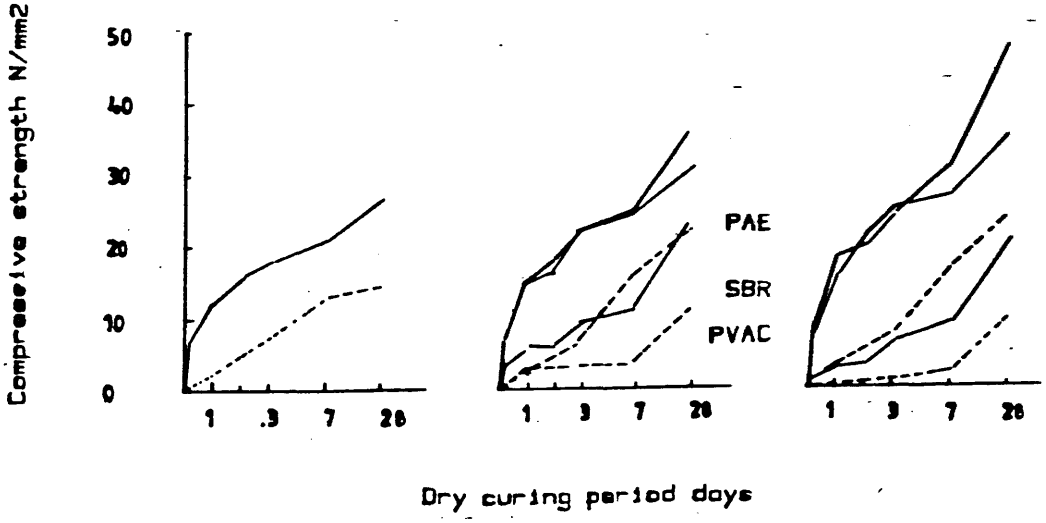

Fig. 1.24 Dry curing period versus compression strength of polymer modified mortar

PAE: Polyacrylic ester
SBR: Styrene butodiene rubber
PVAC: Polyvinyl acetate

Fig. 1.25 Example of strength development by transformation of cement concrete into PIC.

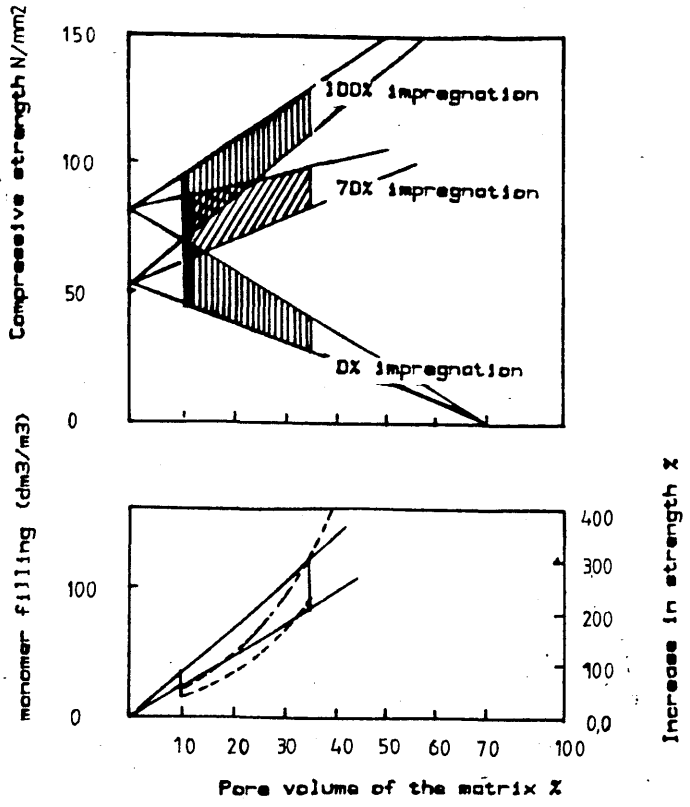

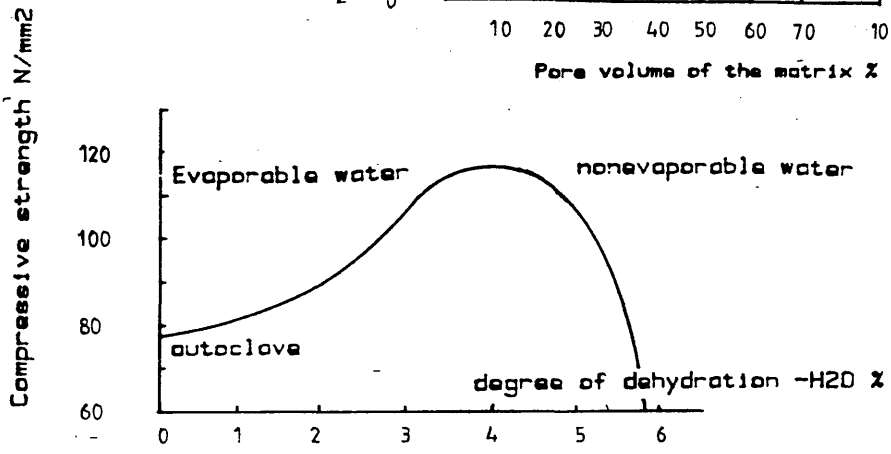

Fig. 1.26 Variation in compresive strength of a thermally treated concrete versus degree of hydration.

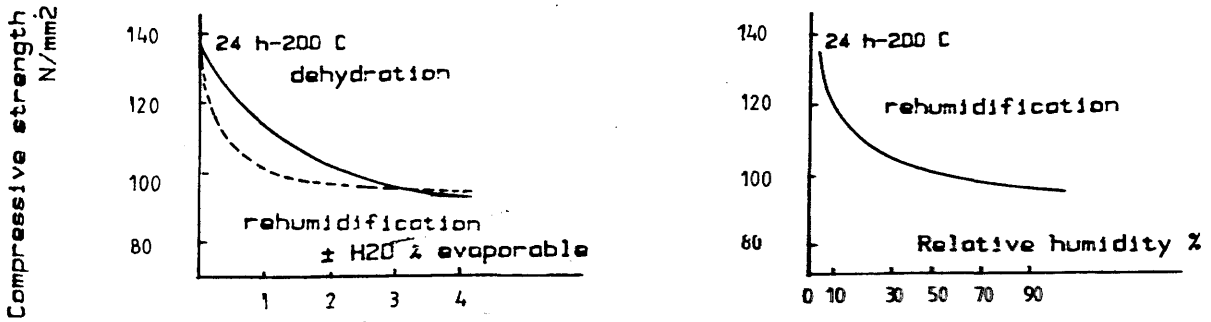

Fig. 1.27 Variation in compressive strength of a mortar versus degree of dehydration and rehumidification.

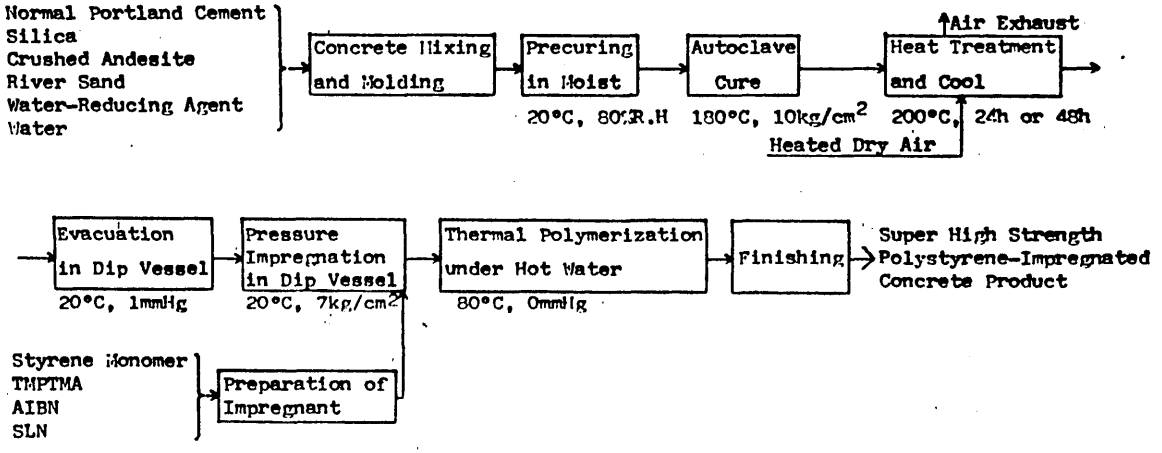

Fig.128 Process for Production of Super High Strength Concrete Product

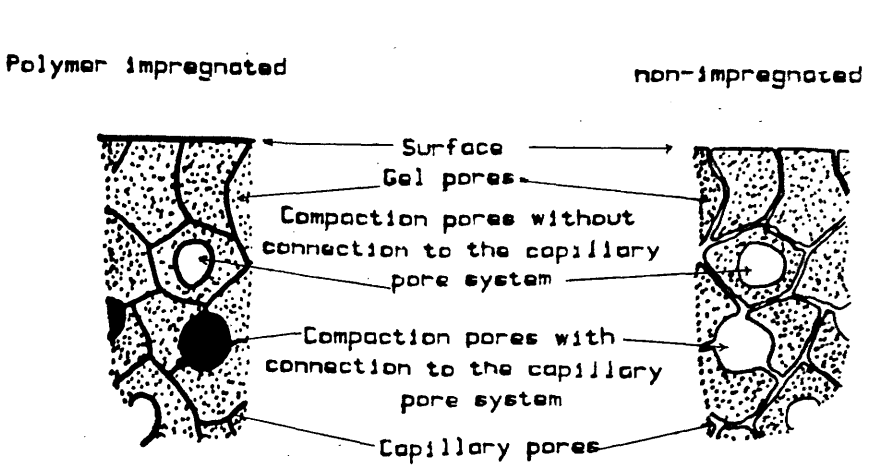

Fig. 1.29 Types of pores in a hardened cement paste.

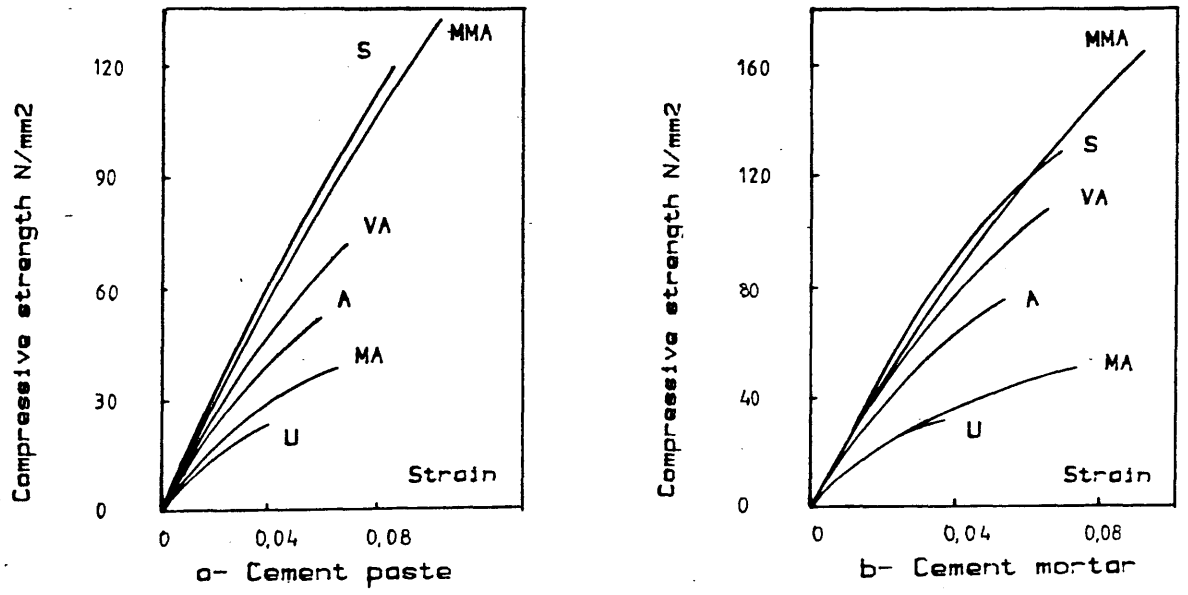

MMA: Methyl methacrylate VA: Vinyl acetate A: Acrylonitrile
MA: Methyl acrylate S: Styrene U: Untreated

Fig. 1.30 Effect of various polymers on stress-strain relationship.

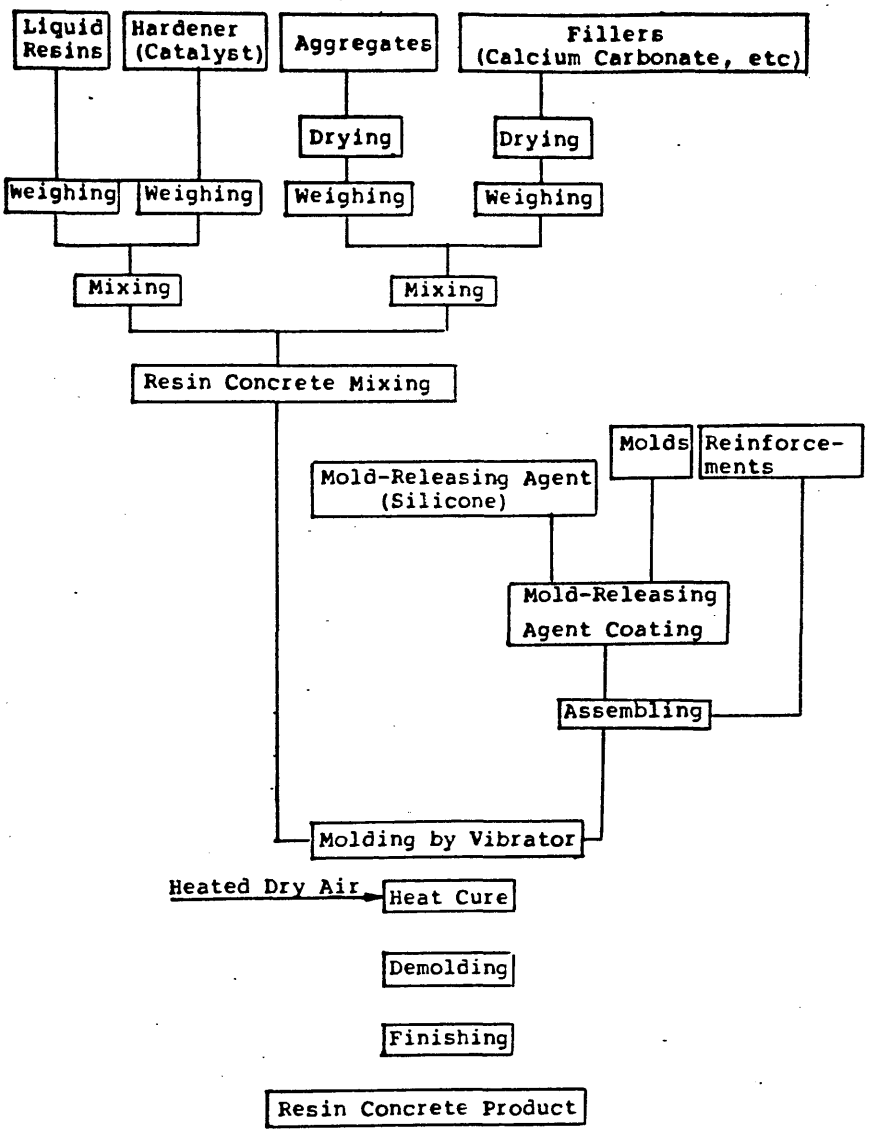

Fig. 1.31 Typical Process for REC Procast Product (Casting Method)

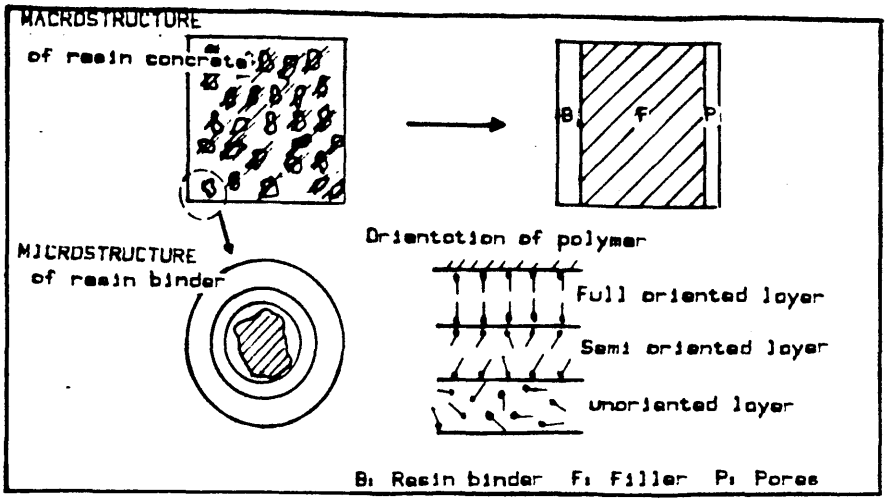

Fig. 1.32 Schematic illustration of the structural system of PC

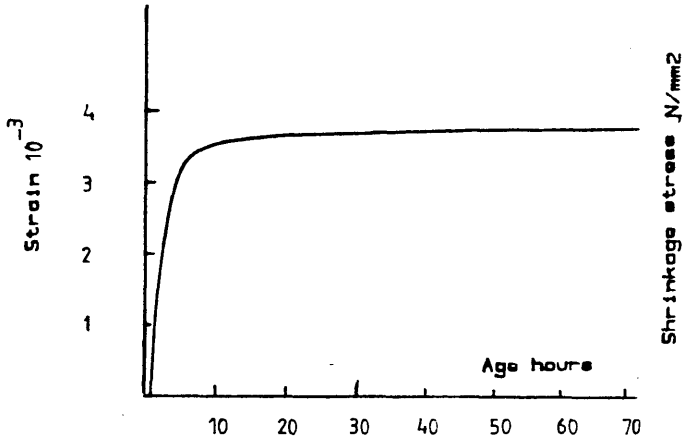

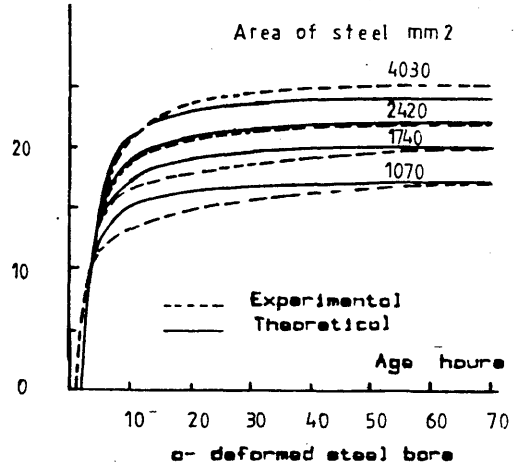

Fig. (1.33-a) Development of hardening shrinkage strain of resin concrete.

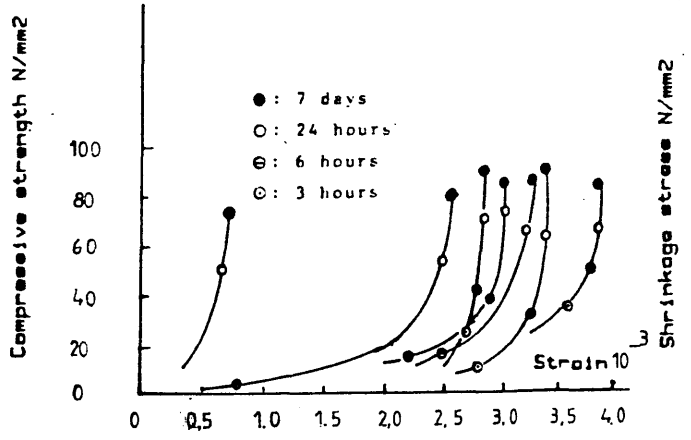

Fig. 1.33-b Relationship between compressive strength and hardening shrinkage strain

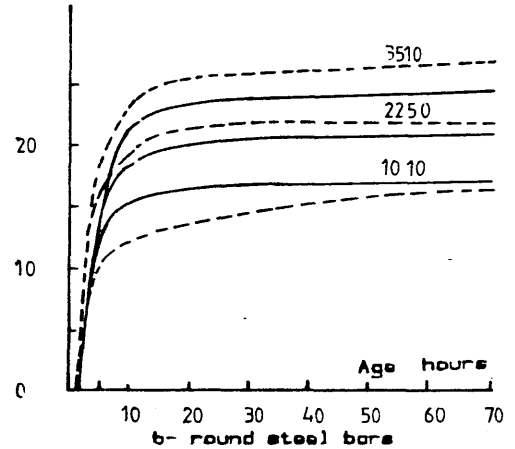

Fig. 1.34 Development of hardening shrinkage stresses of resin concrete.

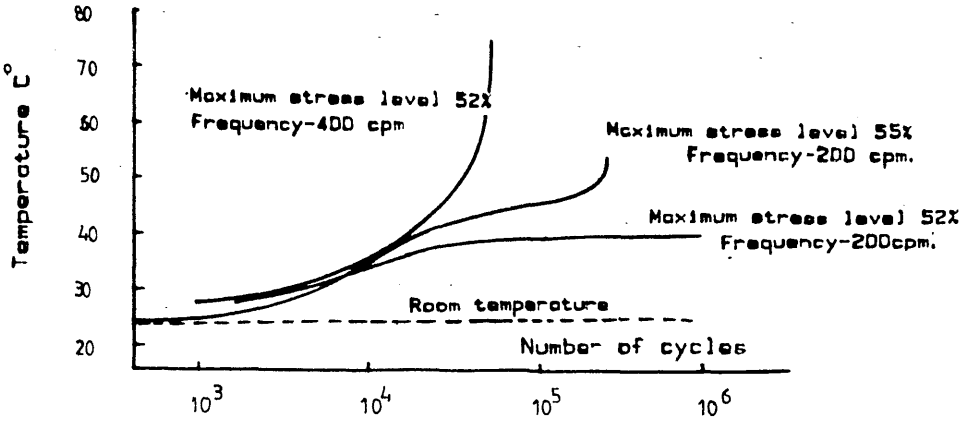

Fig. 1.35 Variation in internal temperature with number of cycles of loading for resin concrete.

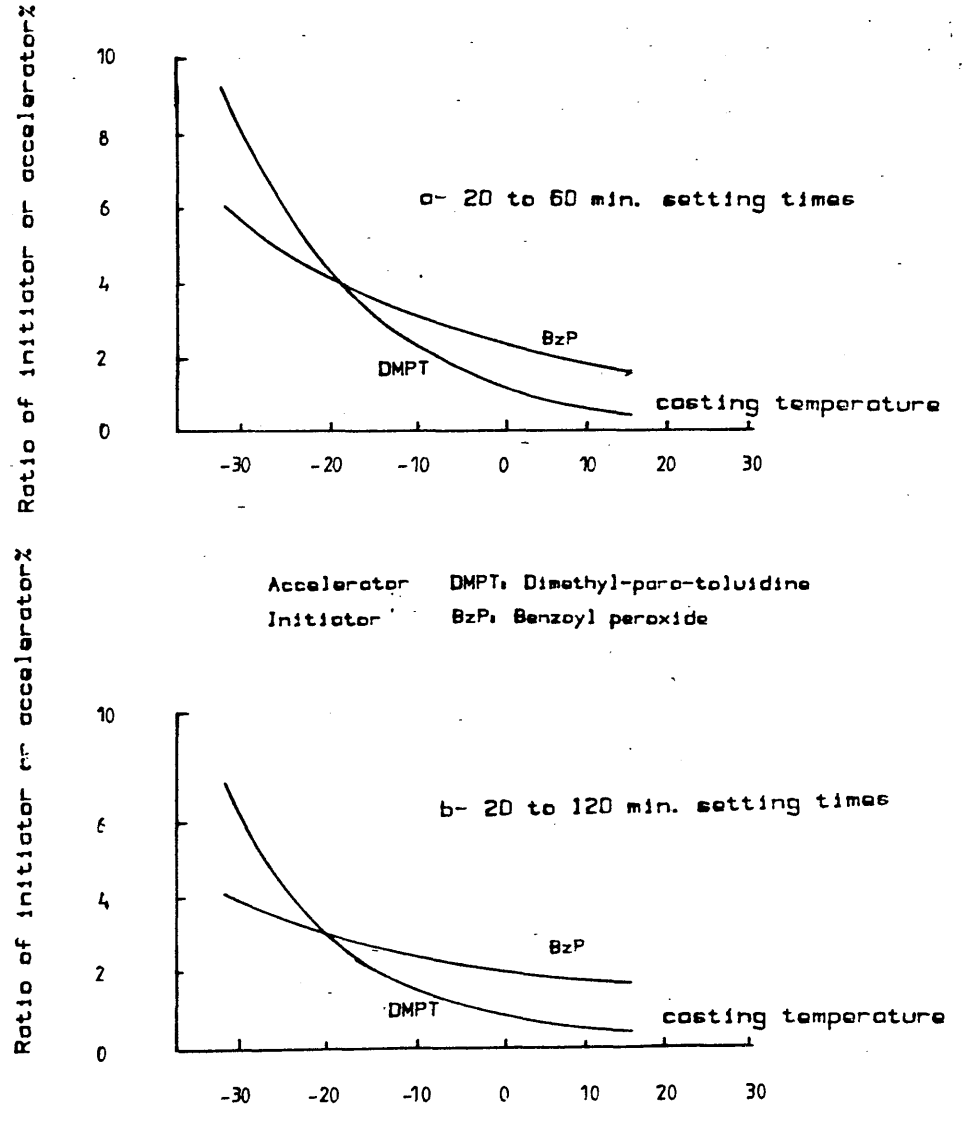

Fig. 1.36 Variation in optimal formulation of the binder with casting temperature to yield PC with a desired setting times (70% MMA, 30% TTEGDA).

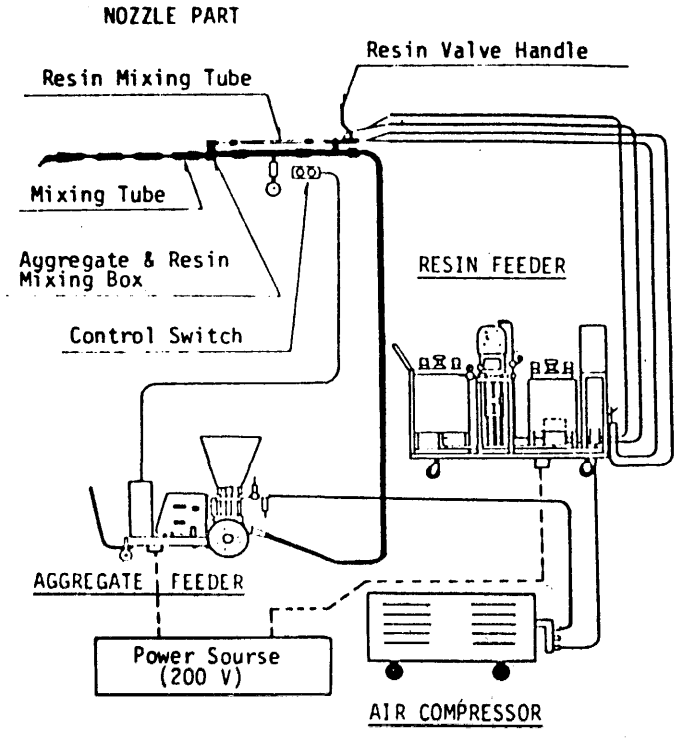

Fig.1.37 SHOT REM Basic System

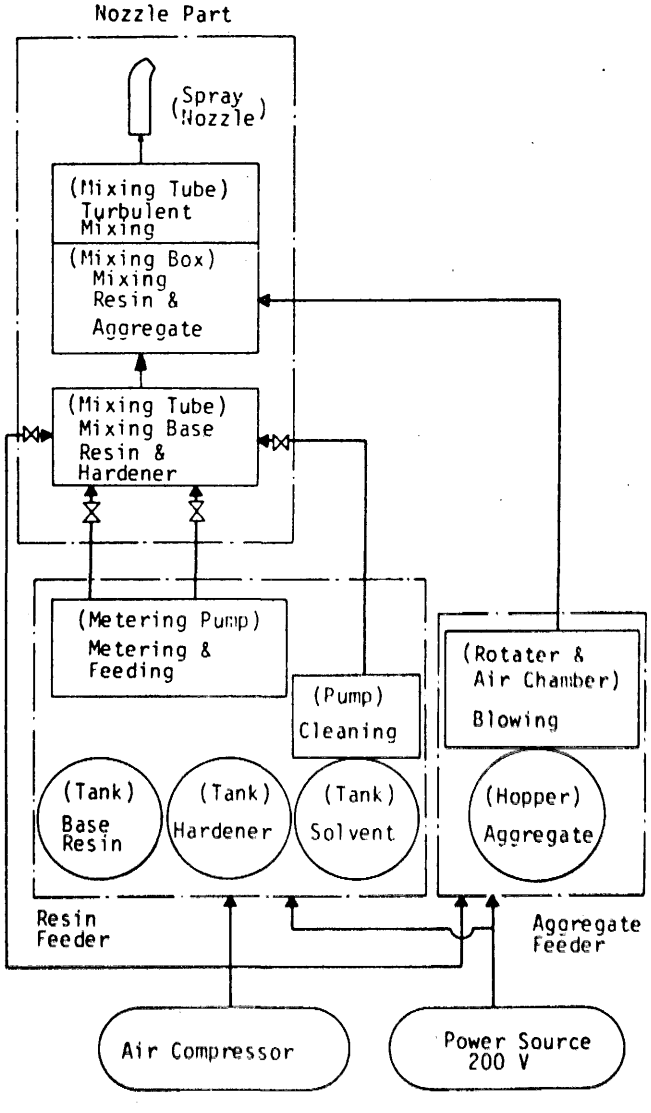

Flow Chart of SHOT REM Basic System

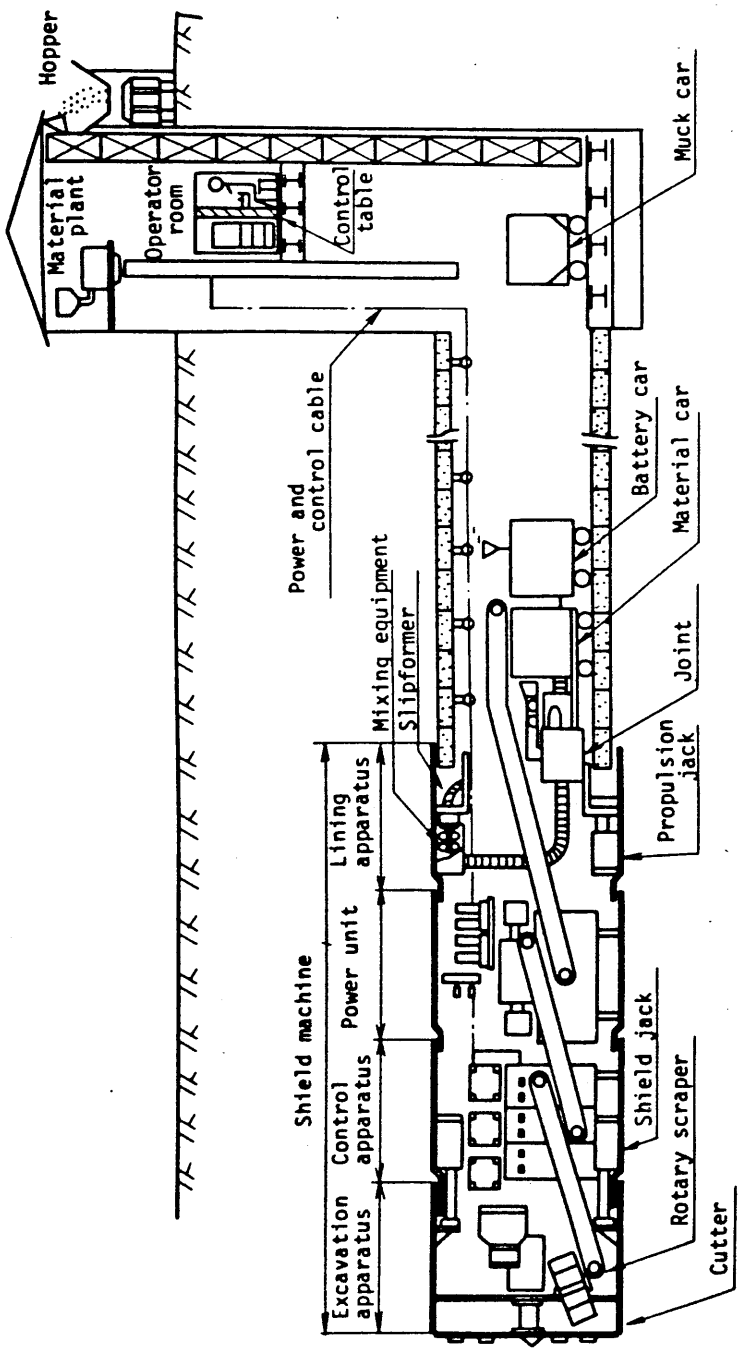

Fig.1.38 Outline of tunnelling method

CHAPTER TWO

MIX PROPORTIONING AND OPTIMIZATION OF POLYESTER RESIN MORTARS

2.1. Introduction

Polymer-concrete mix design in its widest sense means the selectionof suitable ingredients of PC, and the consequent determination of their relative quantities. As with conventional concrete, mix design is a way of reaching the cheapest mix that will have appropriate workability, strength and durability. Portland cement is usually the highest cost ingredient used in making cement concrete. For this reason, the main concern of the mix designer is to keep cement content as low as possible without diminishing other properties of the fresh or hardened concrete.

With PC it is evident that cost depends primarily on the polymer or resin used. It is worth mentioning that on average the cost of resin is twenty times as much as portland cement on a weight basis. Hence it is vital to keep the resin content as low as possible. Several methods have been investigated to fulfill this prerequisite. Carefully selected gradings of aggregates that would give minimum voids and specific surface area were tried. Aggregates with as large a maximum size as possible were also adopted. For good workability and low resin contents, some researchers recommend the addition of fine fillers that would lubricate the aggregates and allow for easier flow. Because of the nature of resin itself, much more viscous than cement slurry, recent trends are aiming at diluting the resin and reducing its viscosity by as much as would not degrade its physiochemical and other mechanical

properties. Interest is now gaining ground in using resins that are initially much lighter and less viscous.

As far as PC workability is concerned, the same definitions as with conventional concrete still apply. One of these is that workability can be defined as the amount of useful internal work necessaryto produce full compaction (52). Itis well known that a sufficiently workable PC would not only allow good placement with minimum vibration in its fresh state, but would also produce a high-performance concrete when hardened. With PC made of polyester-styrene resin, the ratio of styrene /polyester is very similar to the W/C ratio in cement concrete (53). So styrene content or more specifically resin viscosity, has a dominating influence on workability. Resin content in PC determines the mix richness just like cement content with PCC.

Aggregate shape and texture has an effect on PC workability, especially with the lean mixes which are usually the case with PC. Maximum aggregate size has also an effect on PC workability as well as the grading and entrapped or entrained air. Very little has been done regarding the development of different methods of measuring PC workability. A clear distinction between workability and consistency has yet to be defined. Some of the conventional tests for measuring workability might provide a rough idea about the flowability of PC mixes. However, most of these tests would fail in measuring various parameters controlling PC stiffening. Stiffening of PC fresh mixes is made apparent by the loss in solvent content by evaporation and the onset of the polymerization process. All resins have their individual gel

times and final setting times, which change greatly when mixed with other PC ingredients. The traditional troubles with poorly designed cement concrete mixes like segregation, bleeding and nonuniformity are just as likely to happen with PC mixes if not given due attention.

Abram's law relates concrete strength to W/C ratio for given materials in cement concretes. This law should remain applicable for PC strength by substituting W/C ratio with styrene/polyester ratio. Resin viscosity may be used as a measure of this ratio (53).

Very little information is available about proper mixing times, proper mixer types, best vibration techniques and the consequent strength variations for PC. The relationships between the required minimum strength and the mean or the characteristic strength are not established yet. Furthermore, methods of testing and specimen dimensions are still awaiting standardization in most countries. Little is known about strength 'frequency-distribution' for PC. The need for reliable mix-design methods and quality control still calls for greater research efforts.

2.2. Chemistry of polyester-resin

Although the chemistry of Polyester resin is primarily the field of organic chemists, the basics of polyester manufacturing and polymerizing processes will be briefly dealt with.

Regardless of having a neutral charge, an atom will only be stable when its outer electron-shell is filled to its capacity

by electrons (54). This can be done either by ionic bonds in which atoms are held together by opposite electrostatic attractions, or by covalent bonds in which atoms share electrons. Elements in the central groups of the Periodic Table (P.T.), or on the same side of the table tend to share electrons rather than to transfer them. Carbon is an element near the P.T. centre, so it is always covalently bonded.

Organic chemistry is the chemistry of carbon compounds and might for this reason be named as the chemistry of covalent-bond reactivities. These covalent bonds have a wide variety and a rather specialized terminology. However, it may be useful to stress some of them here. The simplest covalent bond is 'sigma-bonding', in which the resulting molecular orbitals contain two electrons as is the case with methane, see Fig.(2.1). In the same figure, examples of double and triple bonds are given. The important thing to notice is that with all double and triple covalantly bonded molecules, there is a reactive or unstable site known in organic chemistry as a 'pi' bond. These sites are principally responsible for crosslinking long-chain molecules. As will be seen later, any resin type containing these sites is called 'unsaturated resin'.

2.2.A Polyester-resin manufacture Polyesters are formed by the reaction of an organic dibasic acid with a dihydric alcohol (glycol). As shown in Fig.(2.2-a) an ester is formed by condensation. In this case the acid has just one carboxylic group (CO.OH), and the alcohol has just one hydroxyl group (OH). The more general case is represented in Fig.(2.2-b) where each alcohol and acid molecule has two end functional groups. The resulting ester in this case has hydroxyl and

carboxyl end groups which allow for more reaction and much longer polyester chains as shown in Fig.(2.2-c). This type of polyester is termed as a 'thermoplastic saturated' resin. Terylene is an example of this type of resin.

If the acid used in processing is of the reactive 'unsaturated' type, the resulting polyester will still be thermoplastic, Fig.(2.2-d); if catalysed the reactive sites are caused to link together and a polymer network is formed, Fig.(2.2-e), with thermosetting properties (does not flow on heating while under pressure). This type of polyester is very viscous and when hardened is very brittle due to the high degree of crosslinking in the final product. That is why most manufacturers use a ratio of saturated/unsaturated acids to reduce the frequency of crosslinking.

Usually another component is added in the manufacture of thermosetting polyesters. This is often a reactive monomer such as styrene, methyl methacrylate or diallyl phthalate. As shown in Fig.(2.3), the reactive monomer (styrene) has two reactive sites which are capable of crosslinking polyester chains at the sites of the reactive acid. Styrene serves in two ways; one is to make the resin more liquid in the prehardened state, the other is to allow less brittle products in the hardened state.

2.2.B Polymerization of polyester-resins While the manufacturing process is essentially a condensation reaction in which water results as a by-product, polyesters are said to be polymerized when they have transferred from the liquid to the solid state. To start polymerization liquid resin should

first be given a small amount of energy or otherwise activated. Thereafter it proceedss spontaneouslyto full polymerization. Energy can be provided either by heat or radiation. Activation is provided by the addition of catalysts (initiators) and accelerators (promotors).

When the catalyst is added to the liquid resin, it can be decomposed either by an energy supply or by the addition of accelerators. When the catalyst is decomposed ,'free radicals' are formed and they initiate the chain-reaction polymerization and crosslinking at the reactive sites of polyester chains through a process called 'addition-reaction'. Under accidental energy application to the liquid resin, this reaction can take place without the addition of catalysts. For this reason most manufacturers add inhibitors to the resin. These inhibitors must be neutralized first if full curing is to be reached.

2.2.C Properites of polyester resins During the manufacture of polyester, cooling will stop the condensation reaction at any desired acid number, molecular weight or viscosity. The higher the molecular weight of the polyester resin and the more points of unsaturation in it, the more rapidly will the polyester-monomer combination gain strength during the curing process. Higher mechanical properites of cured resins are attained with increased molecular weight.

The ratio of saturated /unsaturated acids affects the final product properties. Increasing this ratio gives a more loosely polymeric structure, a slower curing rate, more flexibility, lower heat-distortion temperature and less resistance to chemical attack.

The type of acid used in manufacture has a dramatic influence on the finished product properties. Phthalic saturated acid can be used in the isophthalic or terephthalic form. Use of the former would result in substantially higher molecular weight with superior strength, toughness and increased heat and chemical resistance over standard phthalic-acid resins. If the acids used were all of the saturated type, the result would be a resilient-polyester type (plasticizer) with improved toughness and flexibility suitable for coatings and plastic products. Fumaric-based unsaturated acids give better mechanical and chemical properties than maleic-based ones.

Water and heat resistance are properties which are particularly affected by the choice of the alcohol. Monomers used have also certain effects. While styrene is preferred for its low price, good reactivity and compatibility, others might be used for special applications. Even the type of inhibitor incorporated has some effect on the performance of the hardened product.

Specially-formulated polyester resins are now available for particular applications that require superior weatherability, high flame-resistance, high heat-resistance and low shrinkage strains, etc.

The dominant constituent in the resin polymerization process is by far the catalyst, which is usually an organic peroxide. Its selection depends on temperature of curing and its desired rate, incorporated inhibitors, desired degree of polymerization and the activating means (heat, accelerator,

ultraviolet light, etc.). For any given resin-catalyst system there is an optimum temperature at which the resin can utilize all the free radicals formed by the peroxide decomposition at that temperature. Above this temperature peroxide is wasted and below it too much time is required for completing curing. As catalysts are very expensive, the temperature ranges within which catalysts are effective must be fully investigated.

2.3. Resins used in the present work

The polymeric binder chosen for the PC of this work was of the Polyester resin type. This was mainly because of its high physical and mechanical properties, its low viscosity, its simple curing techniques at ambient temperature and its comparatively low cost compared to other resins.

Initially two different types were investigated and the best one adopted throughout the whole work. The first polyester resin chosen was "Crystic 196" which is a versatile, rapid-curing and general purpose one. It is said to have excellent mechanical properties. It also conforms to B.S. 3532 Type B. Another preaccelerated, low-viscosity version of this resin, "Crystic 196 PLAV", was also chosen. Typical properties of these two versions of "Crystic-resin" are shown in tables (2.1 & 2.2).

The second polyester-resin type chosen was "Cellobond A2661", which is a heat-stable and chemical resistant resin. It has a medium viscosity suitable for both cold and hot applications where heat stability is essential. Typical test results on liquid "Cellobond" resin are shown in table (2.3), while properties of the cured resin are shown in table (2.4).

2.4. Materials Used In The Present Work

2.4.A Chemicals

(1) Resins As mentioned above "Crystic 196", "Crystic 196 PLAV" and "Cellobond A2661" resins were used.

(2) Catalysts Out of the large variety of organic peroxides that are suitable for use, the chosen one was that recommended by the manufacturer. It is a 60% solution of methyl ethyl keton peroxide (MEKPO). This catalyst was used with the chosen resins at room temperature.

(3) Accelerators As cobalt derivatives are the most effective promotors for use with the already chosen catalyst type, a 0.6% cobalt solution was selected as an accelerator. As will be seen later, the preaccelerated version of "Crystic" resin was much more convenient for use as it did not require the addition of accelerator.

2.4.B Aggregates and fillers

(1) Fillers Very fine fillers like calcium carbonate powder, fly ash, portland cement and aluminium silicates may be used with PC. Those fillers have a vital role to play in PC manufacture and performance. They permit the use of high curing temperatures, where they tend to reduce the exothermic-reaction temperature by reducing the concentration of reactive materials. In addition to being a filling material at a very low cost, they also improve workability and act as lubricants when mixed with the resin by reducing the required internal work to overcome internal friction in the mix. Fillers also

provide smoother finished products, with reduced setting and volumetric shrinkage cracking. They also provide along with the resin the system matrix giving it a lower coefficient of thermal expansion, a higher modulus of elasticity and much lower internal strains on setting and final hardening. Resin absorption by aggregates and mix bleeding are greatly reduced by using fillers.

Two main filler-types were chosen for this work; calcium carbonate powder and fly ash. Their properties are shown in tables (2.5 & 2.6) respectively.

(2) Aggregates All the aggregates used in the present work, with few exceptions, were supplied by Hyndford Quarry, near larnak, Scotland. As will be shown later, different classifications and particle shapes of natural sands and irregular gravels were used. Wide ranges of gradings were investigated. Crushed basalt stone supplied by Cairneyhill Quarry, near Airdrie was also used.

Physical, chemical and mechanical properties of the different fine and coarse aggregates used are shown in tables (2.7 to 2.9). For the whole work aggregates and fillers have been oven-dried overnight unless otherwise mentioned.

2.5. Resin-mortar (RM) investigation

For the highest performance concrete, one should first find the highest performance mortar. Different parameters were investigated to discover their influence on RM properties in regard to workability and strength. As will be seen, the experimental work on resin mortars (RM's) was divided into

three groups. These groups were designed to study the following :

(a) The effect of sand grading and its content.
(b) The effect of filler type and its content.
(c) The effect of resin type and its content.
(d) The effect of moisture content.
(e) The effect of resin formulation in terms of styrene/ polyester ratio.
(f) The effect of elevated temperatures.

2.5.A Specimens For the investigation of RM, small specimens were manufactured to allow small batches and to provide more quality control on the reproduceability of them. Small specimens reduced the required number of batches and allowed for collective mixing, casting, vibrating and curing.

For the evaluation of compressive strength and its 'frequency distribution', the two sizes of cubes chosen were 70 and 50 mm. respectively. For tensile strength (splitting strength), cylinders of 50 mm. diameter and 100 mm. length were used. All moulds were made of PVC which allowed good demoulding when silicone grease and other releasing oils were applied.

2.5.B Mixing, casting and curing As the specimens were small, the size of batch was small enough to allow mixing to be carried out manually using an impermeable hardboard base. To ensure consistent batching the resin viscosity was measured before mixing using a viscometer of the type shown in Fig.(2.4). Catalysts and accelerators were first added to the resin at the ratio recommended by the resin-suppliers. Dried fillers and sand were dry-mixed and the formulated resin added

to them.

Manual mixing continued until a uniform mix was reached. Moulds painted with releasing agents were then filled and vibrated for 3 min. on a vibrating table. Specimens were allowed to cure at ambient temperature until the day of testing.

2.6. Tests and their results

Different groups of tests were made to investigate the effects of the previously mentioned parameters on resin mortar performance as follows.

2.6.A First group of RM In this group seven different mixes were studied collectively and general comparisons were made on the basis of their results. Four of these mixes used calcium carbonate powder as a filler, while the other three mixes used fly ash. The various mixing ratios are shown in table (2.11). The sand grading was as shown in Fig.(2.5-a) and lies within the second zone of sand gradings' standards (B.S.882).

For this group "Crystic 196 PLAV" resin was used. The effects of different mix-proportioning parameters were studied as well as the effect of elevated temperature on strength. Elevated temperatures were applied by keeping specimens for 30 min. at 80 C°, followed by 90 min. at 100 C° in an electric-fan oven. Table (2.12) shows the results obtained through this group, which are represented as shown in Fig.(2.6)

From mixs (1) and (2) it is clear that increasing resin content will for a given temperature result in an increase in

strength, but the deleterious effect of increased temperature becomes more apparent as resin content increases. For low resin contents, the filler had a very clear effect. By referring to mixes (2) and (4) it can be seen that as filler content was decreased from 16% to 5% by weight, compressive and tensile strengths decreased by 20% and 30% respectively. This effect is once again pronounced with mixes (5) and (7) in which another type of filler (fly ash) was used. This confirms the importance of the filler regardless of its type. It is noteworthy that increasing resin content by 5% resulted only in a 10% and 15% increase in compressive and tensile strengths respectively,see mixes (1) and (2). This increase could well be exceeded by adjusting the filler content to its optimum fractional volume in the mix.

As no standard testing equipment was available for assessing mortar workability, it was judged visually by the ease of mixing, casting, vibrating and the surface finish of cured specimens. Improved workability was noticed in both low and high resin content mortar mixes by the increase of filler content. Mixes (1), (2) and (7) produced almost void-free specimens. This suggests that filler has similar effects in PC proportioning where resin contents used are much less than in RM.

By comparing identical mixes which differ only in filler type, it is apparant that calcium carbonate powder is better than fly ash; for example see mixes (2) and (7) or (4) and (5). It is probable that fineness may be responsible for that, but also differences in chemical properties and their compatibility with the resin used are the main reasons for the

better performance of calcium carbonate as a filler.

2.6.B Second group of RM This group was designed to help find out the best resin type to be used with PC. In this work, the sand available in the laboratory with the grading shown in Fig.(2.5-b) was used. Another grading was used in which sand finer than 150 umm. is removed as shown in Fig.(2.5-c). Mixing ratios and different resin types used are shown in table (2.13). The results of the six different mixes are given in table (2.14), in terms of compressive and tensile strengths.

It was found that "Crystic 196 PLAV" resin type had the highest potential and viability for manufacture of RM, see mixes (1), (2) and (3). It gave the best mechanical properties , the best workability and the most well finished specimens. Also this type of resin has the advantage of being preaccelerated which necessarily simplifies mixing and reduces the risk inherent in dealing with pure catalysts and accelerators in the mixing area.

Although "Cellobond " resin is a specially formulated one capable of coping with elevated temperatures, it was found that specimens made out of it, mixes (3) and (5), still suffered heat deterioration. Despite the fact that this deterioration was less than that given by "Crystic" general purpose resin, the difference was not large enough to justify the use of "Cellobond" whose performance at ambient temperature is inferior to "Crystic" resin, see Fig.(2.7).

It was also found that continuous-grading sand with fine particles included, gives better results than uniform size or

gap-graded sands, even with the use of fillers, see mixes (2) and (4). A parallel study on the strength development rates within this second group, confirmed that RM's gain strength at a rate which decreases with time. As shown in table (2.15), compressive strength for mix (1) was 100 N/mm2 at 3-days of age, increasing to 104 and 108 N/mm2 at 14 and 21-days respectively. However, this rate depends principally on the resin formulation and the ambient temperature during curing, as it can be made very fast or very slow.

To clarify the process of polymerization for the two different types of the resins used, the following test series was carried out within this second group. Three cylinders of 150 mm. diameter and 300 mm. in length, were cast of mixes (1) and (3) which are made of "Crystic" and "Cellobond" resins respectively. During casting a well protected thermocouple was inserted in the centre of each cylinder. Immediately after vibration, the internal temperature of the mix was recorded at 5 min. intervals up to the maximum temperature, and at 10 min. intervals thereafter up till two hours from the start of mixing. From that time, readings were taken every 30 min. until the temperature became once again equal to the ambient one.

As shown in Fig.(2.8), the 'induction interval (Ti)' ,(57), is bigger for "Cellobond" resin than that of "Crystic" resin; this indicates a higher amount of inhibitor in the former. The rate of polymerization is indicated by the higher rate of heat evolution than heat dissipation , and is shown as an increase in the recorded mix temperature, through the 'propagation interval (Tp)'. It is evident from the same figure that

"Crystic" resin has a higer rate of polymerization. The 'gel time (Tg)' which is the time elapsed to reach the peak exothermic temperature was about 70 min. for "Crystic" resin and 90 min. for "Cellobond" resin. If the temperature gain in the mix is a function of the polymerization rate, it is clear that "Crystic" resin is more reactive.

Based on the same figure, it can be said that curing of the mix usually continues after the peak temperature is reached. However, it is impossible to tell precisely when the polymerization might stop, as it is completely dependent on the existence of reactive free radicals and the polymer chain end-functional groups. When the rate of heat dissipation becomes greater than the rate of heat supply from the exotherm reaction the mix temperature falls as shown in Fig.(2.8), until it reaches the ambient temperature. If that temperature is high enough (15 C° for most resins), polymerization would continue for a much longer period than indicated in the figure. This is proved by the experimentally observed strength development rate. The time when this rate reaches zero should be the real termination of the polymerization or curing process.

From these exothermic tests, it was also found that gel time and curing rates given for pure resins by the manufacturers, are not particularly reliable or applicable to the same resin type when it is mixed with aggregates. This is obviously because of the transfer of heat evolved in the process from the resin paste to the dispersed aggregates.

2.6.C Third group of RM This group was designed to study in

detail the effect of sand grading, moisture and styrene content on compressive strength and its 'frequency distribution'. Because of the large number of specimens used, 50 mm. cubes were prepared for this group.

2.6.C.i Effect of grading Five different gradings of sand were prepared with nominal specific surface areas (SSA's) varying from 2800 to 6700 mm2/gm. These five gradings are shown in Fig.(2.9) and table (2.16) as well. The SSA was calculated from sieve test analyses. Assuming that the natural sands used had spherical-shaped particles, the surface area (SA) could be found for each weight of sand retained on different successive sieves. The overall SSA was calculated as the sum of SA's of different sizes divided by the overall weight of the sand sample.

As shown in table (2.17), the first three mixes made in this group were proportioned identically. To clarify the effect of grading in terms of SSA's and moduli of fineness (MF) on the performance of RM's, these three identically proportionated mixes used different sand gradings. On testing the compressive strength varied widely. Mix (1) gave a higher strength than mix (2) which is made using a finer sand, and a higher strength than mix (3) which is made with a coarser sand. Based on the findings of the first three mixes, more work on the effect of sand-SSA was undertaken as will be shown with the following four mixes in this group.

Using the coefficient 'k' to express the mix richness as the ratio of the mix resin weight in gm., to the SA in mm2 of the sand used, four different mixing ratios were calculated on the

basis of equal k-value and variable SSA's as shown in table (2.17). To make the comparison on SSA-basis valid, the type of the four different gradings used with these four mixes was of the continuous-type grading. Uniform or gap-graded gradings were not used, see Fig.(2.9). The coefficient k was found to have three values with the first three mixes (1), (2) and (3). The value chosen for the last four mixes was that of mix (1); as it gave the highest strength. This value of k which is $5x10^{-5}$gm/mm2 produced four different mixing ratios for mixes (4), (5), (6) and (7), which differed in the SSA's values of the sand used with them, as shown in table (2.17).

Fig.(2.10) shows the relationships between 24-hour compressive strength and SSA for the first three mixes , curve (A), as well as the last four mixes, curve (B). In the same figure, using another ordinate, the relationship between RM unit-weight and SSA is shown. Curve (E) represents mixes (1) to (3), while curve (F) represents mixes (4) to (7). It is clear from this figure that whether k is a variable as in curve (A) or constant as in curve (B), there is a certain range for SSA within which a maximum strength can be obtained. The intersection of these two curves should satisfy the requirements of both of them. Using this condition and the other available points (each is the average of twenty-five results), these two curves (A & B) were plotted as shown in Fig.(2.10). Despite the fact that these two curves represent one value of k and a particular mixing ratio, numerous different values of k can be deduced from curve (A), and a wide range of mixing ratios can be found from curve (B). For instance any point on curve (A) can be translated into a

corresponding k-value depending on the SSA given. Any point on curve (B) can also be translated into a distinct mixing ratio. The only provision to be considered is that the filler content is 15% by weight, i.e., the same filler content as that employed in the mixes on which these test results are based. Bearing in mind this provision, curves (C) and (D) were calculated and plotted as shown in Fig.(2.10), with two different ordinates drawn in a downward direction. From curve (C), the value of k is shown to vary from around 3.5×10^{-5} to 7.5×10^{-5}gm/mm2. These two values of k were experimentally found to represent the upper and the lower limits within which RM would be workable. Higher values than the upper limits imply very sloppy mixes with high bleeding tendencies. Lower values than the lower limit imply very harsh RM with poor finishing properties. The range of SSA's in this chart, as investigated, is from 2500 to 6500 mm2/gm.

The chart can be used for mix-proportioning of RM's made of "Crystic 196 PLAV" resin type, with 15% by weight calcium carbonate powder as a filler and continuously-graded sands. It can also be used for mix-optimizing and prediction of the 24-hour compressive strength and density as will be shown in the following example.

Example Find the optimum mixing ratio and the expected 24-hour compressive strength and density for resin mortar made of the same materials given above and sands with SSA's of the value (1) 2900 mm2/gm. (2) 3800 mm2/gm.

Solution

(1) Using the given chart in Fig.(2.10), draw a vertical line

at SSA = 2900. Find its intersections with the six given curves. Intersections i, i' and i'' for a constant mixing ratio of 15:15:70, give a strength of 102 N/mm2 at a k-value of $7.4x10^{-5}$gm/mm2. with a corresponding density of 2.11 gm/cm3. Intersections ii, ii' and ii'' for a constant k-value of $5x10^{-5}$, give a strength of 90 N/mm2 at a mixing ratio of 12:15:73, with density of 2.07 gm/cm3. For the highest strength, intersection (i) should be considered which means a mixing ratio of 15:15:70. As the corresponding k-value is almost equal to its upper limit, no higher resin content can be used and the given mixing ratio is the optimum one.

(2) Following the same procedure with sand SSA = 3800 mm2/gm , one will have two sets of values representing intersections (i) and (ii) which are as shown in table (2.18). From this table it is clear that neither of the mixing ratios is the optimum one. The shown value of k still can be increased up to the upper limit , at which a new mixing ratio can be found and would give a higher strength . This mixing ratio can be calculated as follows.

The ratio of the sand in the mix by weight Ws can be calculated from the equation;

$$Ws = (1 - Fc)/(1 + k.SSA)$$

in which Fc is the filler content (15% as assumed), then substituting for $k = 7.5x10^{-5}$, SSA = 3800, then Ws = 0.66. Hence the optimum mixing ratio is 19:15:65 (resin : filler : sand by weight.). Extrapolating the values of intersections (i & ii) to the new mixing ratio , the corresponding strength was found to be 120 N/mm2 with 2.25 gm/cm3 -density. It is

important to stress that the previously made extrapolation was found to be valid through various experimental results as long as the limiting k-values are not exceeded. That is to say that for any RM the strength is directly proportional to the resin content within the suggested limits of k-value.

The applicability of this chart could be extended . If six families of curves like curves (A, B, C, D, E & F) were constructed RM's could be proportionated to give a desired strength and density at a given sand SSA. Due to limitations in time and the existance of other objectives to be fulfilled in this present work, experimental investigation of resin mortars was stopped at this stage. However, the basic principle of mix proportioning of RM's on an SSA basis is believed to be clear enough for any one wishing to undertake any further work in this field.

2.6.C.ii Effect of moisture To clarify the influence of water on the degree of polymerization and the consequent performance of RM, the following set of specimens were made. Four identical mixes made with mixing ratios 15:15:70 were used in making sixteen 50-mm. cubes for each mix. The sand used was of the continuous-grading type as shown in Fig.(2.9-I). Four different moisture contents (Mc) were used namely 0.0, 0.5, 1.0 and 1.5% of the sand weight. The mixing ratios and the results are shown in table (2.19) as well as in Fig.(2.11).

The deterimental effect of moisture on the strength of RM is evident as is the fact that loss of strength is not proportional to the water content. Increasing Mc from 0.0 to 0.5% of sand weight resulted in a decrease in the compressive

strength of about 22.5%. While a moisture content of 1.5% caused a strength reduction of 41.5%.

As shown in Fig.(2.11), it can be seen that there is a certain Mc-value above which no further significant loss in strength will be caused. Generally speaking, this set of tests showed that wet aggregates can be used in batching RM and PC, and still can give high mechanical performance.

The question of whether to use dry, surface-dry or wetted aggregates depends primarily on the drying-energy costs and the available types of aggregate. It is not possible to set a particular limit for the allowable Mc of aggregates used; but a compromise between required performance and allowable Mc in the mix would be required.

Recent attitudes call for improved performance of resin itself in a wet environment. Many chemicals are now being used for this purpose such as silane coupling agents and different water absorbents. In Japan, it is reported that up to 3% Mc-aggregates have been successfully used in making RM's without loss in strength (56). Due to the nature of this controversial and chemical specific point, no further work was made in this present work.

The main conclusion drawn from this set of tests was that moisture content can have a damaging effect on the mechanical performance of resin mortars and consequently on resin concretes. This is mainly because the water existing in the aggregate lessens the effect of the incorporated initiators. In that case polymerization speed is reduced and curing may

interfere with curing in one way or another (55). Water has two effects, the first is prolonging or preventing complete polymerization and the second is reducing strength. Prolonging the polymerization process leads to further disruption as other chemical factors may exercise a more marked influence which is not apparent in the course of normal-speed polymerization. One of these is the oxidation of reactive styrene monomers into styrene peroxide instead of acting as a crosslinker. Eventually this peroxide degrades into organic components which act as inhibitors (55).

2.6.C.iii Effect of styrene content It is well known that by increasing the content of styrene, which acts as a diluent for a polyester, the setting time or gel time becomes shorter due to the increased reactivity. Styrene decreases the liquid resin viscosity with a consequent increase in the mix workability. At the same time, increased styrene content (Stc) reduces the strength, as the micromolecular distance (54) between polymer chains increases and the binding matrix becomes much more flexible and looser. To clarify this effect on the performance of polyester resin, the following tests were carried out using "Crystic 196 PLAV".

Four identical mixes were prepared using a mixing ratio 15:15:70. The sand grading used was that shown in Fig.(2.9-I). The only difference between mixes was in resin formulation. Four styrene/polyester ratios (ST/UP) by weight were tried as follows; 0.0, 5.0, 10.0 and 15.0%. The same amount of catalyst (2% of resin weight) was used for the four mixes. Out of each mix sixteen 50 mm.-cubes were cast, cured at ambient

temperature and tested at 24-hours of age. As shown in table (2.20) and Fig.(2.12), strength decreased almost linearily at the rate of 1.2 N/mm2 for each 1% increase in ST/UP ratio. Obviously the rate will depend on the resin used and its properties, but the general trend of strength degradation by increasing Stc is still applicable to any RM or PC.

"Crystic" resin has reasonable workability and gel time as delivered by the manufacturer so that there was no need to alter or interfere with its properties. In the tests which follow no styrene or any other diluting agent was incorporated.

2.6.C.iv Statistical interpretations of RM results At this stage it may be useful to examine some of the experimentally observed variables and their uncertainities, which usually arise from the complex of variations termed as errors. No matter how precise the experimentation and measurements are, different-source errors usually creep into all observations. Full statistical analysis that would help in reaching reliable and safe confidence limits through statistical interpretation of the laboratory findings, is not within the scope of this work. However, interpretation of some of the laboratory data regarding RM's will be discussed.

Out of the previous RM mixes, six were chosen for statistical analysis. For each mix, twenty-five cubes (50 mm.) were cast and tested in compression. To minimise errors, one mix was prepared and all twenty-five cube moulds were filled, vibrated and cured together. For each mix, the compression tests were carried out on the same testing machine and with the same

instrumentation. The specimens of each mix were tested at the same age, temperature and rate of loading.

Table (2.21) shows the arithmetic mean, the standard deviation and the coefficient of variation for the six different mixes. The full results are reproduced graphically for each mix as shown in Fig.(2.13). In this figure the strength frequency distribution is presented by a histogram, in which the horizontal axis represents group interval in N/mm2. The heights of the rectangles shown represent the number of specimens within the interval. Because of the limited number of observations, this graphical presentation may not accurately represent the distribution of the whole population.

Before any further statistical interpretation of data, it was necessary to check the 'normality' of the strength frequency distribution. The Shapiro test for normality (58) was applied and its results are represented in table (2.22). It was found that four mixes are normally distributed with a significance level (Sl) less than 0.01 (more than 99% confidence level). It was also found that five mixes out of six were normally distributed with Sl less than 0.05. Only two mixes did not qualify for normal distribution for Sl = 0.01. However, the general frequency distribution for these resin mortars could be regarded as a 'normal ' distribution.

Values derived from any one set of observations will be subjected to some uncertainity, and can be considered only as estimates of the unknown true values. Such estimates should always be accompanied by measures of their uncertainity (59), by giving two limits and asserting with a certain probability

that they include the true values (confidence limits). Table (2.23) shows the mean and the standard deviation for each mix with their confidence limits for 95% and 99% probability. Also it is usually useful to have a simple procedure with which one may test the homogenity of observations. The British Standards (B.S. 2846 Part 1: 1975) provide 'controlling charts' for such a procdure. These charts have inner and outer limits as shown in Figs.(2.14 & 2.15). The inner and outer limits correspond to probabilities of 1:40 and 1:1000 respectively. The occurance of points outside the outer limit or of more than one or two points outside the inner limits is considered to be evidence that data are not homogeneous. As shown in Figs.(2.14 & 2.15), the observations for each mix were divided rationally into five subgroups. The mean and the range of each subgroup was found and the general means and the mean ranges were calculated and used in constructing the charts. For each mix the group mean and range were plotted and compared to the set limits.

Some conclusions can be drawn from the previous statistical analysis. The variance in compressive strength for resin mortars tested ranges from 2 - 3.4%, a range which is well below the accepted value for conventional concretes and mortars in different standards (60). The true compressive strength values are found to have maximum confidence limits ranging from +0.99 to +1.85 with 99% probability. This suggests the reliability of the derived means for the different mix strengths. The homogenity test for the given observations confirmed once again the consistency and validity of those observations. In addition, it is shown that RM can be

fairly regarded as a material with a 'normal frequency distribution' strength. So all the rules applied in deriving the characteristic strength statistically for conventional concretes and mortars, should remain applicable to resin mortars and resin concretes. This is an important conclusion that will be used later in chosing different PC grades.

Table 2.1: Typical properties of liquid CRYSTIC 196

Viscosity at 25°C	9 poise 3.5 poise PALV
Specific gravity at 25°C	1.12 1.11 PALV
Acid value	21 mg KOH/g 19 mg KOH/g PALV
Volatile content	33% 38% PALV
Appearance	light straw pinkish PALV
Stability in the dark at 20°C	6 months
Gel time at 25°C (determined under laboratory conditions using: CRYSTIC 196 100 pbw. Catalyst Paste H 3 pbw, Accelerator E 4 pbw)	8 minutes
Gel time at 25°C (determined under laboratory conditions using: CRYSTIC 196 PALV 100 pbw. Catalyst M 2 pbw)	14 minutes PALV
Test methods as in BS 2782: 1976	

Table 2.2: Typical properties of cured CRYSTIC 196 (unfilled casting)

Barcol hardness (Model GYZJ-934-1)	45
Water absorption	16.5 mg
Deflection temperature under load (1.80 MPa)	72°C
Elongation at break*	2.3%
Tensile strength	69 MPa+
Tensile modulus	3.8 GPa
Specific gravity at 25°C	1.22
Refractive index n $\frac{20}{D}$	1.560
Dielectric loss (tan δ at 1000 Hz)	0.006
Dielectric constant (at 1000 Hz)	3.0
Residual styrene content (Measured by BPF-approved method for freight containers)	0.01%
Test methods as in BS 2782: 1976	

* Filtered resin, void-free casting

Table 2.3: Typical Test Results

Specific gravity at 25°C		1.117
Viscosity at 25°C	10^{-6} m²/s	475
	cS	475
Volatile content	%	37
Gelation time at 25°C (using 2 mls of liquid catalyst 60% MEK peroxide LA+3 mls of 0.6% Cobalt solution on 100g resin)	minutes	35

Table 2.4: Cellobond A2661 typical properties of cured cast resin.
Test methods as in BS 2782 and BS 3532.

Test		Cured cast resin
Tensile strength	MN/m²	49.3
Young's modulus in tension	MN/m²	3450
Flexural strength, dry	MN/m²	96.5
After immersion for 2 hours in boiling water	MN/m²	79.3
Young's modulus in flexure	MN/m²	3725
Izod impact strength	J/m	12.3
	ft.lbf/in notch	0.23
Heat Distortion Temperature at 1.81 MN/m² (264 lb/in²)	°C	130
Water absorption 1 day	mg	32
Power factor at 23°C at 1 MHz		0.004
Permittivity at 23°C at 1 MHz	pF/m	30
Volume resistivity	ohm m	> 1.2×10^{13}
Surface resistivity	ohm	> 3.74×10^{14}
Electric strength	MV/m	15.0
Electric strength	Volt/mil	380

Table 2.5: Properties of calcium carbonate powder used.

Chemical analysis of the raw material	$CaCO_3$	99.75%
	MgO	traces
	Fe_2O_3	0.02%
	SO_4^{2-}	0.06%
	Colloidal aluminium silicate	0.1%
	Loss on ignition (DIN 55918)	43.34%
	Moisture (DIN 53198)	below 0.2%
Fineness	Residue on a 40 micron sieve (DIN 53195)	0.1%
	Top cut	25 microns
	Mean particle size	5 microns
	Finer than 2 microns (Sedigraph)	10%
Technical data	Density (DIN 53193)	2.7
	Refractive index	1.65
	Hardness (Mohs)	3
	Particle shape	crystalline rhombohedral
	Packed bulk density (DIN 53194)	1.4 g/ml
	Dry brightness: Elrepho green filter (FMY/C)	91
	pH value (DIN 53200)	9
	Oil absorption (rub-out, ASTM D 281-31)	16 g per 100g powder
	DOP absorption (rub-out, ASTM D 281-31)	25 g per 100g powder

Table 2.6: Typical properties[1] of fly ash* used

Chemical analysis of the raw material	SiO_2	52.0	
	AL_2O_3	30.4	
	Fe_2O_3	7.23	
	TiO_2	0.87	
	Mn_3O_4	0.06	
	CaO	2.55	
	MgO	0.79	
	Na_2O	0.49	
	K_2O	0.97	
	SO_3	0.64	
	P_2O_5	0.28	
	Combustible + moisture		3.36
	Loss of ignition		21%
Specific gravity		2.25	
Fineness:			
Effective size D_{10} mm		0.0053	
Uniformity coefficient $\frac{D_{60}}{D_{10}}$		2.5	
% finer than 0.02		79%	
Specific surface area cm^2/gm		4960	

* Barony fly ash, Ayrshire, Scotland.
(1) Research report No.01038, CEGB, the Univ. of Glasgow, by Prof. H.B. Sutherland and P.N. Gaskin.

Table 2.7: Properties of the natural sand* used

Relative density:		
Saturated surface dried basis	2.59	
Apparent basis	2.75	
Bulk density:		
Loose density	1545	kgs/m^3
Rodded "	1680	kgs/m^3
Water absorption[1] (% of dry mass)	1.6	
Alkaline reactivity (innocuous)[2]		
Reduction in alkalinity Rc	90	(mmol/l)
Dissolved SiO_2 in (mmol/l) Sc	16.4	

(1) B.S. 812: Part 2: 1975
(2) ASTM C289-81
* Hyndford Quarry, Near Lanark.

Table 2.8: Properties of the natural gravel* used

Flakiness index	8.0%
Elongation	1.0%
Crushing value	24 %
Impact value (2)	22 %
Content of clay, silt and dust	0.2%
Relative density:	
Saturated surface dried basis	2.6
Apparent basis	2.77
Bulk density:	
Loose density	1495 kgs/m3
Rodded density	1565 Kgs/m3
Water absorption (2) (% of dry mass)	2.7

(1) B.S. 812: Part 2: 1975
(2) B.S. 882: 1983
* Hyndford Quarry, near Lanark

Table 2.9: Properties of crushed basalt stone*

Impact value(1)	10
Crushing value	15
10% Fines value*	260 kN
Abrasion value	4.8
Polished stone value	61
Relative density:	
Oven dried basis	2.74
Apparent basis	2.90
Bulk density (surface dry):	
Uncompacted	1285 kg/m3
Compacted	1420 kg/m3
Water absorption (% of dried mass)	2.0

(1) B.S. 812: Part 3: 1975
* Cairneyhill Quarry, near Airdrie, Scotland

Table 2.10: Gradings for the natural sand, natural gravel and crushed basalt used.

A: Sand grading

Sieve size (mm)	% passing
4.75	95.5
2.36	83.5
1.18	62.5
0.600	40.0
0.300	8.0
0.150	1.5

B: Gravel grading

Sieve Size (mm)	% passing
16.0	100
10.0	89.5
6.7	37.5
5.0	9.5
2.36	0.5
1.18	0.0

C: Crushed basalt

Size (mm)	% by wt.
6	25
10	55
14	20

Table 2.11: 1st group mixing ratios of resin-mortars

Mix No.	Percentage by Weight		
	Resin*	Filler	Sand
1	20	15	65
2	15	16	69
3	20	10	70
4	15	5	80
5	15	5**	80
6	15	10**	75
7	15	16**	69

* Used resin: Crystic PLAV 196 unsaturated polyester resin.

** Filler: fly ash, otherwise calcium carbonate powder.

Table 2.12: 1st Group results*.

Mix No.	Compressive(a) strength in N/mm^2			Tensile (b) strength in N/mm^2		
	at room temp.	at elevated(c) temperature	strength loss %	at room temp.	at elevated temperature	strength loss %
1	126	83	34	15.5	10.5	32
2	114	80	30	13.5	9.5	30
3	126	91	28	14.5	10	31
4	97	80	17.5	10.5	8.2	22
5	87	58	33	10.5	7.5	28
6	101	72	29	12.0	8.2	34
7	109	77	34	12.5	8.5	32

(a) Average of 6 cubes (40 mm - size)

(b) Average of 6 cylinders (d = 50 L = 100 mm)

(c) Specimens kept for 30 min in $80^{o}C$, 90 min in $100^{o}C$, then immediately tested.

* Tests were made at 14 days of age.

Table 2.13: 2nd group mixing ratios of resin mortars

Mix No.	Resin type used	Resin formulation[a]	Mix ratio by weight		
			Resin	Filler[b]	Sand
1	Crystic PLAV 196	2: -: 98	16	16	68
2	Crystic 196	2: 2: 96	16	16	68
3	Cellobond A2661	2: 2: 96	16	16	68
4	Crystic 196	2: 2: 96	16	16	68[c]
5	Cellobond A2661	2: 2: 96	20	15	65
6	Crystic PLAV 196	2: -: 98	15	15	70

(a) Formulation in weight% of catalyst: accelerator: resin

(b) Calcium carbonate powder.

(c) Available sand in the laboratory of the shown grading in Fig.(2.5-b), All other sand used are of the grading shown in Fig. (2.5-c).

Table 2.14: 2nd group results*.

Mix No. / Strength in N/mm^2	(1)	(2)	(3)	(4)	(5)	(6)
Compressive[a] strength	105	92	100	98	102	106
Tensile[b] strength	12.0	12.0	9.5	12.5	12.0	11.0

* At 14-days age.

(a) Average of 6 cubes (70 mm size)

(b) Average of 6 cylinders (d = 50 mm, L = 100 mm).

Table 2.15: Strength development of resin-mortars

Age	Compressive[a] strengths (N/mm^2) for Mix no.[b]		
	(1)	(2)	(3)
3 days	100	92	82
14 days	104	97	92
21 days	108	102	94

(a) Average of 6 cubes (70 mm size)

(b) Mixes used in 2nd group.

Table 2.16: Different sand gradings used with 2nd group

Sieve No. (S.I.)	Percentage retained for different grades				
	I	II	III	IV	V
10	0.0	0.0	0.0	0.0	0.0
5	16.6	34	5	25	10
2.36	16.6	19	5	15	5
1.18	16.6	20	5	20	5
0.6	16.6	3	15	15	20
0.3	16.6	7	45	10	45
0.15	16.6	12	25	15	15
S.S.A.[a]	4200	2800	6700	3600	5600
M.F.	3.5	4.3	2.35	2.95	2.7

(a) Specific surface area in mm^2/gm.

Table 2.17: Mixing ratios and compressive strengths for resin-mortars (3rd group).

Mix No.	Sand Grading	Mix ratio (by wt) Resin** : filler*: sand	K gm/mm^2 $\times 10^{-6}$	Compressive strength (1) N/mm^2	standard deviation N/mm^2
1	I	15 : 15 : 70	50.0	1103.8	2.5
2	III	15 : 15 : 70	32.0	92.5	1.8
3	II	15 : 15 : 70	75.0	101.7	3.3
4	II	10.4 : 15 : 74.6	50.0	88.1	2.8
5	IV	13 : 15 : 72	50.0	95.3	3.2
6	V	18.5 : 15 : 66.5	50.0	104.7	3.0
7	III	21 : 15 : 64	50.0	97.8	2.6

* Calcium carbonate powder.

** Cystic PLAV - 196.

(1) 24 hours - age, 50 mm cubes, average of 25 specimens.

Table 2.18: Mixing ratios and results for different M_c-resin mortars.

Mix No.	Mix ratio (by wt) Resin : filler : Sand***	Moisture content %	24-hour comp.strength N/mm^2 *
1	15 : 15 : 70	0.0	104.0
2	15 : 15 : 70	0.5	81.0
3	15 : 15 : 70	1.0	59.0
4	15 : 15 : 70	1.5	61.0

* Average of 4 specimens, 50 mm cubes, 24-hour age.

** Percentage of sand weight.

*** Used grading curve I Fig.2.9.

Table 2.19: Mixing ratios and results for different Stc-resin mortars.

Mix No.	Mix ratio (by wt)			Styrene content %	24 hours compressive strength N/mm^2
	Resin	Filler	Sand		
(1)	15	15	70	0.0	104.0
(2)	15	15	70	5	97.0
(3)	15	15	70	10	91.0
(4)	15	15	70	15	87.0

Table 2.20: Statistical interpretation of 6 resin-mortar mixes

Mix No.	$\bar{x}$	σ_{n-1}	σ_n	v
(1)	92.524	±1.77	1.73	1.9
(2)	101.684	±3.31	3.24	3.25
(3)	88.1	±2.87	2.81	3.25
(4)	95.28	±3.24	3.18	3.4
(5)	104.70	±3.024	2.96	2.88
(6)	97.80	±2.57	2.53	2.6

$\bar{x}$: Compressive strength arithmetic mean in N/mm^2 , average of 25 observations.

σ_{n-1} : estimate standard deviation in N/mm^2.

σ_n : population " " " "

v : variance percent.

Table 2.21: Results of Shapiro Test for Normality.

Mix No.*	Correlation factor**	Conclusion	
		*** α = 1%	α = 5%
(1)	0.986	N	N
(2)	0.940	NN	NN
(3)	0.961	NN	N
(4)	0.987	N	N
(5)	0.988	N	N
(6)	0.991	N	N

***α : significance level (confidence level = 1-α)

N : normal distribution

NN : not normally distributed

* : a complete sample of 25 observations

** : factor that relates original observation values to those of normal order statistics.

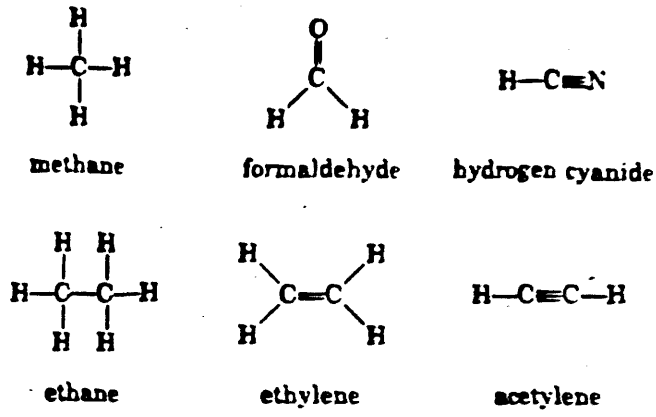

Fig. 2.1 Examples of different carbon covalent bonds.

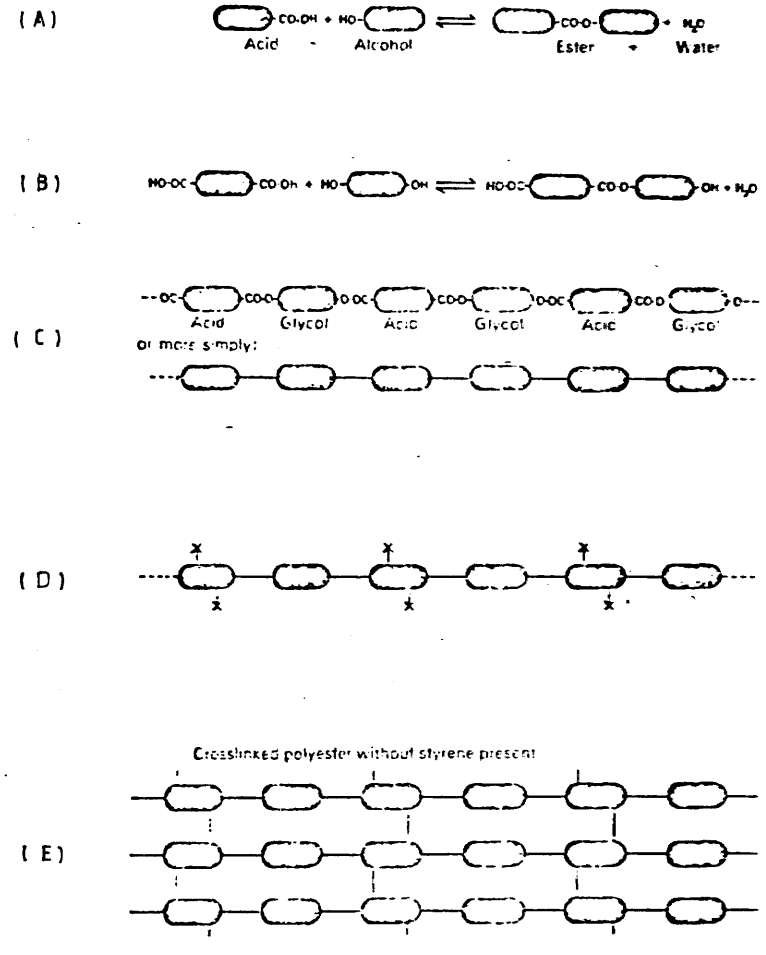

Fig. 2.2 Schematic representation for the manufacture of polyester resin.

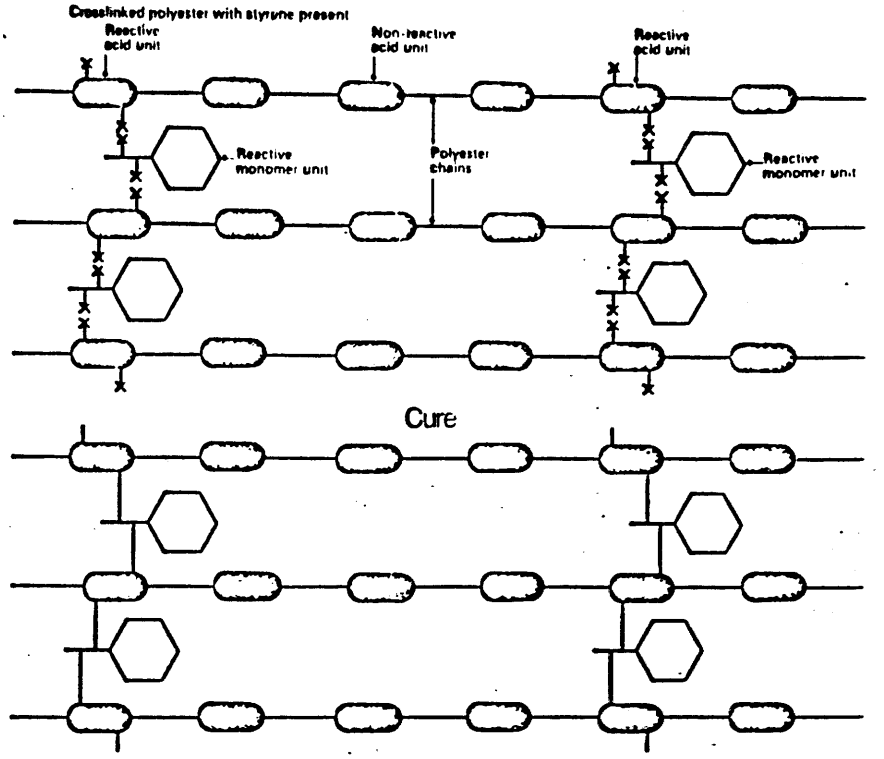

Fig. 2.3 Effect of styrene monomer on the physiochemical properties of polyester.

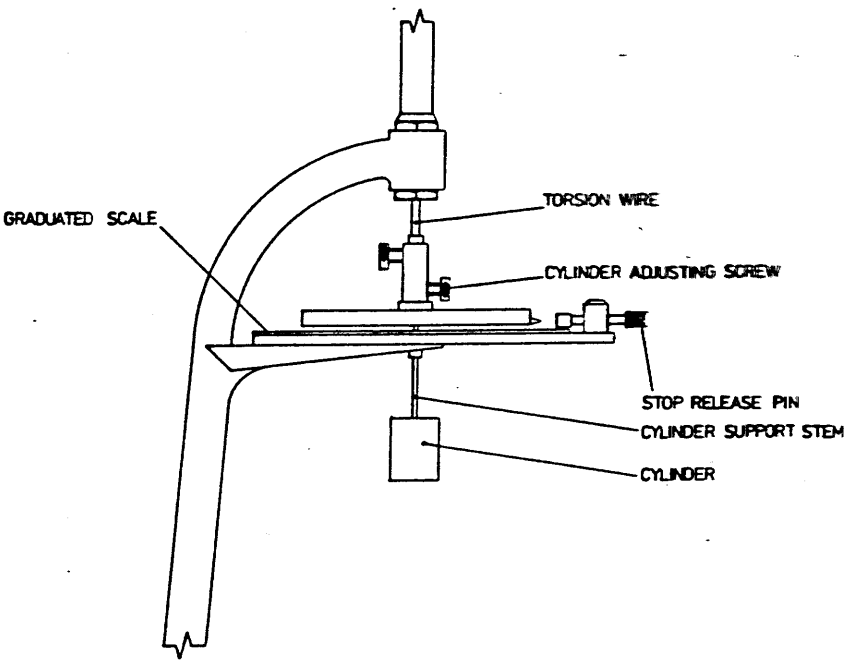

Fig. 2.4 Universal Torsion Viscometer (Assembly Diagram).

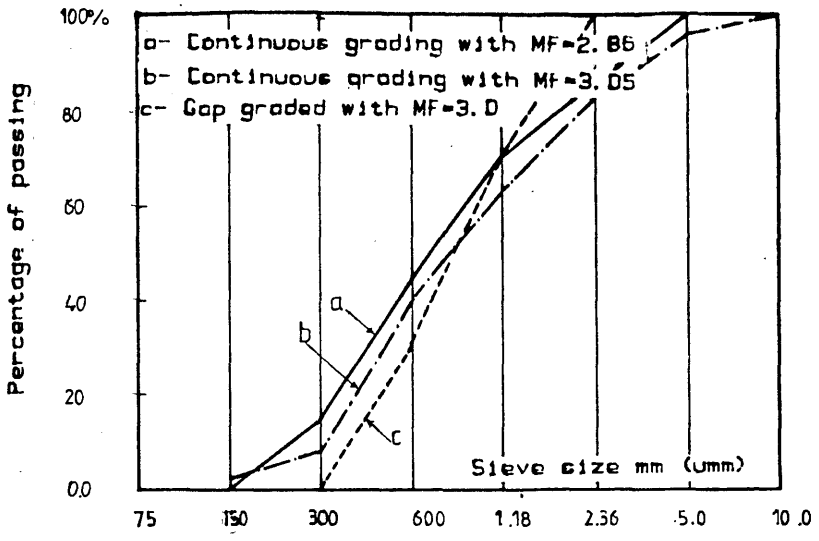

Fig. 2.5 Various sand gradings used with the first and second groups of resin mortars.

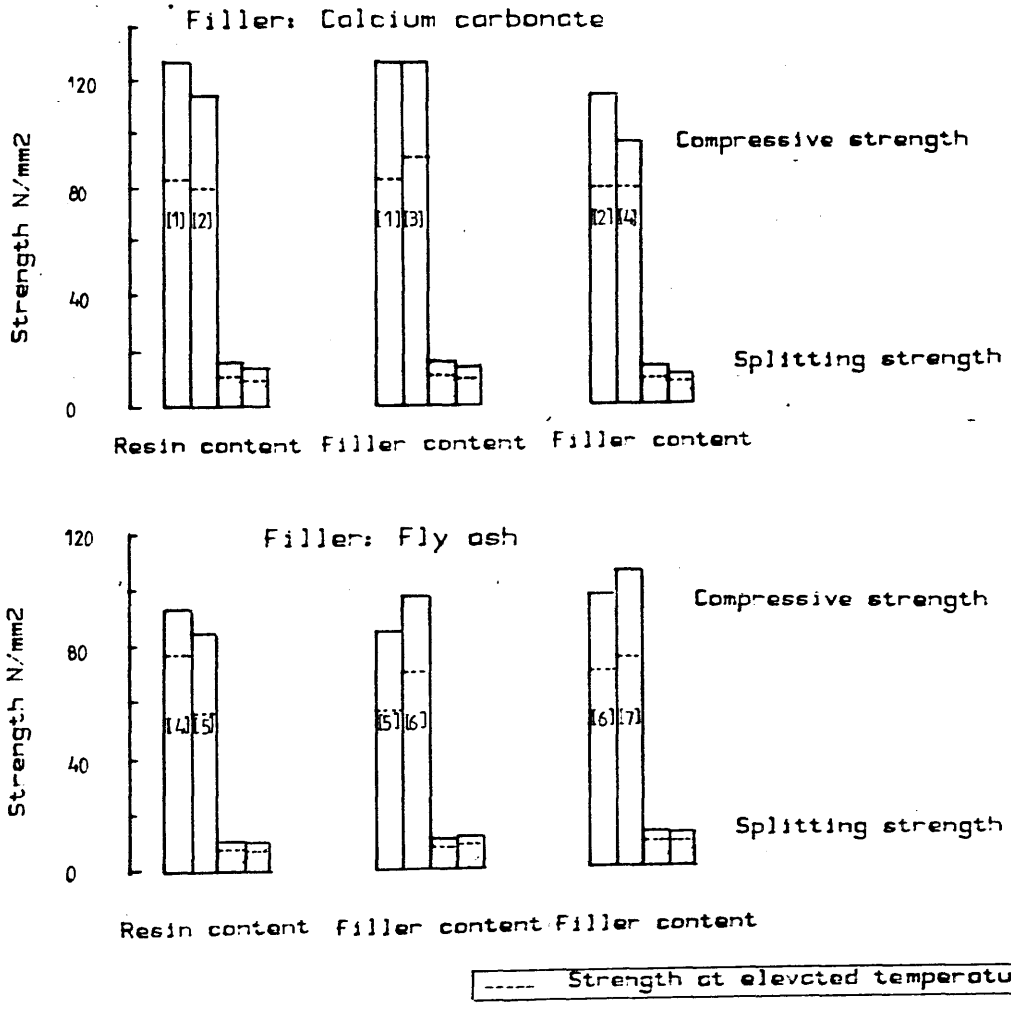

Fig. 2.6 Test results of the first group.

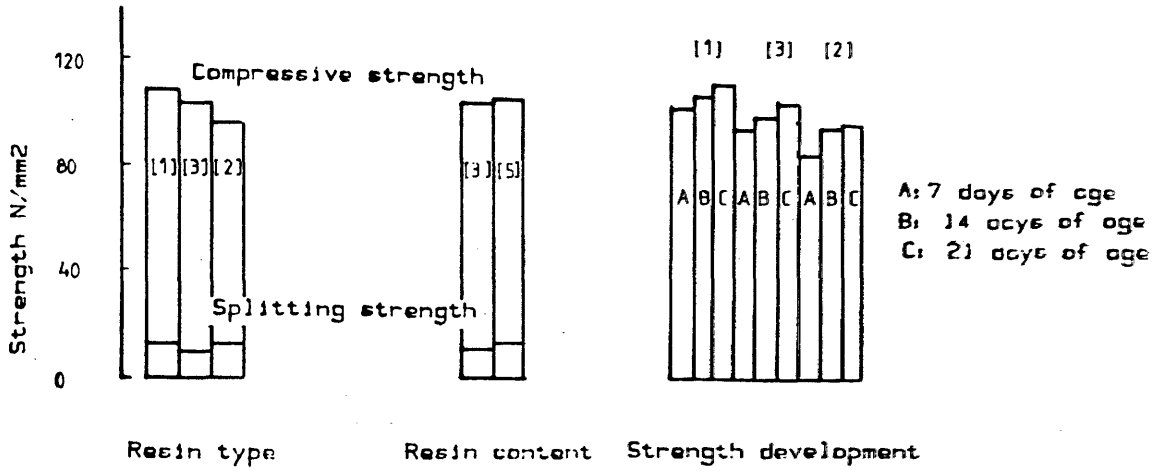

Fig. 2.7 Test results of the second group.

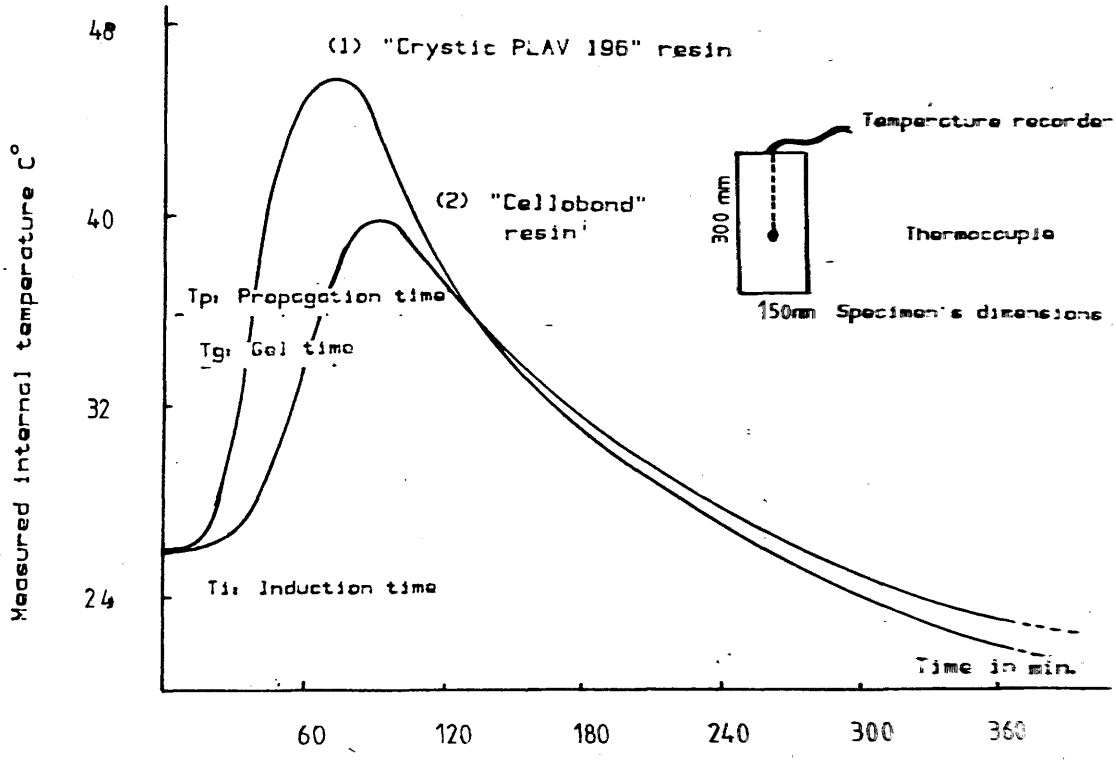

Fig. 2.8 Reactivity of the two resin types used.

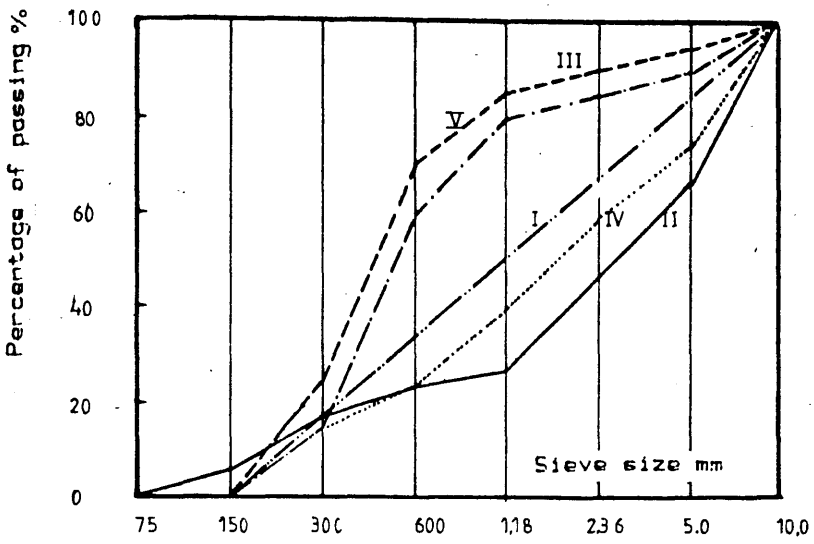

Fig. 2.9 Differtent sand gradings used with 3rd group of resin mortars

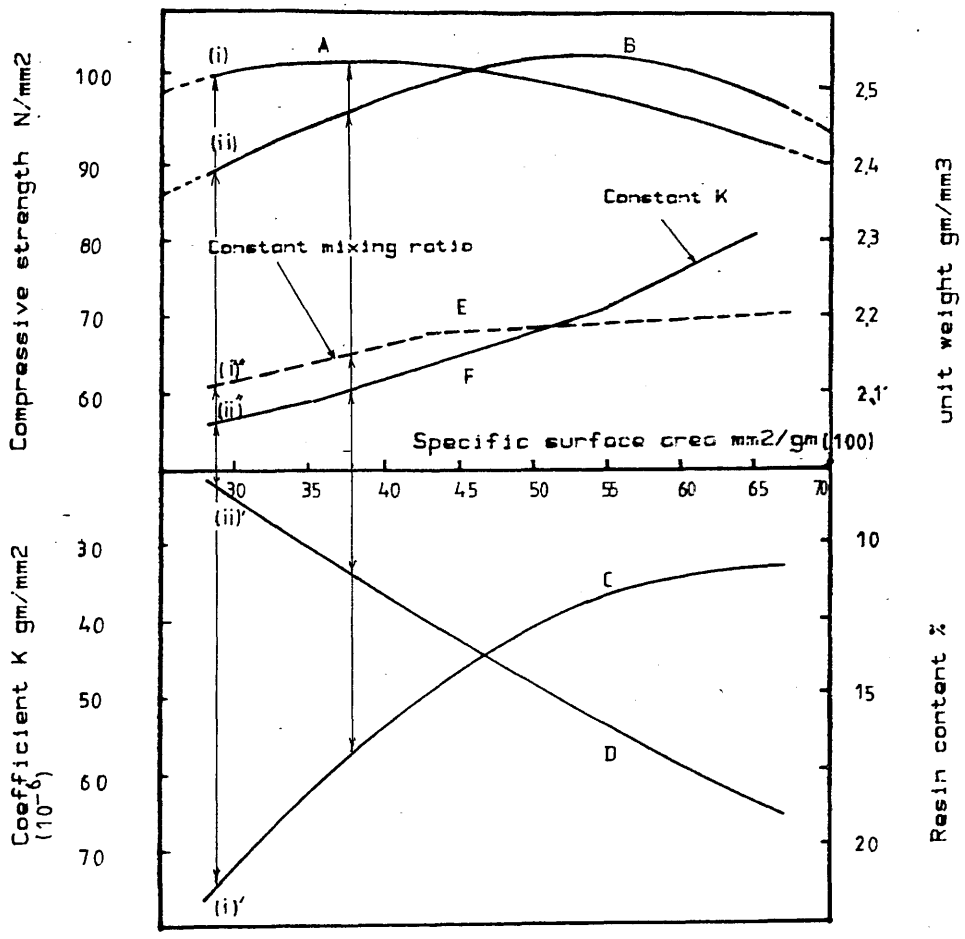

Fig. 2.10 Chart for mix-design of resin mortars made of "Crystic" resin with 15% calcium carbonate as a filler.

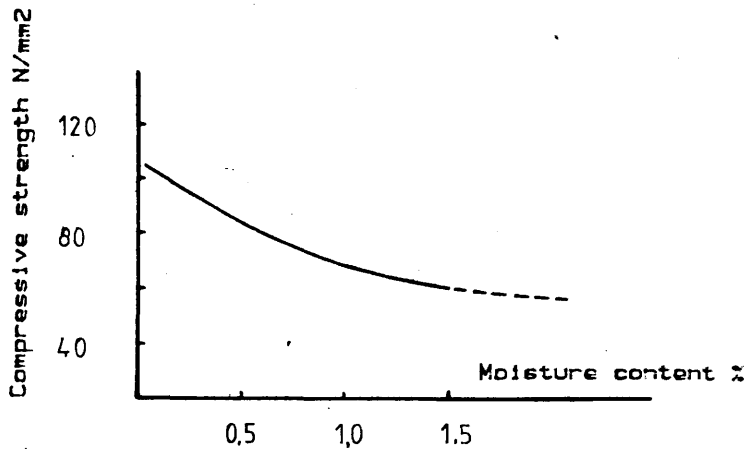

FIG. 2.11 Effect of moisture content of sand on the compressive strength of resin mortar.

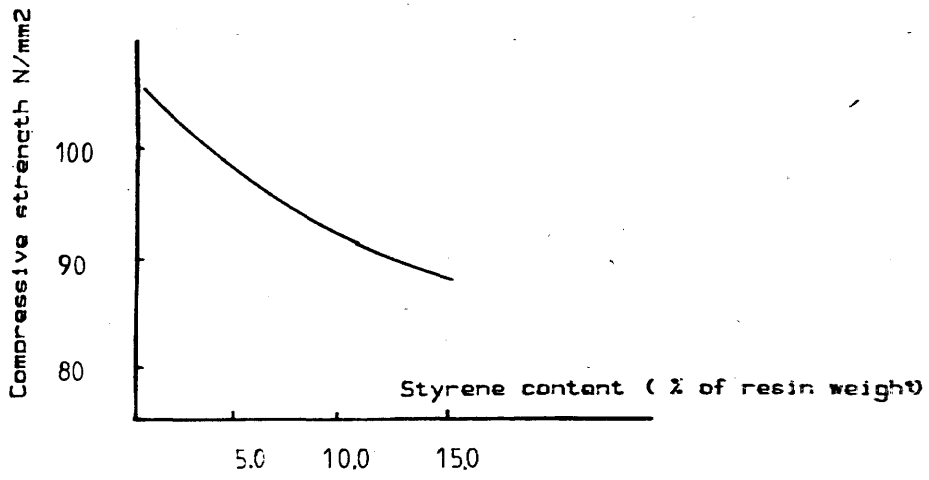

Fig. 2.12 Effect of styrene content on the compressive strength of resin mortar

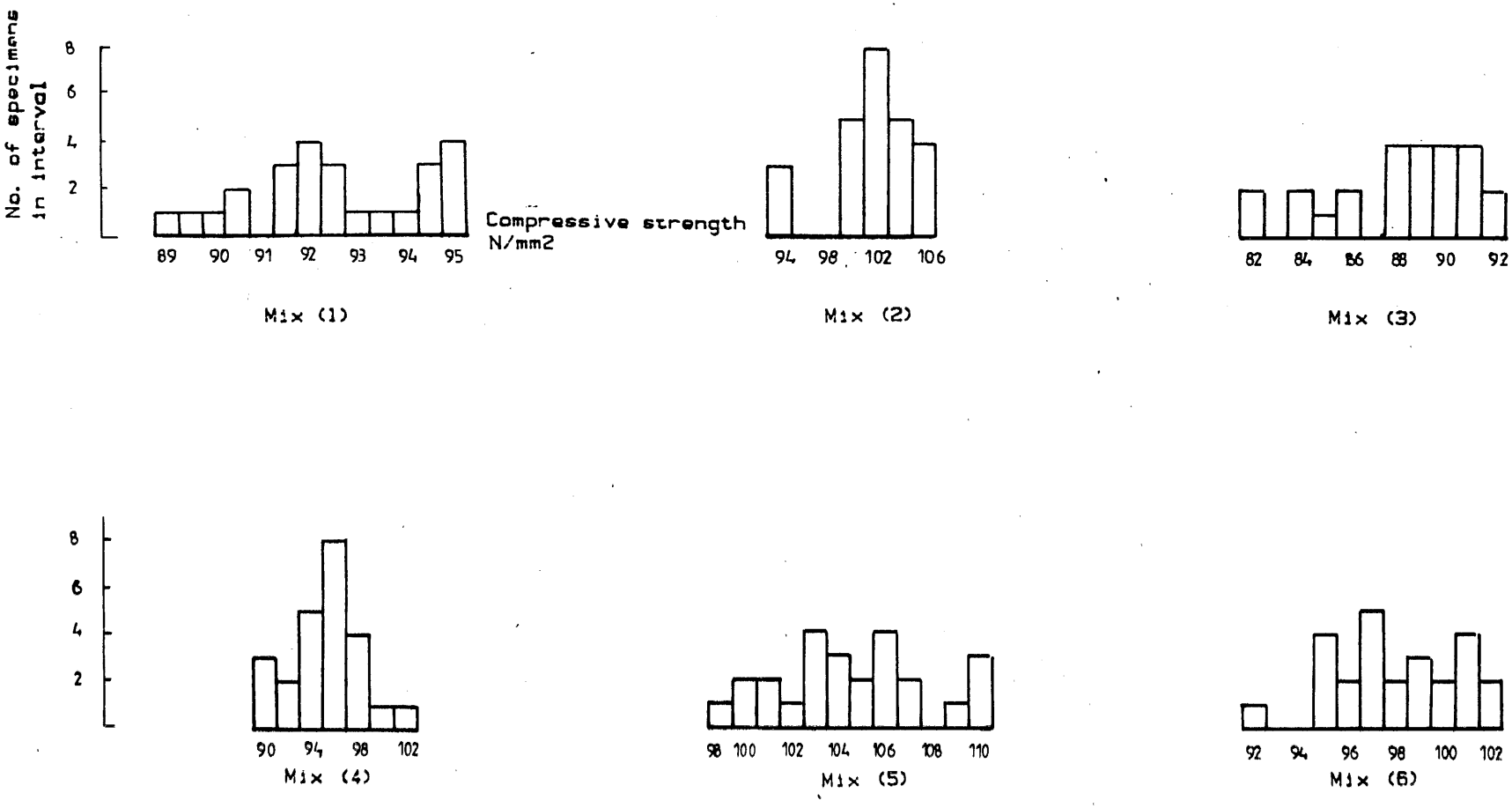

Fig. 2.13 Histograms of strength values for various resin mortars.

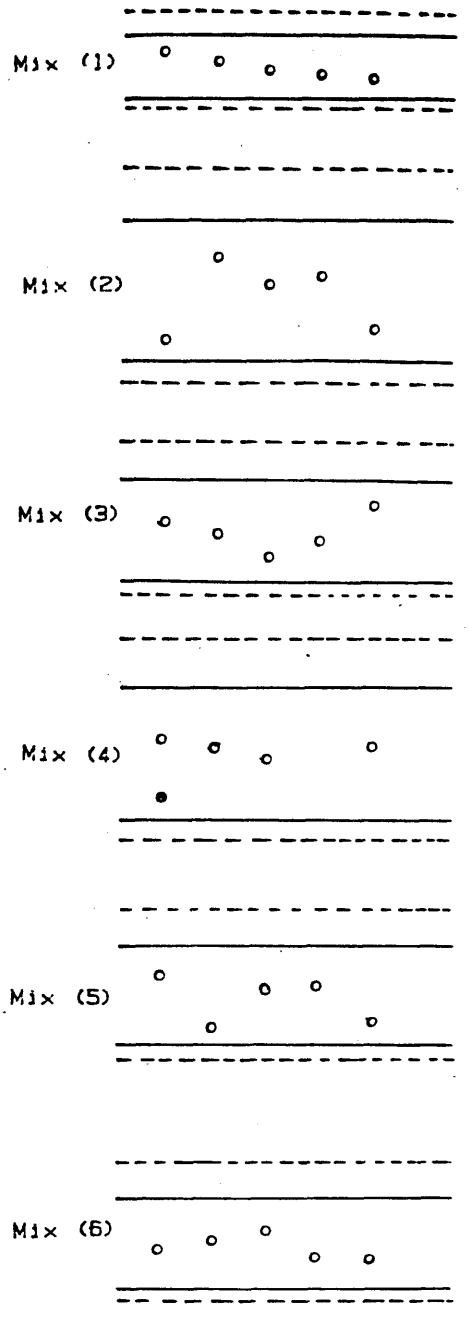

Fig. 2.14 Controlling charts constructed for the subgroups' range.

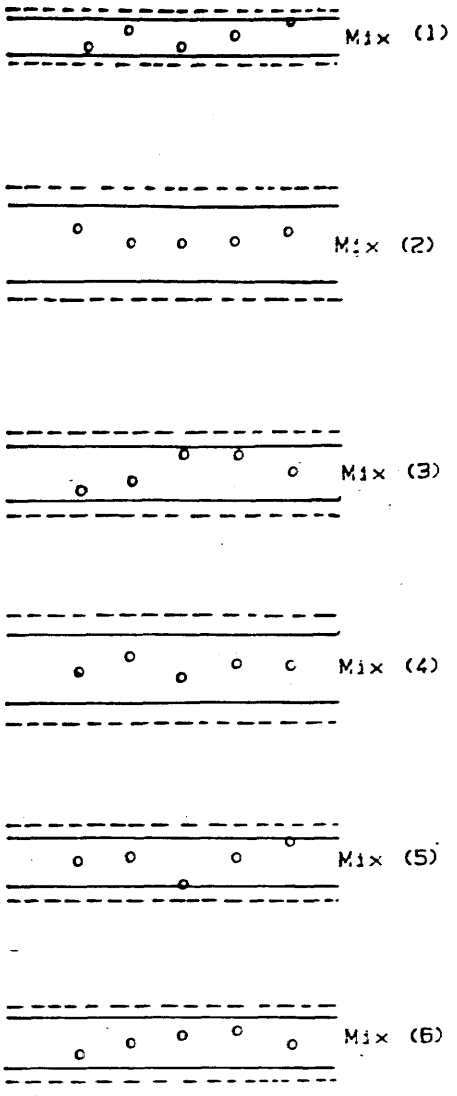

Fig. 2.15 Controlling charts constructed for the subgroups' mean.

CHAPTER THREE

SHORT TERM MECHANICAL PROPERTIES OF POLYESTER RESIN CONCRETE

3.1. Introduction

One of the basic prerequisites of this present work was to obtain different structural grades of PC's. These grades were intended to be used in the structural analysis of PC. when reinforced. They varied in strengths, moduli of elasticity, cracking strains and ultimate compressive strains. As will be shown various mix proportions were tried to obtain five distinct PC grades.

The properties of PC as a composite material can be regarded as the superposition of the additive and synergetic interactions between different components (61). These components affect the performance of PC on micro and macrostructural levels. On the micro level, the component surface properties are responsible for all possible interfacial interactions whether they are physical or chemical ones. On the macro level, the fractional volume and the bulk properties of the component do have a dominating influence on PC properties. Numerous bulk models have been developed for PC and most of its mechanical properties could be calculated accordingly using the additive-mechanism concept. These bulk models which depend on the law of mixture were used after introducing some modifications and new concepts (61). They could be used successfully in predicting strength and other mechanical properties from knowledge of the technical characteristics of PC and the boundary conditions relevant to

them.

As shown in Fig.(3.1), PC can be generally divided into a continuous matrix phase and a dispersed-inclusion phase. The variables in structure that would affect the performance of PC, as shown in Fig.(3.1), are numerous and can result in a wide range of PC performance. For example it was found (61) that pores represent an important macrostructure factor. The formulation and type of resin used has another important influence. Different aggregates may result in a variation of PC compressive strength of almost 50% while keeping all other mix variables constant. A quantitative representation of the effect of the main PC-structure components on the macrostructural level is shown in Fig.(3.2) after Gamski and Bares et al (62) & (63).

On the microstructural level , many polymer-morphology studies have been undertaken to clarify the effect of synergetic interfacial combinations. The most important outcome is the fact that the creation of polymer-aligned layers or envelopes around filler particles produces PC performance (64) essentially different from those in which alignment has not taken place. Chemists are involved in modifying the interfacial layer between matrix and filler. Their main task is to help keep the polymer envelope around the particles as thin as possible with as large an aligned-polymer volume fraction as possible. The effect of the thickness of the aligned polymer envelope on the mechanical performance is shown in Fig.(3.3), along with the effect of PC porosity.

A study made in the U.S.S.R. on the physiochemical structural

formation of PC reached several interesting conclusions (64). One of these was that there is an optimum filler-surface area in the binding matrix ranging from 3000 to 5000 cm2/gm, at which the binder can be used efficiently. In addition there is an optimum ratio of binder which can only be reached with the highest possible degree of aggregate-compaction. Different morphology studies of the microstructre of globular or fibrillar polymer macromolecules showed that its formation depends upon: (a) polymer and filler ratio, (b) monomer chemical composition and (c) the properties of filler itself. These studies revealed the possibility of modifying and/or controlling polymer macromolecule structures along with the asssociated shrinkage strains and stresses. Some newly developed PC's were produced using active-surface fillers (65). These PC's are termed as expansive resin concretes and may expand rather than suffer shrinkage on setting. Several phsiochemical studies undertaken in the U.S.S.R. (66) & (67) suggested different material models with different component-structure-properties to suit different applications. The importance of such models is that they primarily help provide technical information for the development and production of PC. The high cost and the sophisticated applications of PC necessitate such models to serve as a tool in PC design. One of the suggested procedures for establishing design characteristics of PC is shown in Fig.(3.4).

3.2. Review of PC mix proportioning

Before proceeding towards mix-proportioning of PC, different mix variables and their influences on PC performance as found in various researches were revised along with their

experimental findings. Optimizing PC mix-design could be achieved by improving either the continuous-matrix phase or the dispersed-inclusion phase. Improving the continuous phase (the binder) is usually achieved by modifying its formulation and chemical composition. This is done by the addition of special high-cost additives. They are mainly coupling agents, shrinkage reducing agents and flame retardants. On the other hand, improving the dispersed phase is made by much simpler and cheaper techniques. It is simply achieved by proper choice of sound, strong, dry and well-compacted aggregates. Fine fillers or powders of inert or active-surface nature have been tried. Methods of mixing and casting may also have an effect on the final perfomance of PC. In the U.S.A., use of a vibratory mixer equipped with evacuation techniques to remove entrained air improved remarkably PC performance (68).

One of the relevant works on polyester resin concrete mix-design is that undertaken by Y.Ohama in Japan (69). In this work the development of PC mix-design was based on the properties of both binder and aggregate. From his previous work (53), Ohama found that most of the mechanical properties of PC are related to the styrene/polyester ratio (ST/UP) regardless of the resin type and its formulation. In a trial to find a rational PC mix-design method that work was extended (70) and variables other than ST/UP ratio were investigated as will be shown in the following paragraphs.

Mix variables studied were the amount of catalyst and accelerator, binder content, required workability and strength for given resin and aggregate types. Properties of aggregates

and resin used are shown in tables (3.1) and (3.2). The range of mixing ratio investigated is shown in table (3.3) with the following binder formulation;

ST/UP ratio was 2/3, 1.0, and 3/2.
Accelerator content (Co.Oct): 0.3, 0.5, 0.75 and 1.0 % of resin weight.
Catalyst content (MEKPO): 2/3 to 2 times the accelerator content.

Experimental findings showed that the binder working life as a fluid (Wlb) is inversely proportional to the accelerator and catalyst contents. As shown in Fig.(3.5), a linear relation could be found and expressed as follows;

$$Wlb = a + b/(cc.cm)$$

where cc and cm are the percentages of accelerator and catalyst contents. The constants a and b could be found and expressed for each ST/UP ratio as follows;

$$a = 2.211 + 19.87 \log (ST/UP)$$

$$b = 1/[0.0978 + 0.0613 (ST/UP)]$$

This binder working life in minutes measured according to JIS-A1101, could be related (71) to PC working life Wlc in another linear relation as follows;

$$Wlc = 2.59 + 1.01 Wlb.$$

The workability of PC itself was measured by the conventional slump test. As shown in Fig.(3.6), the binder content has a great influence on the slump particularly at low resin contents. However the accuracy and reliability of this test is

not satisfactory, where as shown in Fig.(3.7) resin viscosity had no effect on slump. In addition Ohama made slump tests for neither accelerated nor catalysed PC which makes the findings lose their practical importance as a real measure of PC workability.

The relations between the compressive strength fc in N/mm2 and ST/UP ratio for differing accelerator content are shown in Fig.(3.8). They are mathematically expressed as follows;

$$fc = A + b\,(ST/UP)$$

where $A = 165.4 - 3.605\,(cc)$, $B = 1/[-0.0147 - 0.0466\,(cc)]$

Based on the previous findings, Ohama suggested the mix-design chart (70) shown in Fig.(3.9). The main resin formulation can be selected from Fig.(3.10) according to the desired working life as a fluid. Mix proportions can then be found from Fig.(3.11), which is experimentally derived and can only be applied to the given types of the materials shown in table (3.1).

From the previous discussion of Ohama method of mix-design, it is clear that it does not consider the effect of aggregate grading on the strength or workability, which can be considered as a major drawback.

Another detailed experimental study made in Egypt (72), on PC mix proportioning showed that the aggregate grading with all its parameters (max. aggregate size, fineness, shape and texture, etc.) does have an important role in mix-design. In this study different aggregate types gave different strengths while keeping all other mix variables constant, as shown in

Fig.(3.12). This dependency was emphasized repeatedly in many other studies, as shown in Fig.(3.13) after Ohama. The main objective of this study was to choose the best aggregate grading and to relate it with the mechanical properties and workability of PC. The resin used was a polyester-resin type formulated by using MEKPO and Co.Oct as a catalyst and accelerator respectively. The coarse aggregate used was crushed basalt with a maximum aggregate size of 20.0 mm, while the fine aggregate used was natural sand, along with calcium carbonate powder as a filler. Three main gradings were prepared which had low, moderate and high specific surface areas depending on coarse:fine aggregate ratios of 0.4, 0.6 and 0.8 respectively. These gradings are shown in Fig.(3.14), while table (3.4) represents the mixing ratios for the different mixes investigated.

Using three different mixing ratios for three gradings, nine distinct PC mixes could be individually studied and collectively compared. Two different parameters that could measure workability were considered. Penetration depth and penetration resistance were chosen. Using a pocket concrete-penetrometer with the proper needle size, the pressure needed to obtain 20.0 mm depth in the fresh cylindrical specimens (150 mm diameter and 300 mm length) was recorded. Fig.(3.15) shows the relation between penetration resistance and elapsed time estimated from the moment when catalyst and accelerator were first added to the resin. The second workability parameter, the penetration depth, was measured for the nine mixes by allowing a steel bar to penetrate the fresh PC cylinders under its own weight. Measurements of the

penetration depth versus the elapsed time are shown in Fig.(3.16).

Compression tests were made and their relative values (values as percentages of the highest recorded strength) are shown in table (3.5). From the two quoted figures, Figs.(3.15 & 3.16), it is clear that irrespective of the resin formulation or its content, mixes which used finer aggregates offered lower penetration resistance and depth. This implied that finer aggregate-mixes would have required an increased amount of resin due to the high specific surface area. The poor consistency and consequent poor compaction were reflected as a decrease in the strength as shown in table(3.5) and Fig(3.17). The compressive strength was found to decrease with an increase in the fineness of aggregate for any given mix ratio. This decrease amounted to 30% for either high or low resin content mixes. Out of this work the recommended coarse:fine aggregate ratio for the investigated aggregates was found to be 4:5 by weight. This ratio is suggested to be 3:5 by Ohama, see Fig.(3.11).

Out of this work (72), it can be said that both strength and workability of PC depend strongly upon the type and grading of the aggregate used. The quoted values of coarse:fine aggregate ratios do not, however, preclude the use of much higher or smaller ratios depending on the available aggregate and the purpose for which PC is intended to be used. Yet they imply the importance of this ratio in mix-design.

3.3. Considerations for PC mix-design in the present work

Some considerations had to be taken into account in the proportioning of the various PC constituents to obtain five distinct and consistently reproducible PC grades, as follows;

3.3.A Economy To keep the production cost as low as possible, local aggregates were used after proper selection. Available aggregates were given first priority in proportioning. No special chemicals were used as additives, as the enhancement given by most of them can be obtained by proper mix-design and their costs are usually unjustifiable. Only the catalyst recommended by the manufacturer of the resin was used. No accelerator was required where the resin used was already preaccelerated. General-purpose unsaturated polyester resin was used as the binder. The resin content was kept as low as possible. For that purpose and others, coarse:fine aggregate ratios considered were as high as consistency and other workability requirements would allow. Curing of all PC specimens was at ambient temperature and no oven curing or any other technique of accelerated curing was applied.

3.3.B Performance The required performance of those five PC grades was such as to represent sufficiently the average range of performance dealt with by other researchers. This would make any likely comparison between the findings of this present work and the others more useful. It would also allow for a more realistic representation of PC performance. The absence of this approach precluded the beneficial use of many results obtained in several studies, each of which was concerned with improving one specific mechanical or physical property. Being very keen to obtain high compressive strengths, many researchers have neglected other structural

requirements for the successful use of PC in construction. For example, little concern was given to the stiffness of PC, the internal strains and stresses on setting and the rheological behaviour, etc. High compressive strength in itself can not be regarded as an advantage, where it might create problems of deflections, flexural rigidity and elastic instability. From an economic point of view, effective and efficient utilization of a high portion of the available strength is more importrant than the use of a smaller portion of a much higher strength. Most of the available work on PC mix-design often quotes the compressive strength as the only quality-indicator parameter. To show how far compressive strength is misleading, Fig.(3.18) shows different stress-strain curves for pure resin, resin paste, resin mortar and resin concrete. These curves were found experimentally at the outset of PC proportioning.

Compressive strength values from 100.0 to 120.0 N/mm2 are suggested (73) to be the ceiling that can be economically employed in construction. Above these values deflection is likely to control or cross-sections be too small to accommodate reinforcement. As will be shown later, setting shrinkage with consequent internal stresses and cracking have limited the structural use of many reinforced applications of PC. The excessive creep strains and other inferior rheological properties dictated a very high margin of safety in most of those applications. It is believed that these inferior rheological properties are mainly attributed to the very nature of the binder-matrix phase of PC. Hence reducing its fractional volume in the mix should enhance these properties at the expense of the compressive strength. That is to say

that by increasing the fractional volume of the dispersed phase (aggregates), the viscoelastic flow of PC under load will be reduced and strength will inevitably be reduced. This can be done by increasing the coarse:fine aggregate ratio and the microfiller content as well. There is another advantage given by increasing dispersed phase content in the mix which is reflected as less setting shrinkage, less internal tensile stresses and shrinkage cracks especially when the mix is used for reinforced applications.

It was decided to find the highest possible strength and stiffness by optimizing the available PC constituents. Thereafter it was possible to obtain the five different grades which were made to represent a wide range of PC performance. These grades as will be seen later, were obtained by controlling the resin content, the filler content, the coarse:fine ratio and by changing the type of aggrgate itself.

3.3.C Reproduction of mixes To keep those five grades consistent over all the the work to come, several precautions were taken. All fillers and aggregates were ovendried. The required amounts of aggregates and fillers for the whole work were estimated, ordered and stored. The maximum amount of resin which could be used within its permissible storage-life time was ordered and received with the same batch number. The mixing procedure was kept as consistent as possible. The releasing agents and the vibrating techniques were the same for the whole work. The ambient temperature was around 18 - 22 C with the only exception of the few summer weeks when temperature rose to 28 C. The viscosity of the resin was

checked and verified before mixing by the previously shown viscometer. The same testing machines were used for the different grades and throughout the whole work.

3.4. Description of the experimental work

The descriptions of the five grades of PC's. which were made to serve as base materials for the structural analysis of reinforced PC, are given below.

3.4.A Materials used

[1] Filler : Calcium carbonate powder whose properties are given in table (2.5).

[2] Resin : Crystic 196-PLAV unsaturated polyester resin with the properties shown in tables (2.1) and (2.2).

[3] Sand : Available sand in the laboratory supplied by Hyndford Quarry, near Larnak, with the properties and grading shown in table (2.7) and table (2.10-a) respectively.

[4] Coarse aggregate : Two main types were used; an irregularly shaped gravel with the properties given in table (2.8) and the grading shown in table (2.10-b). The second type was crushed basalt stone with the grading shown in table (2.10-c), and whose properties are given in table (2.9).

3.4.B Mixing ratios

Five different mixing ratios were chosen, as shown in table (3.6), in a way that is believed to represent fairly average PC properties. As said earlier, the mix variables on the micro and macro-levels were adjusted in proportioning these five grades. Their microstructure was controlled by incorporating

three different resin contents and three resin:filler ratios. The macrostructure was modified by using three different coarse:fine aggregate ratios as well as different types and textures of the coarse aggregate itself.

Based on the previous reviews of PC mix-design, and its incorporated constituents and their influence on performance, it was possible to predict performance before testing. As shown in table (3.6) and on a quantitative basis, grade "E" should give the highest compressive strength because of its high resin content and its high filler:resin ratio. As the coarse:fine aggregate ratio is lower than other mixes, grade "E" is predicted to be more workable (more paste and less aggregate internal friction). The hardened elasticity of "E" is also low because the fractional volume of the continuous matrix-phase is high. Hence the expected ultimate and failure strains should be higher than those with other grades. At the other extreme, grade "C" was predicted to give the lowest strength since it had the lowest resin content and the lowest filler:resin ratio. Reduced strength was also due to the use of the gravel in mix "C". This gravel was much weaker than the basalt stone used with other mixes. The workability of this grade and that of grade "D", was expected to be poor due to the limited amount of paste available for eliminating the internal friction of the much bigger volume of the coarse aggregate used. Grade "C" was also found to be much stiffer than grade "E" for the same previous reasons. The type and texture of the coarse aggregate should be reflected in the mechanical performance as well. For instance, grade "A" and "B" have the same mixing ratios but the former is made with

gravel having much smoother texture and much lower mechanical strength than basalt crushed stone used with the latter. So grade "A" should be more workable than "B" while "B" should have higher structural stiffness and ultimate compressive strength than "A".

From a statistical point of view, as PC workability diminishes, reproducibility of tests becomes more difficult and results less consistent. That is to say that "the variance" in any estimated property increases with the decrease of workability and the decrease of strength. Many codes and standard specifications allow for higher "dispersion" for poor quality concretes than for high quality ones because of the same reason (60). As poor-workability PC essentially produces poor quality PC, it was known from the beginning that such concretes, grade "C" and "D" for example, would have a higher degree of variance and that this would affect the interpretation of their test results. Where these grades are supposedly new materials and there is no sufficient statistical history available for their performance , it was imperative to adopt a few assumptions that might keep interpretation of results simple enough yet avoid the usual risk involved in simplification. These assumptions are derived from the previous resin mortar investigation (Chapter Two), and the available provisions for cement concrete quality control(60) & (74), as follows:

(1) The mechanical properties of these grades have a "normal frequency distribution" charcteristics.
(2) The coefficient of variation in the compressive strength is 5% for grade "E" and is increased by 1% for the other

grades "B", "A", "D" and "C" respectively.

(3) The nominal value of any property is the value exceeded by 84% of test specimens, i.e., one standard deviation below the mean value, hence;

$f_n = f' - s/ n^{0.5}$

where f_n and f' : nominal and mean value of number (n) of specimens, s :standard deviation.

3.4.C Specimens for different tests Table (3.7) shows the dimensions of the specimens used for different tests. The properties tested for each grade were compressive strength, splitting strength, flexural strength, moduli of elasticity in compression and flexure, shear strength and bond strength. Fig.(3.19) shows the specimen chosen for shear testing, while Fig.(3.20) shows the pull-out test arrangements for estimating bond strength.

3.4.D Casting and curing For each mix all-in aggregates were dry-mixed with the filler in a rotary mixer for five minutes. The catalyst was added to the resin, stirred by a steel bar for two minutes and then poured over the mixed aggregates in a rotary mixer. This mixer (5 ft^3) has a pan that rotates around two axes, vertically and horizontally. Using this facility of the mixer, PC ingredients could be uniformly mixed within five minutes. Moulds painted with the releasing agent were immediately filled and then vibrated for a time just sufficient to allow good finish by trowelling the top surface of the specimen. All specimens throughout this work were left to cure at the ambient temperature for 24-hours then demoulded

and stored until tested without any special curing techniques.

3.4.E Testing All tests for each grade were carried out at three days of age. A universal testing machine was used for all these tests. The recommended rates for testing conventional cement concrete were used. The chosen rate for compression tests was 15 $MN/m^2/min$. For each grade three specimens were prepared for measurement of different moduli of elasticity. To eliminate creep effects on the measurements cyclic loading was first applied at the same given rate of loading (three cycles from zero to 40% of the ultimate strength). Then the load was increased from zero up to failure load. The planeness of the test surface was attained by grinding, where no structurally compatible material could be employed for capping or packing. The testing machine was equipped with a rigid non-rotating platen for the compression test. The dimensions of the compression specimens were defined to suit the maximum-aggregate size. Cylinders were preferred to cubes or prisms as they have been reported (75) to represent compressive strength more satisfactorily. Depending on the low variance in the strength of resin-mortars investigated in the previous chapter, and assuming that this would more or less be the same with PC, the smallest possible dimensions of the cylinders were considered. The height:diameter ratio was taken to be 2:1 based on other findings (76), which showed that this is the maximum ratio above which no decrease in strength is noticeable, see Fig.(3.21). The same considerations were applied for the dimensioning of all other test specimens, bearing in mind that a high number of small specimens is more representative than a

smaller number of bigger specimens.

For flexure tests, the arrangements shown in Fig.(3.22) were made. Third point-flexure tests were carried out rather than centre-point tests; in the former almost one third of the span is subjected to maximum stresses with more probability of failure initiated by the weakest element. The rate of loading was 1.6 N/mm2/min. Moduli of elasticity and rupture were calculated assuming a linear stress distribution. Their values were calculated only for the comparison of different grades.

Another measure of the tensile strength is the splitting test which was carried out with a similar rate of loading to that of flexure test. Strips of hardboard of 5.0 mm-width and 2.0 mm-thickness were used between the machine platens and the specimen along diametrically opposite generators. For shear tests, as shown in Fig.(3.19), rotating platens were used as in both flexure and splitting tests. The load rate for shear test was similar to that of flexure test. Pull-out tests were operated using the same universal testing machine after replacing the machine platens with suitable grips, as shown in Fig.(3.20). The rate of loading was around 2.3 KN/min.

3.4.F Measurements of strains and deflections For the measurements of different moduli of elasticity in compression, three electric strain gauges of 20.0 mm-length were attached to each cylinder at the middle of its height, making an angle of 120° in horizontal plan to each other. Using an electronic recorder "Data_Logger", continuous recording of strains could be traced until failure. For flexure tests, two transducers with 50.0 mm-travel were attached to the upper surface of the

beam and continuous recording of the deflection was obtained by the Data Logger. The same type of transducers were used for measuring shear slip as shown in Fig.(3.19). For pull-out tests, four 5.0 electric strain gauges were attached to the embedded part of the steel bar; a pair at 50.0 mm distance and the second pair at 150.0 mm distance from the end of the cylinder. By recording the tensile strains at the two levels and knowing the stress-strain curve for the steel used, the corresponding tensile forces could be calculated and as will be shown later, the bond strength could be derived.

3.5. Test results of short-term mechanical properties

3.5.A Results of compression test As the rate of loading was more or less constant, the failure of the specimens was often sudden and sometimes explosive, particularly with grade "C" and "D". The ultimate compressive strength was calculated for each specimen, then the average and the nominal values were found. For the calculations of the different elastic moduli, the stress-strain curves (average of three specimens) were plotted as shown in Fig.(3.23). No falling branch could be traced in these curves.

3.5.B Results of splitting test The nominal values of the splitting strength for the five grades are shown in table (3.8); the splitting strength (f_t) is calculated as follows:

$f_t = 2\ P/(\pi\ d.l)$ where,

P : the ultimate compression load.

d, l : diameter and length of the cylinder.

The nominal value of the splitting strength varied from 8.5 up

to 11.0 N./mm2, which is 11 to 12 % of the nominal compressive strength respectively.

3.5.C Results of flexure test In all flexure tests beams had the fracture plane within the middle third of the span. The following equation was used to calculate the modulus of rupture (f_f) :

$f_f = P\ L\ /\ (b.d^2)$ where,

P : total machine load at failure.

b, d : width and depth of test beam.

The flexural modulus of elasticity $E_f$was calculated using the deflection y at midspan under one fifth of failure load, using the equation :

$E_f=(23/1296).(PL^3)/(yI)$ where I=moment of inertia and L=span.

As shown in Fig.(3.24), the maximum recorded deflection at midspan varied from 0.4 to 0.7 mm. The calculated nominal values of f_f and E_f are shown in table (3.8).

3.5.D Results of shear test The measurements of shear slip versus shear load were not satisfactorily consistent. Within each grade the values varied considerably from a specimen to another. Fig.(3.25) shows different curves obtained for grades "E", "B" and "A" resectively. This wide dispersion in observations may be due to the nature of the shear strength itself, which depends on the interfacial bond and the aggregate interlock at the shear plane. In addition the high dependency of shear strength and rigidity on shrinkage cracking and its width and depth, however small, along the

shear plane might be another reason for this inconsistency. Yet the nominal shear strength derived from the average shear strength of the test results showed the expected trends. For instance for grade "E" it reached 11.0 N/mm2, while for grade "D" it amounted to 8.5 N/mm2. Different moduli of rigidity or shear stiffness could not be reliably derived from these shear tests and the significant value of these tests was only in the evaluation of the shear strength that would serve in the flexure analysis yet to come.

3.5.E Results of bond tests The ultimate anchorage and local bond strengths could be calculated for different grades as represented schematically in Fig.(3.26). The average axial tensile strains were first recorded at positions (2) and (1) at distances of 50.0 and 150.0 mm from the top of the cylinder respectively. Knowing the load-strain curve for the steel used, the axial tensile forces corresponding to different strain values at the two locations were calculated (T1 and T2). The average local bond strength was calculated as a uniform shear stress acting along the embedded surface area of the steel bar between the two positions (1) and (2). The average anchorage bond strength was calculated as the uniform shear stress resisting the whole tensile force along the total embedded surface area of the bar. These values are given in table (3.8), and the curves they are derived from are shown in Fig.(3.27) for grade "A", "B" and "E" respectively. Regarding grades "C" and "D", the measurements of the axial strains in the steel bars varied widely and in some specimens obviously faulty readings were recorded. That might be attributed to the high fractional volume of the coarse aggregate and the

harshness of these two grades which made it very difficult to maintain strain gauges undamaged after casting and vibrating. The anchorage bond strength could be calculated as it depends only upon the total pull-out load resisted by this strength.

Table 3.1: Properties of Filler and Aggregates

Type of Filler and Aggregate	Grading (mm)	Specific Gravity ($20^{o}C$)	Water Content (%)	Organic Impurities
Calcium Carbonate, Heavy	2.5×10^{-3}	2.70	0.1	Nil
Hatsukari Crushed Andesite	10-20	2.53	0.1	Nil
	5-10	2.50	0.1	Nil
Abukumagawa River Sand	1.2 - 5	2.51	0.1	Nil
	< 1.2	2.61	0.1	Nil

Table 3.2: Properties of unsaturated polyester resin.

Specific gravity ($20^{o}C$)	Viscosity ($20^{o}C$, cp)	Styrene content %	Acid Value
1.127	695	28.0	21.3

Table 3.3: Mix Proportions of Polyester Resin Concrete

Material			Binder Content (wt %)		
Binder: Unsaturated Polyester Resin + Styrene			9.00	11.25	13.00
Filler: Ground Calcium Carbonate			9.00	11.25	13.00
Aggregate	Coarse Aggregate	Size			
		10-20mm	15.39	14.55	13.89
		5-10mm	15.39	14.55	13.89
	Fine Aggreaget	Size			
		1.2-5 mm	10.36	9.60	9.17
		1.2mm	41.06	38.80	37.05

Table 3.4: Different mixes investigated

Grading	Coarse: Fine by wt.	Binder ratio by wt % 7	9	11
Fine (A)	2:5	1	2	3
Intermediate (B)	3:5	4	5	6
Coarse (C)	4:5	7	8	9

* Coarse aggregate 3/4", retained on 3/16".

* Fine aggregate passing 3/16", retained on no. 30.

Table 3.5: Relative compressive strengths for different mixes.

Specimen No.	1	2	3	4	5	6	7	8	9
Relative compressive strength	58	67	71	73	80	84	89	94	100

Table 3.6: Mixing ratios by weight % for the five different P.C. grades

Mix	Filler	Resin	Fine agg.	Coarse agg.
A	11.0	10.0	31.5	47.5
B	11.0	10.0	31.5	47.5*
C	10.0	8.0	32.0	50.0
D	10.0	8.0	32.0	50.0*
E	12.0	12.0	38.0	38.0*

* Crushes Basalt stone.

Table 3.7: Dimensions of specimens used.

Property	Dimensions of specimen
Compressive strength	Cylinders, ϕ 75 × 150.0 mm
Compressive mod. of elasticity	"
Splitting strength	"
Flexure strength	Prism 70 × 150 × 650 mm (600 mm test span).
Bond strength	Cylinders, ϕ 100 × 200.0 mm
Shear strength	Shear plane 100 × 100 mm.

Table 3.8: Mechanical properties of the five PC grades

	Grade A	Grade B	Grade C	Grade D	Grade E
Compressive strength N/mm^2:-	85.0	90.0	75.0	80.0	95.0
ultimate strain	0.0073	0.0068	0.0057	0.005	0.0082
Secant modulus of elasticity N/mm^2 (at $1/3$ ultimate strength)	16666.0	17650.0	18870.0	20510.0	15850.0
Flexural modulus of rupture (N/mm^2)	12.95	13.7	12.1	12.6	14.1
Flexural modulus of elasticity N/mm^2	18910.0	20005.0	20615.0	23417.0	16955.0
Deflection at $1/5$ ultimate load in flexore (mm)	0.07	0.07	0.06	0.055	0.085
Ultimate deflection (mm)	0.54	0.46	0.40	0.35	0.78
Splitting strength (N/mm^2)	9.0	10.3	8.0	8.4	10.9
Bond strength (N/mm^2):					
local bond L_{bl}	12.6	11.2	-	-	14.2
Anchorage bond L_{ba}	9.5	9.9	-	-	10.4
Shear strength (N/mm^2)	8.0	9.0	7.0	7.5	10.5

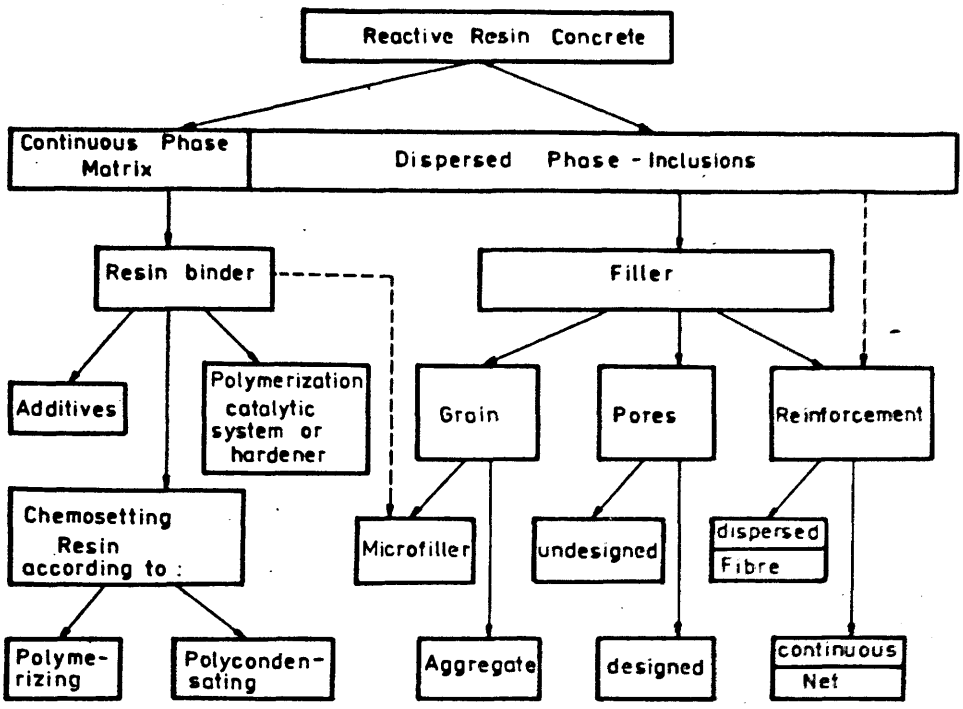

Fig. 3.1 Structural diagram of polymer concrete.

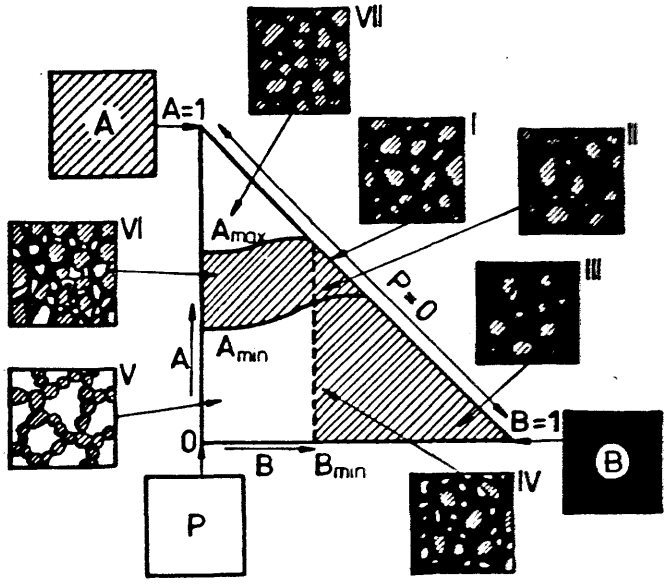

A: Aggregate B: Binder P: Pores

Fig. 3.2 Schematic representation of the macrostructure of PC.

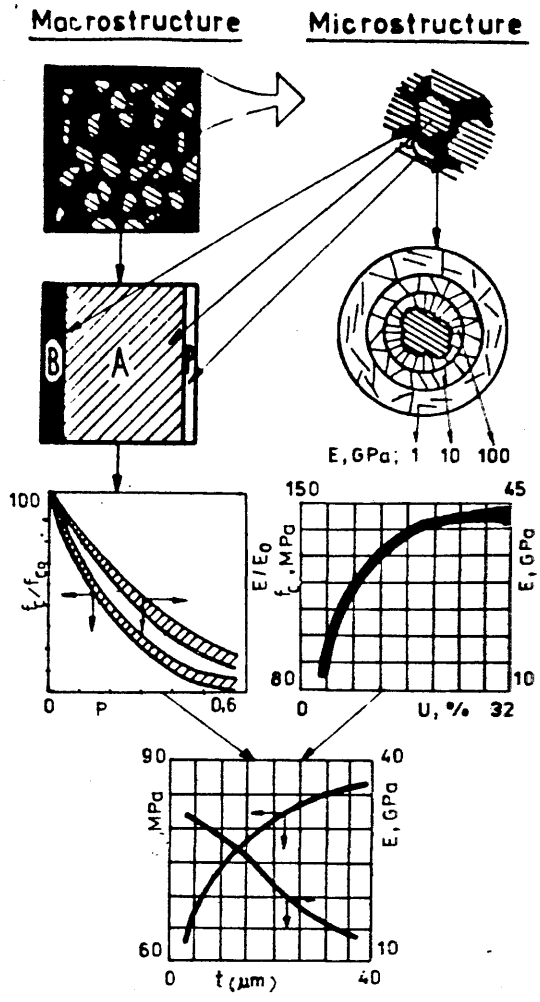

Fig. 3.3 Schematic illustration of compressive strength (fc) and modulus of elasticity (E) versus thickness of resin binder (t) as the superposition of the interaction on the micro and macro structural levels.

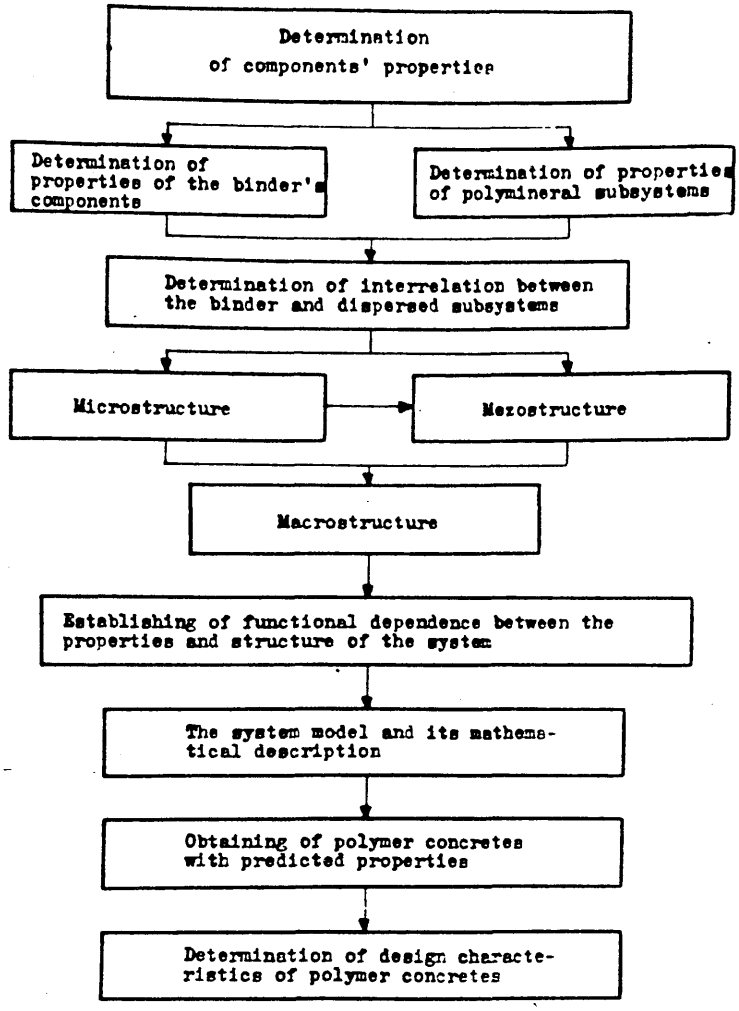

Fig. 3.4 Optimal PC compositions and their design characteristics determination.

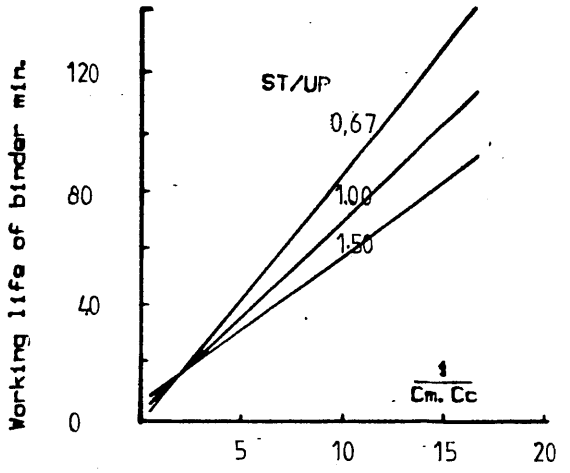

Fig. 3.5 Effect of accelerator and catalyst contents (Cc and Cm) on working life of binder.

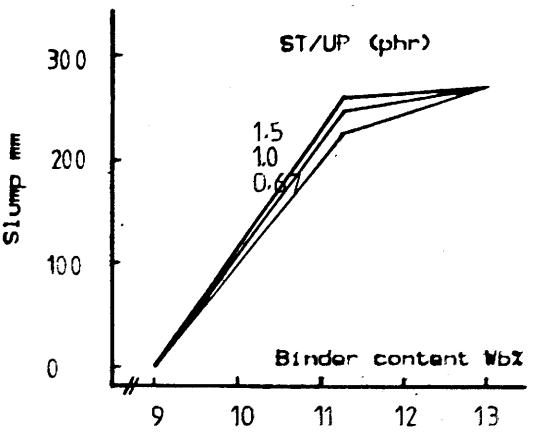

Fig. 3.6 Binder content versus slump of fresh polyester PC.

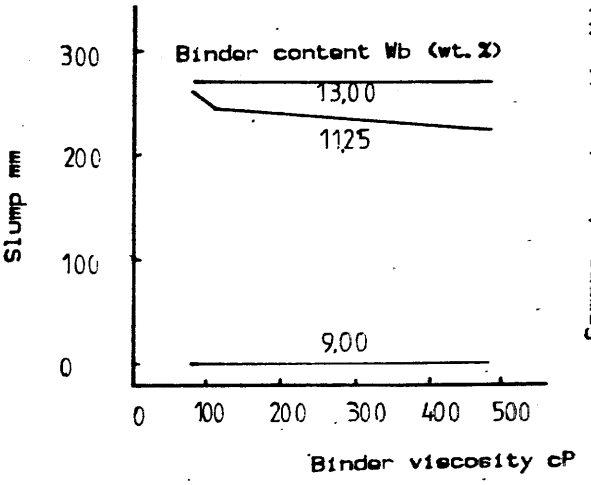

Fig. 3.7 Binder viscosity versus slump of fresh polyester PC.

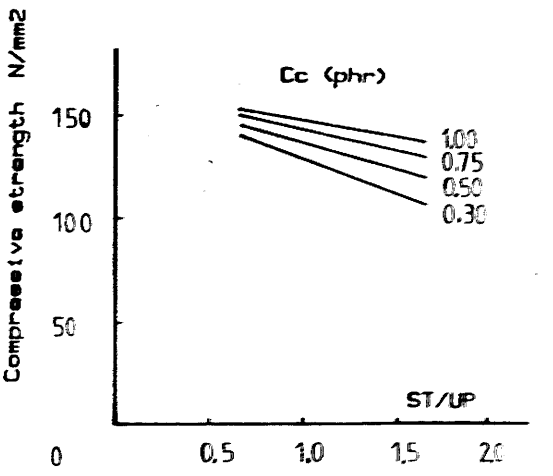

Fig. 3.8 Relationship between ST/UP ratio and compressive strength of polyester.

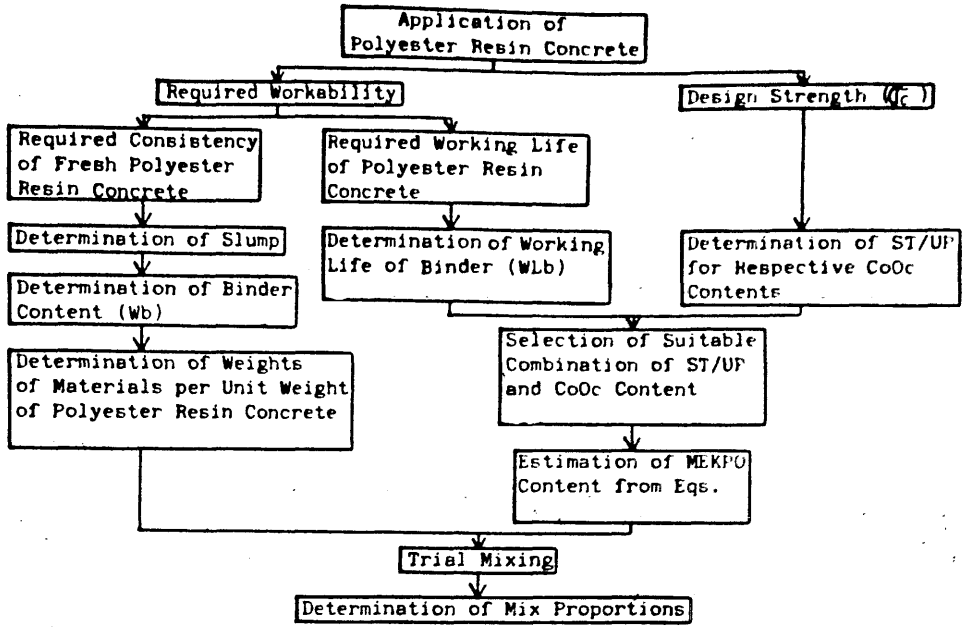

Fig. 3.9 Chart showing mix-design procedure for polyester resin concrete.

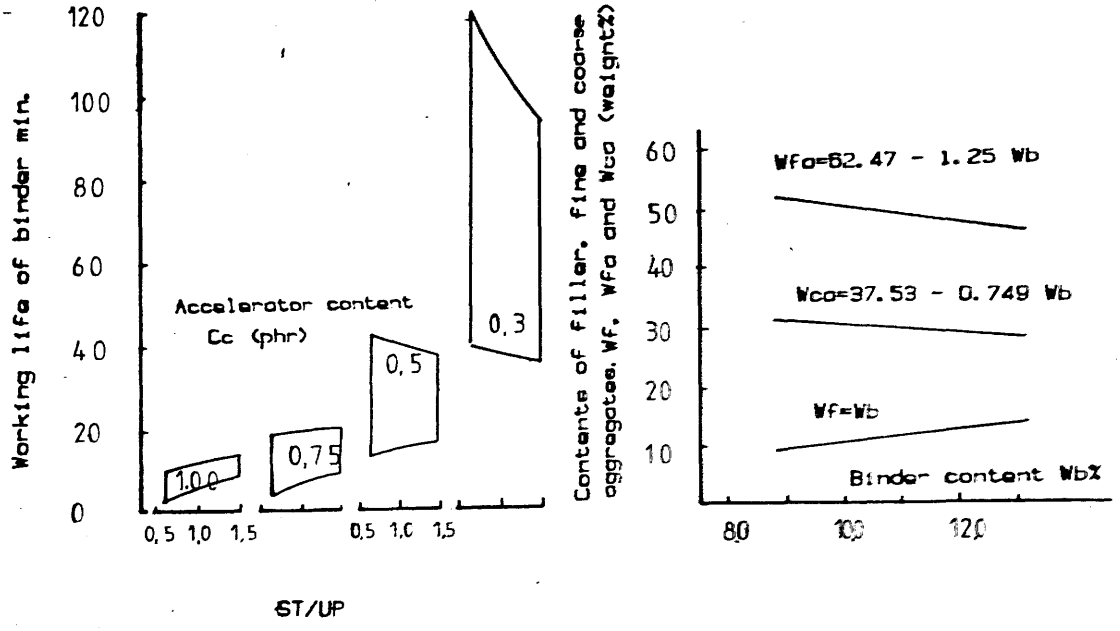

Fig. 3.10 Nomograph for selection of various accelerator content-ST/UP

Fig. 3.11 Nomograph for determining quantities of filler, fine and coarse aggregate per unit weight of polyester PC.

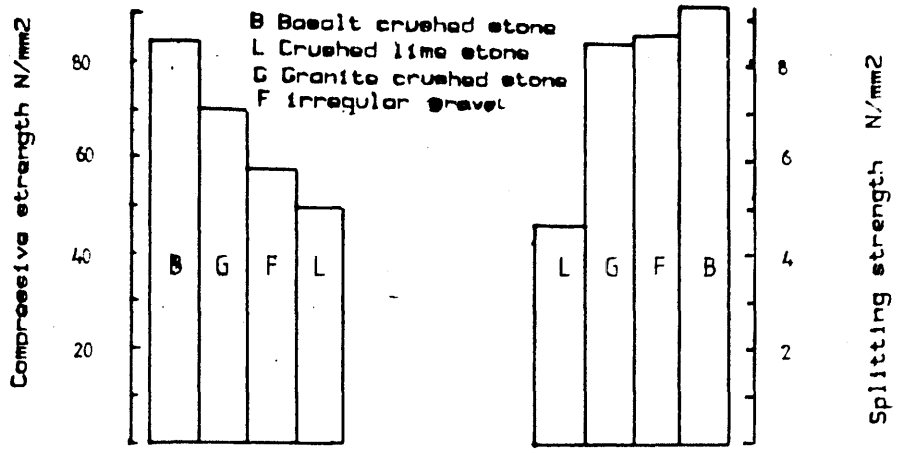

Fig. 3.12 Influence of aggregate type on mechanical strengths of PC.

Fig. 3.13 Volume fraction of coarse aggregate versus compressive strength of PC.

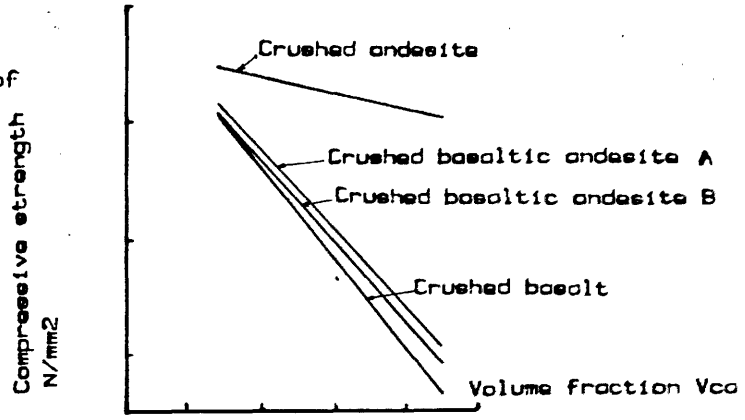

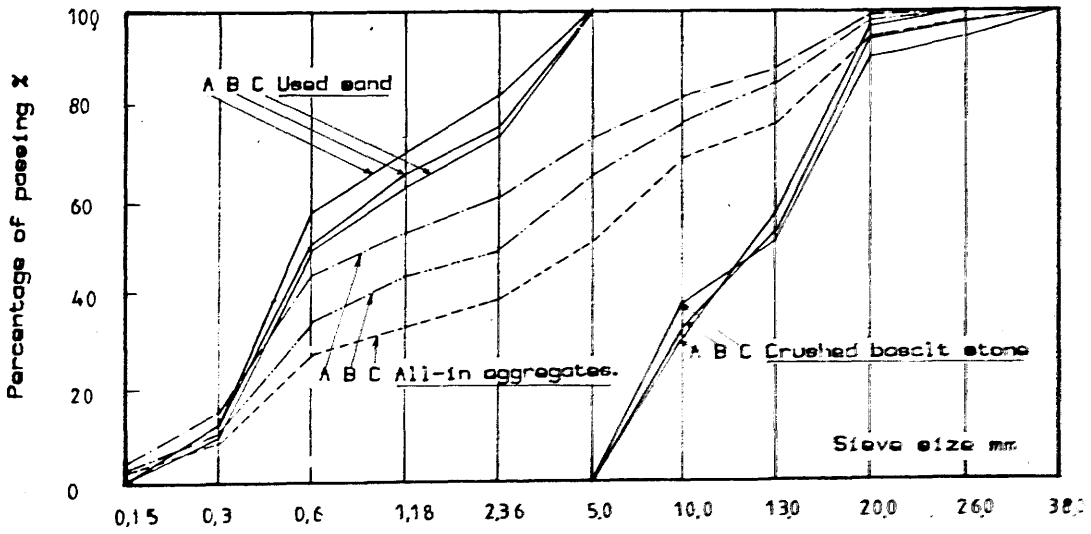

Fig. 3.14 Grading used in making different PC mixes.

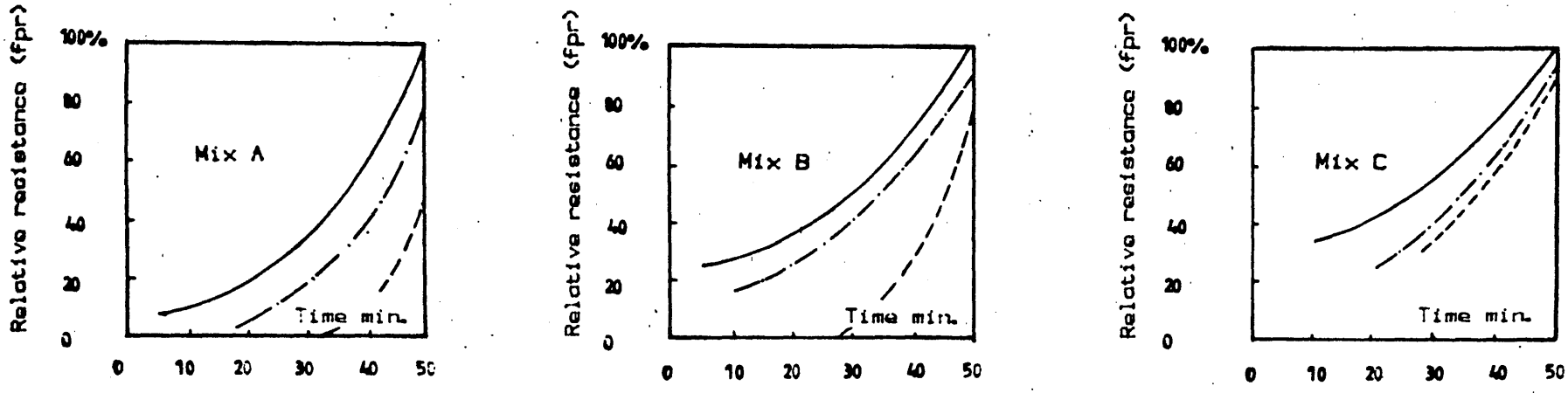

Fig. 3.15 Relative penetration resistance (fpr) versus elapsed time for PC mixe

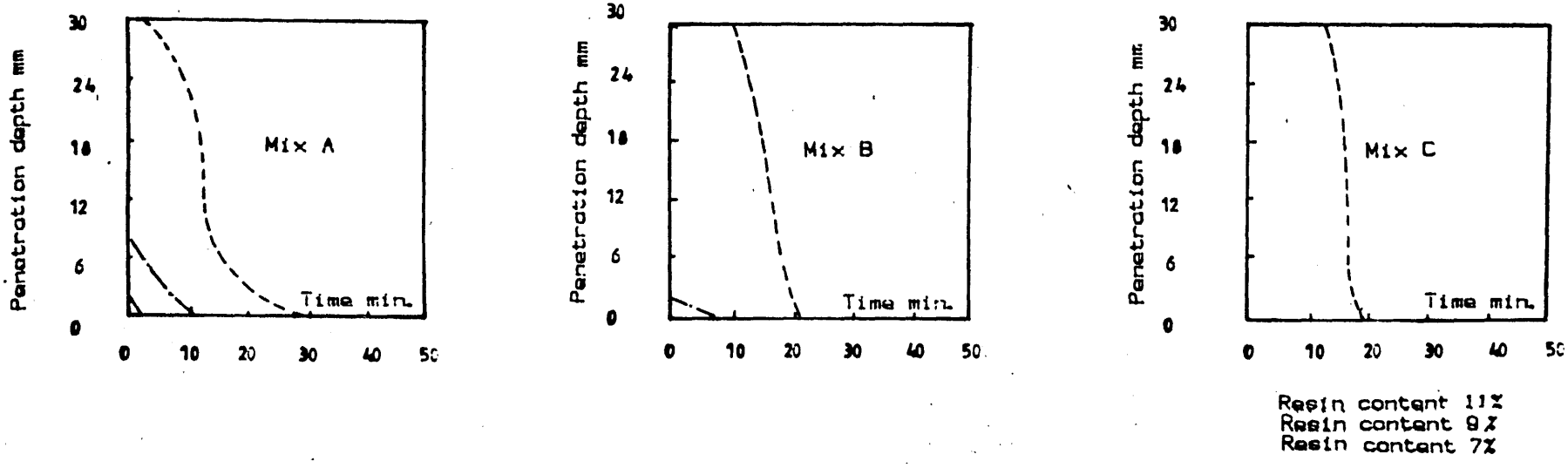

Fig. 3.16 Penetration depth (mm) versus elapsed time for PC mixes.

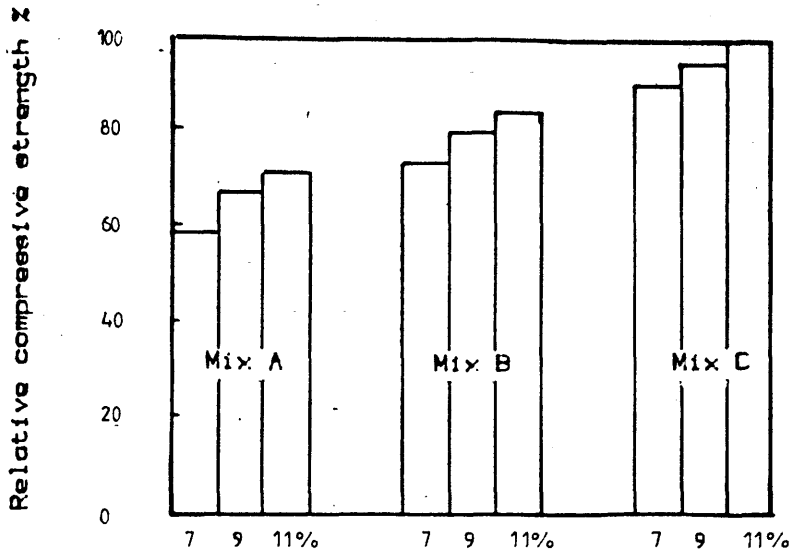

Fig. 3.17 relative compressive strength versus binder content for different aggregate-grading PC mixes.

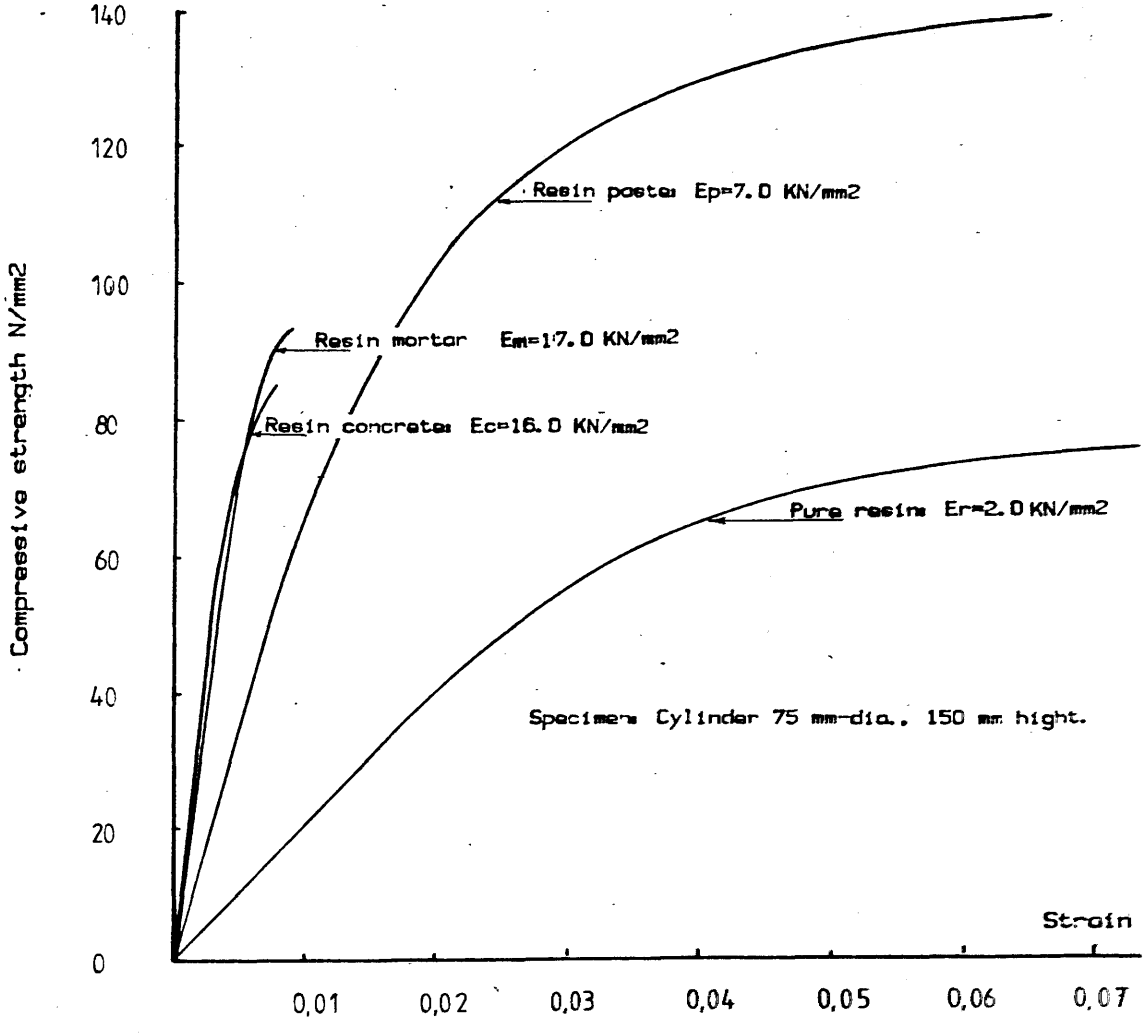

Fig. 3.18 Compressive stress-strain relationships for various resin-based materials.

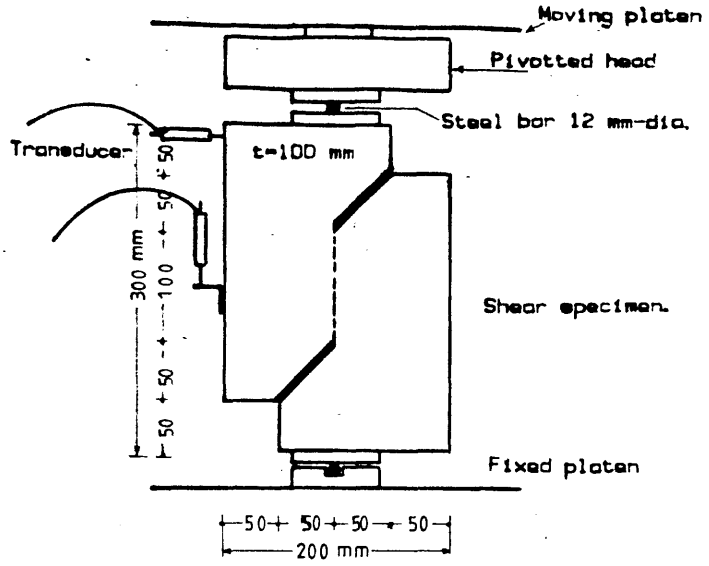

Fig. 3.19 Arrangements for shear test.

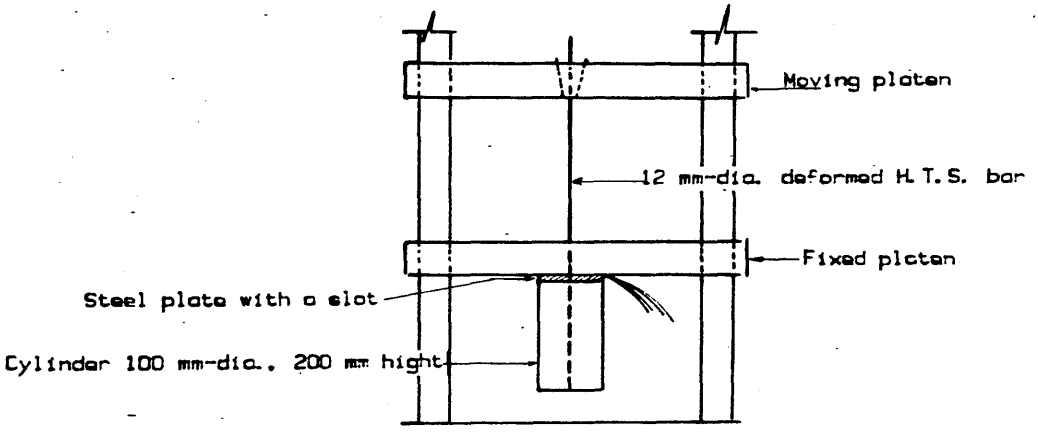

Fig. 3.20 Arrangements for pull-out test.

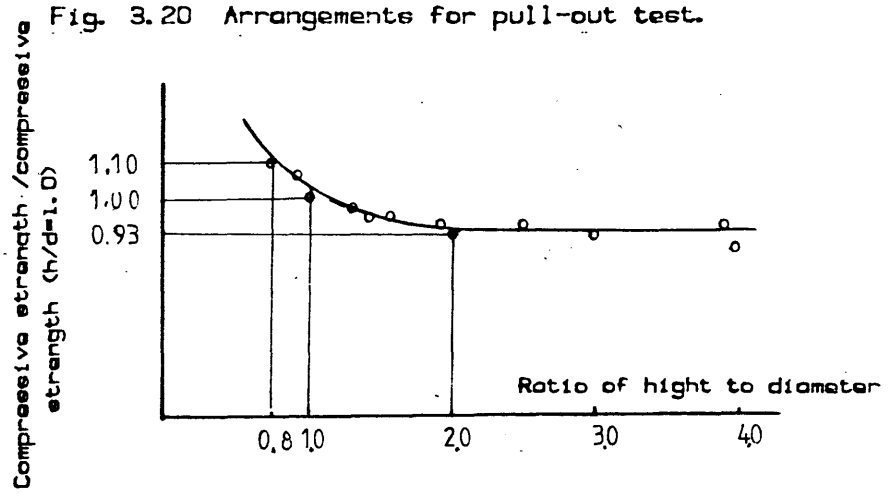

Fig. 3.21 Effect of hight/diameter ratio of cylindrical specimens on the compressive strength of PC.

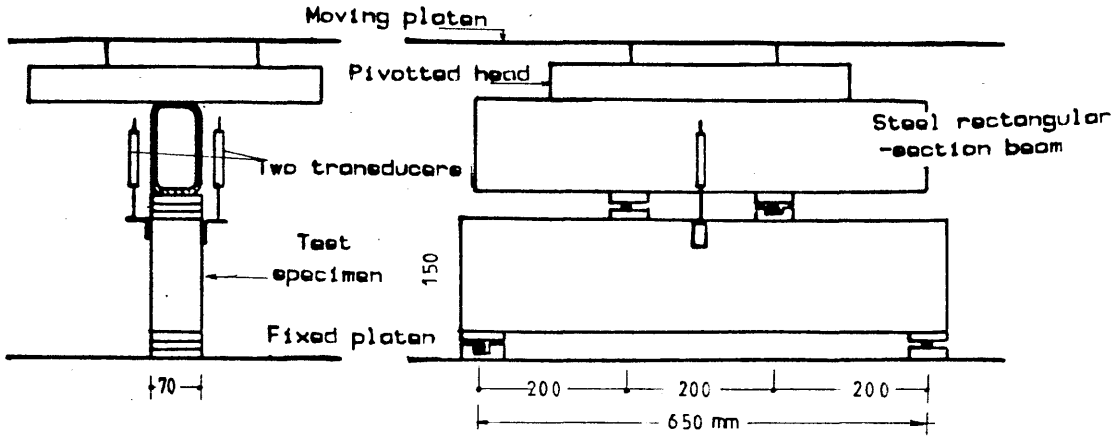

Fig. (3.22) Arrangements for flexure test.

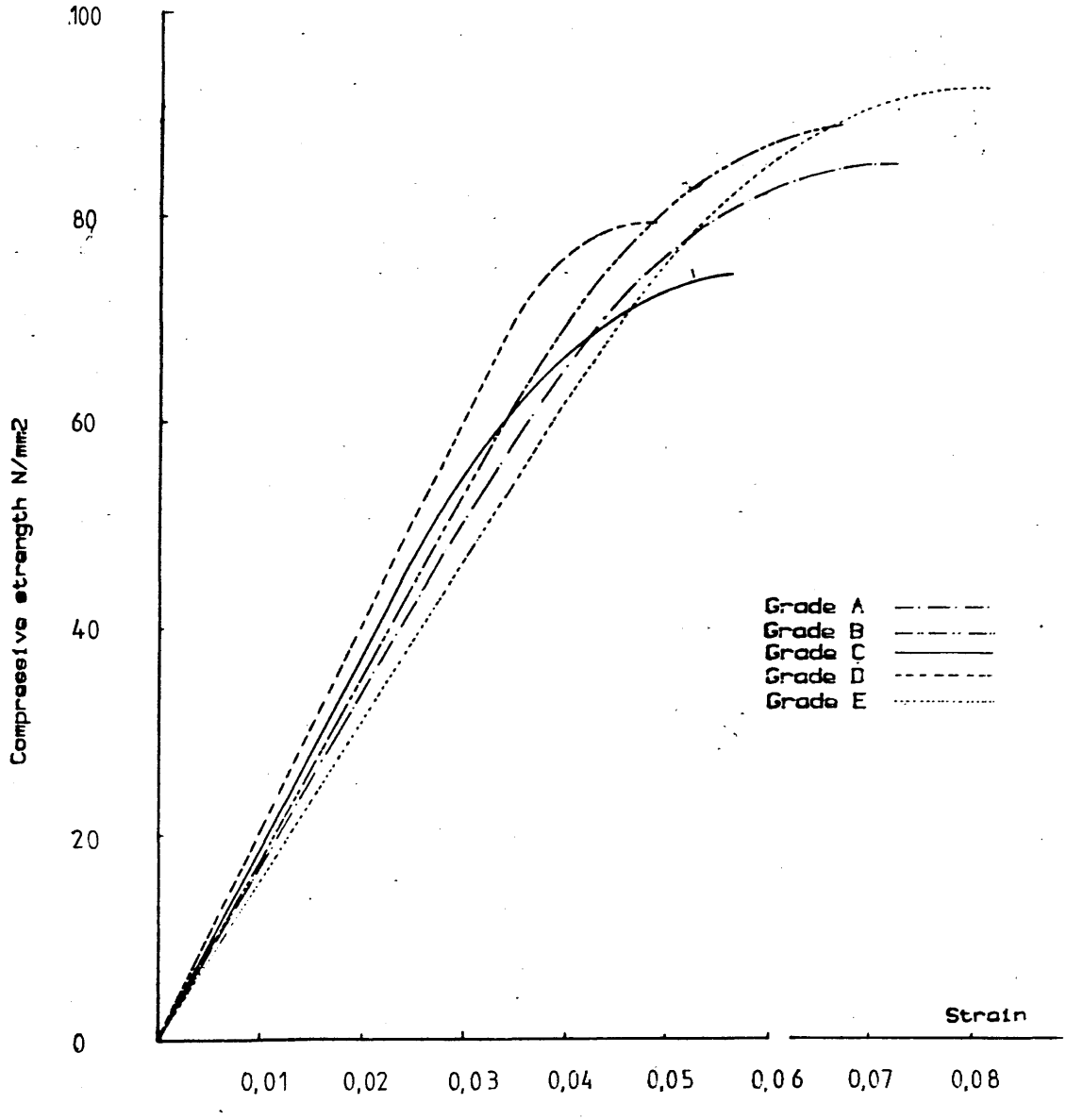

Fig. 3.23 Compressive stress-strain curves for the five PC grades.

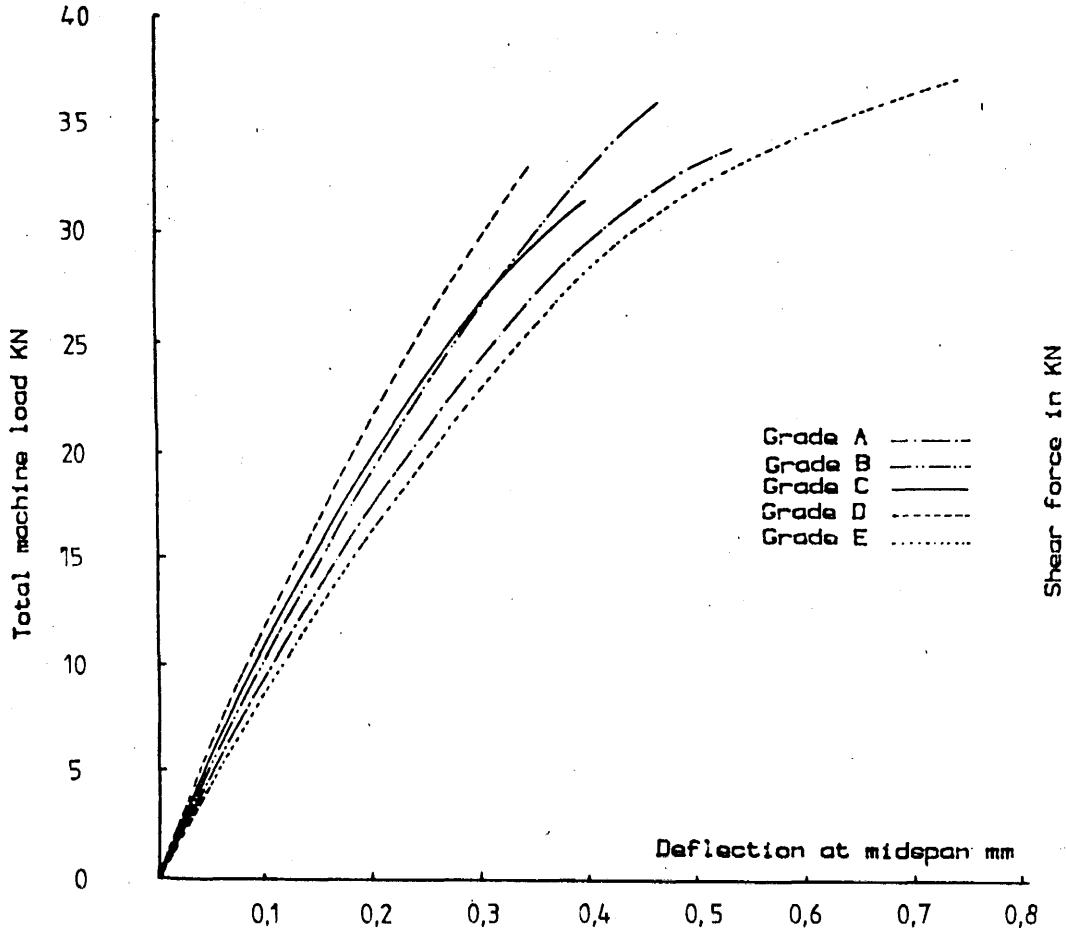

Fig. 3.24 Load-deflection curves for the five PC grades in flexure.

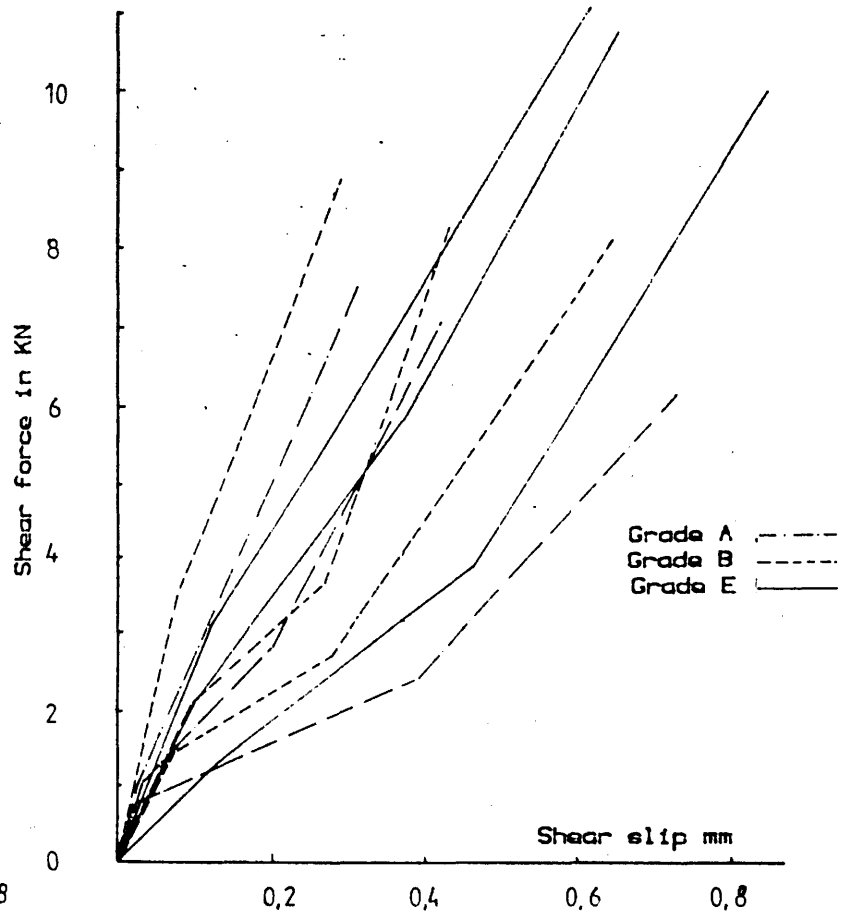

Fig. 3.25 Shear force versus shear slip for the five PC grades.

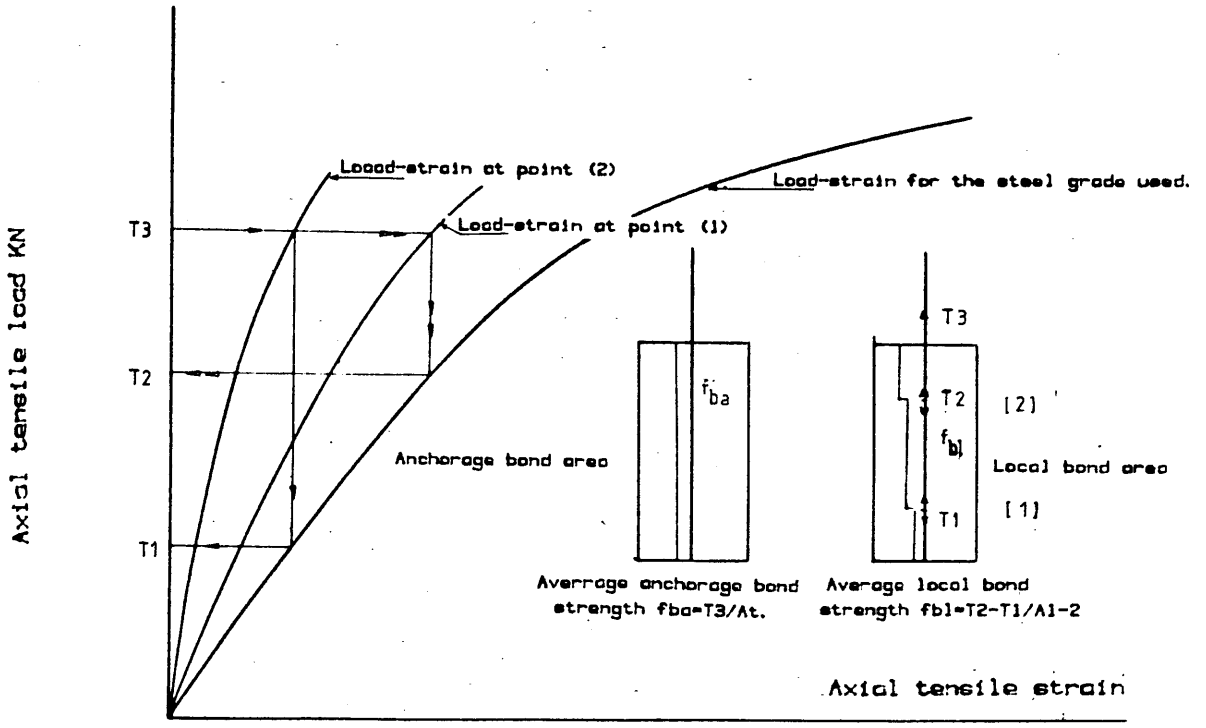

Fig. 3.26 Schematic representation of the derivation of the average anchorage bond strengths.

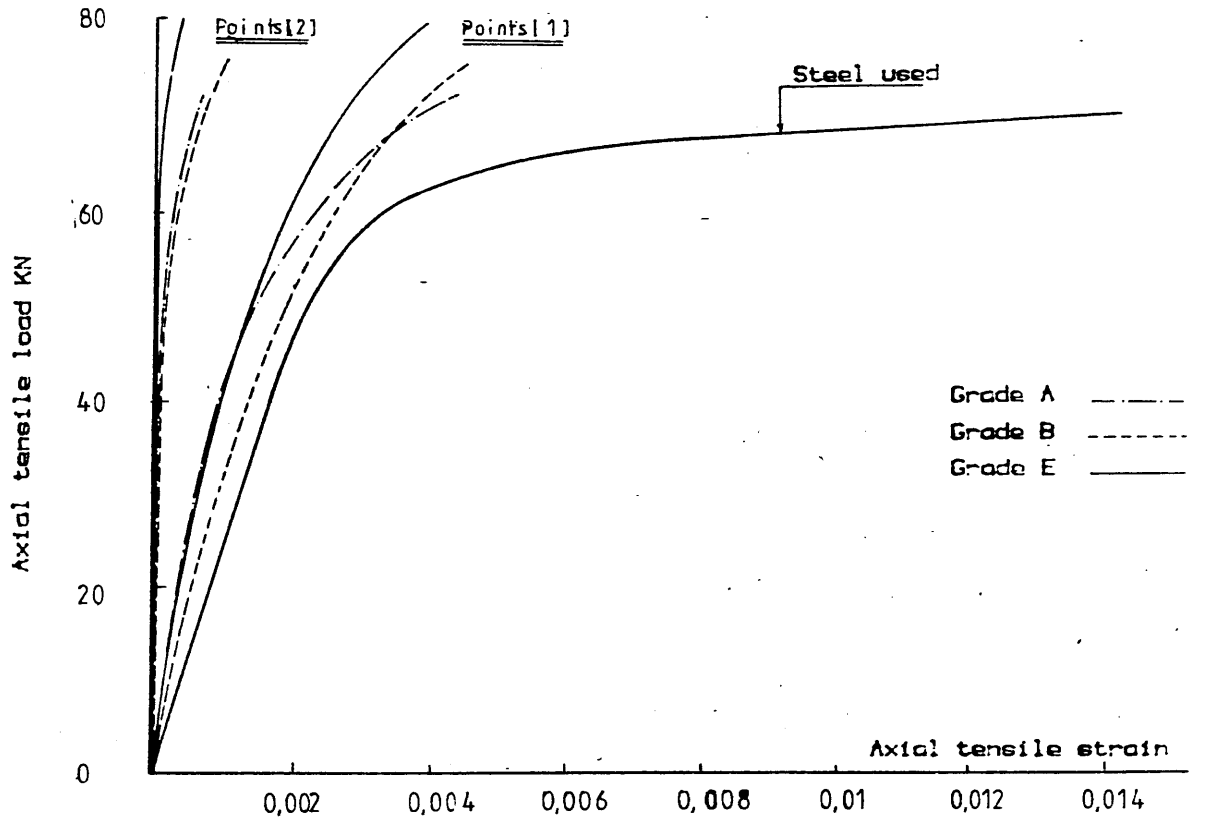

Fig. 3.27 Load-strain curves for estimating bond strengths for PC grades.

CHAPTER FOUR

STRESS DISTRIBUTION IN FLEXURE AT ULTIMATE STRENGTH OF PC

4.1. Introduction

In recent decades progress has been made towards replacing classical elastic structural design methods by new ones which represent actual conditions to a greater degree. Numerous investigations of conventional concrete structures have been carried out leading to several new design theories, these generally show good agreement with test results particularly in the case of pure flexure. However these theories start from different, sometimes even contradictory, assumptions about the physical behaviour of the material employed. An engineer seeks to evaluate the true behaviour of a structure. Approximate results obtained on the basis of widely different assumptions are not satisfactory. The agreement of various theories in design ,however, is understandable when only under reinforced beams have been considered . In such cases the tensile force in the steel at failure is determined irrespective of the concrete quality and the lever arm is not strongly dependent of concrete strength. Only tests of over reinforced members can, therefore, furnish a true measure of the validity of a flexural theory.

For polymer-concrete there is a need for a theory which is not restricted to approximate results in a limited range. Such a theory must be based on the actual limiting properties of the materials and must be valid for all cases of loading. With resin-concrete very little work has been done to clarify its structural behaviour in flexure. Most of that work relies

entirely on beam tests (77), (78) & (79). Three conditins are available for such tests; the equilibrium condition, the deformation condition and the assumption that plane sections remain plane. As the number of unknowns is generally greater than the available number of equations some plausible assumptions had often to be made in the evaluation of certain quantities. As the unknown quantities are closely interrelated it is quite understandable that one may thus arrive at widely different solutions.

The rheological behaviour of hardened PC poses some restrictions on their structural use. Many researchers have studied creep behaviour, stress relaxation and shrinkage strains and stresses of PC. However there is very little interest in applying these findings to the structural behaviour of reinforced PC members and the consequent effects of sustained loading on the ultimate strength of these members. Despite the fact that PC has an inferior long-term performance under load, most of the structural applications were derived disregarding this fact. In consequence, PC designers considered exaggerated factors of safety that would compensate for any hidden influences and the lack of a reliable flexure-theory. As will be seen later, the effect of load application rate can result in a strength variation in PC of up to 20%.

The distribution of concrete stress in the compression zone of reinforced concrete members subject to flexure is of a fundamental importance in theories regarding the ultimate strength and behaviour of such structural members. This stress

distribution often called the "Stress Block" is a powerful tool in furnishing structural relationships in a direct manner for any flexural theory.

For conventional concrete many ultimate strength theories involving a variety of hypothetical stress block shapes have been developed. Generally theories based on stress-strain relations obtained in axial prism tests carried beyond the maximum load have also been presented (80). Some investigators have attempted directly or indirectly to measure the distribution of flexural stresses in tests of reinforced beams. the stress block generally has three main parameters K1, K2 and K3 as shown in Fig.(4.1), which can be used in ultimate strength design. These parameters together with the ultimate strain can be used for different cases ranging from pure flexure to pure compression for reinforced structures or prestressed ones. If the whole shape of the stress block is known and expressed in a certain function it can be used for the design of structures having cross-sections of various shapes or subjected to biaxial moment or any other case of loading. For this reason early researchers paid most attention to finding the stress-strain relationship for conventional cement concrete in flexure.

To find these relationships for PC previous techniques used with cement concrete were revised. Although strains can be directly and easily measured, stresses in the compression zone are difficult to measure and as will be shown direct methods for their measurements are not practical.

4.2. Review of methods for measuring flexural stress

distribution

4.2.A Axial compression test In this method it is assumed that the extreme fibre in bending at ultimate moment is subjected to a maximum stress and a corresponding maximum strain, similar to those found in simple axial compression tests. In most of these the stress-strain curve is traced only up to the maximum load. These relations have been applied to bending of reinforced concrete structures by assuming a linear strain distribution in the compression zone. However some recognized that ultimate strain can have a greater value in flexure than that corresponding to the maximum stress in compression test. So it was believed that the full stress-strain curve in axial compression ,i.e., with the falling branch, can fairly represent stress distribution in flexure. Consequently stiff testing machines that would be less affected by the sudden release of energy at maximum load, were used (81) & (82) and even steel springs around the test specimen were used to enhance the machine stiffness. These special techniques made it possible to trace the stress-strain relation beyond the maximum load.

Neverthless this method of obtaining stress blocks in flexure from compression tests has been vigorously challenged (83) & (84); a plain concrete specimen which has been sustained beyond the maximum load in axial compression is generally cracked and the strain response to load is highly sensitive to time. It has been asserted therefore that concrete strained beyond the maximum point of its stress-strain curve is useless for load carrying purposes in beams and columns.

An opposite view has been expressed by some who pointed out that special testing techniques are required to determine the true stress-strain relationship in axial compression but that the general characteristics of the axial compression stress-strain curve are applicable to flexure of reinforced concrete.

Other experimental work (85) showed an increase in the values of the initial modulus of elasticity and in ultimate strains in flexure tests over corresponding values in axial compression tests. The applicability of this method is approximate and can by no means repesent the actual stress distribution in flexure.

4.2.B Bending simulation test One of the earliest trials to find the stress distribution along the beam cross-section was that made at Imperial College, London 1941 (86); they constructed a special testing machine which had six pairs of horizontal jacks producing axial loads in the test beam at six vertical levels. By assuming a linear strain profile along the beam cross-section, jack loads were adjusted to give that predetermined strain profile. Hence stresses could be calculated from the loads at different stages and up till failure. The low accuracy and the complicated experimentation made this technique impractical.

4.2.C Photoelastic method In this method the stresses have been measured by embedding a piece of special glass in the compression zone of a reinforced beam (87). Photoelastic patterns obtained by passing polarized light through the glass plate at various beam loads gave information from which the stress distribution in the compression zone in flexure was

determined. Major drawbacks such as susceptibility to moisture, humidity , volumetric changes in concrete and others affected the measurements greatly in addition to the difficulties involved.

4.2.D Stress meters method In this method the concrete beam is cast with a stack of eight steel plates embedded at the test zone (88). These steel plates have the same beam width but reduced at the middle to the equivalent area of concrete on a modular ratio basis. By measuring strains in the plates, stresses in them could be calculated and were considered to be the same as the stresses in the concrete at the compression zone. However the results gave a linear stress-strain relationship. A major drawback was the effect of the steel stack on the compression zone which could not be well defined. Also the stress transfer from concrete to steel plates is a function of the bond strength which loses its effect near ultimate loads on crushing or cracking. To eliminate these effects some used pressure cells embedded in the beam instead of the steel plates and satisfactory results were obtained (89). However the complex and expensive instrumentation was probably the reason why the use of this approach has been limited.

4.2.E Tests of reinforced concrete members As said earlier the main parameters of the stress block, and not the whole shape, could be calculated from reinforced members. Strains can be directly measured by using strain gauges. The parameters of the stress block can be generally derived indirectly by computations from the equilibrium conditions.

The main assumption often made was that the strain profile in the cross-section is linear even near failure. This assmption is accepted by most of the investigators. The controversial value was that of the ultimate strain. Some considered it in a direct proportionality with concrete strength while others found it inversely proportional to the strength. Many others took it as a function of load rate only.

This discrepancy led to widely different values of the stress block parameters. Thus interest in the whole block shape was great and a pioneer work regarding the whole shape of the stress-strain curve in flexure was done by Prentis (90), Hamann (91) and Lee (92). They have derived full information about the stress distribution from reinforced beam test data by numerical differentiation. They made four main assumptions as follows:

(1) For the steel used the stress was equal to the strain times E_s up to the yield stress, after which stress is constant

(2) Concrete does not resist tension.

(3) Linear distribution of strain over the beam cross-section.

(4) Concrete compressive stress is a function of strain only.

With the notations of Fig.(4.2) the compressive stress as a function of the extreme fibre strain could be found as follows:

$$C_c = b \int_o^c F(\varepsilon_x)dx = \frac{bc}{\varepsilon_c} \int_o^{\varepsilon_c} F(\varepsilon_x)d\varepsilon_x = F_s \qquad \ldots\ldots(a)$$

where $$\frac{c}{d} = \frac{\varepsilon_c}{\varepsilon_c + \varepsilon_s} \qquad \ldots\ldots(b)$$

Then substituting Eq.(b) into Eq.(a), differentiating with

respect to ε_c and rearranging, two expressions for the stress component in flexure could be obtained as follows;

$$f_{c_f} = \frac{A_s}{bd} E_s \varepsilon_c + (\varepsilon_c + \frac{d\varepsilon_s}{d\varepsilon_c} + 2\varepsilon_s \frac{d\varepsilon_s}{d\varepsilon_c} + \varepsilon_c) \quad \text{for } 0 < \varepsilon_s < \varepsilon_{sy} \quad ..(c)$$

$$f_{c_f} = \frac{A_s}{bd} f_{s_y} (1 + \frac{d\varepsilon_s}{d\varepsilon_c}) \quad ..(d)$$

These equations are valid only for singly reinforced members which are completely cracked in the tension zone. Hence calculated values at low stresses before complete cracking are not correct. Also the equations can only be applied for under-reinforced members. In this method measurements of steel strain depend strongly on the locations of the cracks relative to the position of the strain gauges which might give misleading readings. If this is the case experimental errors will be amplified in the differentiation.

In a trial to avoid the influence of the relative crack position to the strain gauge Prentis (90) applied his differentiation to prestressed beams using unbonded cables and obtained better results. A major enhancement of this procedure was developed by Hognestad (85) in which tensile stresses were avoided in a plain concrete specimen. No need then existed for measurements of steel strains with the problematic effect of concrete crack location relative to the gauges. As shown in Fig.(4.3) a major load was applied by the testing machine (P1) and by further applying a minor eccentric load (P2), the neutral axis could be maintained at the outer face of the plain test region throughout the test. Thereby complications resulting from tensile stresses in concrete were completely eliminated. Steel strain measurements were not required. Using two reasonable assumptions stresses could be calculated; (a)

linear strain profile, (b) concrete steress is a function of concrete strain only. From equilibrium of forces and moments Eq.(a)can be rewritten as

$$C_c = b \int_o^c F(\varepsilon_x)\, dx = \frac{bc}{\varepsilon_c} \int_o^{\varepsilon_c} F(\varepsilon_x) d\varepsilon_x = P_1 + P_2 = F_o\, bc \qquad .....(e)$$

Equating the internal and the external applied moments, then

$$M = b \int_o^c x\, F(\varepsilon_x) dx = \frac{bc^2}{\varepsilon_c^2} \int_o^{\varepsilon c} F(\varepsilon_x)\varepsilon_x\, dx = P_1 a_1 + P_2 a_2 = M_o bc^2 \qquad .....(f)$$

in which $F_o = (P_1 + P_2)/2$ $\qquad$ $M_o = (P_1 a_1 + P_2 a_2)/bc$

By differentiating with respect to εc and rearranging then,

$$f_{c_f} = \varepsilon_c \frac{d\, F_o}{d\, \varepsilon_c} + F_o \qquad .....(g)$$

$$f_{c_f} = \varepsilon_c \frac{d\, M_o}{d\, \varepsilon_c} + 2M_o \qquad .....(h)$$

Eqs.(g) & (h) calculate the concrete stress f_{cf} as a function of the continuously measured concrete strain εc and the measured quantities Fo and Mo. Thus by calculating in small increments the differentials can be closely approximated by the finite difference $dFo/d\,\varepsilon c$ and $dMo/d\,\varepsilon c$. It is worth mentioning that the block parameters can be calculated at any load level from equilibrium requirements as follows;

Where $C_c = bc\, f_{c_y} K_1 K_3 = P_1 + P_2$ $\qquad$ then $K_1 K_3 = \dfrac{P_1 + P_2}{bc\, f_{c_y}}$

Where $M = P_1 a_1 + P_2 a_2 = C_c\, c(1-K_2)$ $\qquad$ then $K_2 = 1 - \dfrac{P_1 a_1 + P_2 a_2}{c(P_1 + P_2)}$

Where $K_3 = f_{c_f} / f_{c_y}$ $\qquad$ then $K_1 = K_1 K_3\, f_{c_y} / f_{c_f}$

It is clear that this method (85) is very powerful and all the stress block parameters as well as the whole stress strain curve in flexure at any stage of loading can be found. This

method is also a very simple one and does not require any special technique. Only a high degree of precision is required for arriving at a reliable interpretation. The interesting thing is that stress can be found either from Eq.(g) or Eq.(h) which provides a double-check process on the validity of the results. For these reasons this method of defining the stress distribution in flexure was adopted for the present work on PC.

4.3. Stress block shape and parameters for resin-concrete

4.3.A. Test specimen dimensions Different considerations were taken into account in dimensioning the specimen. Two main shapes and sizes were chosen. The first was that shown in Fig.(4.4). The cross-sectional area was 100.0x200.0 mm. The required axial load for this area to reach its ultimate capacity was too great. This load produced very high bearing stresses particularly after the bearing plates began to bend and the bearing area reduced sharply near failure. It was far from practical to design a supporting system that would support 1000.0 KN load needed for this size of specimen, without bending of the bearing plates. However the first two specimens were cast using this size. On testing failure of the intended test zone was never reached. Crushing of the specimen under the bearing plates took place first and longitudinal cracks propagated along the specimen length. Eventually failure occured near the end-bracket reinforcement.

The second size and shape was then designed to avoid these troubles. The cross-section of the test zone was chosen to be 100.0x120.0 mm which required the major load to be around

500.0 KN. The cross-sectional area was intended to represent the compression zone in actual full-scale PC structural members. For this reason smaller dimensions were not considered, to avoid any likely troubles in scaling up the results or in applying them to real structures. As shown in Fig.(4.5) the test zone was pre-defined using haunches between the brackets and the longitudinal prism. All specimens made with the shown shape and size failed in the intended test zone.

Sufficient tension, compression and shear reinforcement was provided for the end-brackets, as shown in Fig.(4.6), to obtain failure in the central plain test zone. All such reinforcement ended 100.0 mm from the middle of the specimen, allowing a plain test zone of 200.0 mm length. The end-brackets were designed to be as stiff as possible so that full fixity at the bracket-prism joint could be satisfied. To avoid excessive elastic and plastic deflections at the free edge of the bracket the least possible cantilever span that would provide enough room for the hydraulic jack and other loading instrumentation was considered.

4.3.B Measurements of loads, strains and deflections Where the interpretation of these test results involved numerical differentiation, it was very important to achieve the highest possible degree of accuracy. The net dimensions of each specimen were measured after being demoulded. The strain gauges used were 20.0 mm-length. The choice of these 20.0 mm - electric strain gauges was based on some other tests made with the first specimen size and shape; in those initial tests

100.0 mm -length strain gauges were used with the 20.0 mm ones. Both types gave more or less identical readings. Where the 100.0 mm -gauges are very expensive and did not give any increase in accuracy, the much cheaper 20.0 mm -gauges were used throughout the whole work to come.

As shown in Fig.(4.7) five pairs of strain gauges were used. Pairs 1 & 2 were attached to measure the strain at the extreme fibre and at the experimentally maintained zero strain fibre (neutral axis N.A.) respectively. Pairs 2 & 3, one on each side, were for recording strains at 2/3 and 1/3 the cross-section depth respectively. Pair 4 is used for adjusting the load ratio P2/P1 to maintain the N.A. at the outer face of the test zone throughout the test. Strains recorded were not more than 50.0 microstrain at that face in the worst case. Pair 5 was attached horizontally to the inner face which represents the extreme fibre to measure the lateral strain.

Lateral deflection at the middle of the test zone as well as the vertical displacement of the bracket free end were measured using electric transducers.

The major axial load was applied by a universal testing machine and the minor eccentric load was applied by a hydraulic jack. This load was measured by a calibrated load cell and its value could be recorded continuously as well as all other deflection and strain values by using an electronic Data Logger. The test procedure was to apply an increment of P1 load and hold it. Then watching the displayed strain at the N.A. face, minor load P2 was increased until the negative compressive strain is reduced to zero; at this moment a

reading for the different values is taken. Then another increment of P1 is applied and again strain, gauge 4, was brought down to zero by further increase of P2 and so on. At later stages P2 required to be reduced by controlling the pump pressure.

Bearing in mind that the greater number of load increments means greater accuracy, the increment of P1 was 2000.0 lbs (this is the available scale units of the testing machine). This resulted in around 60-80 readings for the whole test depending on the PC grade. The rate of load application was kept as constant as possible. Each increment of load took on average a time of one minute to apply. Then the load P1 was held constant until the N.A. starins were brought to zero which took another 30.0 seconds on average. Near failure the rate of load application was increased significantly to keep the load increasing while excessive strains were taking place.

4.3C Test results and their interpretation For each grade two specimens were cast using a single batch, cured at atmospheric temperature until testing at seven days of age. The readings of loads, strains and deflections were recorded for each specimen. Then the average values of the two specimens were considered in the analysis of each PC grade. The stress distribution in the test region was found using the previously mentioned two equations [Eqs.(g and h)];

$$f_{cfi} = \varepsilon_{ci} \frac{\Delta F_{oi}}{\Delta \varepsilon_{ci}} + F_{oi} \quad \text{and} \quad F_{cfi} = \varepsilon_{ci} \frac{\Delta M_{oi}}{\Delta \varepsilon_{ci}} + 2M_{oi}$$

in which $F_{oi} = \frac{P_{1i} + P_{2i}}{2}$, $\Delta F_{oi} = F_{oi} - F_{o(i-1)}$

$$M_{oi} = \frac{P_{1i}a_{1i} + P_{2i}a_{2i}}{bc^2}, \quad \Delta M_{oi} = M_{oi} - M_{o(i-1)}$$

$$\Delta\varepsilon_{ci} = \varepsilon_{ci} - \varepsilon_{c(i-1)}$$

a_{1i} = eccentricity of major load from N.A.+lateral deflection.

a_{2i} = eccentricity of minor load from N.A.+lateral deflection.

At each load increment the stress block parameters are calculated as follows;

$$(K_1K_3)_i = \frac{(P_{1i} + P_{2i})}{bc\ f_{cy}}$$

$$(K_2)_i = 1.0 - \frac{(P_{1i}a_{1i} + P_{2i}a_{2i})}{P_{1i}+P_{2i})c}$$

$$(K_3)_i = \frac{f_{cfi}}{f_{cy}}$$

$$(K_1)_i = (K_1K_3)_i \quad f_{c_y}/f_{c_{fi}}$$

Hence at each load level, corresponding to certain extreme fibre strain ε_c, the stress strain curve of the compression zone (all the test zone) in flexure was found with its parameters as shown in Fig.(4.8).

The value K1 is the average uniform stress distribution parameter, it should be equal to 0.5 for a triangular stress distribution; while for 2nd. degree parbola-stress distribution it is 2/3. Therefore the value of K1 was expected to increase with increasing load level and approaching failure where the stress distribution loses its linearity.

The value K2 is the parameter that defines the position of the resultant internal compressive force. If the depth of the compression zone is 'c', then the internal force is at K2.c distance from the extreme fibre. So for very low levels of load when the stress distribution is linear this value of K2 is almost 1/3. As the stress strain curve develops nonlinearity the value of K2 will increase.

Parameter K3 represents the ratio of the calculated flexural compressive stress f_{cfi} at any stage to the axial cylinder compressive strength f_{cy}. This ratio is very small at low load levels and increases until it reaches a peak value in the vicinity of 1.0.

On testing the different five grades the ratio of minor to major load usually decreased. The maximum value amounted to 0.07 while the minimum value amounted to 0.03. Fig.(4.9) shows this ratio as recorded with the different tests of the five PC grades. The minor load was increasing at a decreasing rate until the late stages of the test when its absolute value decreased. This may be due to the excessive lateral deflection near failure at the test zone which caused the lever arm of P2 and P1 to increase rapidly. Thus the value of the external applied moment increased significantly and consequently the resulting tensile strains were very high and required to be restricted by reducing the value of P2.

However the load ratio at any stage was found to be higher for higher compressive strength-grades. The maximum value for the extreme fibre strain recorded for each grade in these tests were completely different from that obtained in axial compression tests of cylinders made of the same grade. This phenomenon will be dealt with later in this chapter. The derived stress strain curves for different grades in flexure are shown in Figs.(4.10 - 14).

The lateral strain is plotted against the calculated stress f_{cf}, as the average value of the readings of pair 5-gauges as shown in Fig.(4.7). This value of lateral strain was used to

calculate the apparent Poisson's ratio as shown in Fig.(4.15) for the different grades. Where the longitudinal and the lateral strains [ε_c and ε_{cl}] are measured at two different positions on the extreme fibre face and not at the same point, Poisson's ratio plotted is just an approximate one. However it was useful in calculating the volumetric strain ε_{cv} approximately as follows;

$$\varepsilon_{cvi} = \varepsilon_{ci} - 2\varepsilon_{cli}$$

The stress values derived were calculated using the two equations given previously. The values derived by using either of the two equations were almost identical which indicated a high degree of reliablity of the experimental measurements. Poisson's ratio had a starting value in the vicinity of 0.27 and as shown in Fig.(4.15) it increased at a decreasing rate until it reached a stabilized value of around 0.4. These values may seem very excessive if compared to conventional concrete. However this is mainly due to the nature of the PC itself and its rheological properties which will be discussed in another chapter.

The parameter K2 is plotted against the extreme fibre strain in Fig.(4.16). The initial K2-values for various grades were within the range of 0.33 to 0.34. This asserts the linear stress distribution at the early stages of strain levels. Parameter K2 increases at a decreasing rate and all grades seem to have a maximum stablized value within the range of 0.42 to 0.44. It is evident that the greater the compressive strength ,the greater is the value of K2, particularly at low strain levels. However by extrapolating the five curves shown

in Fig.(4.16) it was found that the maximum assymptotic value of K2 is inversely proportional to the compressive strength and directly proportional to the secant modulus of elasticity for each grade.

The values of K3 as shown in Fig.(4.17) had a certain peak value Ko3 for each grade. This maximum value is greater for greater PC compressive modulus of elasticity E_c. It is obtained at a value of the extreme fibre strain ranging from 0.0053 to 0.0057. The less stiff grade had a higher value of this strain. Another conclusion is that values of K3 are generally bigger for low f_{cy}-grades than those for higher f_{cy} grades. Maximum values of parameter K3, denoted as Ko3, could be expressed as a function of E_c in KN/mm2 as follows;

$$Ko3 = 0.27 + 0.03775\ E_c \qquad ...(4.1)$$

The corresponding extreme fibre strain ε_{oc} could be expressed as

$$\varepsilon_{oc} = 0.00695(1-E_c/86.55) \qquad ...(4.2)$$

The ultimate value of the parameter K2, denoted as K2u, as found experimentally could also be expressed as a function of E_c as follows:

$$K2u = 0.3 + 0.006\ E_c. \qquad ...(4.3)$$

These three equations are valid for E_c-values within the range tested, i.e., from 15.0 to 25.0 KN/mm2. The importance of having such equations will be shown later when a general expression of the stress strain curve in flexure is to be derived.

The experimental values of parameter K1 were found to be a function only of the extreme fibre strain, irrespective of the PC grade itself as shown in Fig.(4.18). This function could be expressed as

$$K1 = 0.9 - 0.38 \left[1.0 - (\varepsilon_c/0.009)^2 \right] \quad \ldots(4.4)$$

The derived stress-strain curves in flexure differed remarkably from their respective ones in the axial compression tests. As shown in the previous figures (4.10-14), the flexural modulus of elasticity E_f is much higher than E_c. The maximum compressive stress in flexure occurred at a strain lower than that in compression where maximum stress occurred at maximum strain.

The mode of failure differed widely in both methods. For example in axial compression tests the whole specimen cross-section will usually crack considerably if strained beyond the maximum load. These cracks could take the form of either tension diagonal cracks, longitudinal axial-splitting cracks, or combinations of both. The chance for strain or stress redistribution is very limited where the whole cross-section is stressed uniformly.

The mode of failure observed with the eccentrically loaded prisms was quite different. Primarily it is a failure caused by excessive compressive stresses producing principal tensile strains greater than the material can stand. The specimen had one face at virtually zero strain (the outer face) while the inner face was subjected to maximum compressive strains.

The concept of "critical stress" can be of some use in describing the failure mode. As shown in Figs.(4.10-14) the critical stress is defined as the stress at which volumetric strain is equal to zero, i.e., the stress after which the specimen begins to expand volumetrically. The ratio of the extreme fibre strain at the critical stress to that at failure ranged from 0.45 to 0.61, while the ratio of the critical stress to the maximum stress ranged from 0.77 to 0.91 respectively. The strain profile was found, as assumed, to be linearly distributed over the specimen cross-section. So for grade E for example, the critical stress ratio was 82% at a strain ratio of 50%. As shown in Fig.(4.19) it can be said that 50% of the cross-section is subjected to stress up to 18% more than the critical stress. Hence the crushing of the cross-section at failure is expected to extend to 50% of its depth after which the test zone acts as a plastic hinge with excessive rotations around it. Finally failure occurs by tensile cracks propagating from the zero strain-face to the crushing maximum strain area. For grade C the critical stress ratio was found to be 77% while the strain ratio was 46%. That is to say that 54% of the cross-section is subjected to stress higher than the critical stress by 23%. This high margin of stresses over the critical stress produces a rapid crushing and a brittle failure. Experimental observations showed that most of the specimens tested failed in this mode, i.e., lateral tension cracking extending from the outer face until it reaches the crushing zone. This zone had a depth ranging from 0.5 to 0.65 of the whole depth of the test zone.

4.4. General flexural stress-strain curve for different grades

All the previous findings of the stress block shape and parameters of various PC grades are based on certain assumptions. Some of these were proved experimentally to be valid while others were found not to be. The linear strain profile was found to be a valid assumption. However the assumption that stress is a function of strain alone can by no means be a realistic one. The stress in PC is extremely time-dependent. As will be shown later, creep and strength reduction under sustained load are quite significant and should be considered if a general approach for flexural design is to be obtained. Consequently the effect of time in terms of rate of load application and stress history must be paid due attention. Hence these findings so far can be termed as "short-term" flexural behaviour.

Another fact is that simulating the compression zone in real reinforced beams by a plain eccentrically loaded prism might allow for some misleading results. For example, in a reinforced beam, steel stresses between cracks are reduced or even converted into compressive ones near supports and can contribute to the ultimate capacity of the section, i.e., tension stiffening. Thus calculating the ultimate capacity in flexure based only on the compression zone stresses would usually give a slightly lower value than that found if the tension stiffening was considered. In this case neglecting the reinforcement contribution is conservative.

The type of test itself preassumes that the ultimate capacity is controlled by the concrete and not by the reinforcement, a case which is often encountered with over-reinforced sections.

Applying these test findings to under reinforced sections may thereby be misleading. However as PC is a relatively expensive construction material it may be out of the question to use it in under-reinforced sections. Over-reinforced sections are not desirable either due to the unfavourable mode of failure. So PC structural members are probably best designed for crushing of concrete to occur simultaneously with yielding of the reinforcement.

On the other hand if high tensile steel without a well defined yield point is used, the ultimate capacity will be controlled eventually by the concrete reaching its ultimate strain. Bearing this in mind the findings still apply to balanced ,or over-reinforced sections made of mild steel, or to sections reinforced with cold-drawn steel at any reinforcement ratio. In addition they can be applied to under-reinforced sections if the PC strain level is known in these sections.

The test zone also was not laterally confined, while in real structures stirrups are often used. The effect of lateral confinement is such that it would increase the ultimate capacity of the section particularly for high loads with small eccentricities. So once again, neglecting this effect means additional safety over the present findings and does not preclude their validity.

The only apparent reservation may be faced in the mode of failure itself. For instance in a real reinforced beam the strain can not strictly be plane for there is a discontinuity at every crack in the tension zone; a case which is not simulated in the present test. Regarding the statistical

effects, the specimen would fail at the weakest section in compression selected from only those sections which have developed tension cracks. Despite this reservation it was found that the present findings are applicable to reinforced structures and the effect of tension crack propagation on the compression zone depth is felt only at the very late stages of the test and even beyond the ultimate capacity. Hence this reservation is practically outside useful structural limits.

From the previous paragraphs the validity of the present findings are evidently acceptable. The assumptions appear to allow the derivation of reasonably accurate and reliable stress strain curves in flexure. The only remaining, yet controversial, point is that regarding the ultimate capacity of the section and how it is defined. The controlling parameter is the ultimate concrete strain if the section is balanced, under or over-reinforced. This value of ultimate strain for cement concrete was expressed in many different ways. Some related it directly, or even indirectly, to concrete strength while others considered it as completely independent of concrete strength (93). In addition other researchers found it to be a function of the loading rate and the associated rate of strain. Higher rates of strain would produce ultimate conditions at lower values of strain .

At the present stage and regarding the "short-term" stress-block in flexure the ultimate strain was defined purely on a mathematical basis. The different derived stress-strain curves could be expressed as a 'sine-function' with the notations given in Fig.(4.20) as follows;

$$f_{cf} = Ko3 \; f_{cy} \sin \left(\frac{\pi \varepsilon_c}{2 \varepsilon_{oc}} \right) \qquad \ldots(4.5)$$

In which Ko3 can be calculated from Eq.(a). The ultimate strain ε_{cu} is that strain that would give maximum internal moment Mu; Where $M = b \int_o^c x \, f_{cf} \, dx$

Substituting for $x = c.\varepsilon x / \varepsilon c$ and rearranging, the ultimate moment can be obtained using the simple differentiation $dM/d\varepsilon c = 0.0$.

This expression of the the ultimate moment can thus be used to calculate the ultimate strain value as a ratio of ε_{oc}. This ratio $\varepsilon_{oc} / \varepsilon_{cu}$ was found to be 0.75. So for each grade ε_{oc} can be calculated from Eq.(4.2) and then ε_{cu} can be found. Knowing the value of Ko3, ε_{oc} and ε_{cu} the full stress-strain curve in flexure at ultimate strength can be traced for each grade with a given f_{cy} by using Eq.(4.5). These theoretical curves for the different grades are plotted against the experimentally derived ones. They appear to be in good agreement and should be useful in calculating the ultimate capacity of any section under any case of loading. It is important to stress the fact that the mathematically derived value of the ultimate strain preassumes that the ultimate carrying capacity of the cross-section is controlled by the concrete and not by the reinforcement, a case which is often encountered when cold-drawn steel is used for reinforcement.

Other effects were overlooked for simplification, such as the effect of the cross-section shape, and the position of the neutral axis (N.A.). With conventional concrete, ultimate strain was found to increase by reducing the compression zone area; either by decreasing the N.A. depth or by reducing the

concentration of the area above the N.A. as shown in Fig.(4.21). For a constant compression zone area and depth it was also found that irrespective of the steel type or the reinforcement ratio, the ultimate strain is a function of time or rate of strain by which the load is applied as shown in Fig.(4.22).

In one of the early researches (92) the ultimate strain value of cement concrete members varied from 0.0022 to 0.0048 for the same concrete strength,rate of strain and load duration ,by changing only the cross-section shape and N.A. position. This suggested that with other concrete qualities , other rates of deformation and load duration, even more pronounced differences might be expected. This qualitatively explains the wide divergence in the ultimate strain values arrived at by different researchers on cement concrete as shown in Fig.(4.23). It could even be argued that all these reported values, though apparently contradictory, can actually occur. They were probably recorded under widely different conditions and the fundamental error consisted in generalization. Concrete ultimate strain has not and can not have one permanently fixed value.

For PC the ultimate strain value can be even more controversial. All the previously mentioned effects can result in the same, if not more, divergence in ε_{cu} values. Bearing in mind the lack of accumulated data of PC structural performance and its high time-dependency, it is necessary to accept an approximate average value even if a certain amount of error would exist in it. These errors should be taken into account in setting the safety factors in the actual design and

practice of PC. The extent to which the chosen values of ε_{oc} and ε_{cu} give acceptable results or not will be demonstrated in more detail later in the analysis of results for reinforced members.

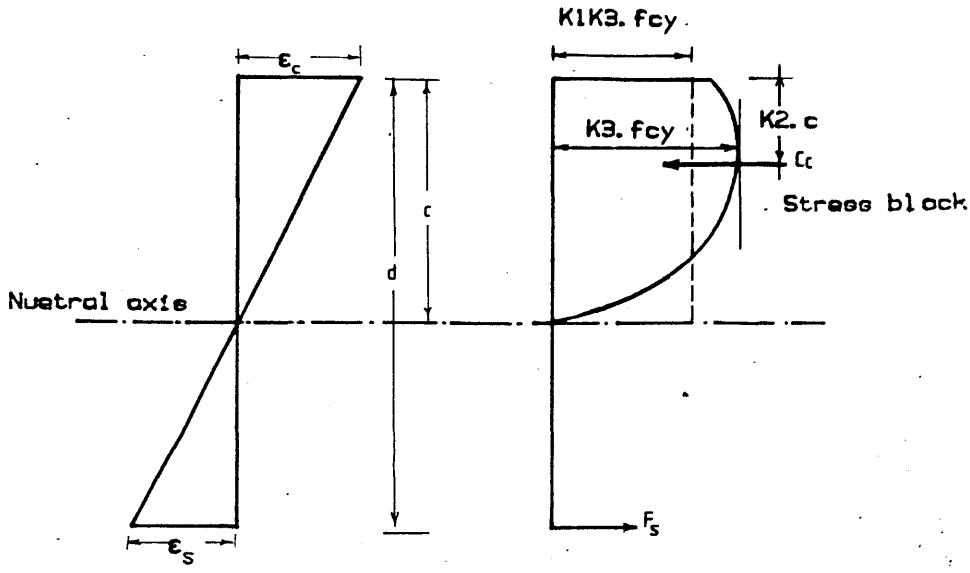

Fig. 4.1 Definition of the three main parameters of the stress block in flexure

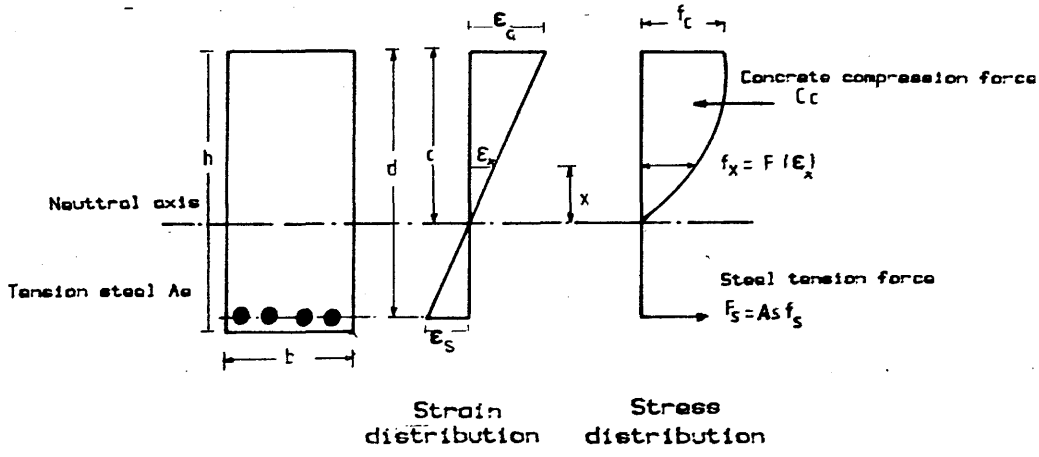

Fig. 4.2 Notations for a singly reinforced rectangular section in flexure.

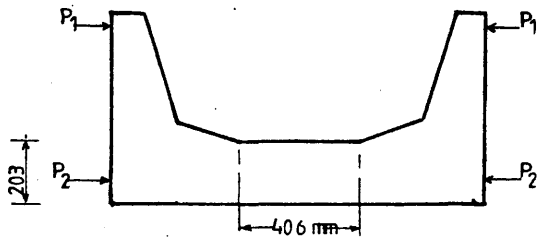

Fig. 4.3 Test specimen of Hognestad.

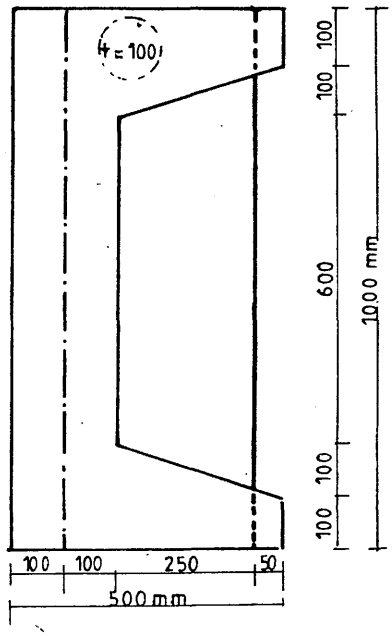

Fig. 4.4 The first specimen chosen for the derivation of the stress block

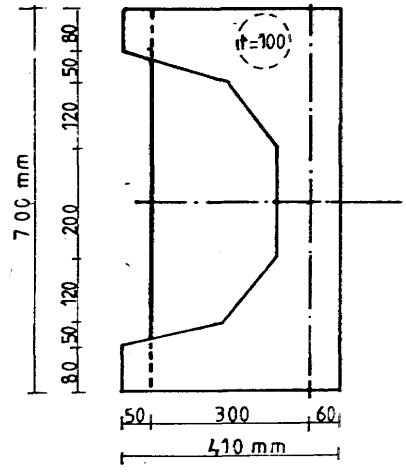

Fig. 4.5 The second specimen chosen for the derivation of the stress block

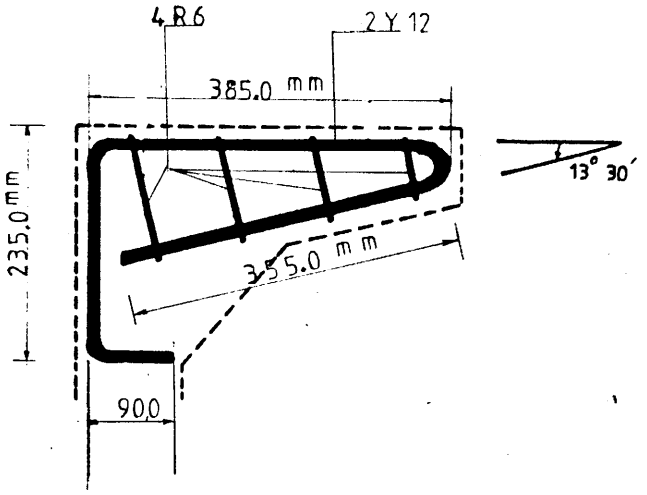

Fig. 4.6 Details of reinforcement of the end bracket.

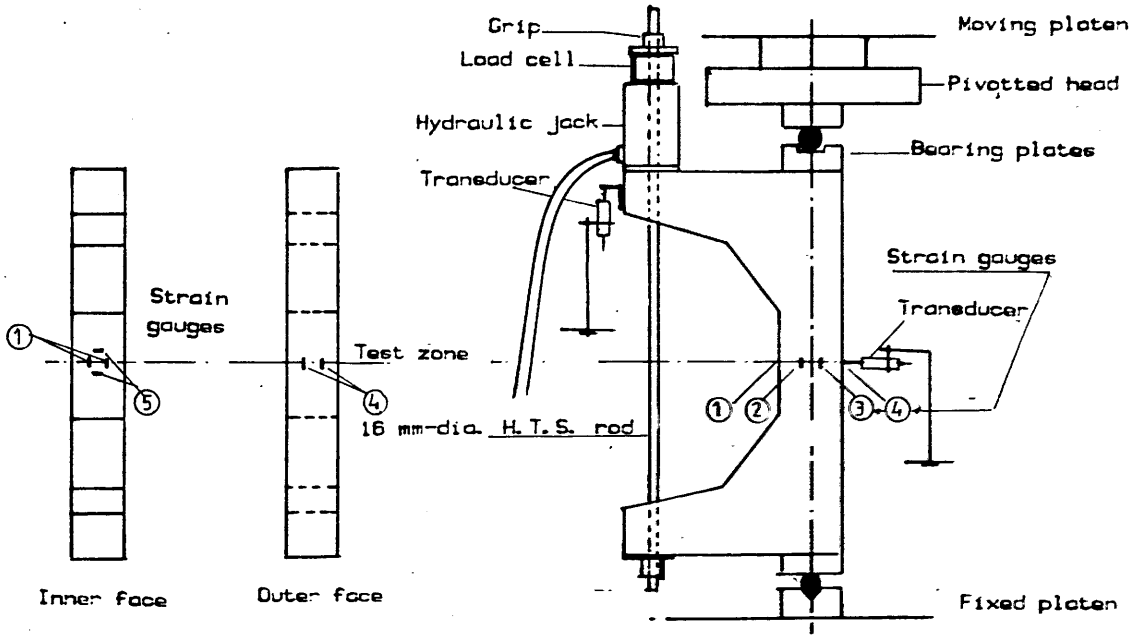

Fig. 4.7 Testing instrumentation and arrangements.

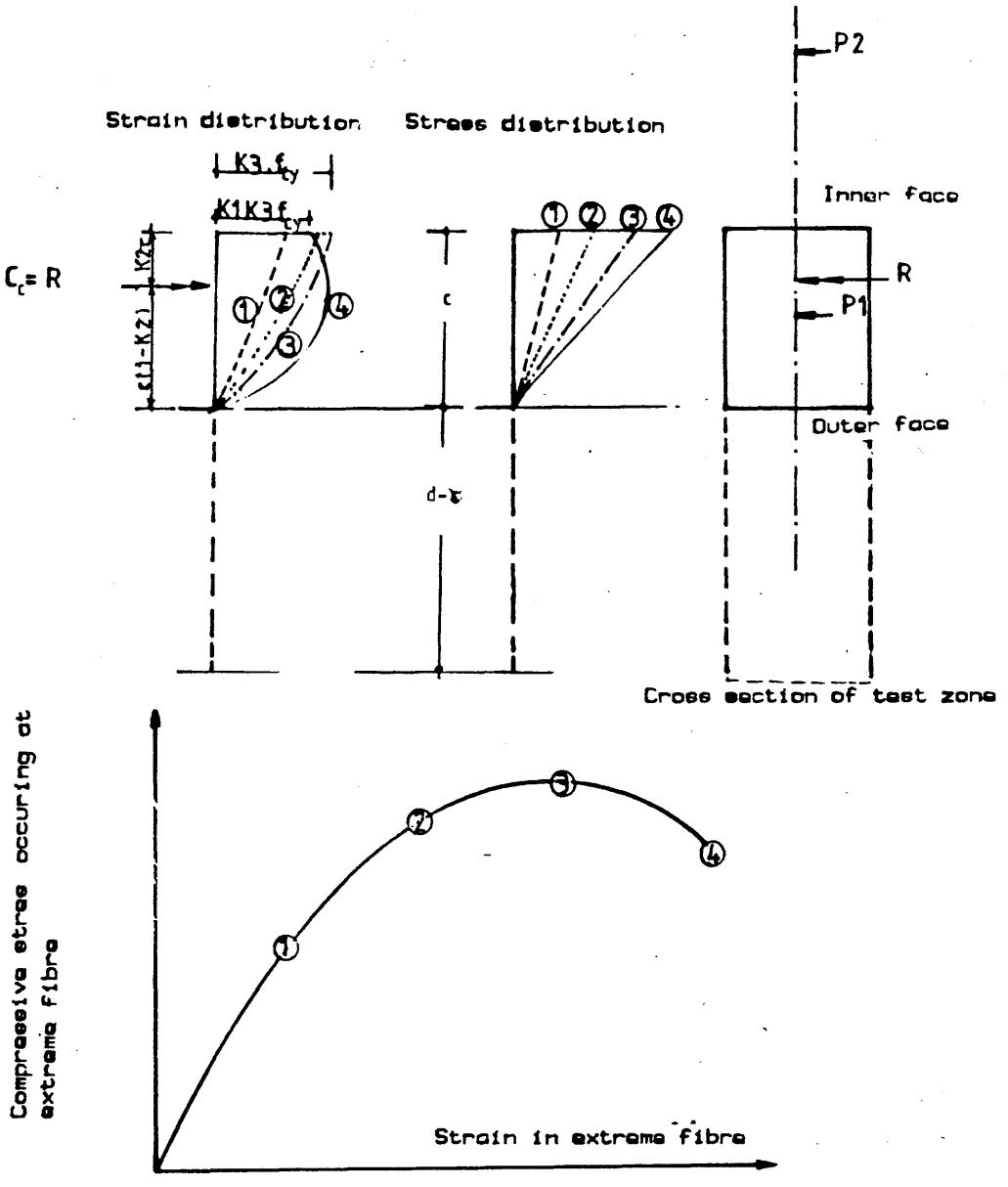

Fig. 4.8 Development of stress-strain relationship in the test zone.

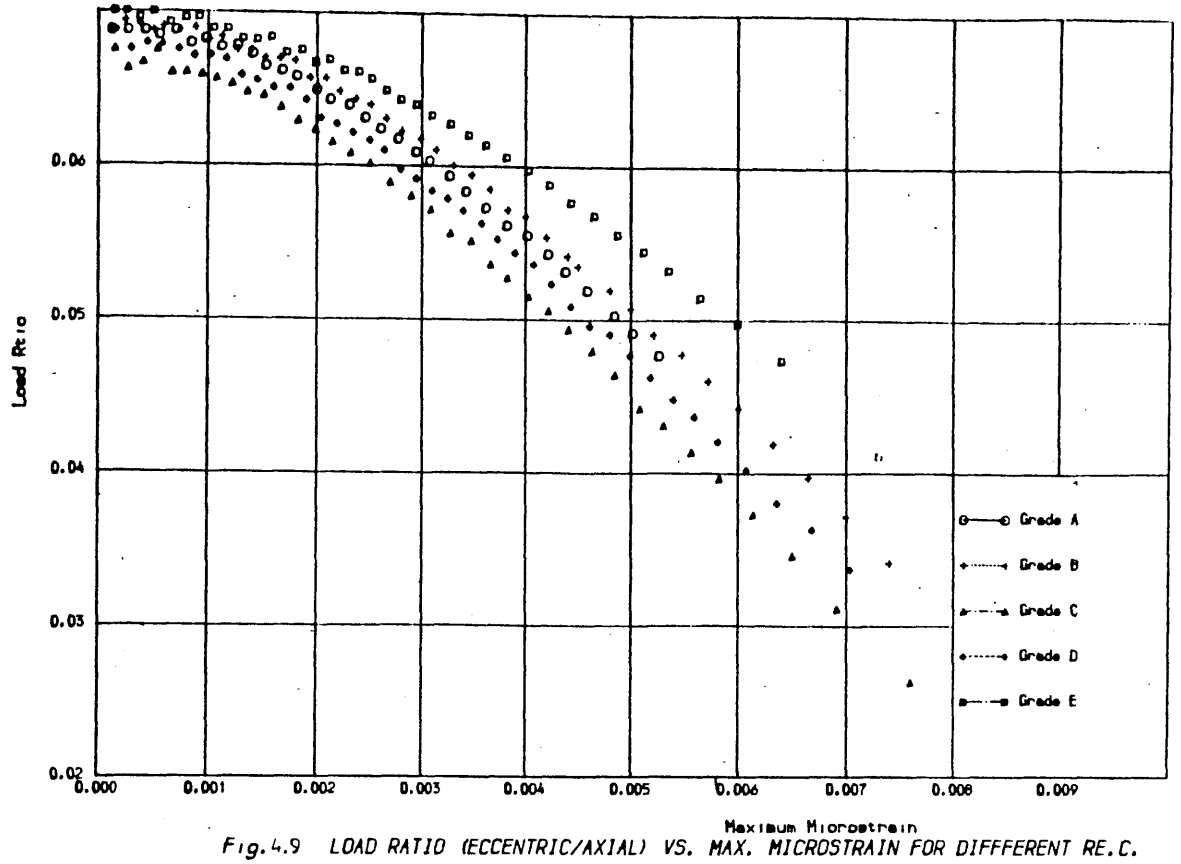

Fig. 4.9 LOAD RATIO (ECCENTRIC/AXIAL) VS. MAX. MICROSTRAIN FOR DIFFFERENT RE.C.

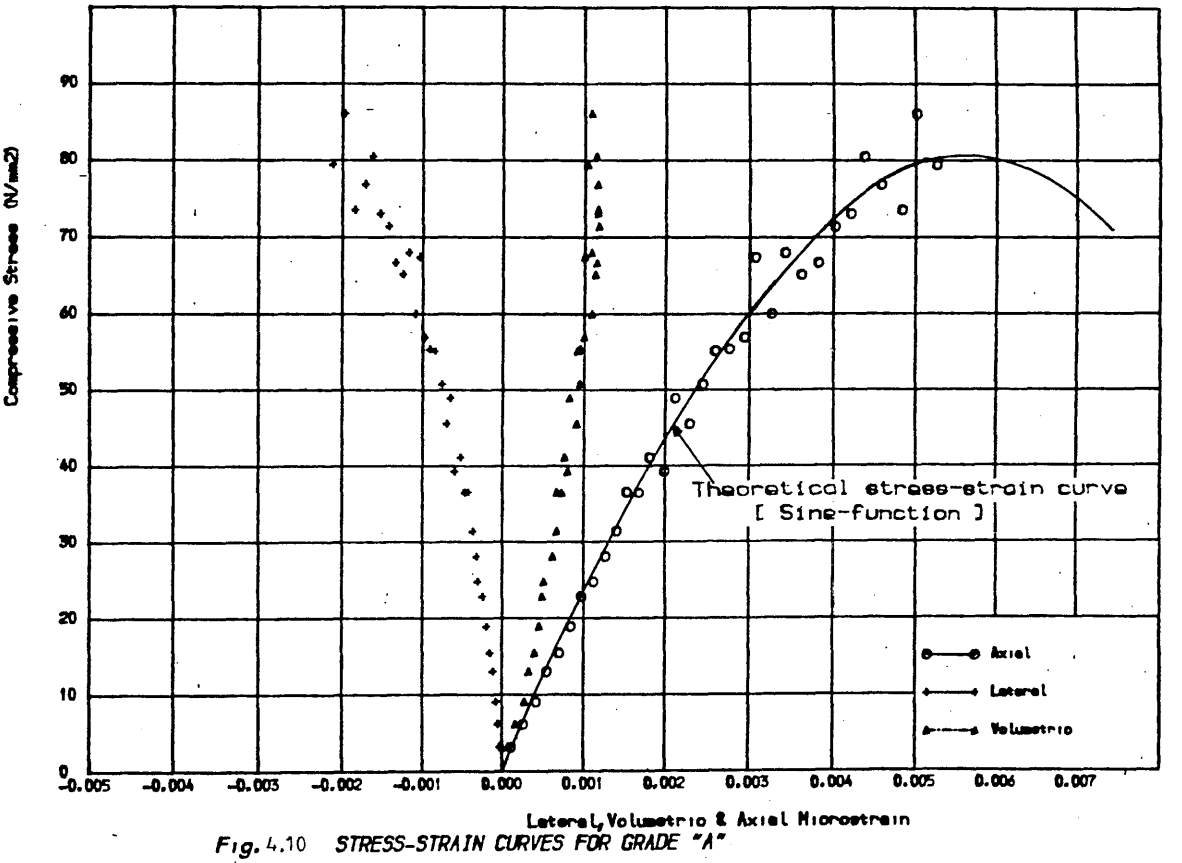

Fig. 4.10 STRESS-STRAIN CURVES FOR GRADE "A"

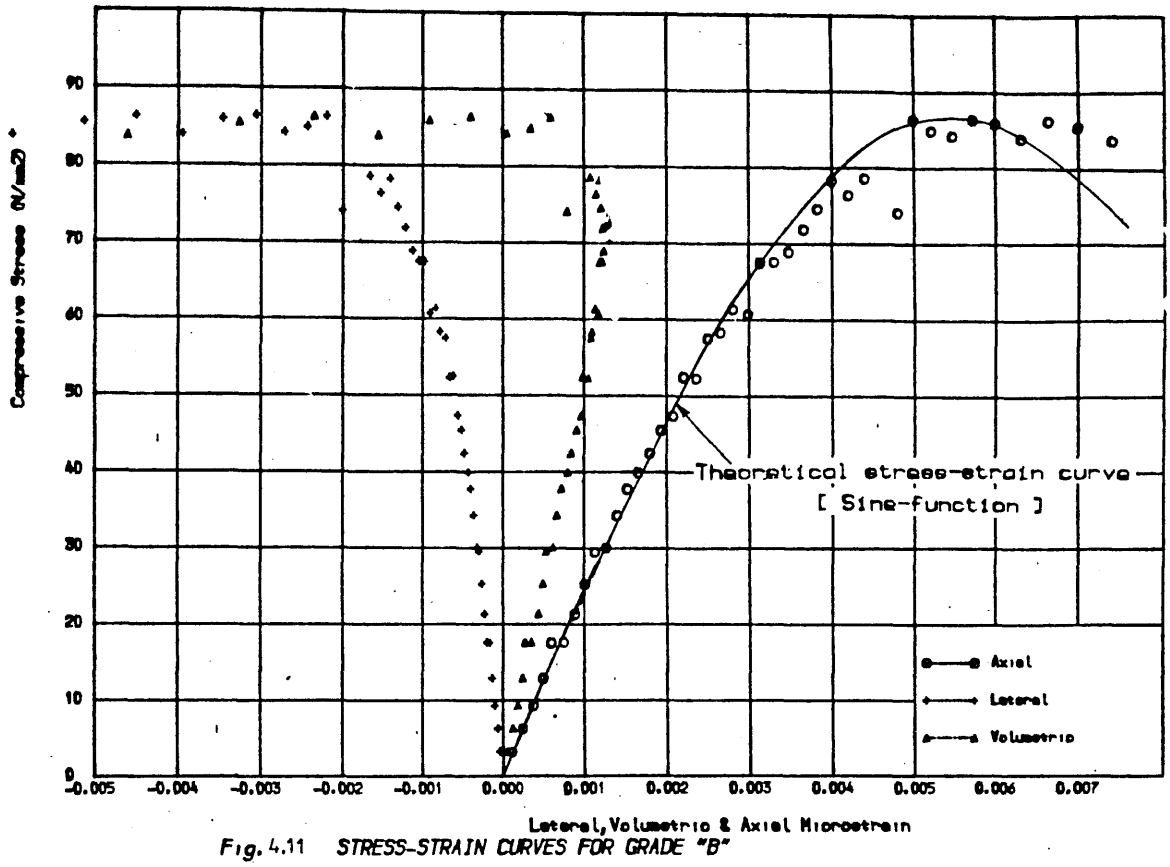

Fig. 4.11 STRESS-STRAIN CURVES FOR GRADE "B"

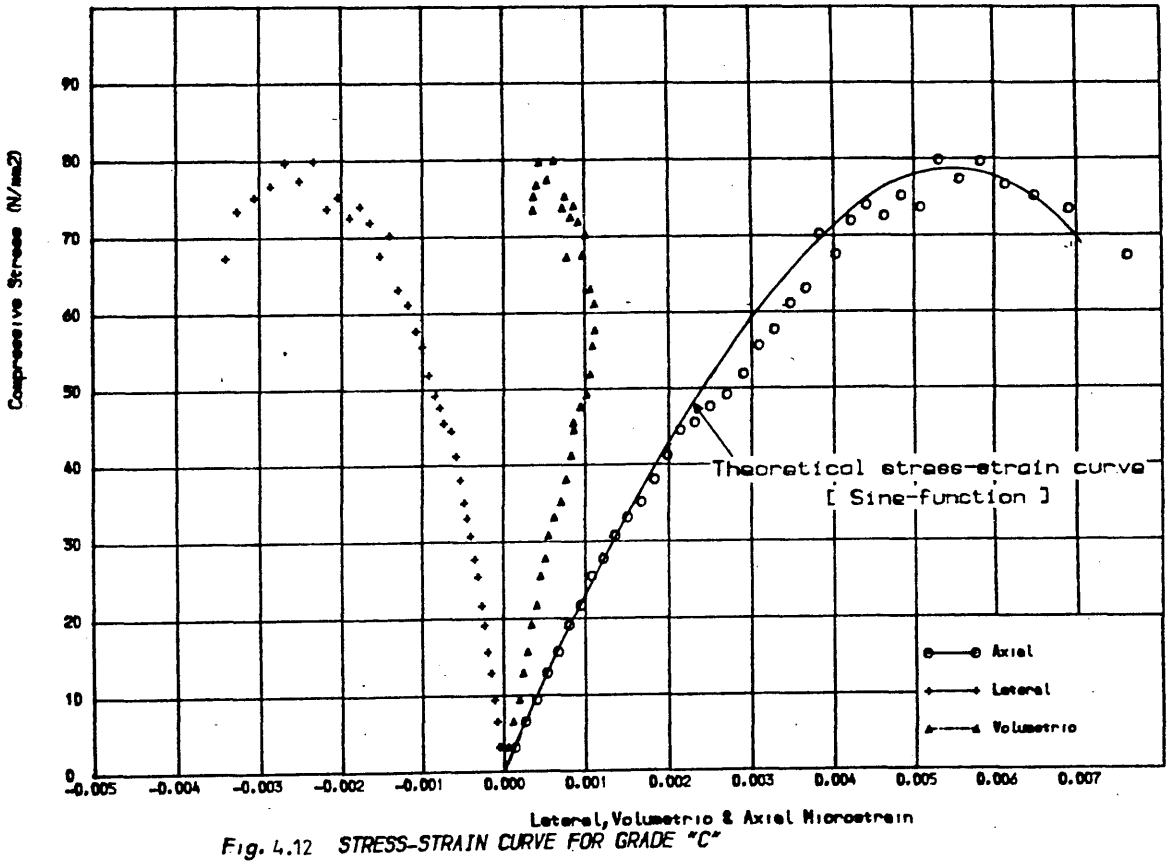

Fig. 4.12 STRESS-STRAIN CURVE FOR GRADE "C"

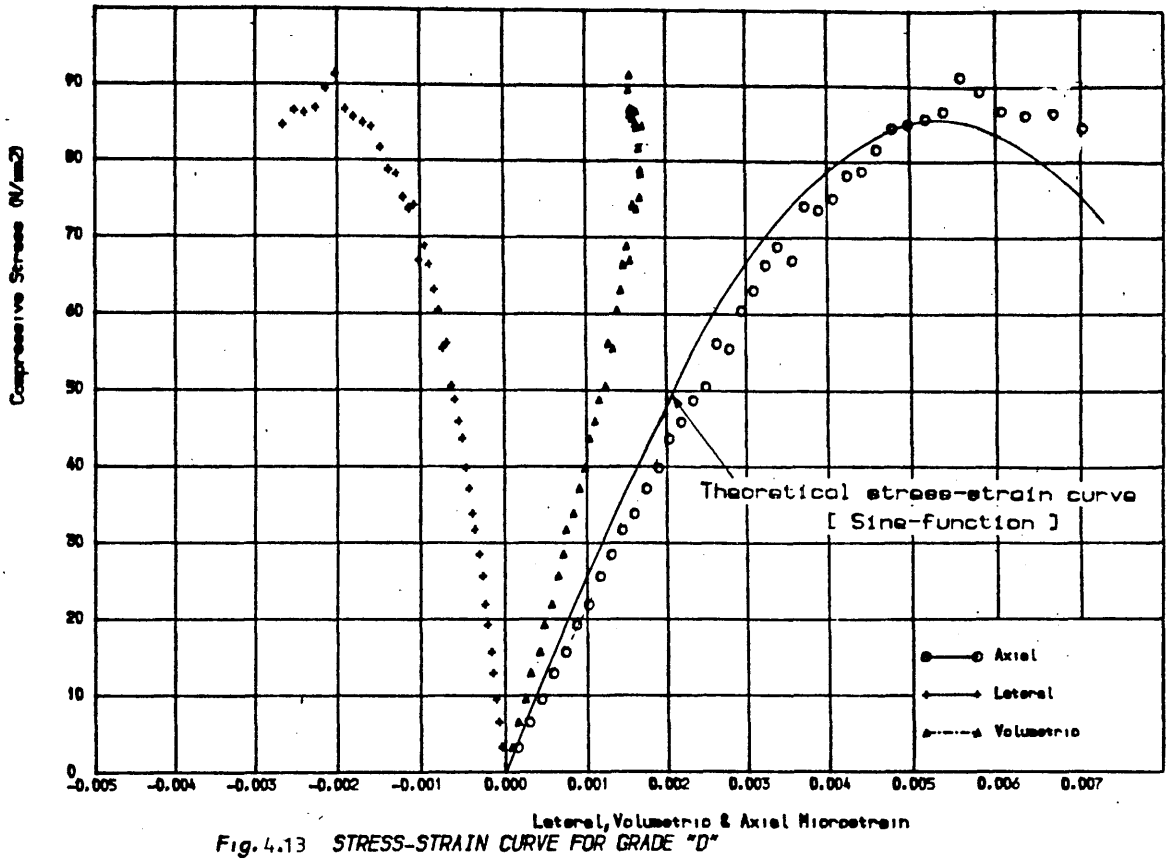

Fig. 4.13 STRESS-STRAIN CURVE FOR GRADE "D"

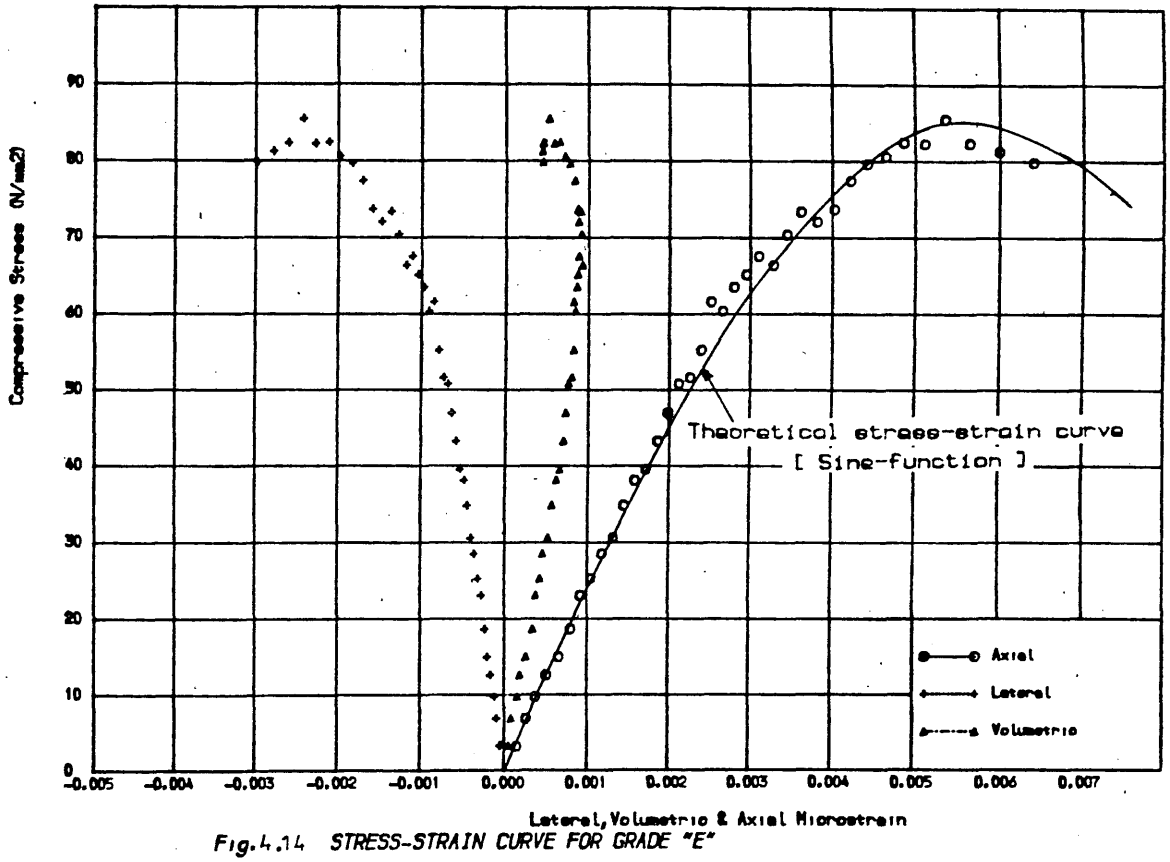

Fig. 4.14 STRESS-STRAIN CURVE FOR GRADE "E"

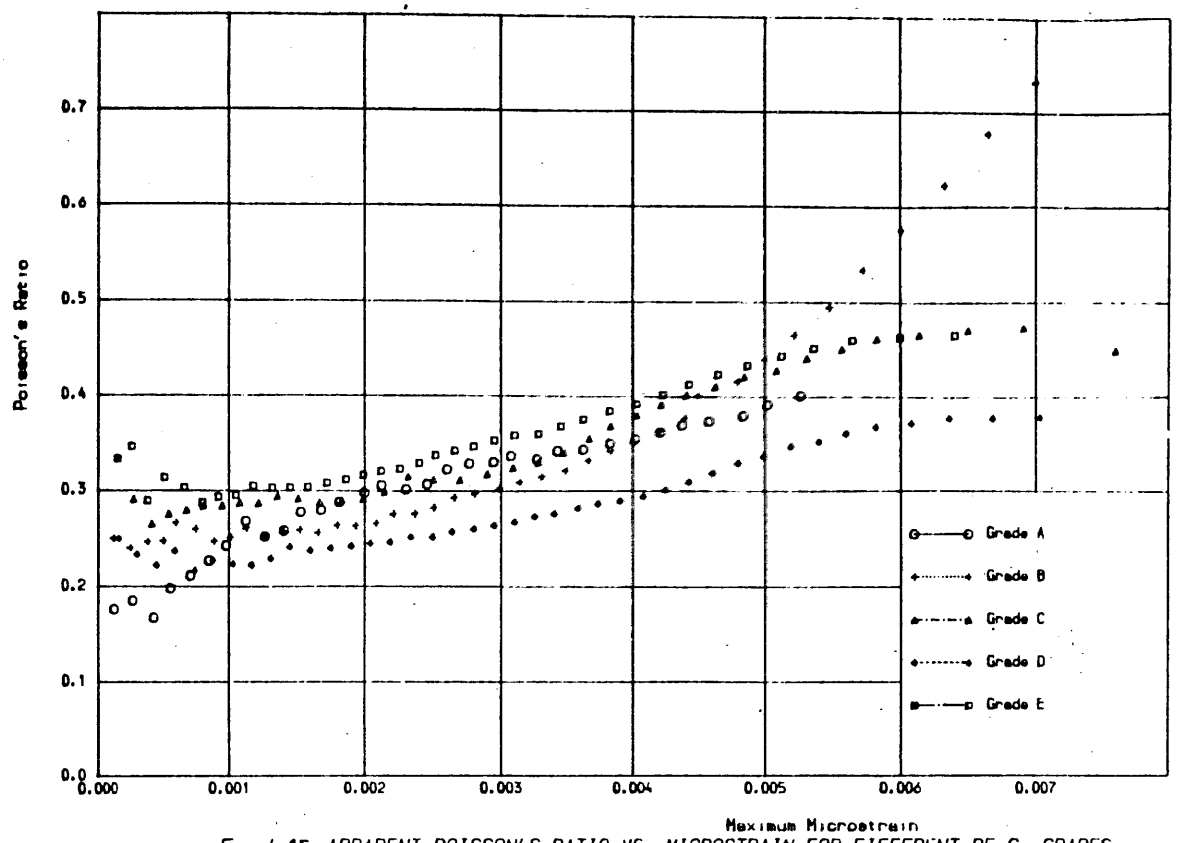

Fig. 4.15 APPARENT POISSON'S RATIO VS. MICROSTRAIN FOR FIFFERENT RE.C. GRADES.

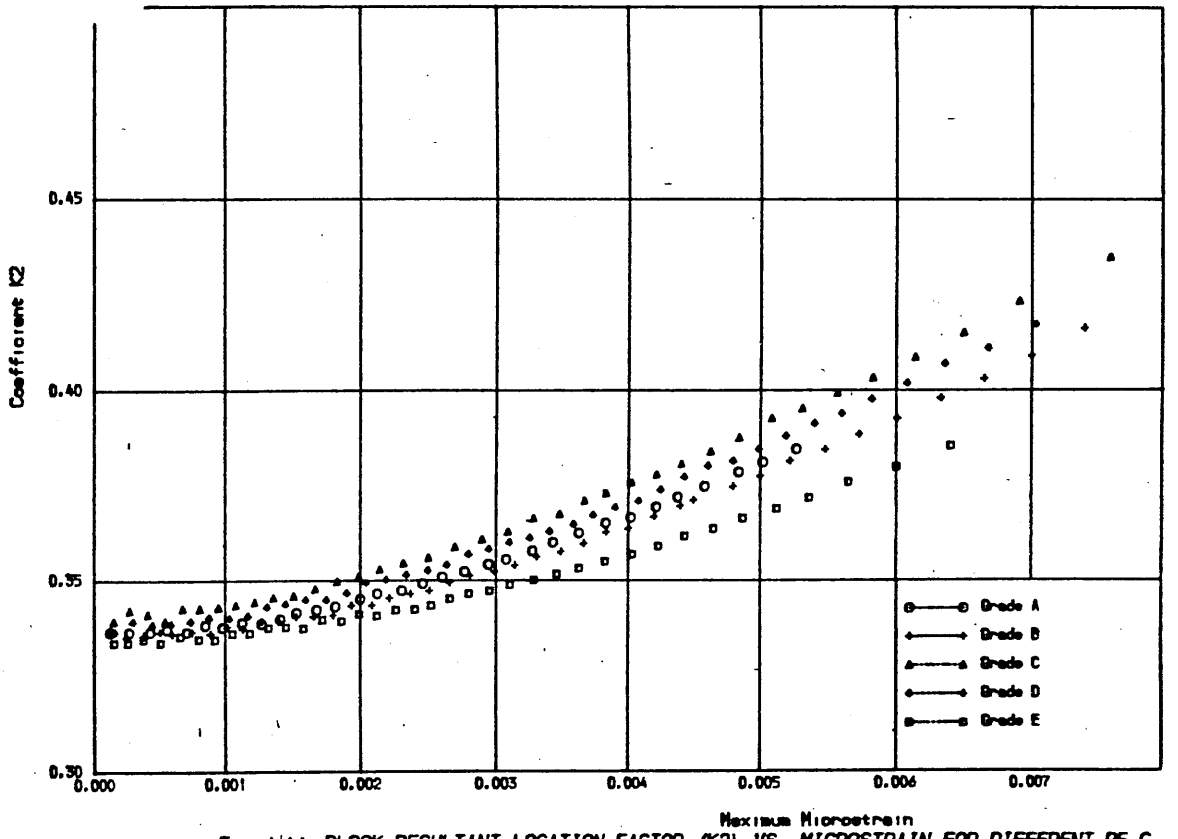

Fig. 4.16 BLOCK-RESULTANT LOCATION FACTOR (K2) VS. MICROSTRAIN FOR DIFFERENT RE.C

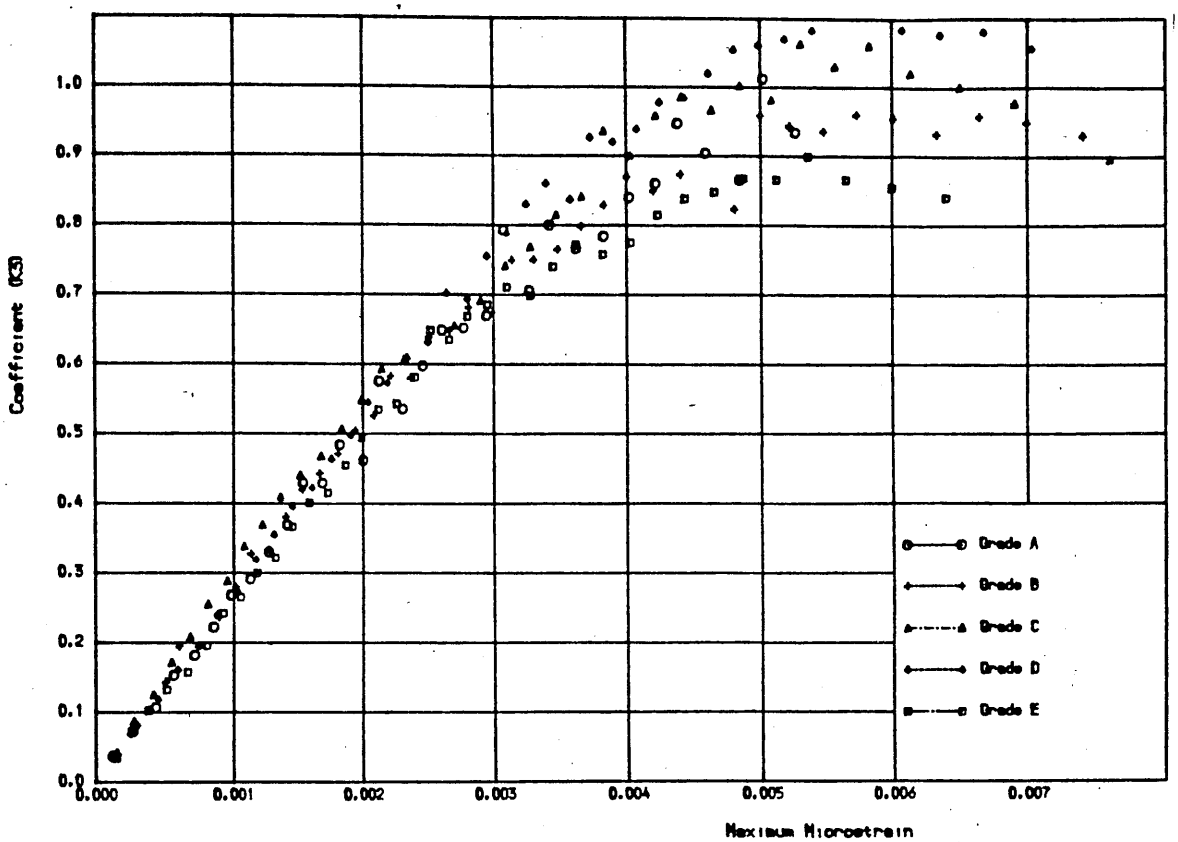

Fig. 4.17 MAXIMUM STRESS FACTOR (K3) VS. MICROSTRAIN FOR DIFFERENT RE.C. GRADES.

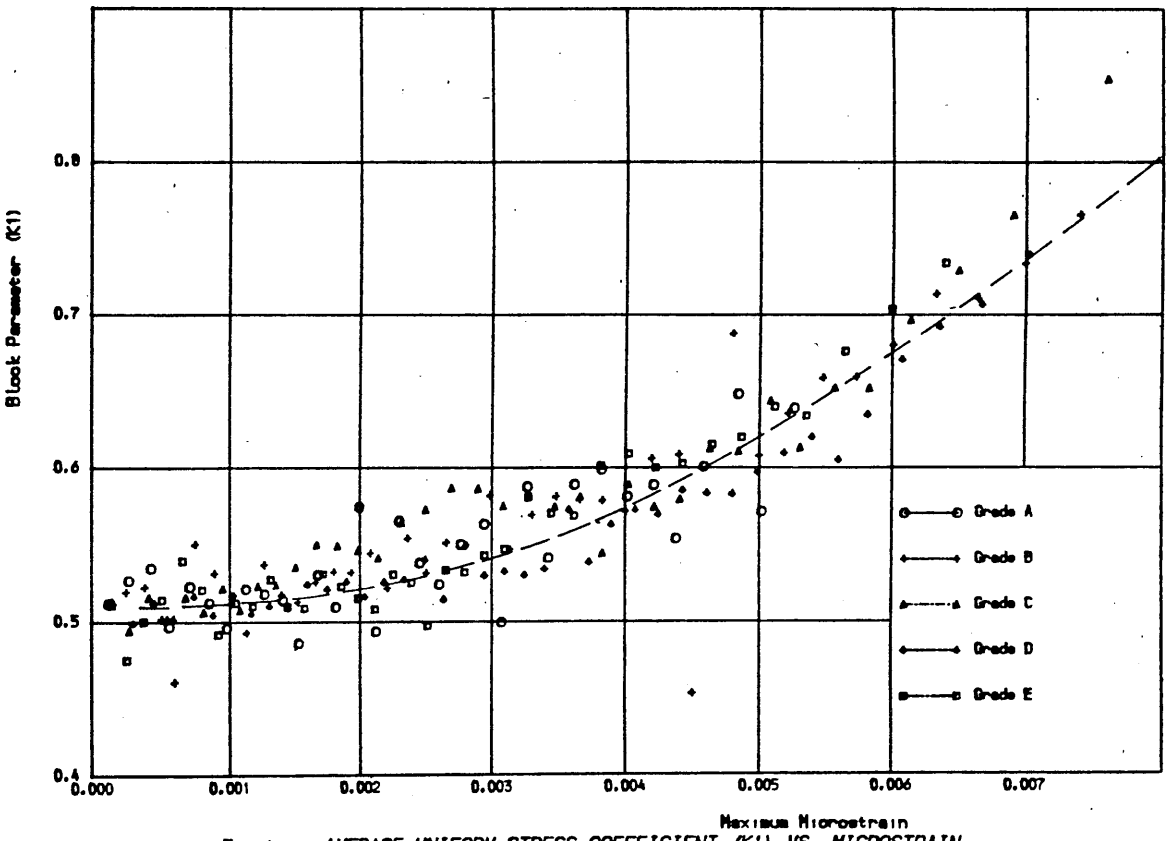

Fig. 4.18 AVERAGE UNIFORM STRESS COEFFICIENT (K1) VS. MICROSTRAIN.

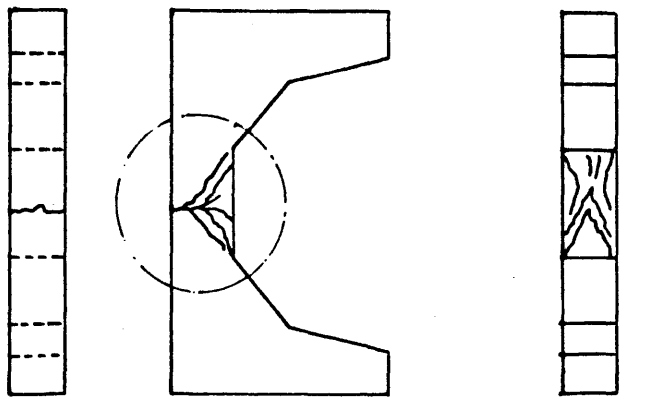

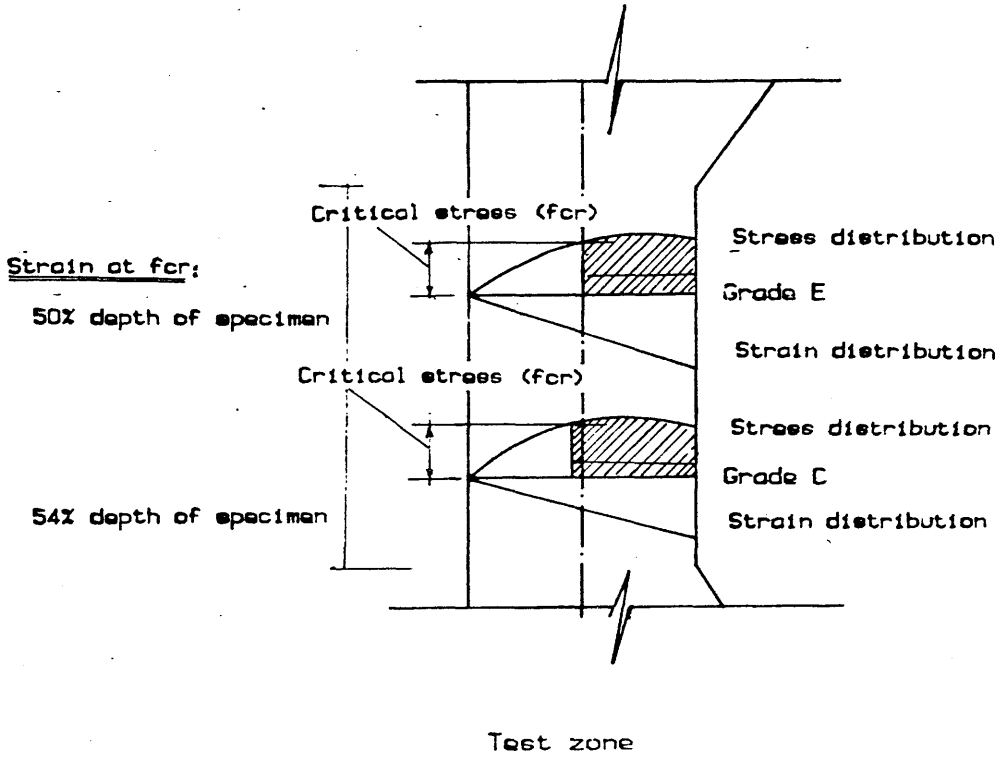

Fig. 4.19 Mode of failure as related to the compression zone depth subjected to stresses higher than the critical stress.

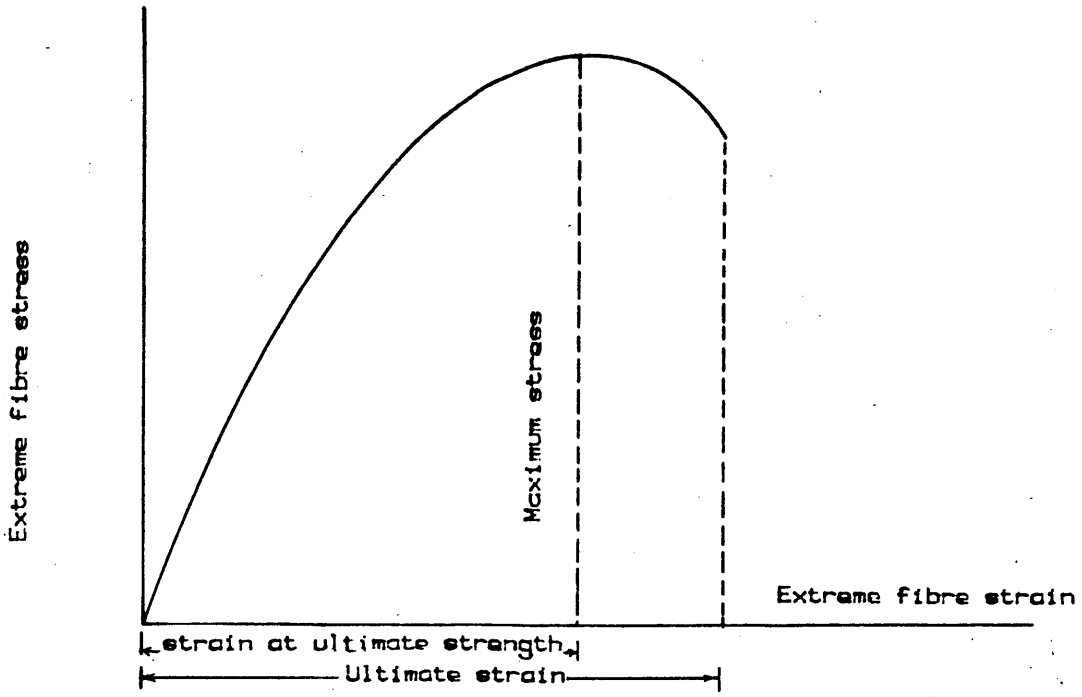

Fig. 4.20 Theoretical stress-strain relationships for the five PC grades in flexure.

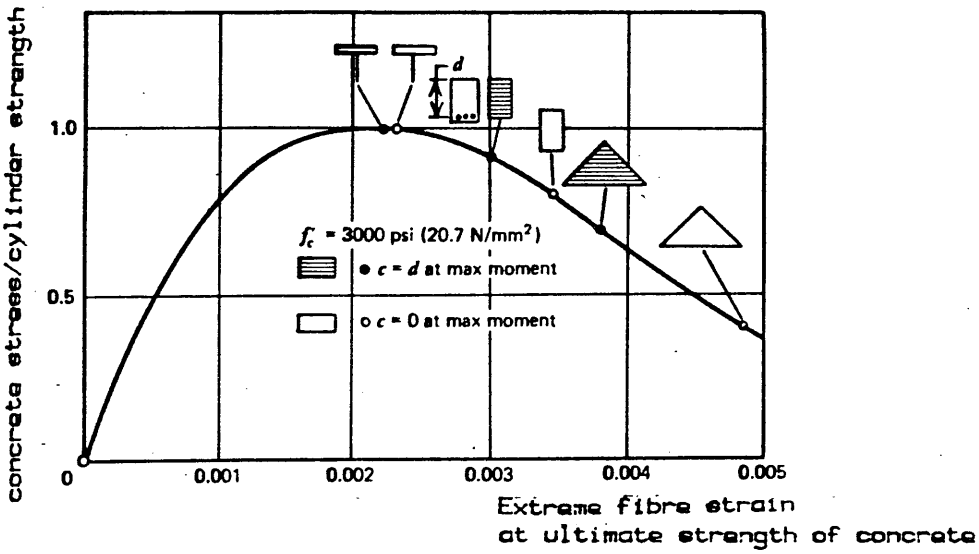

Fig. 4.21 Ultimate strain as a function of cross section and position of neutral axis.

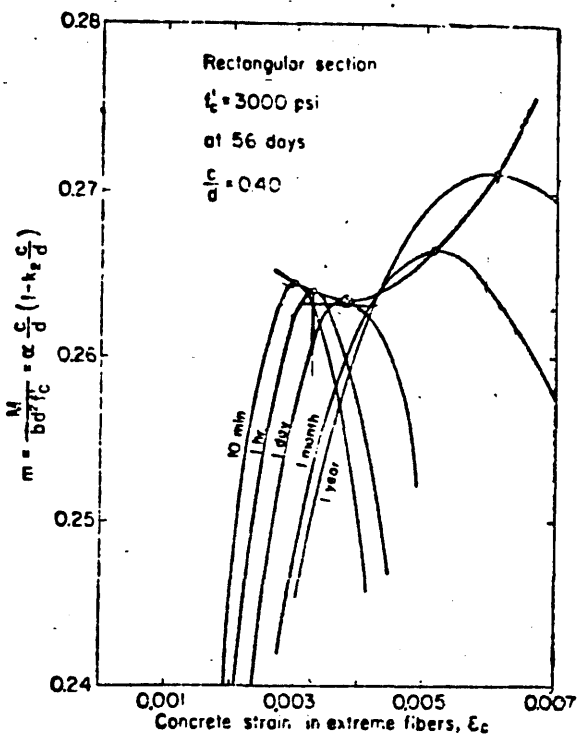

Fig. 4.22 Variation in reduced moment with concrete strain and time.

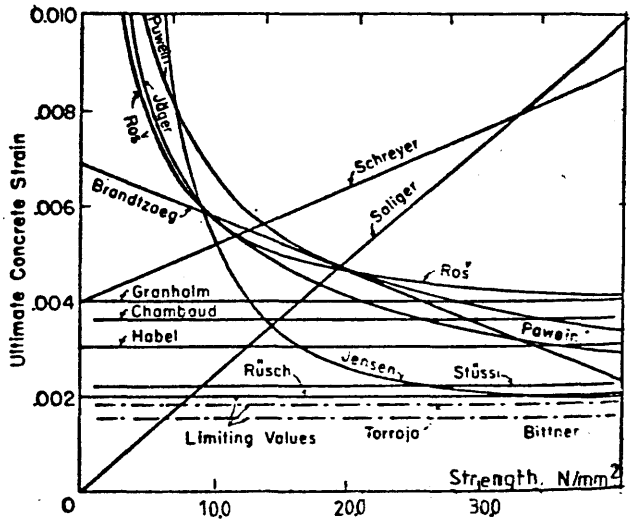

Fig. 4.23 Relationships between ultimate strain and concrete strength.

CHAPTER FIVE

REINFORCED PC BEAMS AND THEIR TEST ANALYSES

5.1. Introduction

Knowledge of the structural performance of PC's when reinforced, is the major prerequisite for the design of reinforced PC structures. Yet the work done to clarify it is surprisingly limited. Little research has been reported on the structural behaviour of PC reinforced beams (77), (78) & (79). As stated earlier most of that research has been directed towards mechanical and durability properties. The effects of different steel types, reinforcement ratio, PC ultimate strength and strain were not studied. In addition most of the reported work on reinforced PC was for reduced-scale members which did not help in the derivation of general design equations or produce reliable conclusions (94).

Recognizing the importance of the stress-strain relationship in flexure, little research has been carried out on PC to obtain different stress-block parameters. Generally the stress distribution in the compression zone at ultimate capacity was often expressed as a rectangular uniform distribution. This simplification led to some misinterpretation of the experimental results obtained by the researchers. The full behaviour of a reinforced PC beam from small load-levels up to failure, including flexural deformations, can not be obtained without a general expression of the stress value at any strain level in the concrete. The ultimate carrying capacity of a member made of a given PC grade depends on the reinforcement

ratio R and the type of steel used. Consequently the type of failure is governed by these two factors. If steel with a well-defined yield point is used, the concepts of over, under and balancd reinforcement can be dealt with theoretically and experimentally. On the other hand, when using high tensile steel without a well-defined yield point, these concepts can not exist. In this case there is a specific reinforcement ratio R_s at which steel strain would not exceed a prescribed value, if the whole section is to develop its ultimate strength. Increasing R normally implies an increase in the ultimate carrying capacity and a reduction in the resulting strains in steel. However, there is obviously a certain maximum R that will result in a desirable mode of failure and would allow the efficient use of steel.

The present work was carried out primarily in an attempt to specify this specific reinforcement ratio R_s and to check the validity of the previously found stress-block shapes and parameters for different PC grades.

5.2. Fundamental equation for pure flexure

For any rectangular cross-section with the notations shown in Fig.(5.1), There are three conditions. Two of these are concerned with equilibrium of forces and moments, while the third is that of strain compatibility. Using these conditions, the ultimate moment or rather the moment at any chosen concrete strain can be expressed as follows:

(1) Equating internal and external forces then,

$P = C_c + Cs - F_s$, which can be rewritten as

$P = K1.K3.f_{cy}.c.b + A'_s.f'_s - A_s.f_s$

Substituting for K1.K3 = G, then

$P/(b.d.f_{cy}) = G.c/d + A'_s/(b.d).f'_s/f_{cy} - A_s/(b.d).f_s/f_{cy}$

Let $A'_s/(b.d) = R'$, $A_s/(b.d) = R$, and $P/(b.d.f_{cy}) = L$, then

$L = G.c/d + R'.f'_s/f_{cy} - R.f_s/f_{cy}$

$L = T + T'_s - T_s$ ...(5.1)

(2) Equating externaland internal moments:

$P.e = M = C_c\ (d - K2.c) + Cs\ (d-d')$, then

$M = G.f_{cy}.c.b\ (d-K2.c) + A'_s.f'_s\ (d-d')$

$M/(b.d^2.f_{cy}) = G.c/d\ (1-K2.T/G) + R'.f'_s/f_{cy}\ (1-d'/d)$

Substituting for $Y = K2/G$ and $M = b.d^2.f_{cy}.Z$, then

$Z = T\ (1-Y.T) + T'_s\ (1-d'/d)$ ...(5.2)

(3) Assuming a linear strain profile over the cross-section:

$c/d = \varepsilon_c/(\varepsilon_c + \varepsilon_s) = T/G$

Then $c = T.d/G$ ...(5.3)

$\varepsilon_s = \varepsilon_c\ (G/T - 1)$ ...(5.4)

$\varepsilon_{s'} = \varepsilon_c\ (1 - d'/c) = \varepsilon_c\ (1 - d'/d.G/T)$ ...(5.5)

Equations (5.1 to 5.5) apply to any section subjected to combined moment and axial load. For the case of purs flexure Eq.(5.1) can be rewritten as

$T + T'_s - T_s = 0.0$ from which $T = T_s - T'_s$ ...(5.1-a)

It is evident that the problem is now reduced to finding only the value T. From T the strains in the steel can be calculated and the reduced moment value Z can also be found. The value Z is dependent on Y and G which are the two characteristic parameters of the stress block and vary from one grade to another. They are also dependent on concrete strain. Thus depending on the chosen values of Y and G one can estimate the

internal moment developed in any section at any load or concrete strain level. The values of G and Y as derived experimentally are shown in Figs.(5.2 and 5.3) for the five grades investigated.

Where the steel used has no definite yield point, its stress-strain curve had to be idealized. The chosen idealisation was a trilinear stress-strain curve as shown in Fig.(5.4). This idealization was based on the experimental findings of various tension tests carried out using the same type of steel as that used throughout this present work. As shown in Fig.(5.4), the steel stress in each of the three linearly idalized zones can generally be expressed as

$f_s = A + B.\ \varepsilon_s$. or $f'_s = A' + B'.\varepsilon_s'$

where A, B, A' and B' are constants and change from zone to zone in the steel stress-strain curve. Now by using Eq.(5.1-a) and Eqs.(5.3, 4 and 5), then

$$T = R.\ f_s/f_{cy} - R'.f'_s/f_{cy}$$

$$T = R/f_{cy}\ (A + B.\varepsilon_s) - R'/f_{cy}\ (A' + B'.\ \varepsilon_s')$$

$$T = R/f_{cy}\ [A+B\ (G/T -1)] - R'/f_{cy}[A'+B'(1-d'/d.G/T)] \quad ...(5.6)$$

Equation (5.6) can be rewritten in the following general form,

$$T^2 + 2.S.T = Q \quad ...(5.6-a)$$

Solving for T, the reduced moment factor (Z) and compression zone depth can be calculated for any assumed maximum concrete strain level. The only remaining provision is that steel stress constants have to be assumed first and the derived steel stresses should lie within the assumed zone. If this is not the case, another zone should be assumed and the

calculations repeated. The process should be continued until constants and stresses are compatible. Examples of the use of these equations will be given later during the evaluation of the experimental data for different reinforced beams.

5.3. Description of PC reinforced beams

5.3.A Dimensioning Five reinforced beams were cast and tested, one for each PC grade. The beam dimensions were chosen such as to represent full scale structural members and to be suitable for the available facilities in the laboratory. Bearing in mind the maximum volume of a single batch that could be mixed, the number of batches,the required time for placing each batch and the time of setting, the beam volume was calculated to suit these conditions.

Because of the heavy reinforcement, vibration had to be carried out using a vibrating table rather than other techniques. The size of the table and the limited space around it set a limit to overall dimensions. The overall length of the beam was thus chosen to be 2600 mm. The minimum width was chosen such that it could accommodate four steel bars of up to 20 mm-diameter. In addition by consideration of the maximum aggregate size used with different grades, the beam width was eventually chosen to be 150 mm.

The beam depth was defined such that no more than two layers of tension reinforcement would be required for failure to take place in concrete at and not before 0.2% proof stress was reached in the tension reinforcement. This last condition was taken into account to ensure efficient use of the

reinforcement. The initial calculations of the beam depth gave a value of 250 mm to satisfy the previous prrequisites.

These dimensions proved to be convenient in mix batching, placing, vibrating and testing. Each beam was cast using two batches, each of which took around 20 min. to mix, place and vibrate. The beam was supported across the vibrating table diagonally with its two overhanging ends supported by two struts each the same height as the table.

5.3.B Reinforcement arrangements The reinforcement ratio for each beam was calculated on the basis of the previous findings on PC stress-block parameters. As said earlier, no balanced reinforcement ratio R_b can be found with steel not having a well-defined yield point. A wider range of possible R's was thus available. As the main purpose of this series of tests was to check the validity and reliability of the previously given findings, specific reinforcement ratios R_s were chosen. These values of R_s were estimated on the basis that concrete strain and not steel strain is the limiting factor for the beam to attain its ultimate carrying capacity. That is to say that failure should be forced to be by the concrete reaching its ultimate compressive strain before excessive steel strains have reduced the compression zone depth in so called tension failure. This makes the best use of PC. Thus R_s was chosen to ensure at least a compression zone depth at failure of 45% of the effective depth. On calculation, different R_s values ranged from around 6% to 8%.

No compression reinforcement was used in the five beams made from the five PC grades. The internal compression force was

supplied by the concrete only as there was no steel in the compression zone. Shear reinforcement was provided in the shear span. No such reinforcement was used in the middle third of the beam to avoid any effect of lateral confinement. Details of the reinforcement of the five beams are demonstrated in Figs. (5.5-a,b,c,d&e). Although the nominal shear stresses at failure were very high the total capacity of the bent up bars and links together with the PC itself was more than sufficient to prevent any shear cracking. Failure always occurred as intended in the middle third test zone.No single shear crack was observed in the shear span for the five beams up to failure at which nominal shear stresses reached levels in the vicinity of 10.0 N/mm2.

5.3.C Measurements and testing Each beam was tested using a third point flexure test as shown in Fig.(5.6). The two-point load was applied using a suitable steel beam with two bearings. To measure strains in the tension reinforcement, eight pairs of 5.0 mm strain gauges were attached to the four middle bars (two bars for each layer). Each bar had two pairs of gauges located 400.0 mm apart (one gauge on top of the bar, the other on the bottom). The average reading of each pair was calculated. In this way each of the two steel layers gave eight readings, whose average was taken to represent strain level in that layer. As shown in Fig.(5.7-a), the strain gauges were distributed in such a way that any single crack which might occur accidentally at the location of one strain gauge would not affect more than a single pair of strain gauges. In this way reliable strain readings were maintained throughout the whole test.

For measuring concrete strains, electric strain gauges of 20 mm. length were used as shown in Fig.(5.7-b). Twenty strain gauges , ten for each side , were attached to the concrete surface at five levels. The highest level was as near to the compressive extreme fibre as possible (5 mm. from the top), while the lowest coincided with the centroid of the lowest steel layer. The distance between these two extreme levels was divided into four equal divisions and five pairs of gauges attached on each side of the beam. Deflections at the centreline of the beam were measured using two electric transducers as shown in Fig.(5.7-a). For each beam there were sixteen gauges for measuring steel strains, twenty gauges for concrete strains and two transducers for deflections. All these gauges and transducers were connected to a Data-Logger.

Flexure tests were carried out at a rate of loading initially equal to 1.0 KN/min. In the later stages near failure the rate of machine platen movement had to be increased to compensate for the excessive deflections. Readings were taken at 2000.0 lbs.-incremental load.

5.4. Test results

Concrete strain at each load level was calculated as the average of the four readings at the same level. The steel strain value for each layer was taken as the average of the eight readings of the strain gauges at the same layer. Strain profiles for each beam as found experimentally are shown in Figs.(5.8-a,b,c,d&e) for grades "A" to "E" respectively. Curvature of each beam is shown in Figs.(5.9) for the five

grades. The strain profiles are more or less linear even near failure for all beams. The change in the compression zone depth c was insignificant in the early test stages as was the curvature of the beam. At final stages near failure, the neutral axis moved rapidly upwards and the curvature increased in proportion with consequent high deflections at failure.

Steel strains in the two layers plotted against concrete maximum strain, at the extreme fibre, for the different beams tested are shown in Figs.(5.10-a,b,c,d&e). To help analyse the results, the maximum compressive concrete strains at which steel tensile strain in either of the two layers, reached its proprortional limit, its 0.1 % proof stress or its 0.2 % proof stress, were defined using the actual stress-strain curve of the steel used. These stages are denoted respectively as I, III, V and II, IV, VI for the first and second steel layers.

The steel strain was found to be linearily relatedto the concrete strain at the early stages and up to stage I and II for the first and second layers. After exceeding its proportional limit the steel strain increased rapidly and at a higher rate than the increase in the concrete strain. Near failure, the first steel layer often reached a strain beyond that corresponding to 0.2 % proof stress. The second steel layer always reached a stress greater than its 0.1 % proof strength. This shows that steel was used efficiently despite the very high reinforcement ratios chosen.

The effect of the chosen R on the behaviour of the steel can be seen by comparing, for instance, beam "E" with beam "B". With beam "B" which had R equal to 0.07, concrete strain at

the compressive extreme fibre amounted to 0.0029 and 0.004 for the first and the second layer to reach their proportional limits (I, II). In Beam "E", with R = 0.078, concrete strains for the same two stages amounted to 0.0035 and 0.0047.

The change in the compression zone depths as calculated from the steel and concrete strains are shown in Figs.(5.11-a,b,c,d&e) for the respective beams. As shown in these figures, the depth c was almost constant up to the proportional limit of the first steel layer (I). A decrease in c was initiated when stages I and II were reached. This decrease was very apparent after the steel reached stages V and VI, when the two layers reached 0.2 % proof strength. However, the final value of c was never less than 50% of the effective beam depth.

The tension force in the steel was calculated using the idealized stress-strain curve of the steel, from which the stress at any corresponding recorded strain could be obtained. Figs.(5.12-a,b,c,d&e) show the development of the steel tensile forces for the two layers plotted against the concrete strain. The large difference in the tension forces between the two layers for beam "A" is mainly due to the large difference in the steel areas used for each layer.

Maximum deflections varied from 37.0 mm. for beam "A", to 50.0 mm. for beam "E". The full load-deflection curves as recorded experimentally are shown in Fig.(5.13). The ultimate moment calculated from the maximum recorded machine load also changed significantly from one beam to another. The lowest machine load and moment at failure was recorded with beam "D" where

they amounted to 418.0 KN and 167.2 KN.m respectively. The highest values were recorded with beam "E" with a maximum machine load and moment of 533.0 KN and 213.5 KN.m respectively. Table (5.1) shows the recorded values of the maximum machine load and the associated applied moment for the different beams tested.

5.5. Analysis of results

For each beam the internal forces, the internal moments, the ratios of the applied to the calculated moments and the ratios of internal tension forces to compression forces were calculated. The curvature of each beam was also calculated. These relationships could be found fully from the beginning of load application up to failure. The concrete stress distribution in the compression zone for each beam was already known. So the values of the compression force and its location at any concrete strain level could be readily calculated.

In an attempt to check the applicability and accuracy of the previously derived stress distribution in flexure, the block parameters were used directly in the different calculations without any idealization.

For any value of compressive extreme fibre strain ε_c, the internal compressive force C_c , see Fig.(5.14), can be found as follows:

$C_c = b.c.K1k3.f_{cy}$ where

$c = \varepsilon_c/(\varepsilon_{s1} + \varepsilon_c) .d_1 = \varepsilon_c/(\varepsilon_{s2} + \varepsilon_c).d_2$

The tension forces in the two steel layers and the total internal tension force in each beam could be calculated

knowing the average strain in each layer ε_{s1} and ε_{s2} as follows :

$F_{s1} = A_{s1} (A1 + B1.\varepsilon_{s1})$ and $F_{s2} = A_{s2} (A2 + B2.\varepsilon_{s2})$

in which A1, A2, B1 and B2 are the constants of the idealized steel stress-strain curve as given in Fig.(5.14). The total internal tension force F_s was calculated then as follows :

$$F_s = F_{s1} + F_{s2}$$

The calculated internal forces are plotted against each other in Figs.(5.15-a,b,c,d&e). In these figures it is evident that the equilibrium condition of internal forces is satisfied especially at early stages of testing. Up to the proportional limit of the reinforcement, the tension force is almost identical with the compression force as calculated. Slight divergence between the two calculated forces existed after the steel had exceeded its 0.2% proof stress. This can be attributed to the approximation involved in the idealization of the steel stress-strain curve and to the hardening of the steel causing differences from that curve.

Internal moments could also be found using the derived block parameters. As shown in Fig.(5.14), the moment M at any stage concrete strain level could be expressed as :

$$M = C_c . (d1 - K2.c) - F_{s2} (d'')$$

Using this equation a comparison between the calculated internal moment and the actual applied one could be found as shown in Figs.(5.16-a,b,c,d&e). Generally the calculated internal moments were found to be slightly less than the

corresponding applied ones at the early test stages. This is due to the assumption previously made that the whole concrete cross-section below the neutral axis resists no tensile stresses. The two moment values are almost equal for all beams with the exception of beam "A". The analysis of moments in beam "A" gave a noticeable divergence between the calculated and the actual moments, despite the fact that force equilibrium condition was satisfied for the same beam, see Fig.(5.15-a).

As a clearer demonstration, the ratios of the total tension forces to the compression ones as calculated, and the ratios of the internal moments to the actual moments are plotted in Figs.(5.17-a,b,c,d&e). These ratios fluctuated in the vicinity of 1.0 +/- 10%. This is mainly due to the various sources of probable errors involved in the strain readings, the idealization of the steel stress-strain curve and other flexural parameters neglected in simplifying the calculations.

The curvature of the different beams tested could also be calculated from zero to failure load. Knowing the compression zone depth c and ε_c, the curvature ϕ could be found from the equation; $\phi = \varepsilon_c/c$, see Figs.(5.9-a,b,c,d,&e).

As ϕ is strongly dependent upon c, the value of ϕ increased disproportionately after the reinforcement steel exceeded its proportional limit. Beams with low R offered higher ϕ at any stage of loading than those with higher R, despite the latter having much lower PC moduli of elasticity than the former.

5.6. Theoretical calculation of the ultimate moment and the

specific reinforcement ratio

All the previous calculations of the internal forces and moments were based on the experimental readings of the strains in concrete and steel. However, it is possible to calculate these different forces and moments theoretically. Using the fundamental equation given before, Eq.(5.6) , the parameter T and the reduced moment factor Z can be estimated for any given concrete strain. As will be seen, this equation could be used for the calculation of the specific reinforcement ratio R_s. This ratio by definition would provide an ultimate moment at a specific, predetermined steel strain and mode of failure.

For the beams tested, some simplifications could be introduced to Eq.(5.6); where no compression reinforcement is used, Eq.(5.6) can be rewritten as :

$$T = R/f_{cy} \ (A + B.(G/T - 1.0)) \qquad ...(5.6\text{-b})$$

Knowing T, the reduced moment factor Z could be expressed as:

$$Z = T \ (1.0 - YT) \qquad ...(5.2\text{-a})$$

From Eq.(5.2-a), it is clear that there is a single value for the coefficient T that would give maximum Z. This value is at T = 0.5/Y and is equal to 0.25/Y. The parameter Y is dependent on the concrete grade and strain value reached at ultimate carrying capacity for different grades as given in table (5.2). The variation in Y as derived experimentally for any point on the whole stress-strain curve of concrete in flexure has been demonstrated before in Fig.(5.13). As this work is concerned with the ultimate moment, only a single value corresponding to this limiting state was quoted in table (5.2). The maximum value of Z however, can not be practically

attained as it would require an extremely high value of R. This would imply a heavily reinforced section, in which even if enough room could be provided to accommodate the steel, most of this steel reinforcement would not be used efficiently. In addition, the mode of failure would be extremely sudden and explosive.

On the other hand, using a much lower R than that which would give the maximum Z is not an economic approach in design. With a low R the strain in the reinforcement steel would be very high and the compression zone depth would be so small as to give an inefficient use of the PC itself. There would also be severe curvatures and flexural deformations. This situation dictated the search for such a specific reinforcement ratio that would allow the economic use of both concrete and steel, and would provide an acceptable structural behaviour and mode of failure.

To find R_s for each grade, several relationships had to be first clarified. The value of T was calculated as a function only of R, by using Eq.(5.6-b), as follows;

- Given PC grade and f_{cy}, find G and Y at the theoretical value of ultimate strain ε_{cu}, or by using the empirical equations previously given, [Eqs.(4.1-4.4)].
- Assume R and the steel stress constants A, B (each can take any of the three values in the idealized steel curve).
- Using Eq.(5.6-b), calculate T.
- Using Eq.(5.4), find steel strain ε_s.
- Check the value of ε_s which must be within the assumed constants zone, otherwise chose another set of constants and

repeat the calculations until the assumed constants apply to the same zone in which ϵ_s lies.

- Fix the last value obtained for T.
- Using Eq.(5.2-a), calculate Z.
- Using Eq.(5.3), find the compression zone depth c.

Following this simple procedure, the coefficient T for various grades could be found and plotted against R as shown in Fig.(5.18). The investigated range of R-values was from 0.0 to 10%. The highest value of T corresponding to that range chosen, amounted to 0.55 which is well below 0.5/Y that would give a maximum Z. By extrapolation, it was found that to reach this maximum value at T = 0.50/Y, the required R would be 16.0% which, as said earlier, is a very high value. With this high value of R , neither would there be enough room for accommodating steel, nor would the steel be used efficiently. The resulting steel strain and its dependency on R to reach the ultimate concrete carrying capacity is shown in Fig.(5.19). While the values of Z versus R are plotted in Fig.(5.20). The change in the compression zone depth expressed as a percentage of the whole beam depth, is shown in Fig.(5.21) for different R-values.

All these curves, Figs.(5.18-21), for the five PC grades tend to have a horizontal assymptote which obviously corresponds to T = 0.5/Y at an R = 16%. Hence, within the investigated range of R-values, the factor Z, the ratio c/d and the coefficient T are directly proportional to R. Whereas steel strain is inversely proportional to R.

The two decisive factors for an efficient and an economic

design that would also give a desirable mode of failure, can be concluded from the paragraphs above. They are the steel strain, Fig.(5.19), and the compression zone depth, Fig.(5.21).

The value R_s can be calculated by setting certain limits according to the design requirements. In this work, when calculating R_s for different grade-beams, two main prerequisites had to be satisfied, as follows :

[1] The steel strain shall not be less than 0.004 and not more than 0.01.
[2] The compression zone depth shall not be more than 65% of the beam depth and not less than 50% .

The first requirement implies an efficient use of the reinforcement without allowing for excessive tensile strains that might initiate a tension failure mode. While the second requirement primarily implies an economic use of the PC itself with full use of the high compressive strength of the material. To illustrate how these R_s's were calculated, beam "E" is taken as an example, as follows.

Referring to Fig.(5.19), an R-value that can satisfy the first requirement, may take any value from 0.05 to 0.082. From Fig.(5.21), the same R-value can be in the range from 0.085 to 0.006. As the ultimate moment is a direct function of Z which is directly proportional to R, the highest possible value of R = 0.082 was initially considered. This value required slightly more space for steel than that already available with the beam cross-section chosen. The highest value of R that could be accommodated was 0.078, and this was taken as the R_s for beam

"E".

Beam "D" is taken as another example. Following the same procedure R was found to be within the range from 0.05 to 0.081, and from 0.062 to 0.088 by using Figs.(5.18) and (5.21) respectively. As grade "D" is a very brittle one, it was decided to take an R_s-value lying in the middle of these ranges, to avoid excessive sudden and explosive failure. The R_s-value chosen was 0.0637 which allowed for around 52% of the beam depth above the neutral axis and steel strain of about 0.0072 at the ultimate capacity.

In this way, different R_s's were calculated and employed in the design of the different beams. Needless to say the value taken for R_s is optional and depending on the limits set and these might vary from one structure to another or from one design code to another.

To see how precise the experimentally-derived stress-block parameters are, the ultimate moment for each beam as well as the steel strain and the compression zone depth were calculated theoretically using the previously found values of the parameter T. Their values are compared with the direct experimental ones as shown in table(5.3). Using Fig.(5.20), the reduced moment Z for each beam was calculated according to the value of R_s employed. One interesting fact about Figs.(5.18-21), is that the ultimate capacities of the members are assumed to be attained at a certain maximum compressive concrete strains (ε_{cu}). These limiting strain-values have been established earlier mathematically using the idealized sine-curve for the flexural stress-strain

relationships for different PC grades. The ratio of the theoretical to the experimental ultimate moment for all beams, ranged from 0.925 to 1.035, as given in table (5.3). The compression zone depths and the steel strains for different grades as calculated theoretically by using Figs.(5.18 and 5.21), were verified experimentally and almost identical values were obtained.

5.7. Mode of failure for the five beams tested

The specific reinforcement ratios chosen, varied from one beam to another depending on the parameters G and Y for each beam grade. They were mainly determined such that steel and concrete would be efficiently utilized. This efficient utilization of both steel and concrete should allow for concrete crushing after and not before the steel has attained its 0.2% proof strength. As there was no definite yield point for the steel used, the failure of these beams could not be described in terms of initial tension or compression failure.

In all beams the load-deflection relationships, Fig.(5.13), were almost linear up to 60-75% of the failure load, with corresponding small values of midspan deflection. Clear dependency of flexural stiffness on PC modulus of elasticity Ec can be seen in Fig.(5.13). Where, irrespective of R, beams made from higher Ec-grade had higher stiffnesses and lower deflection values at failure, than beams made from lower Ec-grades.

Failure in all beams was reached after the two tension steel

layers had developed stresses more than the 0.2% proof strength. As shown in Fig.(5.22), flexural stiffnesses at the six previously defined stages of steel (I to VI), can predict the failure mode. Deflections at stage I (first steel layer reaching its proportional limit), amounted to 14.5 and 18.4 mm. for beam "A" and "E" at associated maximum concrete strains of 0.003 and 0.0035 respectively. The machine load values at this stage for these two beams were 258 and 320 KN. Up to stage I, concrete and steel could be considered to be in an elastic state. By the time that the second steel layer had reached its proportional limit (stage II), stress in the first layer had exceeded its proportional limit and began to develop nonlinearity which affected the load-deflection linearity itself. After stage II, deflection began to increase and stiffness began to decrease but the applied load was still far below its ultimate value. Excessive increases in steel and concrete strains were recorded after the two steel layers had reached their 0.1% proof strength, stages III and IV. At the beginning of stage IV,concrete had a maximum strain, for example, of 0.005 and 0.0067 for beam "C" and "E" respectively. The recorded deflections at this stage for beam "D" and "E" were 25.7 and 37.2 mm. respectively at load values of 95% of the ultimate load of each beam.

Tension cracks began to develop immediately after stage I was reached and a sharp drop in the compression zone depth took place. However these cracks could not be seen or traced before stage IV when failure was imminent. For safety reasons, the propagation of these cracks was not traced while the beam was under test. After the test had stopped these cracks were

investigated and copied for further analysis. When steel had reached stages IV and V, at strain values of not less than 0.004, maximum concrete strain became very great and a rapid increase in deflections took place. This resulted in a significant decrease in c, which led to excessive increases in steel strains. At these two stages, flexural stiffness dropped ,for example, to 0.6 and 0.8 of their initial values at stage I for beam "E" and "C" respectively.

In the last few load increments tension cracks widened and severe crushing of concrete became apparent. Eventually deflections reached such values that the machine load began to decrease. Rate of movement of the machine platens had to be increased to compensate for these high delection values. By doing this, load could be slightly increased until the ultimate value was obtained, at which tension cracking and concrete crushing propagated rapidly and machine load could not be increased or maintained. However, the machine platens were kept moving to allow for all the existing cracks to be clearly traced at the end of the test. This movement of the machine platens induced concrete and steel strains much higher than those expected at the ultimate load, Figs.(5.23 a,b,c,d, and e).

As shown in these figures, a plastic hinge developed in each beam at the location of the deepest, longest and widest crack or group of cracks. The centres of these hinges coincided with the recorded compression zone depth at failure. After the development and failure of these hinges the machine load dissipated and the flexure test came to its end.

On close inspection of the crack pattern on both sides of each

beam, almost no cracks could be found outside the test zone, i.e., the beam middle third. Cracks on both sides were almost identical. Cracks on each side, and opposite to each other, were connected by a horizontal crack running through the beam width. The test zone of each beam was subjected to pure flexure with no associated shear stresses. Thus tension cracks in this zone propagated, as expected, more or less vertically from the onset of the cracking process. A few of these cracks were inclined, and most of them eventually propagated through the weakest and shortest path heading towards a common point near the neutral axis .

The interesting thing about crack formation was that when crack spacing and width were calculated using a classical approach (95), they gave good agreement with the experimental observations. To illustrate this , take beam "B" as an example. The calculated minimum crack spacing was 66.5 mm. with a corresponding minimum crack width of 0.15 mm. The maximum spacing of cracks accordingly is twice the min. spacing, with an average value for crack spacing and width of 3/2 the minimum spacing and minimum width. These two average values ,i.e., 100 and 0.22 mm., agreed well with the crack spacing and depth observed with beam"B". By referring to Fig.(5.23-b), the minimum and maximum crack spacings are around 40.0 and 90.0 mm. respectively.

As shown with all other beams the cracks were distributed almost uniformly at spacings within the minimum and maximum values of spacing for each beam. The important thing to be stressed here is that the possible prediction of crack

spacings and widths can be of outstanding significance in controlling the crack formations often required for srviceability limit state design.

Table 5.1: Ultimate machine loads and moments recorded for the five PC beams

Beam	A	B	C	D	E
Machine ultimate load KN	427.0	507.0	422.5	418.0	533.0
Ultimate moment KN.m.	170.8	203.0	169.0	167.2	213.5

Table 5.2: Theoretical values of ultimate concrete strain and coefficients Y,G at ultimate conditions.

Grade	A	B	C	D	E
Ultimate strain	0.0075	0.0073	0.0072	0.0071	0.0076
Coefficient Y	0.57	0.56	0.55	0.536	0.57
(experimental)	(0.614)	(0.582)	(0.568)	(0.54)	(0.627)
Coefficient G	0.70	0.72	0.75	0.789	0.686
(experimental)	(0.66)	(0.706)	(0.751)	(0.783)	(0.643)

Table 5.3: Comparison between theoretical and experimental ultimate capacity for the five PC beams

Grade	A	B	C	D	E
Ultimate moment KN.m					
M_u.theoretical	177.2	194.3	160.0	176.8	197.6
M_u-Experimental	171.0	203.0	169.0	167.2	213.5
Ratio of M_u th./$M_u$exp.	1.035	0.96	0.95	1.06	0.93
Compression zone depth (mm)					
C_u - theoretical	124.0	120.0	110.0	110.0	133.0
C_u - experimental	130.0	120.0	113.0	114.0	128.0
Ratio of C_uth/$C_u$exp.	0.95	1.0	0.97	0.96	1.04

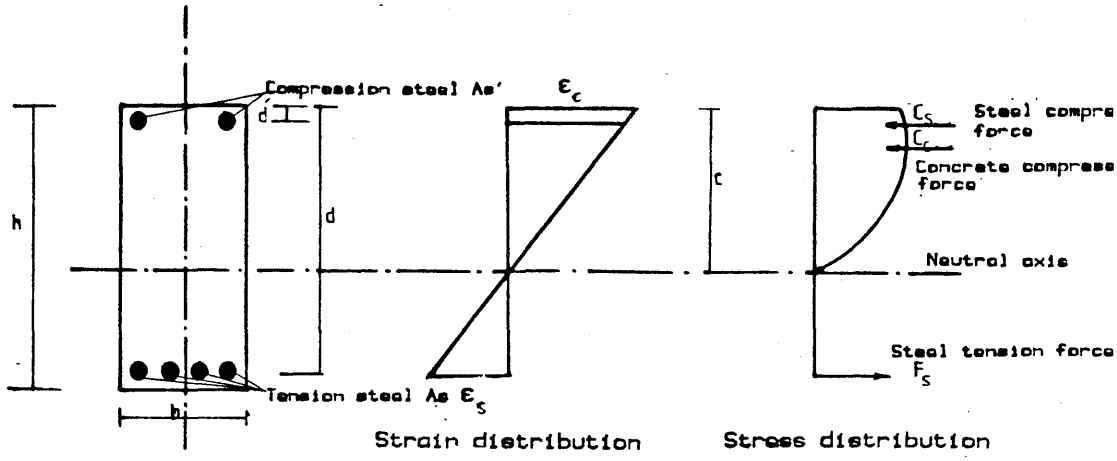

Fig. 5.1 Notations of doubly-reinforced section at ultimate strength.

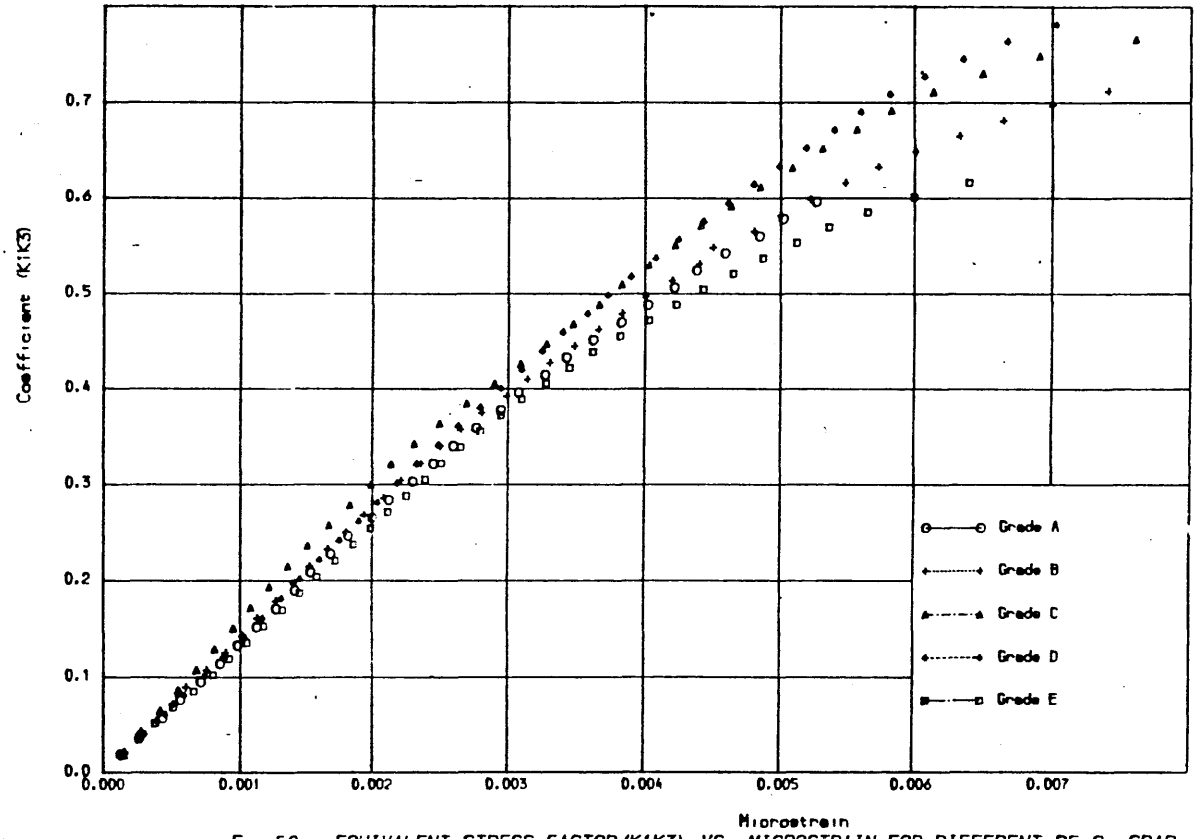

Fig.5.2 EQUIVALENT STRESS FACTOR (K1K3) VS. MICROSTRAIN FOR DIFFERENT RE.C. GRAD

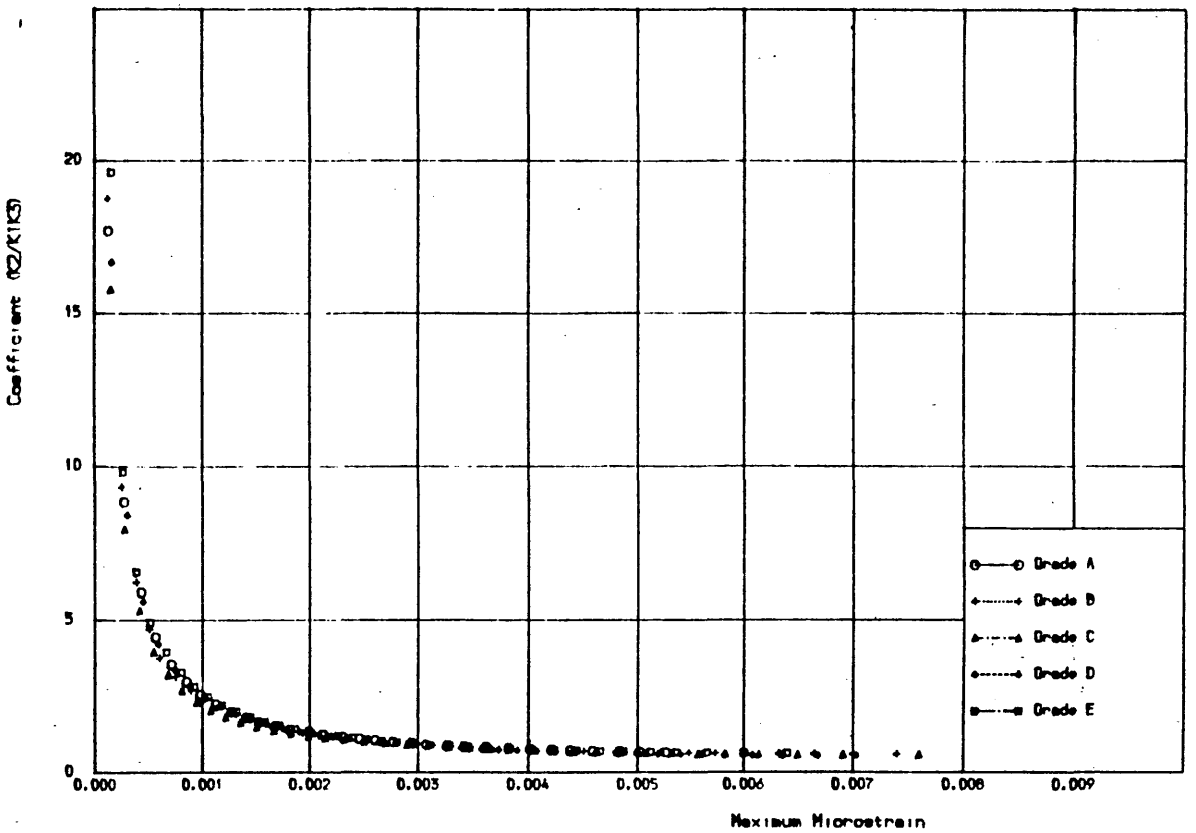

Fig. 5.3 STRESS-BLOCK RATIO (K2/K1K3) VS. MICROSTRAIN FOR DIFFERENT RE.C. GRADES.

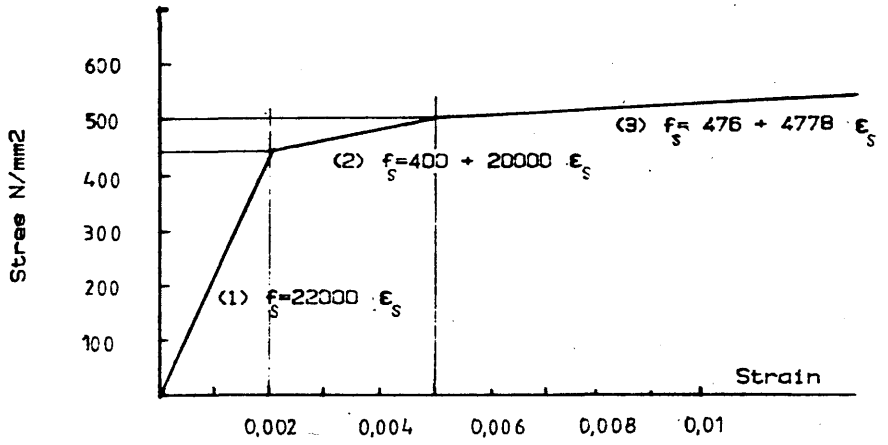

Fig. 5.4 Idealized trilinear stress-strain curve for the steel used.

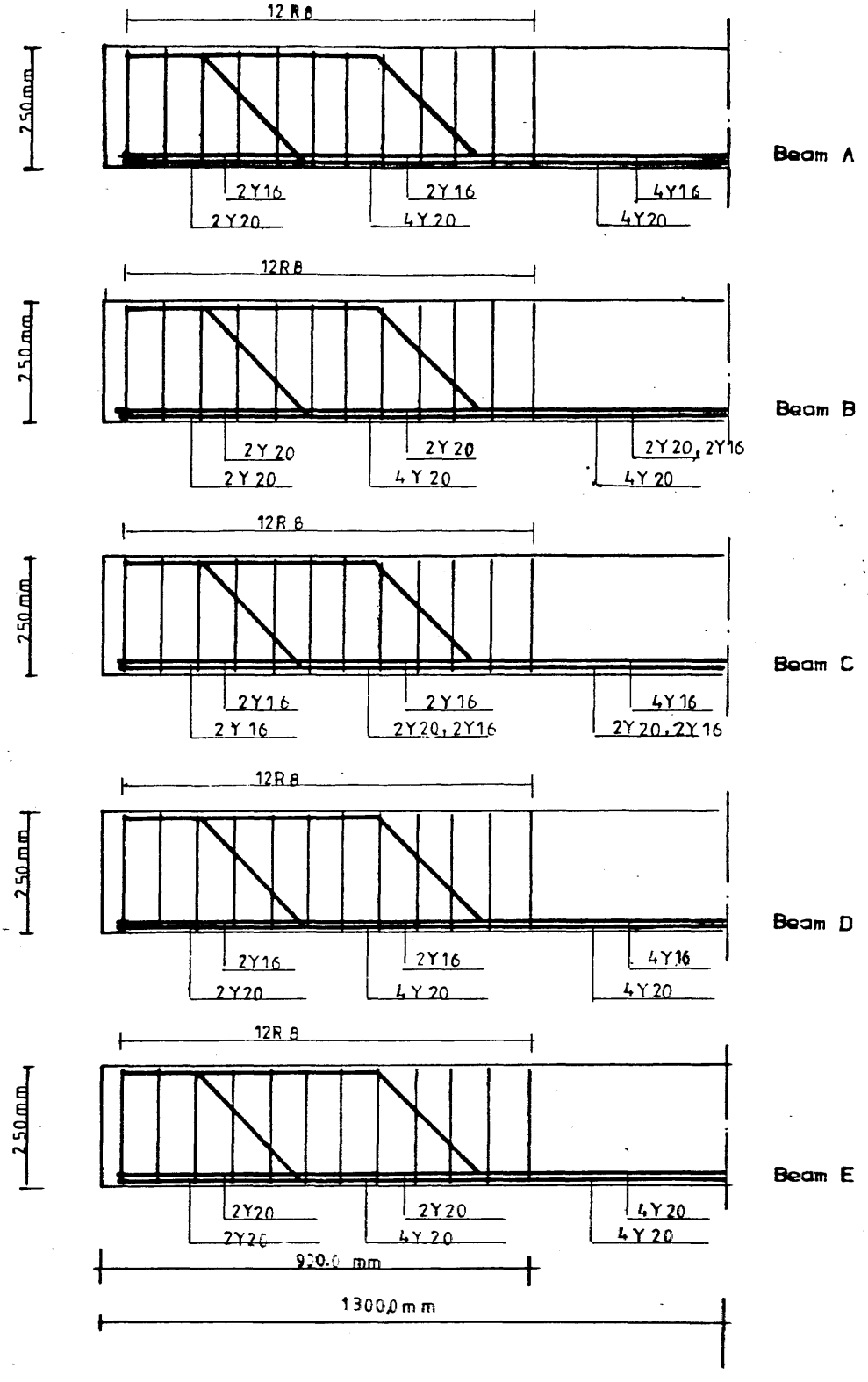

Fig. 5.5 Details of reinforcement of the five PC beams.

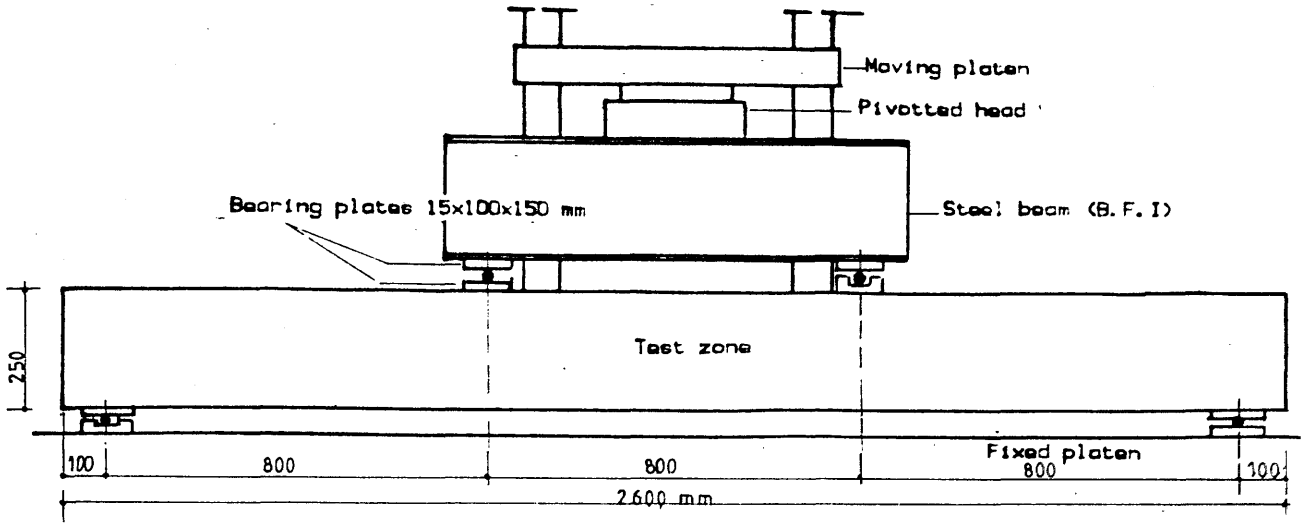

Fig. 5.6 Arrangements for third-point flexure tests of the five PC beams.

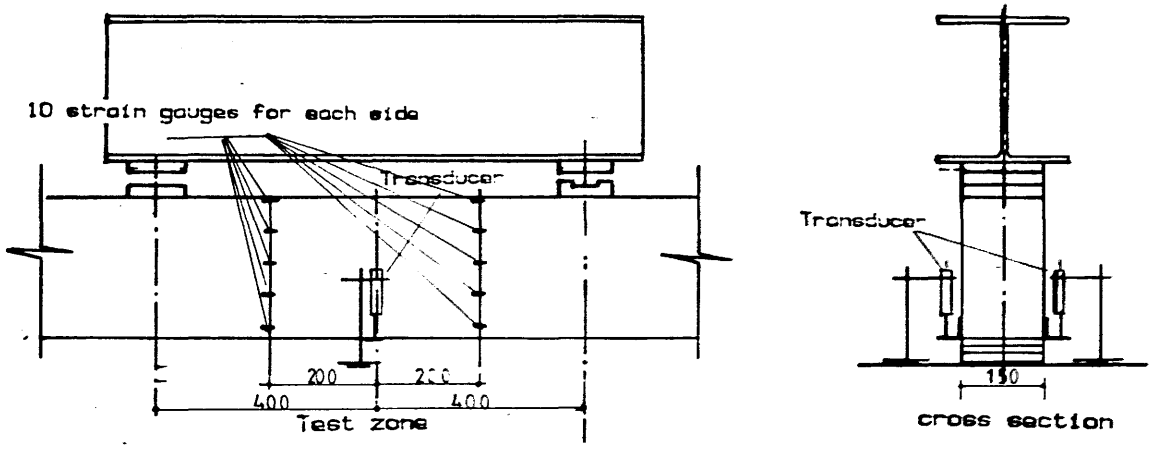

(a) Measurements of PC strains and max. deflecttion

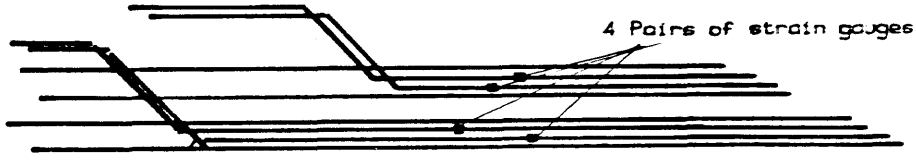

(b) Measurements of steel strains.

Fig. 5.7 Measurements of str ains and deflections.

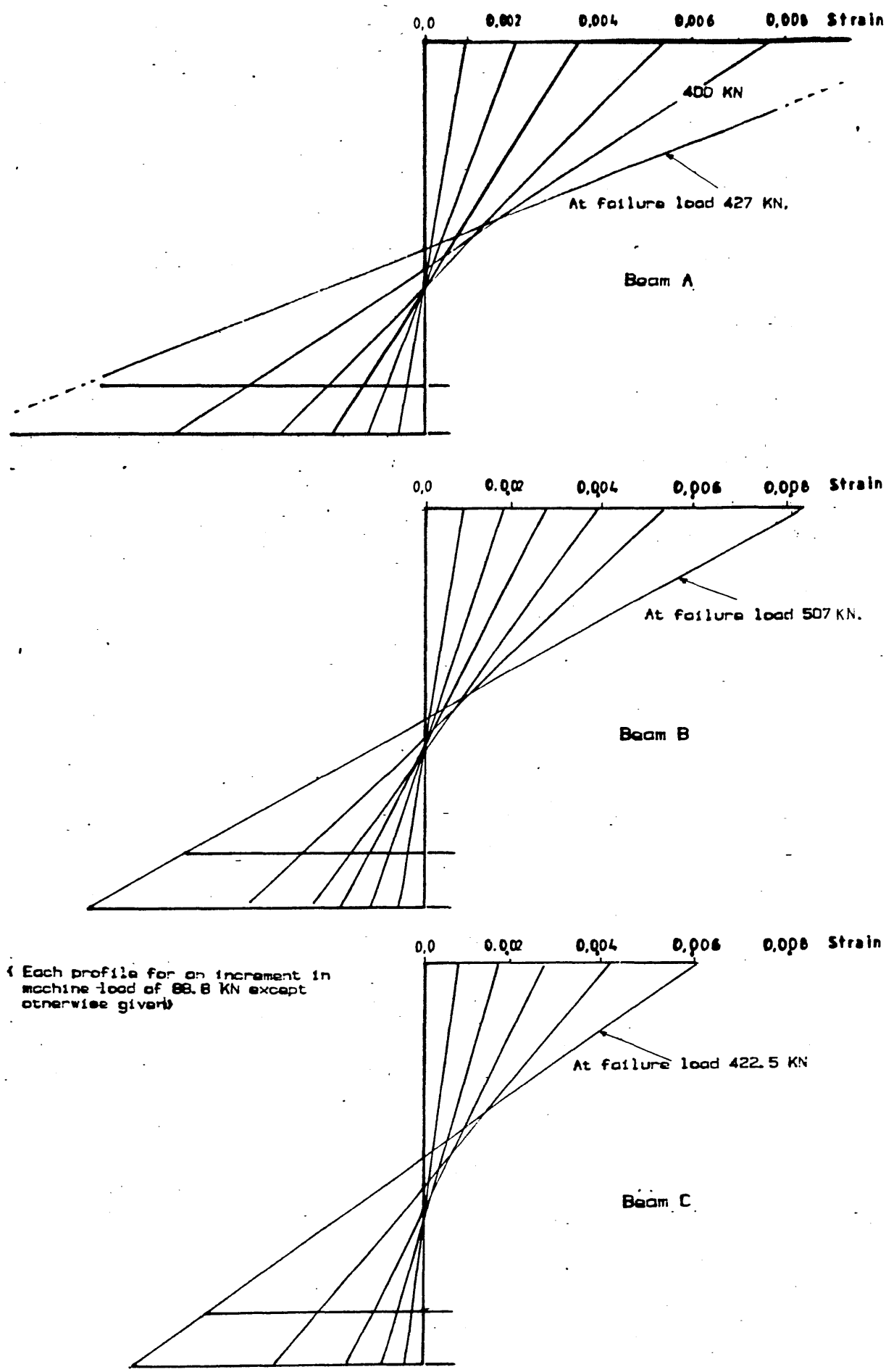

Fig. 5.8 Strain profiles at various testing stages for the five PC beams tested (A, B & C).

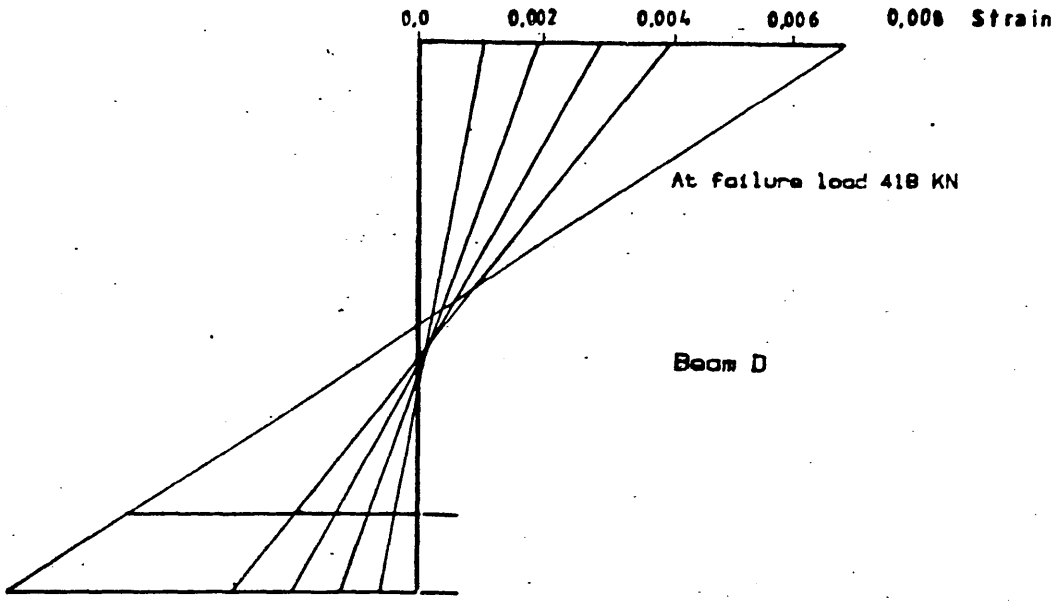

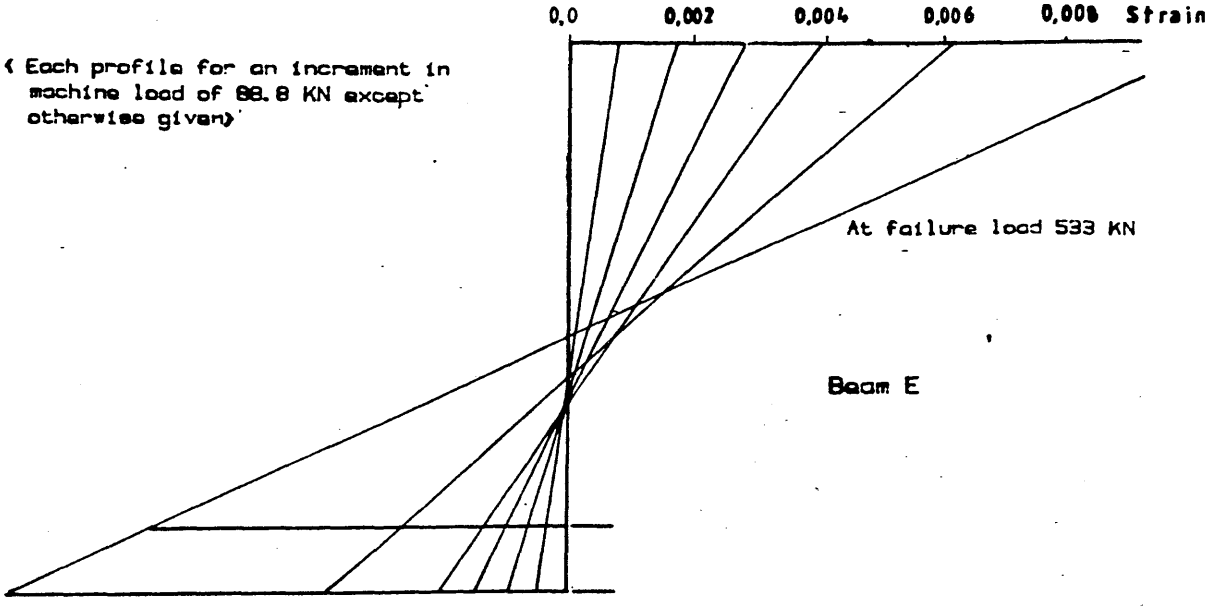

Fig. '5.8' Strain profiles at various testing stages for the five PC beams tested (D & E).

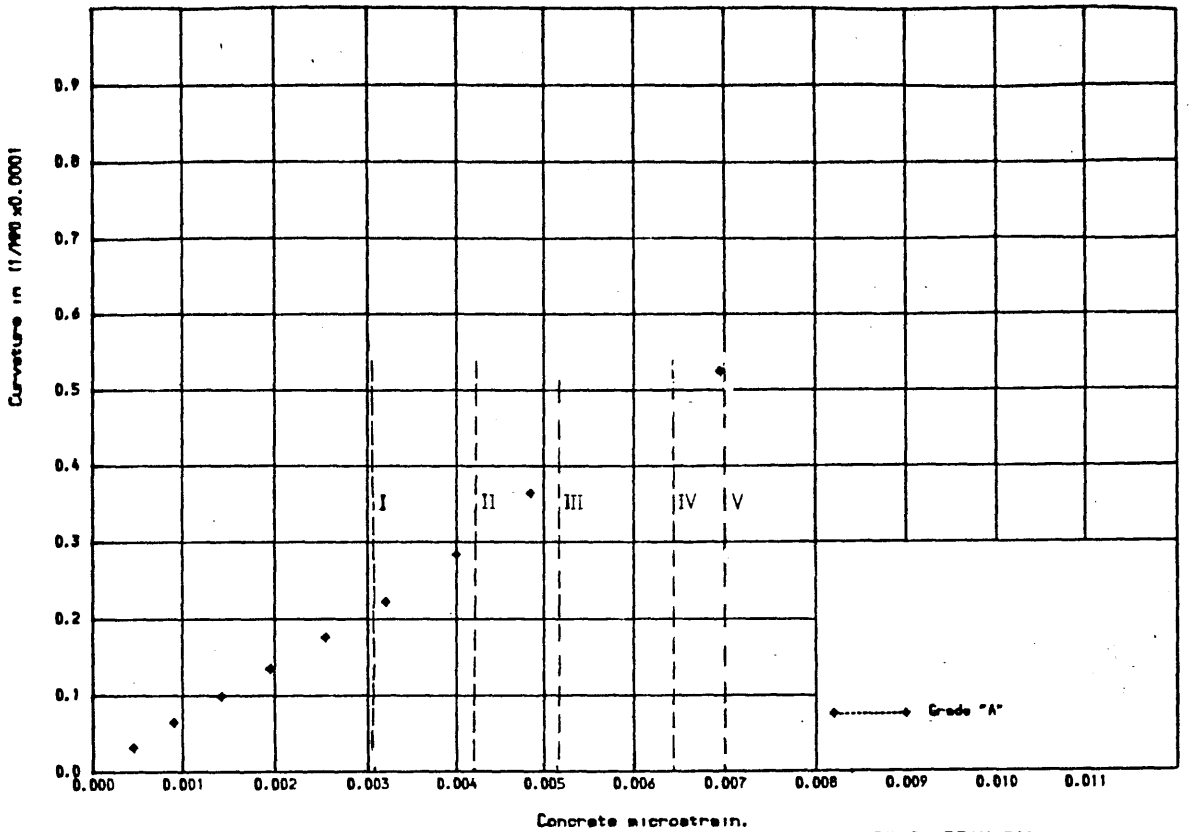

Fig. 5.9-A *CURVATURE VS. CONCRETE STRAIN FOR REINFORCED RE.C. BEAM "A".*

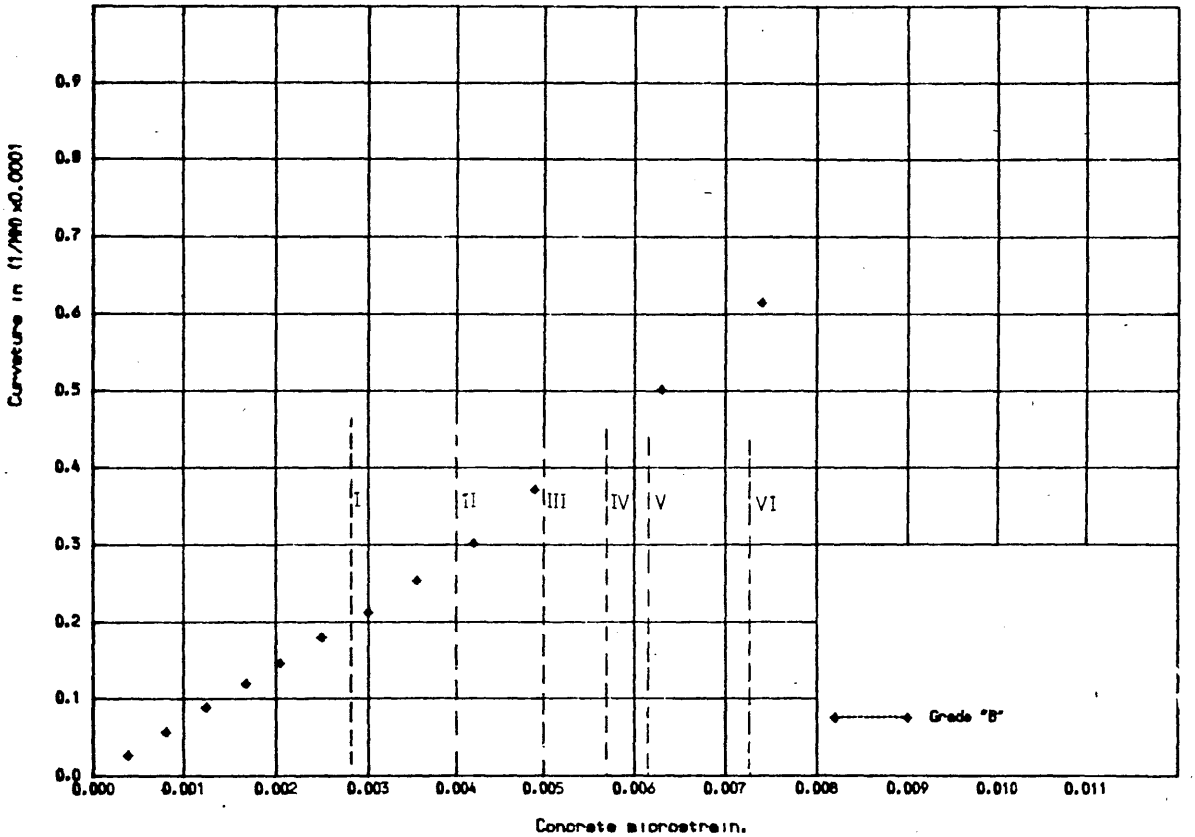

Fig. 5.9-B *CURVATURE VS. CONCRETE STRAIN FOR REINFORCED RE.C. BEAM "B".*

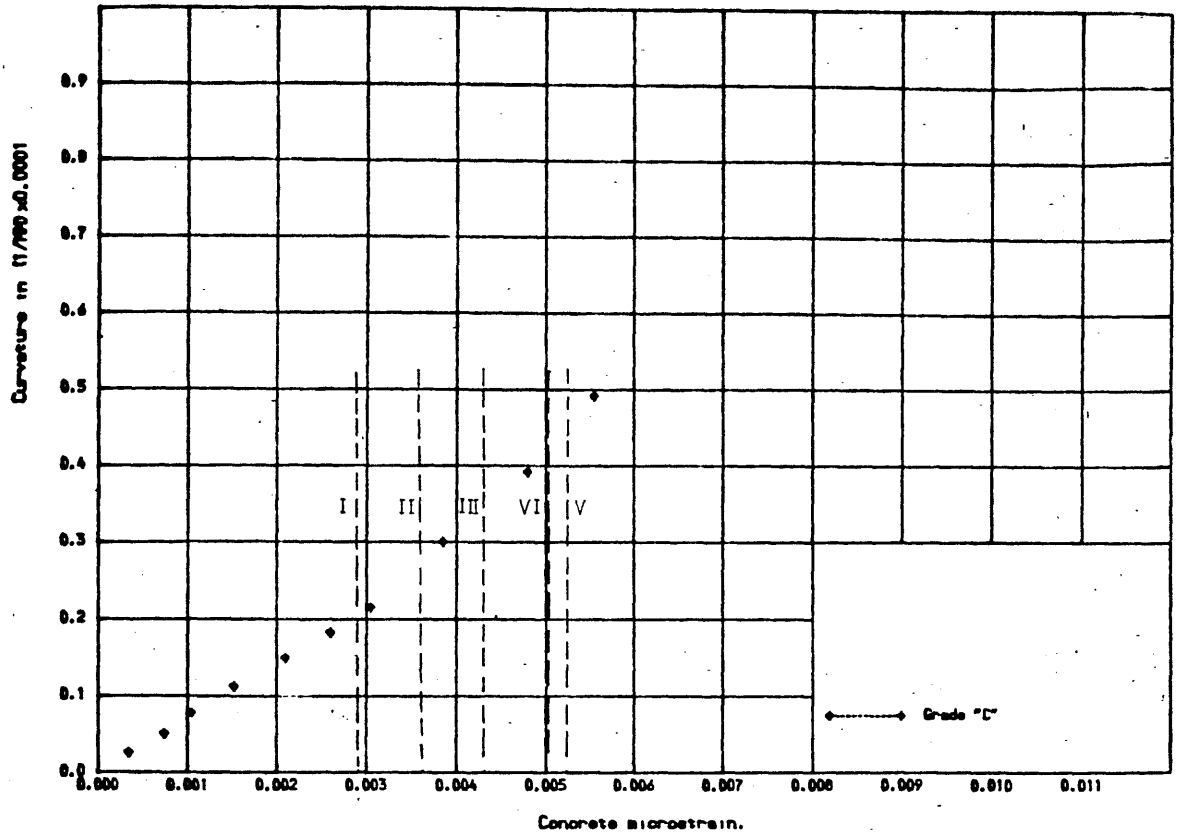

Fig. 5.9-C CURVATURE VS. CONCRETE STRAIN FOR REINFORCED RE.C. BEAM "C".

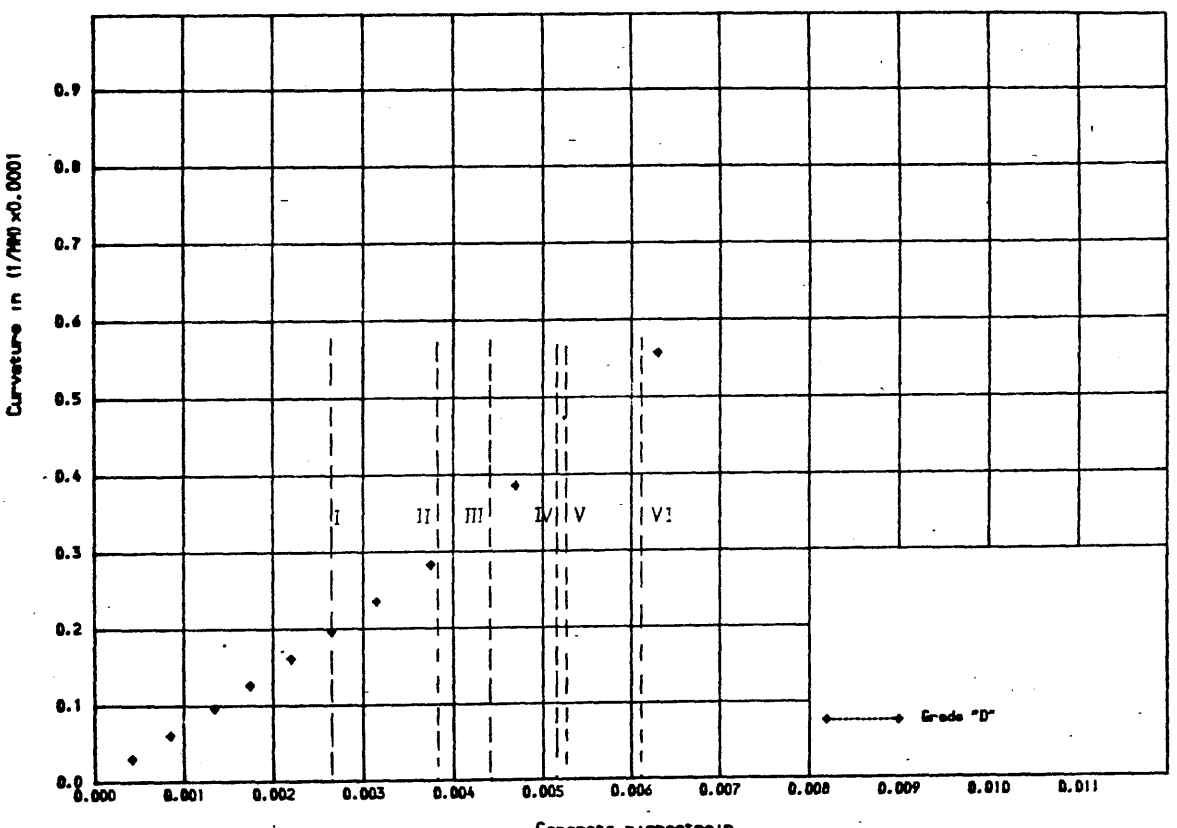

Fig. 5.9-D CURVATURE VS. CONCRETE STRAIN FOR REINFORCED RE.C. BEAM "D".

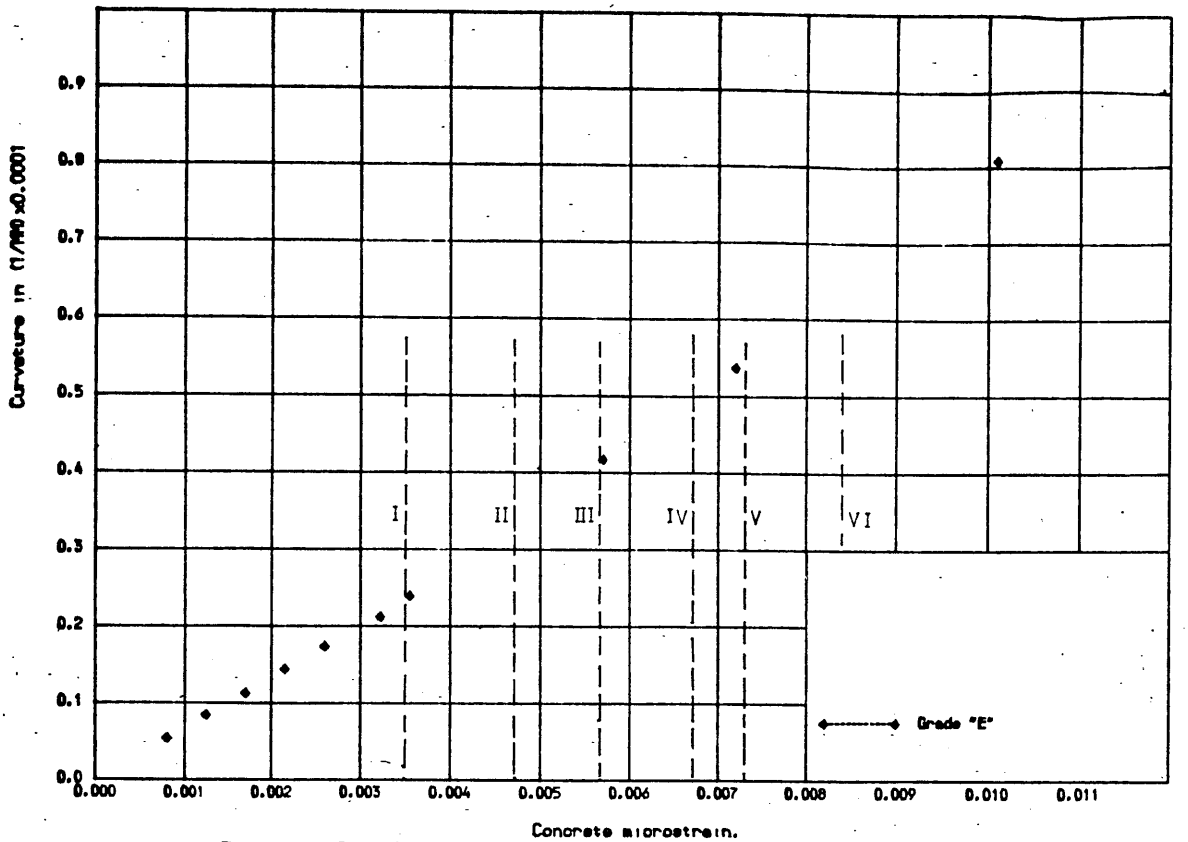

Fig.5.9-E CURVATURE VS. CONCRETE STRAIN FOR REINFORCED RE.C. BEAM "E".

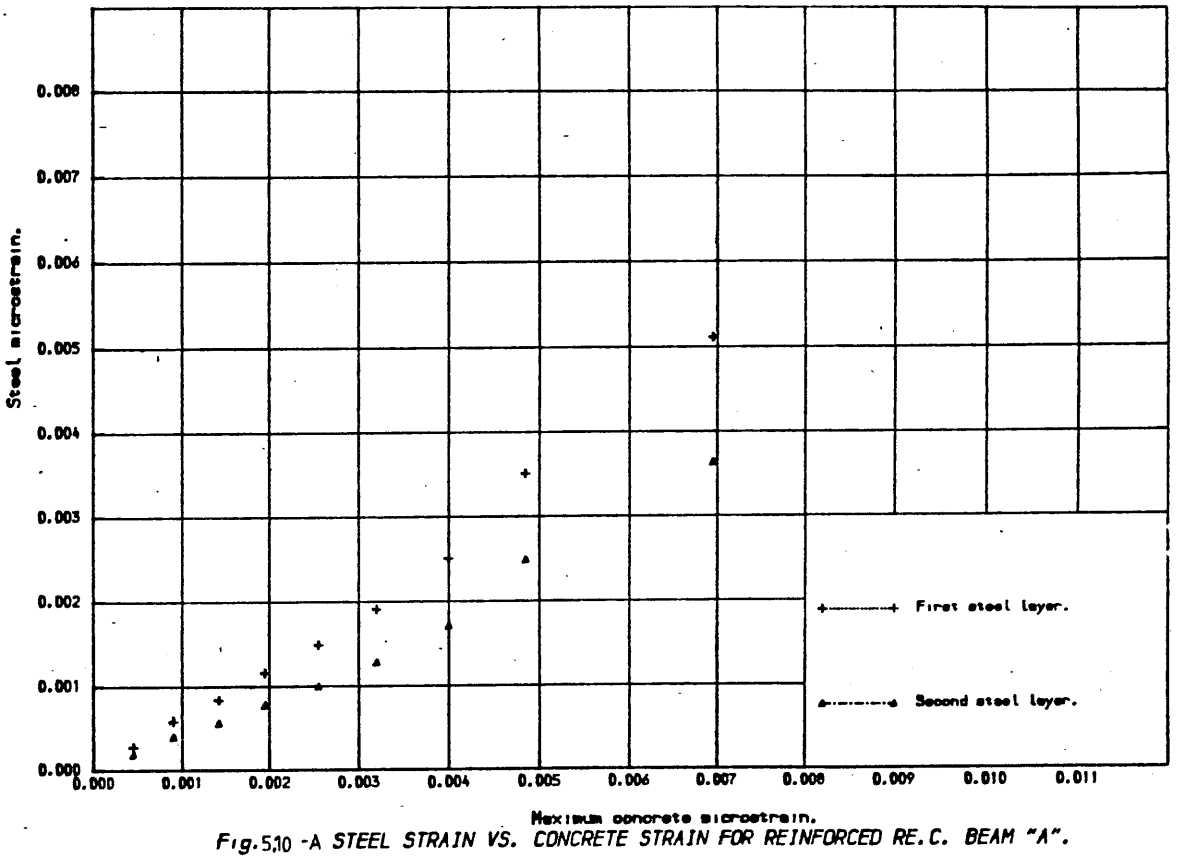

Fig.5.10 -A STEEL STRAIN VS. CONCRETE STRAIN FOR REINFORCED RE.C. BEAM "A".

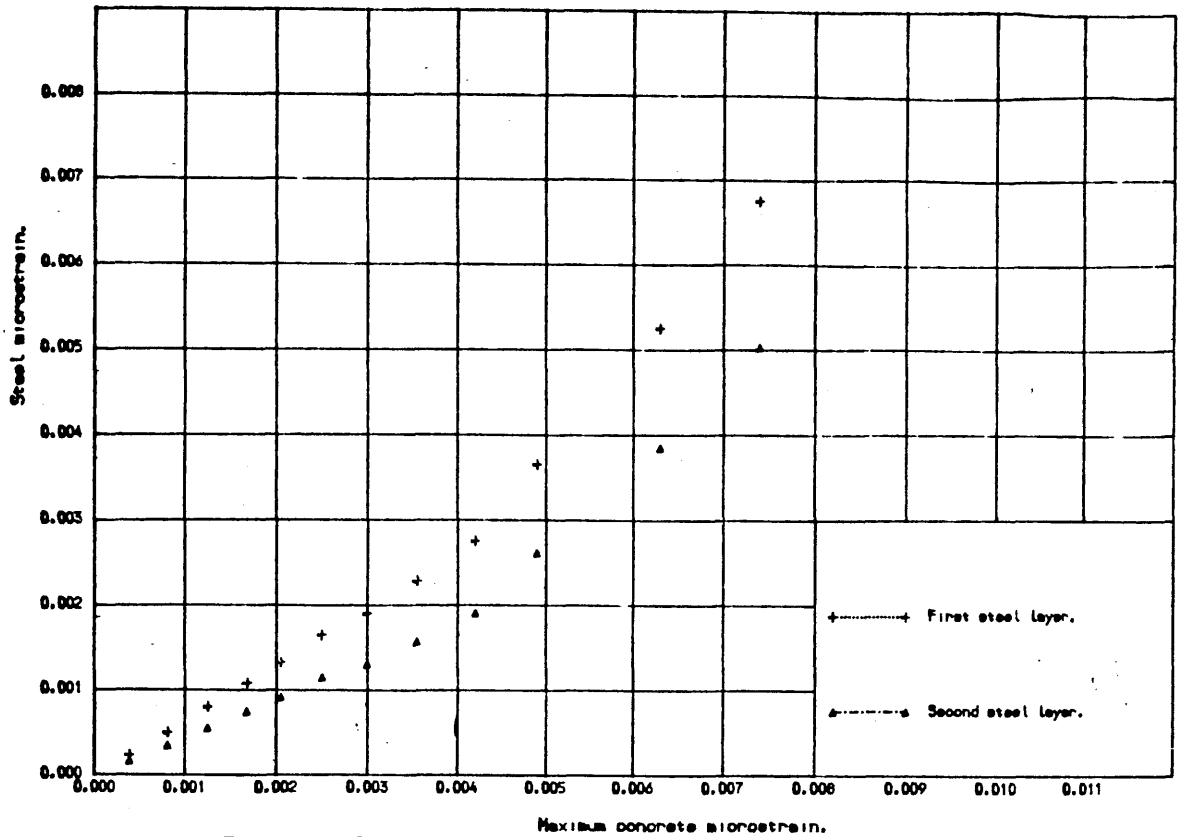

Fig. 5.10-B STEEL STRAIN VS. CONCRETE STRAIN FOR REINFORCED RE.C. BEAM "B".

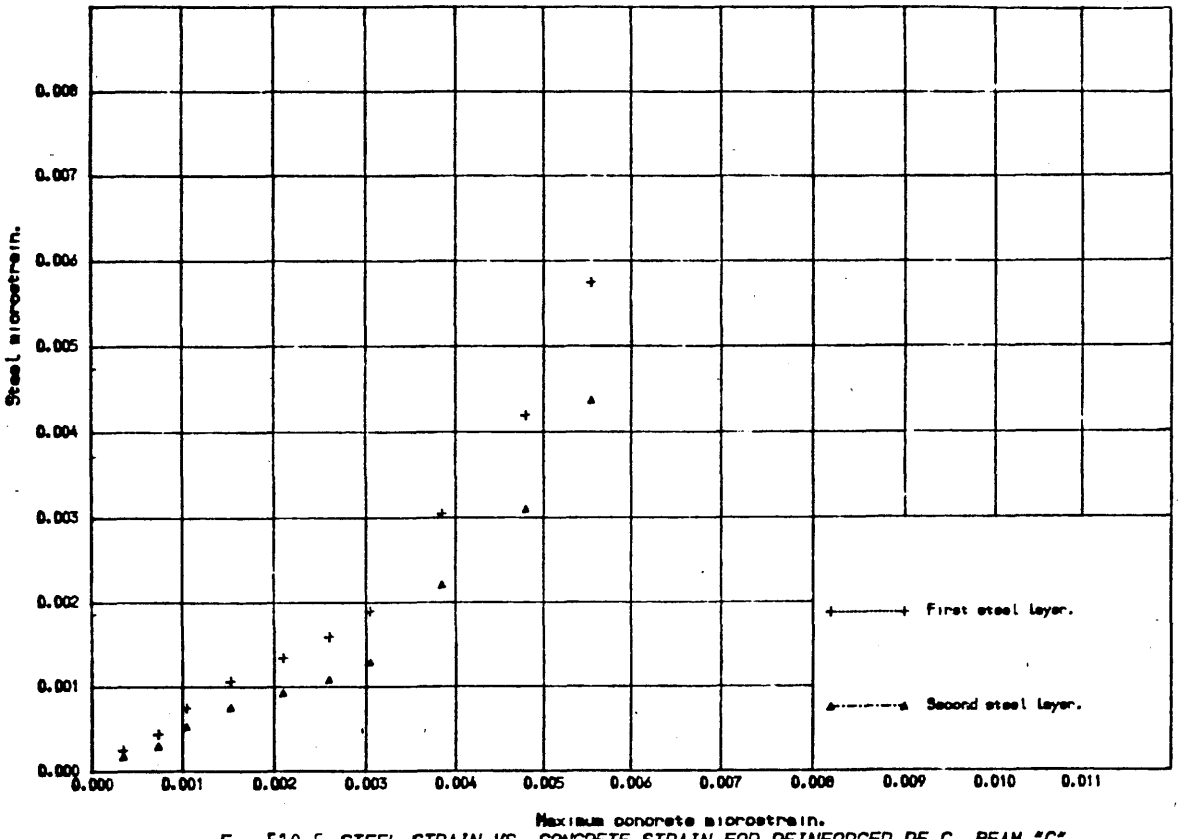

Fig. 5.10-C STEEL STRAIN VS. CONCRETE STRAIN FOR REINFORCED RE.C. BEAM "C".

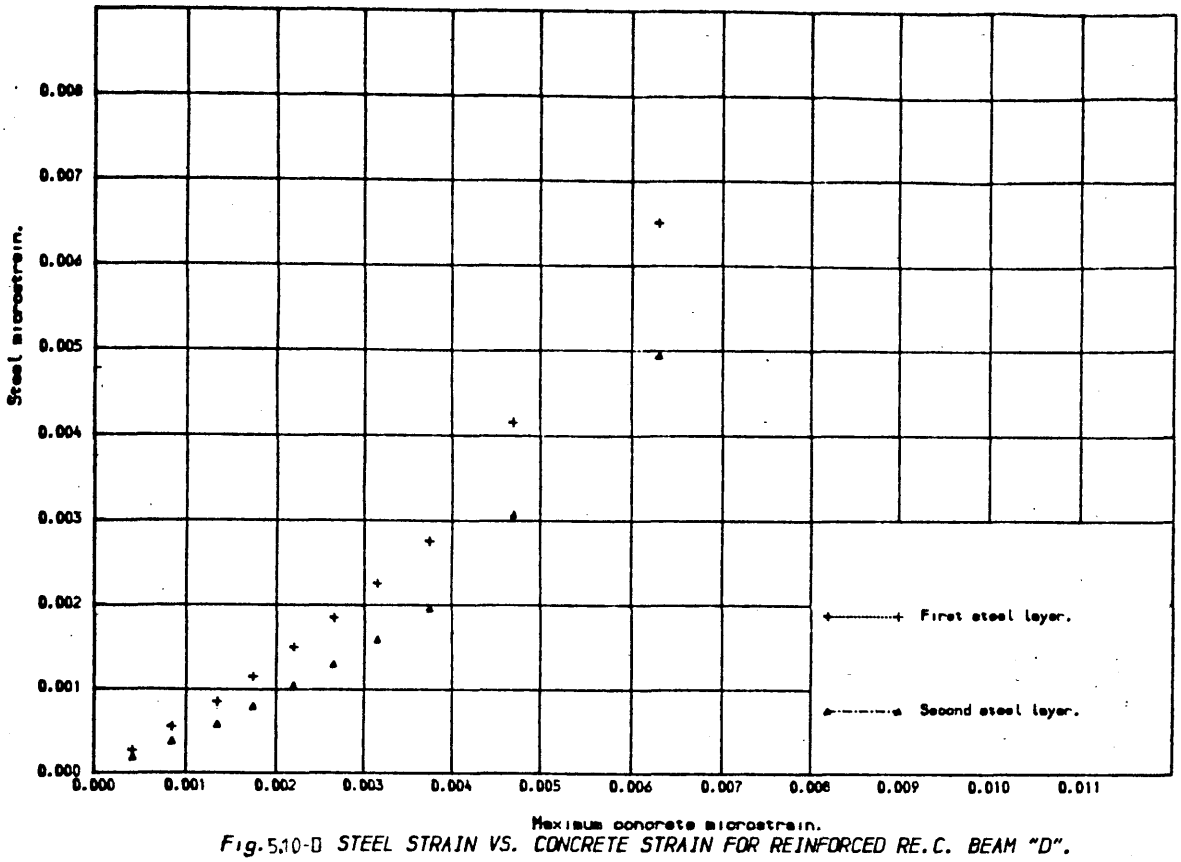

Fig. 5.10-D *STEEL STRAIN VS. CONCRETE STRAIN FOR REINFORCED RE.C. BEAM "D".*

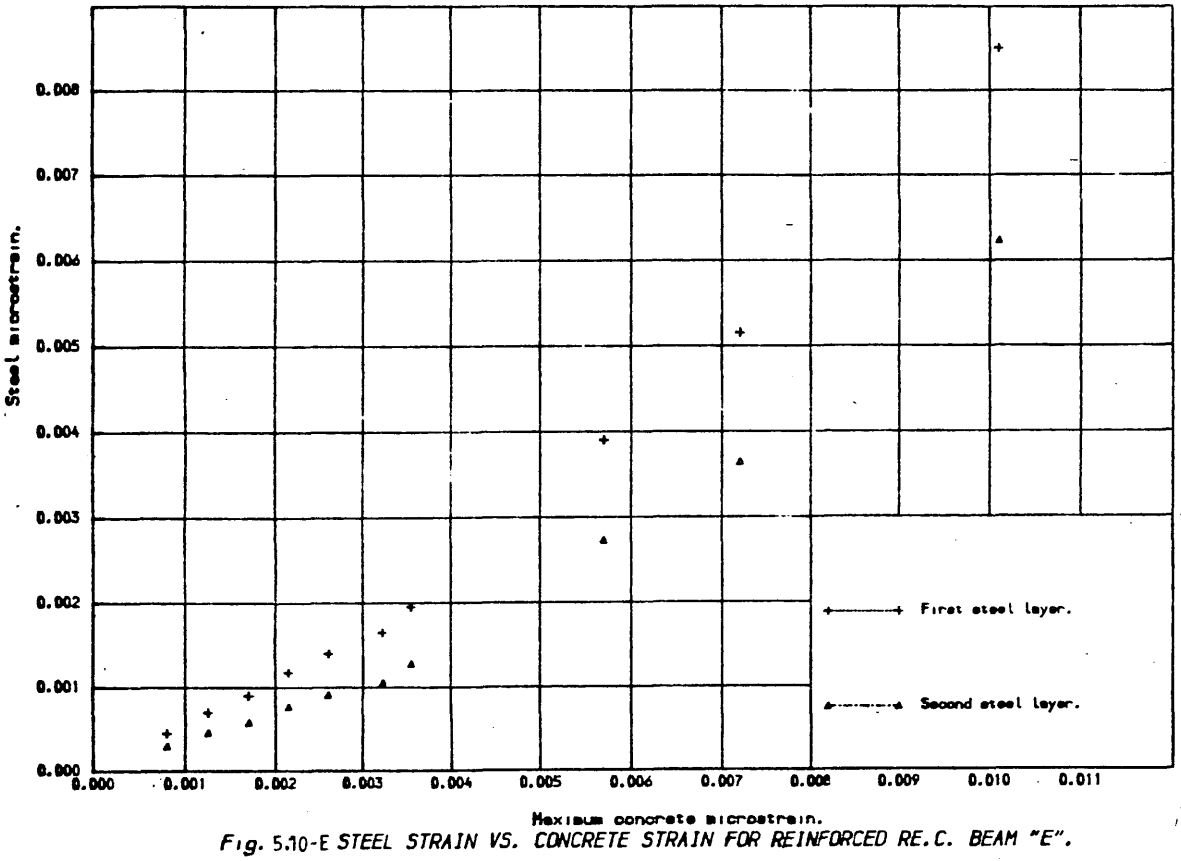

Fig. 5.10-E *STEEL STRAIN VS. CONCRETE STRAIN FOR REINFORCED RE.C. BEAM "E".*

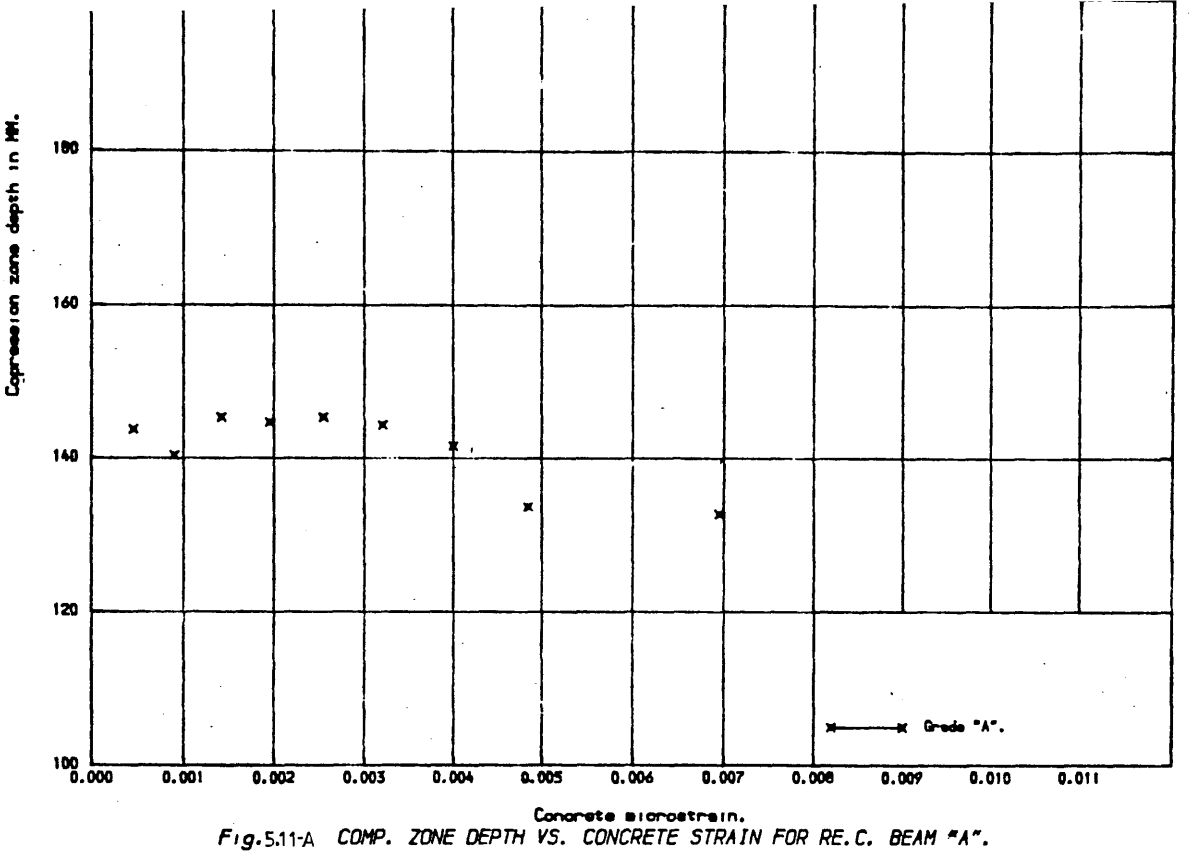

Fig. 5.11-A *COMP. ZONE DEPTH VS. CONCRETE STRAIN FOR RE.C. BEAM "A".*

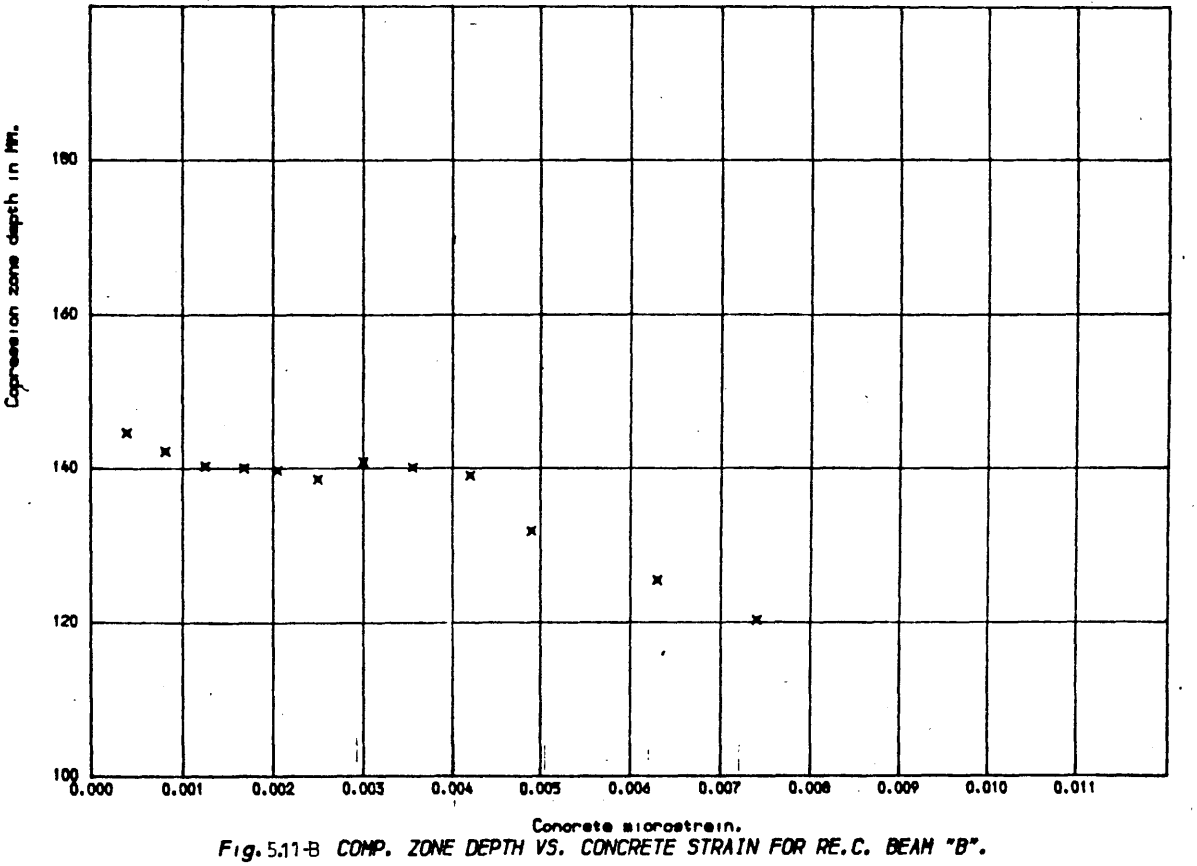

Fig. 5.11-B *COMP. ZONE DEPTH VS. CONCRETE STRAIN FOR RE.C. BEAM "B".*

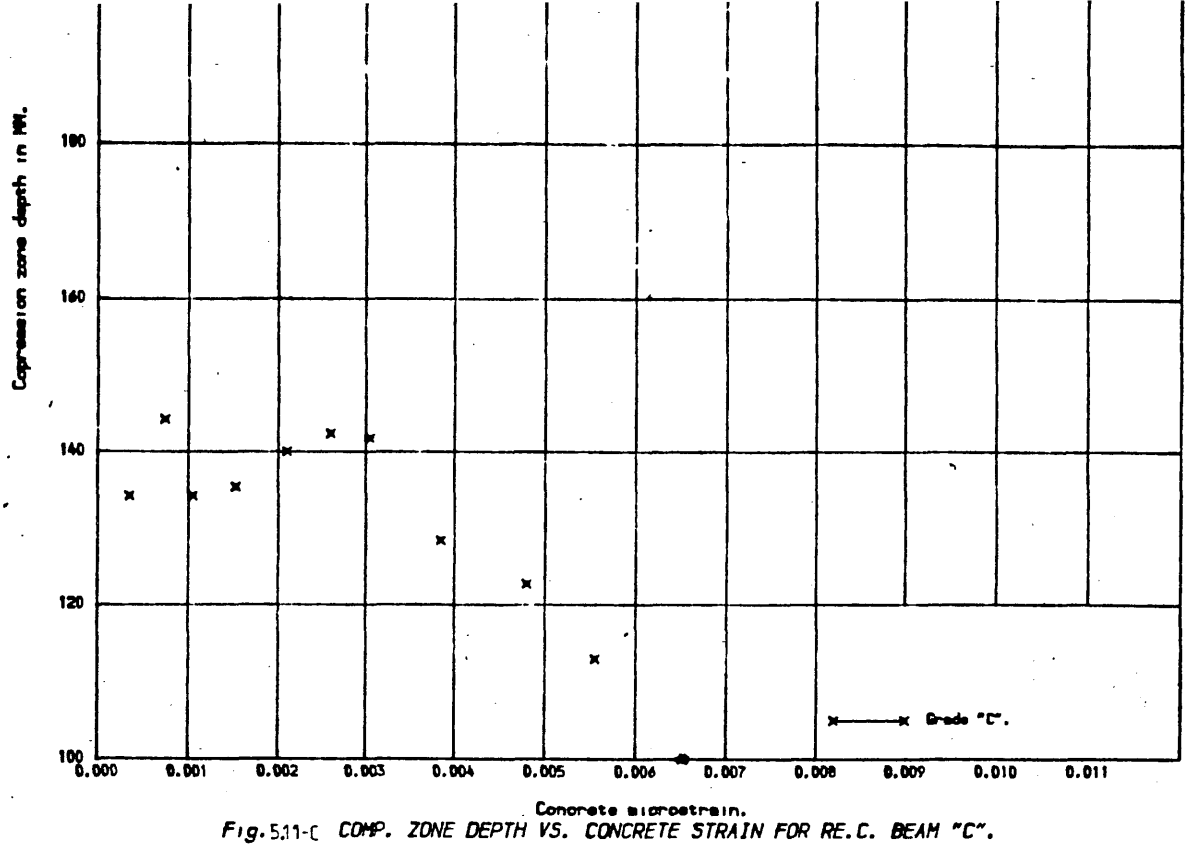

Fig. 5.11-C COMP. ZONE DEPTH VS. CONCRETE STRAIN FOR RE.C. BEAM "C".

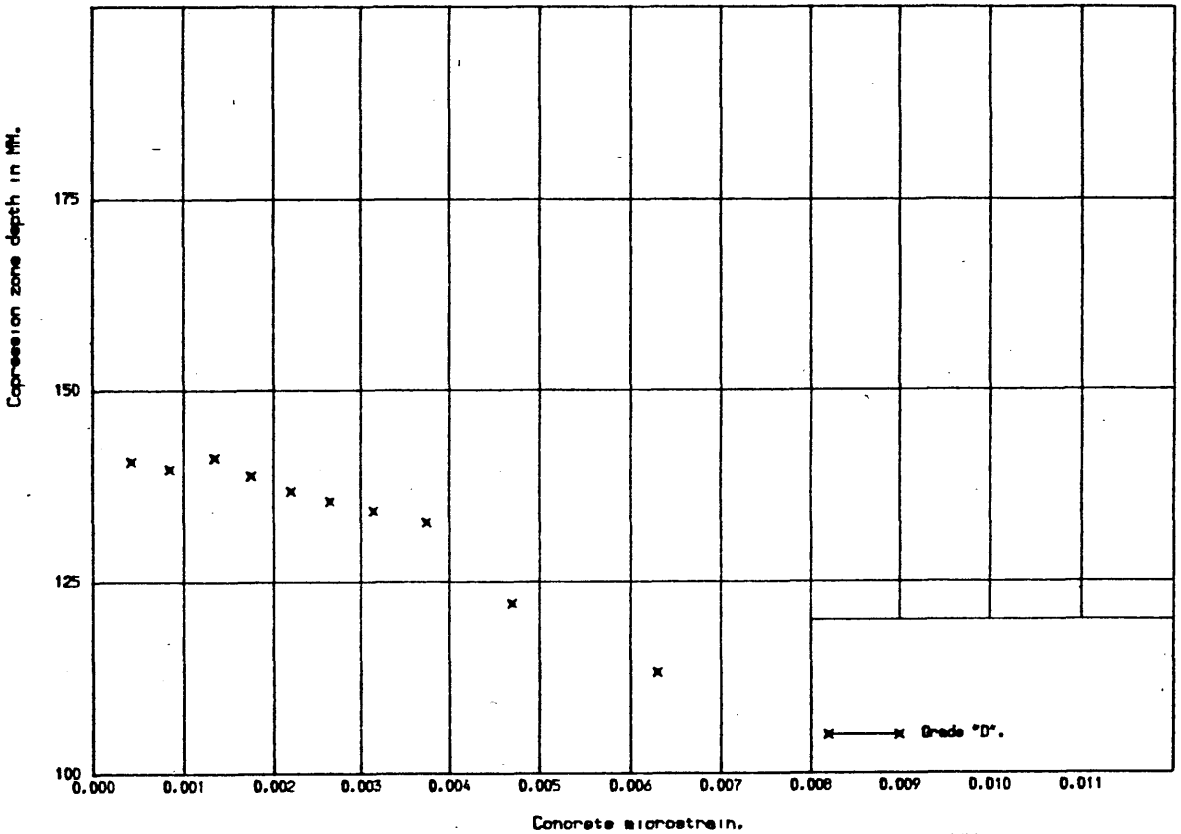

Fig. 5.11-D COMP. ZONE DEPTH VS. CONCRETE STRAIN FOR RE.C. BEAM "D".

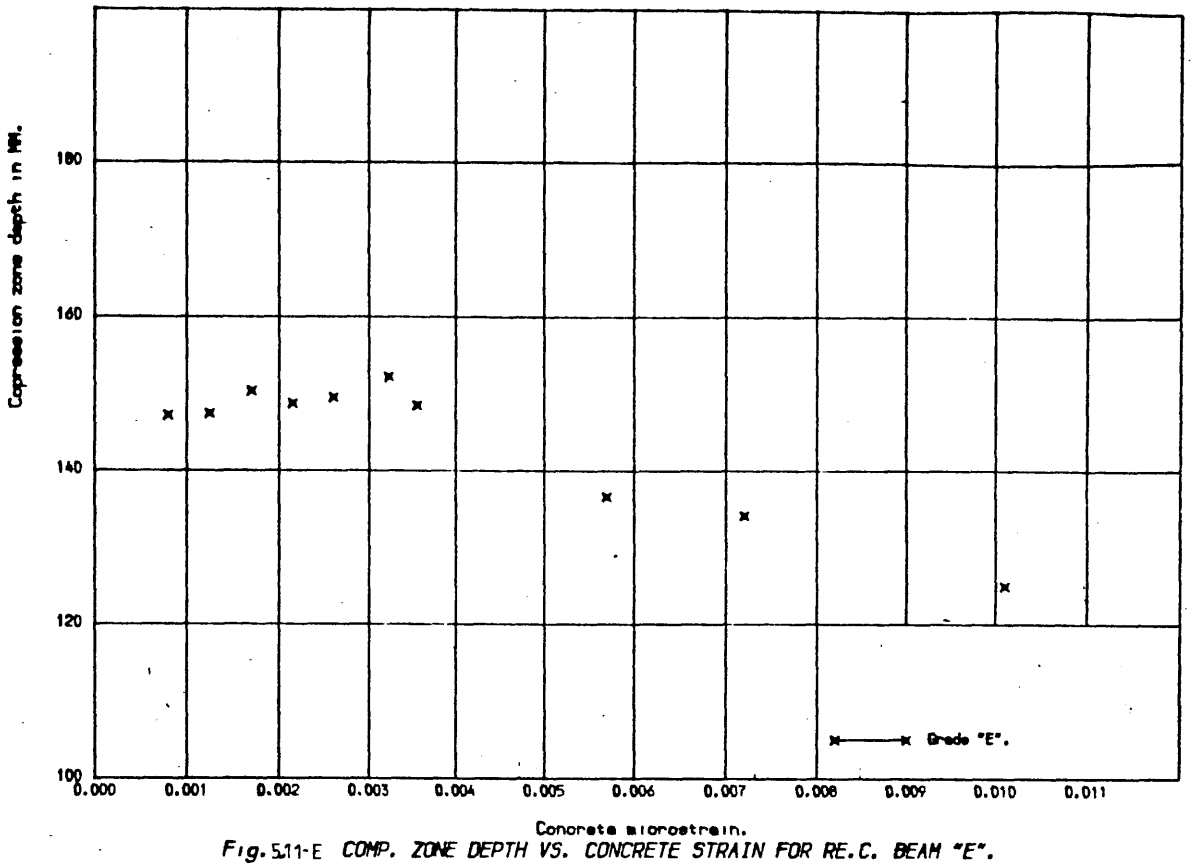

Fig. 5.11-E *COMP. ZONE DEPTH VS. CONCRETE STRAIN FOR RE.C. BEAM "E".*

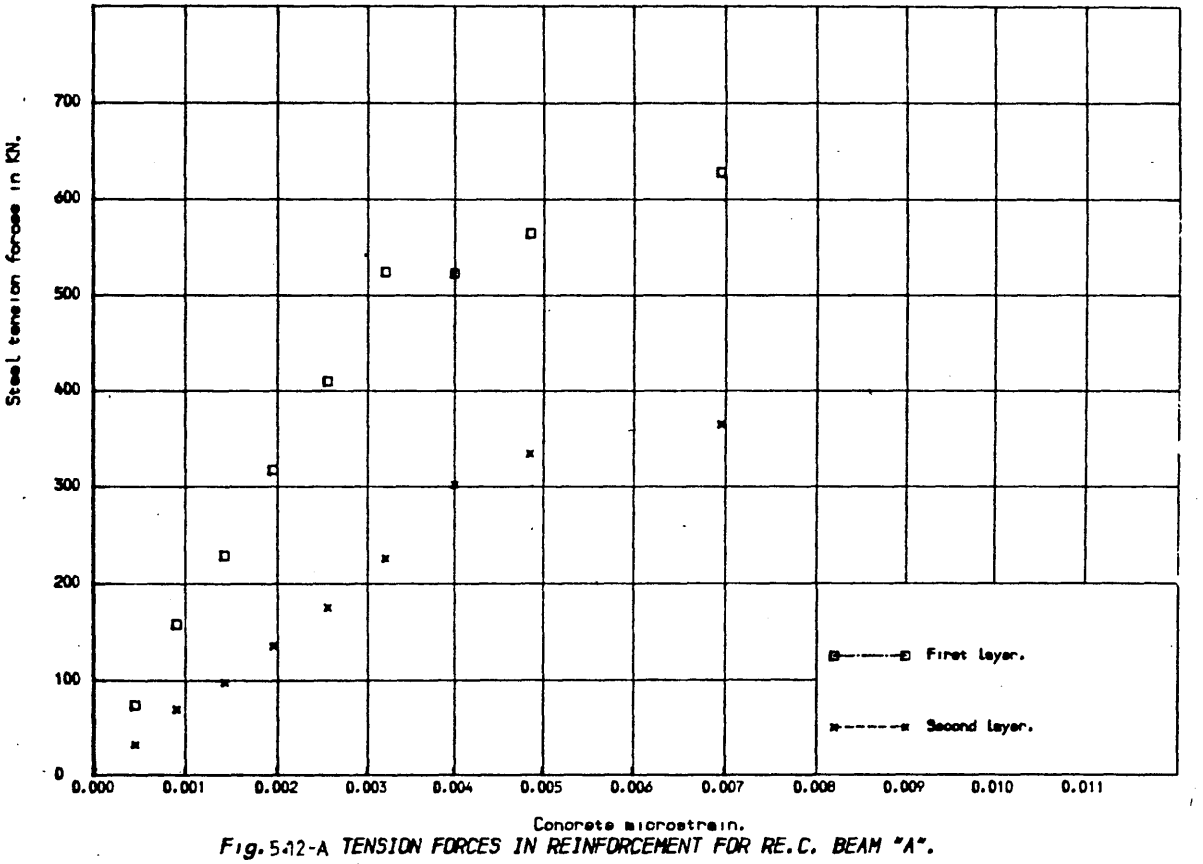

Fig. 5.12-A *TENSION FORCES IN REINFORCEMENT FOR RE.C. BEAM "A".*

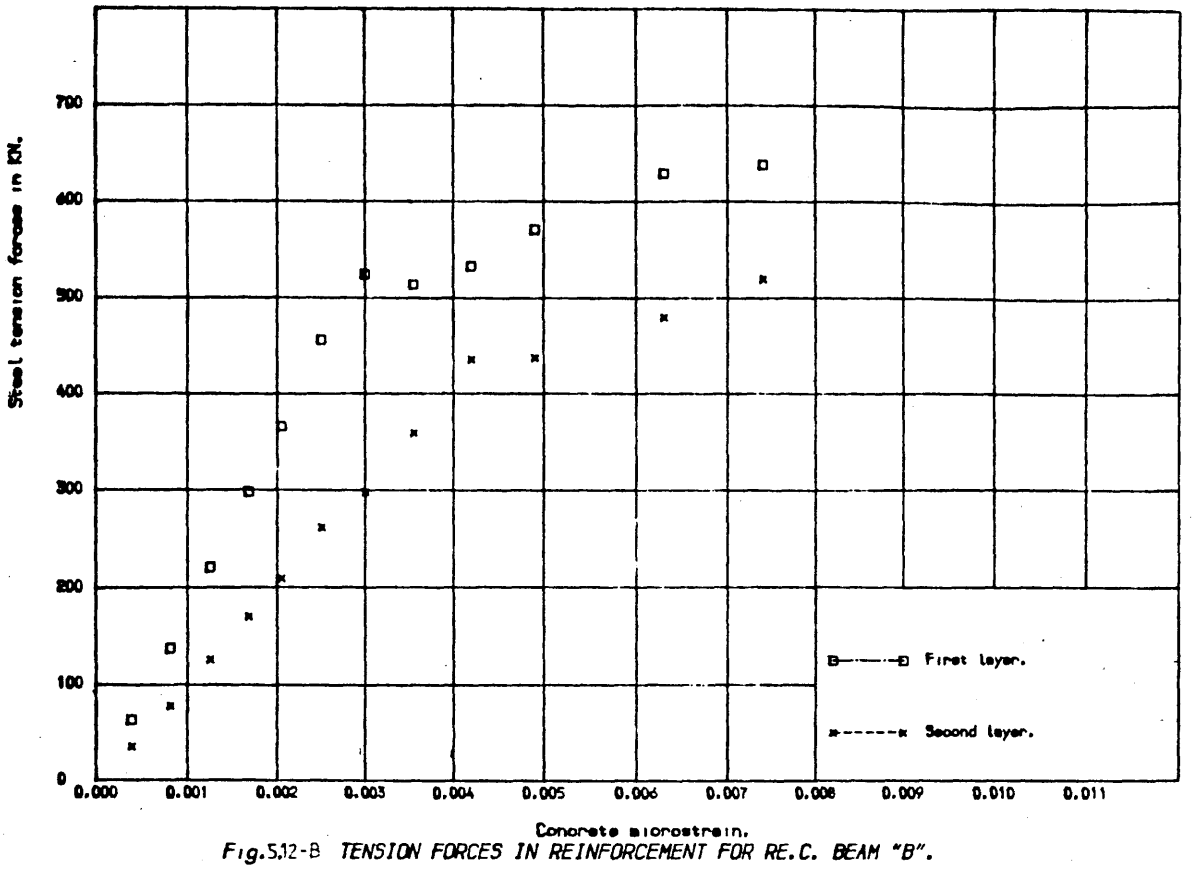

*Fig.*5.12-B *TENSION FORCES IN REINFORCEMENT FOR RE.C. BEAM "B".*

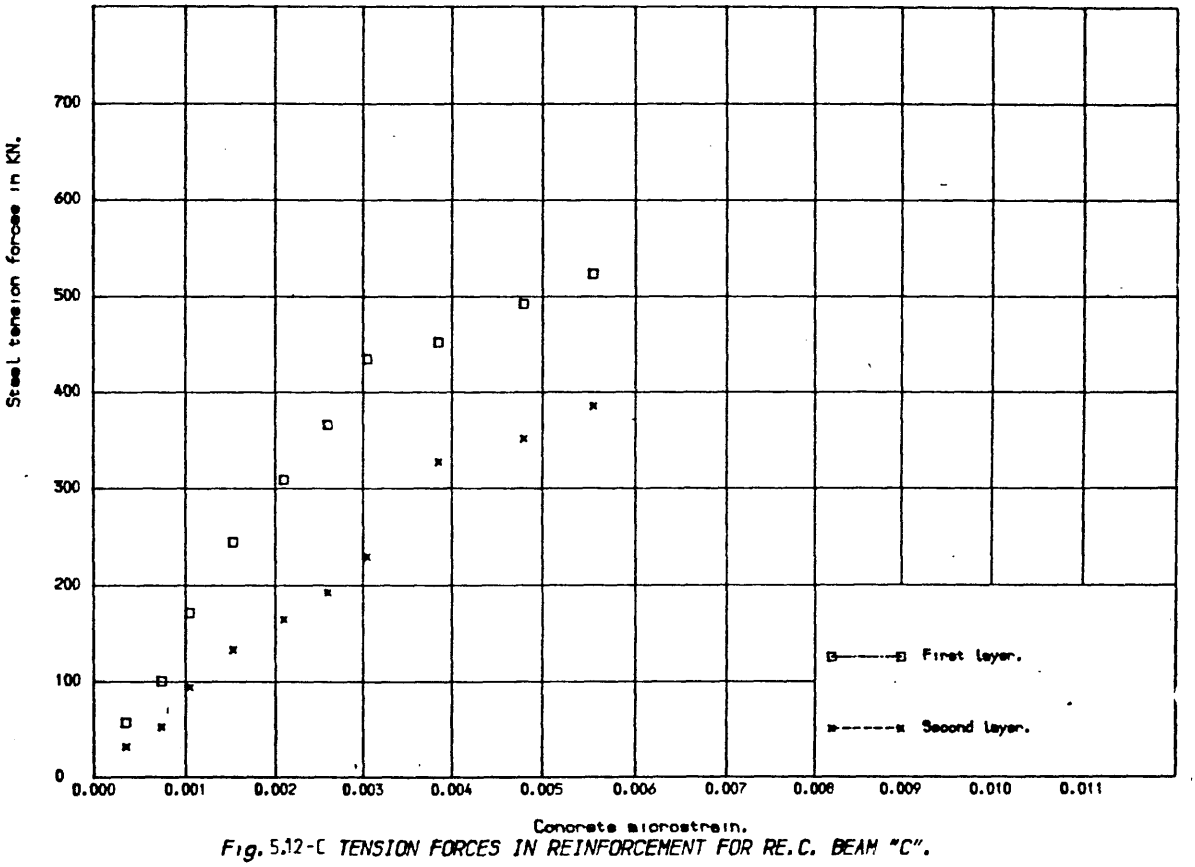

Fig. 5.12-C *TENSION FORCES IN REINFORCEMENT FOR RE.C. BEAM "C".*

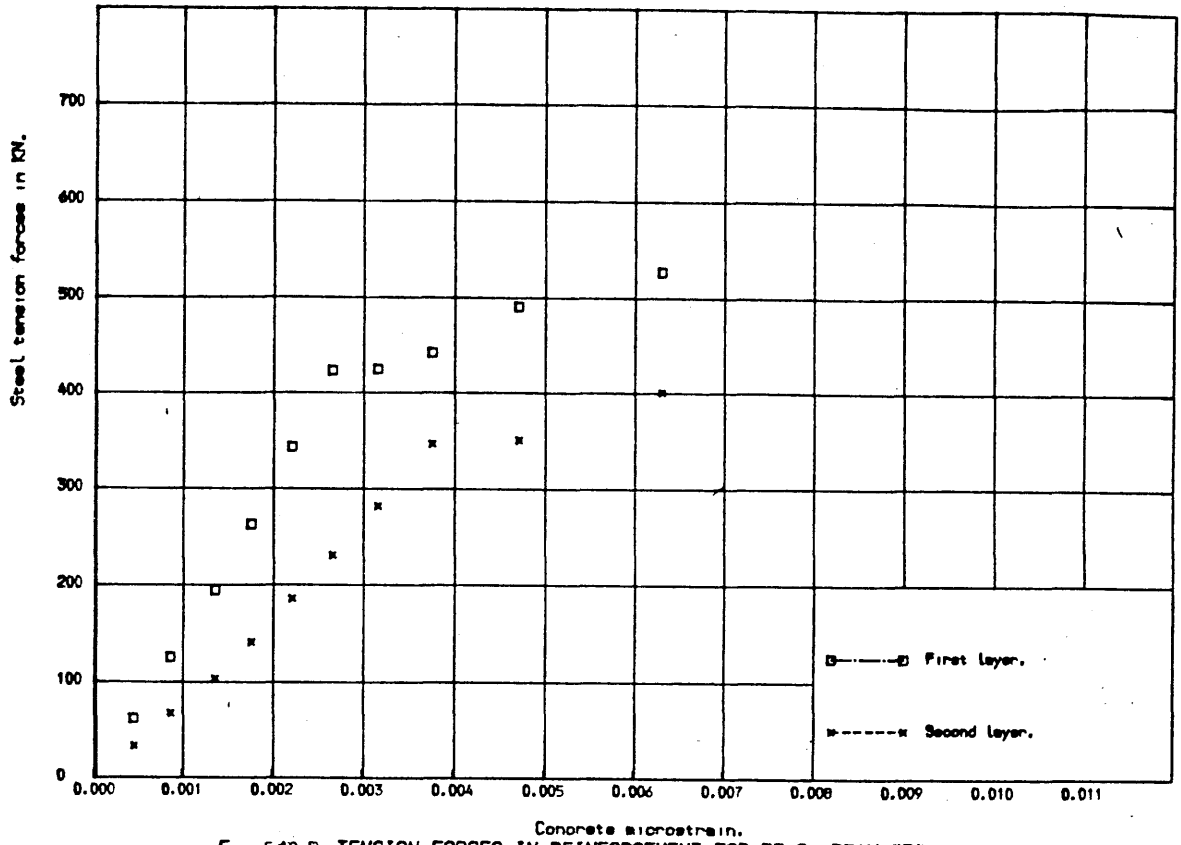

*Fig.*5.12-D *TENSION FORCES IN REINFORCEMENT FOR RE.C. BEAM "D".*

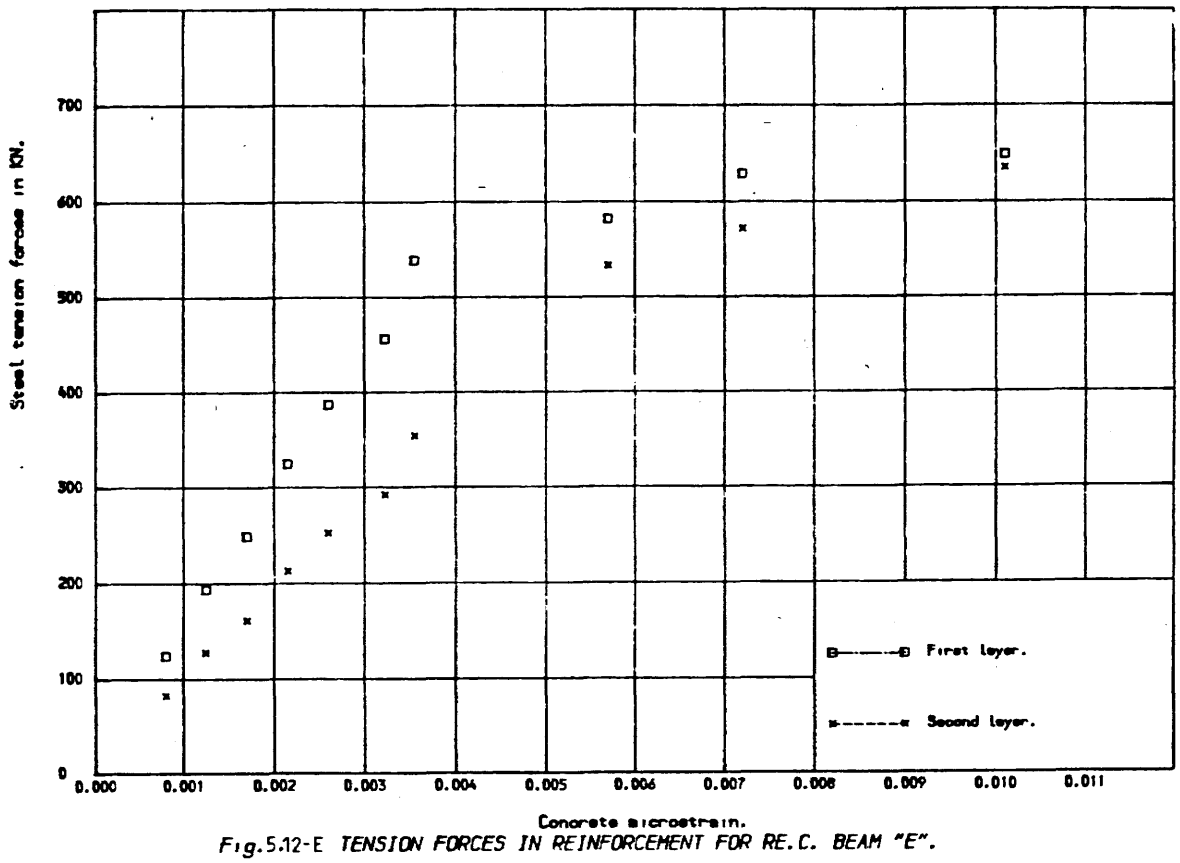

*Fig.*5.12-E *TENSION FORCES IN REINFORCEMENT FOR RE.C. BEAM "E".*

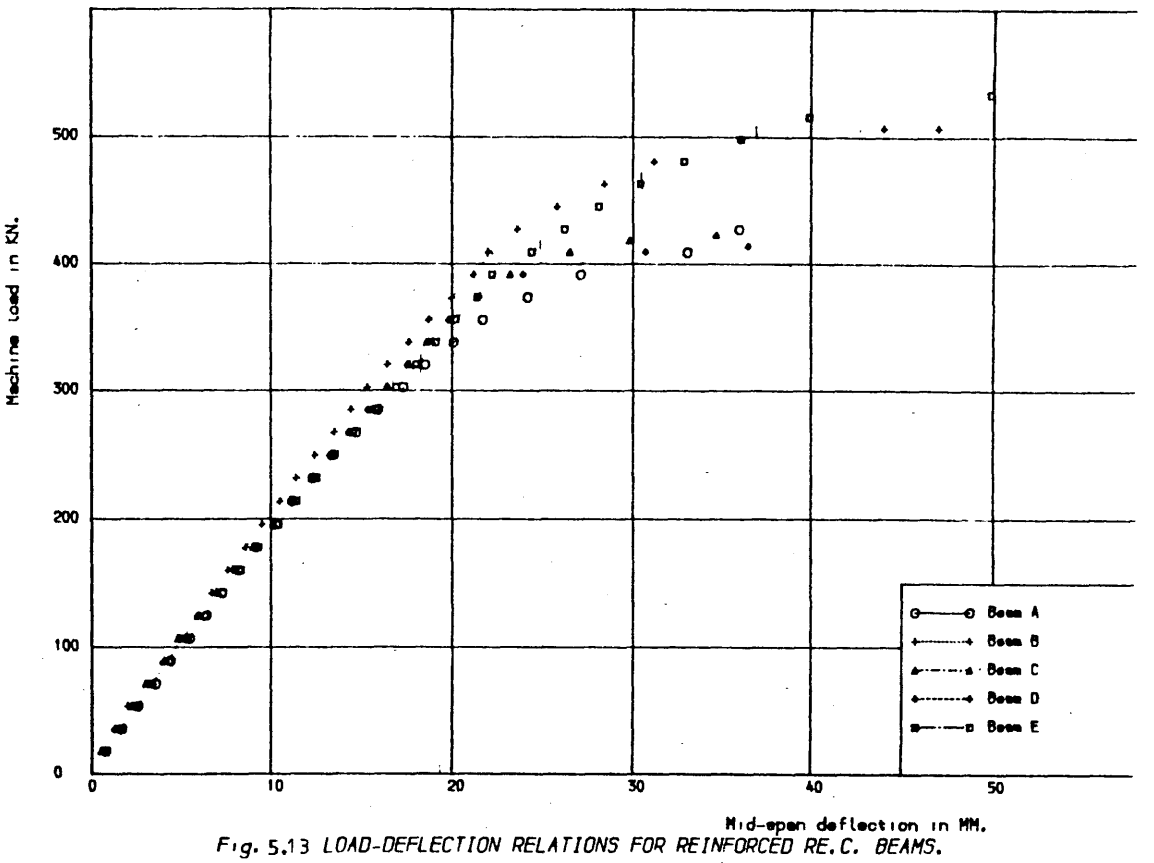

Fig. 5.13 LOAD-DEFLECTION RELATIONS FOR REINFORCED RE.C. BEAMS.

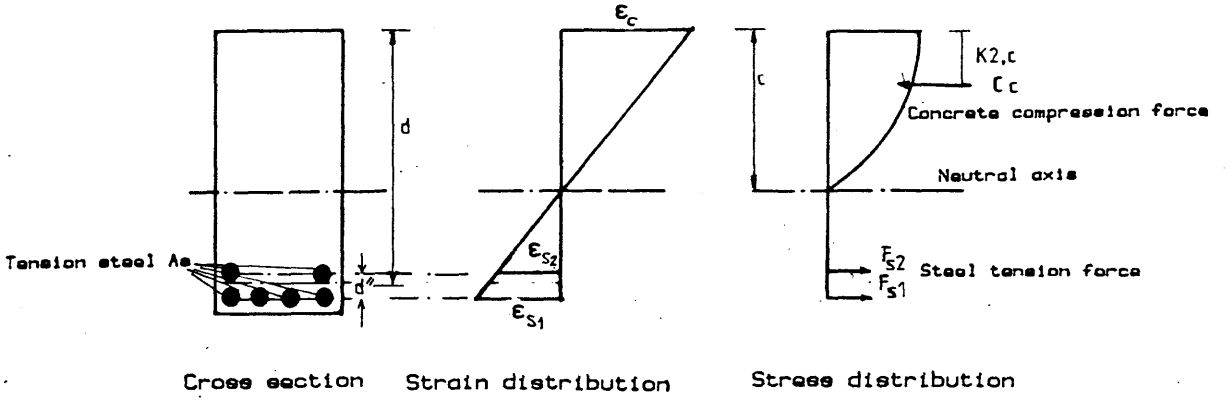

Fig. 5.14 Notations of rectangular cross section at ultimate strength in pure flexure.

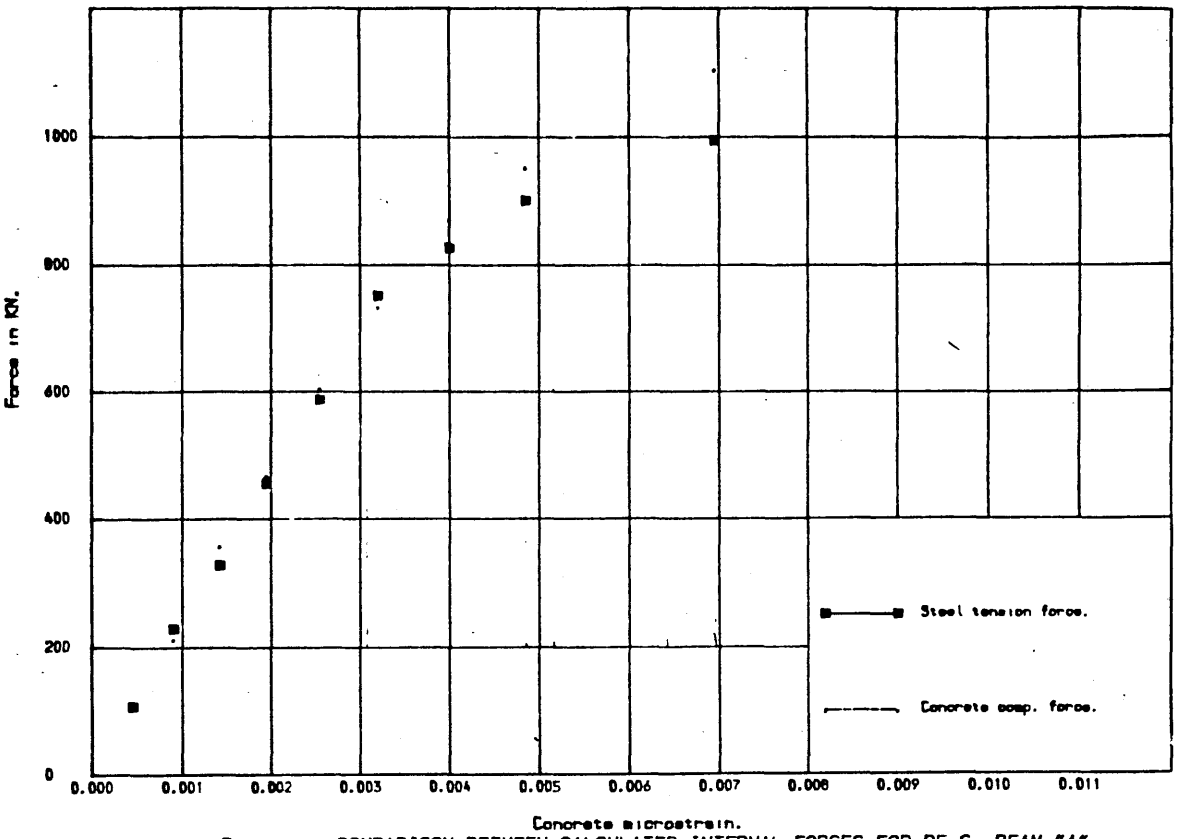

Fig. 5.15-A *COMPARISON BETWEEN CALCULATED INTERNAL FORCES FOR RE.C. BEAM "A".*

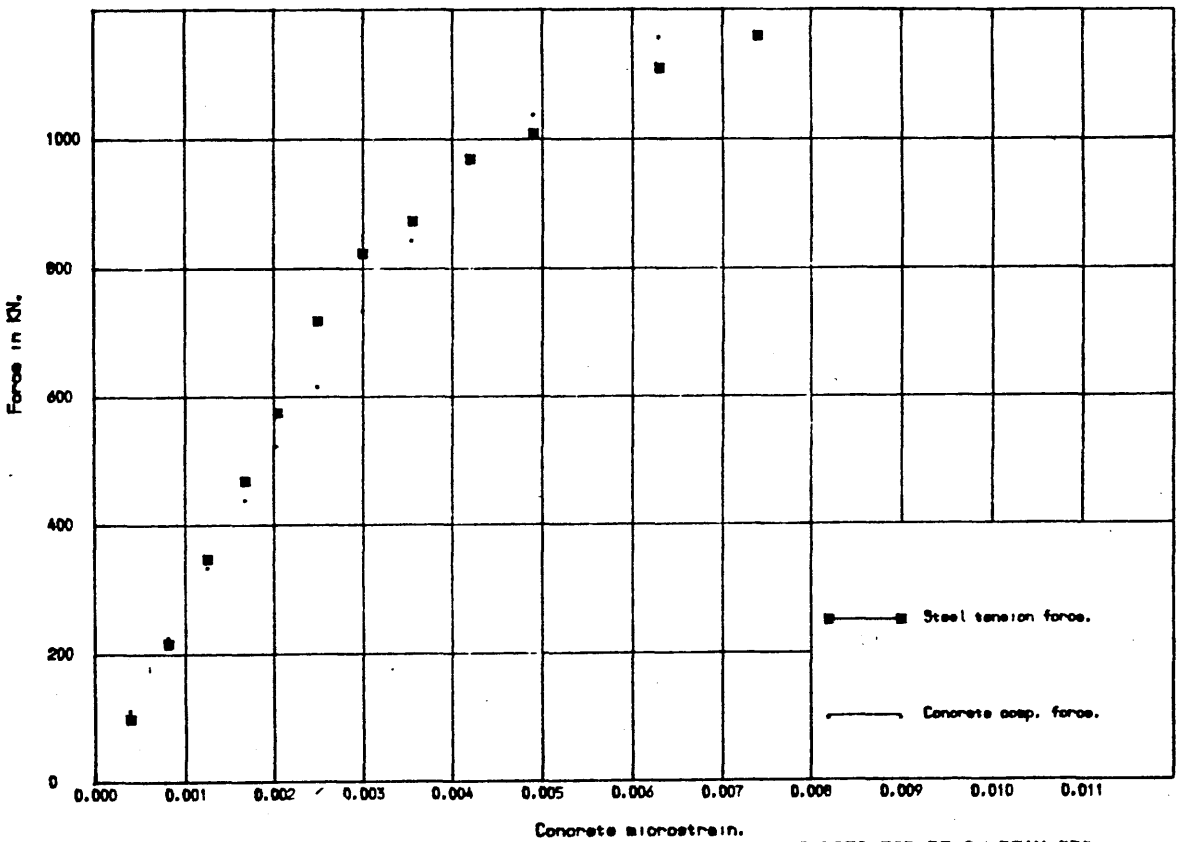

Fig. 5.15-B *COMPARISON BETWEEN CALCULATED INTERNAL FORCES FOR RE.C. BEAM "B".*

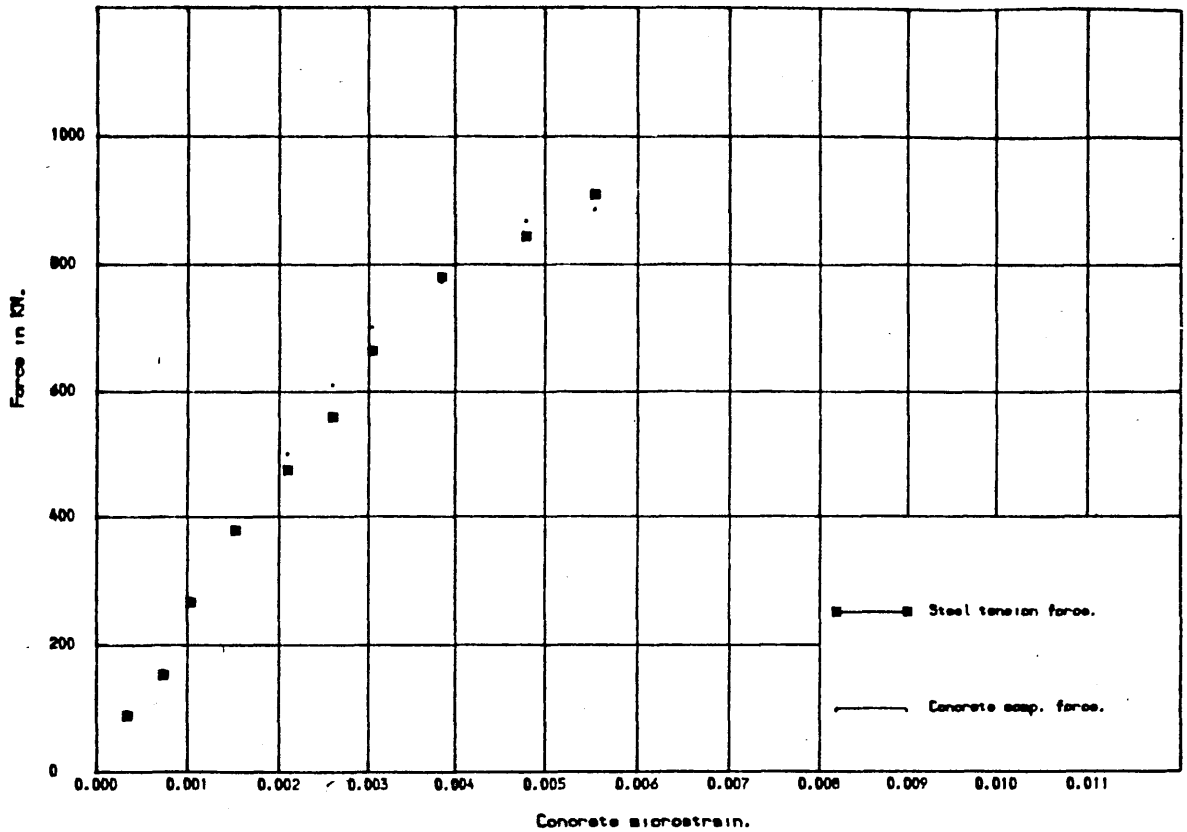

Fig. 5.15-C *COMPARISON BETWEEN CALCULATED INTERNAL FORCES FOR RE.C. BEAM "C".*

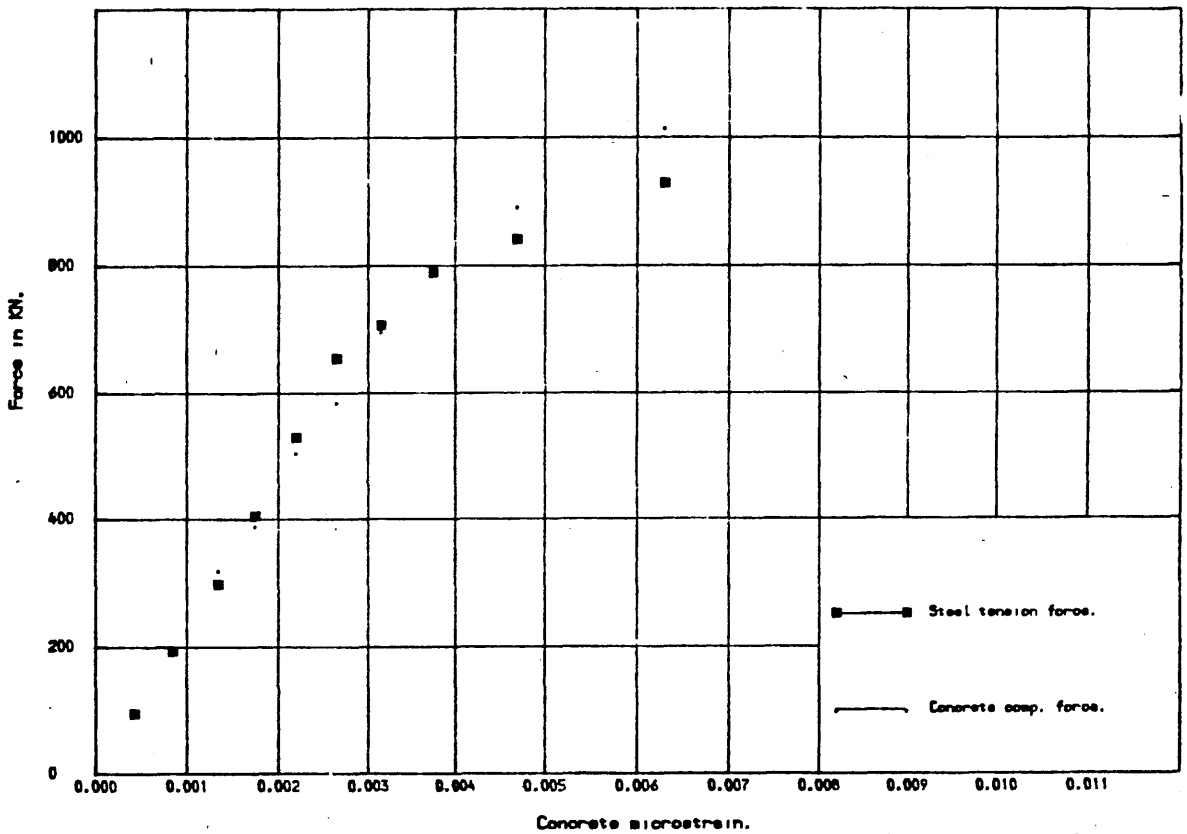

Fig. 5.15-D *COMPARISON BETWEEN CALCULATED INTERNAL FORCES FOR RE.C. BEAM "D".*

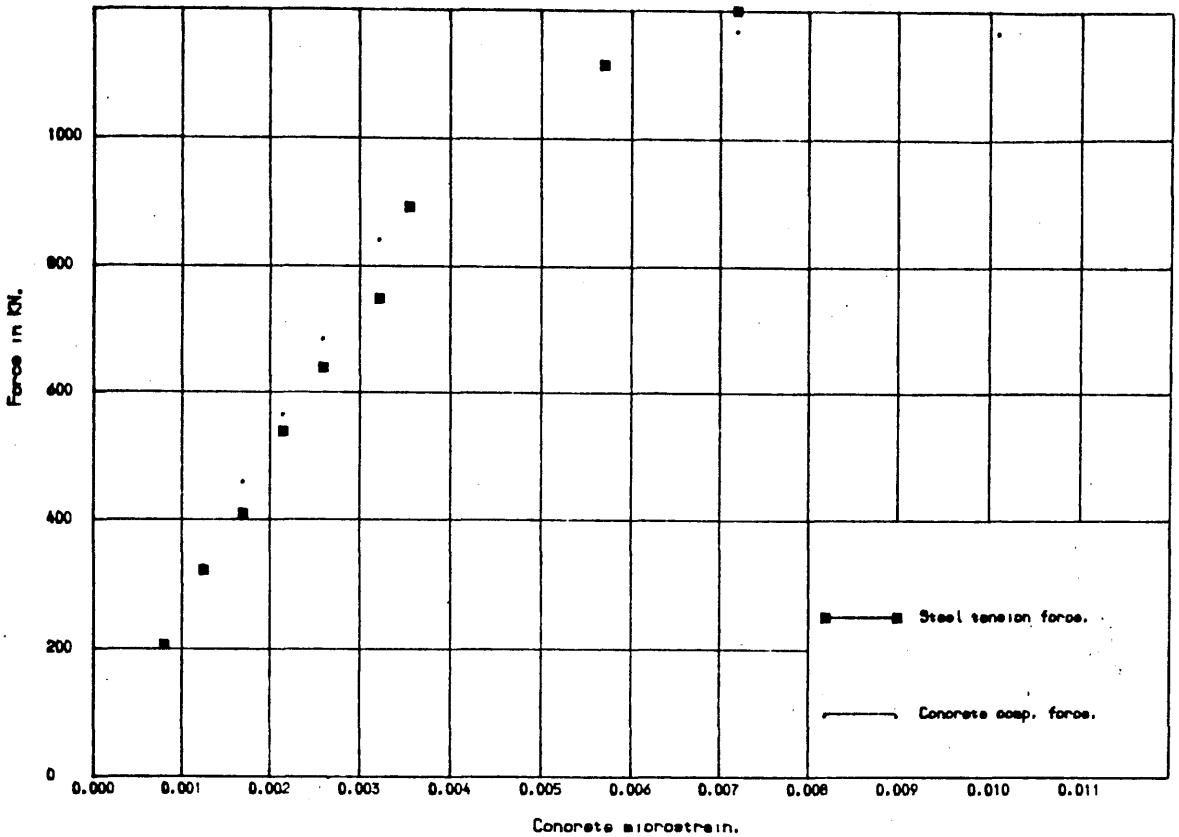

Fig. 5.15-E *COMPARISON BETWEEN CALCULATED INTERNAL FORCES FOR RE.C. BEAM "E".*

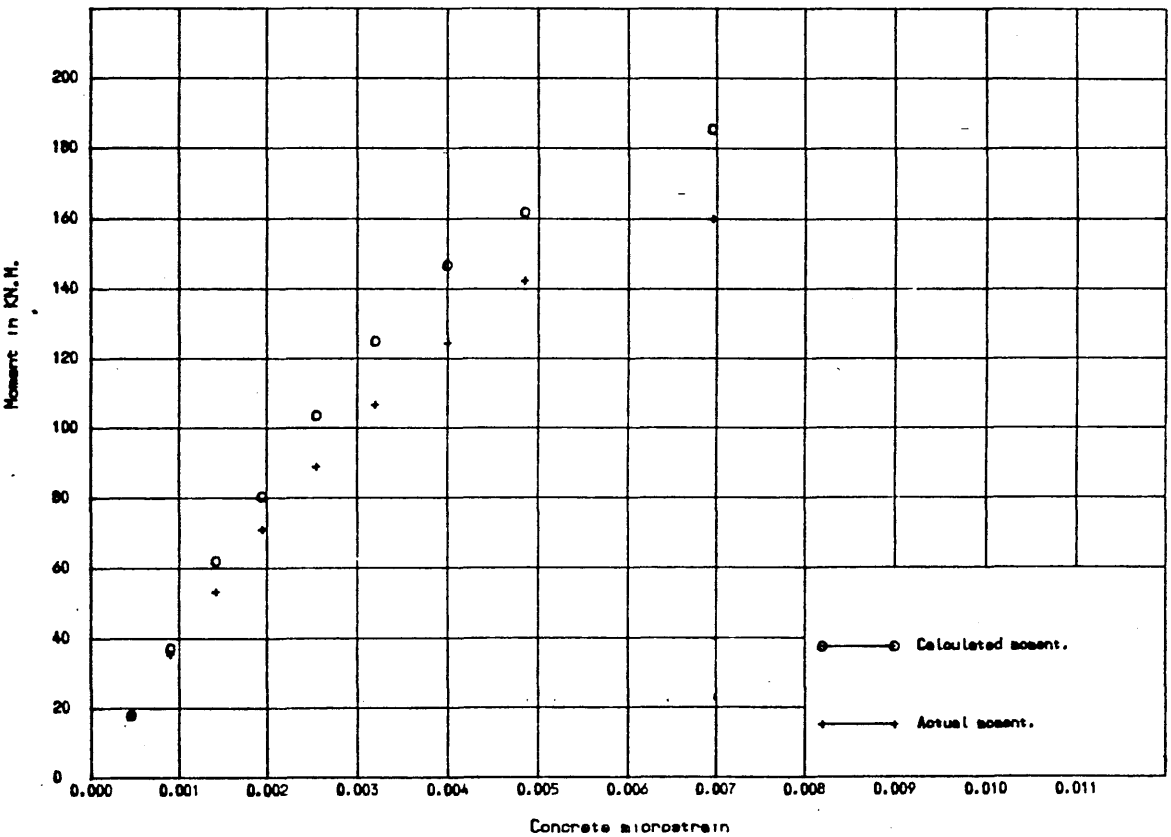

Fig. 5.16-A *COMPARISON BET. CALCULATED & ACTUAL MOMENT FOR RE.C. BEAM "A".*

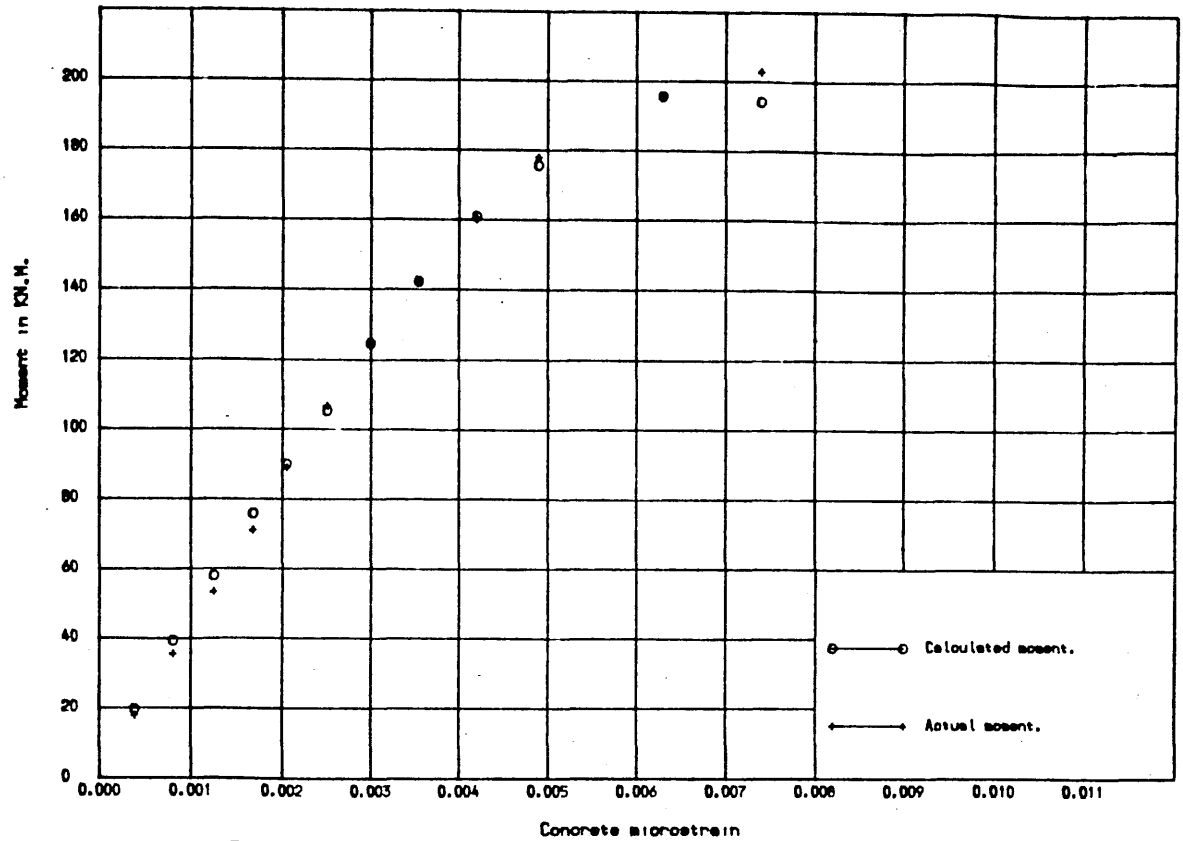

Fig.5.16-B COMPARISON BET. CALCULATED & ACTUAL MOMENT FOR RE.C. BEAM "B".

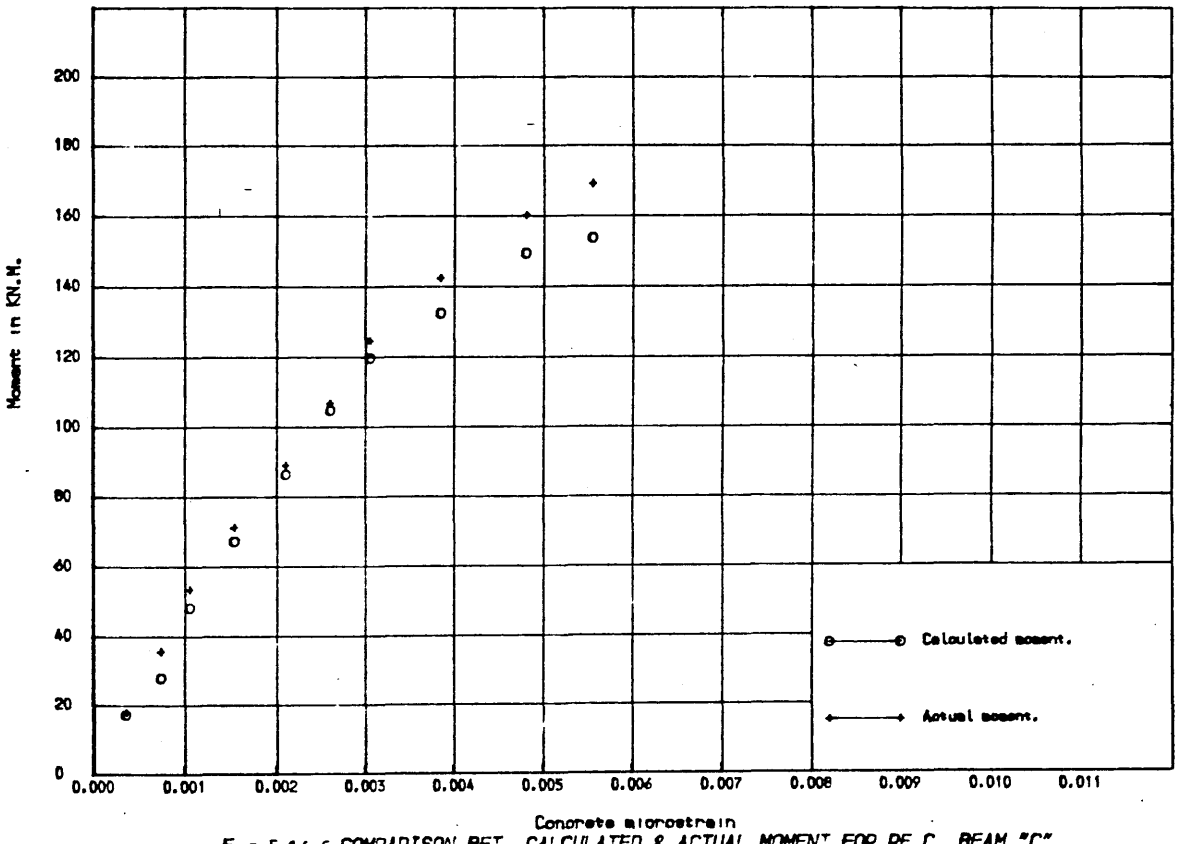

Fig.5.16-C COMPARISON BET. CALCULATED & ACTUAL MOMENT FOR RE.C. BEAM "C".

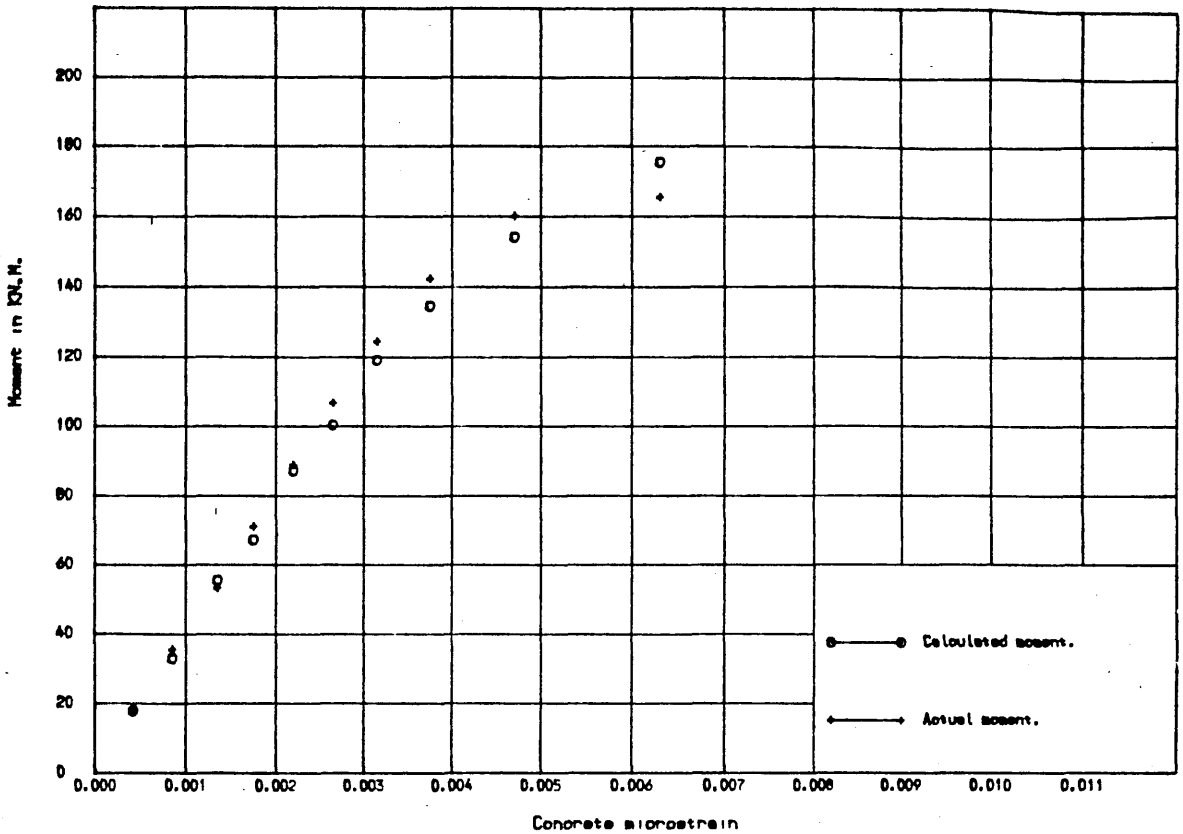

Fig. 5.16-D *COMPARISON BET. CALCULATED & ACTUAL MOMENT FOR RE.C. BEAM "D".*

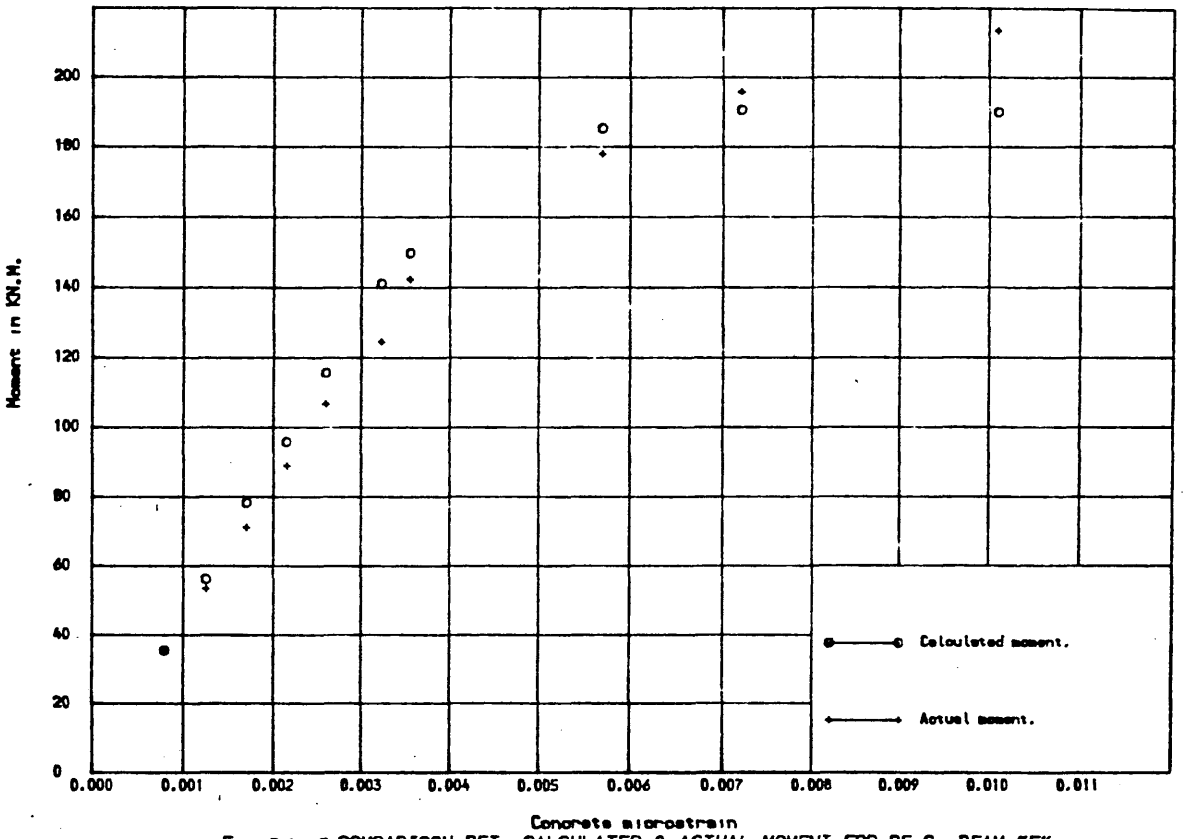

Fig. 5.16-E *COMPARISON BET. CALCULATED & ACTUAL MOMENT FOR RE.C. BEAM "E".*

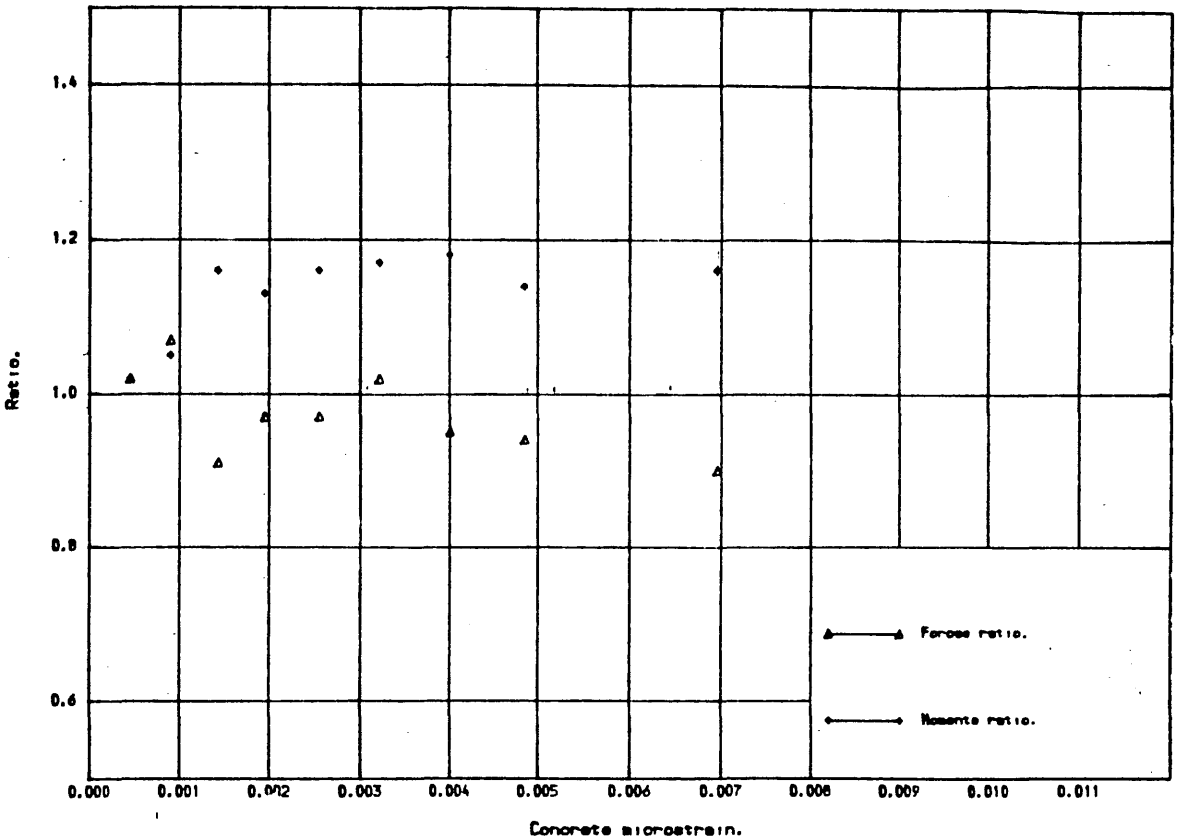

*Fig.*5.17-A *FORCES & MOMENTS RATIOS FOR RE.C. BEAM "A".*

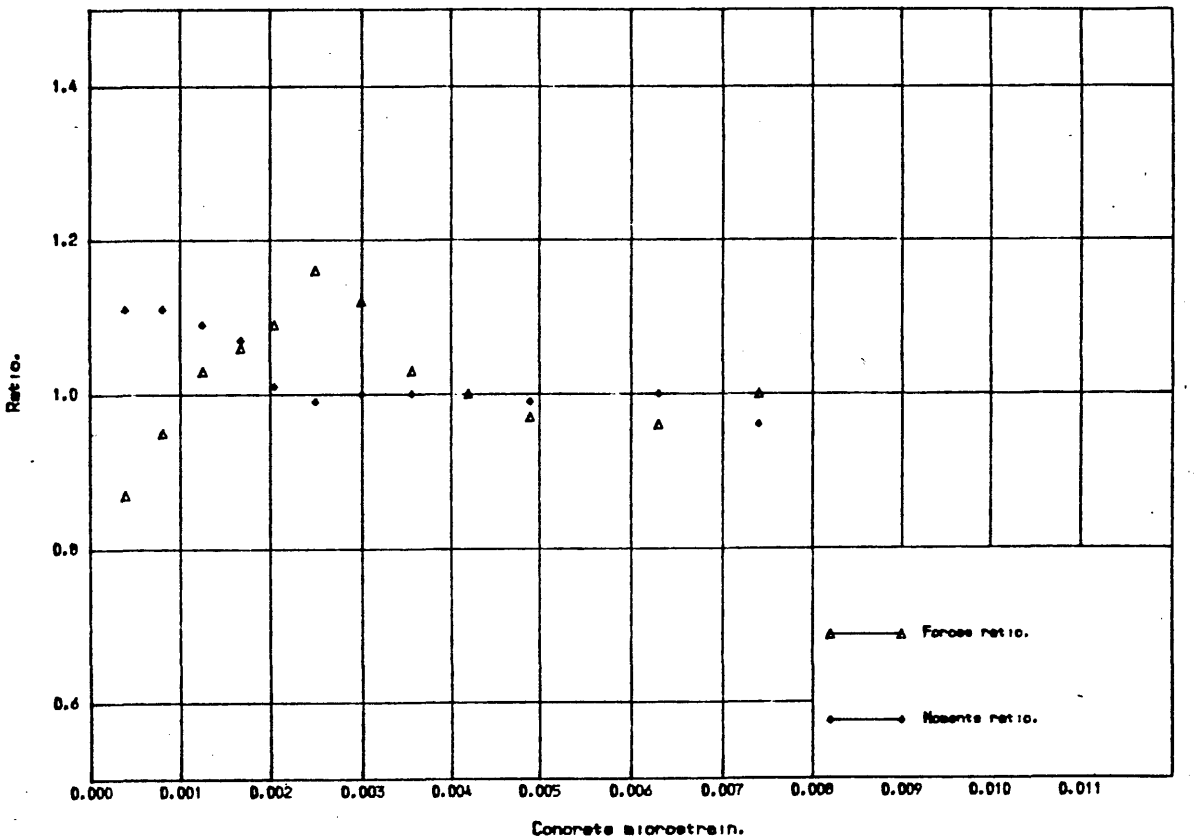

*Fig.*5.17-B *FORCES & MOMENTS RATIOS FOR RE.C. BEAM "B".*

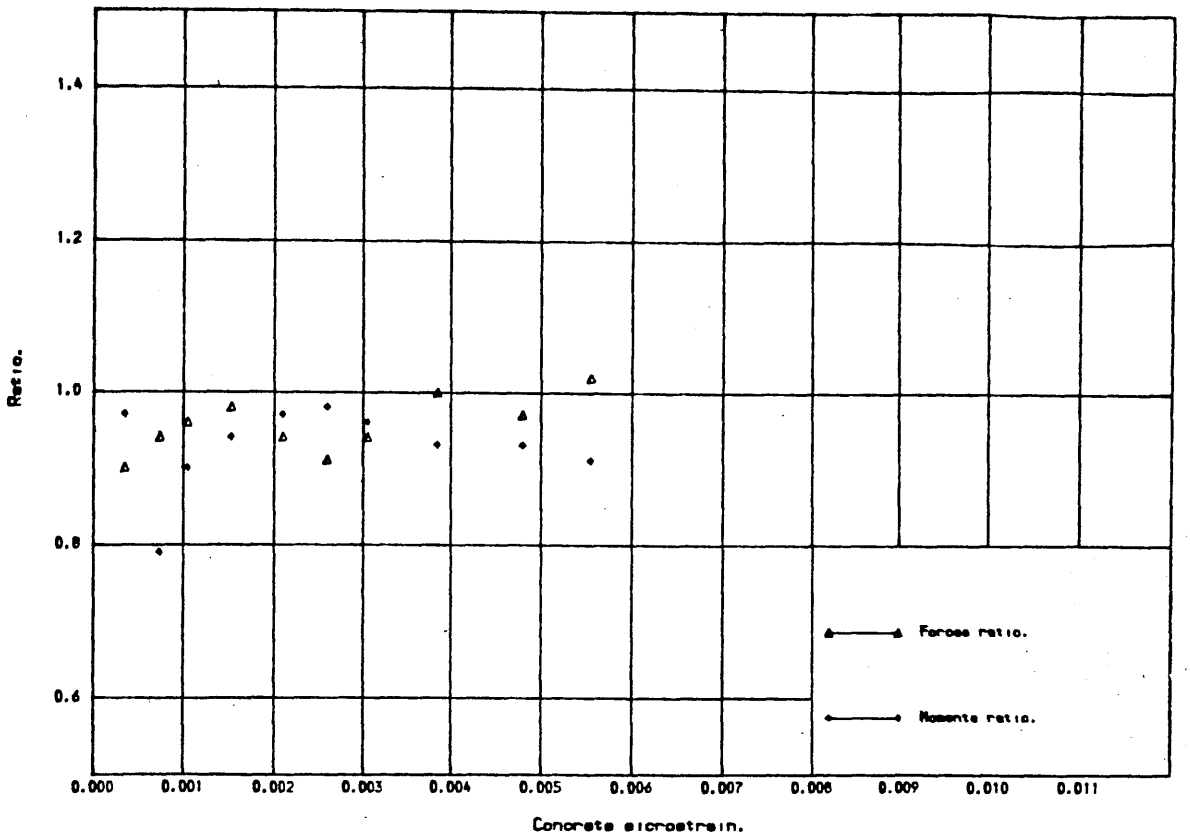

Fig.5.17-C FORCES & MOMENTS RATIOS FOR RE.C. BEAM "C".

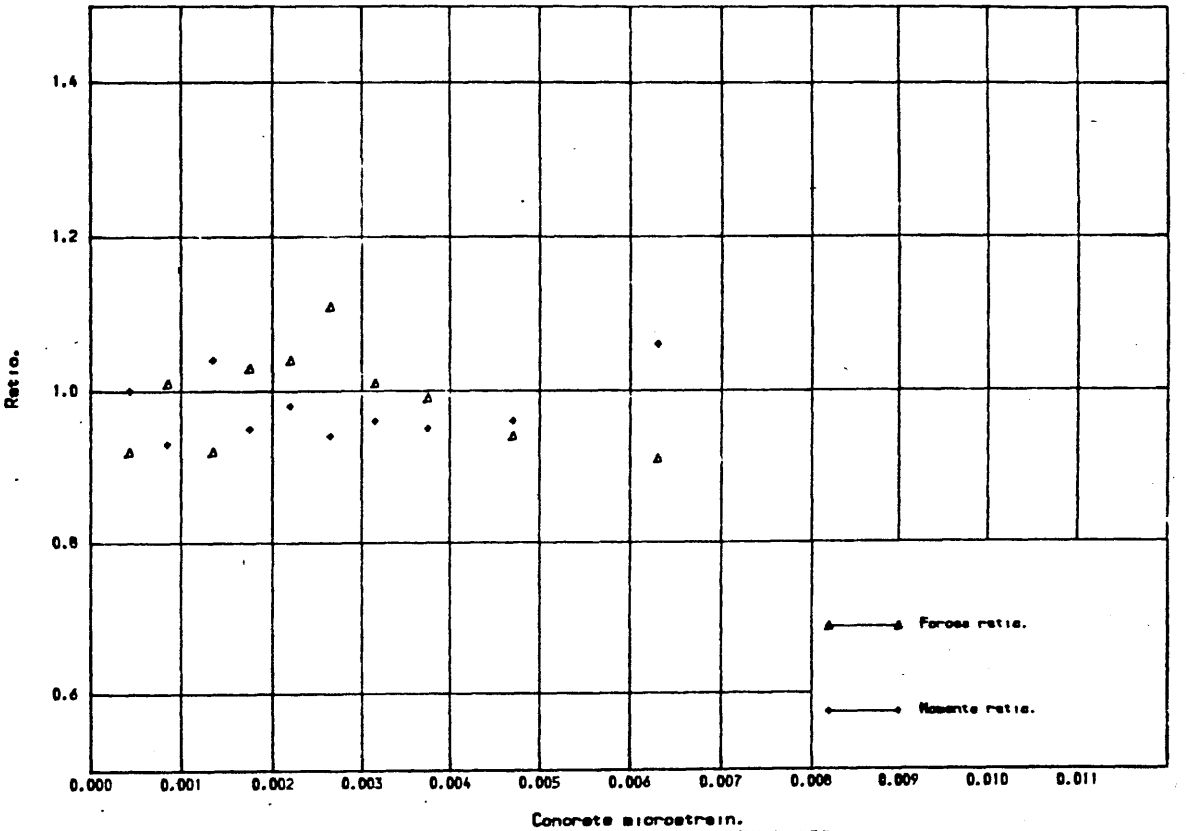

Fig.5.17-D FORCES & MOMENTS RATIOS FOR RE.C. BEAM "D".

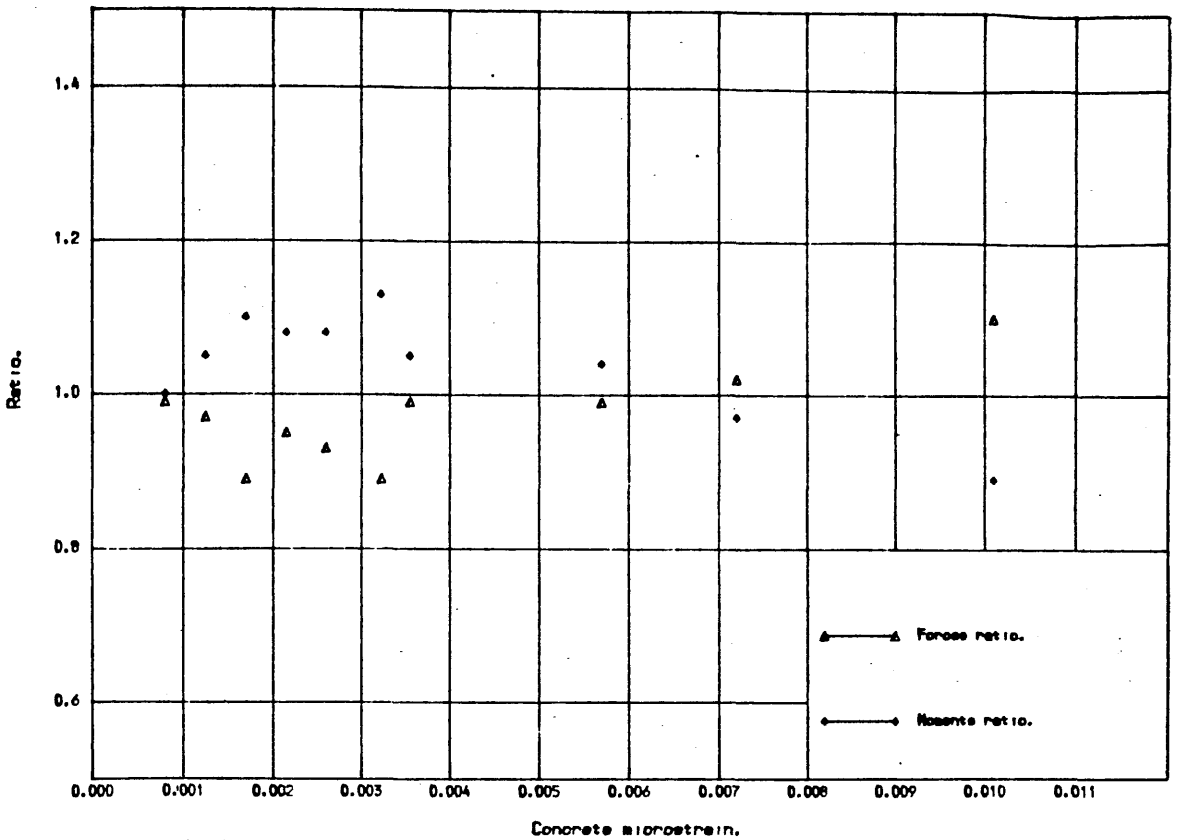

Fig. 5.17-E FORCES & MOMENTS RATIOS FOR RE.C. BEAM "E".

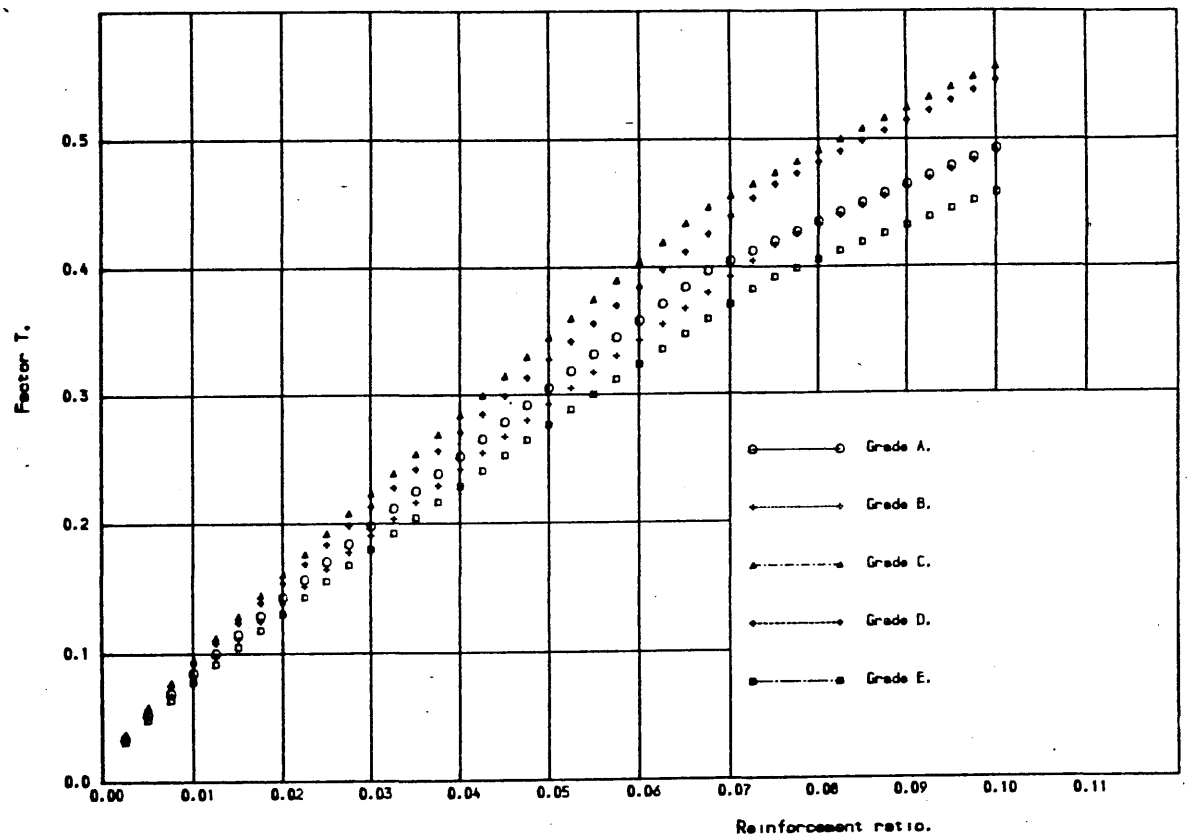

Fig. 5.18 EFFECT OF REINFORCEMENT RATIO ON THE FACTOR 'T'.

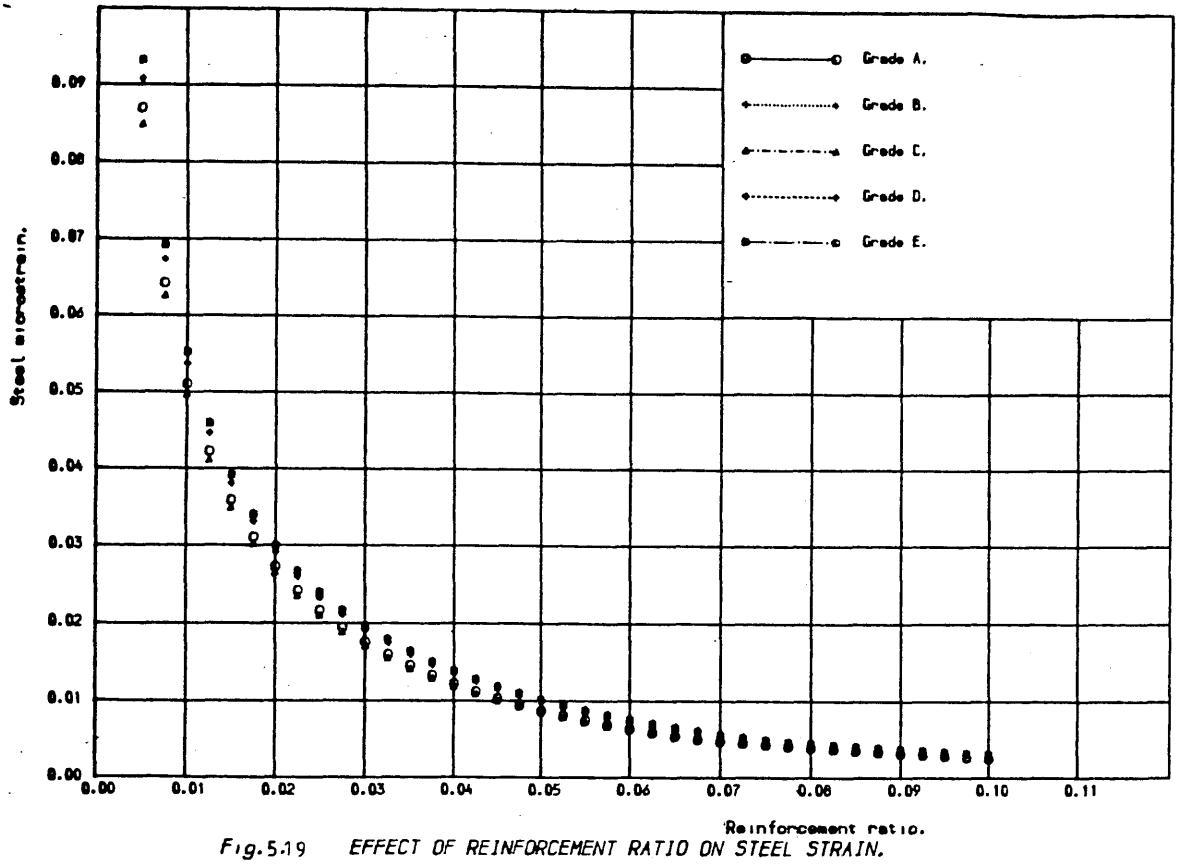

Fig. 5.19 EFFECT OF REINFORCEMENT RATIO ON STEEL STRAIN.

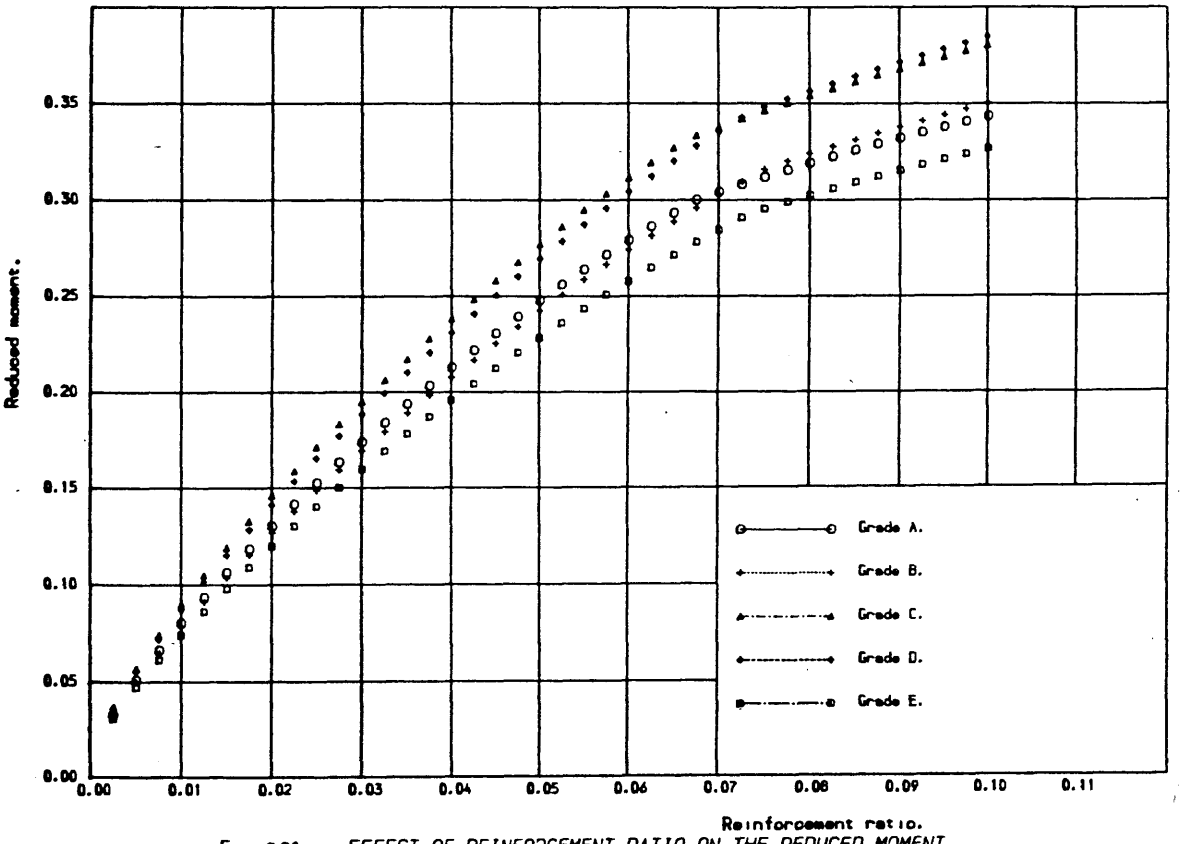

Fig. 5.20 EFFECT OF REINFORCEMENT RATIO ON THE REDUCED MOMENT.

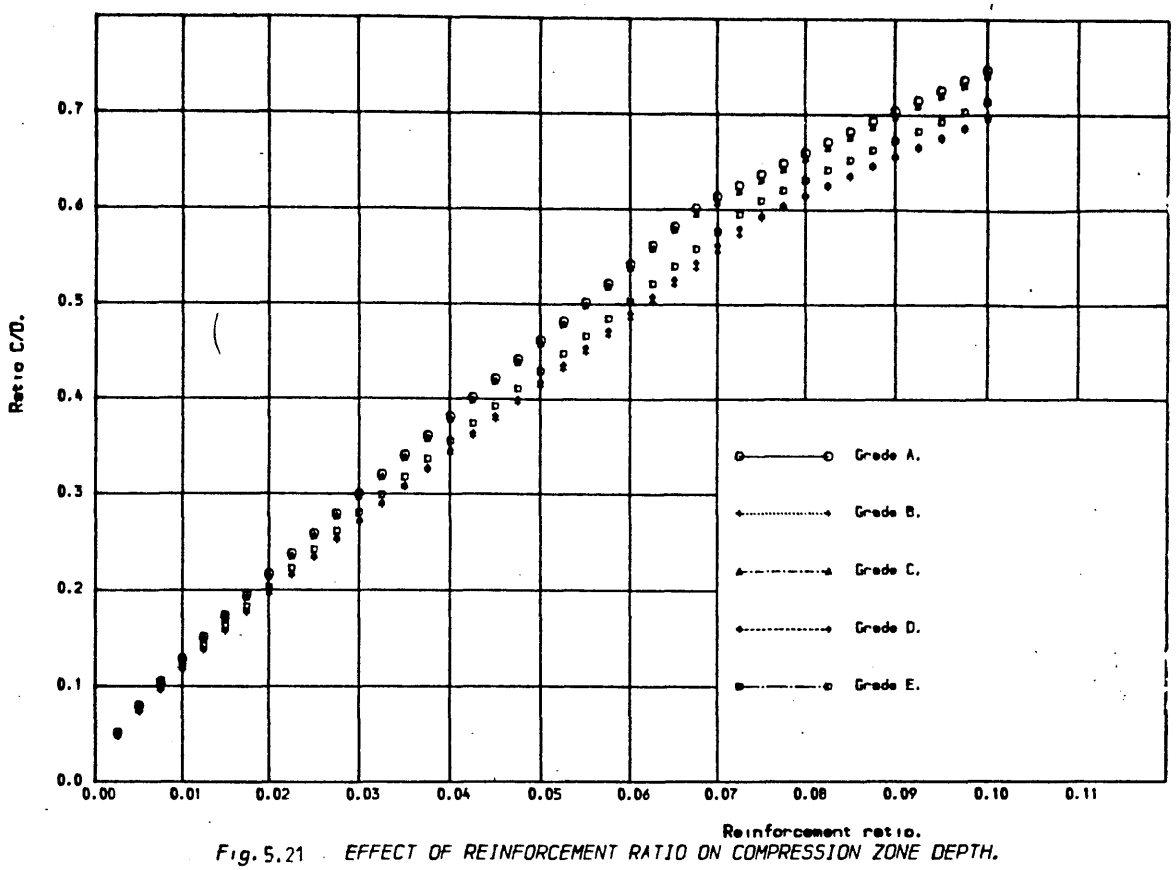

Fig. 5.21 EFFECT OF REINFORCEMENT RATIO ON COMPRESSION ZONE DEPTH.

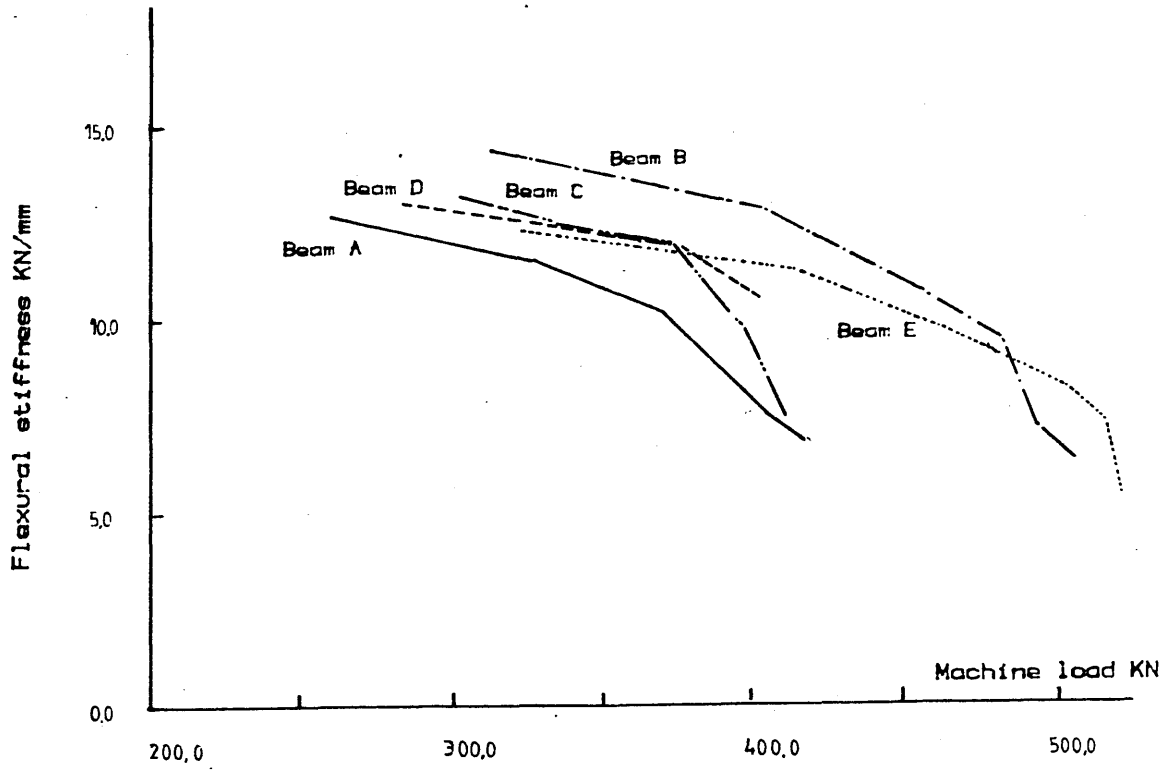

Fig. 5.22 Variation in flexural stiffness versus machine load at the six steel stages for the five PC beams tested.

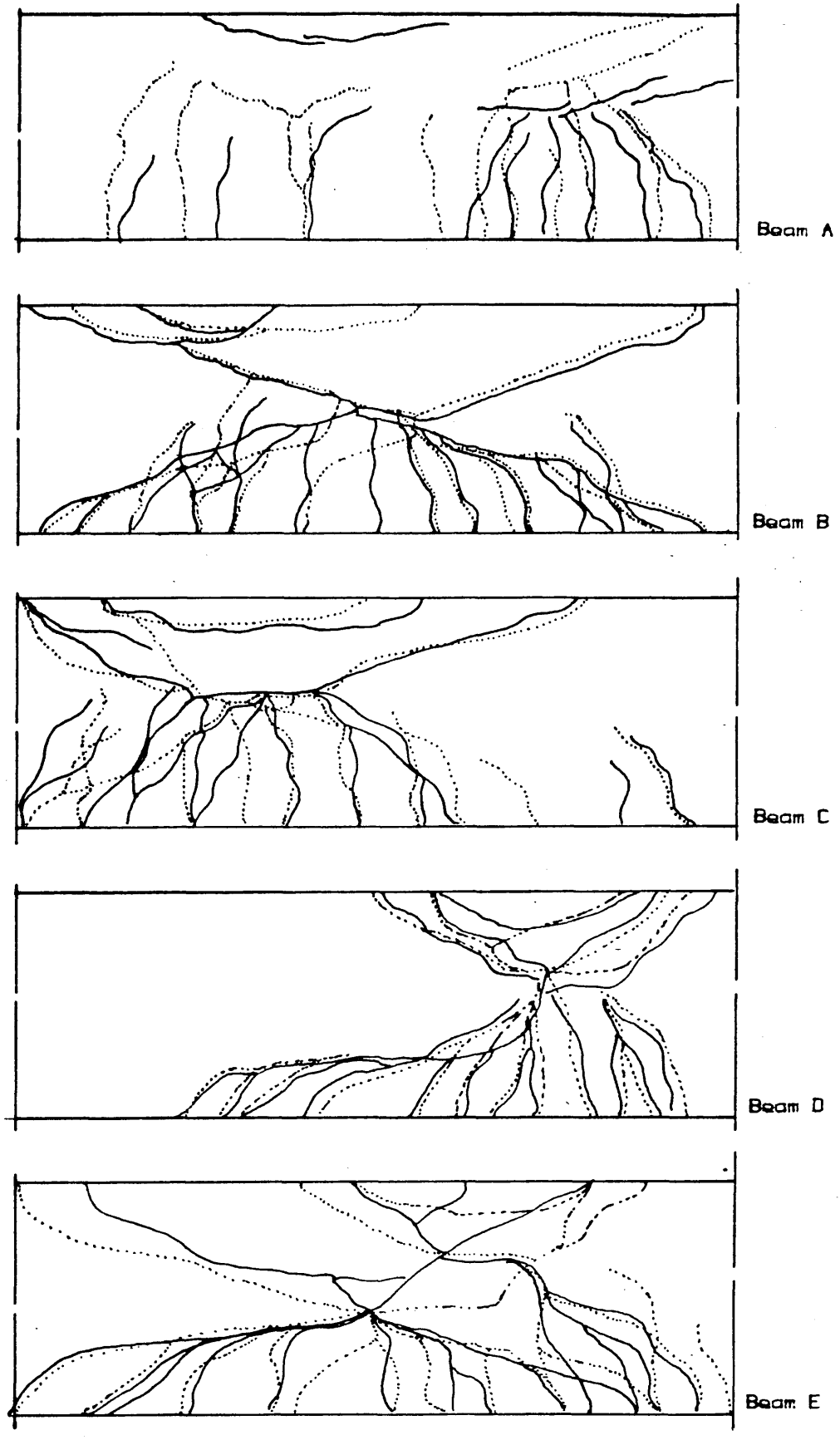

Fig. 5.23 Crack pattern within the constan moment span for the five PC beams tested (Dotted lines represent the back side crack pattern).

CHAPTER SIX

REINFORCED PC COLUMNS AND THEIR TEST ANALYSES

6.1. Introduction

Any ultimate flexure theory should cover loadings other than pure flexure. The most common case of loading is probably that of combined moment and axial load. Members subjected to this type of loading are encountered in almost any structure. Hence, the methods for structural analysis and design of reinforced PC members under this loading should first be reliably established. Thereafter any case of biaxial moment, with or without normal force, can be dealt with. In this present work, short columns with small eccentricities were investigated. Proper interpretation and extrapolation of the findings should allow a general approach for dealing with short or slender columns with any degree of eccentricity.

As columns generally have compression reinforcement, its influence on the ultimate capacity must be thoroughly investigated. The reinforcement steel used in the present work had no definite yield point and its strength continued to increase up to very high strain values. This type of steel has dictated, as said before, the concept of the specific reinforcement ratio 'R_s', at which a prescribed value of steel strain can take place at the ultimate capacity. These values of R_s were determined in the analysis of pure flexure in beams on the basis of the efficient use of steel and the desired mode of failure. However, and as will be shown later, with columns R_s can not be determined in this way. This is mainly

because of the fact that efficient use of steel is not a matter of only adjusting tension and compression reinforcement ratios.

For a given section under the action of combined moment and direct axial load the ultimate moment capacity depends on the magnitude of the axial load; this capacity depends on the eccentricity of loading defined as the ratio of moment to axial load. This mutual dependency between the normal force and its eccentricity for the ultimate moment capacity, prevents the possibility of setting a general R_s for any section without consideration of the eccentricity level. For any given section, an infinite number of values of R_s can exist depending on the eccentricity of the normal force. In other words, for a section having tension and compression reinforcement ratios R and R', there is only one value of eccentricity that would allow the development of certain prescribed value of steel strain at ultimate condition.

As said earlier in Chapter Five, The so called tension or compression failure had little significance in describing the failure mode. All columns made of this type of steel would fail when the ultimate compressive concrete strain ε_{cu} has been reached. Hence, columns that might have very small R will still fail eventually when the concrete develops its ε_{cu} in the compression zone , no matter how high the tension steel strains might be.

As will be shown in this chapter, the different parameters of the stress block for various PC grades were employed along with the concept of specific reinforcement ratio for specific

eccentricities in the design of the five columns tested. To simplify derivations and calculations the effect of lateral confinement and its contribution to the stress block parameters was neglected.

6.2. Fundamental equation for uniaxial eccentric loads

For any rectangular cross-section, and with the notations given in Fig.(6.1), the previously derived Eqs.(5.1 - 5.5) still can be applied. Dividing Eq.(5.2) by Eq.(5.1) then,

$Z/L = [T(1-YT) + T'_s(1-d'/d)]/(T+T'_s-T_s)$, from which

$(e/d)(T+T'_s-T_s) = T(1-YT) + T'_s(1-d'/d)$ ...(6.1)

in which T_s, T'_s and T are as follows,

$T_s = R.f_s/f_{cy}$, $T'_s = R'.f'_s/f_{cy}$, $T = G.c/d$

and e is the eccentricity measured from the centroid of the tension steel to the applied load.

Using the idealized steel stress-strain curve and Eq.(5.4) & Eq.(5.5), the stresses in the tension and compression steel f_s and f'_s can be expressed as follows;

$f_s = A + B.\varepsilon_s = A + B(G/T - 1)$

$f'_s = A' + B'.\varepsilon_{s'} = A' + B'(1- d'.G/(d.T))$

By substituting in Eq.(6.1) and rearranging then

$AT^3 + BT^2 + CT + D = 0.0$ ...(6.2)

in which : $A = Y$, $B = e/d - 1.0$

$C = (R'/df_{cy})[(A'+B'.\varepsilon_c)(e-d+d') - (R.e/R')(A-B\varepsilon_c)]$ and

$D = (R'.B'.\varepsilon_c.G/df_{cy})(d'-d'^2/d-R.eB/R'B'-e\,d'/d)$

Eq.(6.2) can now be used to calculate the value of the factor T for any cross-section having a certain R, R' and e . It is

clear that this equation is similar to Eq.(5.6-a) which was derived for pure flexure. While the factor T in the case of pure flexure is defined by a second degree function, this is increased to a third degree in the case of combined direct force and moment. This increase in the function order is due to the additional effect of the normal force which does not exist in the case of pure moment.

The factor T can be used for calculating T_s and T'_s. Knowing these three factors , the normal force and the moment at any value of ε_c can be calculalted (Eqs.(5.1 &5.2)); the ultimate values can be found if ε_c is substituted by ε_{cu}.

As with Eq.(5.6-a), the constants of the steel stress-strain curve should first be assumed and then checked. Several cycles might be required until the assumed constants are verified. The PC stress block parameters affect Eq.(6.2) in terms of G,Y, ε_c and f_{cy}, which express each PC grade explicitly. One major difficulty is the solution of the third degree equation which can be solved graphically or mathematically. Computer programmes can easily provide such solutions.

On being solved, this fundamental equation (Eq.(6.2)) can provide the calculation of not only the ultimate moment but almost any other value in the section. The compression zone depth c, the strains in tension and compression steel ε_s & $\varepsilon_{s'}$, the internal forces in PC and steel, and the curvature can be calculated at any maximum compressive strain in PC.

6.3. Tests of reinforced PC columns

6.3.A Dimensioning Five reinforced PC columns were tested,

one for each grade. The same considerations taken into account in dimensioning the beams were applied to columns. In addition the test-zone cross-sectional area was chosen in such a way that not more than 2000 KN would be required as an eccentric load. This was to allow the design of the supporting system to be practically possible.

The width of the cross-section was taken to be 150 mm. as was that of the beams. Cosidering the maximum load value set before, the total depth was taken to be 200 mm. For this area of cross-section, the expected ultimate load necessitated a minimum bearing area of 150x250 mm2. To allow for this increased area at the two ends of the column, haunches of 1:1 slope had to be made as shown in Fig.(6.2). The column-end dimensions and the bearing plates dimensions gave a possible maximum eccentricity of 75 mm measured from the geometrical centroid of the test zone cross-section.

The shear force in the vertical haunch-column plane for the chosen loadings and the given dimensions was found to be 800 KN. This high shear force required a minimum shear plane of 150x500 mm2. As was experimentally verified, this shear area in addition to the shear reinforcement was sufficient and no shear failure took place in any of the five columns.

The columns were cast horizontally with the tension side being the top level. Before casting the column mould was painted with silicone grease which helped provide sound demoulding and well finished surfaces when hardened. Because of the heavy reinforcement used, a vibrating table and steel tamping rods had to be used during PC placement and for prolonged periods.

Each column required one batch which took around 30 min. to mix, place and vibrate.

6.3.B Arrangement of the reinforcement The stress block parameters found previously are based on a plain prism in which no compression reinforcement nor lateral ties were used. Therefore it was essential to check the applicability of these parameters to columns whose compression zone is reinforced and laterally confined. Generally compression reinforcement R' has a little role to play in beams where its contribution can only be of significance near failure and only with associated high tension reinforcement R. Conversely, in columns with small eccentricities, R' has more effect on the ultimate capacity and behaviour. Unlike beams, compression failure can not be avoided by limiting the tensile steel area. A major factor controlling the failure mode and the contribution of R or R' is the eccentricity level.

For any given section reinforced with the type of steel adopted in this work, the ultimate axial load and the ultimate moment are inversely proportional to eccentricity e . This effect of e can be more clearly seen when R is small, R' is high or both. Consequently steel strains are strongly related to the chosen value of e for any given section.

In the five columns tested, a range of R' values was employed, varying from 2.4% to 4.6%. Although these varying ratios were determined to suit the P.C. grades they also helped in the analysis and investigation of the effect of compression reinforcement on the ultimate structural performance of these columns. As will be shown later, for the cross-section chosen

increasing R theoretically from 0.5% to 10% can result in an increase in the ultimate load or moment of only about 15%.

With the available range of e , around 120 to 150 mm. from the tension reinforcement centroid, the influence of R was limited. The value of R has a significant effect on the resulting stresses and strains in the tensile steel only at high e values. This implies that only for such cases will R have a dominant effect on the associated deformations and the lateral buckling of the column. The chosen values of R were based on the concept of the specific reinforcement ratio which would allow prescribed strains in steel to develop at failure. These ratios varied from 2.9% to 7.7% and it will be shown later how they were reached.

To limit the buckling of the longitudinal steel and to allow for full use of PC up to its ε_{cu}, ties were provided. As shown in Figs.(6.3-a,b,c,d&e), these ties were closely spaced. The lateral confinement given by the ties and its contribution to the ultimate carrying capacity will be dealt with later. Sufficient shear reinforcement was provided as shown in the same figures for each column and no shear failure took place.

6.3.C Testing and measurements The eccentric load for each column was applied using a 1000-Tonne Los System Testing Machine. The required loads were high and no single-roller supporting system could be provided for them. As shown in Fig.(6.4), three rollers made of high tensile steel were used; each is 50 mm diameter and 150 mm long. The rollers only allowed lateral movement where no rotation could have been tolerated as the three rollers were assumed to support the

load equally; see details in Fig.(6.5). The chosen thickness of the bearing plates was proved sufficient to prevent any local bending in them that could have initiated local crushing failure.

Steel strains were measured using 5 mm. electric strain gauges. For each column, strains in two tension and two compression steel bars were recorded within the test zone. Two pairs of strain gauges were attached to each of these four bars at two positions, 100 mm. apart. The two gauges at each position were attached opposite to each other (right and left sides of the bar, not inner and outer faces). In this way each column had eight strain gauges for either tension or compression reinforcement, which were kept away from direct contact or friction with the lateral ties by attaching the gauges to faces remote from them. The average values of strains were calculated (out of eight individual readings) and used in the analysis.

PC strains were measured using 20 mm. electric strain gauges. Eight strain gauges were attached to each column, two on each side or face at the midheight of the column. Strains recorded at the inner and outer faces measured the maximum compressive and tensile strains in PC respectively. As shown in Fig.(6.6), the concrete strain profile along the cross-section could be traced by recording these strains and those at one third and two thirds of the total depth of the test zone. The average value of each of two opposite gauges was calculated and used in the analysis. The tensile strains in PC at the outer face were small enough to enable the gauges at this face to

continue operating into the late test stages. In some columns no tension cracks developed before concrete crushing had taken place in the inner side (the compression zone).

The strain gauges and the machine load readings could be recorded incrementally by the use of a Data-Logger. Load increment was 50.0 KN every 2 min. At the end of each increment, instantaneous reading of all values of strain and the machine load were taken. Tests continued at this rate until failure. There was no need to increase the rate of the platen movement where no excessive deflections occurred near failure.

6.4. Test results

Using the average strain values in concrete and steel at different positions, the strain profiles for various load levels could be plotted for each column. These incremental strain profiles are shown in Figs.(6.7-a,b,c,d &e). In all these figures increase in curvature was almost at a constant rate, until at late stages when failure was imminent and this rate increased rapidly. The neutral axis always lay between the two 'tension 'steel layers (column B, C & E). Columns A and D which had only one tension steel layer, had their neutral axes lying below and above this layer respectively throughout the test. Columns E, B and C had generally tensile strains in the outermost layer and compressive strains in the innermost layer. The 'tension'steel was subjected to tensile and compressive strains in columns D and A respectively. Figs.(6.8-a,b,c,d & e) show the steel strains as experimentally recorded and plotted against the maximum

compressive concrete strain (ε_c).

The compression zone depth (c) as calculated from the strain profiles at different stages are plotted against ε_c in Figs.(6.9-a,b,c,d &e). Column A which had the smallest eccentricity (e), had a c-value in the vicinity of 190 mm.,which is greater than the effective depth (d). The change in c for column A was almost zero which is mainly due to the small value of e applied rather than the values of tension and compression reinforcement ratios (R & R') employed.

As the tension steel strains were generally much smaller than the compressive strains in the compression steel, three stages of that steel's stress-strain curve were defined to help analyze the results. These stages are;[i] compression steel reaching its proportional limit,[ii] compression steel reaching its 1.0% proof strength and [iii] compression steel reaching its 2.0% proof strength.

For column A, c is almost constant at any stage. The strain in compression reinforcement after reaching stage [i], increased slightly and when this steel reached stage [ii], ε_c amounted to around 0.004. At stage [iii], ε_c was 0.0055 after which it increased rapidly until failure.

Column B had a constant compression zone depth of around 170 mm. up to stage [i], which kept the innermost layer of tension steel continuously under compression strains, while the other outer layer developed tensile strains. Despite grade B having 90 N/mm.2 compressive strength, the ultimate load recorded with column B was much lower than that of column A whose compressive strength was 85 N/mm2. This can well be attributed

to the higher e used with column B. This relatively high value of e produced a value of c much smaller than that with column A, with a consequent smaller ultimate load. Full analysis and interpretation of results for the five columns will be given later. However, what should be stressed here is that the value of c decreased for all columns (except column A) as the test load was increased.

Knowing the steel strains and using the idealized stress-strain curve for the steel , the axial tensile and compressive forces could be calculated at various load levels. Figs.(6.10-a,b,c,d &e) represent these steel forces plotted against ε_c. These figures show how beneficial compression steel might be in short columns with small eccentricities. On average, the compression force provided by this steel amounted to 25% of the total internal compression force at any load level. This indicated that R' contributes to the section carrying capacity even at the elastic stages and long before the initiation of concrete crushing (compression failure).

The ultimate failure load recorded varied from a one column to another. The highest value was recorded with column A (2250 KN), while the smallest was recorded with column C (1750 KN). The recorded ultimate compressive concrete strain ε_{cu} well exceeded the theoretically derived value for each grade. Values of up to 0.01 were recorded near failure. This implies that the theoretical values are conservative although they are within the range from 0.0072 to 0.0076.

6.5. Analyses of results

By using the results of the five columns tested, the previously given strain profiles were produced. These strain profiles are almost linear at any load level and even near failure. From these profiles steel and concrete strains could be obtained and used in the analysis of each column. As shown previously, by knowing the steel and concrete strains and having the stress-strain curve for each of them, the internal forces could be calculated on these bases. The internal concrete compressive force, the total internal force and the external eccentric machine load are plotted against ε_c for each column as shown in Figs.(6.11-a,b,c,d,&e). The internal moments calculated on the above bases are plotted along with the actual applied moment at various test stages for each column as shown in Figs.(6.12-a,b,c,d,&e). The ratios of the calculated to the actual applied loads and moments are also derived and shown in Figs.(6.13-a,b,c,d,&e).

As tension steel strains were small and within the elastic stage, compression steel strain was used in describing the behaviour of the different columns tested as this steel generally developed much higher strains. In addition to the three previously defined stages [i, ii & iii], a fourth stage [iv] will be used in the analysis of results. This stage represents the stage at which a column will develop a maximum concrete compressive strain equal to the theoretical ultimate value (ε_{cu}) set for its PC grade.

Table (6.1) shows the various reinforcement ratios and the eccentricity values employed in the five columns tested. The high tension reinforcement ratios (R) were those chosen primarily to ensure as large a compression zone depth as

possible, and to control the mode of failure. The high compression reinforcement ratios employed were mainly to help increase the ultimate carrying capacity of the columns. These prerequisites had to be taken into consideration due to the small range of eccentricity available.

With small eccentricity-columns, a compromise has to be made between the efficient use of tension steel and the economic use of PC itself. In such a case, using tension steel efficiently so as to develop a high proportion of its ultimate strength by reducing R, would imply a great reduction in c and a consequent waste of the merit of PC in compression. This would also allow for uncontrolled propagation of tension cracking and in general would cause a reduction in the ultimate carrying capacity. Hence to keep this capacity as high as possible, and to control tension cracking development high values of R had to be icorporated even if tension steel would develop only a small proportion of its ultimate strength.

As shown in the given profiles, the outermost tension steel layer developed strains amounting to 0.0003 and 0.001 at stage [iv], for column A and D respectively. Despite column A having R=2.94% and column D having R=4.65%, tension steel strains recorded with the latter were much higher than with the former (almost three times as much). This is mainly because column A had e =127 mm., while column D had e =155 mm. So it is evident that the tension steel strains are not only dependent on R, but probably to a greater extent, on the eccentricity level itself. This mutual relationship between R and e will be

dealt with later in more detail. But the conclusion here is that the definition of small or large eccentricity- columns must be considered and introduced on the bases of the mutual effects of R, R' and e on the ultimate behaviour of the column.

The values of R' employed, as shown in table (6.1), are high . This was to provide the maximum possible internal compressive force resisted by the cross-section. This would necessarily give a maximum ultimate moment. As shown in the given strain profiles, recorded strains in compression steel at stage [iv] ranged from 0.00645 with column E to 0.0069 with column A. These high strains confirmed the importance of this compression steel, where they provided forces which contributed considerably to the total internal compressive force of the cross-section , particularly at early stages. For example, with column A the ratio of the compression force resisted by this compression steel to that resisted by concrete amounted to around 70%, 50%, 45% and 40% at stages i,ii,iii and iv respectively.

At early stages of loading, the associated strains in both concrete and compression steel are small. For instance, at stage i column A developed an ε_c=0.0022 while steel strain was 0.002. At these small strain values, compression steel develops almost 75% of its ultimate strength, while PC develops only 30% of its ultimate strength. On further increase in test load, PC develops its ultimate strength at a much higher rate than that of steel and the proportion of compression steel force in the total internal force is reduced. This trend of compression steel contribution in terms

of the internal forces provided obviously applies to all other columns tested.

The applicability of the different stress-block parameters found previously with various PC grades, can now be closely examined. Referring to Figs.(6.11 and 6.12),the calculated total internal direct forces at any test-load level were generally less than the actually applied external forces, in columns A, B and E. Conversely , columns C and D had generally higher calculated direct forces than the actual ones. These calculated total internal forces are the sum of the compression force in PC and the forces in the tension and compression steel. On the other hand, the calculated moments were less than the actually applied ones for all columns. The difference between the actual and the calculated values of either forces or moments was almost negligible at early test stages (stage i). Thereafter a significant divergence began to take place. This situation can be partially attributed to the steel used and the PC itself, where assumptions for simplifying the analyses are made. The idealized stress-strain curve of the steel used , no matter how precise it is, should reflect some errors in the derivations of the steel stresses on the basis of the experimentally recorded strain values.

PC stress-block parameters which were used with the previous calculations are so far based on the plain prism findings where no compression steel existed. As these findings applied well to the beam analyses where no compression steel was involved and did not apply well to present column analyses, some modifications have to be carried out on these parameters

when considering PC columns.

The stress-block has two main parameters namely K1.K3 (G) and K2. The reliability of the first of these is reflected only in the calculations of the internal forces, while both factors affect the calculated values of the internal moments. The parameter K1K3 is dependent on the ultimate cylinder compressive strength f_{cy} nominated for each grade, and on the concrete strain ε_c reached at any stage. The special vibrating techniques used when casting the five columns might be a reason for a variation in the values of f_{cy}. As said before, because of the heavy reinforcement employed, prolonged periods of vibration using steel rods and a vibrating table were required and must have had effects on the actual value of f_{cy} in these columns. Resin bleeding occurred in columns A,B and E which were made of high resin content-PC grade. This bleeding was probably responsible for decreasing f_{cy} in the respective columns. This effect was persistently reflected by the actual loads being less than the calculated ones which are based on the higher nominal f_{cy}-values.

On the contrary, columns C and D seem to have gained an increase in their f_{cy}-values by the elongated vibrating times. With these two columns, the actual loads were generally higher than the calculated ones. These two grades in particular, have the stiffest consistency as they had the largest fractional volume of coarse aggregate and the lowest resin content. The results for columns C and D in terms of the internal forces confirmed this gain in strength due to better compaction and the consequent limited voids resulting in the composite as a whole resulting from the prolonged vibrating periods.

The same reasons can be held responsible for the greater divergence in the actual and the calculated values of moments , where not only the value of K1K3 but also that of K2 are used in the calculations. In addition the calculations of the moments included that part provided with compression steel which being idealized could cause a magnification in the errors when multiplied by the lever arm. The actual and calculated moments up to stage [i] were slightly different and changed almost linearily with ε_c as shown in Figs.(6.12). After the compression steel has reached stage [ii], the rate in moment increase decreased (actual or calculated value); when this steel exceeded its 0.2% proof strength, no remarkable increases in these moment values took place.

The tension steel did not develop strains in any column tested more than those within its proportional limit. This was mainly due to the small applied eccentricity. In addition the innermost layer of tension steel was under compressive strains. As will be shown later these columns had a compression failure-mode. Considering Figs.(6.8), it is clear that tension steel in itself was not used economically. But as said before high values of R helped maintain a high value of c, which provided high ultimate carrying capacity.

For the columns tested and with the given small range of eccentricity, it was theoretically found that the ratio of c/d can be caused to vary from around 0.6 to 0.9 by mutual changing of R and R'. Generally the greater R the greater the compression zone depth is, irrespective of e . Column A for example, can have its tension steel strained up to 0.0033 at

R=R'=0.5% with ultimate eccentric force of 1090 KN. at e =140 mm. The same column could support an ultimate load of 1515 KN. at the same e if R and R' are increased to 10% and 3% respectively; in this case tension steel strains would be only 0.00038. The 50% increase in the normal force and moment can well justify the use of high values of R even if tension steel has low strains. This was the main consideration when choosing the specific values of R with different columns tested.

Stresses and strains in compression reinforcement were fully developed and this reinforcement contributed greatly to the internal force provided by each column section. This steel has little effect on the value of c particularly in columns with small eccentricity level ratios er (er =e /d), as had the columns tested. This effect almost vanishes completely with cross-sections having high er-values. The compressive strains recorded in the compression steel with the five columns reached well beyond those strains corresponding to its 0.2% proof strength. For example,at stage [iv], these strains as experimentally observed, amounted to 0.00644 and 0.0069 for columns B and E respectively. At this stage, the machine loads were generally smaller than the recorded failure loads except for column D. This increase in the failure load over the theoretically defined ultimate load (stage [iv]), could be partially attributed to the additional effect of the heavy lateral confinement.

The compression zone depth was generally constant until stage [i], afterwhich a decrease in c took place in all columns, except column A. This decrease took place at a decreasing rate

and after stage [iii], c became once again more or less constant. With column A, which had er=0.69, compression steel could not exercise any significant effect on c-value. This value was experimentally found to be constant at all stages, see Figs.(6.9).

6.6. Theoretical calculation of the ultimate carrying capacity

In the previous analyses of results, values of internal forces and moments, steel strains and values of c were calculated using the experimental readings of the strains in the concrete and steel at various test stages. Having the idealized steel stress-strain curve and the concrete stress-block parameters, the recorded strain values could be used in the analysis of the different columns from the first load increment up to failure. As it is the main objective of this work to clarify the ultimate behaviour of PC, the theoretical deriviation of the ultimate capacity of short PC-columns with small eccentricity will be given.

The previously given Eq.(6.2) can be used for calculating the coefficient T for any given section made from any PC grade with a certain e at any desirable value of ε_c. This equation can thus estimate the single ultimate value of T at the theoretically defined ultimate compressive concrete strain ε_{cu} for any given section. This coefficient T can be used in the calculations of the reduced normal force and moment coefficients L and Z, by using Eqs.(5.1 & 5.2).

The following paragraphs demonstrate how T can be derived and used in the calculations of all the other relevant quantities to the ultimate carrying capacity of a given cross-section.

6.6.A Theoretical calculations of T The previously derived equation (Eq.(6.2)) is of the third degree in T and its constants A, B, C and D have been defined above. Constant A is equal to the stress-block parameter Y= K2/ K1K3, which is dependent on PC grade. Constant B is a function of the applied eccentricity e , and the effective depth d (e/d= er). While each of the constants C and D is a function of R and R', f_s and f'_s, d and d', assumed maximum concrete strain ε_c and e. Hence constants A and B can be given fixed values for each PC grade and each value of er. While the other two constants, depending primarily on the state of stresses in the steel used, will vary even for a given cross-section.

In addition these stresses which are derived from the idealized steel stress-strain curve can result from any one of three different functions of the steel strain. Each of these three functions has different stress constants depending on the zone in which the steel strain lies. Generally if the constants of Eq.(6.2) are known, its solution should be mathematically possible. On solving this third degree-equation, T can have any of three different values, out of which one is relevant.

For any section made of a certain PC grade, having a known er ratio, the following steps can be followed to obtain the ultimate value of T (Tu), if ε_c was substituted by ε_{cu}. After obtaining Tu the whole analysis for the section can be carried out.

(1) Depending on the PC grade fix the constant A.

(2) Depending on the value er fix the constant B.

(3) Depending on R, R', er, d, d' and ε_{cu}, and assuming the stress constants for tension and compression steel, calculate the values of constants C and D.

(4) Using Eq.(6.2) solve for Tu, and by elimination find the relevant value of Tu.

(5) Using Eqs.(5.4 and 5.5) calculate strains in tension and compression steel ε_s and $\varepsilon_{s'}$ respectively.

(6) Check the assumed values of the steel constants to ensure that they are compatible with the derived values of ε_s and $\varepsilon_{s'}$. If not, assume another set of steel constants and repeat steps (3) to (6) until the check is positive.

(7) Fix the last value of Tu, ε_s and $\varepsilon_{s'}$.

(8) using Eqs.(5.3, 5.4 & 5.5) calculate c.

(9) Using the idealized stress-strain curve calculate the steel stresses f_s and f'_s.

(10) Using Eq.(5.1) calculate the coefficient Lu.

(11) Using Eq.(5.2) calculate the coefficient Zu.

This procedure could be carried out using computing facilities to solve for Tu for a wide range of R and R' ratios. The range of R chosen varied from 0.5% to 10%, while that of R' was from 0.5% to 3%. The calculations were carried out for the five PC grades. In addition these calculations were repeated with various er ranging from 0.6 to 2.4. The theoretically derived values of Tu are applicable to any rectangular cross-section made of these five grades, provided it has the same er, R and R'.

The output of this computing work helped greatly in clarifing the effect of each individual parameter on the ultimate

behaviour of short columns in general. However, to make direct use of these calculations in examining the ultimate structural performance of the five columns tested, another set of calculations based on the er values actually used with each column was carried out. In this set the reinforcement ratios R and R' varied from 2.5% and 0.5% to 12% and 5% respectively.

The variation in Tu for different R values with R' as a parameter is shown in Figs.(6.14-a, b, c, d &e) for the five columns respectively. The value of Tu increased at a decreasing rate with the increase in R. The effect of R' on Tu was almost negligible for columns having high values of er. In column A which had er as small as 0.69, R' had a much more evident effect on Tu. In such a case, a greater increase in Tu can be obtained by increasing R' rather than increasing R.

Irrespective of er, the decreasing rate in the increase of Tu by either increasing R or R', makes it approach a maximum value for each cross-section. Unlike beams, this maximum value depends on the stress-block parameters, er and to a lesser extent on R and R'. This dependency can be closely examined by referring , for instance, to Fig.(6.14-d) and Fig.(6.14-e). Columns made from grade D and E had exactly the same er, however, the value of Tu is much higher with grade D than with grade E for any given R and R'. As grade D is much stiffer than grade E, it is quite evident that Tu depends on the stiffness of PC which is reflected in the values of stress-block parameters. For example, at R=6% and R'=3% the values of Tu were 0.568 and 0.68 for columns made of grade E and D

respectively. Grade D, as discussed before in Chapter 3, relative to all grades and in contrast to grade E has the highest stiffness, highest modulus of elasticity and the smallest concrete compressive ultimate strain ε_{cu}.

As said above, a maximum value of Tu does exist theoretically, but would require very high values of R and R'which are far from being practical. That is in addition to the fact that the increase in the ultimate carrying capacity near this maximum value of Tu by increasing R or R', is insignificant and can not justify the use of the extremely high values of R and R' required for it.

Figs.(6.15-a, b, c, d & e) show the variation in the reduced load coefficient Lu as plotted against R, and R' as a parameter. From these figures the effect of R and R' on the ultimate structural behaviour can be partially understood. It was found that increasing R' has a greater effect on the ultimate load than that of increasing R, particularly at small values of er. Columns made from grade A with er = 0.69 had an increase in Lu of around 5% for each 0.5% increase in R', while the same increase amounted to 0.1% for a similar increase in R. When the value er increases, the effect of R' on Lu decreases and that of R becomes more dominant as shown in the same figures. If er is infinity (case of pure moment), the situation is completely reversed and the effect of R becomes far greater than that of R'. So for the available small values of er adopted in this work, it is clear that ultimate capacity in terms of the normal force is more practically and economically enhanced by increasing R' and not R. In such cases the compression reinforcement ratio is the

decisive one.

The definition of small or large eccentricity has therefore to be established or reconsidered on these bases, where it can provide an initial evaluation of tension or compression steel contribution to the cross-section. This definition is that for any given section the eccentricity ratio er at which changing R results in a higher effect on Lu than when changing R', is considered to be a large eccentricity and vice versa. In between these two limits a balanced eccentricity ratio e*r will exist. The derivation of this ratio will be given later on in this chapter.

Having calculated Tu, the reduced moment Zu could be found using Eq.(5.2). The variations in Zu with different R and R' values are shown in Figs.(6.16-a, b, c, d & e). This coefficient Zu showed the same dependency on R, R' and er as that of Lu. That is, the factor Zu is more dependent on R at high values of er and R'. Once again a certain value of er that would make the effect of either R or R' more dominant for a given section should be mathematically definable.

Another conclusion regarding the mutual relationship between Lu and Zu at any value of er can be drawn. This is that a maximum value of Zu can only exist when a maximum value of Lu is reached and not before. In other words, for a given e, there is only one value of Zu corresponding to each value of Lu. With ordinary cement concretes reinforced with steel having a well-defined yield point, there can exist a maximum value of Zu at a certain eccentricity irrespective of Lu-value. If this eccentricity was decreased the value of the

column load would increase and the lever arm would decrease in such a way that Zu will eventually decrease (compression failure). Conversely, if this eccentricity is increased the column load will decrease and the lever arm will increase in such a way that Zu will eventually decrease (tension failure).

This situation can not take place in columns made of PC and reinforced with steel having no yield point. The block-parameters of PC and the stress-strain curve of the steel are such that if the compression zone depth is increased by decreasing e, the partial reduction in Zu by the reduction of the lever arm will still be smaller than the partial increase in Zu by the increase in the internal compressive forces.

To check the applicability of these theoretical findings to the five columns tested, the ratios of the ultimate theoretical load to that actually recorded were calculated for each column. These ratios varied from 75% with column C to 95% with column A. These big differences showed that the adopted values of Y, G and ε_{cu} in this theoretical approach are very conservative. It should be noticed that ε_{cu} for each grade was first fixed mathematically and then used in the derivation of Y and G from their idealized and experimentally found curves. The actual ultimate loads were reached at concrete strain values much greater than ε_{cu}.

The steel strain either in the tension or in the compression sides for the investigated range of cross-sections could be calculated using the coefficient Tu. Figs.(6.17-a, b, c, d & e) show the tension steel strains as plotted against R with R'

as a parameter. Similar curves for compression steel are shown in Figs.(6.18-a, b, c, d & e). From these figures it is evident that for a given PC grade and er, steel strains are strongly related to R and R'. Increasing R while keeping all other variables constant, would obviously reduce the resulting strains in tension steel; this is mainly because c will increase. In addition this increase in c would necessarily increase the associated strains in the compression steel, but to a lesser extent. This effect of R on steel strains becomes more dominant at high values of er and at small values of R'.

The effect of R' on the steel strains can be significant in sections where R and/or er are very small. if R is high, c will usually be big enough to make any small variation in it by changing R' have virtually no effect on steel strains.

The value of c at ultimate (c_u) could be found for various R and R' by using the equation; c_u=d.Tu/G. Figs.(6.19-a, b, c, d & e) show the dependency of c_u on R and R'. Generally c_u will increase at a decreasing rate by increasing R. It will also increase by increasing R' only at small er; while it will decrease at a very low rate at high er by increasing R'. In the case of pure flexure R' has almost no effect on c_u.

On comparing these c_u-figures to the five columns tested, it was found that they agree well with the experimental observations. The maximum value was 178 mm. for column A, and the smallest value was 149 mm. with column C. The other three values for columns B, D and E were 152, 153 and 154 mm. respectively. Unlike the values of Lu, c_u seems to be less affected by the idealization, assumptions and ε_{cu}-values

involved in the analyses.

6.6.B Small and large eccentricity-columns Before proceeding towards how the specific reinforcement ratio can be defined, the definition of small or large eccentricity has to be first clarified. As said before, it was found that irrespective of PC grade, there is a certain ratio of eccentricity e*r at which the influence of R or R' on the ultimate column load is equal. Ratios smaller than e*r cause a higher rate of change in L with respect to R', dL/dR' , than that with respect to R, dL/dR , and vice versa. This ratio e*r can therefore represent a clear distinction between large and small eccentricity-sections on the previous bases. It should be noticed that the corresponding rate of change in Z (or the ultimate moment), with respect to R or R' can be used as an alternative method for the definition of e*r.

So to specify any reinforcement ratio, the eccentricity level has first to be defined on the bases of the suggested definition. Knowing e*r for any given cross-section and the eccentricity level to which it is subjected, the question of whether tension or compression steel will be the controlling steel on the ultimate capacity, can be answered. Using this controlling, or rather decisive, steel and other provisions similar to those regarded in calculating R_s for beams, the specific tension and compression steel can be conveniently obtained.

For the determination of e*r a comprehensive partial differentiations of the values dL/dR and dL/dR' were carried out using computing facilities. For any given cross-section R

was kept constant and R' was changed. The value dL/dR' was then calculated for a wide range of er. The same was done by keeping R' constant and changing R. In this way the ratio er at which dL/dR = dL/dR' could be derived. This ratio e*r was found to be equal to unity irrespective of PC grade, dimensions of the cross-section and the reinforcement ratios themselves. This implies that the ultimate capacity of any given cross-section having an eccentricity measured from the centroid of the tension steel to the applied force less than the effective depth will depend more powerfully on R'. In such a case the section can be termed as having a small eccentricity. On the other hand if e is bigger than d the same cross-section will be more dependent on R and is therefore classified as having a large eccentricity.

The variation in c as discussed earlier can now be easily accounted for. Where er is less than e*r, increasing R' would increase c significantly. While in sections where er is bigger than e*r, increasing R' would decrease c rather than increase it. On the other hand increasing R usually increases c whether er is less or more than e*r.

Now the specific reinforcement ratios can be dealt with on a firm basis. For short columns two cases are likely to exist; small or large eccentricity. For large eccentricity- columns the case is very much like that of pure moment and similar provisions can be considered depending on the structural performance required. In this case the tension steel reinforcement is the one to be specified first to satisfy those requirements. Having done that, R' can be calculated

accordingly.

In the other case of the small eccentricity, R' will be specified first. Provisions to be satisfied in calculating R' and then R, can vary in their limits and significance as required. For example regarding the failure mode, a clear distinction between initial tension and compression failures has to be made. This distinction can be related to the yield strength of the steel if it has such a definable strength. With other steel types having no yield point, a limiting tensile steel strain has to be set at which c/d will not be less than certain ratio. In this present work this limiting steel strain and c/d at ultimate capacity are considered to be 0.01 and 0.5. Accordingly, sections having lower values of steel strain and/or higher values of c/d at ultimate capacity will have an initial compression failure.

Using the above definitions of the eccentricity level and failure mode , the reinforcement ratios were chosen to allow for only initial compression failure. This failure mode was aimed at as it represents the more general mode of failure with short columns having small eccentricity.

Column A can be taken as an example of how these specific reinforcement ratios were calculated. In this column, er was less than e*r, therefore R' is the ratio to be specified first. As increasing R' would necessarily increase the ultimate carrying capacity, R' must be as high as possible. For the available cross-section the maximum R'-value that could be accomodated was, the chosen one of 4.6%. As the initial failure mode was chosen to be a compression one, the

value of c/d had to be not less than 0.5. This provision would primarily dictate the chosen value of R. However, as er employed with column A was a very small one, R had virtually no effect on c and could have been chosen to be zero. The actual value of R was 2.94%. This value was mainly employed to control tension crack-propagation after the ultimate load had been reached and to help eliminate any sudden rotation at failure.

This procedure of choosing R_s and R'_s was followed with all the other columns. Their values varied depending on PC grade and the applied er for each column. It should be emphasized that with the beams tested previously, the specific reinforcement ratios were determined on the bases of prescribed steel strain values and c/d ratios only while with columns a third factor related to the eccentricity level had to be considered.

6.7. Mode of failure

Due to the small applied eccentricity and the relatively high R_s-values employed, the five columns failed by concrete crushing in the compression zone. The five columns were short ones and the resulting strains in the tension steel were small so that c_u was always very large. These large values of c_u allowed only very small values of curvature. The small curvature and the short lengths of these columns did not produce any significant deflections at the test zone. The small deflection values kept the eccentricity level close to its initially set value for the whole test up to stage [iv].

In the five columns tested, the machine load was applied at a

constant rate by providing a constant rate of platen movement. No increase in this rate was required even near failure. After the ultimate capacity was reached, the test load began to decrease as the rate of the platen movement was not changed. For safety reasons, no crack tracing was conducted while the test was in progress. These crack patterns were traced and copied only after the test had come to an end.

Figs.(6.20-a, b, c, d & e) show the crack pattern for the five columns after failure. In these columns crushing of the concrete started immediately before the maximum recorded load was reached. On further application of load, the maximum compressive concrete strains increased rapidly and the test zone acted as a plastic hinge allowing high rotation and curvature values about it. This rotation induced high tensile strains in the tension steel and in the concrete below the neutral axis which until that stage had been very small. Thus horizontal tension cracks began to develop in the tension side and these propagated towards the compression zone. This resulted in a decrease in c_u and consequently further increase in concrete compressive strains. Had the columns had little or zero tension steel, a sudden and possibly an explosive failure would have occurred in the form of quick rupture by cracks propagating in the tension zone and travelling towards the compression one. However, as there was a considerable amount of tension steel in each column, this steel could exercise its intended role by controlling the failure process. This steel could take the tensile forces lost by the concrete and redistribute the strains in the form of many horizontal tension cracks almost uniformly distributed along the middle

third of the total column length. As shown in Figs.(6.20), these cracks reduced c and allowed for large curvatures only at the final stages of the test.

On further maintaining the load, the concrete in the compression zone began to spall. All the five columns had their inner faces (at maximum compressive strain) spalled off completely at the end of the test. Parts of the compression zone along the two sides of each column also spalled.

It should be noticed that the column load began to decrease immediately after the concrete began to crush. After this stage , and by the time when tension cracks began to develop and propagate, the column load had sharply decreased. Thereafter, the columns began to behave more or less like a beam. The horizontal tension cracks tilted and became diagonal cracks heading eventually towards a specific point at the centre of the plastic hinge at the failure zone.

This mode of failure was observed with all columns except column A. In this column the tensile strains in the concrete and the steel were not large enough to produce any significant curvature or reduction in c at the final test stages. The load began to decrease with concrete crushing in the test zone and beneath the supporting plates under high local bearing stresses. This local bearing failure did not allow for increase in the test load to the extent required to produce a significant reduction in c at failure. The tension cracks in this column were distributed along a relatively small length of the column (the middle sixth); their propagation was also very limited in depth.

As seen from the crack patterns of the five columns, tension cracks on each side of any column were almost identical and pairs of cracks in opposite sides were joined with a horizontal crack across the outer tension-face.

As said earlier, the links must have contributed to the carrying capacity of each column by their lateral confinement effects. This contribution, however, was found to be very limited. To clarify this effect, associated measurements of tensile strains in the lateral ties of column A in particular were carried out. Column A was a prime candidate for examining the lateral confinement effect, as it had the smallest er. Strains in four lateral ties were experimentally recorded for the whole test range of column A. These four ties were distributed as the third one from the top, the third one from the bottom and two at the middle of the test zone.

Recorded strains in these ties and their locations are shown in Fig.(6.21). At any load level, the middle pair of ties developed lower tensile strains than the other top and bottom pair. The recorded strains in the middle ties were as small as 0.0007 up to around 90% of the ultimate load. At this ultimate load, they developed strains of about 0.001. The significant increase in the strains recorded took place only after the ultimate load has been reached and the concrete has begun to crush. By maintaining the load after this stage, the machine load decreased and the strains in the ties began to increase excessively. At the time when the load was down to 90% of the ultimate value, the strains reached 0.0022. However, by further reduction in the machine load strains in the ties

began to decrease and at complete failure the strains recorded were almost zero.

Based on these experimental findings, it can be said that the real contribution of the lateral confinement to the compressive strength and consequently the column load is of little significance with these rectangular ties before the ultimate capacity is reached. It can only exercise some influence at early failure stages. In other words rectangular lateral ties can only enhance the carrying capacity of columns after these columns begin to fail and not before. So in terms of ultimate carrying capacity, lateral ties can not be effective and their effect can be completely ignored. They can only help produce additional lateral stability to the longitudinal steel, by supporting it.

Table 6.1: Details of the five PC columns.

Column	A	B	C	D	E
d mm	182.0	170.7	173.3	180.0	170.6
d' mm	20.0	18.0	16.0	18.0	18.0
As mm^2	804.0	1884.0	1206.0	1256.0	1884.0
As' mm^2	1256.0	804.0	628.0	804.0	804.0
e mm	127.0	145.7	148.3	155.0	145.5
e r	0.698	0.853	0.855	0.861	0.853

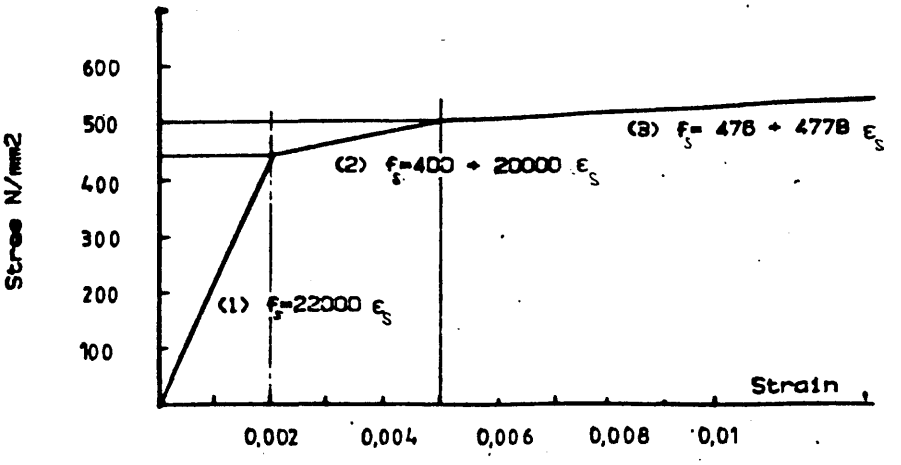

Fig. 6.1 Idealized trilinear stress-strain curve for the steel used.

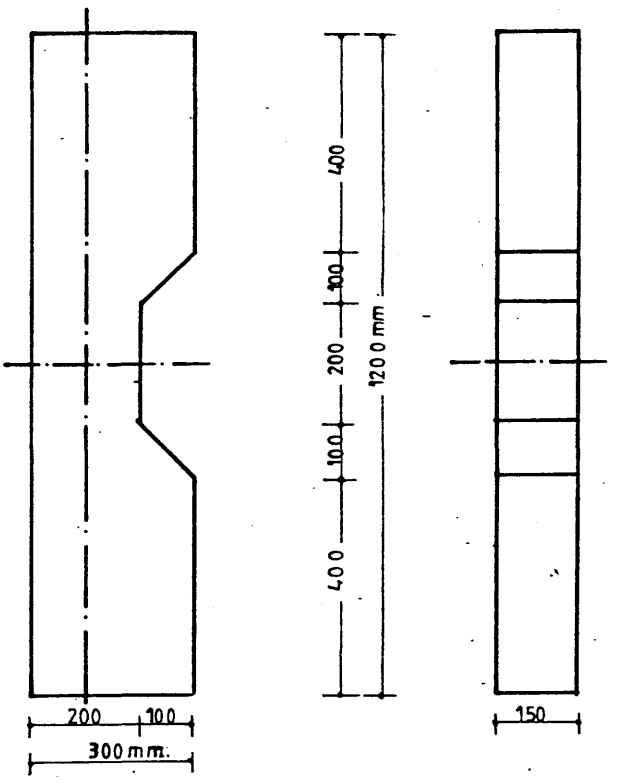

Fig. 6.2 Dimensions of the reinforced PC columns.

Fig. 6.3 Details of reinforcement for the five reinforced PC columns.

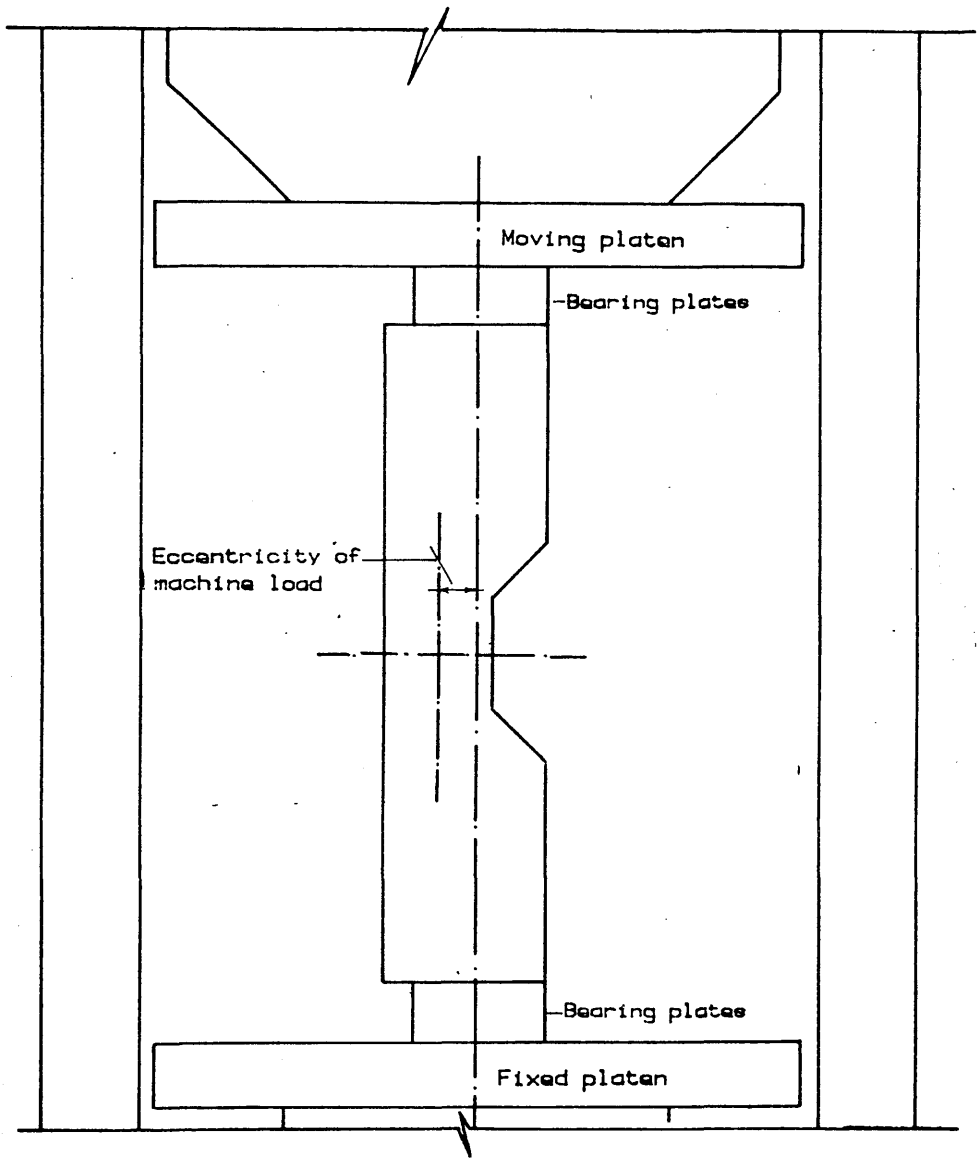

Fig. 6.4 Testing of reinforced PC columns.

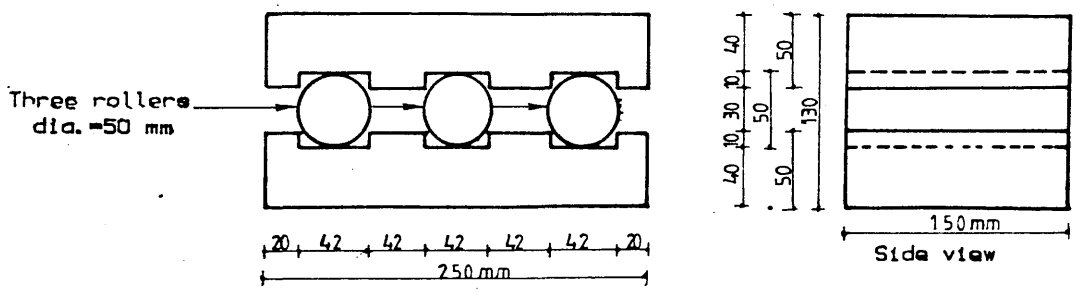

Fig. 6.5 Details of the bearing plates.

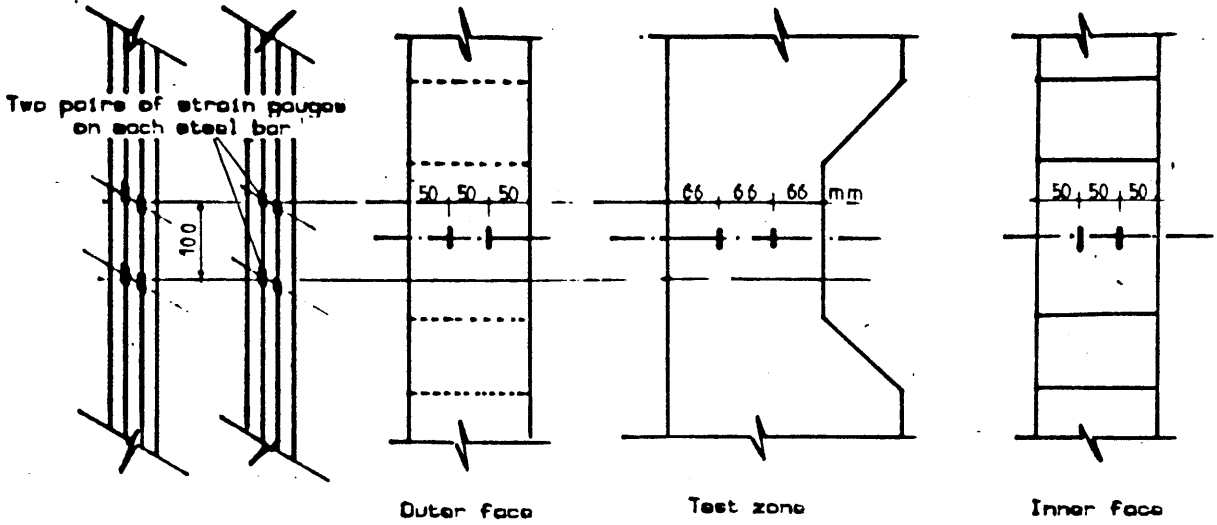

Fig. 6.6 Locations of strain gauges for measuring strains in PC and steel.

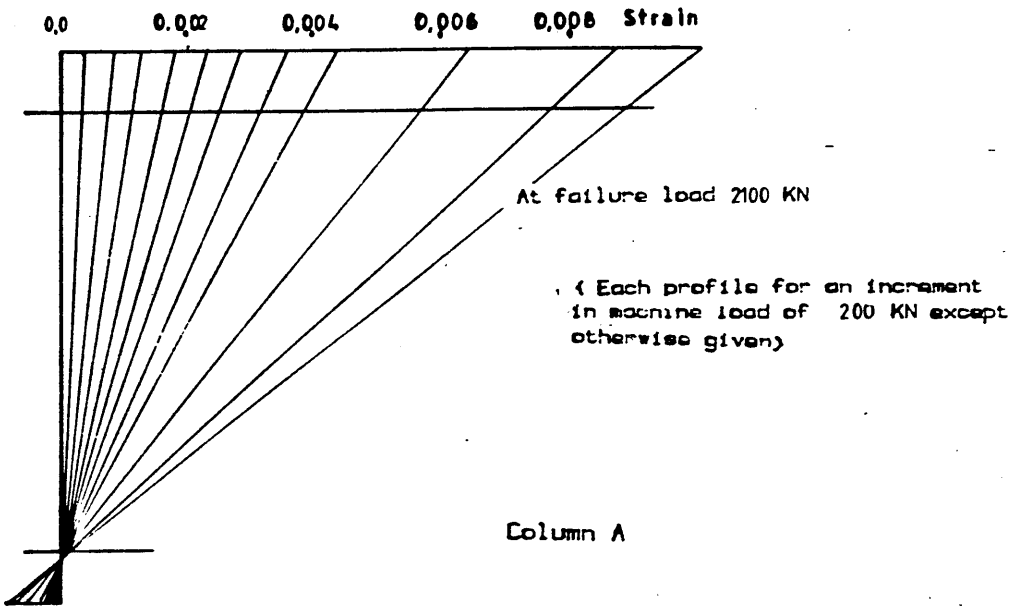

Fig. 6.7 Strain profile at various testing stages for the five reinforced PC columns. (Grade A)

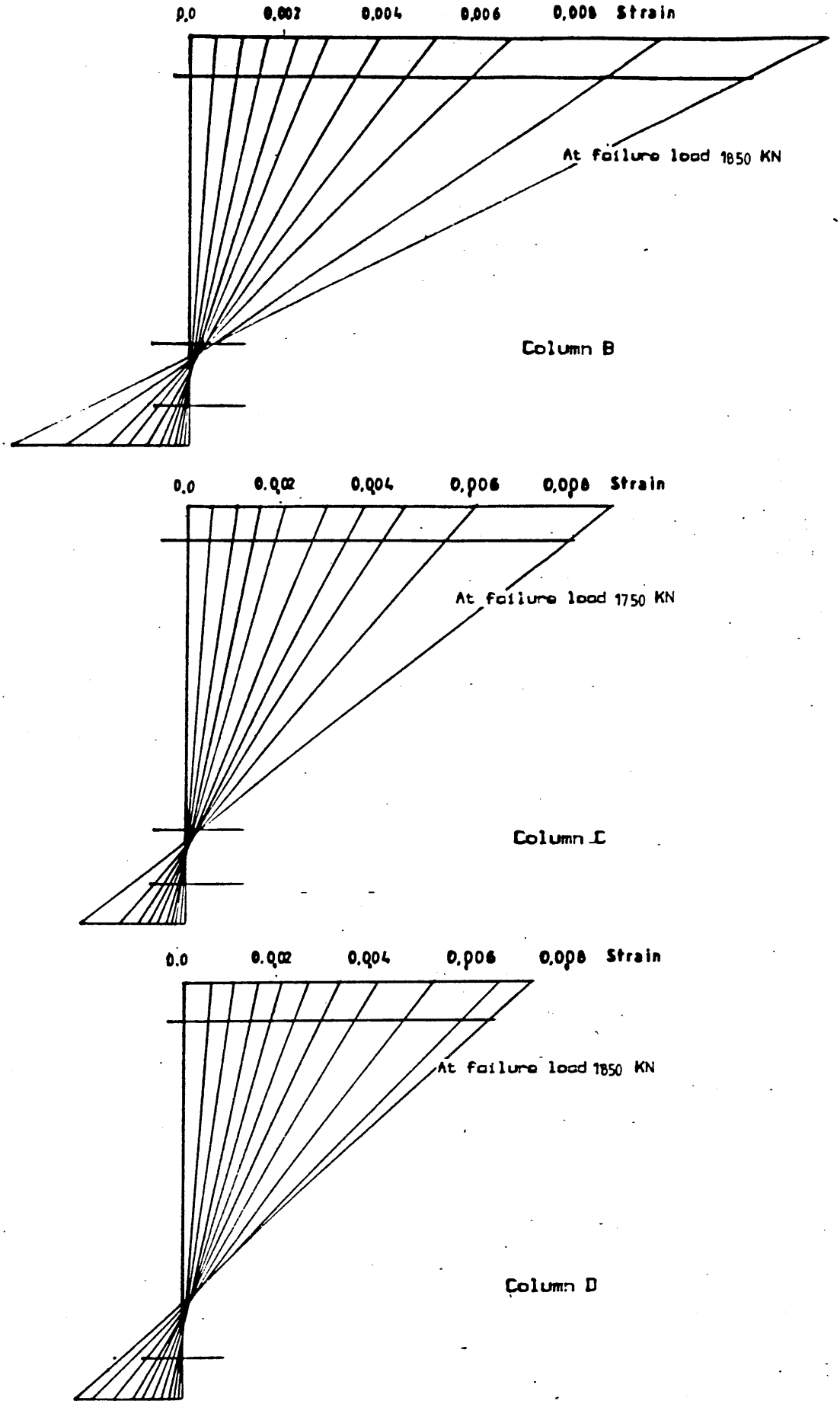

Fig. 6.7 Strain profile at various testing stages for the five reinforced PC columns. (Grade B,C & D)

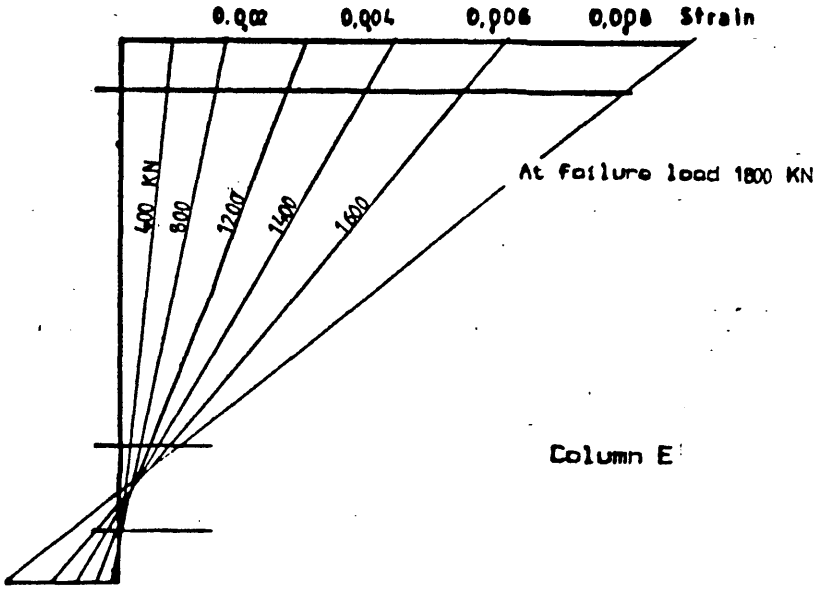

Fig. 6.7 Strain profile at various testing stages for the five reinforced PC columns. (Grade E)

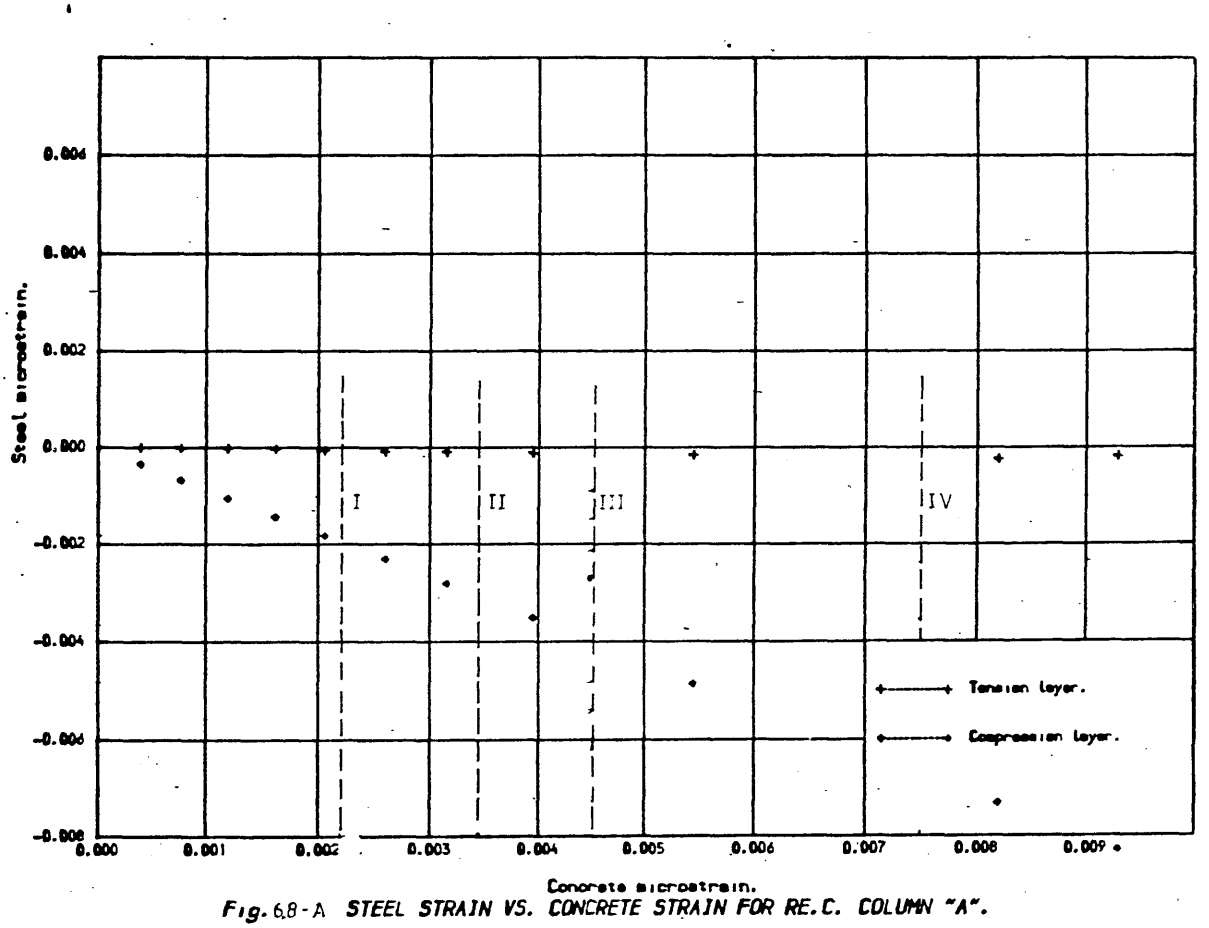

Fig. 6.8-A STEEL STRAIN VS. CONCRETE STRAIN FOR RE.C. COLUMN "A".

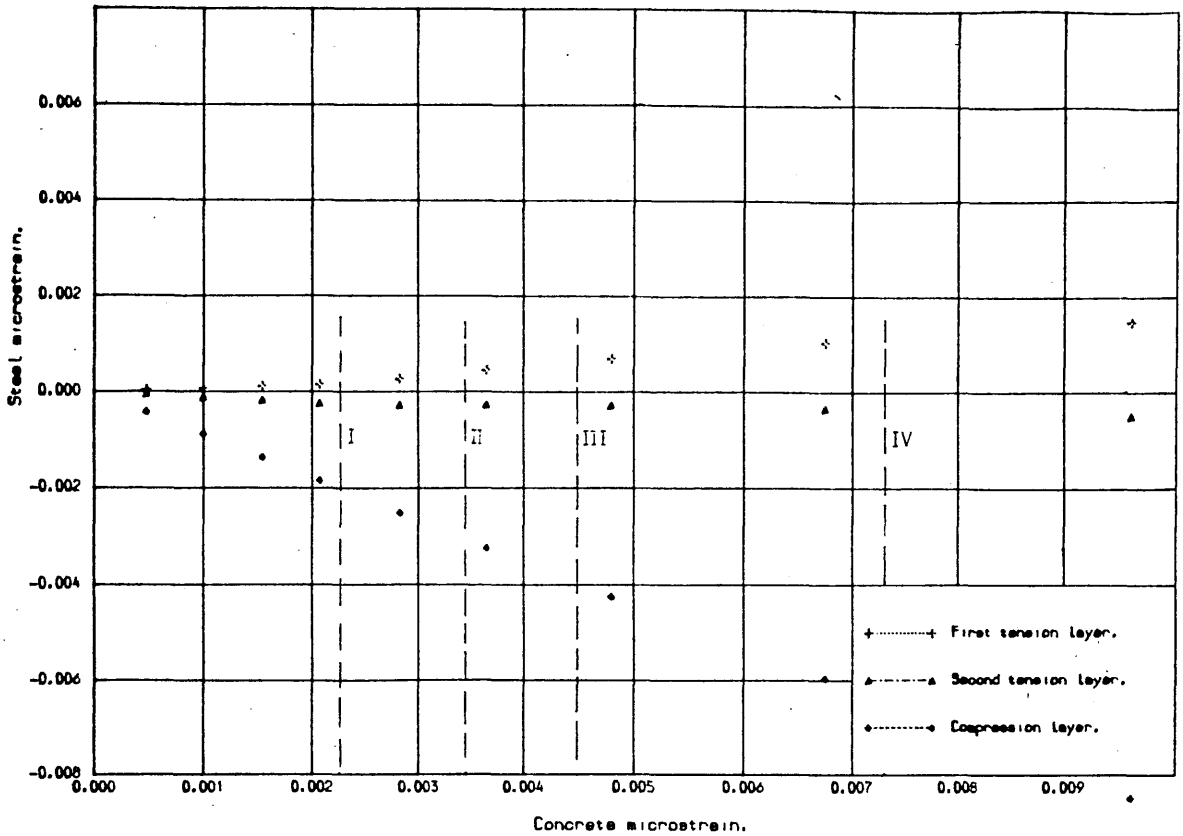

Fig. 6.8-B *STEEL STRAIN VS. CONCRETE STRAIN FOR RE.C. COLUMN "B".*

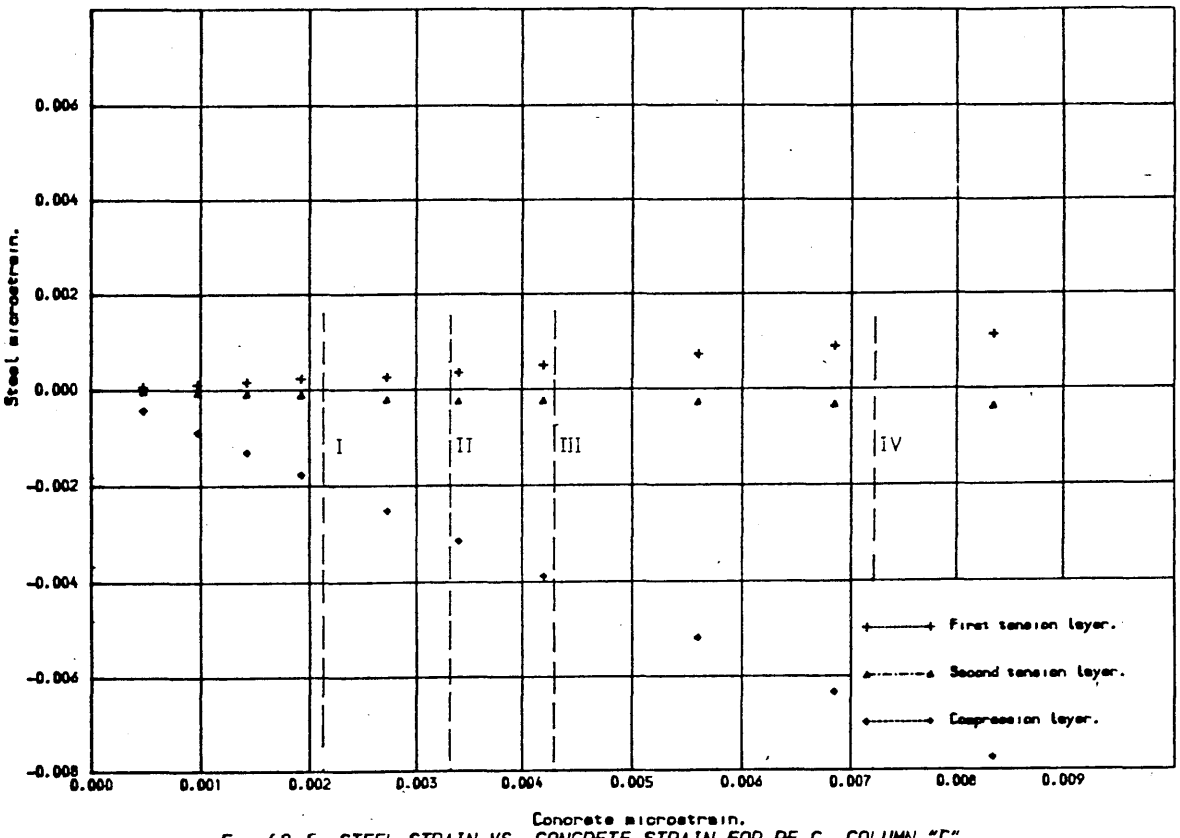

Fig. 6.8-C *STEEL STRAIN VS. CONCRETE STRAIN FOR RE.C. COLUMN "C".*

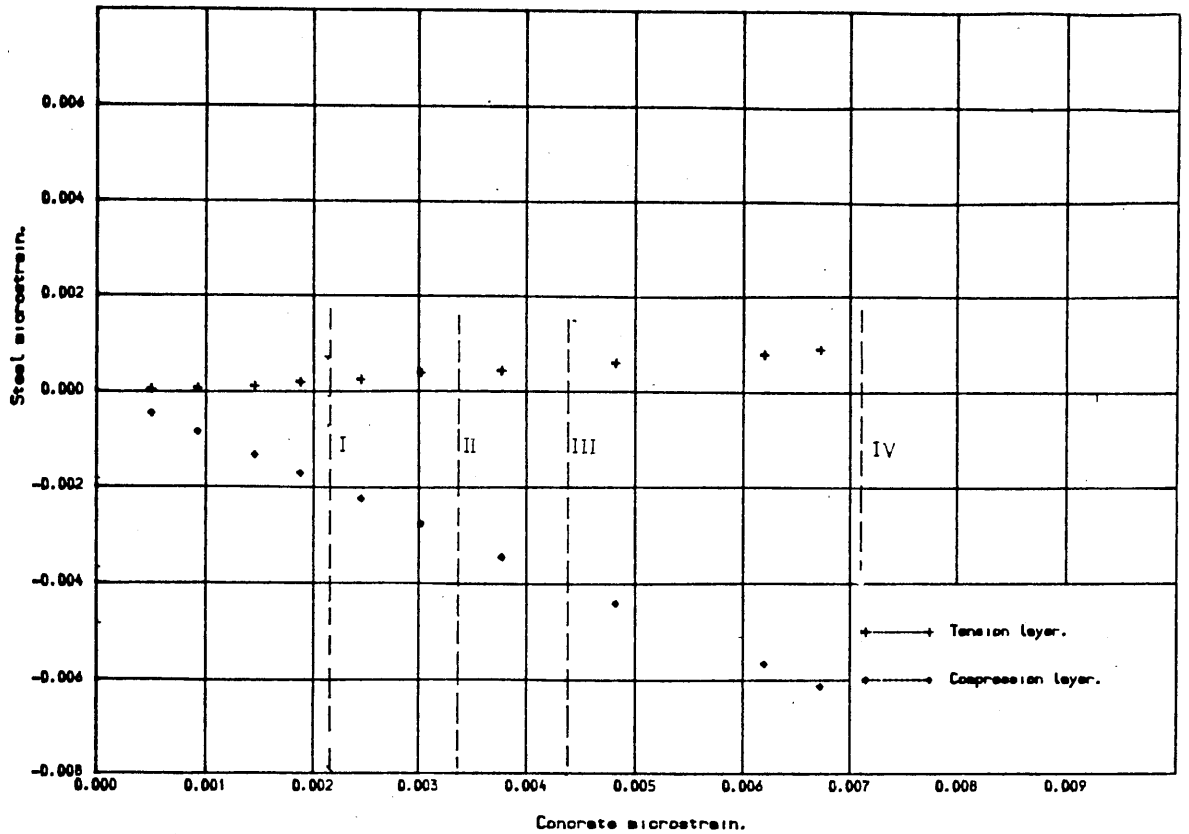

Fig. 6.8-D *STEEL STRAIN VS. CONCRETE STRAIN FOR RE.C. COLUMN "D".*

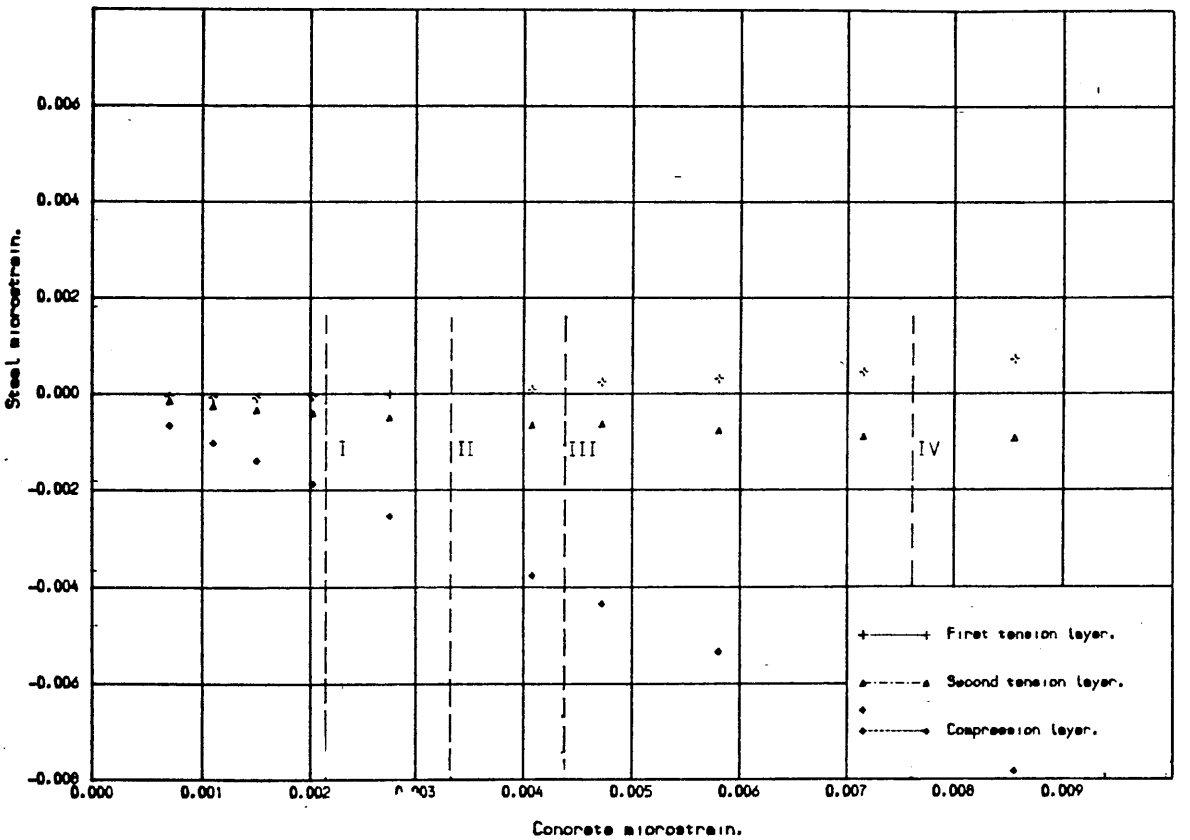

Fig. 6.8-E *STEEL STRAIN VS. CONCRETE STRAIN FOR RE.C. COLUMN "E".*

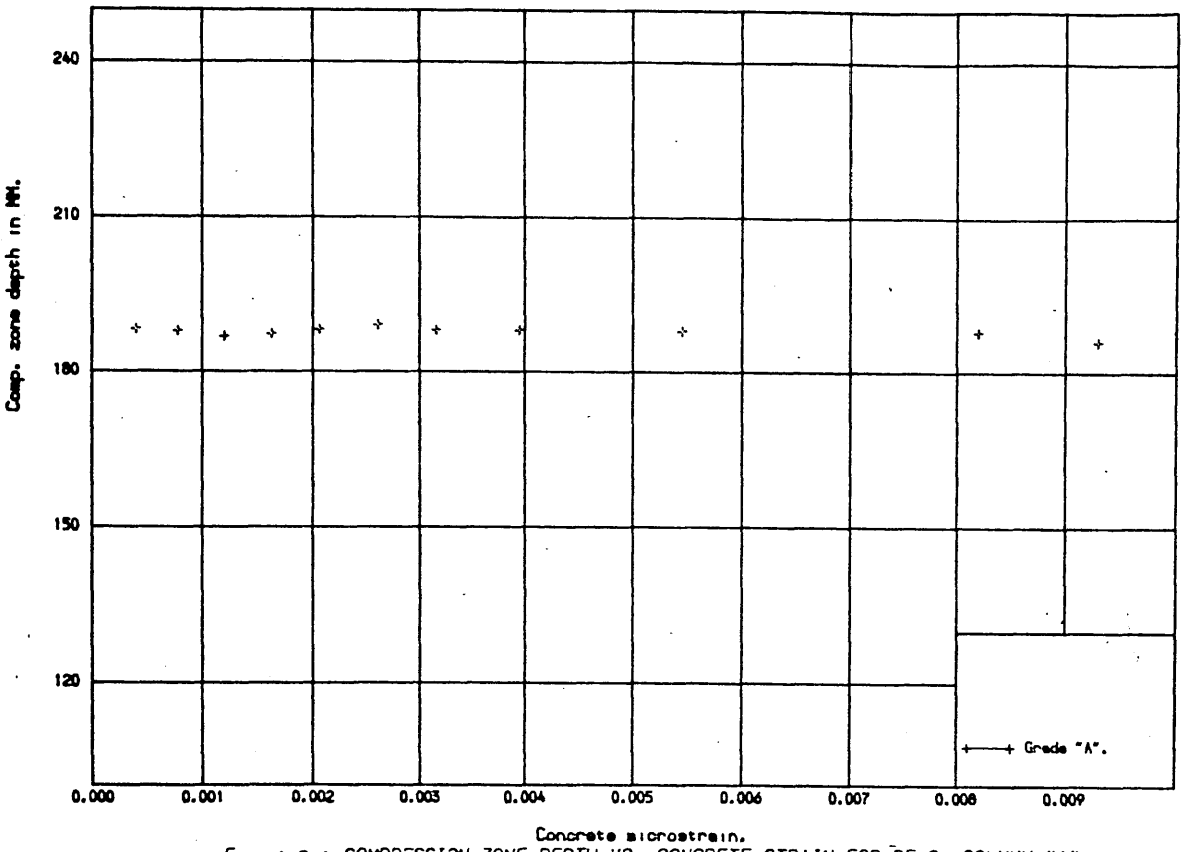

Fig. 6.9-A *COMPRESSION ZONE DEPTH VS. CONCRETE STRAIN FOR RE.C. COLUMN "A".*

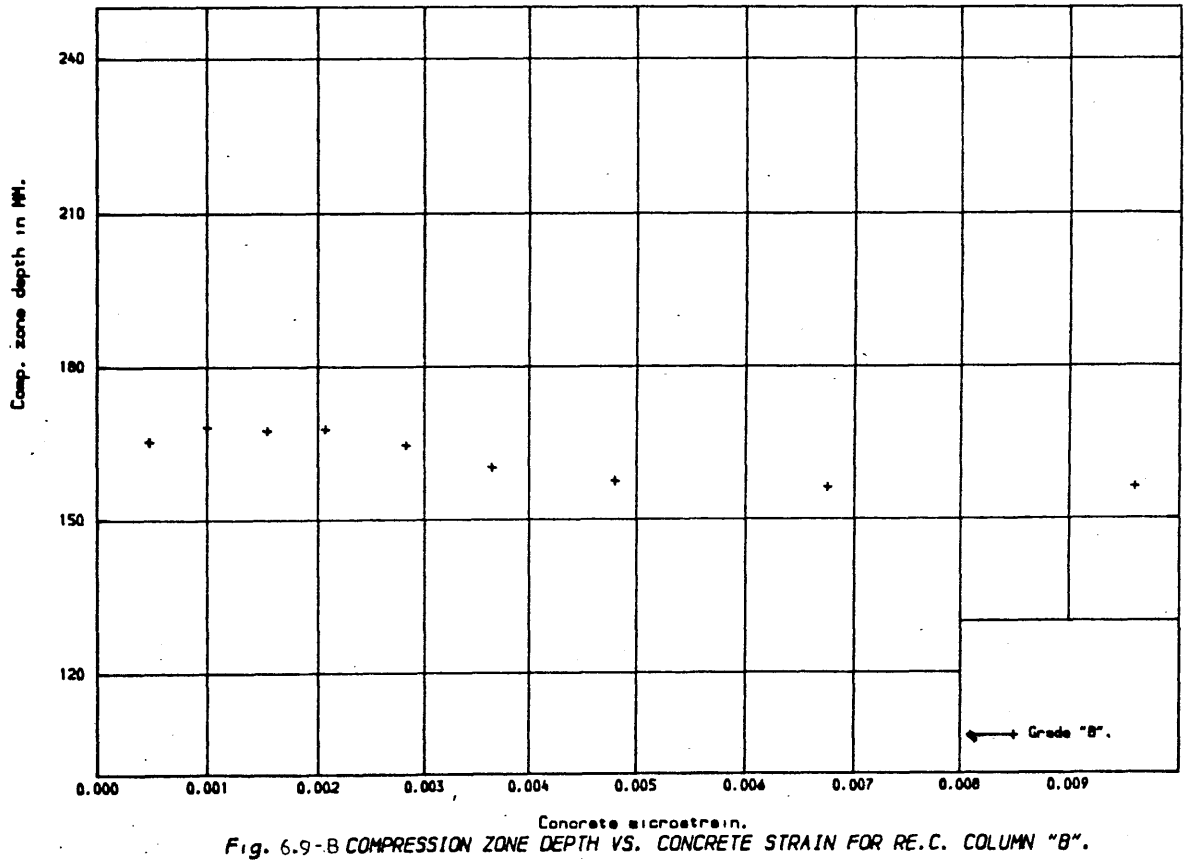

Fig. 6.9-B *COMPRESSION ZONE DEPTH VS. CONCRETE STRAIN FOR RE.C. COLUMN "B".*

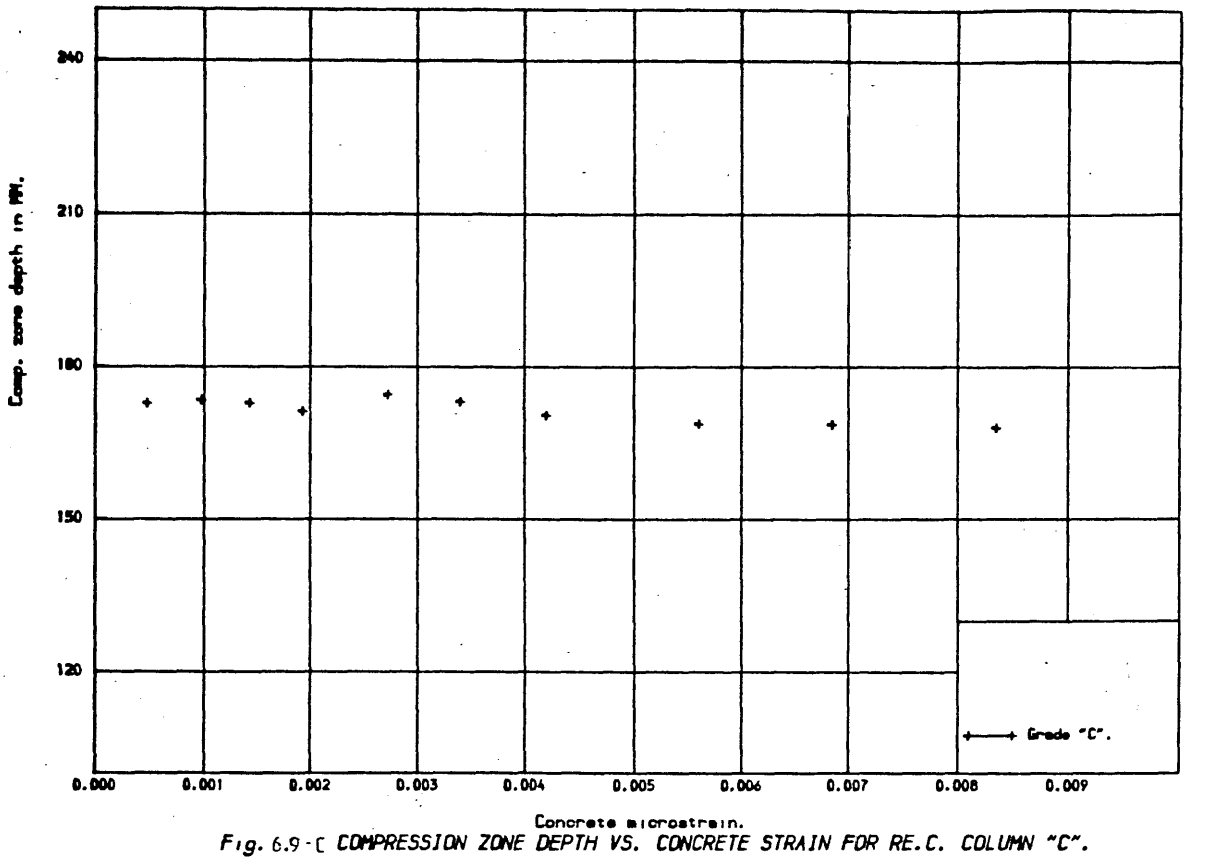

Fig. 6.9-C COMPRESSION ZONE DEPTH VS. CONCRETE STRAIN FOR RE.C. COLUMN "C".

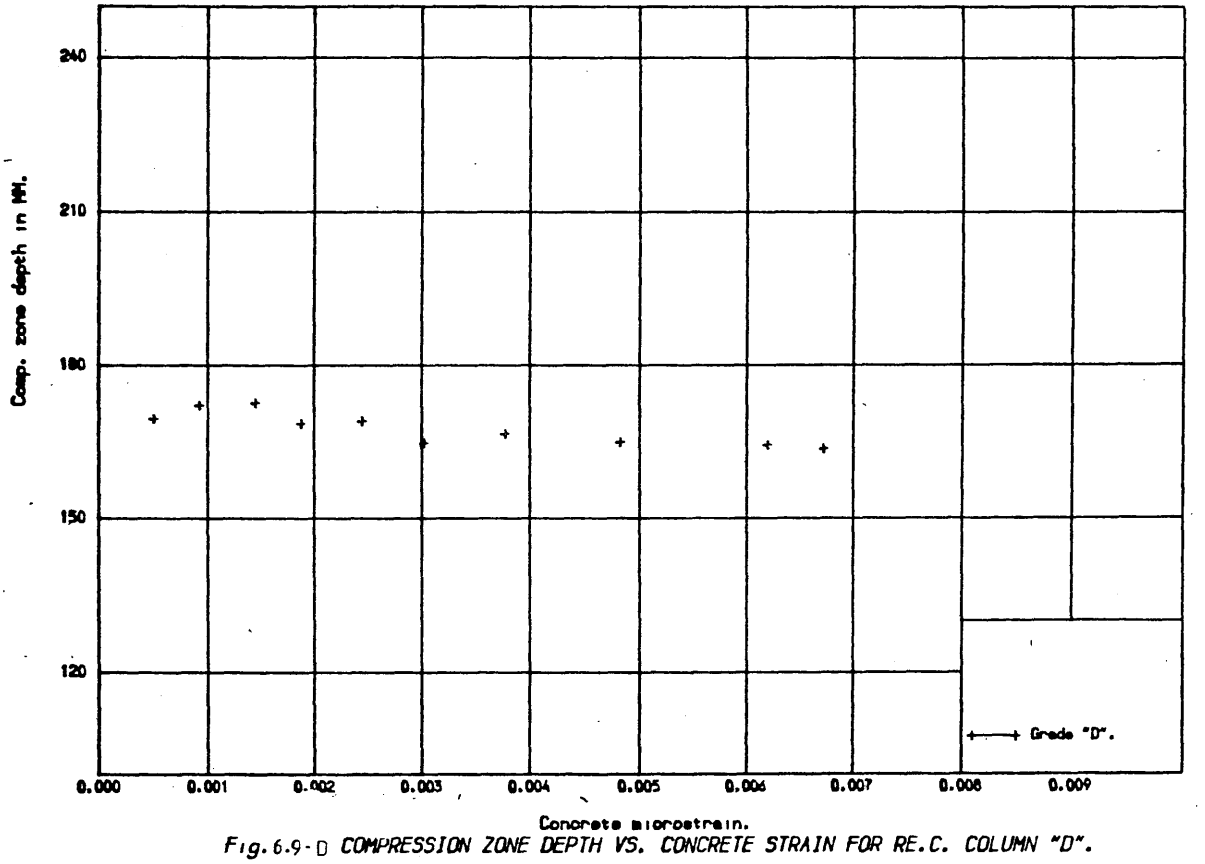

Fig. 6.9-D COMPRESSION ZONE DEPTH VS. CONCRETE STRAIN FOR RE.C. COLUMN "D".

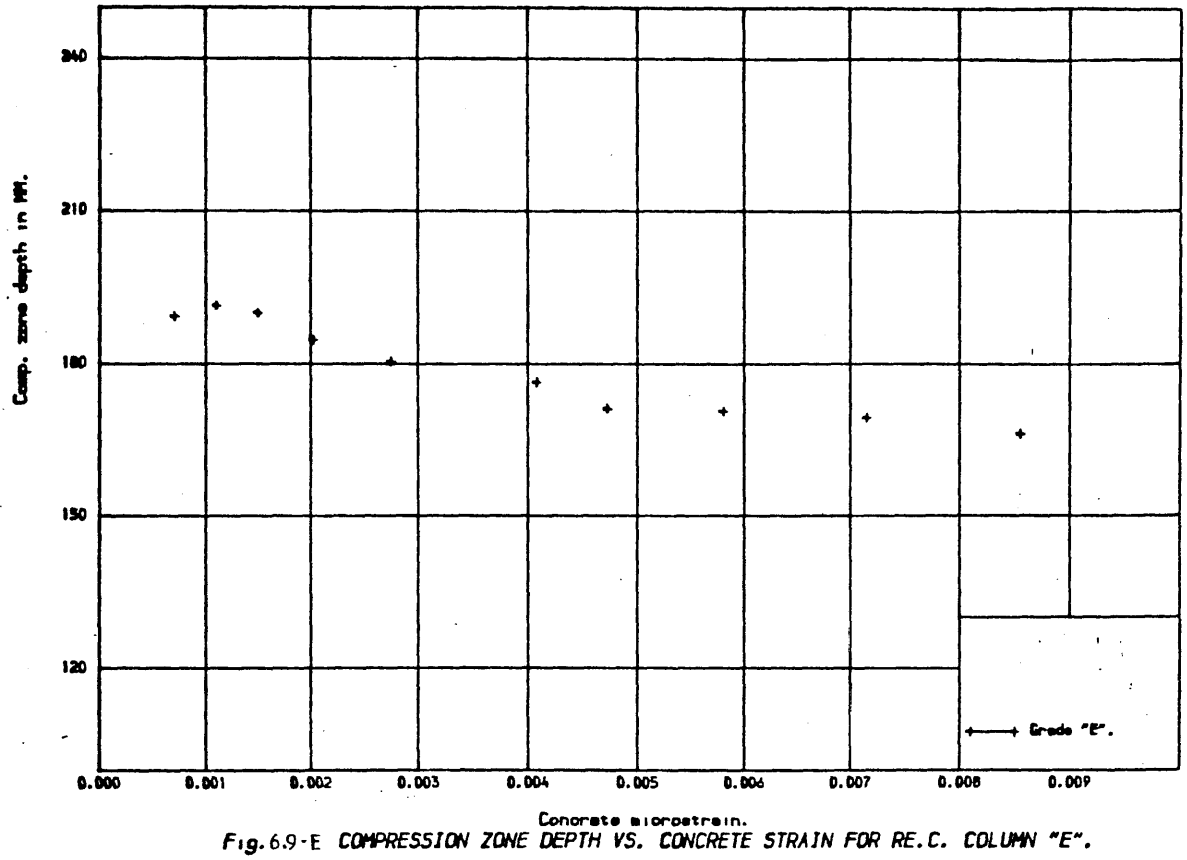

Fig. 6.9-E *COMPRESSION ZONE DEPTH VS. CONCRETE STRAIN FOR RE.C. COLUMN "E".*

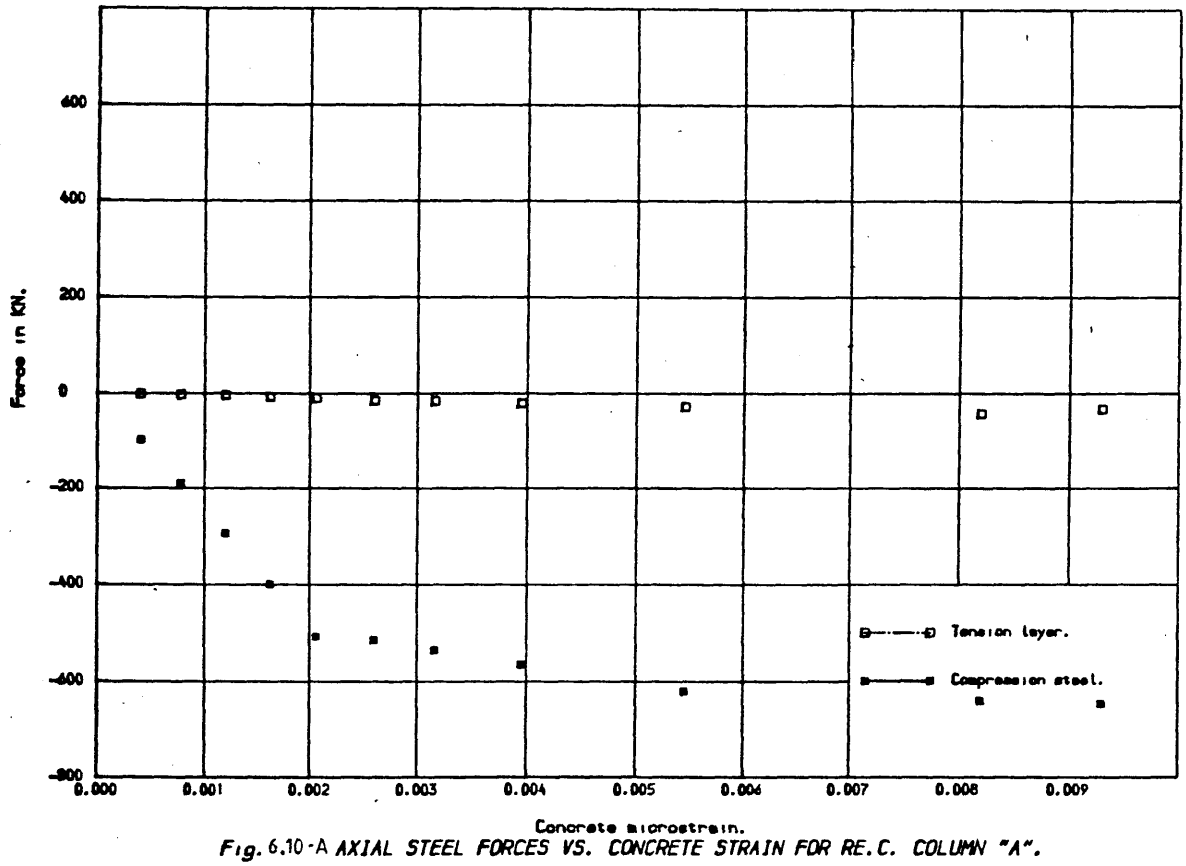

Fig. 6.10-A *AXIAL STEEL FORCES VS. CONCRETE STRAIN FOR RE.C. COLUMN "A".*

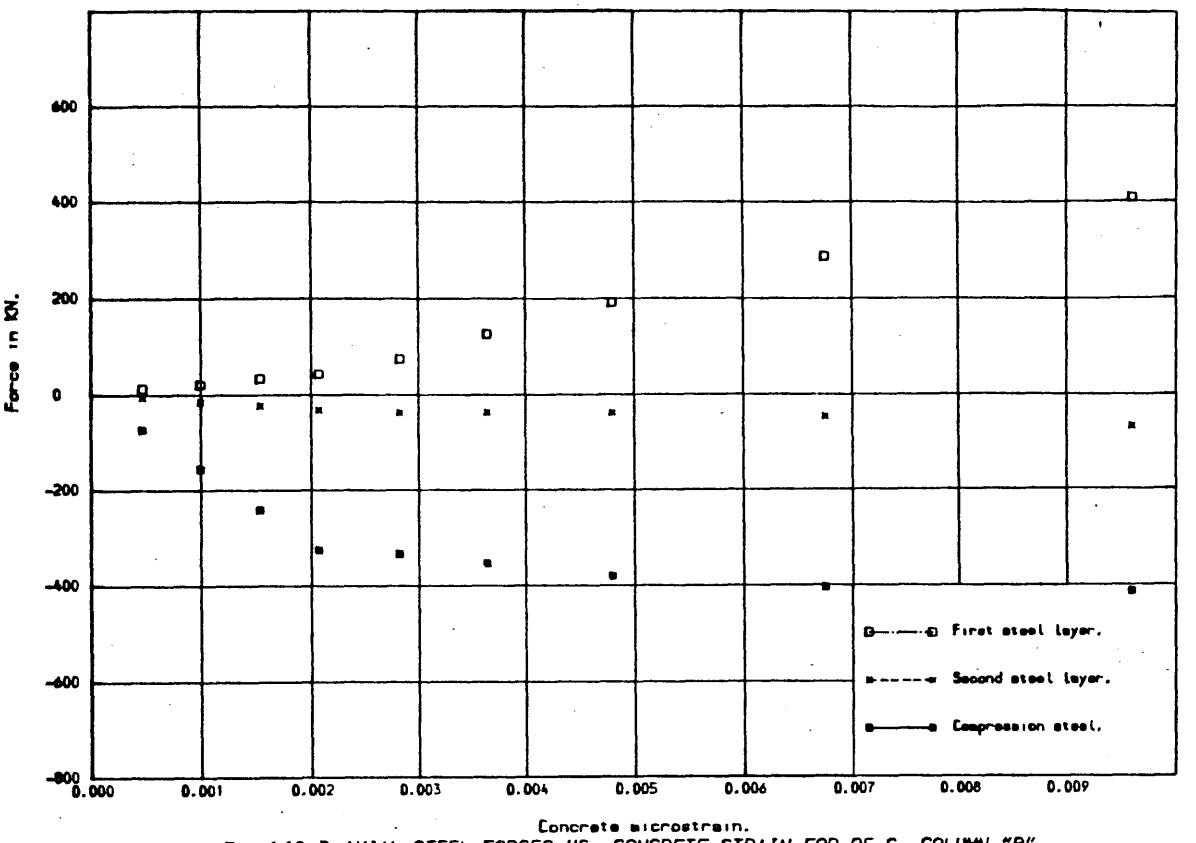

Fig.6.10-B AXIAL STEEL FORCES VS. CONCRETE STRAIN FOR RE.C. COLUMN "B".

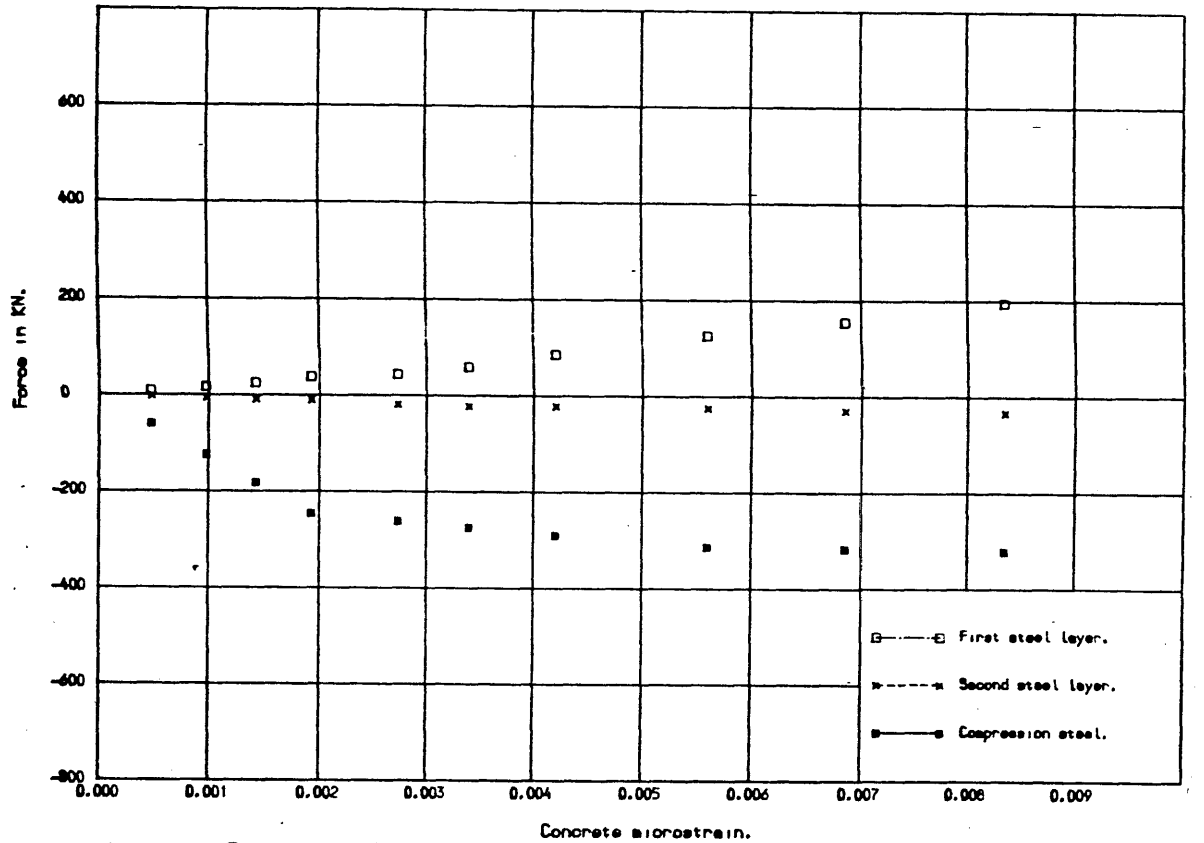

Fig. 6.10-C AXIAL STEEL FORCES VS. CONCRETE STRAIN FOR RE.C. COLUMN "C".

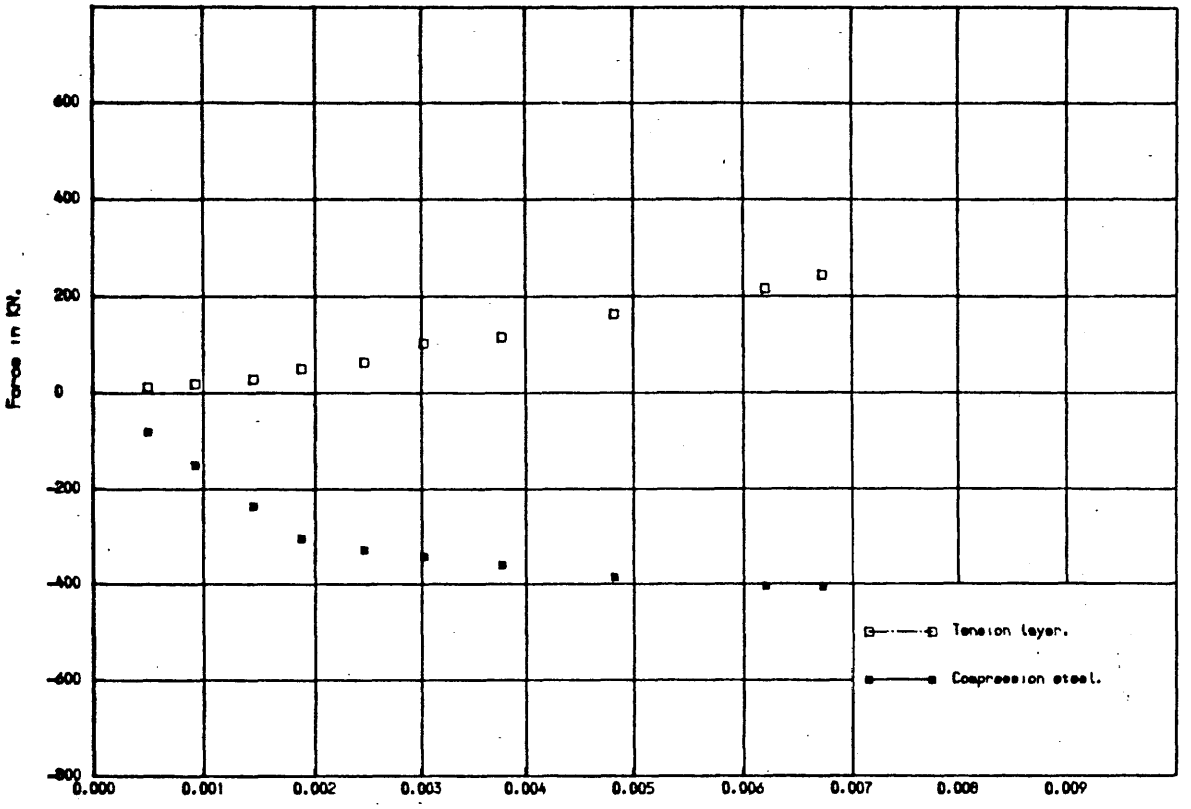

Fig.6.10-D AXIAL STEEL FORCES VS. CONCRETE STRAIN FOR RE.C. COLUMN "D".

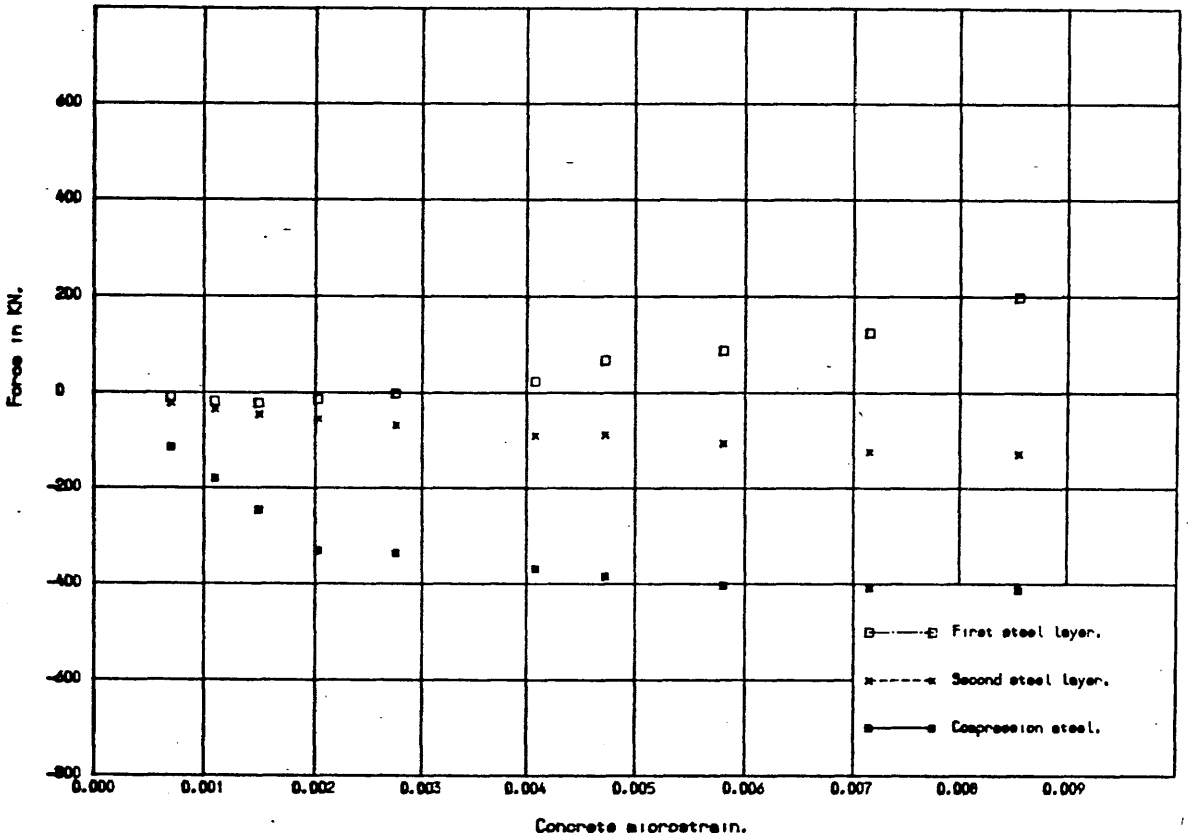

Fig.6.10-E AXIAL STEEL FORCES VS. CONCRETE STRAIN FOR RE.C. COLUMN "E".

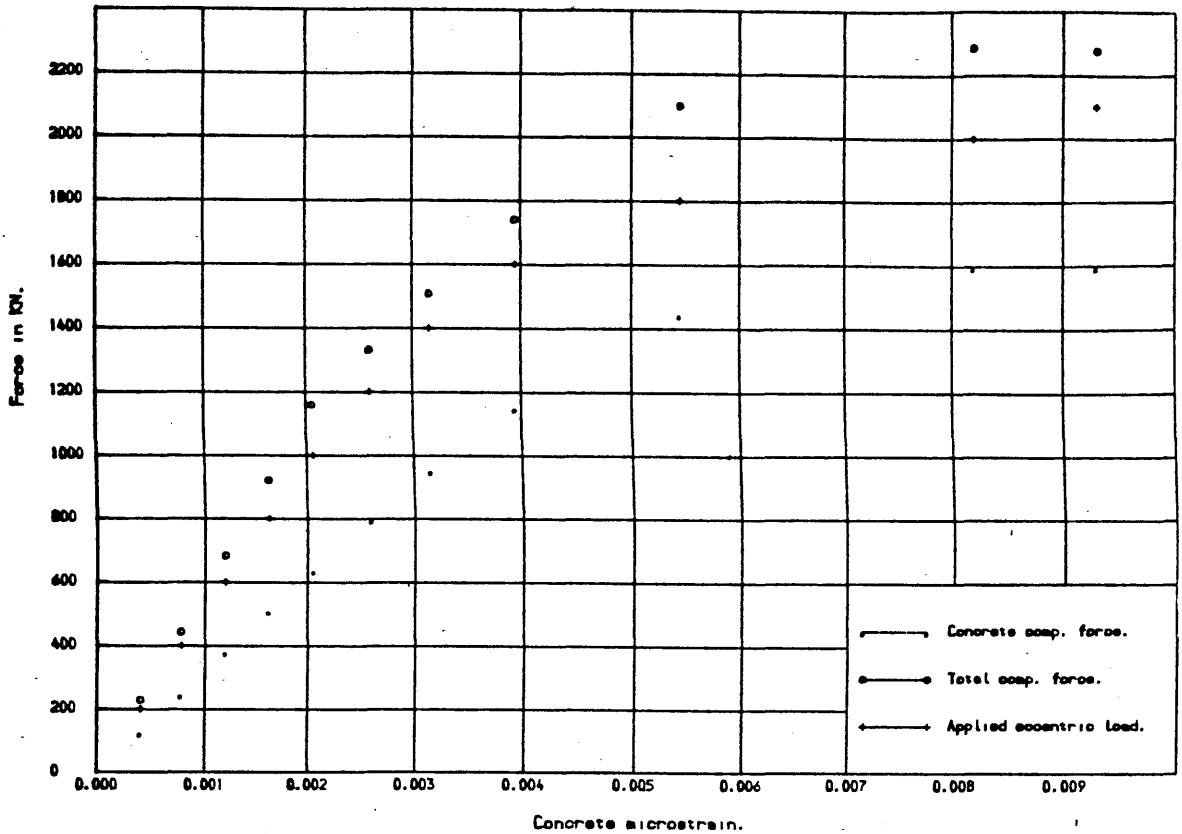

Fig. 6.11-A INTERNAL & APPLIED FORCES VS./ CONCRETE STRAIN FGOR RE.C. COLUMN"A".

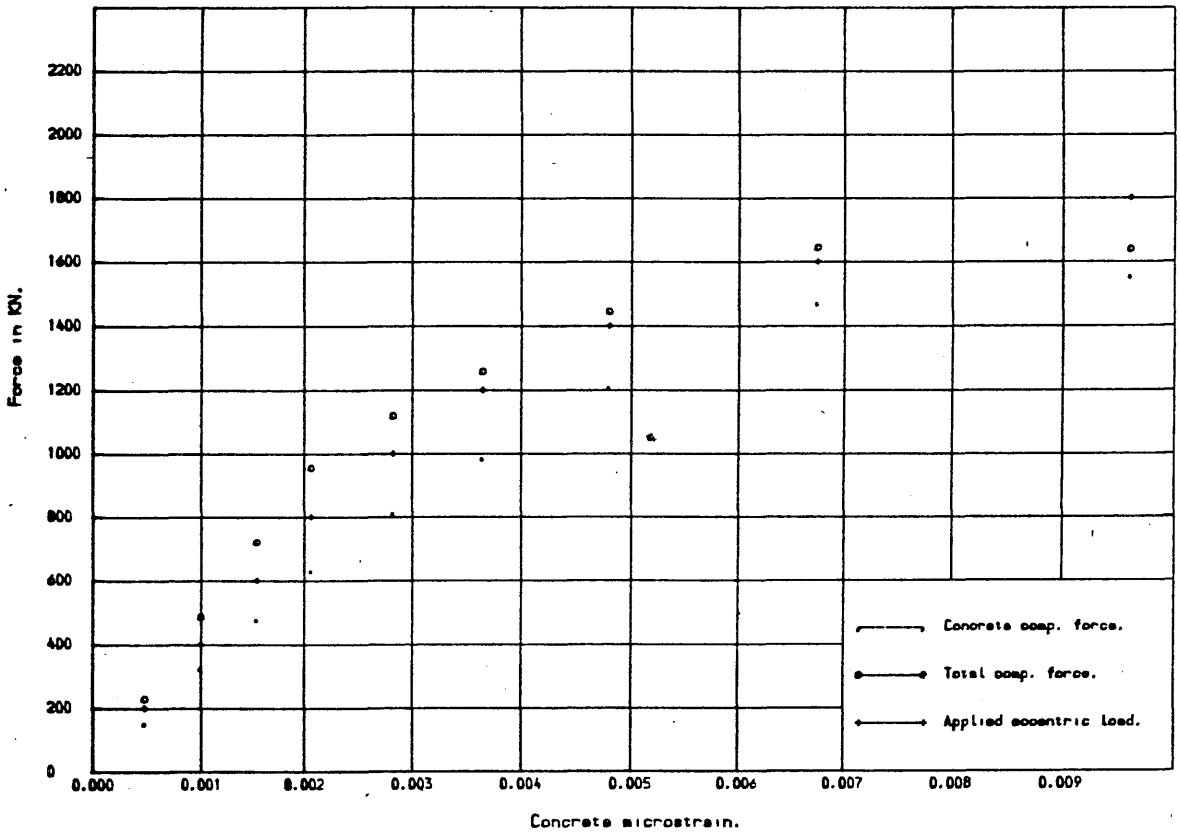

Fig.6.11-B INTERNAL & APPLIED FORCES VS./ CONCRETE STRAIN FGOR RE.C. COLUMN"B".

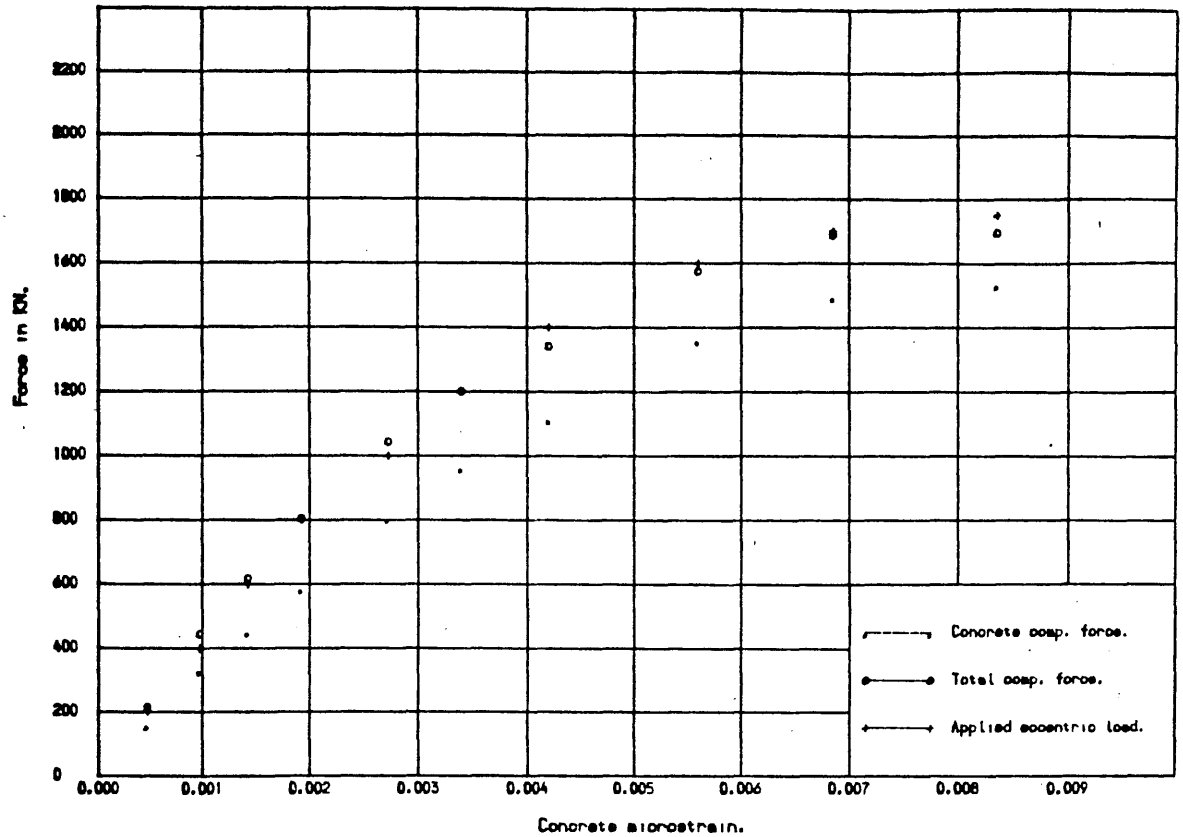

*Fig.*6.11-C *INTERNAL & APPLIED FORCES VS./ CONCRETE STRAIN FGOR RE.C. COLUMN"C".*

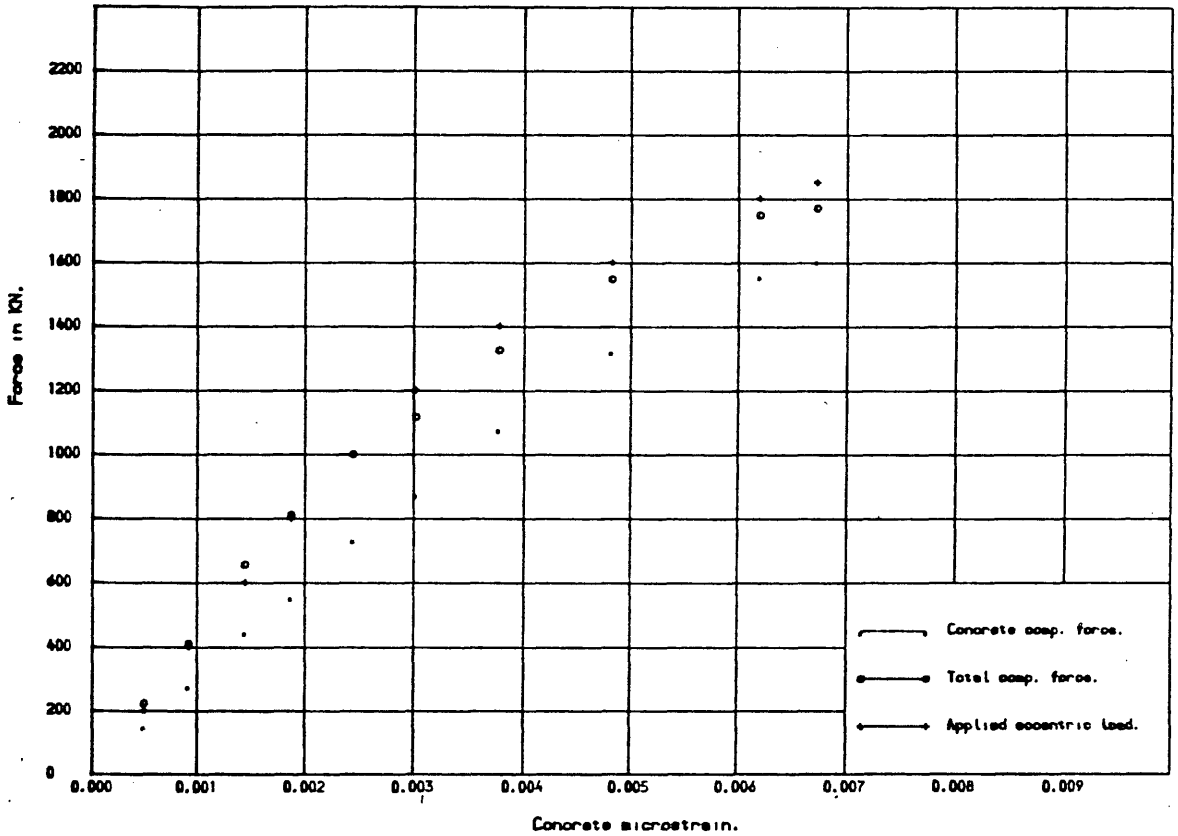

*Fig.*6.11-D *INTERNAL & APPLIED FORCES VS./ CONCRETE STRAIN FGOR RE.C. COLUMN"D".*

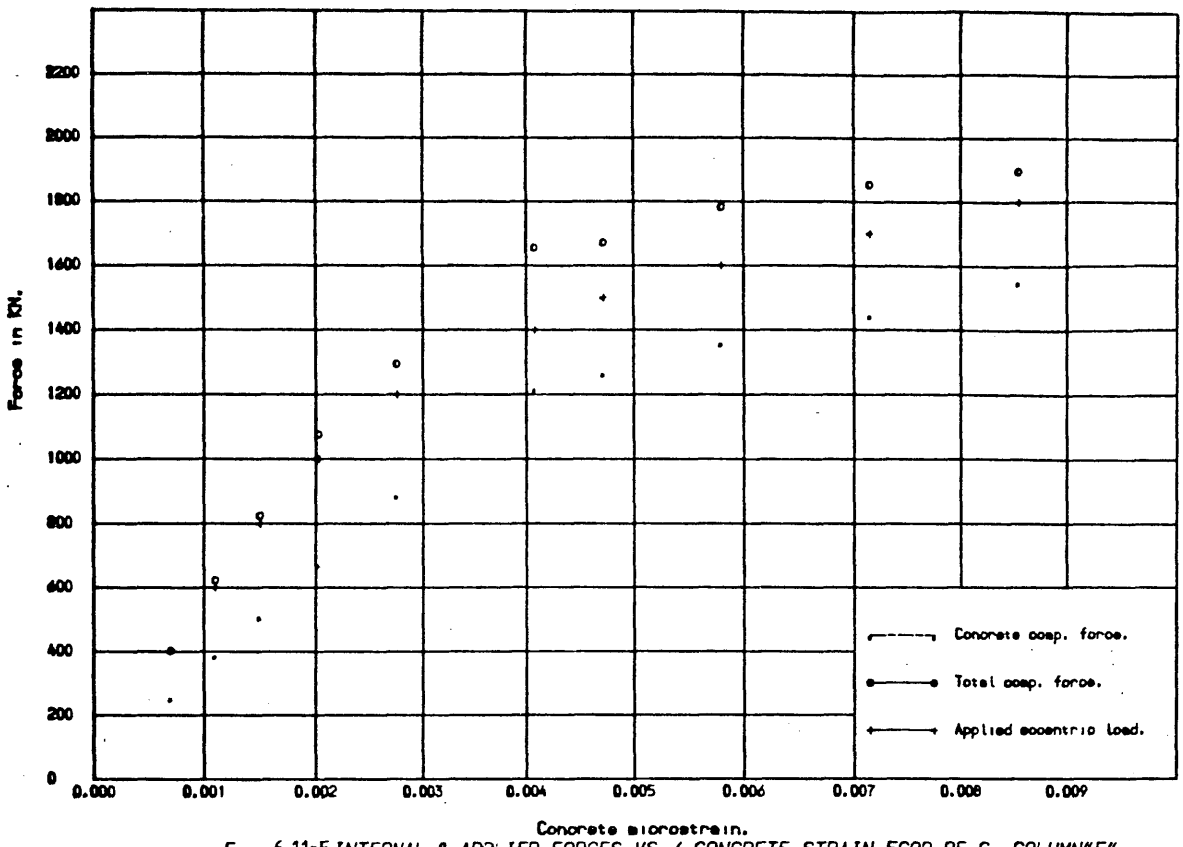

Fig. 6.11-E *INTERNAL & APPLIED FORCES VS./ CONCRETE STRAIN FGOR RE.C. COLUMN"E".*

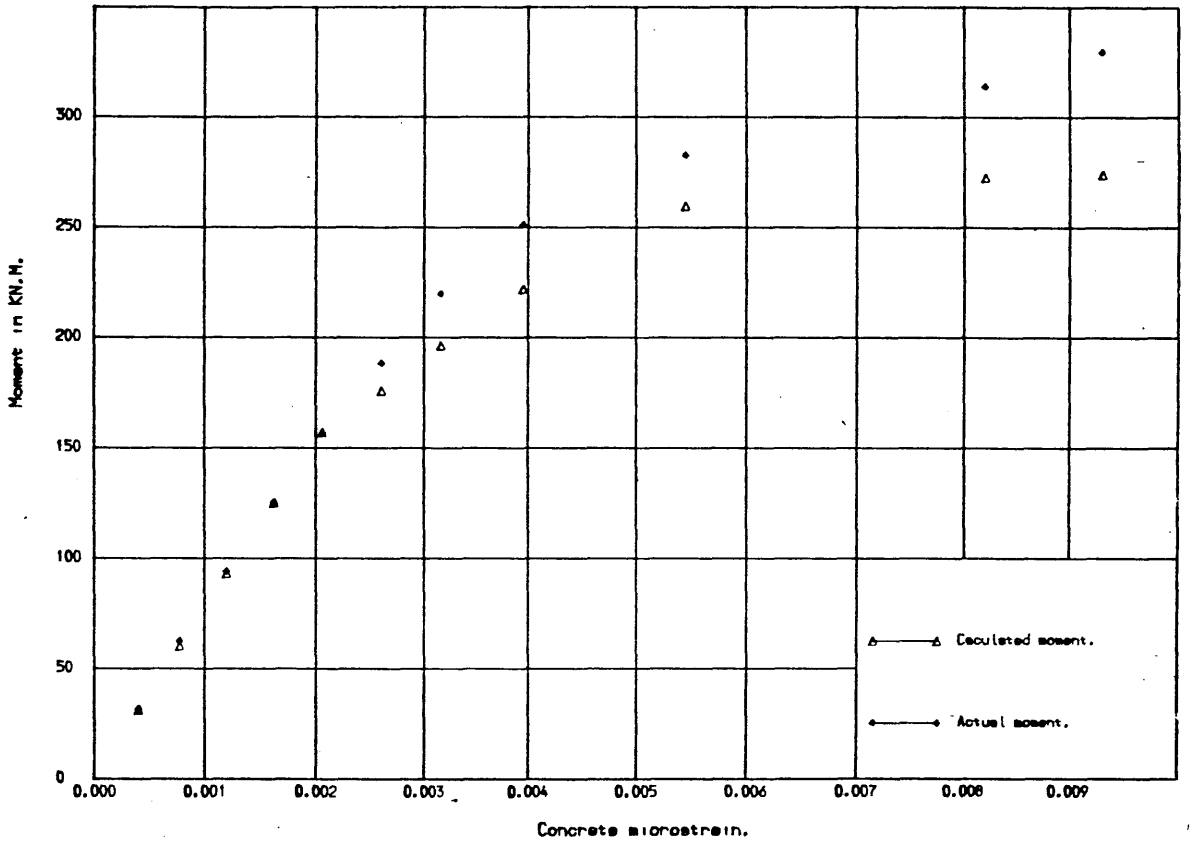

Fig. 6.12-A *CALCULATED & ACTUAL MOMENTS VS. CONCRETE STRAIN FOR RE.C. COLUMN "A".*

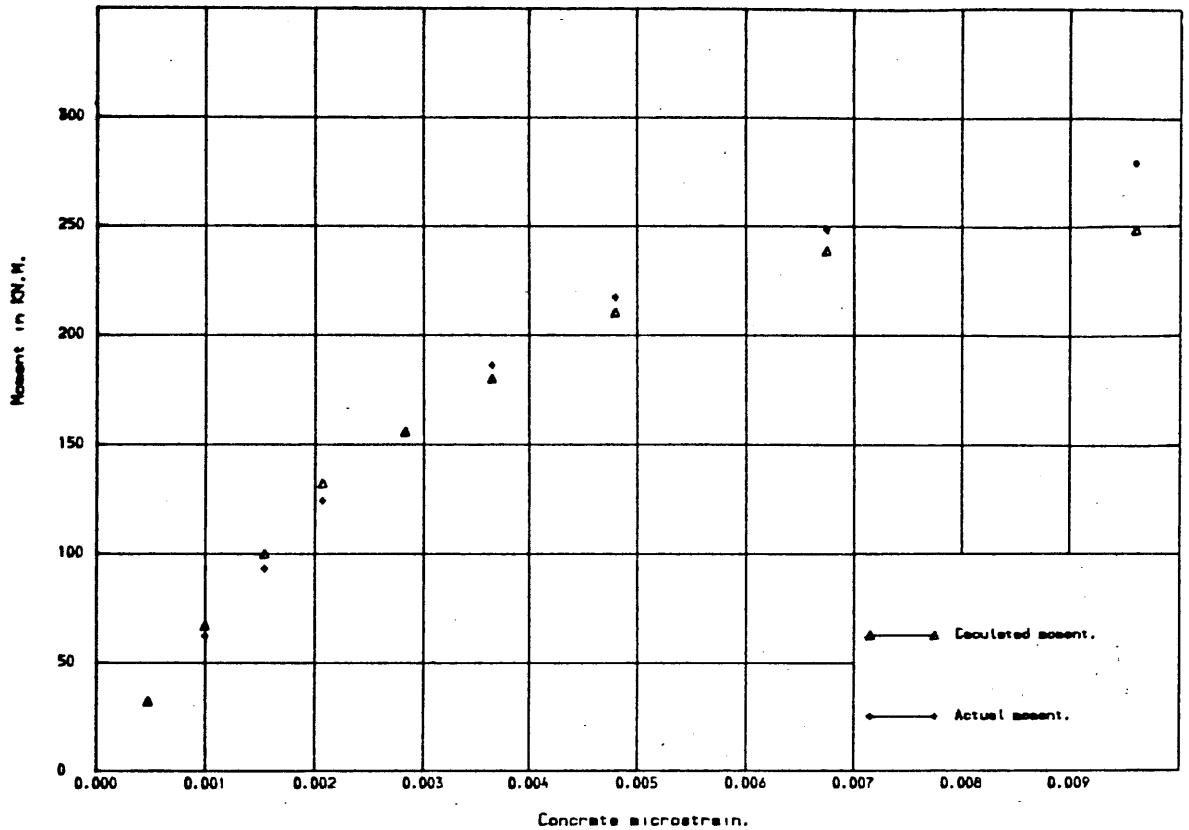

Fig.6.12-B CALCULATED & ACTUAL MOMENTS VS. CONCRETE STRAIN FOR RE.C. COLUMN "B".

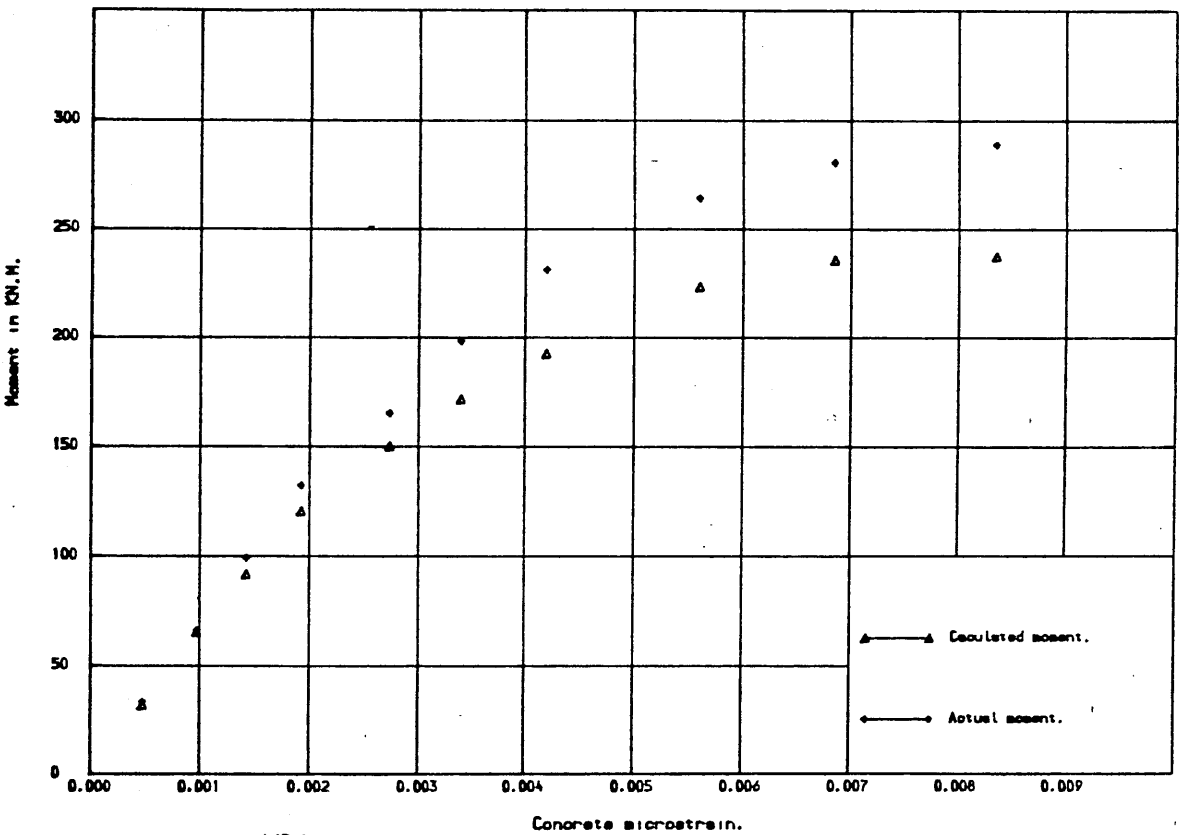

Fig.6.12-C CALCULATED & ACTUAL MOMENTS VS. CONCRETE STRAIN FOR RE.C. COLUMN "C".

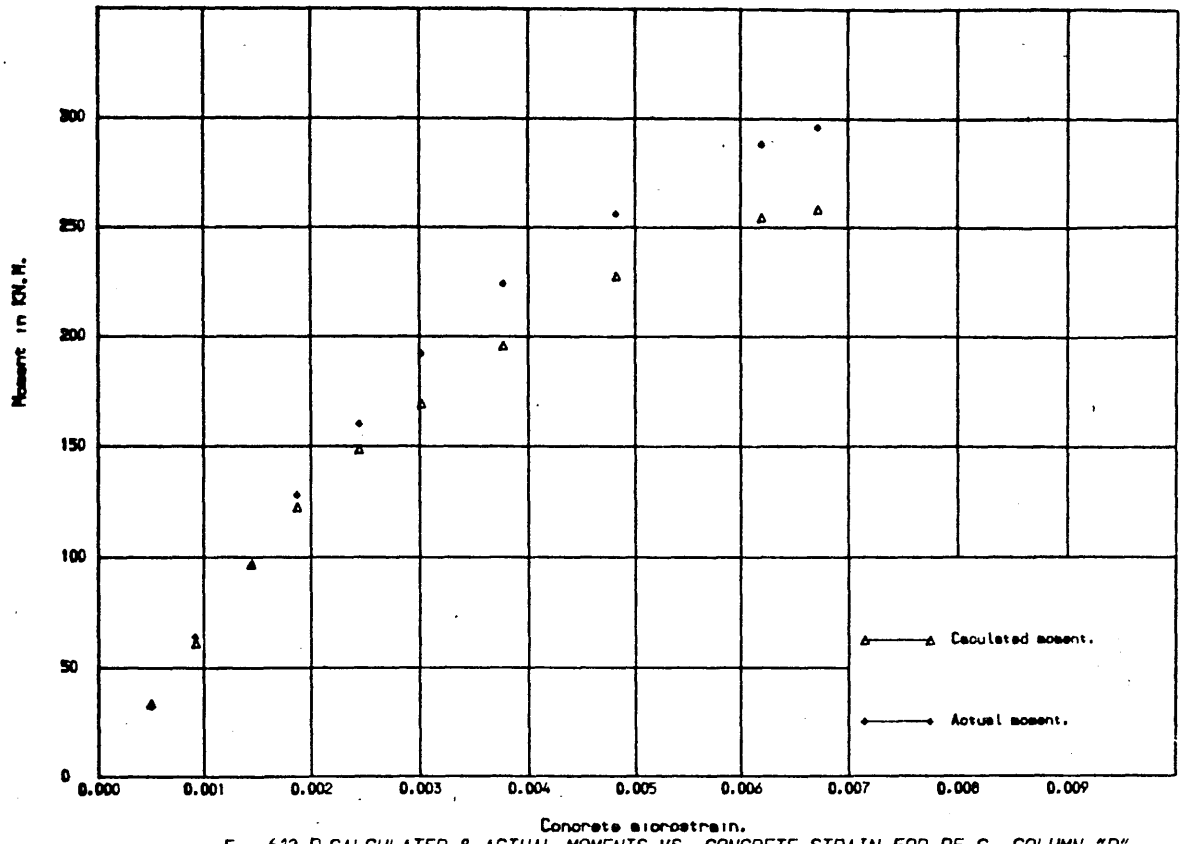

Fig.6.12-D CALCULATED & ACTUAL MOMENTS VS. CONCRETE STRAIN FOR RE.C. COLUMN "D".

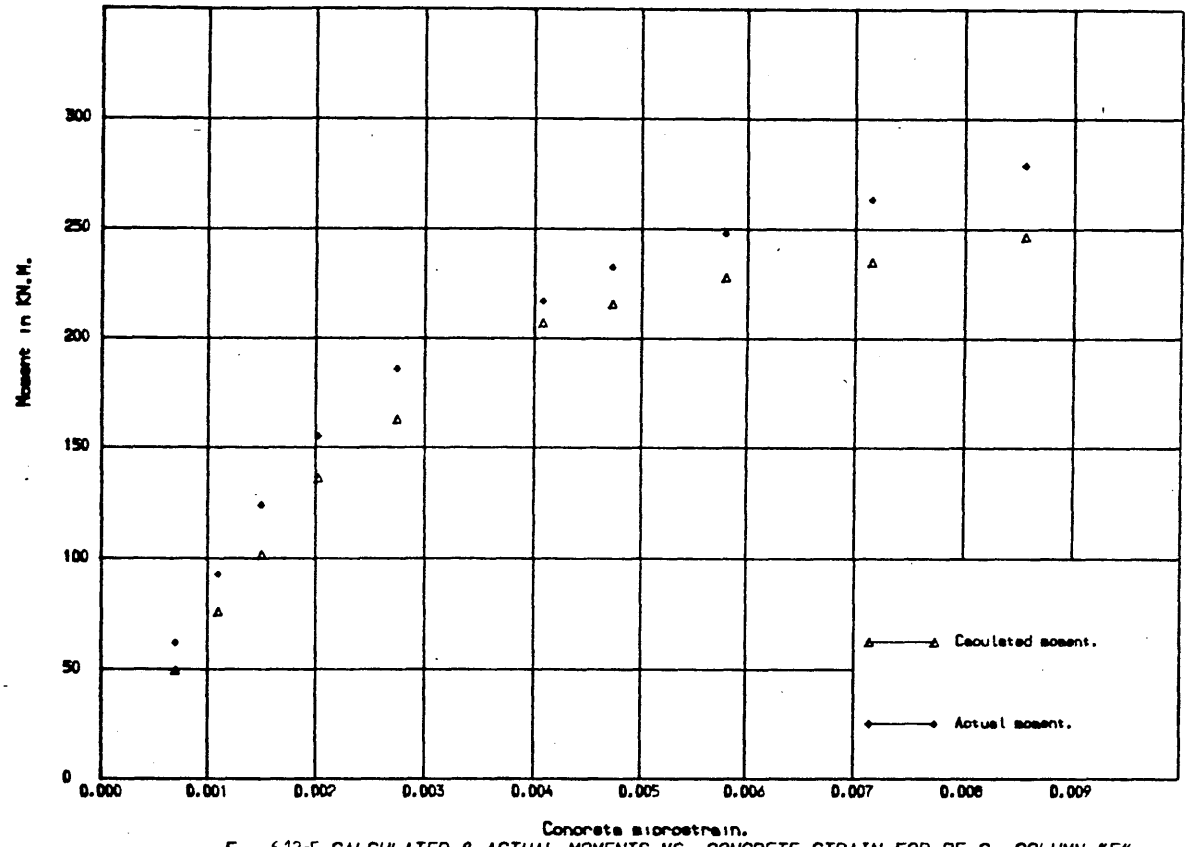

Fig.6.12-E CALCULATED & ACTUAL MOMENTS VS. CONCRETE STRAIN FOR RE.C. COLUMN "E".

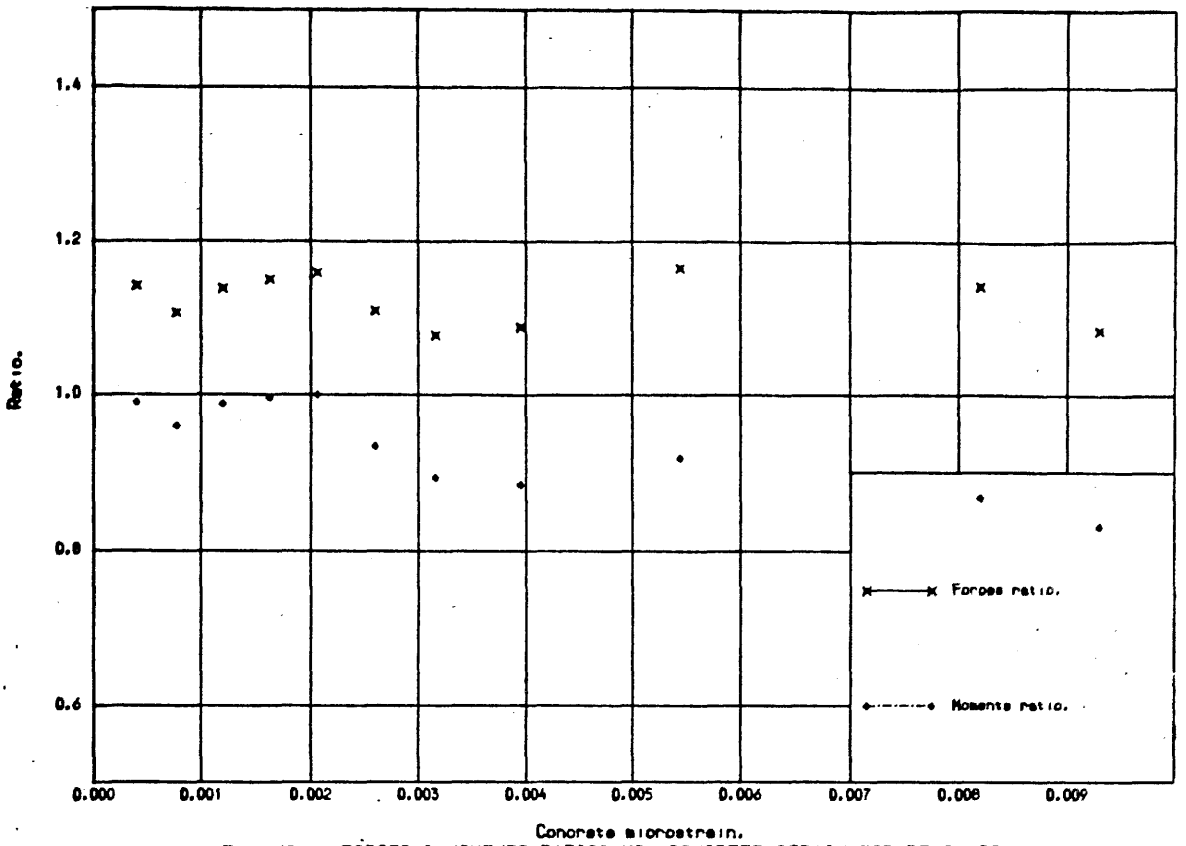

Fig.6.13-A FORCES & MOMENTS RATIOS VS. CONCRETE STRAIN FOR RE.C. COLUMN "A".

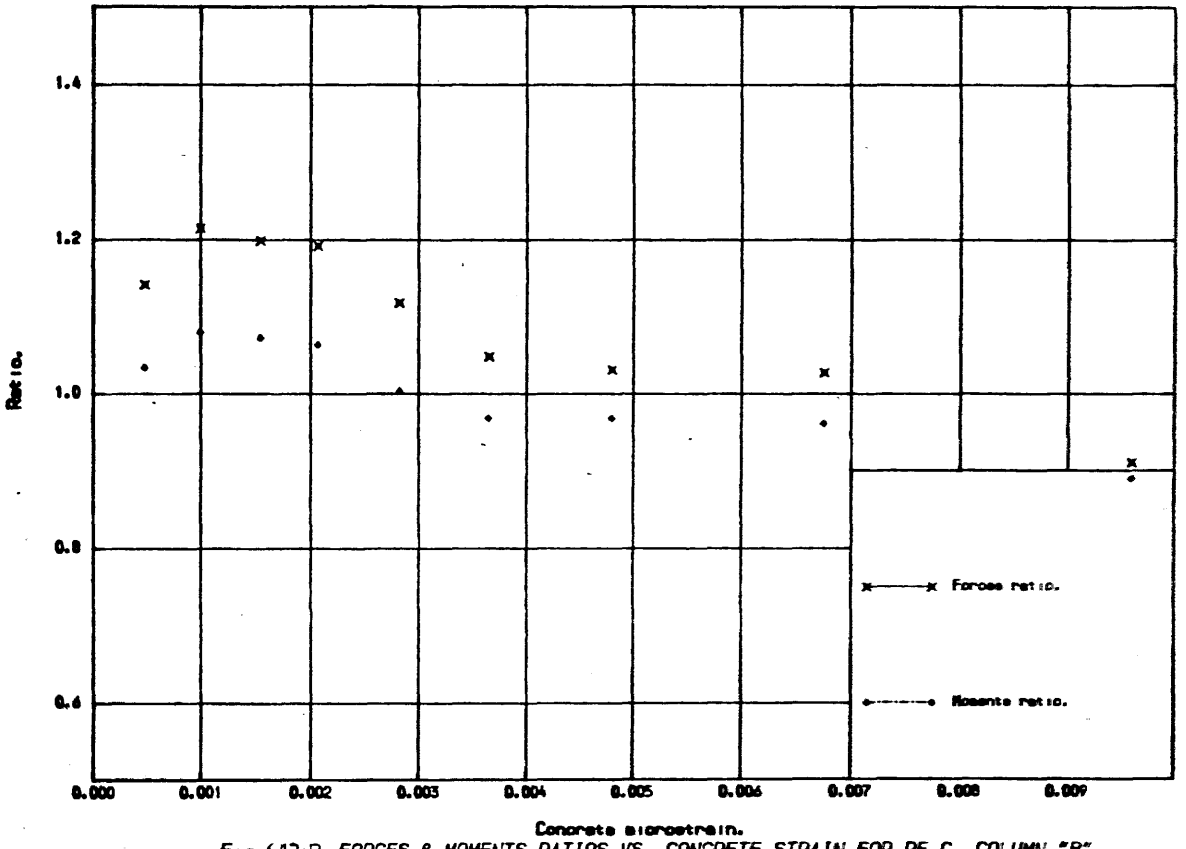

Fig.6.13-B FORCES & MOMENTS RATIOS VS. CONCRETE STRAIN FOR RE.C. COLUMN "B".

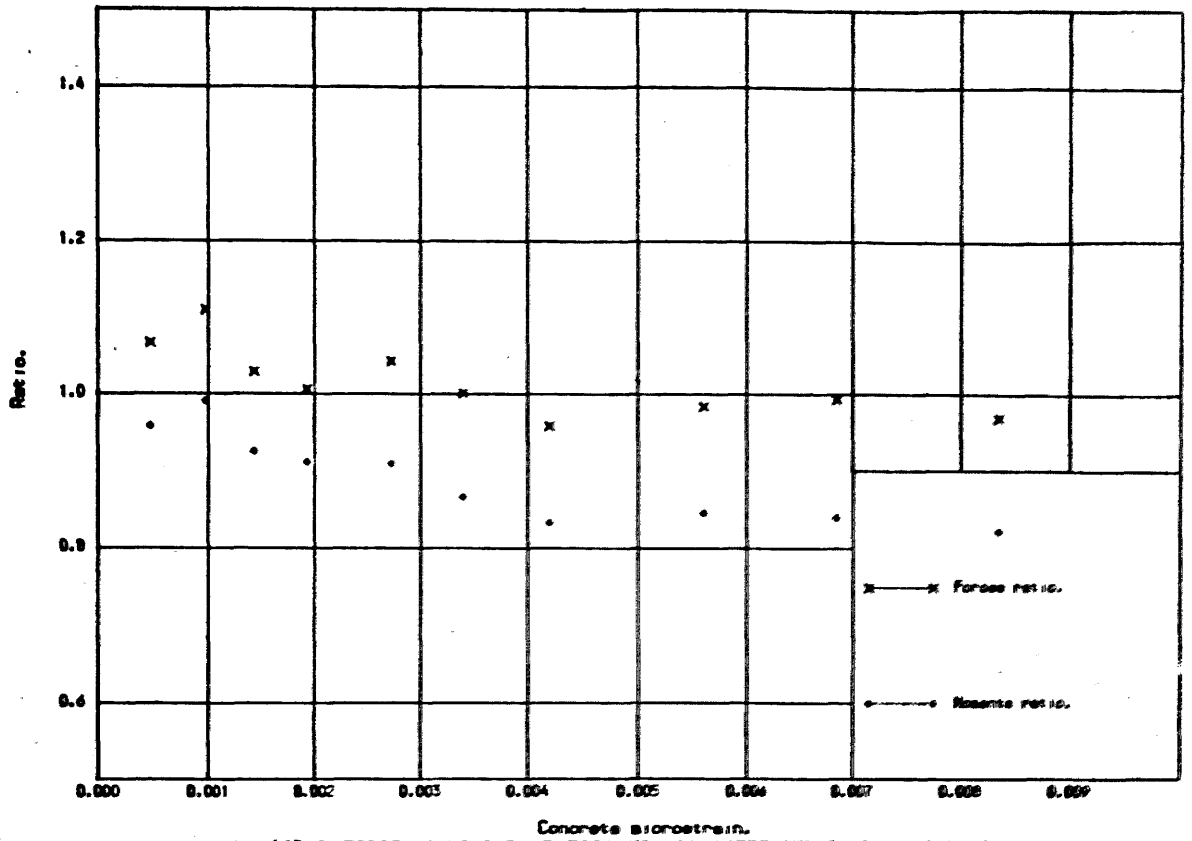

Fig.6.13-C FORCES & MOMENTS RATIOS VS. CONCRETE STRAIN FOR RE.C. COLUMN "C".

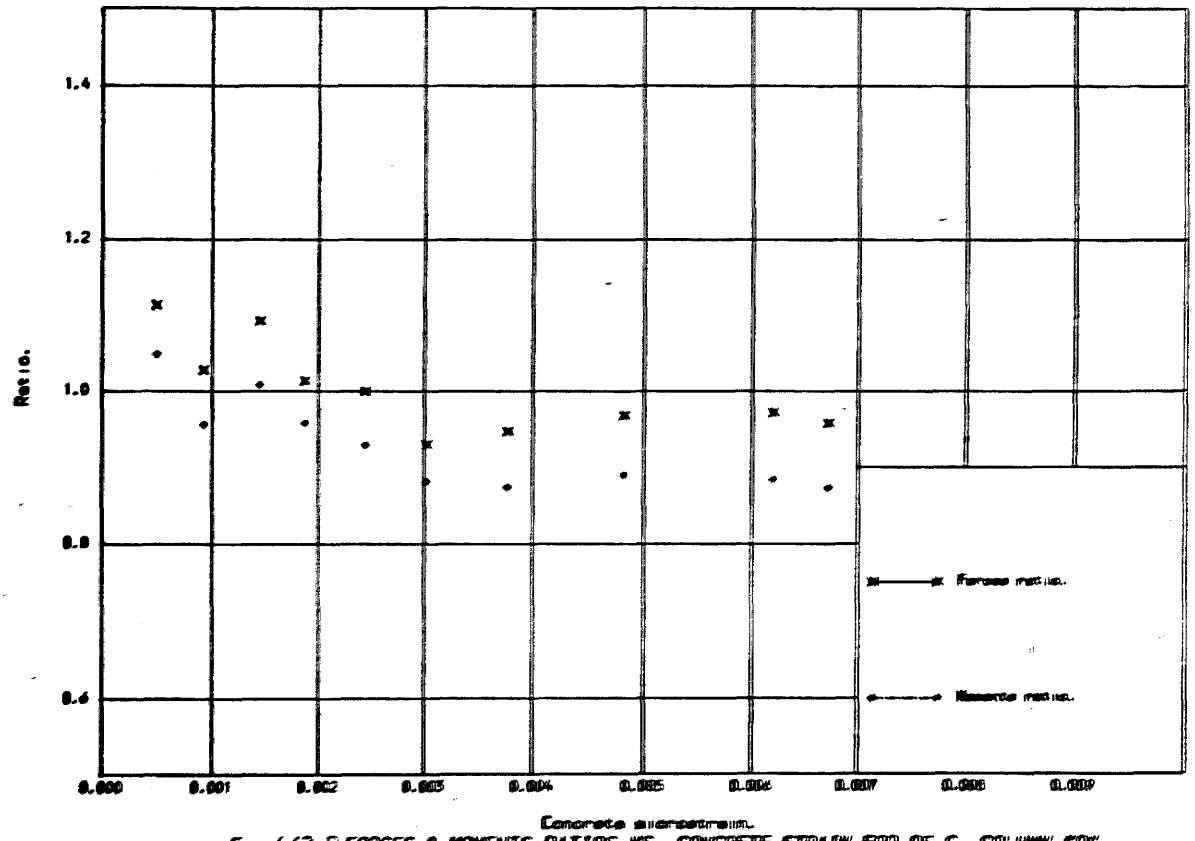

Fig.6.13-D FORCES & MOMENTS RATIOS VS. CONCRETE STRAIN FOR RE.C. COLUMN "D".

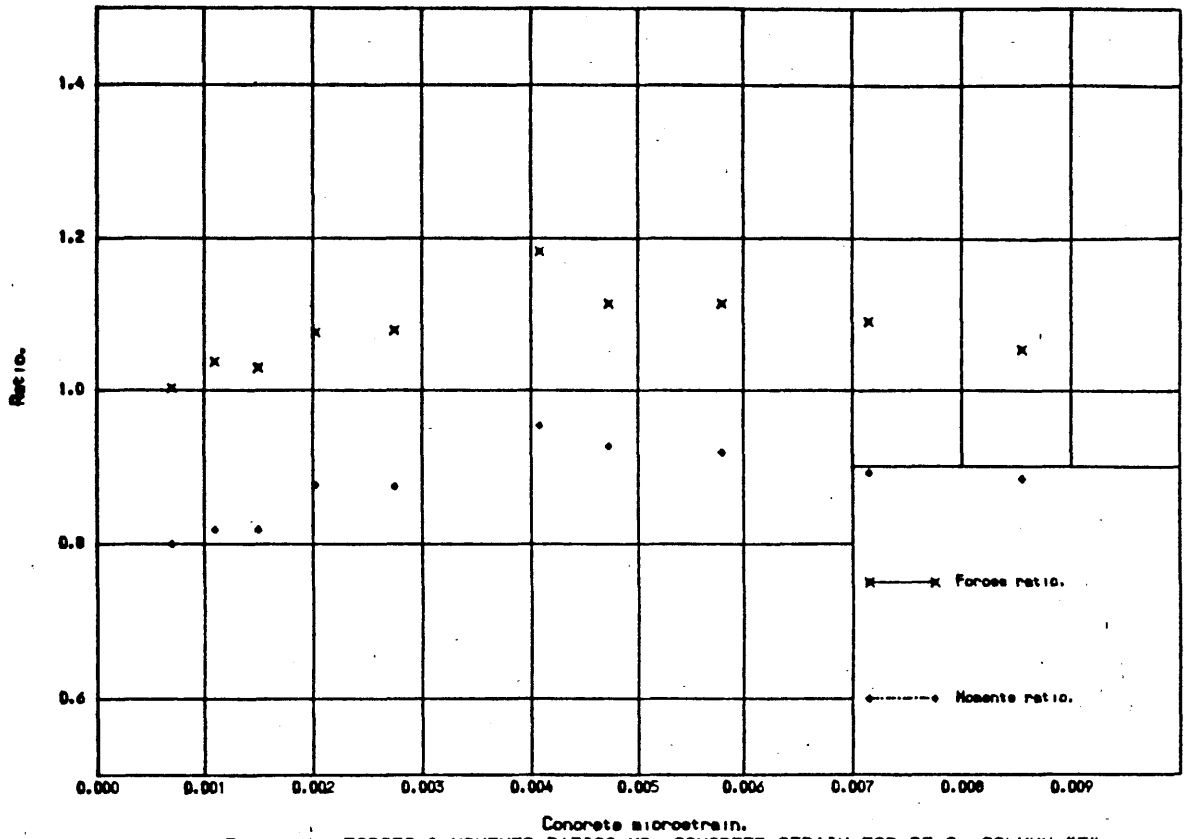

Fig. 6.13-E *FORCES & MOMENTS RATIOS VS. CONCRETE STRAIN FOR RE.C. COLUMN "E".*

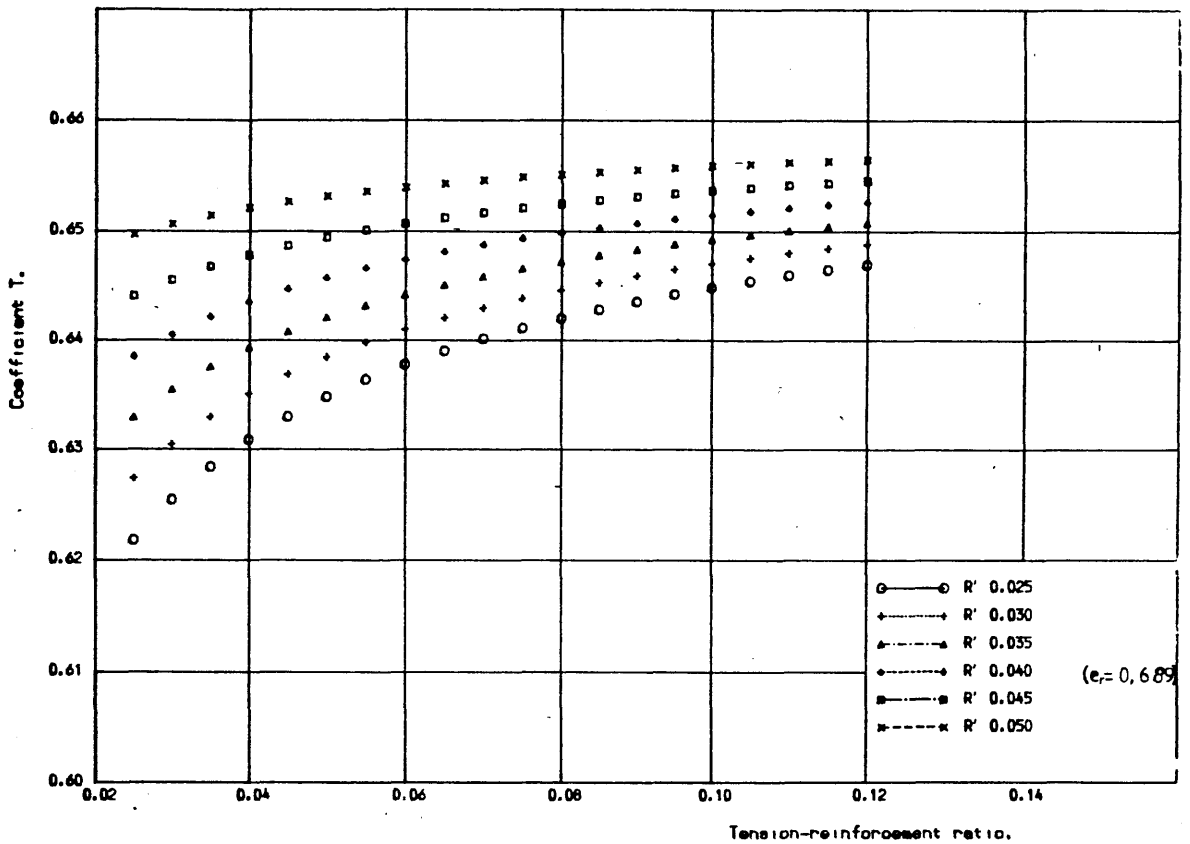

Fig. 6.14-A *VARIATION IN "T" COEFFICIENT FOR COLUMN "A".*

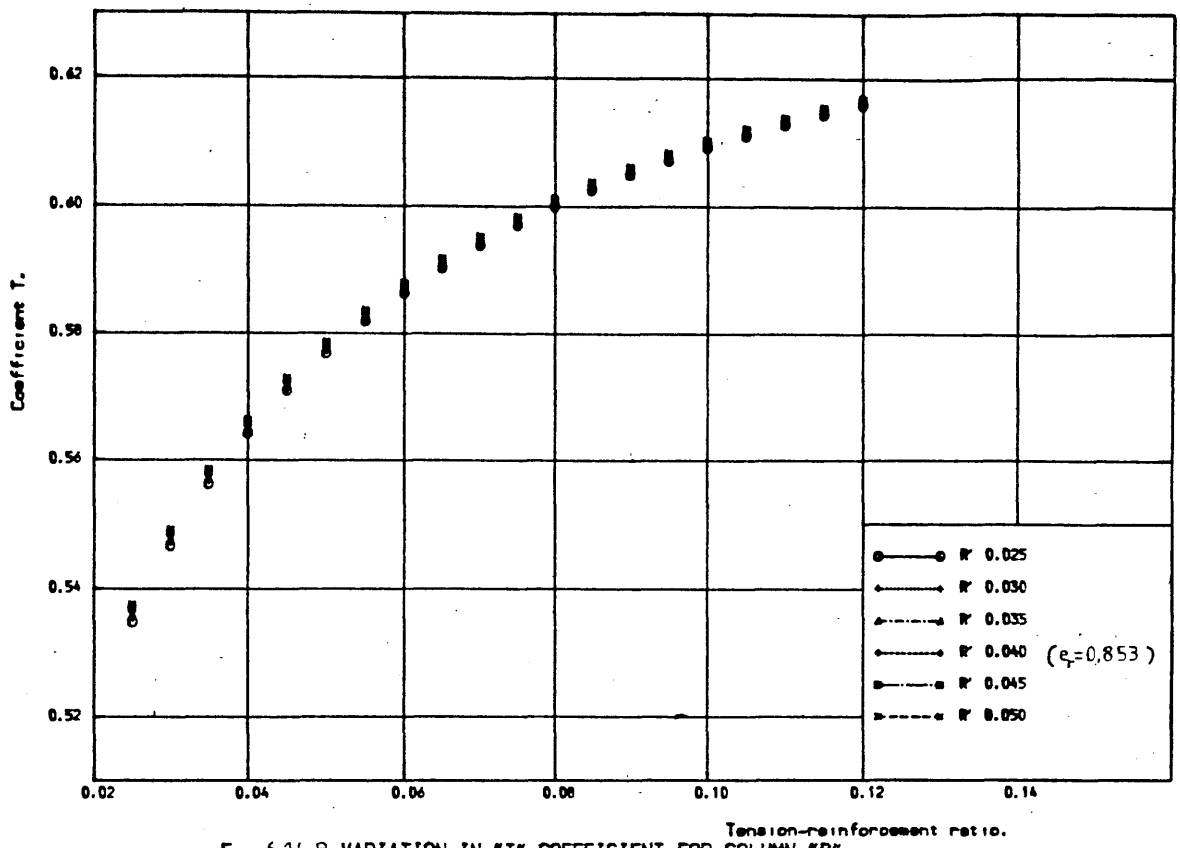

*Fig.*6.14-B *VARIATION IN "T" COEFFICIENT FOR COLUMN "B".*

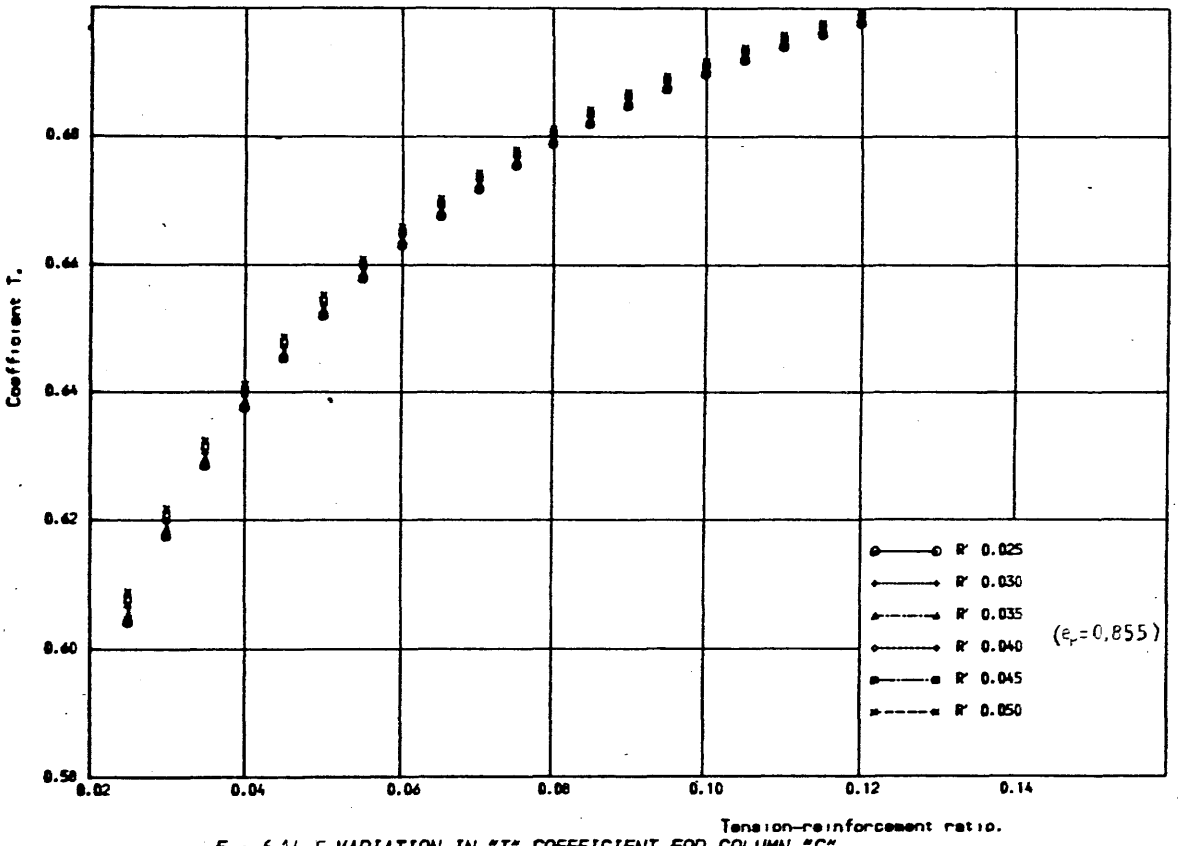

*Fig.*6.14-C *VARIATION IN "T" COEFFICIENT FOR COLUMN "C".*

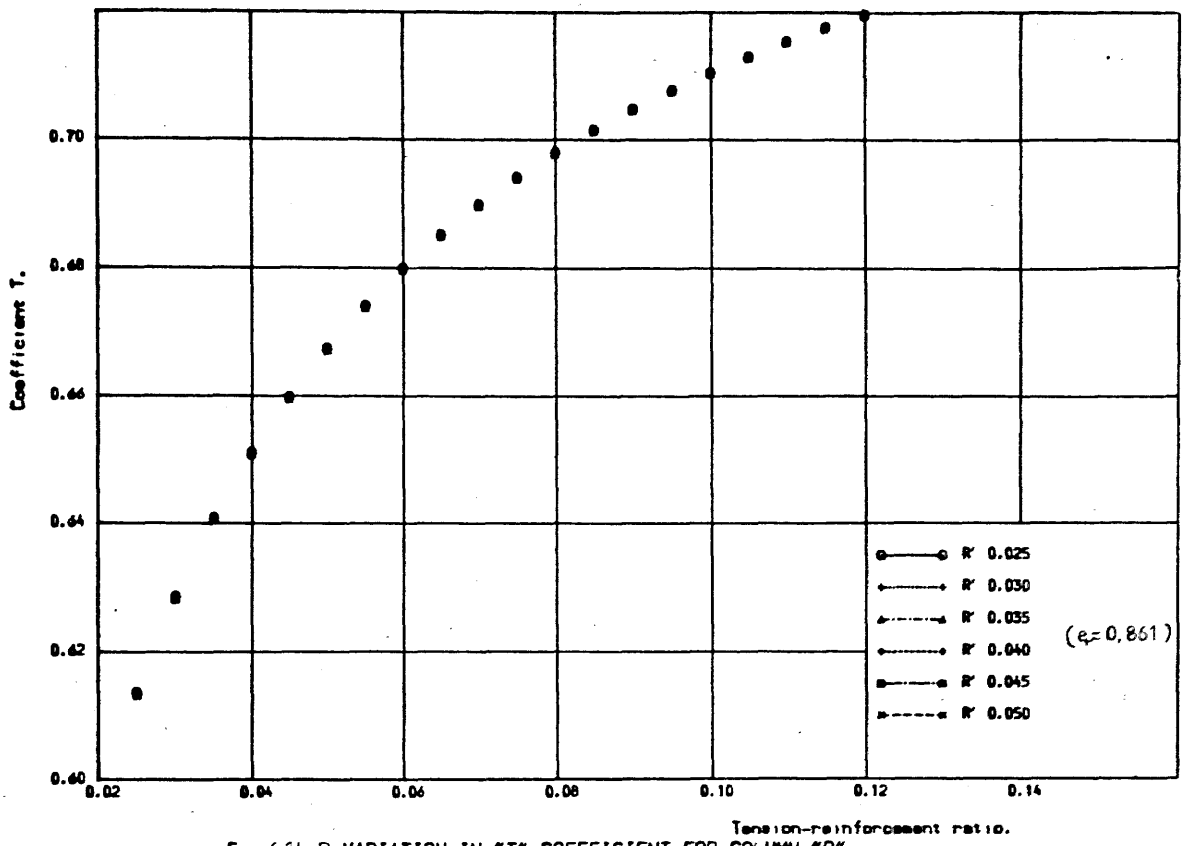

*Fig.*6.14-D *VARIATION IN "T" COEFFICIENT FOR COLUMN "D".*

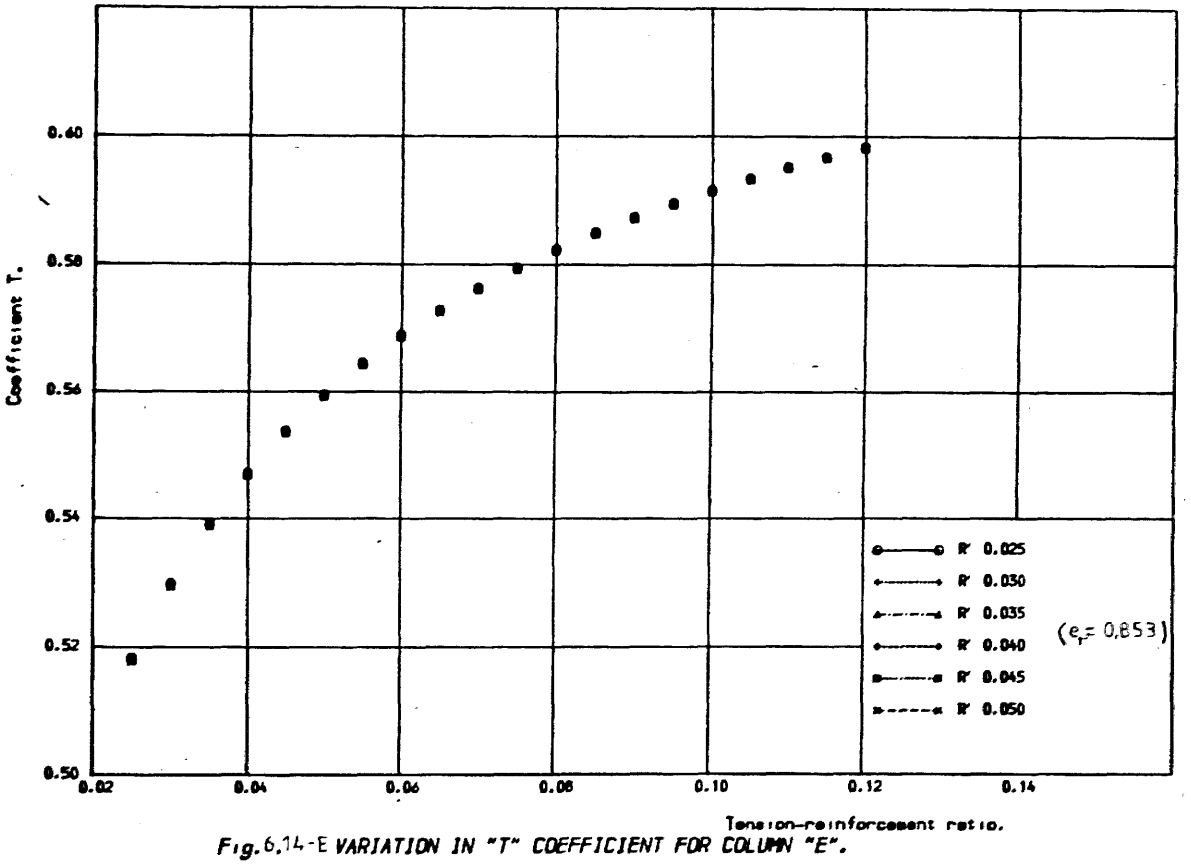

*Fig.*6.14-E *VARIATION IN "T" COEFFICIENT FOR COLUMN "E".*

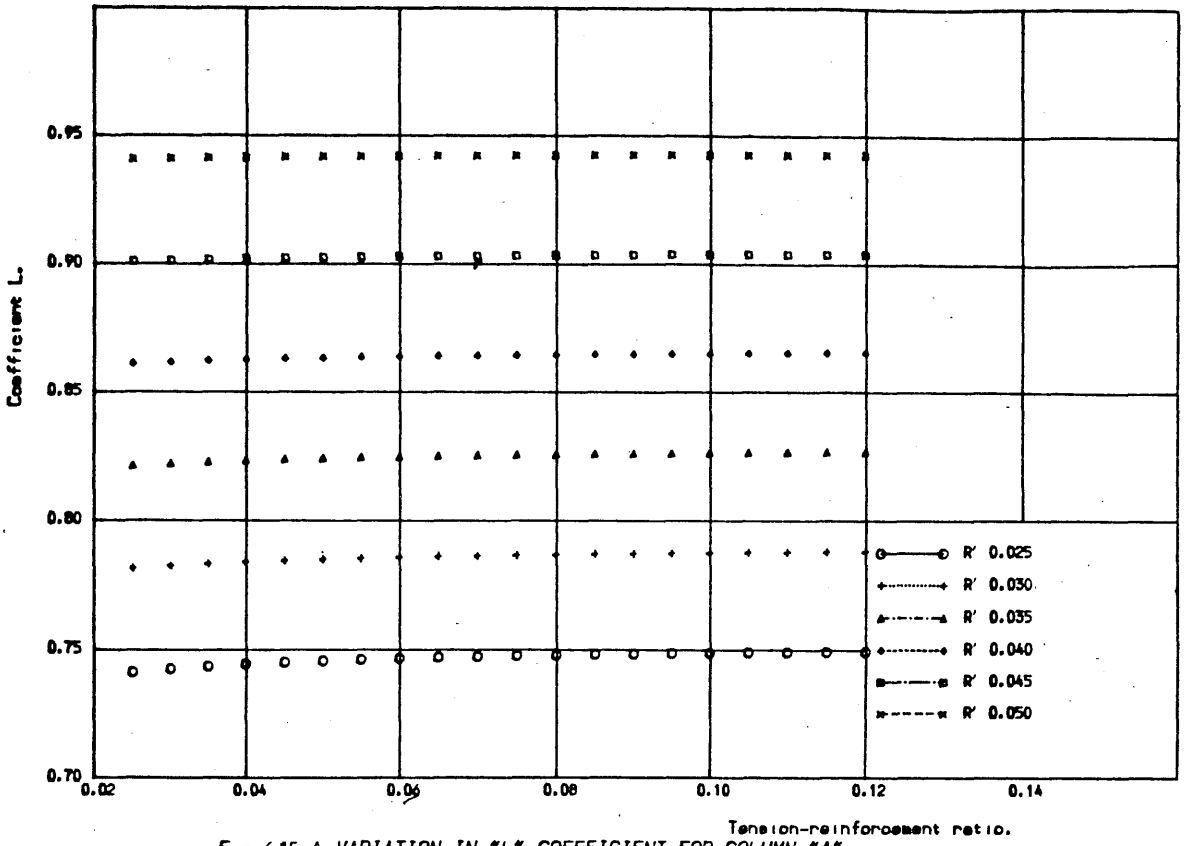

Fig. 6.15-A *VARIATION IN "L" COEFFICIENT FOR COLUMN "A".*

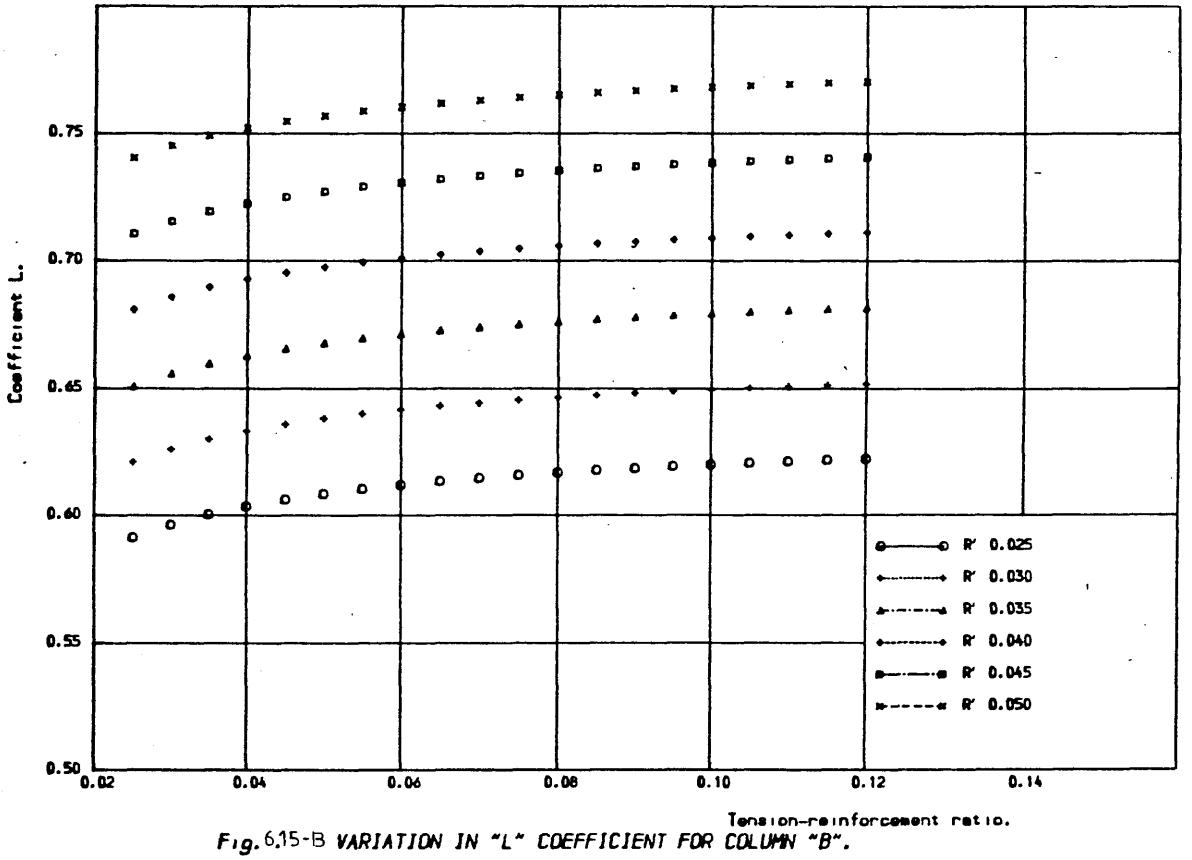

Fig. 6.15-B *VARIATION IN "L" COEFFICIENT FOR COLUMN "B".*

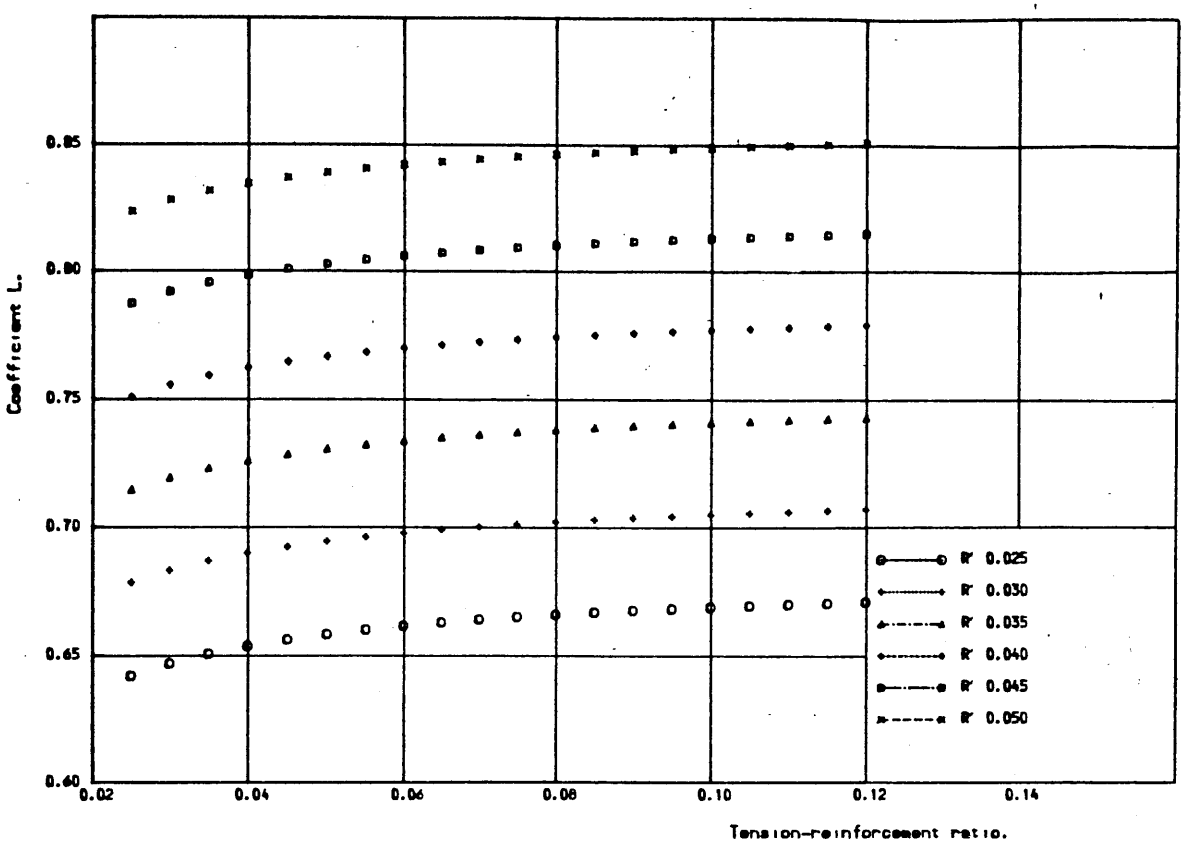

*Fig.*6.15-C *VARIATION IN "L" COEFFICIENT FOR COLUMN "C".*

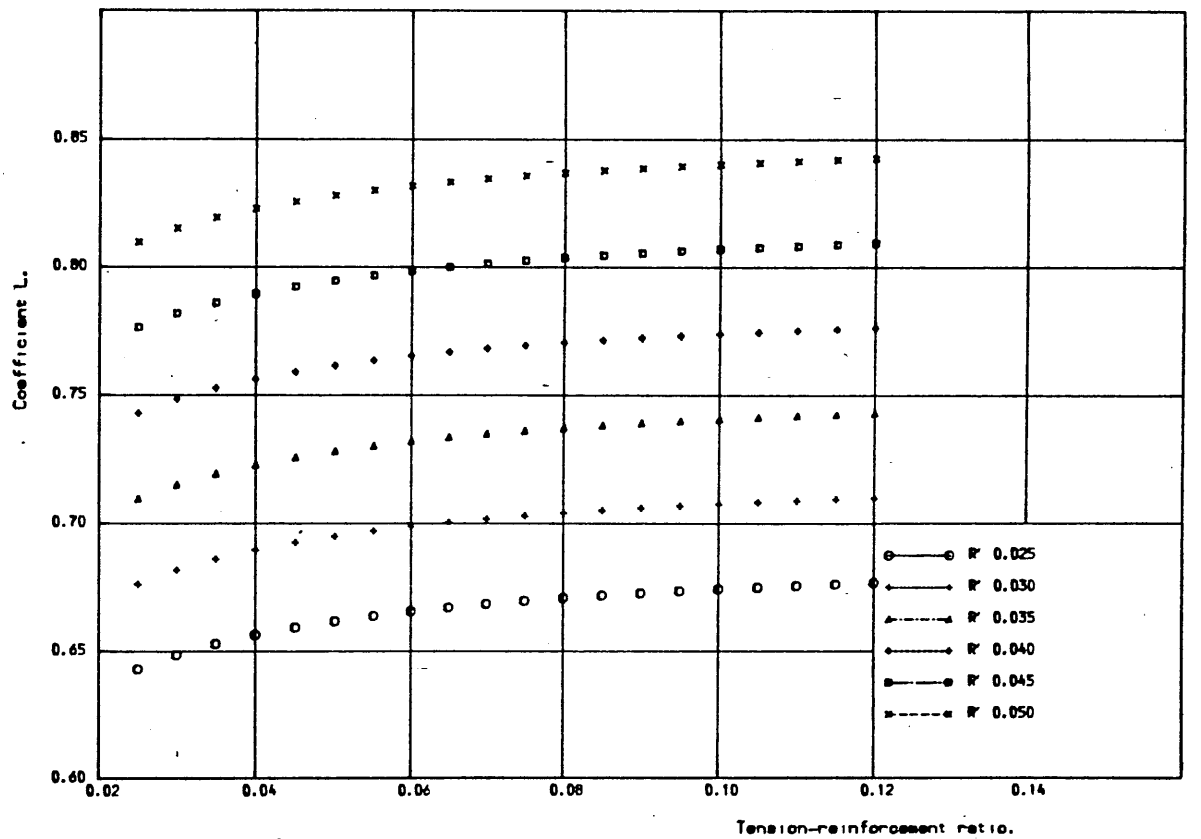

*Fig.*6.15-D *VARIATION IN "L" COEFFICIENT FOR COLUMN "D".*

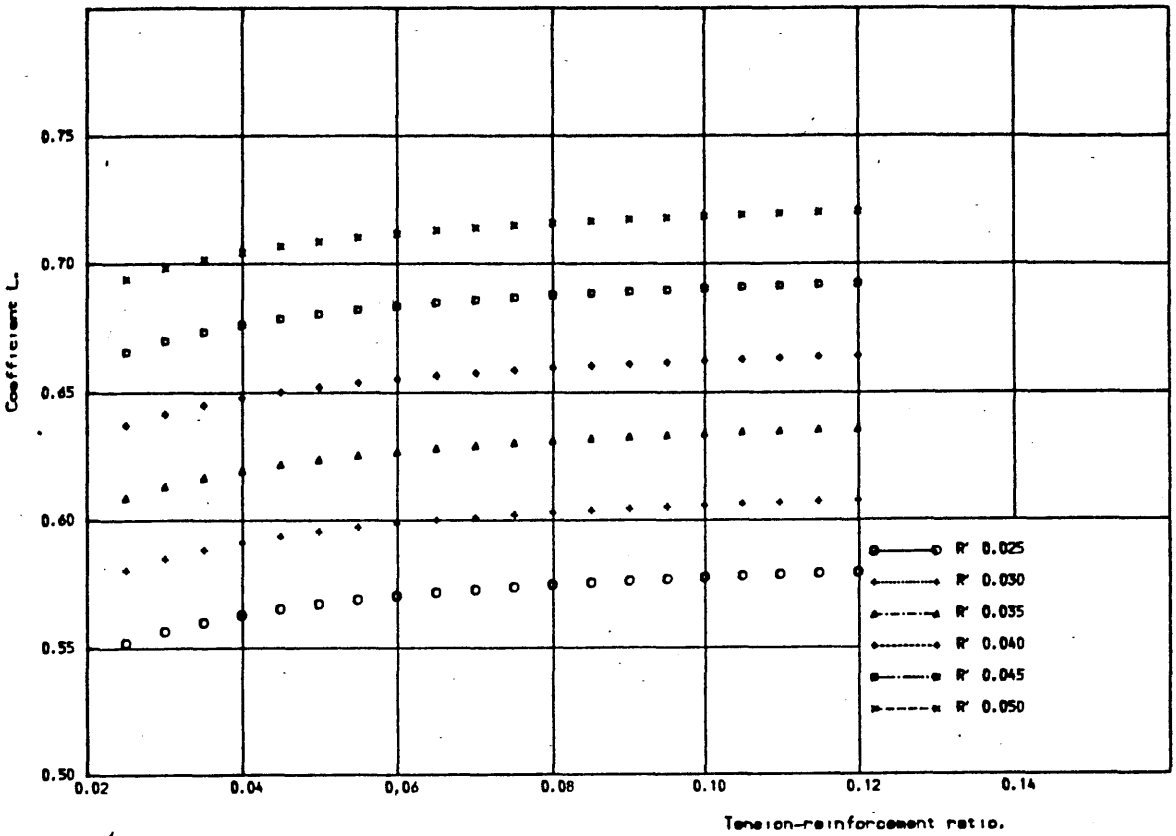

Fig. 6.15-E *VARIATION IN "L" COEFFICIENT FOR COLUMN "E".*

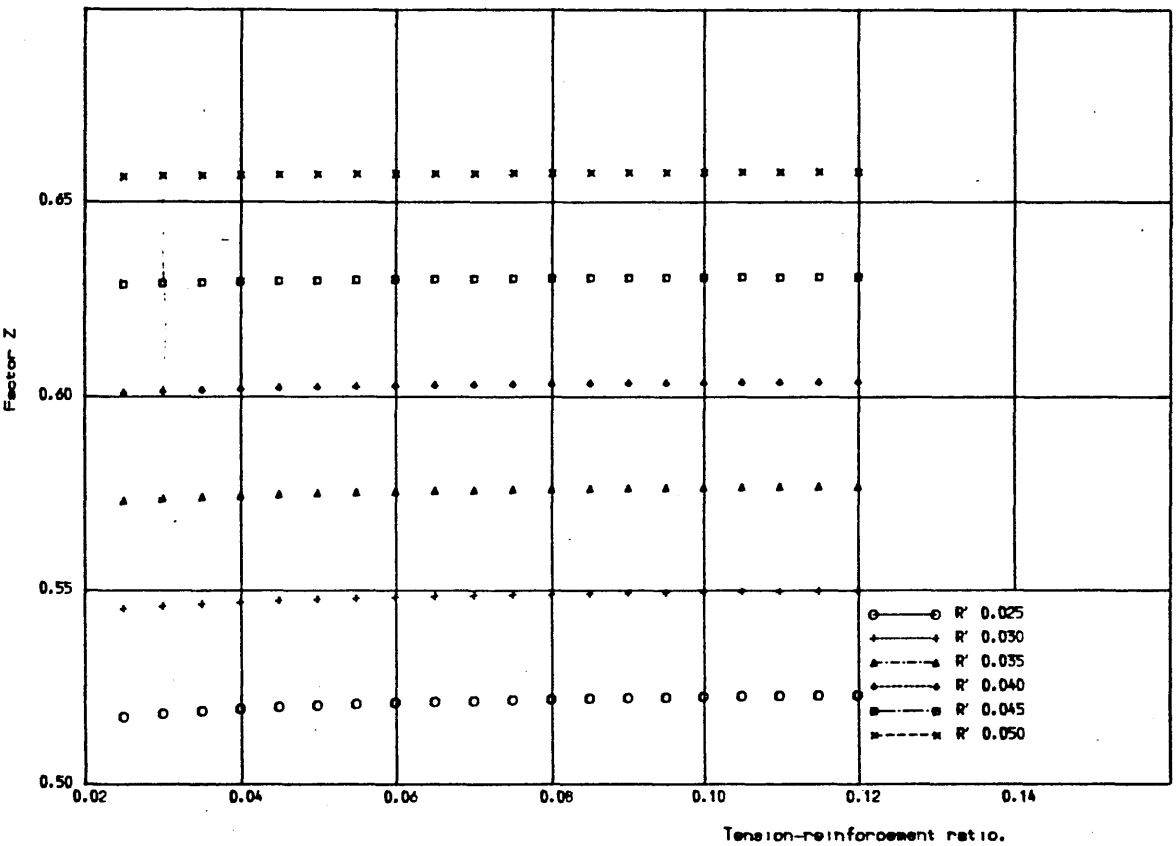

Fig. 6.16-A *VARIATION IN THE REDUCED MOMENT FACTOR Z FOR COLUMN "A".*

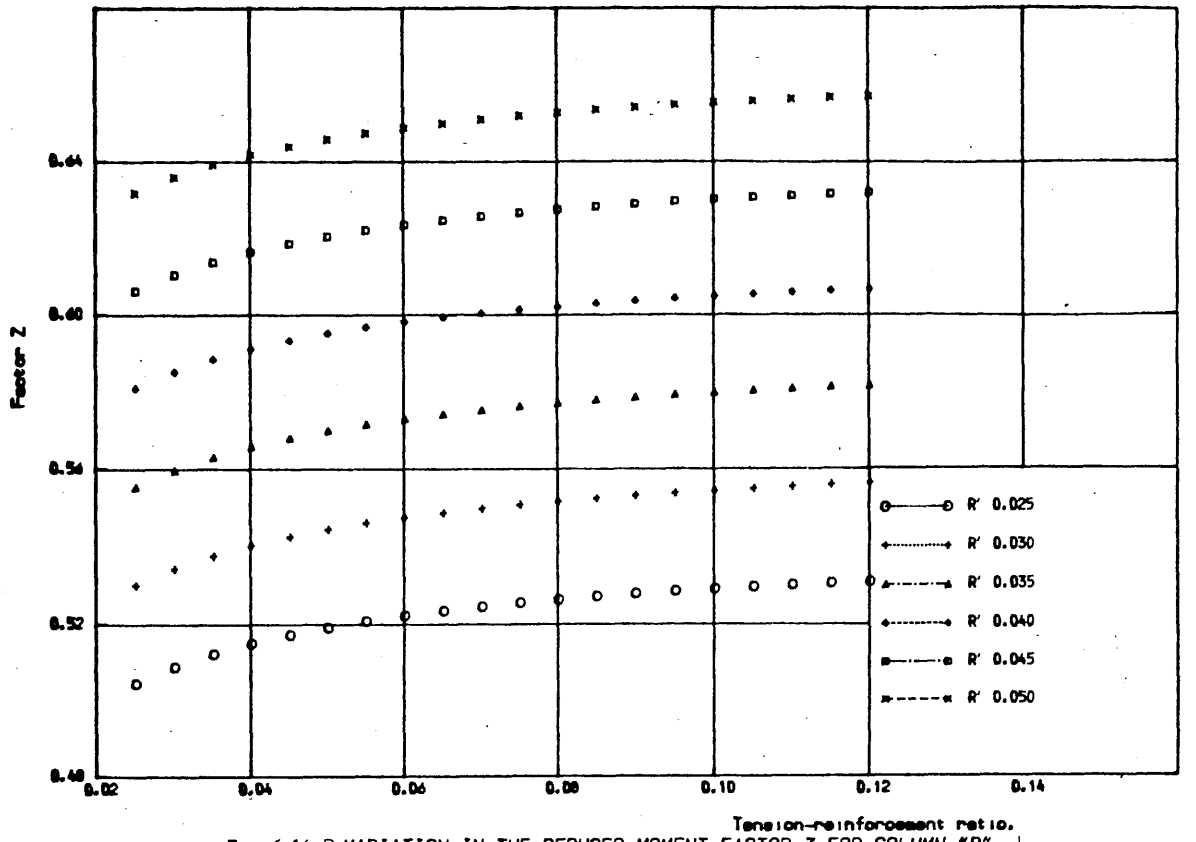

Fig. 6.16-B *VARIATION IN THE REDUCED MOMENT FACTOR Z FOR COLUMN "B".*

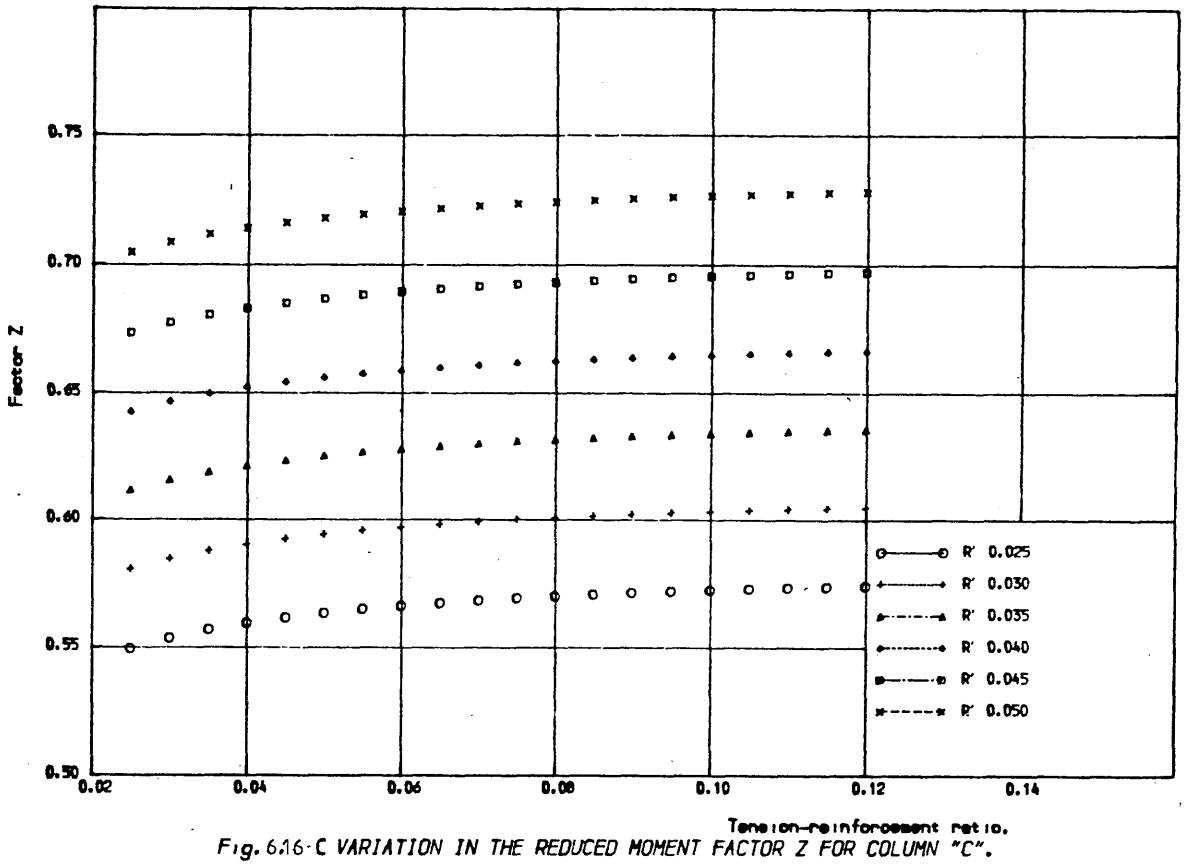

Fig. 6.16-C *VARIATION IN THE REDUCED MOMENT FACTOR Z FOR COLUMN "C".*

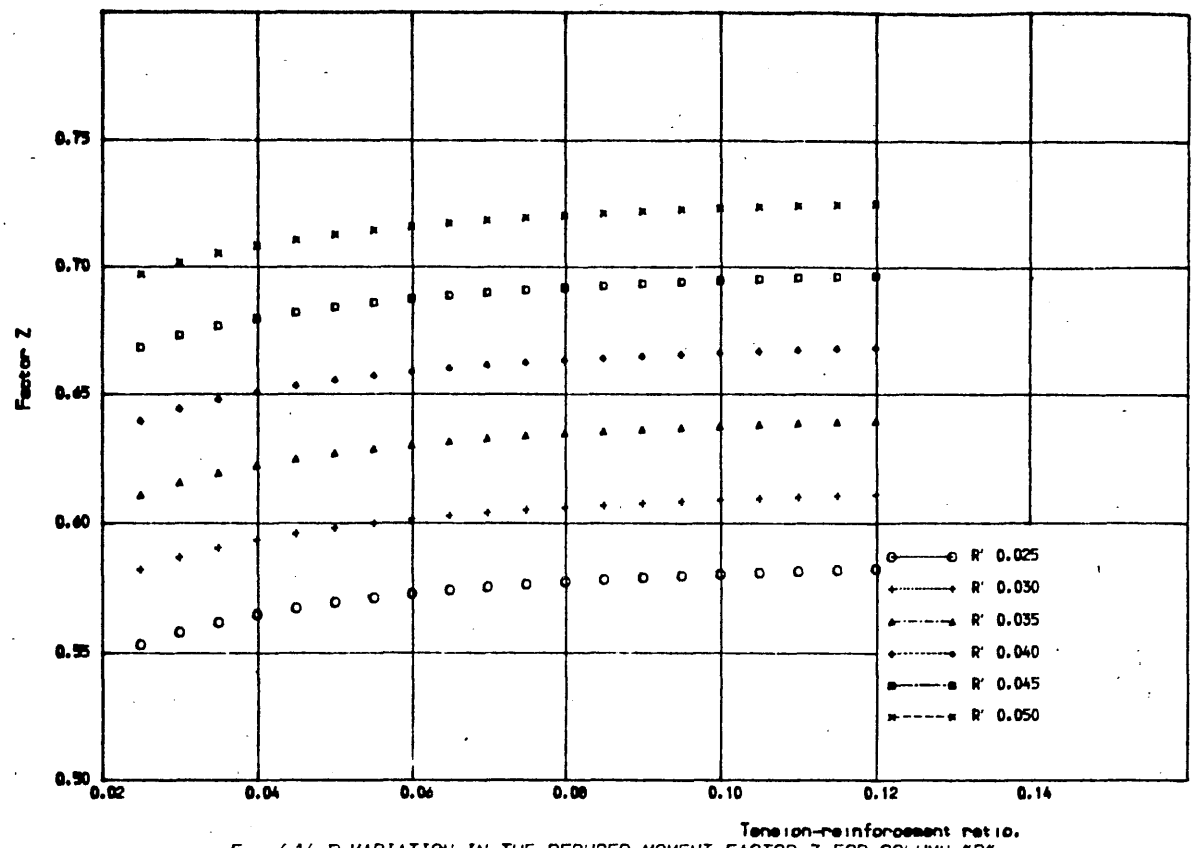

Fig. 6.16-D *VARIATION IN THE REDUCED MOMENT FACTOR Z FOR COLUMN "D".*

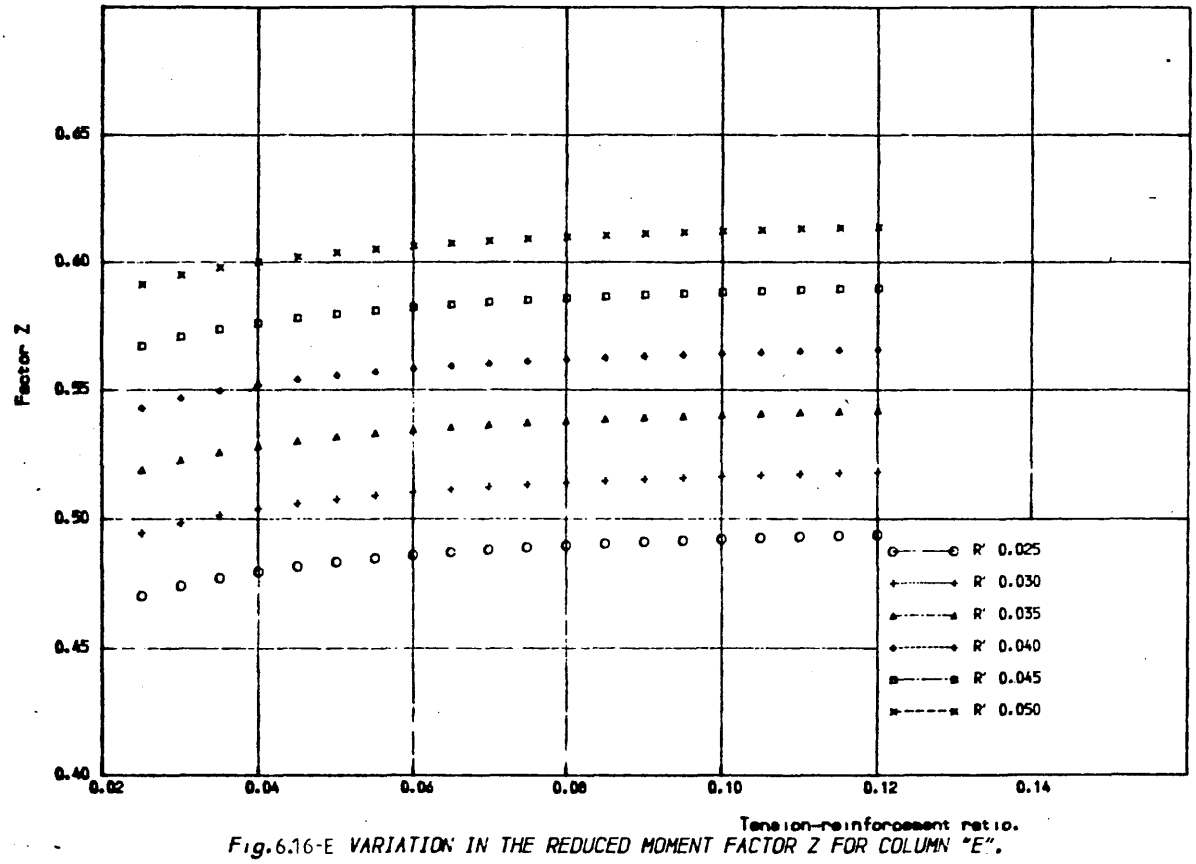

Fig. 6.16-E *VARIATION IN THE REDUCED MOMENT FACTOR Z FOR COLUMN "E".*

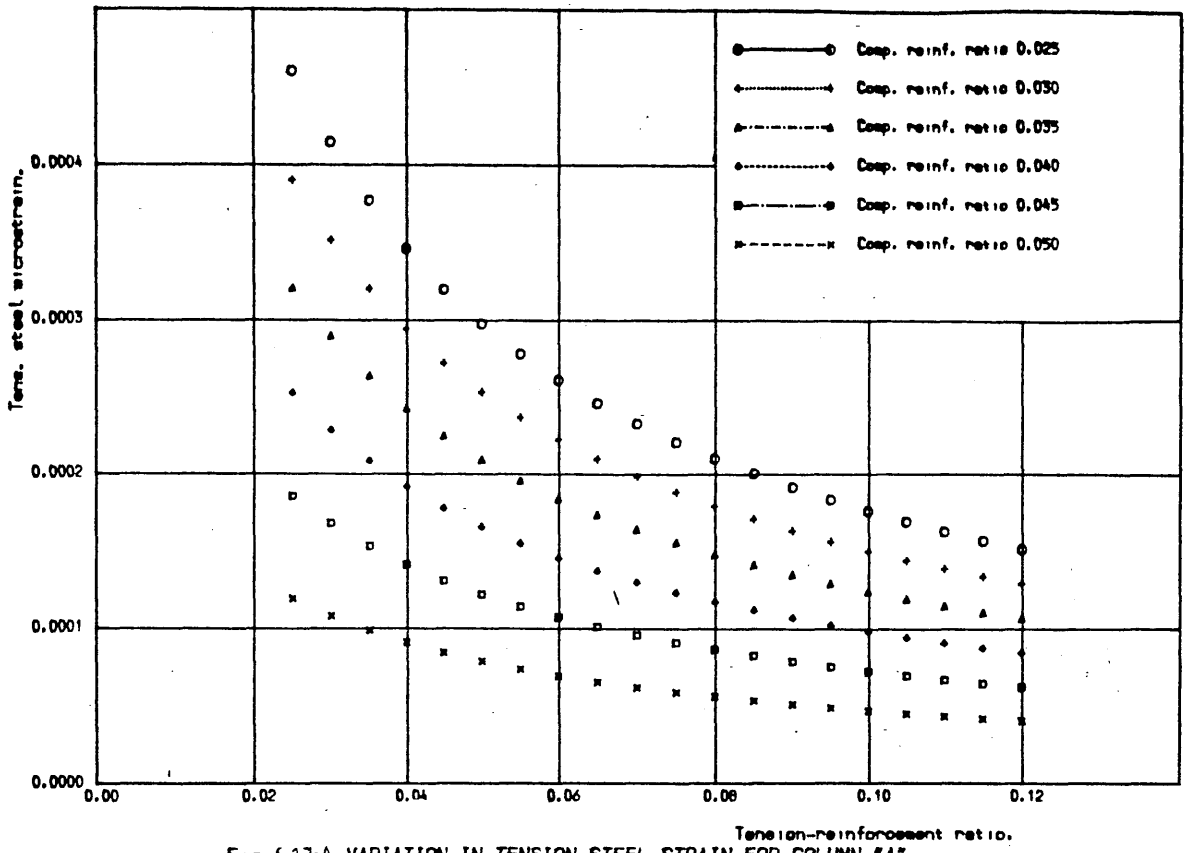

Fig. 6.17-A *VARIATION IN TENSION STEEL STRAIN FOR COLUMN "A".*

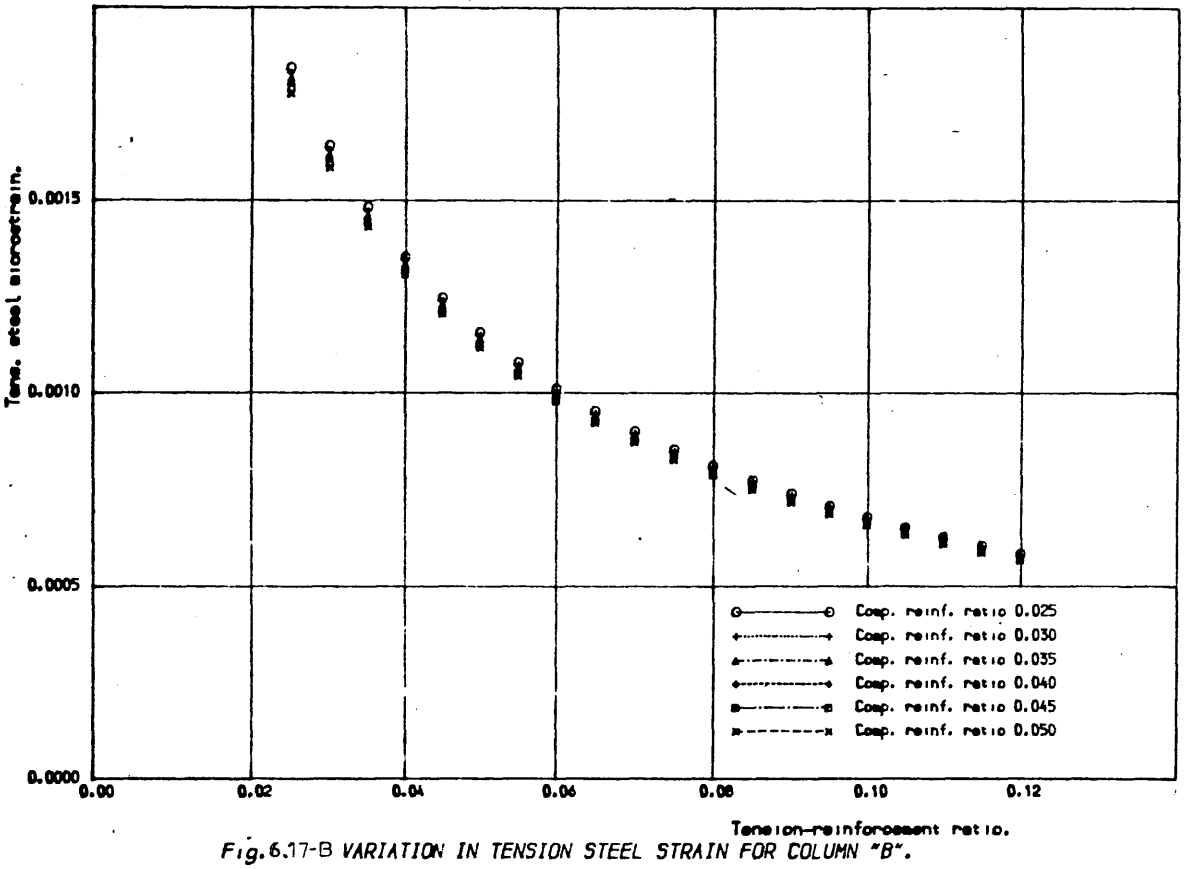

Fig. 6.17-B *VARIATION IN TENSION STEEL STRAIN FOR COLUMN "B".*

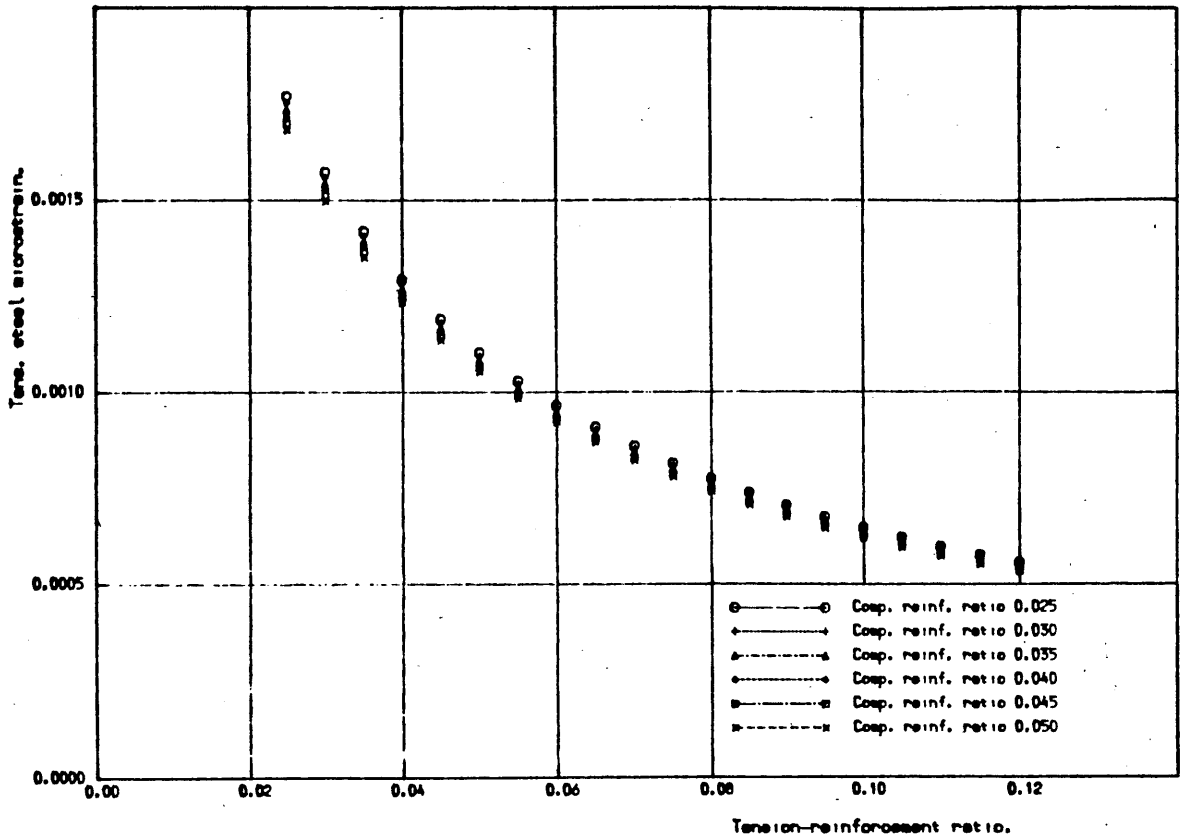

Fig. 6.17-C *VARIATION IN TENSION STEEL STRAIN FOR COLUMN "C".*

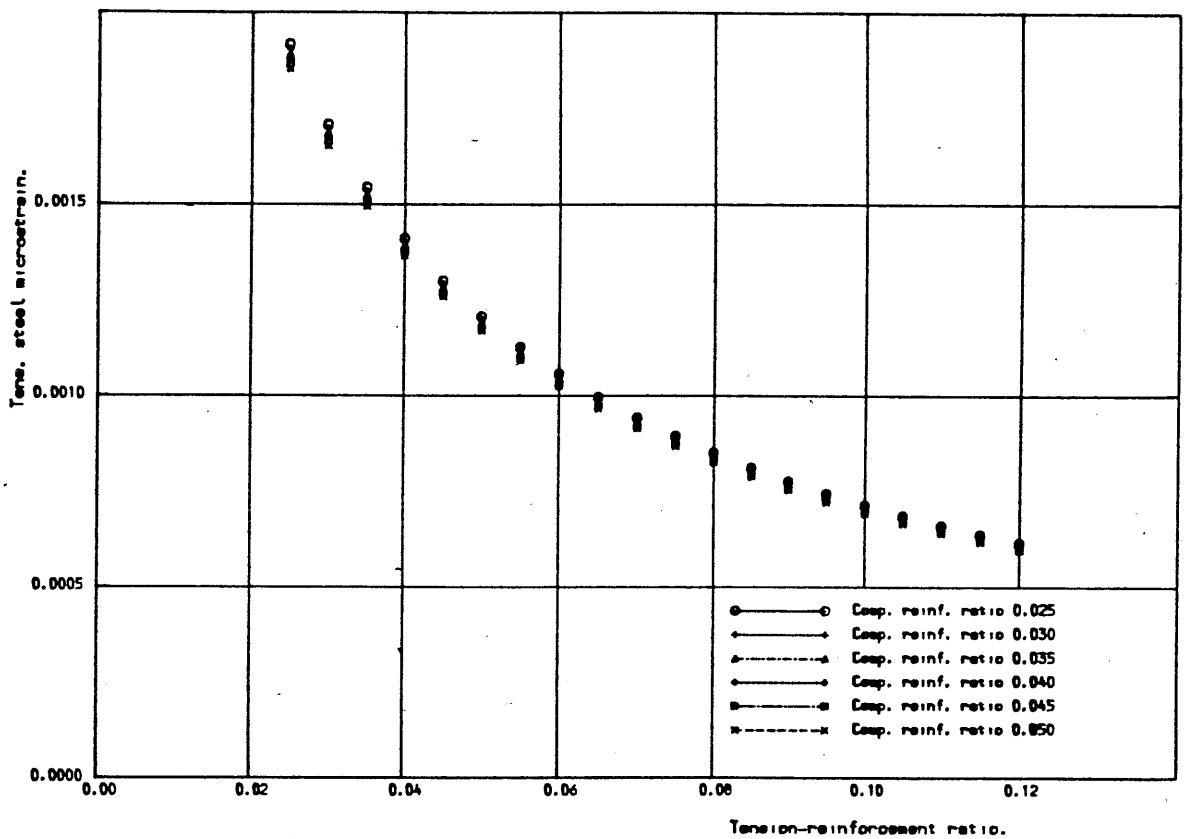

Fig. 6.17-D *VARIATION IN TENSION STEEL STRAIN FOR COLUMN "D".*

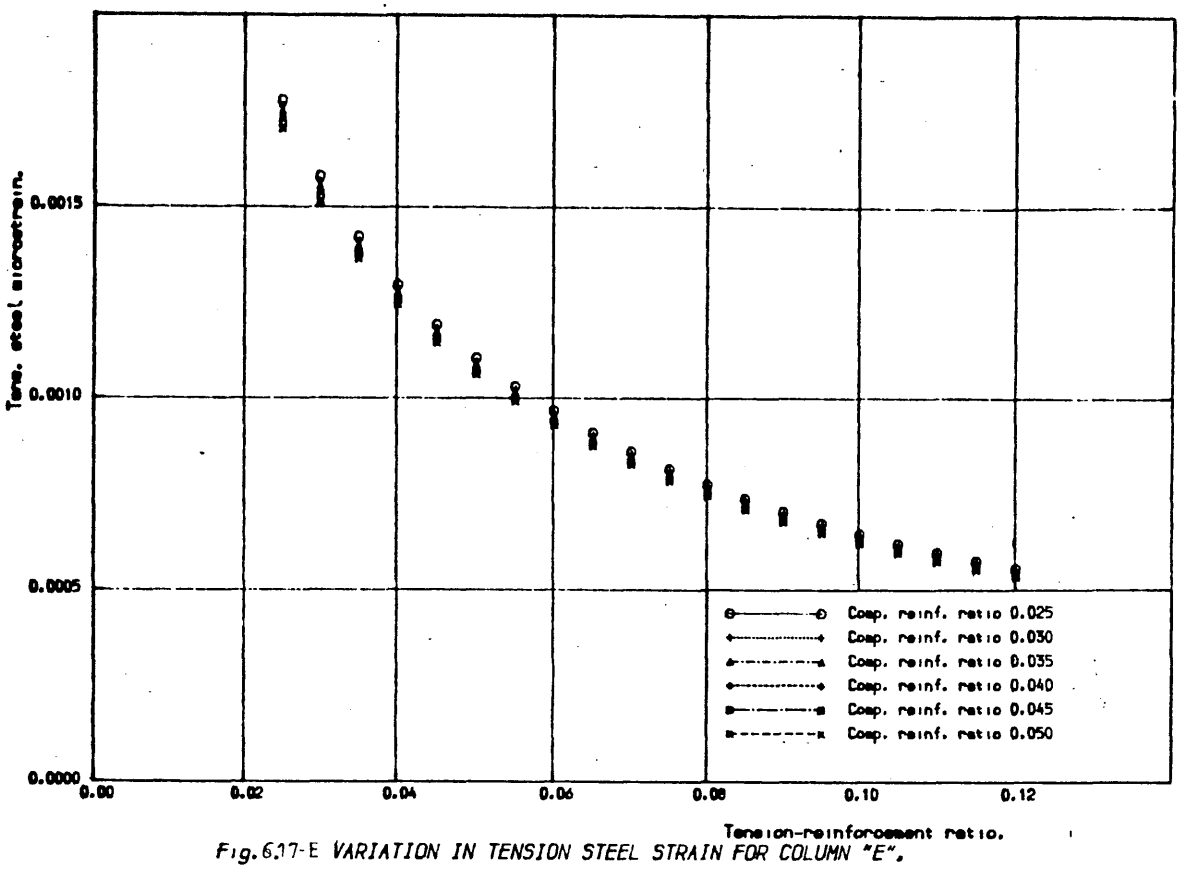

Fig. 6.17-E *VARIATION IN TENSION STEEL STRAIN FOR COLUMN "E".*

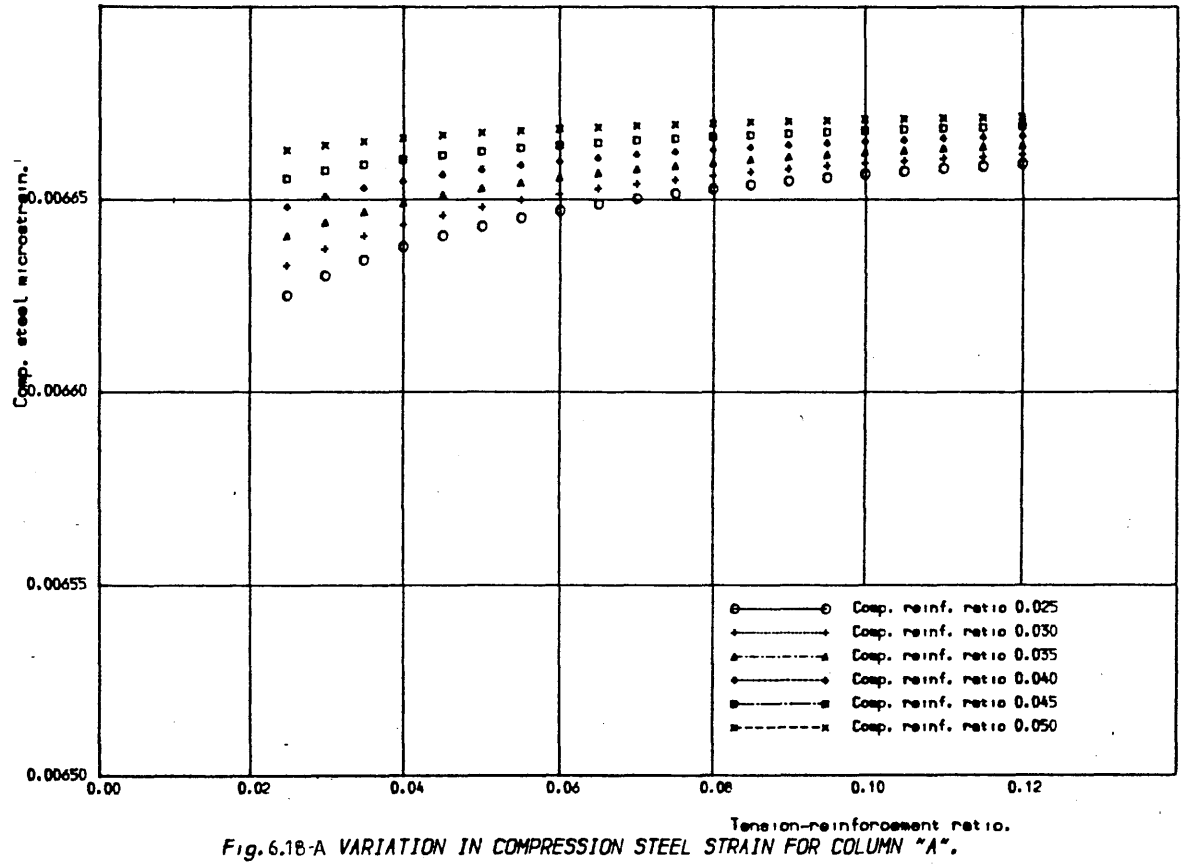

Fig. 6.18-A *VARIATION IN COMPRESSION STEEL STRAIN FOR COLUMN "A".*

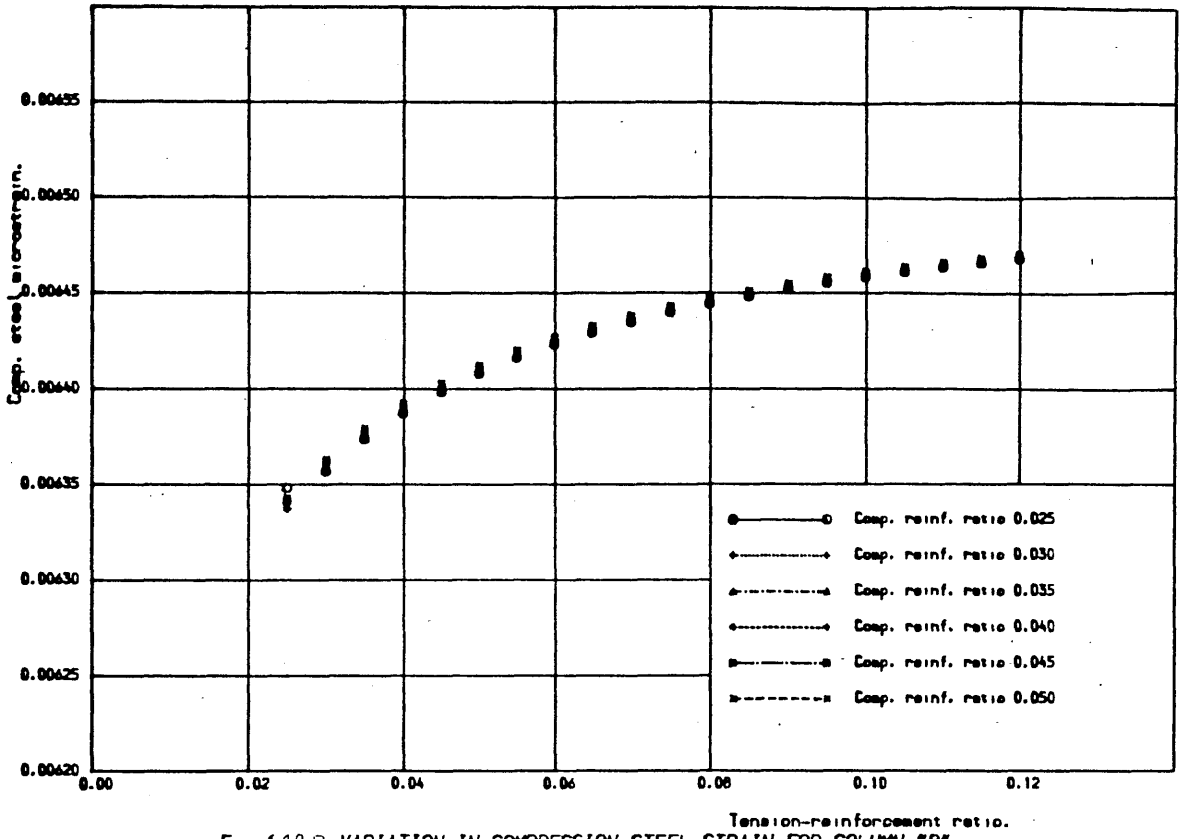

Fig. 6.18-B *VARIATION IN COMPRESSION STEEL STRAIN FOR COLUMN "B".*

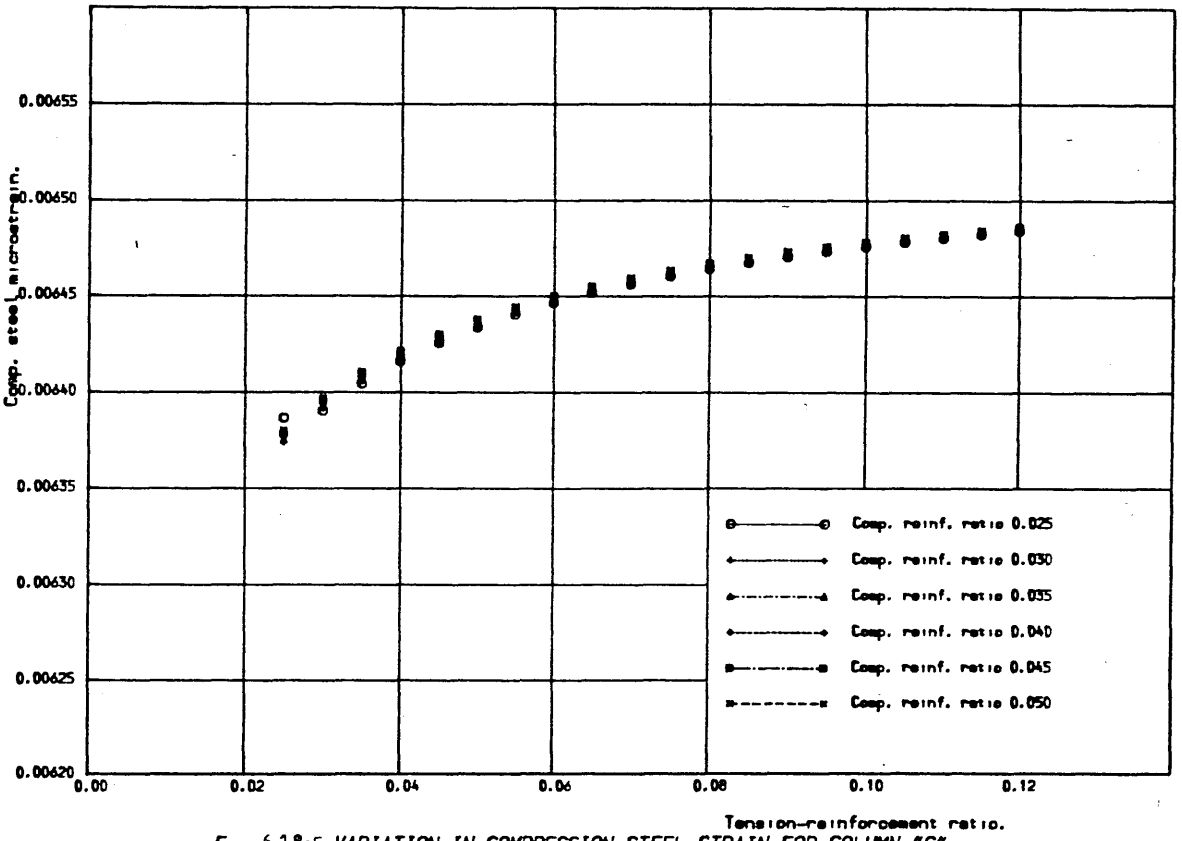

Fig. 6.18-C *VARIATION IN COMPRESSION STEEL STRAIN FOR COLUMN "C".*

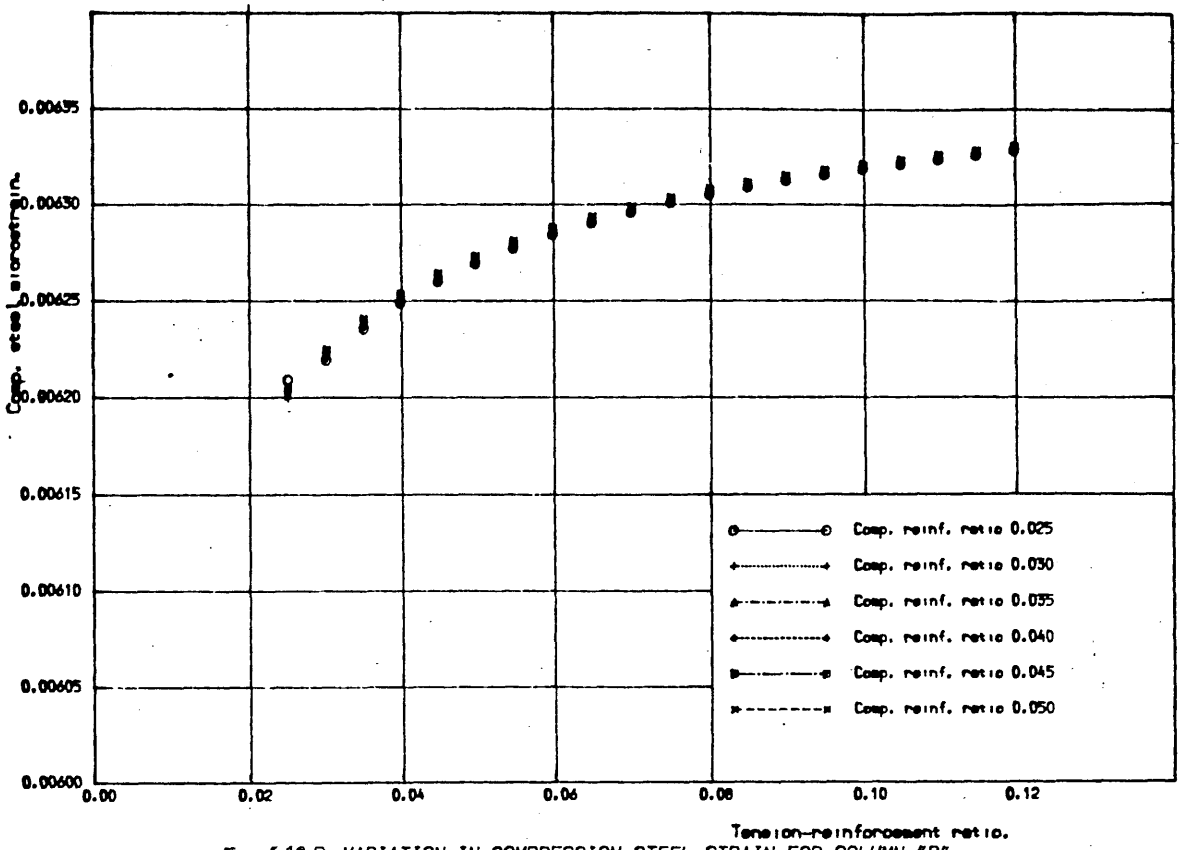

Fig.6.18-D VARIATION IN COMPRESSION STEEL STRAIN FOR COLUMN "D".

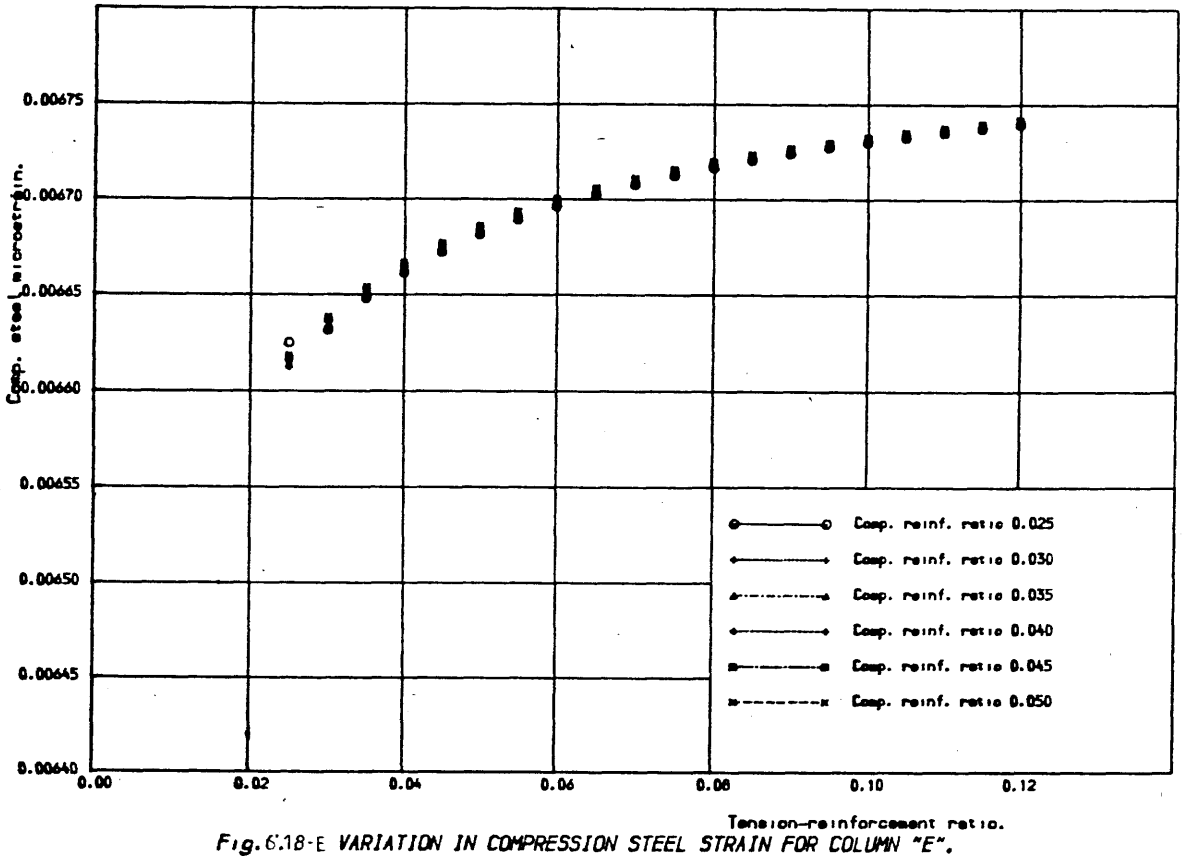

Fig.6.18-E VARIATION IN COMPRESSION STEEL STRAIN FOR COLUMN "E".

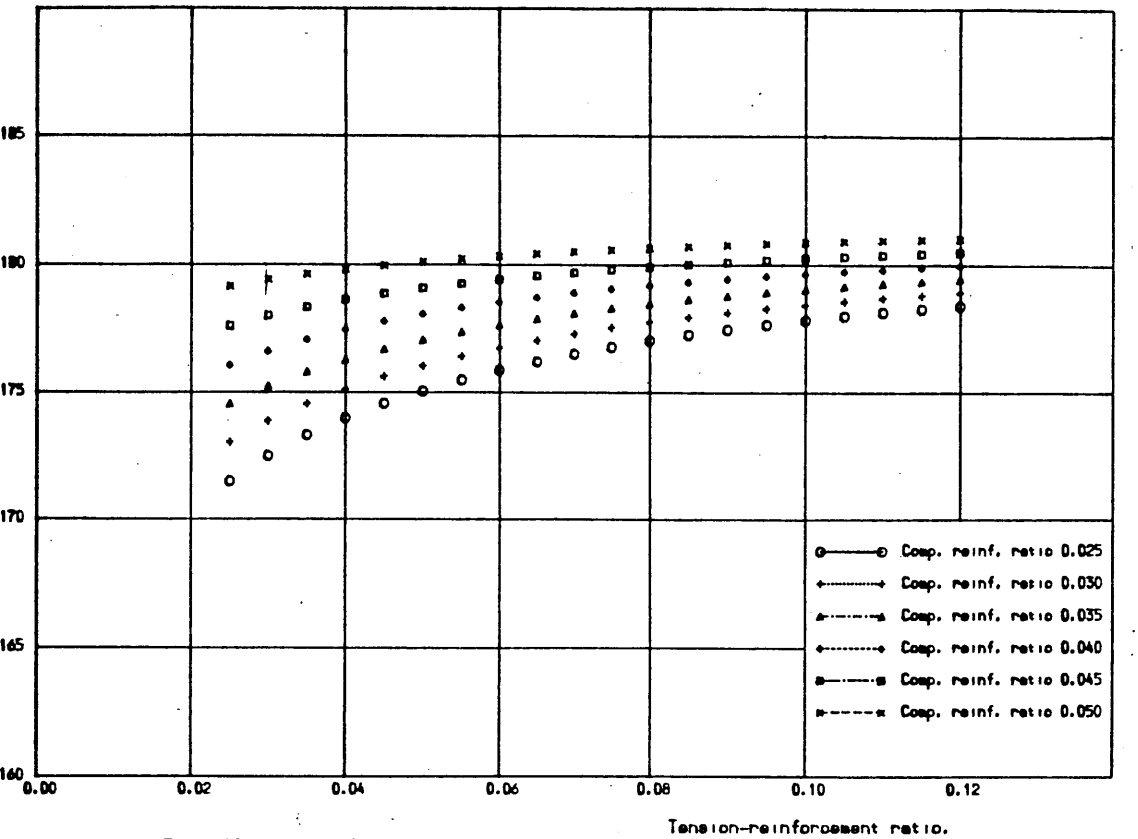

*Fig.*6.19-A *VARIATION IN COMPRESSION ZONE DEPTH FOR COLUMN "A".*

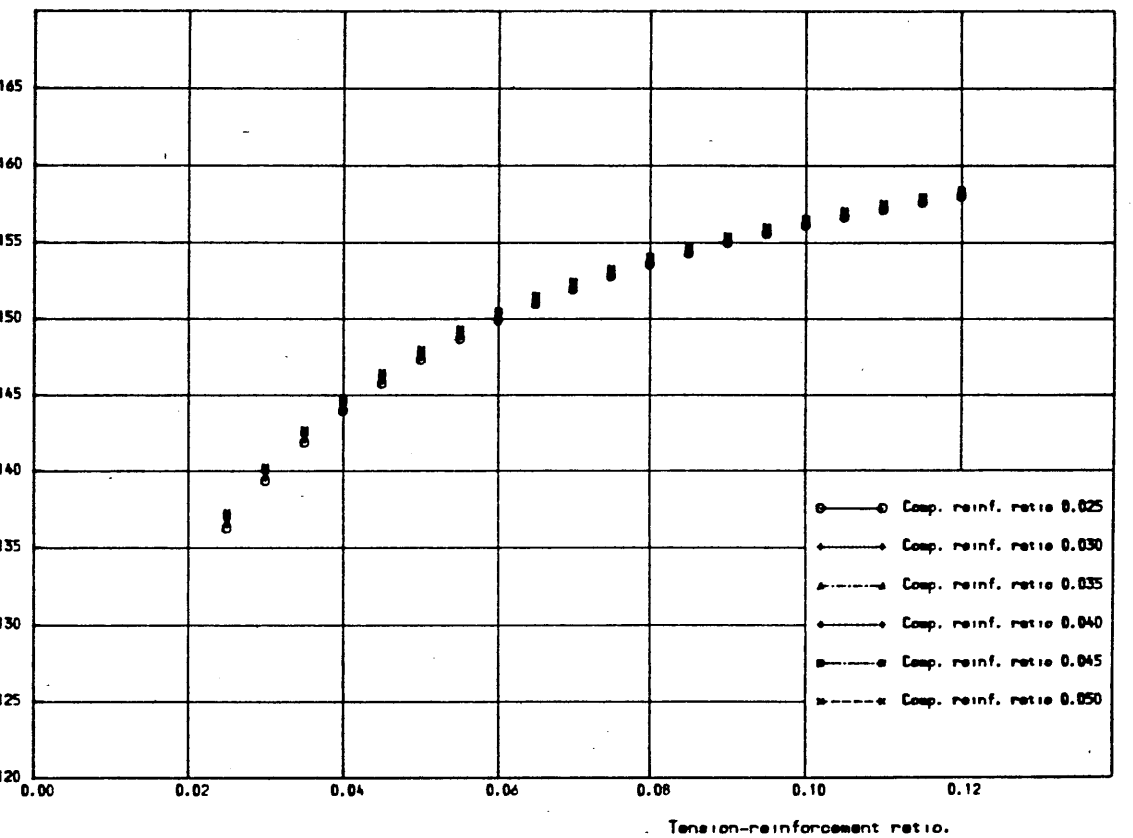

Fig. 6.19-B *VARIATION IN COMPRESSION ZONE DEPTH FOR COLUMN "B".*

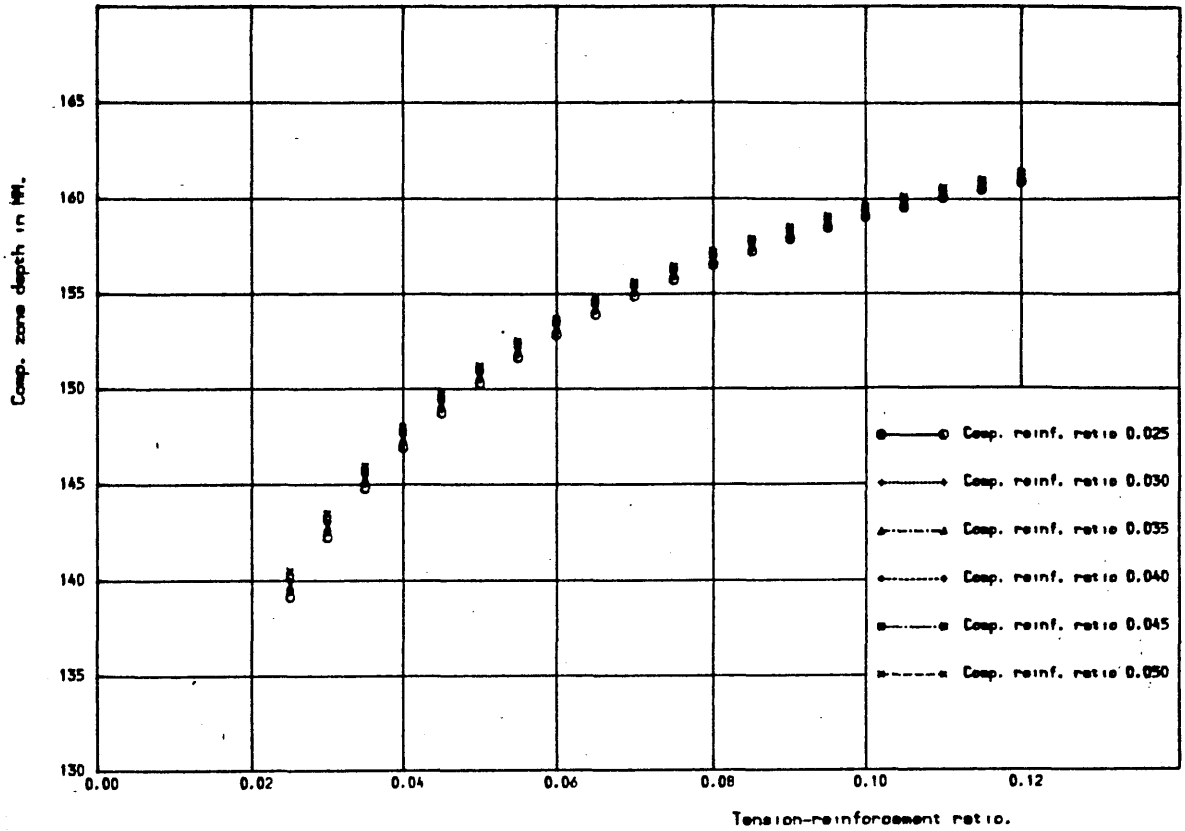

*Fig.*6.19-C *VARIATION IN COMPRESSION ZONE DEPTH FOR COLUMN "C".*

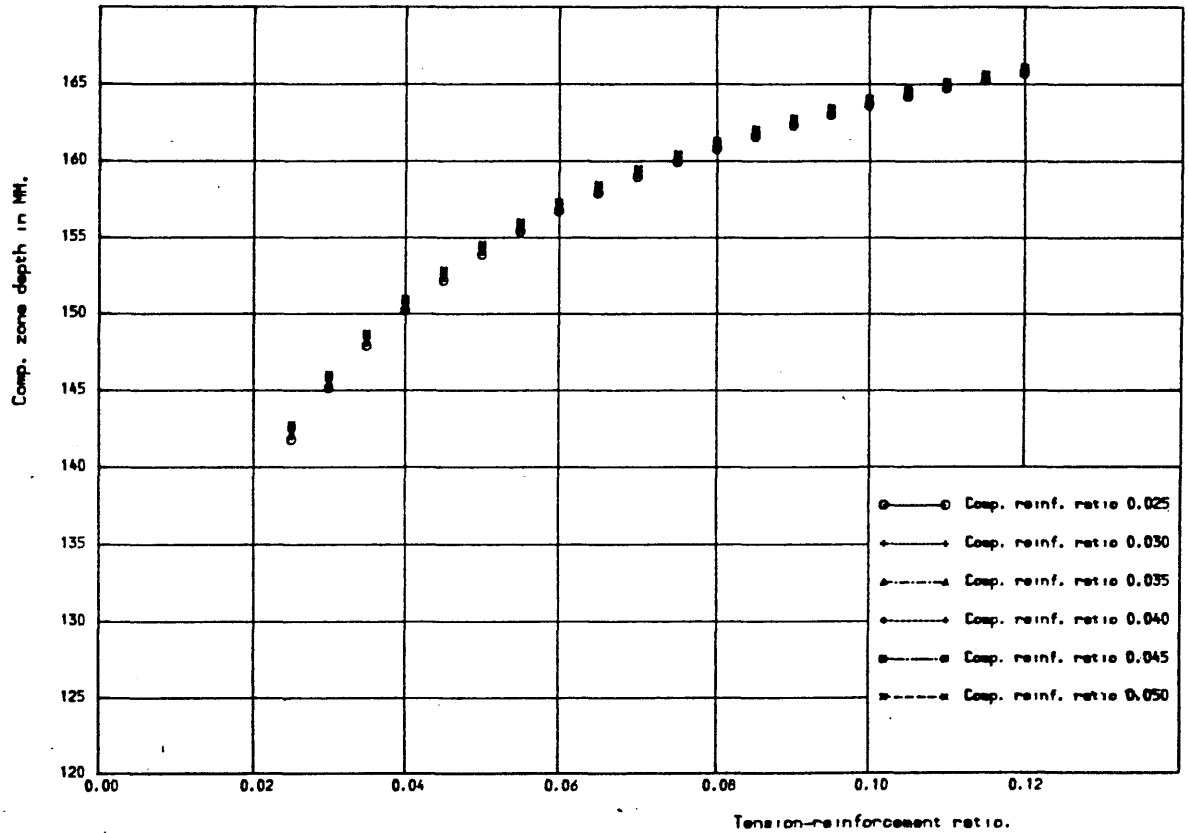

*Fig.*6.19-D *VARIATION IN COMPRESSION ZONE DEPTH FOR COLUMN "D".*

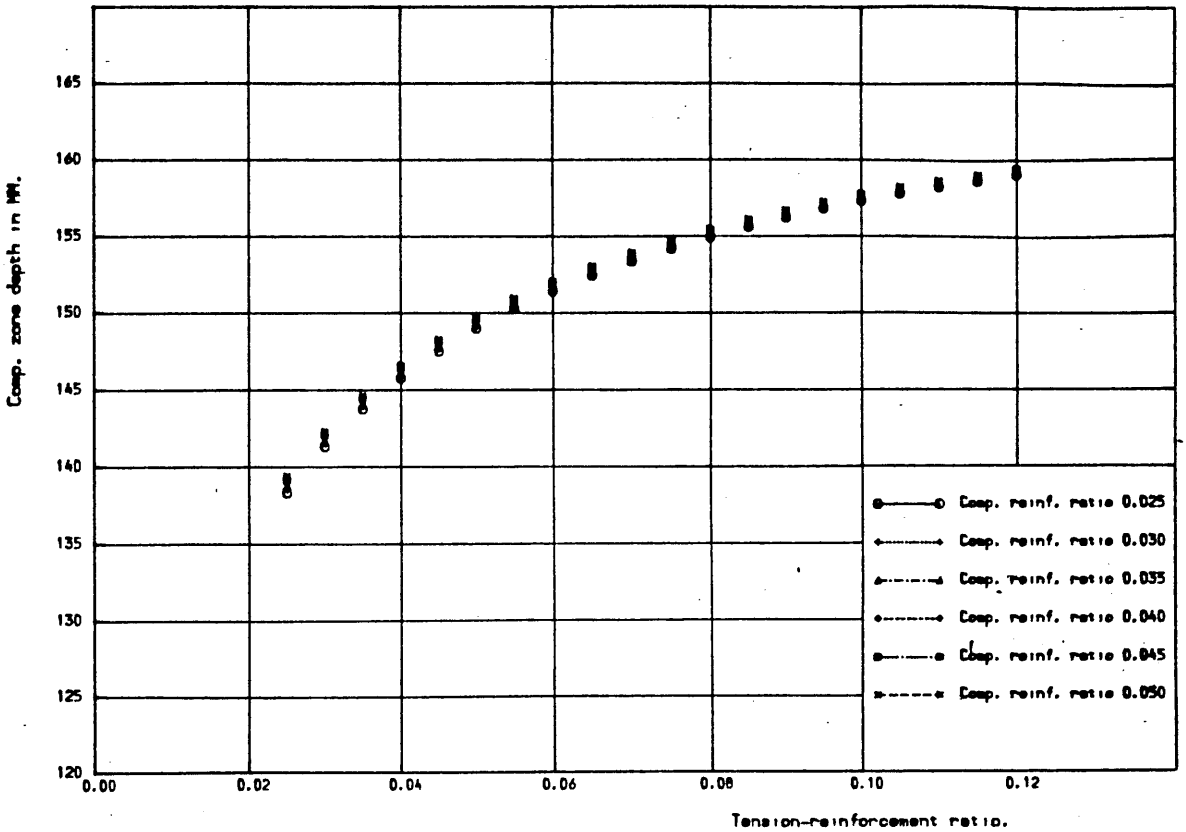

Fig.6.19-E VARIATION IN COMPRESSION ZONE DEPTH FOR COLUMN "E".

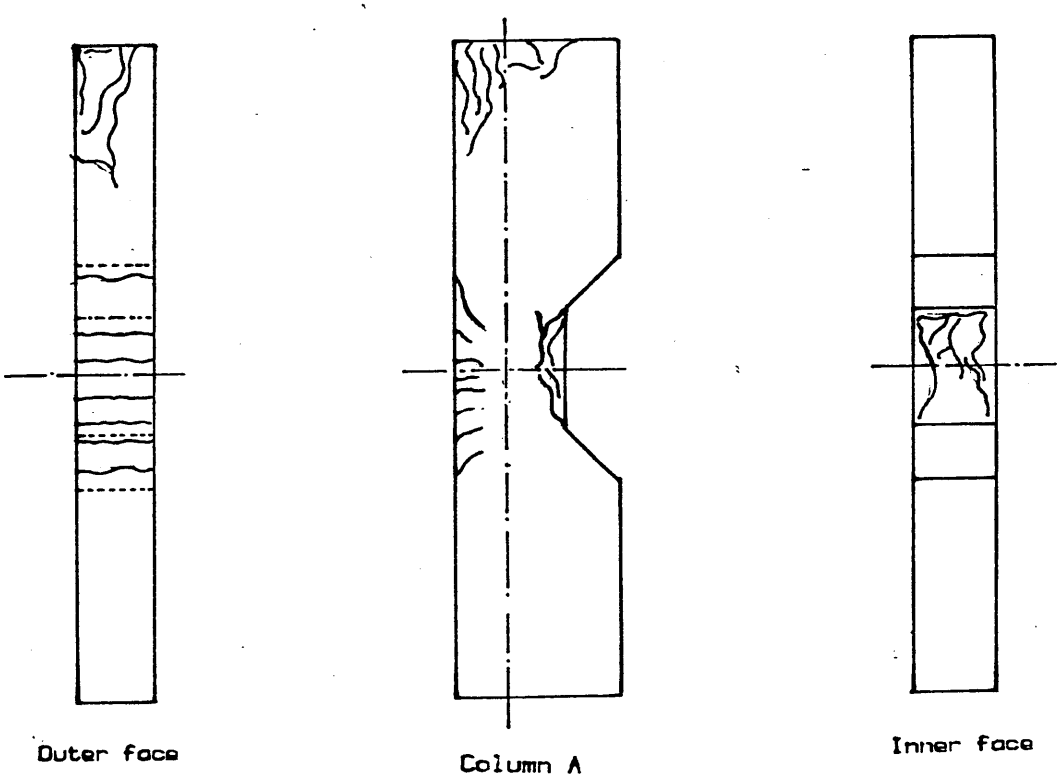

Fig. 6.20 Crack pattern for the five PC columns. (Grade A)

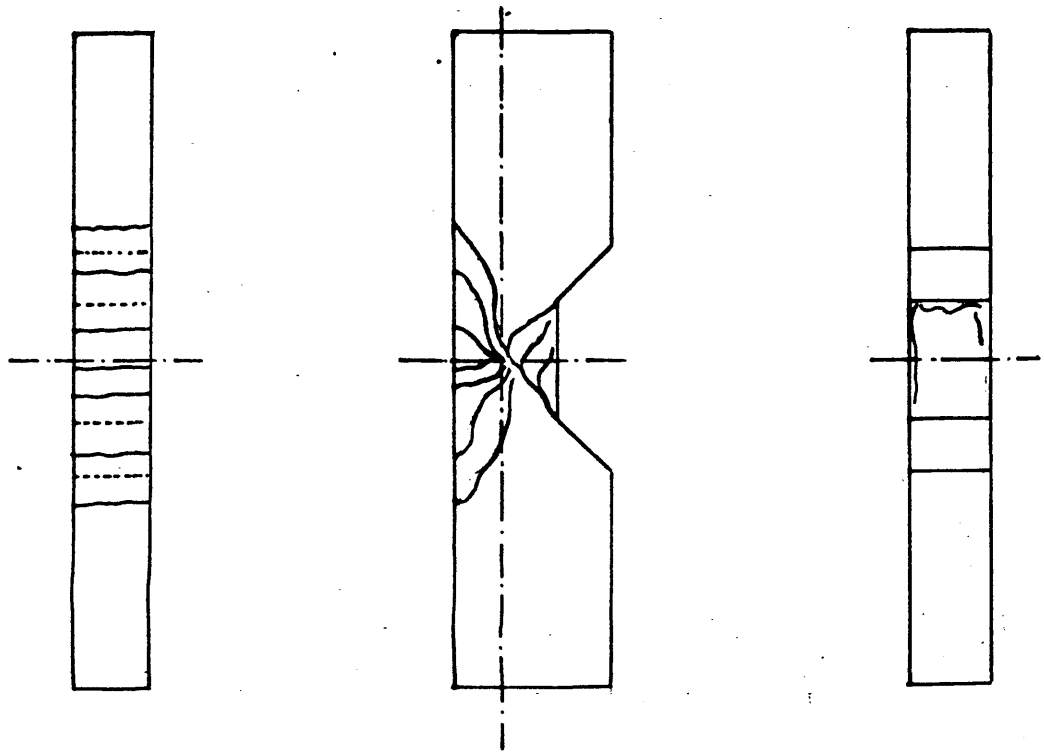

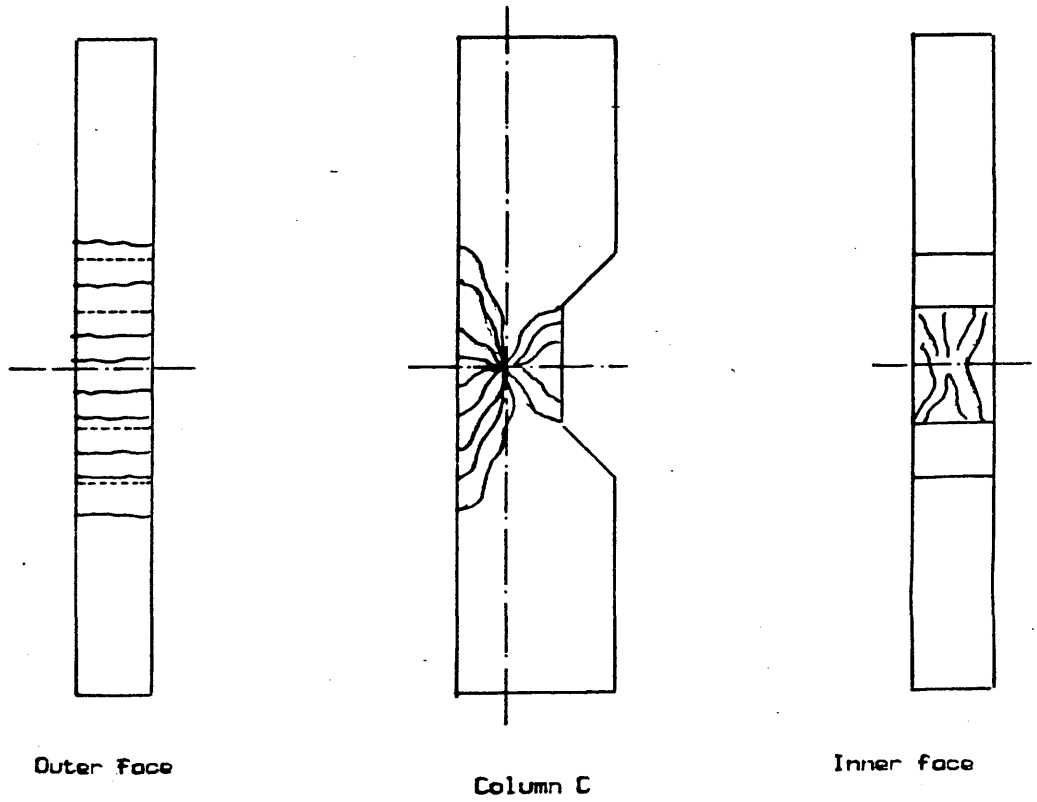

Fig. 6.20 Crack pattern for the five PC columns. (Grade B & C)

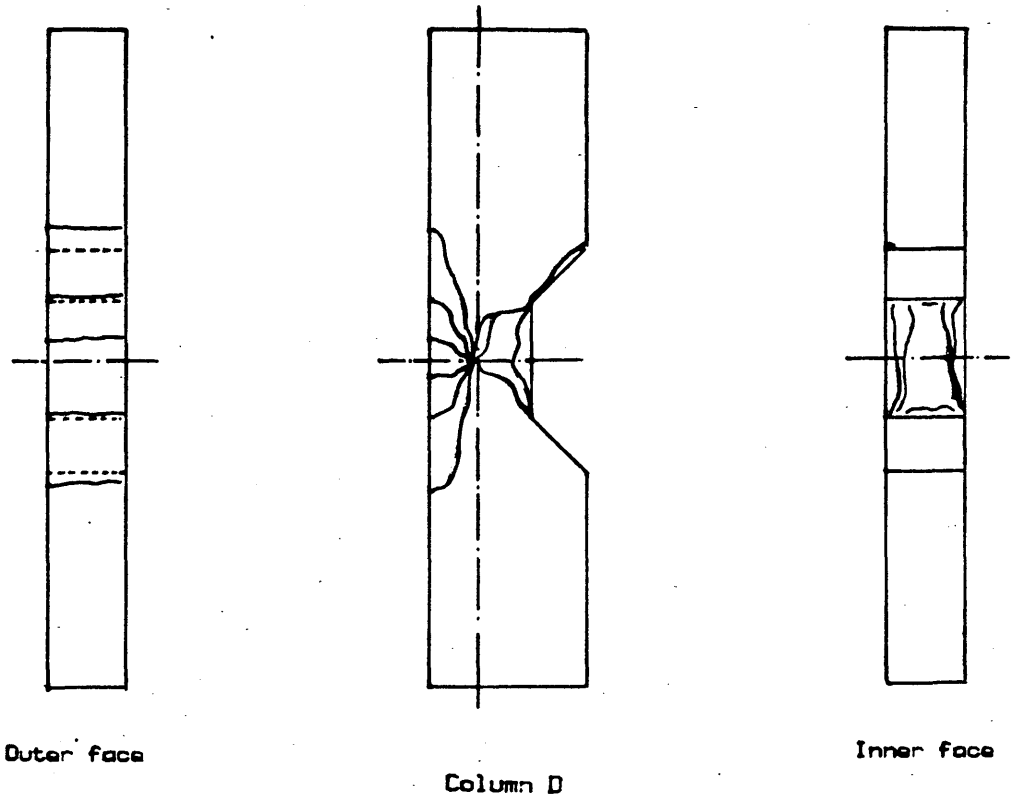

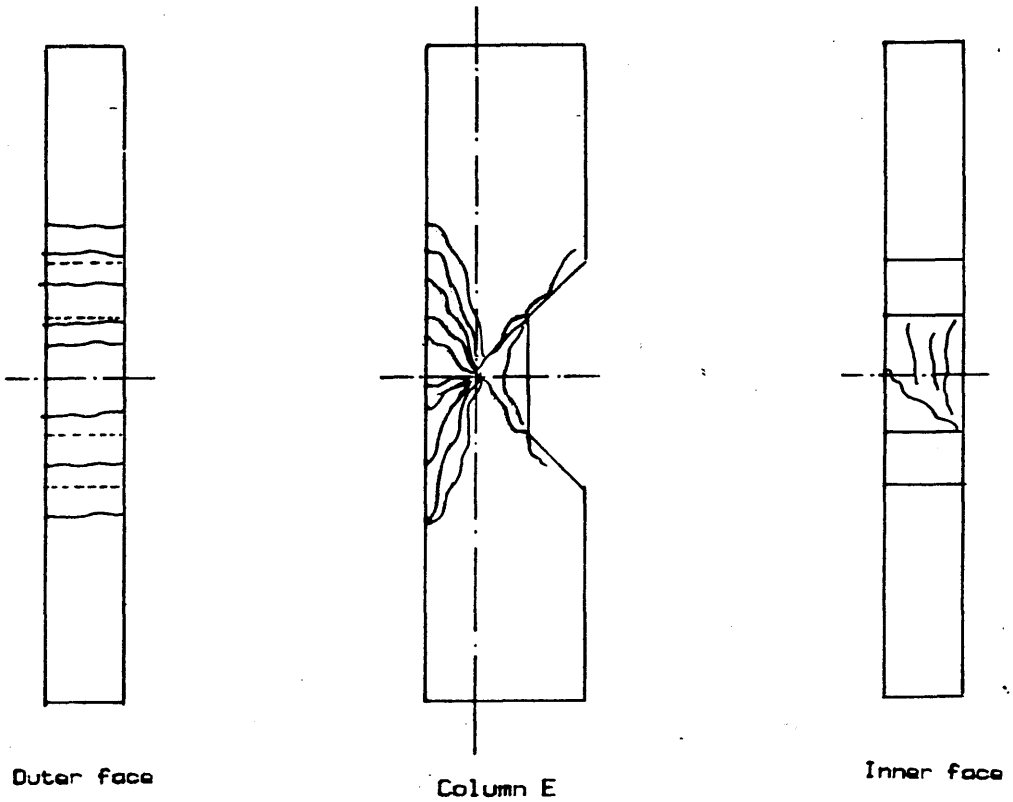

Fig. 6.20 Crack pattern for the five PC columns. (Grade D & E)

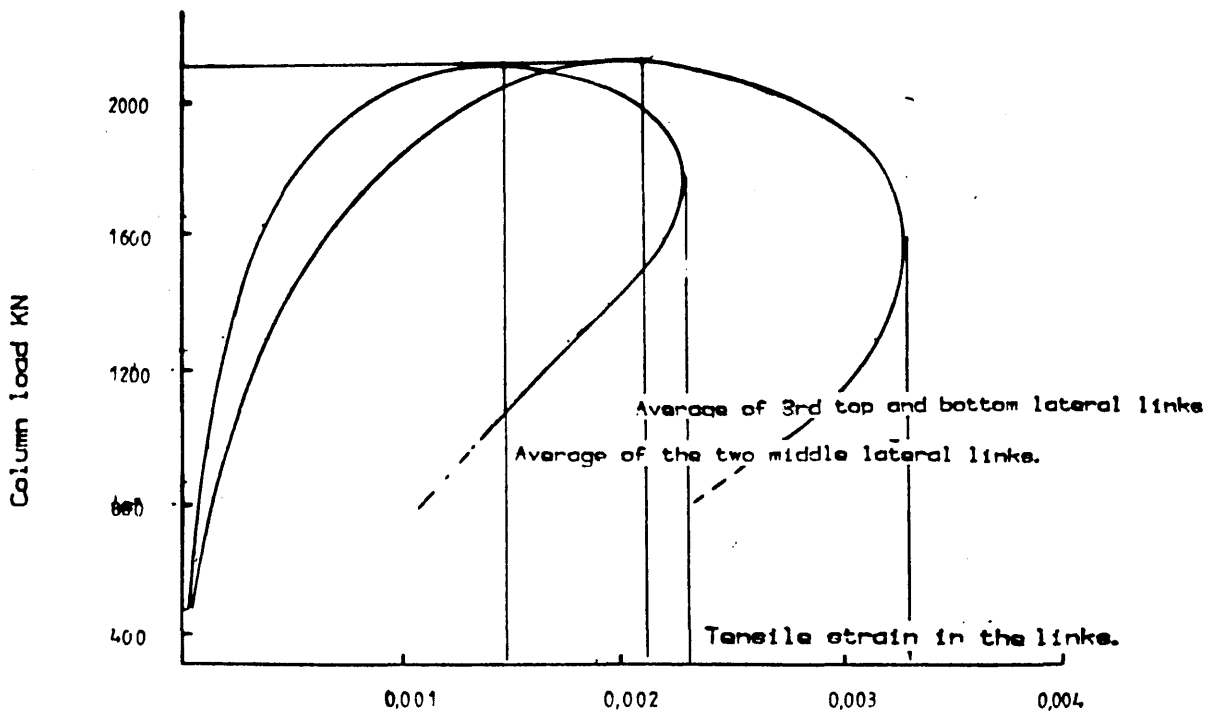

Fig. 6.21 Relationship between tensile strains in laterla links and the column load

CHAPTER SEVEN

LONG-TERM MECHANICAL PERFORMANCE OF POLYMER CONCRETE

7.1. Introduction

Time-dependent deformations play a vital role in the mechanical performance of any structural material and can lead to failure if the associated stresses are high enough to initiate microcracking. These deformations can be either recoverable viscous or irrecoverable plastic ones. The nonlinearity observed with most concrete stress-strain curves is mainly due to microcracking in the interface between paste and aggregate (96). The initiation of microcracking depends on the stress level; if this level is high the rate of deformation will be high and creep may cause time-dependent failure. On the other hand, linear proportionality between time-dependent deformations and stress level in terms of the short-term strength usually ends at the onset of microcracking (97) & (98). This implies that failure will take place with time if the applied stresses can produce microcracking.

Concrete under sustained stresses fails at a lower stress than the short term strength measured by conventional tests. This led to the early conclusion (99) that failure occurs at a limiting strain rather than a limiting strength and regardless of whether this strain is reached by a rapidly applied high stress or a lower sustained stress. The limiting strain takes place at a 'limiting' stress/strength ratio, often termed the "plastic limit" (100), which can have a value of 0.25 up to 0.85 or more depending on the material itself. Time-dependent

failure can not take place below the "plastic limit". Time-dependent deformations will take place in any case of loading. The relative values of these deformations are high for cases of sustained load, smaller for cases of load increasing at a small rate and even smaller for loads applied at high rates.

A different cause of time-dependent deformations in concrete is the process of hardening on setting. Differential shrinkage strains can sometimes be big enough to induce significant internal stresses. These induced stresses can cause setting and shrinkage cracking with the result of seriously limiting the structural use of PC.

Conventional cement concretes undergo creep and shrinkage deformations essentially due to the relative moisture movement required for hygral equilibrium of the cement paste. Many hypotheses on a phenomenological basis were suggested for describing the mechanism of creep and shrinkage of PCC (101). A theory of visco-elastic flow (102) & (103) was produced on the basic assumption that the hydrated cement paste is a highly viscous liquid. The viscosity of this liquid increases with time as a result of chemical changes within the paste structure. In this theory, cementitious materials are considered to behave in a viscous manner when loaded. The inert aggregates do not flow and in resisting the paste movement they are increasingly stressed with time. If this were the case, creep would progressively reduce with time. In addition, a viscous flow by definition requires a constant volume and a Poisson's ratio of 0.5, a case which can not exist in concretes. For these reasons and others, the theory of visco-elastic flow was not widely accepted.

The solid solution theory (103) was based on the assumption that vapour pressure of water in a gel is affected by the applied stress, with the result that the water content of the gel and its volume are altered. However, other studies (102) showed that cement gel in particular shows a remarkable structural stability against external loads to the extent that the solid solution approach can not be reliable.

Probably the most generally accepted theory in this respect is the seepage theory, first postulated bu Lynam in 1934 (104). In this, creep of concrete is taken to be due to seepage of the gel water (dispersion media) under pressure through the elastic skelton of the paste (dispersed phase). This expulsion or viscous flow causes stress redistribution from the viscous component to the elastic skelton. On removing the load such a system will undergo a partial immediate elastic recovery followed by a slow time-dependent recovery often termed as elastic after-effect. In this way creep can be considered to be analogous with shrinkage, but the motive force is an externally applied pressure instead of a direct internal vapour pressure.

Polymer concretes suffer shrinkage and creep to a greater extent than cement concretes. The explanation for these time-dependent deformations in PC is completely different from that of PCC. The cement paste with its combined and free water , cement gel, hydrates and capillary pores are just a few features that do not exist in PC. On the microstructural level, cement hydrates are gels with particles attracted electrostatically at van der Waals' distances,whereas PChas

amorphous molecules distributed at covalent distances. The exact nature of creep and other deformation sources in polymers are not within the scope of this work. However, deformations resulting in PC either due to external or internal stresses are give below.

7.2. Deformations of PC

Deformations of PC can be classified into two general types; load induced deformations and self induced deformations. Both of these are dependent on time. The self induced deformations are mainly related to the physio-chemical properties of PC. They can be either shrinkage or expansion deformations. Shrinkage occurs during the polymerization process. In this two main phenomena can induce shrinkage deformations as follows :

(1) Temperature gradient : The polymerization process of unsaturated polyester (UP) is a highly exothermic process (some 60 Cal/g in 2 hours). In the early reaction stages, heat evolution is usually greater than heat dissipation with the result that a peak mix temperature usually exists. This peak temperature can be as high as 20 C° above the ambient temperature depending on resin formulation and degree of filling, etc. After the peak temperature is reached, PC cools and the lowered temperature causes thermal volumetric shrinkage of as much as 5-8% for the pure resin. The process of thermal shrinkage increases rapidly after the peak temperature is reached and then attenuates slowly for as long time as completion of polymerization might take. This type of shrinkage will decrease as the filler or the dispersed phase

content in the mix increases. Obviously the shrinkage will be very small after these filler particles come into contact.

Internal tensile stresses will begin to be induced at the moment when shrinkage starts and can only take place after gelation which occurs at the peak exotherm. As the modulus of elasticity at this stage is very small, the induced tensile stresses will also be very small. On further hardening, the modulus of elasticity increases and the shrinkage strains become measurable. In some cases, the induced stresses can exceed the tensile strength and cause setting cracking in PC. However, all studies in this context show that the rate of tensile strength development increases rapidly after gelation and the induced stresses at any time are too small to initiate shrinkage cracks. The only possible case of cracking resulting from thermal shrinkage can exist if PC is heavily restrained and can be controlled by casting and curing in a temperature-controlled environment.

The thermal volumetric changes of neat UP resin can be very high as it has a coefficient of thermal expansion of $6\text{-}11 \times 10^{-5}$ /C.° With PC this coefficient is around 1×10^{-5}/C.° This large decrease is caused by the presence of fillers and aggregates used when making PC and the thermal capacity of the system is said to be enhanced or increased. The enhanced thermal capacity will reduce the magnitudes of the resulting tensile stresses in the binder, the compressive stresses in the aggregates and the interfacial shear stresses. It follows that a well-graded and compacted aggregates bound together with the thinnest possible resin layer (smallest resin content

possible) will virtually suffer no more thermal volumetric changes than those encountered with PCC.

(2) Chemical shrinkage : The polymerization process is essentially a process in which individual molecules are caused to be covalently bonded into macromolecules and contraction is induced in the system as a whole. Growth in viscosity is mainly caused by the formation of these macromolecules in the form of long chains. The process of crosslinking these linear chains results in a further chemical contraction.

While thermal volumetric changes can be controlled by resin formulation, mix ratio of PC or controlling the ambient temperature, the chemical reaction can not be controlled by using similar external effects. To avoid chemical contraction several physio-chemical methods have been tried (105). The 'Pore-method' is the most traditional one and has been in use in plastic technology for a long time. A few research trials making use of this method with PC have been carried out (106) & (107). In this method, special foaming agents are used to produce gas which provides a cellular structure in the material and compensates for the chemical contraction. The main disadvantage is the resulting high porosity of the material and the consequent inferior mechanical performance.

More recently it became possible to control the free volume of monomers and polymers by special macromolecule alignment techniques (108) through forming controlled microstructures in the resin binder. Expansion in the resin volume during curing can be obtained by using polyring monomers which help produce ring opening polymerization (109). The main disadvantage of

this method is that it requires the synthesis of highly complicated chemicals which can provide such special potential. Other methods have been developed and used such as 'low-profile method' by Ohama (110) or 'geometrical active-microfiller method' by Czarnecki (105). These methods in general should counteract the chemical contraction and even the thermal shrinkage. There is the possibility that some of these methods could produce an overall expansion in resin concretes made with UP resin and 'expansive PC' could be manufactured (105).

Load-induced deformations can exist after PC has reached its initial set at gelation. When hardened, PC can be regarded as a dispersed phase of inert aggregate in a continuous phase of polymer matrix. This implies that PC can not readily be treated as a homogeneous material for which traditional methods of caculating deformations can be used. Polymer concrete with its amorphous polymerized monomers and unreacted monomers, microfillers, sand and aggregates, composite voids and base-matrix pores is heterogeneous at virtually any observation level; when steel is present it becomes anisotropic as well.

While the theoretical study of molecular or atomic behaviour can provide explanations for deformation, it only applies to materials which are homomgeneous and isotropic. Hence the most practical way of assessing the deformations of PC can only be on a empirical basis. In this, the rheological properties can be approximated to certain physical models whose constants can be derived from associated experimental stress-strain

relationships. This approach has attracted the majority of the very few studies carried out in this field.

In the rheological sense, PC can exhibit elasticity or visco-elasticity. This will primarily depend on the rate of load application and its duration. PC behaves elastically at very high rates of load application or at very small durations of load. Deviation from this linear stress-strain relationship is incurred by interfacial bond microcracking at high levels of stress, which is related to PC heterogeneity rather than energy dissipation. However, Davydov (111) reported that PC has hysteresis which causes this deviation particularly at prolonged load durations. That is to say that the rate of energy dissipation increases with increase in load duration whereas the restored strain energy decreases. It follows that nonlinearity of the stress-strain curve is not fully dependent on the initiation of bond microcracking but probably to a greater extent on rate of loading or its duration (the relative relation between the external potential load energy and the internal thermal energy). Experimental observations (111) suport the view that PC possesses viscoelasticity. All stress-strain curves show recoverable time-dependent strains. The proportionality between stress and rate of strain is satisfied at any stress level before microcracking. On being stressed, PC develops a certain amount of irrecoverable time-dependent deformation. The ratio of this irrecoverable deformation to the instantaneous recoverable and time-dependent deformation is not constant. It varies considerably depending on the applied stress level and the rate at which it is applied. Temperature can have another major effect on the

response of PC to stresses. These combined effects make it difficult to represent PC rheologically on a clear basis.

7.3. Shrinkage strains and resulting stresses of PC

Polymer concretes usually undergo shrinkage strains at early ages. This proceeds at a high rate in the first phase after gelation sets in; thereafter the rate decreases considerably and almost reaches zero after polymerization and thermal balance is attained. Shrinkage induces tensile stresses in the polymer phase and compressive stresses in the aggregate and in the steel if the PC is reinforced. The resulting tensile stresses can in some cases be high enough to initiate tension cracking especially in heavily reinforced members. The shrinkage stresses are intrinsically dependent on the polymerization rate, that is the slower the polymerization the more favourable the state of the induced stresses due to shrinkage. In addition other factors can interfere in shrinkage such as the binder ratio, the degree of aggregate compaction, the resin type and its viscosity .

A.Watanabe (112) carried out a study on the stresses in plain PC resulting from setting shrinkage. In that study most shrinkage strains of polyester resin concrete took place in the first ten hours and no increase in this shrinkage could be traced after PC had reached 24-hrs of age. The shrinkage strains (ε_t) at any time (t) could be expressed as a hyperbolic function of time as follows :

$\varepsilon_t=(t-A)/[B+C(t-A)]$ in which A, B and C are constants.

Theoretical estimation of the tensile stresses in PC could be

derived on the basis that Hook's law is valid for infinitesimally small periods of time. By integrating the stress components corresponding to very small time values , Watanabe could express theoretically the total value of the induced tensile stress f_i within any given time period $t = t_2 - t_1$ as follows :

$$f_i = f_{i2} - f_{i1} = \int_{t=t_1}^{t=t_2} (K_t \frac{d\,\varepsilon_t}{dt})dt$$

in which $K_t = \frac{E_s A_s E_{ct}}{E_s A_s + A_c E_{ct}}$

E_s , E_c : steel and PC moduli of elasticity and,

A_s , A_c: steel and PC cross-sectional areas.

Based on experimental measurements E_c at any time t could be expressed as a single function of time for a given PC type; in this way the coefficient K_t could be expressed for any given reinforced PC section. As creep would have some effect on the resulting tensile stresses, corrections due to creep recession were introduced and rather lengthy equations were obtained. Both theoretical and experimental measurements showed that tensile stresses resulting from shrinkage increase very rapidly at the early stages. This increase then attenuates and eventually reaches a more or less constant value. The noteworthy observation of that study is that the tensile stresses in PC members having 4% reinforcement amounted to 2.0-2.5 N/mm 2 at associated tensile strengths of 7.0-8.0 N/mm 2. This implies that although tensile stresses can develop rapidly they will be smaller than the corresponding values of the tensile strength attained. As with PCC, the induced tensile stresses in PC are inversely proportional to the reinforcement ratio. However, Watanabe (112) observed

experimentally that the resulting stresses in PC decreased when the reinforcement ratio had exceeded a certain value; this value is reported to be 5%. It is also reported that half of the final shrinkage strain takes place while PC is still in a liquid state and when no shrinkage stresses can be induced.

In another relevant study carried out by W.koyanagi (113), the experimentally measured strains in PC and reinforcement steel increased rapidly, after the peak exothermic temperature was reached, for about ten hours after which time the increase became very small. Strains in either steel or PC decreased by increasing the reinforcement ratio as shown in Fig.(7.1). In Koyanagi's work it was found that there is a definite time lag between the occurence of strain in PC and in the steel. This is because strains occurring in PC while still in a liquid state can not produce strains in the steel. It followed that induced stresses can not be explained merely by the total recorded strains in PC based on an elastic analysis; thus inelastic deformations were taken into account.

In this work Koyanagi adopted a rheologicaL model similar to that of Burgers (Kelvin and Maxwill elements in series), see Fig.(7.2). As the deformation equation of this model is a second order differential, some assumptions were made for simplifying the solution. By equating the theoretical deformations of the model δa, δb and δc to similar experimentally-recorded deformations, see Fig.(7.3), the constants of the dashpots and springs could be calculated. Their values as plotted against time for PC are shown in Fig.(7.4). In this figure relaxation time T_{rx}(time required

for the internal stress to relax) increases rapidly with time, whereas retardation time T_{rd}(time required for the strains to be recovered) is almost constant.

Based on these observations, Koyanagi suggested that PC transforms from a viscous liquid to a viscoelastic solid in the course of time. On calculating the induced tensile stresses using the suggested rheological model, it was found that the stress increases with increased reinforcement ratio as shown in Fig.(7.5).

7.4. Creep behaviour of PC

Despite the importance of long term deformations in the structural behaviour of PC, very little work has been carried out on the creep properties and the consequent effects of sustained load. Furthermore, even less information is available regarding the effects of different rates of stress and/or strains on the short term properties of PC.

One of the earliest studies concerned with the creep behaviour of PC was that of T.Broniewski (114), who found deviation from the linear stress-strain relationship as recorded in conventional tests began at almost one third of the ultimate strength of PC. That deviation in addition to the high ultimate strains was reported to be mainly due to the highly viscoelastic nature of the polymer matrix. On conducting a few direct tensile creep tests Broniewski found that creep-time relationships can be expressed using the following equation of Macleod (115);

$e_t = e_i(t/B)^m$ in which e_t and e_i are creep and initial

strain, while B and m are constants. This equation is presented in Fig.(7.6). It is suggested that with viscoelastic materials it is quite sufficient to use a few experimental measurements at the first 100 hours for the derivation of the constants. This is mainly because the material response tends to stabilize in the course of time. In this simple equation, the effect of age at loading is pronounced in the value of e_i, while the effect of the stress level is pronounced in the constants B and m.

This equation can be rewritten as $t = B.\ (e_t/e_i)^{(1/m)}$. For a given PC grade, a limiting failure strain e_1 exists and this equation can be used to predict the time required for PC to reach this limiting strain under a particular stress level. Partial factors of safety can be introduced to the value of e_1 to give the life time of a member under given load conditions so that no more than, for instance, 50% of e_1 should develop.

Other studies of PC creep carried out by K.Okada (28) , showed that creep is proportional to stress level and that it is greatly influenced by temperature. As shown in Fig.(7.7), elevated temperature can induce excessively high creep strains due to the strong thermo-dependency of all the mechanical properties of PC.

Obviously, this dependency is a function of the resin type and the mix proportions. High values of the resin and/or small values of aggregate contents in the mix would allow for higher values of creep; fig.(7.8) shows the effect of these two factors on creep. In this figure, mix M made with high resin content (15% by wt.), high filler and high sand contents gave

much higher creep values than mix R which is made of low resin content and high coarse aggregate contents (10% and 40% respectively).

In another study made by T.Yamasaki (112), the creep coefficient in terms of the true creep relative to the instantaneous strain increased with increase in load duration. The creep coefficient approached a horizontal assymptote after 72 hours of loading. The magnitude of the assymptote of the creep coefficient was found to increase with increased age at loading. However this increase was at a decreasing rate and at ages more than 24 hours a decrease in the creep coefficient was observed.

Yamasaki (112) studied the proportionality between creep and the associated stress level. It was found that the maximum stress/strength ratio that would not produce time related failure was below 57%. At this ratio time induced failure occurred after 43 hours. For stress levels of 60% and 70% failure took place after only 1.5 and 3.0 hours respectively. The relationship between creep and stress/ strength ratio based on the experimental observations was not linear at any stage as shown in Fig.(7.9). This behaviour has been confirmed by other relevant studies in the United States (116). This is unlike the case with cement concretes and mortars, which can exhibit linear creep-stress ratio relationships of up to 0.5 and 0.8 stress/ strength ratios respectively.

In a study made by M.Helal (116), further disimilarity between PC and PCC responses to sustained load was found. It is usually assumed that a final creep strain (ultimate creep)

will be reached in any member under loads. Ultimate creep can be reached in PCC after almost 20 years. With PC Helal found that this ultimate value can be reached within only one year. While with PCC 50% and 75% of ultimate creep can take place approximately after three months and after one year, they are reached with PC after only one week and six weeks respectively. In his experimental work, Helal found that the stress level that can cause time-related failure is 50%; this value is very comparable to the value obtained by Yamasaki (112). It is worth mentioning that the sustained strength for PCC as reported by Neville may vary from 0.7 to 0.9 of the short term strength (117). This implies that PC strength is usually more affected by sustained load than that of PCC.

7.5. Experimental study of time-dependent properties of PC

In the present work, time-dependent properties of PC were investigated using two main approaches. The first of which was to investigate the effect of different rates of strain on the ultimate compressive strength, modulus of elasticity and values of strain at failure. The second approach was to study the effect of the duration of a constant load (creep response) on the resulting strains and the associated sustained strengths.

The fundamental aim is to arrive at a clear interpretation of the time-dependency of PC on which basis reliable partial factors of safety can be drawn up. It should be clear that a general assessment of such dependency would require greater study of the phenomenological and theoretical levels than that undertaken in the present work. However what is aimed at here is an experimental evaluation of those time-dependent

properties of PC which might provide, along with the results of other relevant studies, a starting step towards the production of a practical code of PC structural design.

7.5.A The effect of rate of strain on the properties of PC

7.5.A.i Some structural implications The effect of rate of strain is essentially related to the load duration and creep effects which will tend to increase with decrease in the rate of strain or with increased load duration. A chosen rate of strain is usually more accurately attainable in compression tests than rate of stress. Adjustment of the testing instrumentation to maintain a constant rate of stress over the whole testing period is difficult. Near its ultimate strength PC, like PCC, would develop extremely high rates of deformation. This would necessarily give misleading results even if the testing machine could still provide such a constant rate of stress. In addition the stress-strain curve recorded under constant rate of stress can only be traced up to the ultimate strength, after which no load increase can exist. Any falling branch of the curve would be lost. This falling part can be of fundamental importance for certain applications in assessing the load-carrying capacity of PC near and after its ultimate strength is reached. For these reasons it was decided to carry out the series of axial compression tests using different but constant rates of strain rather than stress.

For a given PCC, increasing the load duration leads to a reduction in the strength and to an increase in deformations. This phenomenon as said earlier is due to the effects of creep

and shrinkage of PCC. The same should apply to PC with the reservation that in PC the effects of creep are more evident and those of shrinkage are less dominant than in PCC. In fact shrinkage of PC becomes of very little significance after one to three days of age, depending on the type of PC. This fact has dictated the study of PC creep rather than its shrinkage as will be shown later.

As different rates of loading affect deformations and strengths, these rates would also affect all the stress-block parameters in flexure which already have been derived. The short-term findings of stress-block shape and parameters at ultimate capacity might therefor require some modifications. These modifications will primarily depend on the nature of the load, whether it is increasing or constant, and on the values of the applied rates of loading or load duration. Consequently the stress-strain curve for a given PC grade can never be given one fixed shape and should differ from one case of loading to another.

In the compression zone of any PC flexural member, strains can be fairly asssumed to be linear. It follows that each fibre will be strained at a different rate from the others and this rate will be proportional to distance from the neutral axis. Based on this assumption, Rusch (93) could derive a stress-strain curve for PCC in flexure from axially tested prisms at different rates of loading. He also suggested a procedure from which various stress-strain relationships, attained at different loading durations, can be derived.

Out of this procedure it can be said that stress-block

parameters whether for PCC or PC, will vary for a given concrete depending on the strain chosen to be reached within a prescribed period of time. Fig.(7.11) shows schematically how Rusch could derive the flexural stress-strain curve from the axial compression stress-strain curve carried out at different rates of loading. This derivation was based on reasonably accurate assumptions the most important of which is that for each rate of strain in various fibres across the compression zone, there will appear the same stresses as in the corresponding fibres of axially loaded prisms at similar rates of strain. In this the effect of anisotropy and strain gradient were not considered.

7.5.A.ii Description of the experimental work

The experimental study of the effect of the different loading rates on the stress-block shape and parameters was carried out for each of the five PC grades. The axially loaded specimens in compression were tested at various constant rates of strain. These rates were made to cover as wide a range as the available testing machine would practically allow. The fastest and the slowest rates that the machine could provide and which are of significance were chosen to be 2.9×10^{-7} and 415×10^{-7}/ second. These chosen rates required loading times in the range from 2 minutes to around 20 hours. Between the fastest and the slowest rates six additional rates were determined as given in table (7.1).

The specimens were cylinders of 100 mm-diameter and 200 mm-length. For each grade and each rate of strain, two cylinders were tested. The sixteen cylinders tested for each grade were

cast altogether using one batch and vibrated on a vibrating table. Curing was the same as that carried out with all previous specimens.

The testing machine is "LOS-SYSTEM UPS.2000". This machine can be adjusted to the required rate of platen movement with the result of producing a constant rate of deformation in the test specimen throughout the whole test.

To overcome any ill effects of uneven end surfaces, all specimens were finely ground at both ends before testing. No capping or packing could be made where it could have affected the readings of the deformations. Having done so, the relative displacement of the two stiff and non-rotating platens of the machine could be taken as the deformation in the test specimen. This indirect method of measuring the deformations should remain correct as long as the specimen is in complete contact with the top moving platen; a condition which was persistently satisfied throughout the test. Fig.(7.12) shows how the displacements of the cylinders were measured and recorded. The displacement was recorded using a transducer.

The machine load and the displacement were continuously recorded using a plotter connected to the machine control console. In addition these values of load and displacement were printed out at intervals using a Data Logger connected to the machine as a second output of the test results. The machine has a safety-limit operational system which made it possible that continuous testing of up to about 20 hours be carried out unattended. This safety system can stop the load increase after a predetermined displacement value is reached

or can stop the displacement increase if a given load is reached.

7.5.A.iii Test results and their interpretation

The curves of load-displacement as given by the plotter were checked against the output of the Data Logger, then reproduced as stress-strain relationships. For each rate, the average curve of two specimens was found and considered in further analysis. Figs.(7.13-a,b,c,d&e) show these curves for the eight chosen testing rates for the five prospective grades. A major reservation on these curves is that the two specimens tested for each rate of strain did not always prove sufficient for drawing up a general stress-strain curve for that rate.

While consistency of the results and their invariability was acceptable for good-workability grades (grade E for instance), poor workability grades like D and C suffered divergence in the results for each of two cylinders tested at the same rate.

As shown in Figs(7.13), all PC grades seem to follow a similar trend in their response to various rates of strains as that of PCC. Irrespective of PC grade, faster rates of strain gave higher ultimate strengths, smaller strains at failure and quicker failure immediately after the ultimate load was reached. Slower rates were associated with smaller ultimate loads, higher strains and greater retained carrying capacities after macrocracking.

The relative retained carrying capacity C_r at any time after the ultimate load is reached, is defined here as the ratio of the retained machine load at that time to the ultimate load. With high rates of strain the drop in C_r was very large and

took place within a few minutes after the ultimate load was reached. For example, with grade D at rates [1] and [2] the reduction in C_r was 100% and 95% respectively after only two minutes. On the other hand, with small rates of strains like rate [8] for instance, C_r calculated for grade E and B had values 60% and 40% respectively, 8 hours after the ultimate load was reached. Quite a few of the specimens tested at rate [8] retained considerable C_r-values and the machine load could be maintained for as long as 16 hours beyond the ultimate load with strain values of as much as 0.015, especially with lower stiffness grades.

The linearity of the stress-strain curves obtained are more evident with fast rates. For each grade, the features of the stress-strain curves obtained at rate [1] are comparable to those of the short term tests carried out previously at a constant rate of stress (see chapter 3). This applied only up to the ultimate load after which the falling branch of the curve in short term tests could not usually be traced.

The stress-strain curves corresponding to rates [1] and [8] for each grade are shown in Fig.(7.13). These two curves represent the boundaries for all possible stress-strain curves carried out at a rate of strain ranging from 2.9×10^{-7}/sec to 415×10^{-7}/sec. Within these two boundary curves, the ultimate strength decreased by almost 16% to 22% depending on PC grade. On the other hand, the axial strains occurring at ultimate load increased by almost 6% to 14%.

The stiffness of the various grades increased with increased rate of strain. For the five PC grades tested , grade E had

the lowest modulus of elasticity while grade C had the highest one. The initiation of microcracking is indicated by the beginning of nonlinearity of the stress-strain curve, whereas macrocracking is made manifest by the test load starting to decrease. Both micro and macrocracking as defined here, required more loading time at small rates of strain. In addition the small rates produced cracking at smaller stress levels than with high rates of loading.

To clarify these effects, Figs.(7.14-a,b,c,d&e) were constructed. In these figures, the time required for each PC grade to develop its macrocracking (t_m) is plotted against the stress level (relative to strength at rate [1]). It is clear from these figures that the strength of PC is strongly dependent on rate of loading or load duration. In the same figures, Figs.(7.14), the axial macrocracking strain ε_{cm} is plotted against tm. The two relationships of stress level and strains with macrocracking time as given in Figs.(7.14), tend to reach stabilized values. Time-dependency is shown mostly in the first two hours of loading, after which neither a significant increase in the axial strain nor a decrease in the strength would occur.

As said earlier, time-dependent deformations are present in all cases of loadings and their magnitude for a given stress level are increased by prolonging the loading times. If the strength recorded with rate [1] is to be taken as the short-term strength, point 1 on curve a, then all other points on this stress level-time curve would represent cases of long-term or time-dependent failure. The smallest stress level which caused such time-related failure according to a- curves

varied from 77% to 84% for different grades, and on average was about 80%.

On the other hand the largest macrocracking strain relative to macrocracking strain for short-term loading was on average 110%. This increase in the strain energy of a given PC grade by increasing the loading time can be useful in the structural applications of PC. Higher strains at failure would allow the initiation and formation of wider warning cracks and can provide more use of the reinforcement steel at failure. The retained carrying capacity as defined before is higher for longer periods and can therefor offer a greater safety margin in structures at failure.

At this stage it should be noticed that if a cylinder is subjected to a gradually increasing load at a constant rate of strain, there will exist a definite stress level corresponding to a particular rate of strain or certain loading time below which no failure would take place. This stress is termed here as the long-term strength f_{cl}. All the given curves of Figs.(7.14) show that for each PC grade there can exist two horizontal assymptotes for the axial macrocracking strain ratio ε_{cmr} and for the stress level f_r. By extrapolating each of these curves the ultimate values of ε_{cmr} and f_r could be obtained and used in deriving the long-term strength and macrocracking strain ε_{ml} for each grade.

For example, with grade E the extrapolated assymptote values ε_{cmr} and f_r, at 10 hours loading, were 105.5% and 83% respectively. As the short term values of the strength and the macrocracking strain (rate [1]) are 0.0078 and 95 N/mm2, it

follows that the respective long-term values are 0.00823 and 79 N/mm2. To attain a strain value of 0.00823 within 10 hours the required rate of strain would be 1.4×10^{-5}/min. This implies that for rates of strains smaller than 1.4×10^{-5}/min., or for constantly increasing loads with duration not less than 10 hours only a stress equal to or more than 79 N/mm2 will cause failure. This value is the long-term strength for grade E. By similar derivations, the long-term strengths for grades A, B, C and D were found to be 78, 73, 70 and 75 N/mm2.

The variation in the ultimate strength versus different rates of strain are shown in Figs.(7.15-a,b,c,d &e). This variation could be expressed using the following equation :

$$f_{cu} = p.r^{v} \qquad (7.1)$$

in which f_{cu} is the ultimate strength in N/mm2 at a given rate of strain r in (1/min.)$\times 10^{5}$. To obtain the constants p and v for each grade, Eq.(7.1) was plotted logarithmically as shown in Figs.(7.16-a,b,c,d &e). The intersection of the line with the ordinate (log f) gives the value of log p, while the slope of the line gives the value of the constant v. The values of these constants for each grade are shown in Figs.(7.16). In these figures the highest rate of strain was fixed for the five grades at a value of 0.0025/min., whereas the lowest rate was that corresponding to the long-term strength of each grade previously derived. Using Eq.(7.1) the ultimate strength at any rate of strain can be calculated. It should be noticed that this equation is valid only within the boundaries set, i.e., within the highest and the lowest rates of strains given for each grade.

As given before in Figs.(7.13), the stiffness of PC dropped considerably with decreased rates of strain or increased load durations. This decrease in stiffness and linearity of PC stress-strain curves might be attributed to the effect of hysteresis of the material itself. Prolonging load duration allows for an increase in the rate of energy dissipation through losses in internal thermal energy, a case which does not exist in fast loading rates. These losses are reflected through a decrease in the strain energy restored (the instantaneous and time-dependent recoverable strain), and this would lead to an increase in the plastic flow and result in reducing the modulus of elasticity and the microcracking stress level (the onset of nonlinearity). The reduction in the elastic moduli was significant within the rates of strain chosen. For example with grade C this reduction amounted to 20%. The variation in the elasticity moduli with different rates of strains could be expressed using a similar equation to Eq.(7.1) as follows :

$$E = q\, r^{w}. \qquad (7.2)$$

in which E is the modulus of elasticity in N/mm2 corresponding to a rate of strain r in (1/min)x10^5. The constants q and w could be obtained from the logarithmic plotting of Eq.(7.2) as done before with constants p and v.

Once again Eq.(7.2) is applicable only within the previously given range of rates of strain. Table (7.2) gives the values of the constants p, v, q and w of Eqs.(7.1 and 7.2) for the five PC grades.

7.5.B Experimental work on creep behaviour of PC

The effect of sustained load on the ultimate strength and the stiffness of PC is of vital importance for its structural applications. Time-dependent deformations can take place under any loading. Here the experimentally found effects on stress-strain relationships with time will be given for constant load levels. In these, the effects of the applied stress level and load duration on various creep parameters were investigated.

Needless to say that many other effects still require to be examined such as the effect of temperature and the effect of different mix ingredients of PC. Nevertheless, several effects which exercise strong influences on the creep behaviour of PCC have little significance with PC and therefore may be disregarded. For instance, as there is no water, the effect of relative humidity movement and associated drying shrinkage does not exist in PC. In other words, apart from the chemical and physical shrinkages that occur in early ages, PC is almost in stable hygral equilibrium and the total changes in deformation under loads can be fairly assumed to consist of only elastic deformations and basic (true) creep. Fig.(7.17) shows schematically the different components of deformations under constant loading versus loading time and their definitions for PC and PCC.

7.5.B.i Description of the experimental work

Creep tests were carried out using 'THE TYLER' portable creep rig as shown in Fig.(7.18). This rig is designed to accept a prismatic specimen measuring not more than 508x108x108 mm. The specimen is sandwiched between two circular platens each 32 mm thick and 203 mm diameter. A hydraulic jack is inserted

between one of these platens and a third outer end platen. Three High Tensile steel rods pitched at 120° running through the three platens provide the loading frame. A nut on each rod above the intermediate platen helps transfer and maintain the jack load. After the jack load is applied the nuts are tightened and the jack pressure is released. The losses in the jack load on transfer to the nuts can be estimated from charts as a function of the applied load. To compensate for creep strains in the specimen, the load is adjusted periodically.

The stress levels in the creep tests were dictated by the loading capacity of the rigs. The maximum allowable load as given by the rig suppliers are 217.5 and 156 KN for rigs with supporting rods 14 and 16 mm respectively. The specimens chosen were prisms and had two sizes measuring 500x100x100 mm and 350x70x70 mm; which will be termed as 'large'and 'small' specimens. For each PC grade, two specimens (one of each size) were cast horizontally, vibrated and cured in the same way as before.

For testing the large size, a rig with 16 mm-diameter rods were used, while 14 mm-diameter rods were used for testing the small specimens. The actual applied jack loads as obtained from a calibrated pressure gauge-jack load curve for the hydraulic system used, were 202 and 172 KN for the large and small specimens respectively. After calculating the losses on load transfer, the effective axial loads were found to be 182 and 155 KN which produced constant stress values of 18.5 and 31.5 N/mm2 respectively. Within the limits of the maximum allowed load set by the rig capacity, and the minimum specimen

cross-sectional area (70x70 mm) set by the maximum aggregate size , a wide range of stress levels was not possible. These rigs are originally designed for testing PCC and in such a case stresses such as those mentioned above would give very high stress levels. Because of the high value of PC strength, these stresses gave maximum stress levels of only 42%.

The strains were measured using mechanical extensometers. Each specimen had three pairs of studs located at the center line of each of the specimen's clean faces. The gauge length was 200 mm for the large specimens and 100 mm for the small ones. As said before the applied constant load had to be adjusted to allow for creep strains and to maintain a constant stress. Each load was adjusted before every reading and the given strain values are the averages of the three strain readings.

Based on the available knowledge of the creep behaviour of PC, these creep tests were made to last for short loading times relative to tests of PCC. For instance, studies made by Ohama (118) showed that rate of creep in resin mortars becomes insignificant after 90 days of loading (ultimate creep e_{cu}), and that about 80% of it occurs during the first 20-30 days. Helal (116), using resin concrete, reported that 50% of e_{cu} (after one year) takes place within the first 7 days and that 75% of it occurs within the first 5-7 weeks of loading. Other researchers carried out creep tests on PC for only 20-30 days and useful results were obtained (119). This is mainly because, as said earlier, the properties of PC develop almost fully in very short times compared to PCC, and because of the lower stiffness of PC which makes its response to time very rapid.

In accordance with these implications, the creep measurements were observed for 64 days. After measuring the instantaneous strain, readings were taken at 1, 2, 4 and 8 hours. Then a reading was taken each day for the first 8 days, thereafter each 2 days for another 12 days. After 20 days, a reading was taken every four days until the load was removed. A similar time table was followed in measuring strain recovery and continued until two successive readings of the residual strains became equal. The test was then stopped.

To help draw some general conclusions regarding the effect of the different mix ingredients of PC and their proportions on creep, four grades were investigated; namely grade A, C, D and E. All the creep tests were carried out at normal ambient temperatures.

7.5.B.ii Results and their interpretations

The total strains (instantaneous + creep) recorded at various constant stress levels for the four PC grades are plotted versus loading times in Figs.(7.19-a,c,d &e). The effect of age at loading is not considered as it was previously found that the rate of strength development becomes very small after the first few days of age. It was found that at ages more than 14 days the strength of PC can be fairly assumed to be fully developed, and no practical gain in elastic moduli or in strength will take place. All the creep tests were carried out at ages not less than 20 days.

On loading, the values of the instantaneous strains e_i were found to be directly proportional to the stress level applied.

The modulus of elasticity calculated as the ratio of the applied stress to the associated value of e_i , at either of the two stress levels provided, were almost identical for each grade. However, the calculated values of the elastic moduli were smaller than the corresponding values previously found for each grade in short-term tests (see Chapter 3).

All the strain-time curves of Figs.(7.19) had the strain increasing at a decreasing rate over a period of time varying from one PC to another. Creep strain taking place within this period of time is often termed as 'primary creep'. The elapsed loading time for primary creep varied from about 5 days with grade D to almost 30 days with grade A. Thereafter creep rate became constant with time and very approximate linear relationships between strain and time were experimentally observed with all curves. This stage of stationary rate of creep is usually termed 'secondary creep'. In all creep tests carried out, only primary and secondary creep stages were observed. No tertiary creep could be reached as stress levels were too small to initiate strains big enough to cause the rate of creep to increase.

The basic creep strain e_c at any loading time is calculated as the difference between the total strain e_t at that time and the instantaneous strain e_i. Similarly, creep recovery r_c is calculated as the difference between the total strain recovery r_t and the instantaneous recovery r_i. The creep coefficient k_c is calculated as the ratio of e_c/e_i, while the creep recovery coefficient k_r is calculated as the ratio r_c/r_i. The coefficient of instantaneous creep recovery k_i is defined as the ratio of the instantaneous recovery to the instantaneous

strain on loading ($k_i=e_i/r_i$). Tables (7.3-6) shows some creep results and the calculated values of e_c, k_c, k_r and k_i at various loading times.

The effect of resin content in the mix on creep behaviour can be demonstrated by comparing the results of grade A to those of grade C, or grade D to E as each pair of these grades are made of the same aggregate type. The values of e_c for grade A at any time were 2-3 times as much as those of grade C, that is despite the nominal stress level in the former being 21% and in the latter 24% (large specimens). With small specimens observed values of e_c with grade C at a stress level of 42% were almost 0.5-.75 times those recorded with grade A at a stress level of 37%.

The same trend was found with grade D and E with the latter consistently giving higher e_c-values. Grade C and A were made with the same aggregate type (river gravel) and the same mixing ratios except that grade A had a resin content of 10%, while in grade C it was 8%. Also grade D and E were made of the same aggregate (crushed basalt stone) with 8% and 12% resin contents respectively, but grade E had only 38% aggregate content by weight whereas grade D had 50%.

From the above it is clear that increasing resin content while keeping all other mix variables constant, leads to an increase in creep strains as would be expected. Referring to grade A and C, it can be seen that an increase in resin content of only 25% gave increase in e_c-values of about 140% and 95% after 64 days of loading at stress levels of 18 and 31.5 N/mm2 respectively.

The effect of aggregate type on creep can be seen by comparing the e_c-values of grade C and D which were made with exactly the same mixing ratio but in which grade C contained river gravel while grade D was made of crushed basalt stone. Grade D always developed higher e_c-values than grade C at almost the same stress levels. After 64 days of loading, grade C had e_c-values of 0.00045 and 0.001 at stress levels 24% and 42%, while the corresponding two e_c-values for grade D were 0.00034 and 0.000687 at stress levels of 22.5% and 39.5% respectively. These findings support the fact that while creep values of PC at a given stress level are essentially a function of the creep strains of the polymer matrix; the higher the modulus of elasticity of the aggregate or the higher its fractional volume, the higher the restraint effect.

The values of the creep coefficient k_c at 64 days of loading for grades C, D, A and E were 0.47, 0.336, 1.08 and 0.76 respectively at a stress value of 18 N/mm2. These values increased at a stress value of 31.5 N/mm2 to 0.625, 0.466, 1.147 and 0.79 respectively. It is clear that k_c-value is as dependent on resin content and on aggregate type and its content as e_c-value is. The relationship between the stress level and e_c or k_c could not be established reliably from the limited data obtained from the small range of stress levels investigated with each PC grade.

The total strain-time curves obtained could be expressed using a power expression similar to that of Mcleod (115), as follows :

$$e_t = e_i\,[(b+t)/b]^m. \qquad \ldots(7.3)$$

in which b and m are constants depending on PC grade and e_t is the total strain after loading time t in hours, under the stress level causing an instantaneous strain of value e_i. The theoretical strain-time curves according to Eq.(7.3) are shown in Fig.(7.19). The constants b and m were calculated for each grade by using its experimental creep data.

As shown in Figs.(7.19), the theoretical and the experimental strain-time curves agreed well throughout the loading period. Using Eq.(7.3), the creep strain e_c at any loading time t can be found as follows;

$$e_c = e_t - e_i = e_i[(1+t/b)^m - 1] \qquad \ldots(7.4)$$

Equation (7.4) can be used for predicting creep strains after any time, and it is clear from this equation that e_c-values would always increase if the load duration is increased. However this increase in e_c occurs at a decreasing rate which can be calculated by differentiating Eq.(7.4) with respect to time as follows;

$$de_c/dt = (e_i.m/b)\,[1+t/b]^{m-1} \qquad \ldots. \ (7.5)$$

The value of the constant m was found to be less than 1 for all PC grades. It follows that the magnitude of the power in Eq.(7.5) is always negative with the result that increasing t would lead to decrerasing de_c/dt. Using Eq.(7.4), the values of creep strain at 50 days of loading e_{c50} could be expressed theoretically in terms of the corresponding e_i-values for each grade. Assuming that the time tu at which the rate of increase in e_c will be equal to 0.01 e_{c50}/day is the time corresponding

to the ultimate creep e_{cu} the values of e_{cu} and tu could be calculated from Eq.(7.5). Table (7.8) gives the values of e_{cu}, tu and the associated ultimate creep values k_{cu} for each grade tested as calculated theoretically on the above bases. Eq.(7.4) can be rearranged to predict theoretical k_c-values at any loading time as follows;

$$e_c/e_i = k_c = (1 + t/b)^m - 1 \qquad \ldots.(7.6)$$

From Eq.(7.6) it is clear that K_c is assumed to be a function of time only for a given PC grade , where the constants b and m depend only on the material and not on the stress level. This implies that if the stress level is increased, e_c and e_i-values would have equal relative increases in such a way that k_c will remain unchanged. This can be demonstrated by Eq.(7.5) where for instance 25% increase in e_i would cause an increase in creep rate of the same value.

Expressing creep in a function that is related to e_i-value, Eq.(7.4), makes the calculations much easier by avoiding the tedious calculations of different constants corresponding to each stress/strength ratio. The instantaneous strain e_i embodies indirectly this effect of various stress levels. As was experimentally verified, the pair of constants b and m derived for each grade applied well to the creep results at the two stress levels used in testing each grade. Eq.(7.4) does not apply at stress levels high enough to initiate failure or to produce 'tertiary creep', and Eqs.(7.3-7.6), are intended to predict creep only when no time-dependent failure can take place.

The working life-time of a PC member subjected to a constant

compressive stress at which a certain value of total strain will occur can be estimated using Eq.(7.3) after being rearranged into the following form;

$$t = (b/24)\ [(e_t/e_i)^{(1/m)}-1] \qquad ...(7.7)$$

in which t is the loading time in days under the stress value that caused an instantaneous strain value e_i on loading. After time t the total strain will be e_t. Partial factors of safety can be introduced into the e_t-value such that its value after time t might not exceed a prescribed ratio of the ultimate strain of the material.

For example, with grade A (b=33, m=0.1944), and for stress level of 37% (e_i= 0.0017), the time required for a strain value of 0.004 to take place is 110 days. At stress level of 21% (e_i =0.00102), the required time for the same strain value is 4 years and 90 days. Table (7.9) gives the working life-times for the different PC grades at various constant stress levels as calculated by Eq.(7.7).

On unloading, instantaneous recovery r_i was found to be less than the corresponding e_i for each PC grade. The value of k_i ($k_i=r_i/e_i$) for low stress levels was always greater than with higher stress levels. The coefficient of creep recovery k_r (r_c/e_c after 64 days of laoding) varied from 0.16 with grade A (large specimen) to 0.625 with grade C (small specimen). The coefficient k_i was always smaller for higher stress levels and k_r was higher for higher stress levels.

This suggests that with small stress levels, most of the strains are elastic and only limited amounts of viscous and

plastic strains exist. When these small stresses are removed, a higher ratio of the elastic strain is recovered (high k_i-values) and the remaining time-dependent recoverable strains will be smaller (small k_r-values) than the case with high stress levels.

While creep was found to increase at a decreasing rate, creep recovery was found to approach assymptotic values and horizontal assymptotes for the various PC grades were reached within as little as 30-50 days after unloading. After that time no measurable creep recovery took place. It was experimentally found that creep recovery is dependent on resin content in addition to the stress level. High resin contents in PC produced considerably lower values of k_r than low resin contents. This can be seen by comparing k_r-values of grades A and C or D and E.

On these bases, it can be said that PC made of high resin contents will undergo high creep strains most of which is irrecoverable and in such a case reversible loads or variations in live loads over a long period would have serious consequnces in terms of excessive irrecoverable time-dependent deformations and the resulting internal stresses. Conversely, k_c-value is higher the higher the resin content, which implies that despite the decreased stiffness and consequently increased value of e_i, the relative increase in e_c is usually higher than that of e_i.

On comparative bases, it can be said that creep strains of PC on average are higher that those of PCC. For instance, at stress levels of about 20% and 40%, PCC would develop creep

strain of the order 0.0004 and 0.0008 respectively after one year under load. At the same stress levels, PC would develop creep strains on average of 0.0007 and 0.0013. While the absolute values of creep strains of PC are twice as much as those of PCC, the specific creep strains and creep coefficients of both concretes are very comparable.

In these creep tests the two stress levels applied were not enough to extrapolate or derive the sustained strength f_{su} for each grade reliably. However, making reasonable assumptions for the definition of sustained strength could help derive such a strength. For this, the sustained strength was assumed to be reached when the total sustained strain e_{su} after one year of loading becomes equal to the axial macrocracking strain ε_{cm} corresponding to the long-term strength f_{cl} found previously in this chapter.

Using this predetermined strain value and using Eq.(7.3), the corresponding value of e_i can be calculated. For a given PC grade with a given modulus of elasticity E, the stress that would produce this instantaneous strain can be estimated and considered as the sustained strength of the material. For example, with grade E we have;

$e_{su} = \varepsilon_{cm} = 0.00823$, $m = 0.0916$, $b = 3.0$, $E_c = 15850$ N/mm2. Using Eq.(7.3) the value of $e_i = 0.00396$, then the sustained strength is $e_i \times E_c = 62.7$N/mm2. If the value e_{su} were to be reached after a shorter loading time the value of the sustained strength would be increased accordingly. For instance, if the sustained strength were assumed to be reached after 100 loading days, its value for grade E would be 70.7

N/mm2.

The question of whether the assumed loading time for the e_{su}-value to develop should be more or less than one year should be related to the partial factors of safety of the material that might be specified in relevant design codes as will be shown later. Nevertheless, it is evident that using such a definition for sustained strengths can result in a considerable simplification in their derivation without resorting to other much more complex functions, and from the practical point of view any small errors resulting from such a simplification are insignificant.

Table 7.1: Chosen strain rates for compression test

Rate	Strain/sec.	Strain/min.	Strain/hr.	Strain/day
[1]	415×10^{-7}	250×10^{-5}	150×10^{-3}	360×10^{-2}
[2]	85 "	50 "	30 "	72 "
[3]	40 "	25 "	15 "	36 "
[4]	15 "	10 "	6 "	14.5 "
[5]	8 "	5 "	3 "	7.2 "
[6]	5.5 "	3.25 "	1.95 "	4.7 "
[7]	4.0 "	2.5 "	1.5 "	3.6 "
[8]	2.9 "	1.75 "	1.05 "	2.5 "

Table 7.2: Values of constants of the expressions of long-term strength and modulus of elasticity

Constant	Grade A	Grade B	Grade C	Grade D	Grade E
P	78	75	70	76	79
u	0.045	0.05	0.052	0.038	0.043
q	12160	12996	11773	13066	13841
v	0.0497	0.0348	0.0527	0.025	0.0205

Table 7.3: Sample of creep test results for PC-Grade A.

	Time of loading (days)	Instantaneous strain	Total strain	Instantaneous strain recovery	Creep recovery	Coeff. of creep	Coeff. of creep recovery	Coeff. of instantaneous creep recovery
Large specimen [stress level 21%]	2.0	0.00102	0.001207	0.00097	0.00018	0.18	0.16	0.95
	8.0	"	0.001407	"	0.00025	0.38	0.222	"
	32.0	"	0.00194	"	0.00031	0.902	0.28	"
	64.0	"	0.00212	"	0.00031	1.08	0.28	"
Small specimen [stress level 37%]	2.0	0.0017	0.00213	0.00156	0.000515	0.253	0.26	0.91
	8.0	"	0.00245	"	0.000687	0.441	0.352	"
	32.0	"	0.00338	"	0.00075	0.981	0.384	"
	64.0	"	0.00365	"	0.00075	1.147	0.384	"

Table 7.4: Sample of creep test results for PC-grade C

	Time of loading (days)	Instantaneous strain	Total strain	Instantaneous strain recovery	Creep recovery	Coeff. of creep	Coeff. of creep recovery	Coeff. of instantaneous creep recovery
Large specimen [stress level 21%]	2.0	0.000953	0.001047	0.00082	0.00022	0.100	0.489	0.86
	8.0	"	0.001203	"	0.00025	0.262	0.556	"
	32.0	"	0.001293	"	0.00025	0.356	0.556	"
	64.0	"	0.001403	"	0.00025	0.472	0.556	"
Small specimen [stress level 42%]	2.0	0.0016	0.00194	0.00128	0.000625	0.2125	0.625	0.8
	8.0	"	0.00213	"	0.00078	0.331	0.78	"
	32.0	"	0.00235	"	0.000875	0.468	0.875	"
	64.0	"	0.026	"	0.000875	0.625	0.875	"

Table 7.5: Sample of Creep test results for PC-grade D.

	Time of loading (days)	Instantaneous strain	Total strain	Instantaneous strain recovery	Creep recovery	Coeff. of creep	Coeff. of creep recovery	Coeff. of instantaneous creep recovery
Large specimen [Stress level 22.5%]	2.0	0.00093	0.001086	0.000895	0.000196	0.17	0.576	0.96
	8.0	"	0.001148	"	0.00024	0.234	0.705	"
	32.0	"	0.001217	"	0.000242	0.308	0.7117	"
	64.0	"	0.00127	"	0.000242	0.366	0.7117	"
Small specimen [Stress level 39.4%]	2.0	0.00154	0.00179	0.001301	0.000478	0.162	0.696	0.84
	8.0	"	0.00195	"	0.00056	0.266	0.815	"
	32.0	"	0.0021	"	0.0006	0.363	0.873	"
	64.0	"	0.002227	"	0.0006	0.446	0.873	"

Table 7.6: Sample of creep test results for PC-Grade E.

	Time of loading (days)	Instantaneous strain	Total strain	Instantaneous strain recovery	Creep recovery	Coeff. of creep	Coeff. of creep recovery	Coeff. of instantaneous creep recovery
Large specimen [Stress level 19%]	2.0	0.00115	0.00146	0.001015	0.000312	0.269	0.356	0.88
	8.0	"	0.00162	"	0.000375	0.408	0.428	"
	32.0	"	0.00187	"	0.00039	0.626	0.445	"
	64.0	"	0.002025	"	0.00039	0.761	0.445	"
Small specimen [Stress level 33%]	2.0	0.00212	0.00296	0.001156	0.000687	0.396	0.408	0.84
	8.0	"	0.003245	"	0.00075	0.5306	0.446	"
	32.0	"	0.00366	"	0.00081	0.726	0.482	"
	64.0	"	0.0038	"	0.00081	0.792	0.482	"

Table 7.7: Values of constants B,m for creep power expression

Constant	B	m
Grade A	33.0	0.1944
Grade C	9.15	0.0756
Grade D	3.60	0.0577
Grade E	3.0	0.0916

Table 7.8: Values of PC ultimate creep strains and the required times for them.

	Ultimate creep strain	Time required (days)
Grade A	2.28 e_i	625.0
Grade C	0.646 e_i	278.7
Grade D	0.523 e_i	220.8
Grade E	1.007 e_i	251.0

Table 7.9: Working life time for PC under various stress levels

Grade	Stress level (%)	Instantaneous strain	Working life time predicted in days [years] for strain of the value				
			0.002	0.003	0.004	0.005	0.006
A	20	0.00102	42.5	35.2	1551	[13.4]	[34.2]
	40	0.00204	-	8.6	42.5	137	352
	60	0.00306	-	-	4.08	15.8	42.5
C	20	0.0008	∞*	∞	∞	∞	∞
	40	0.0016	6.9	[4.26]	∞	∞	∞
	60	0.0024	-	6.9	32.7	[17.2]	∞
D	20	0.00078	∞	∞	∞	∞	∞
	40	0.00156	11.0	[34.3]	∞	∞	∞
	60	0.00234	-	11.0	[4.45]	∞	∞
E	20	0.0012	34.3	[8.2]	∞	∞	∞
	40	0.0024	-	5.8	34.3	∞	[8.16]
	60	0.0036	-	-	0.27	4.5	34.3

* More than 100.0 years.

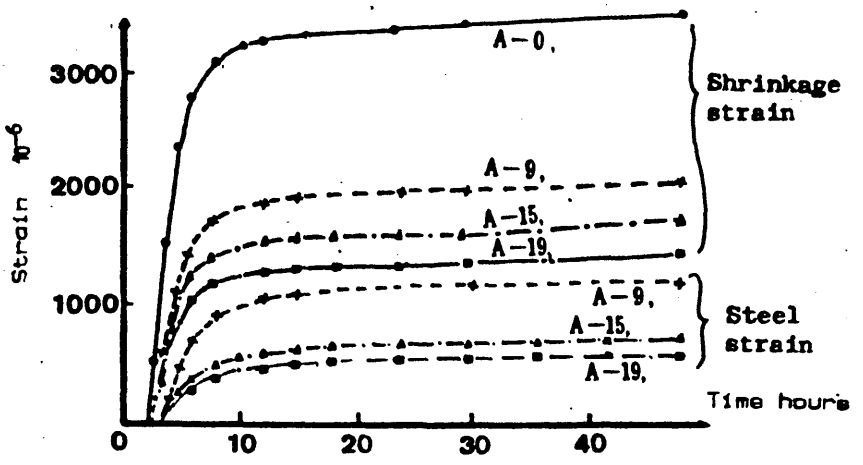

Fig. 7.1 Time-dependent strains of PC and steel versus elapsed time after casting

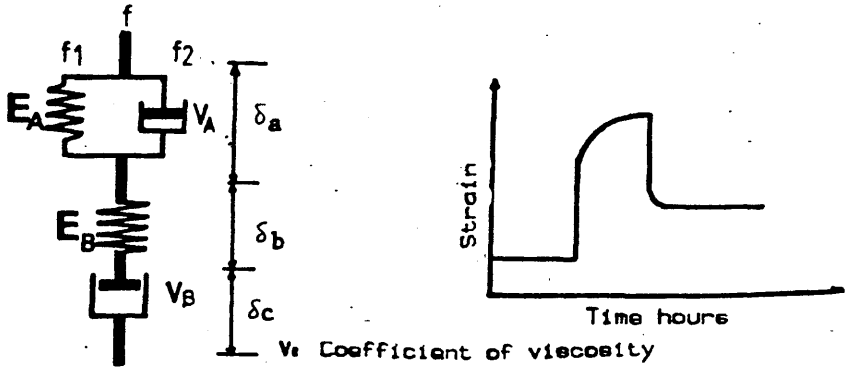

Fig. 7.2 Four element rheological model.

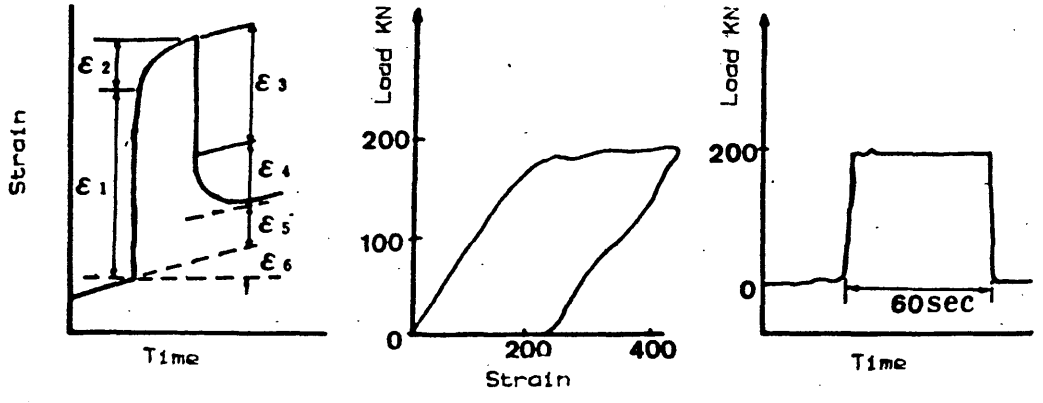

Fig. 7.3 Deformation behaviour of PC within infinitesimal period of time.

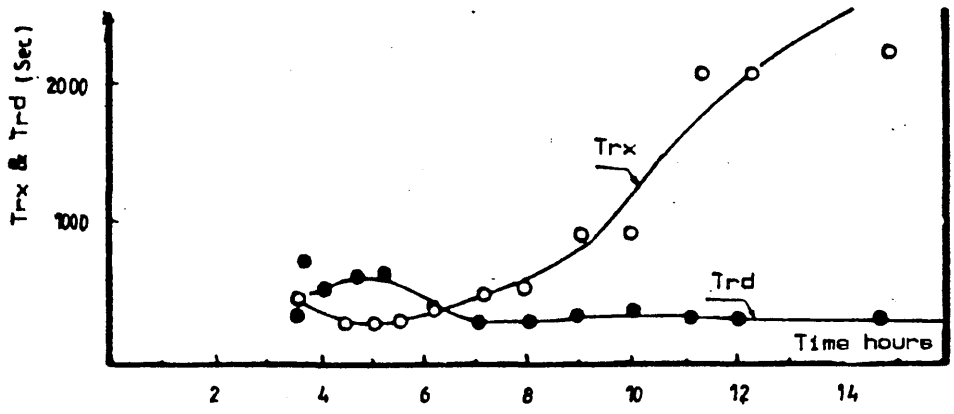

Fig. 7.4 Variation in relaxation time (Trx) and retardation time (Trd) versus elapsed time after casting for PC.

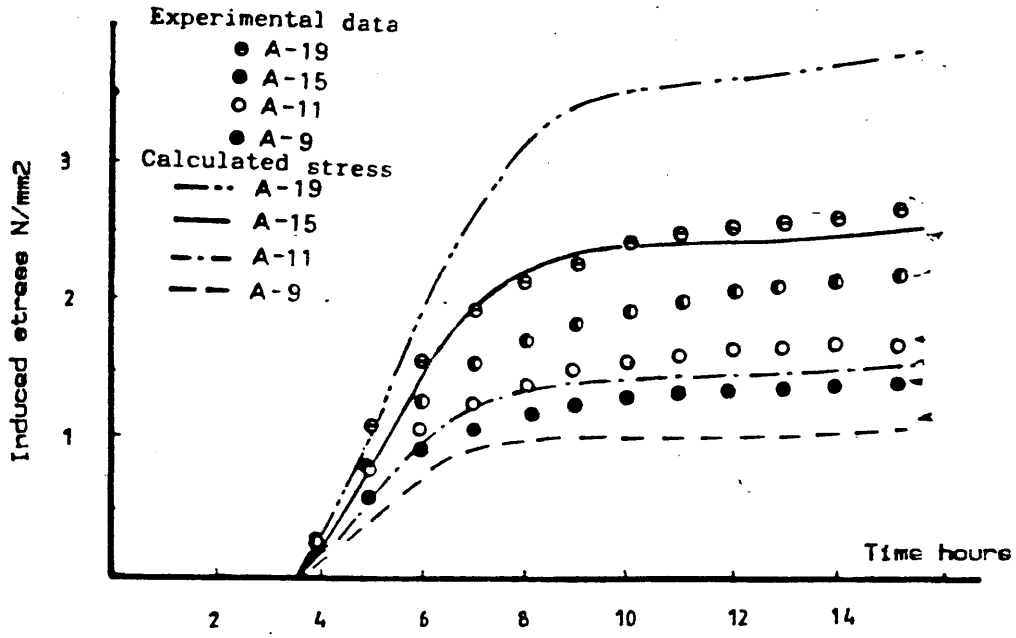

Fig. 7.5 Comparison of the calculated and experimental induced stresses.

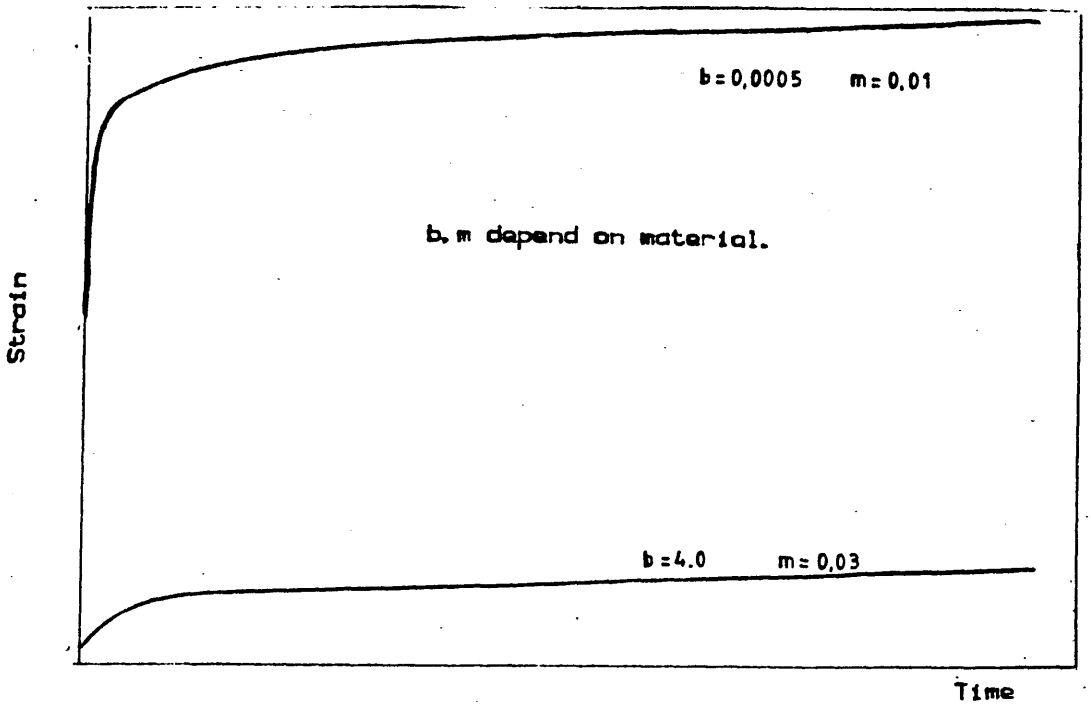

Fig. 7.6 Representation of Macleod expressiofor creep.

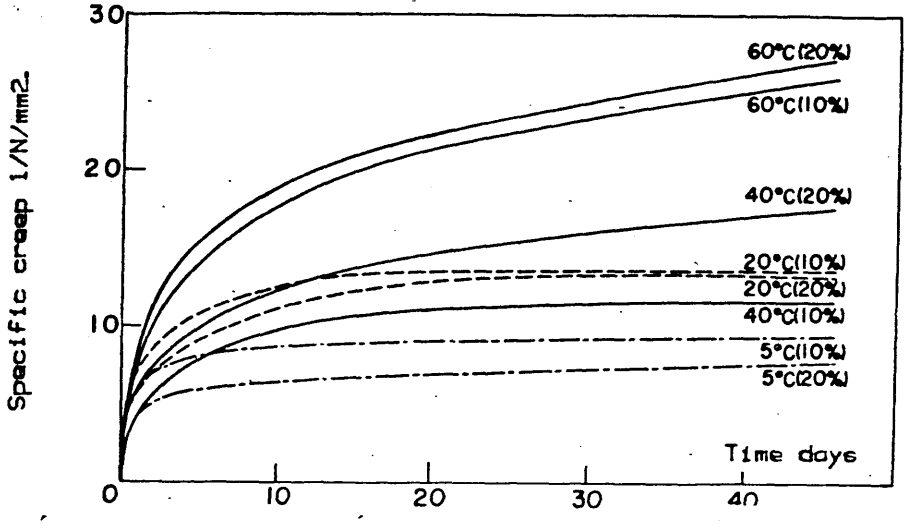

Fig. 7.7 Dependency of creep of polymer paste (polymer+fine filler) on temperature and stress level.

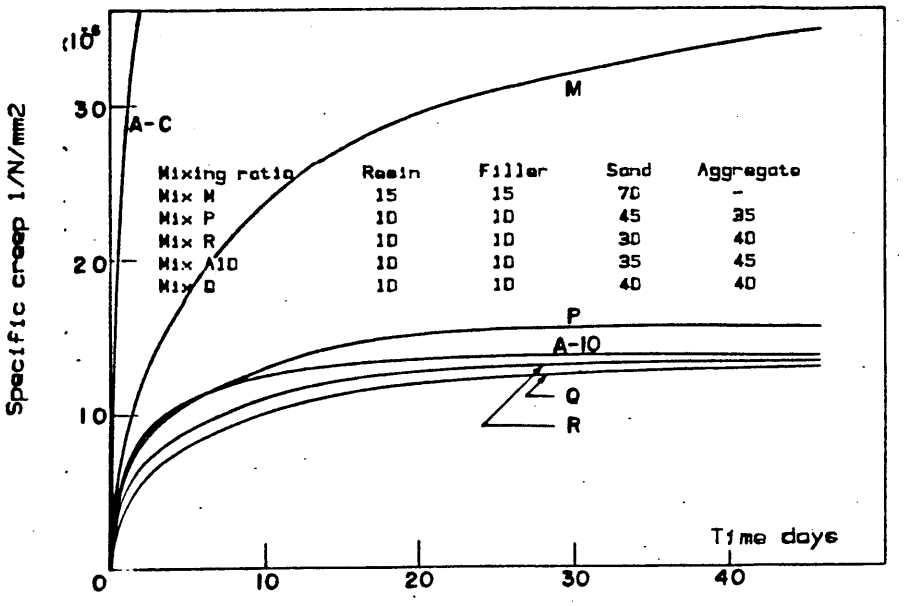

Fig. 7.8 Effect of mix-proportioning on creep of PC.

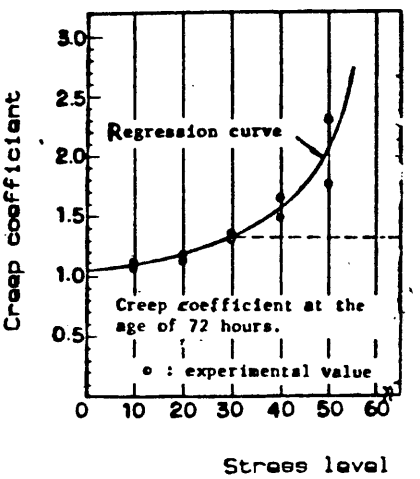

Fig. 7.9 Relationship between creep coefficient of PC and stress level applied.

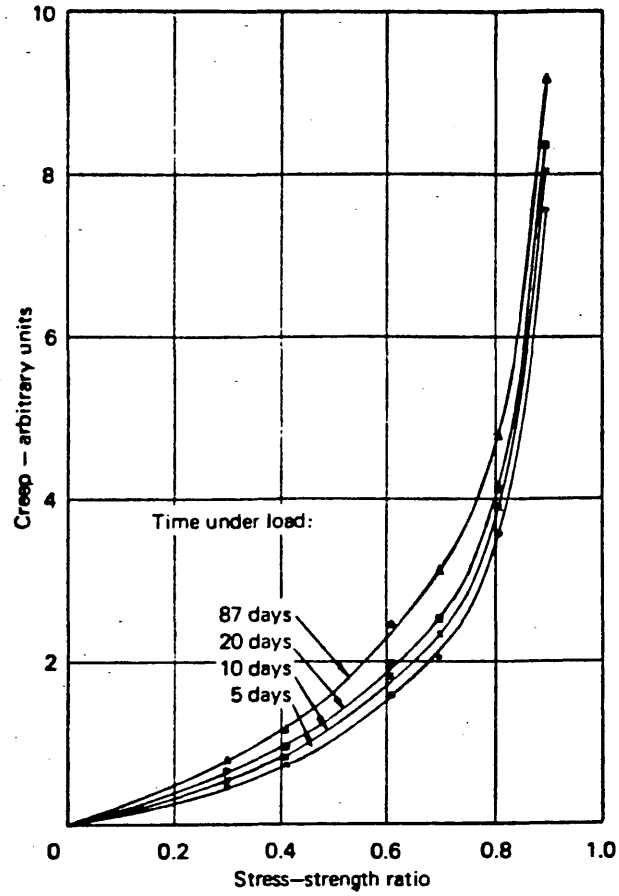

Fig. (7.10) Relationship between creep and stress/strength ratio for some PCC's.

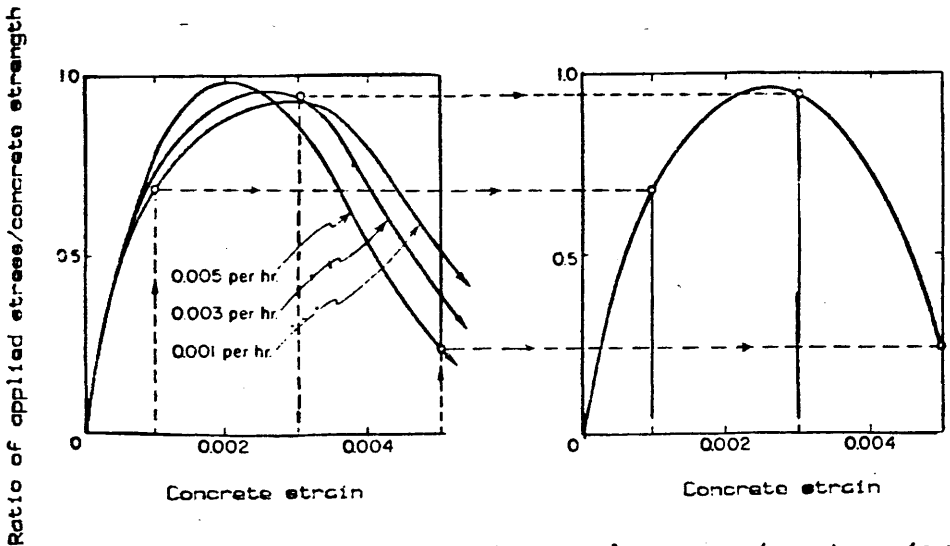

[left] Stress-strain curves for axial compression at various rates.
[right] Stress-strain relationship for eccentric compression after 1 hour of loading at constant rate of strain.

Fig. 7.11 Derivation of stress-strain relationship in flexure (schematically)

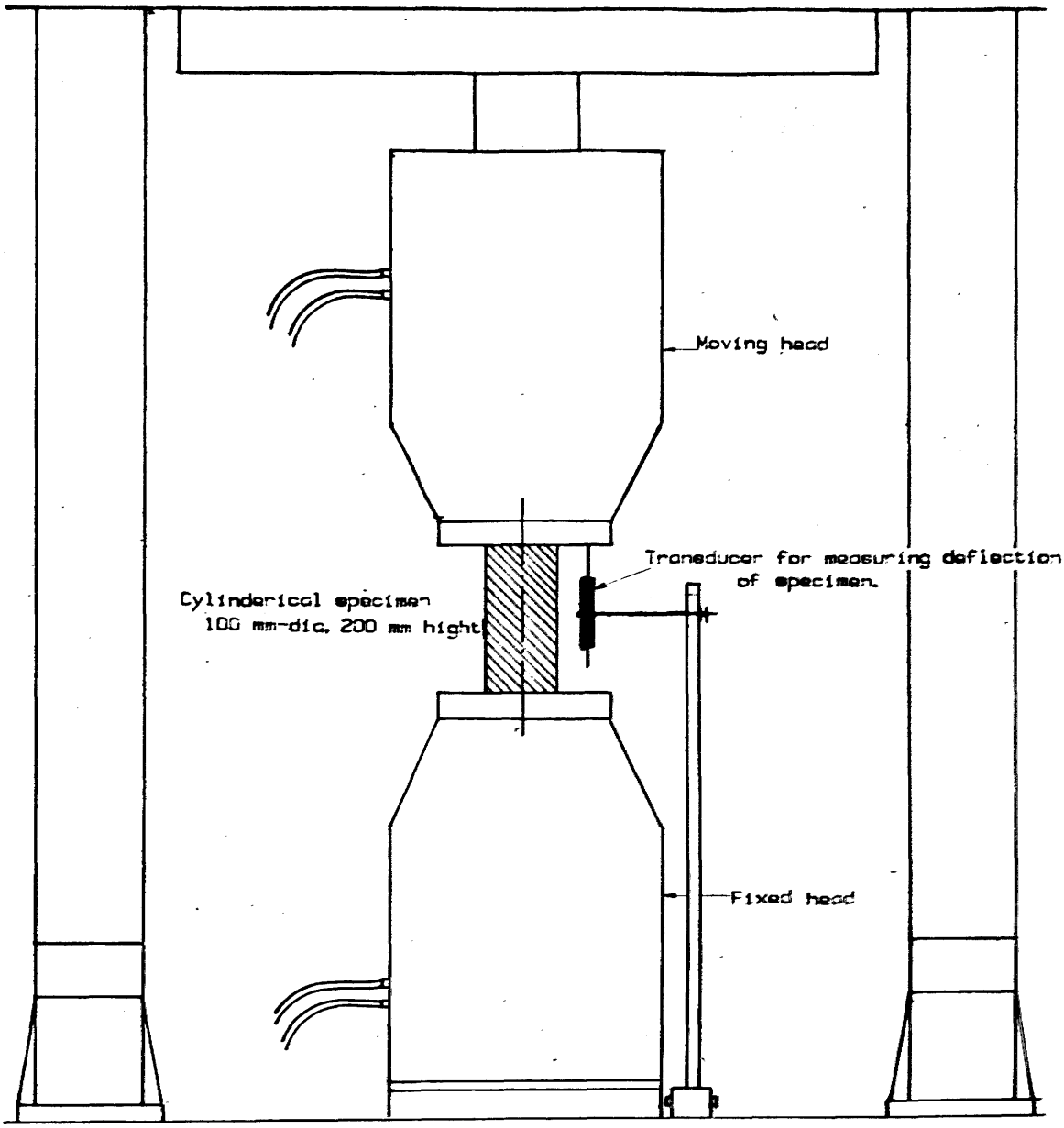

Fig. 7.12 Axial compression testing of PC at constant rate of strain.

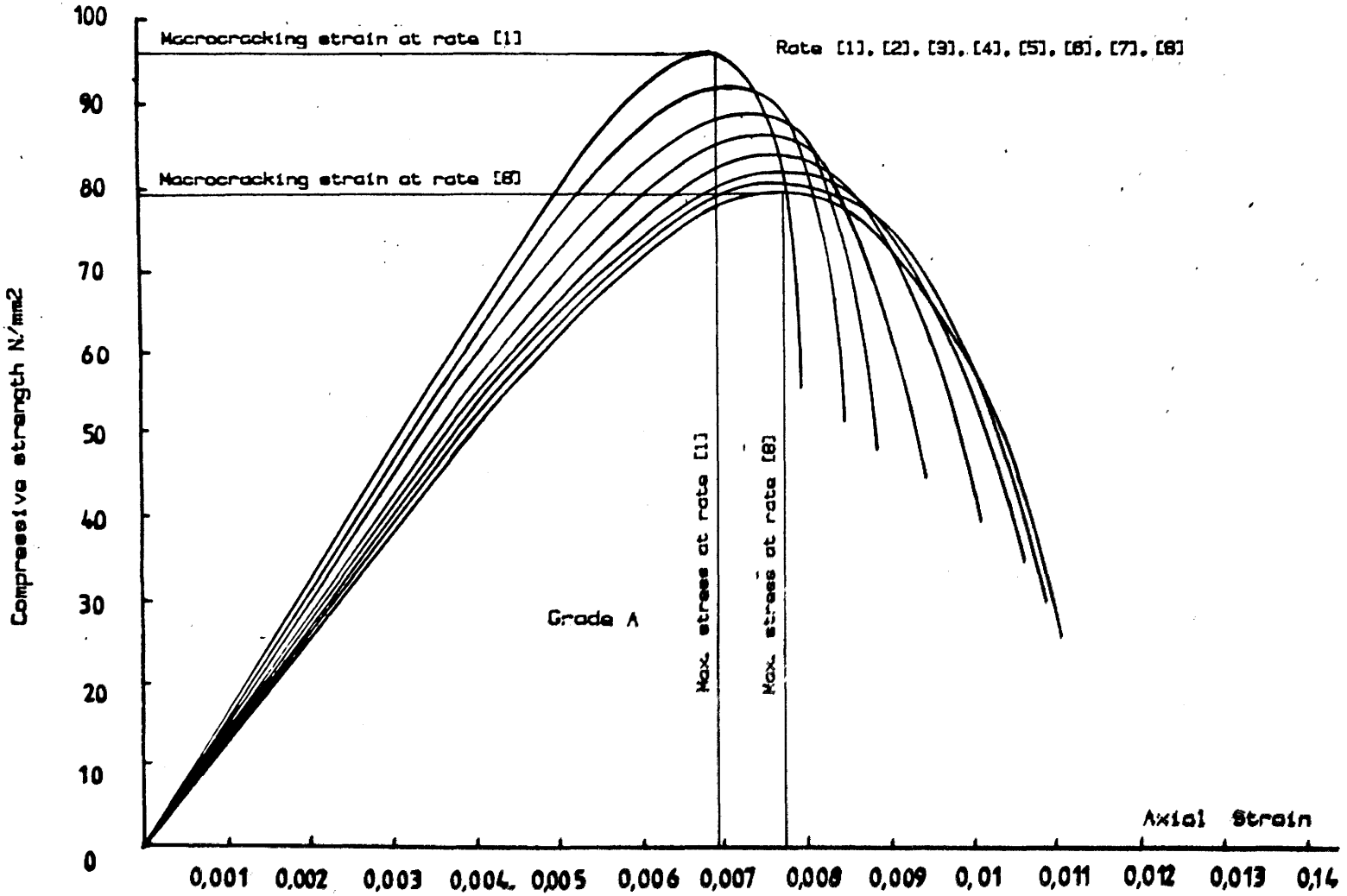

Fig. 7.13 Stress-strain curves as recorded experimentally in axial compression (Grade A)

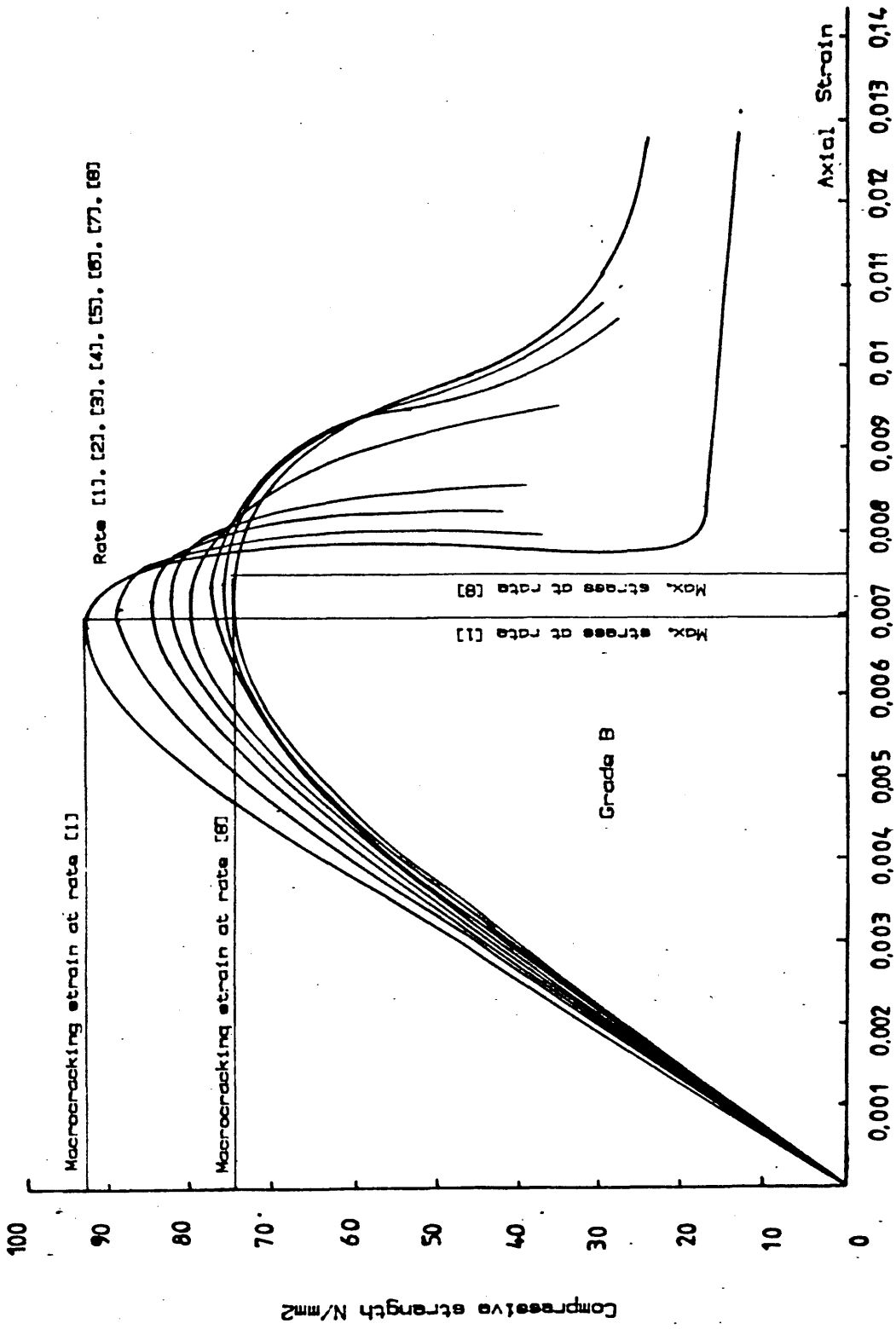

Fig. 7.13 Stress-strain curves as recorded experimentally in axial compression (Grade B)

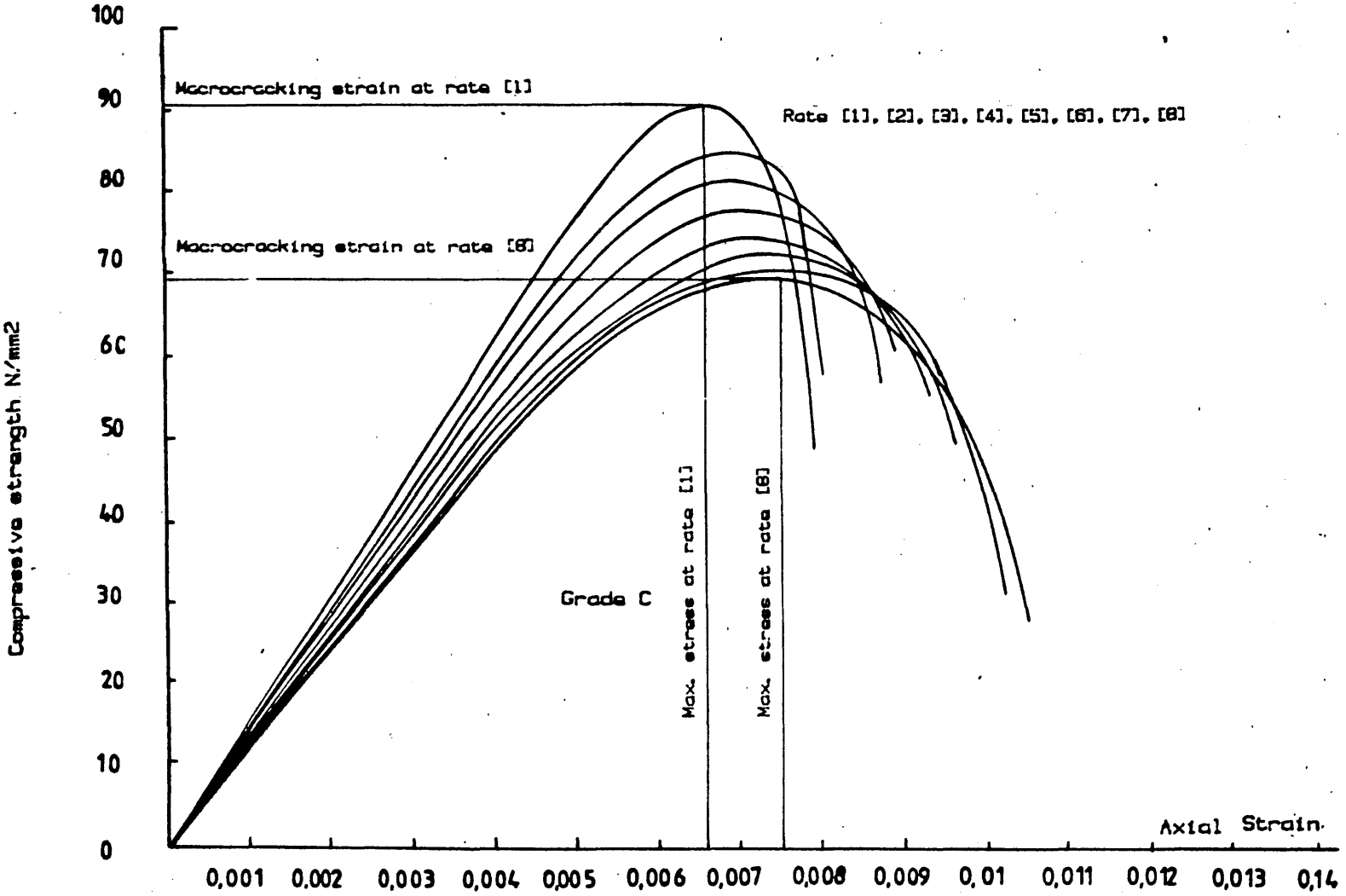

Fig. 7.13 Stress-strain curves as recorded experimentally in axial compression (Grade C)

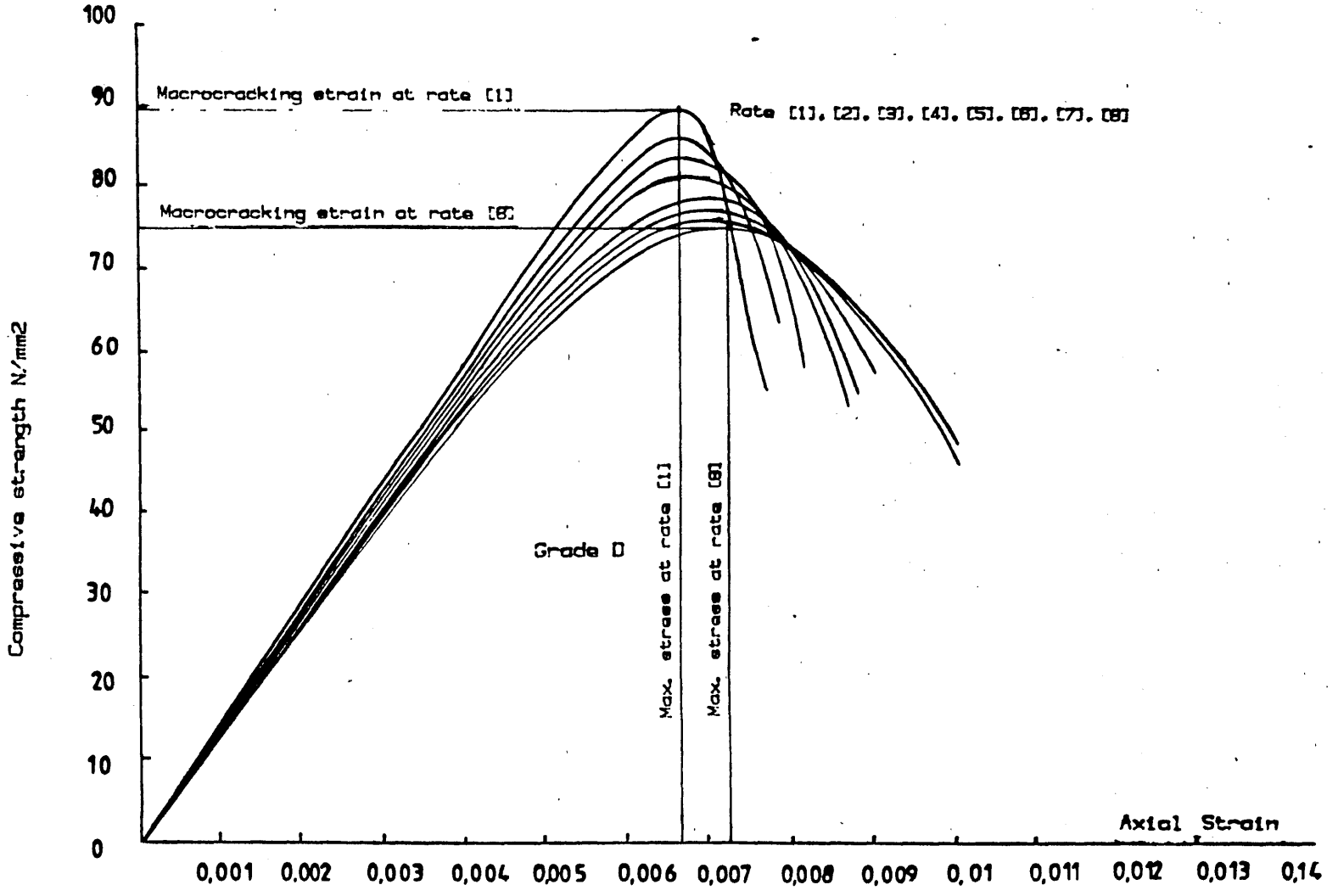

Fig. 7.13 Stress-strain curves as recorded experimentally in axial compression (Grade D)

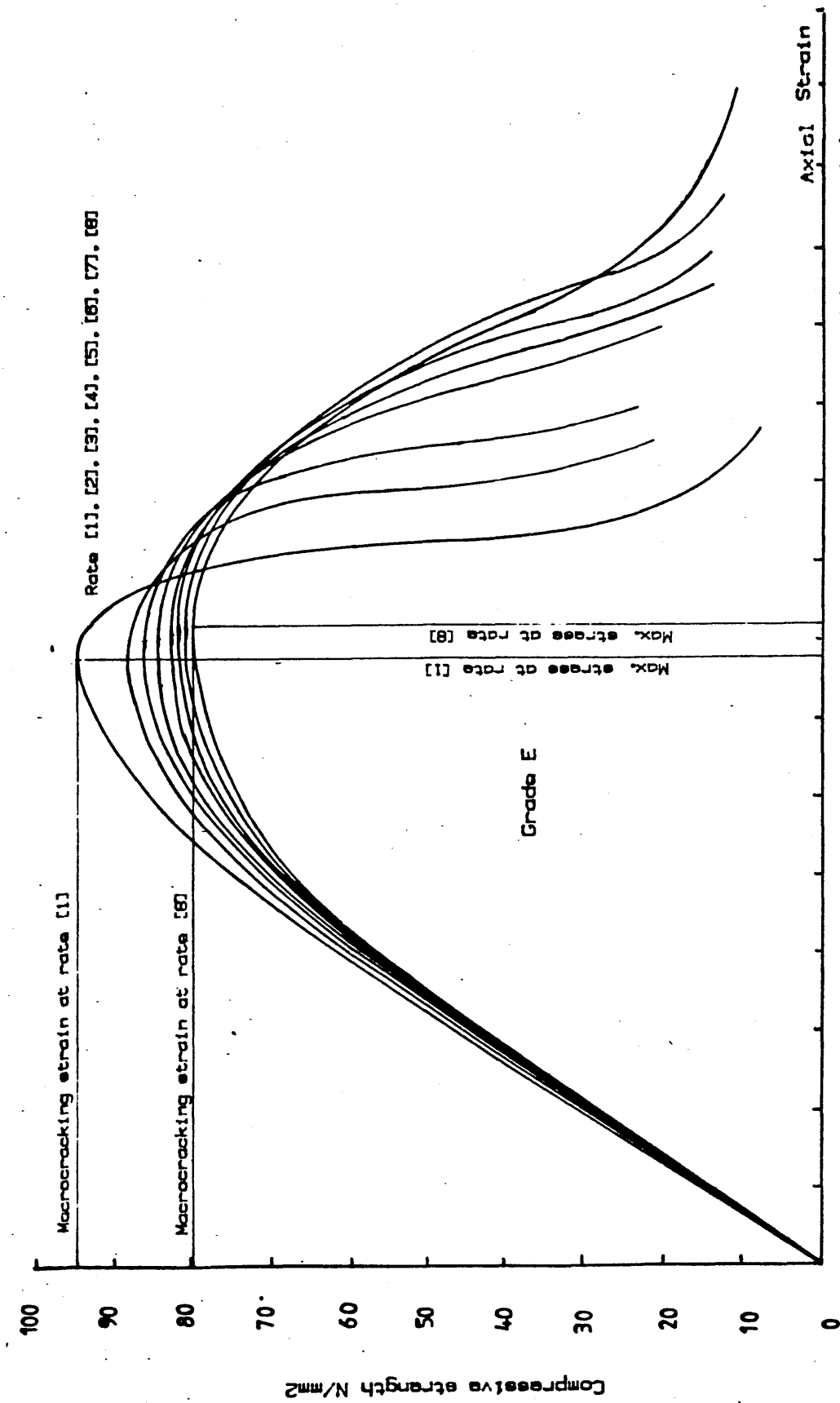

Fig. 7.13 Stress-strain curves as recorded experimentally in axial compression.
(Grade E)

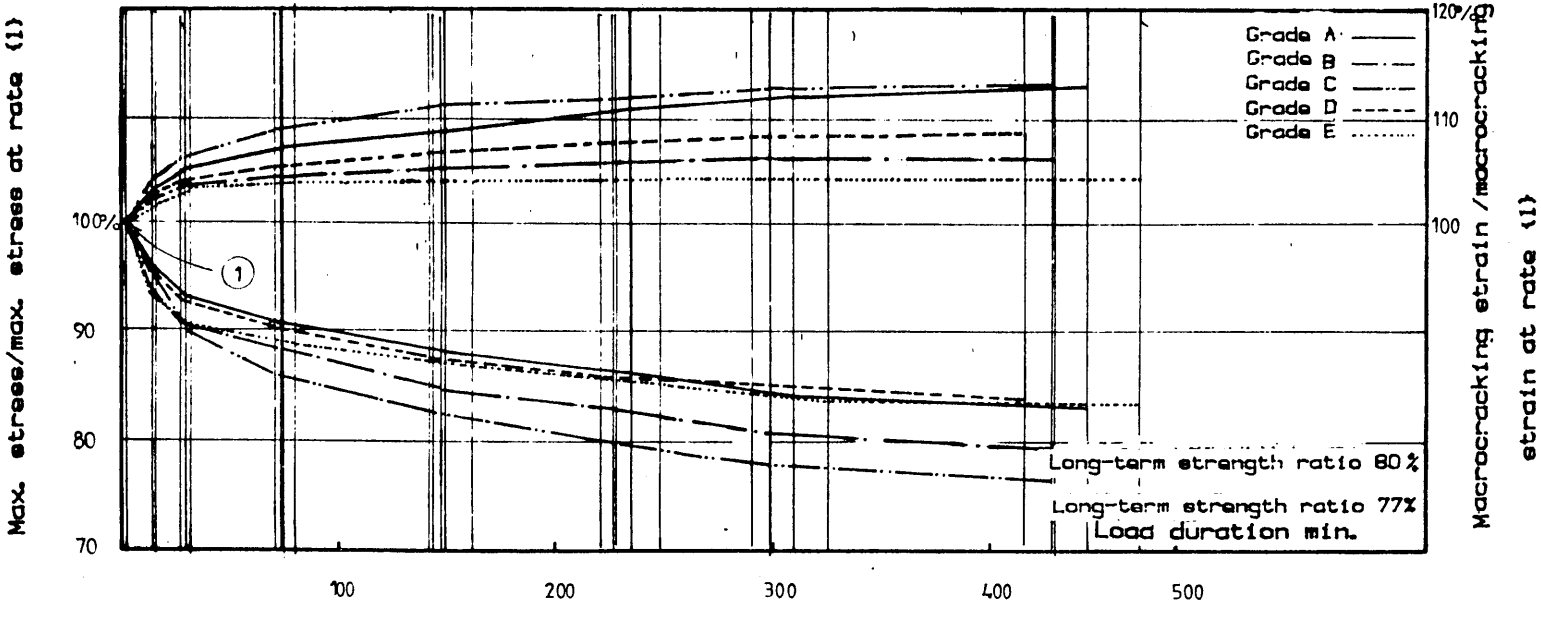

Fig. 7.14 Dependency of ultimate strength and macrocracking strains on load duration.

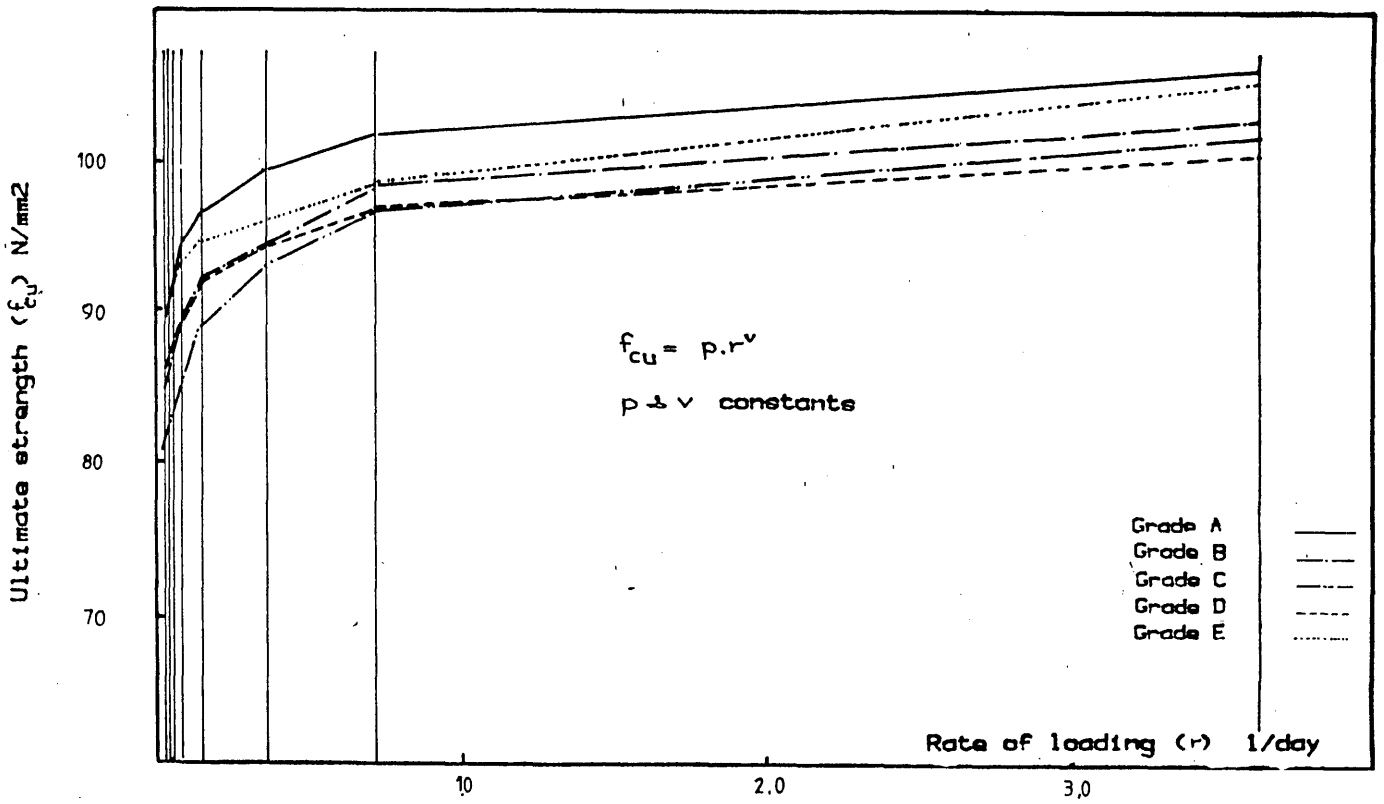

Fig. 7.15 Dependency of ultimate strength on rate of loading.

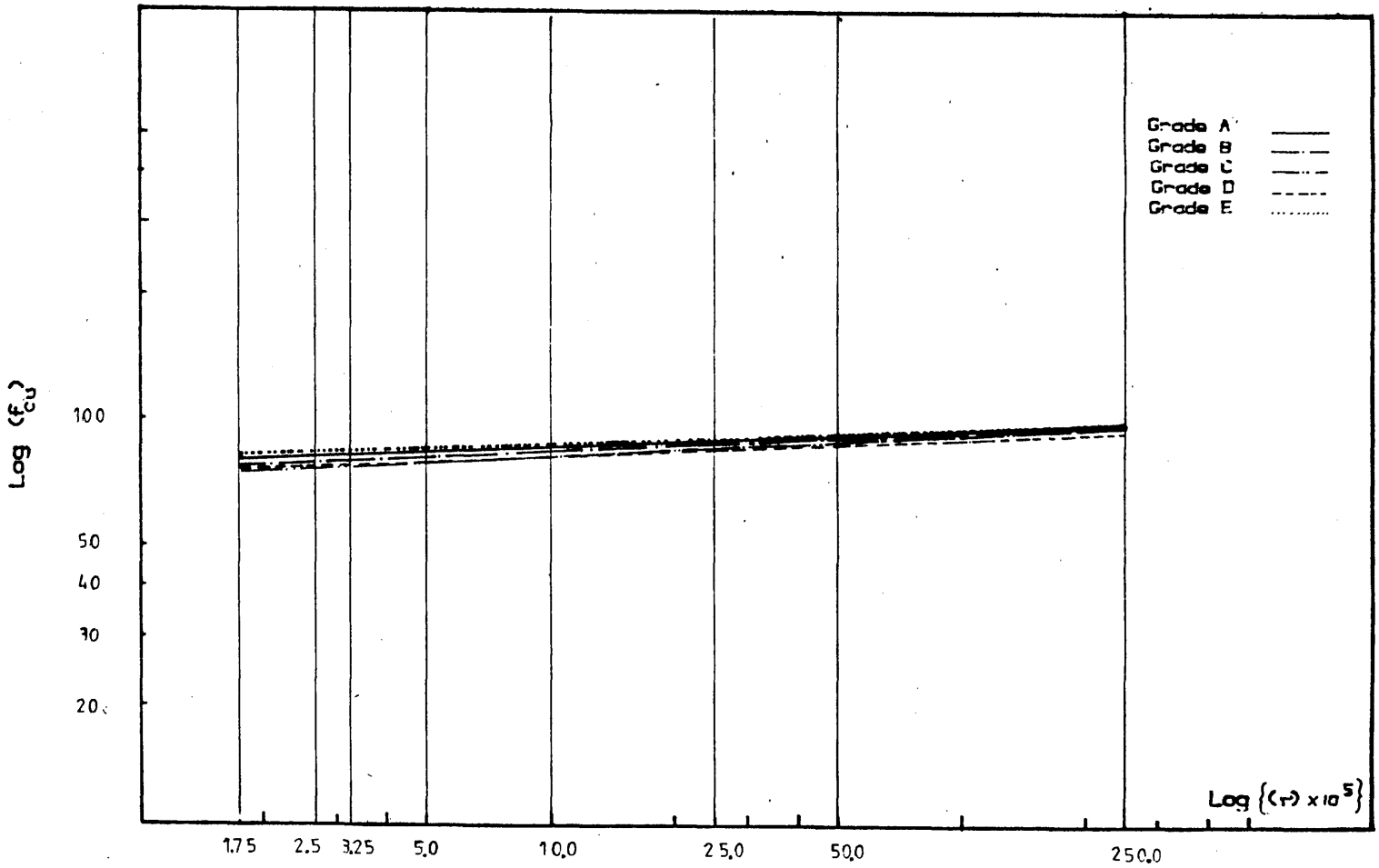

Fig. 7.16 Derivation of the constants and for the five PC grades.

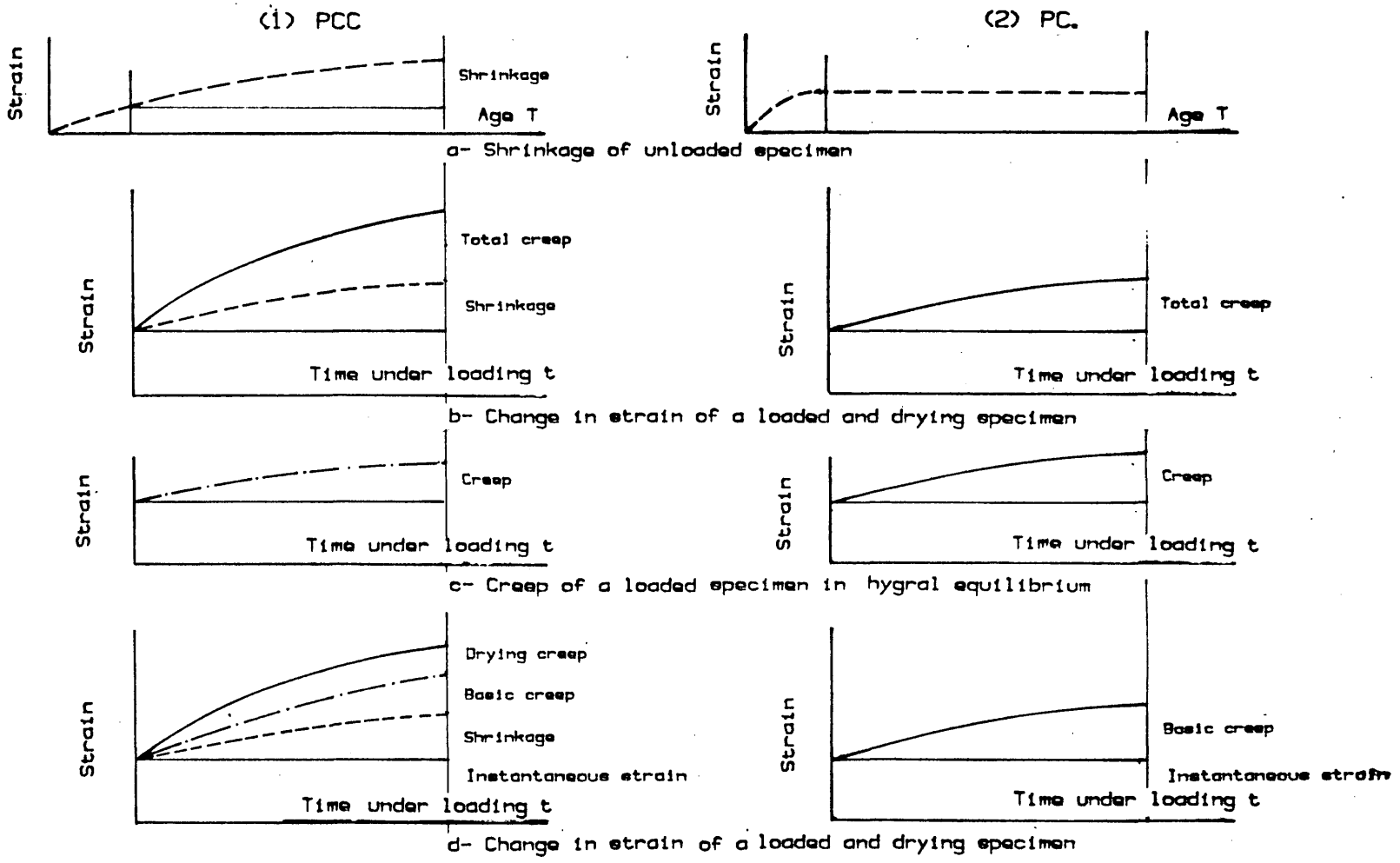

Fig. 7.17 Terms and definitions for creep of (1) PCC (2) PC.

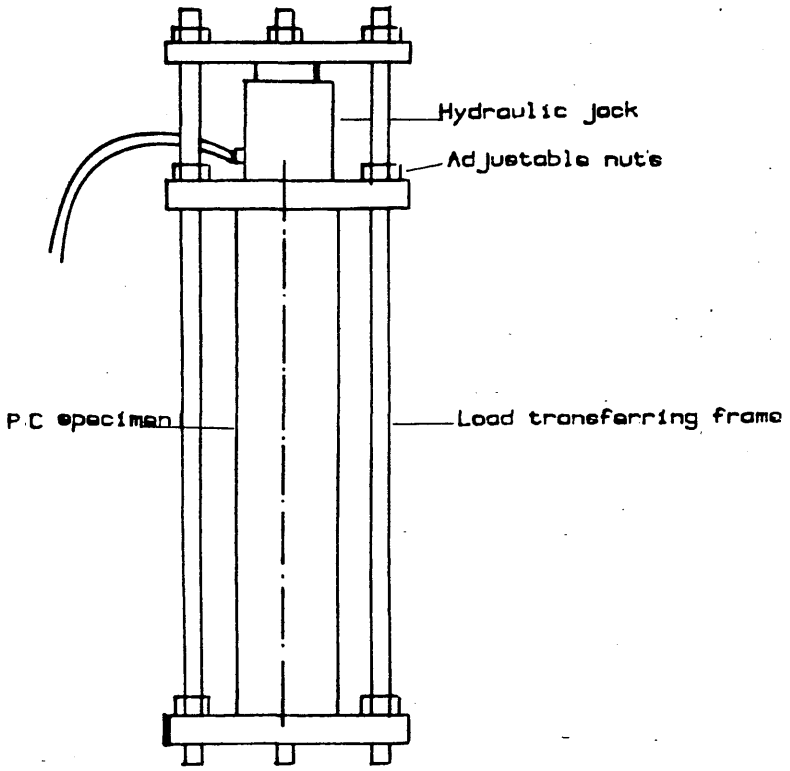

Fig. 7.18 The Tyler portable creep rig.

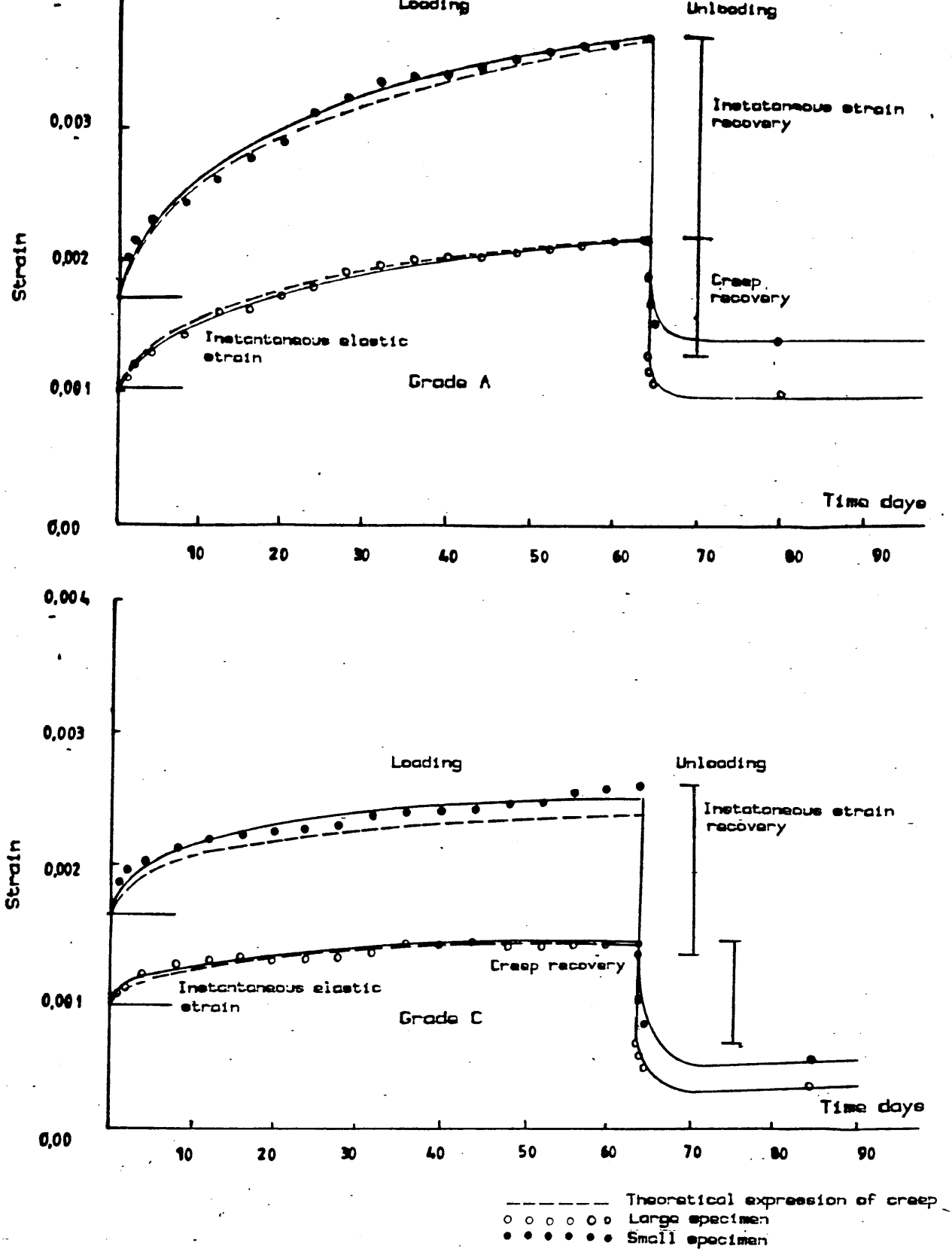

Fig. 7.19 Creep results for PC.
(Grade A & C)

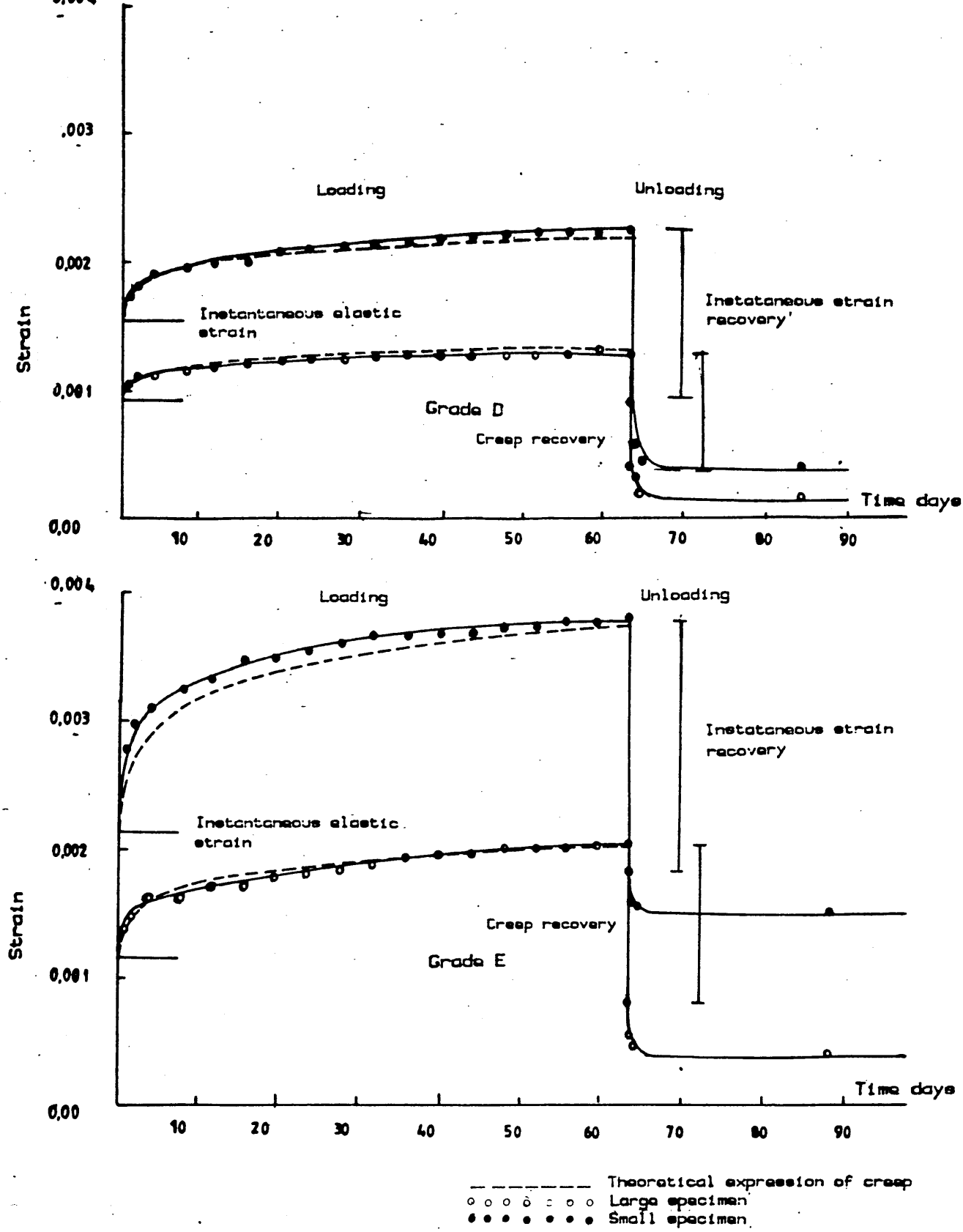

Fig. 7.19 Creep results for PC.
(Grade D & E)

CHAPTER EIGHT

ULTIMATE STRENGTH DESIGN OF REINFORCED PC STRUCTURES IN FLEXURE

8.1 Introduction

The design of reinforced concrete structures based on their ultimate strength has been accepted in many countries and is a viable alternative to the classical design approach of the elastic theory. The reasons for an ultimate strength design method for PCC structures being more favourable than elastic design apply even more to PC structures.

As has been shown, The stress-strain curve for PC is not linear; most of its strains are inelastic and highly time-dependent. Ultimate strength design is not bound to crudely approximated modular ratios. It takes inelastic strains into account and therefore can predict a reasonably accurate load factor. The limit state design method as introduced by the European Concrete Committee in 1964 (120) aimed at combining the best features of ultimate strength and working stress design theories. In this, the ultimate strength approach is used for proportioning the sections and the elasticity theory is used to ensure that deflections or crack widths will not exceed certain values under service load. Crack widths and deflections are considered as the limit state of serviceability.

For reinforced PC structures, the serviceability limit state as a design approach is likely to be of vital importance and therefore has to be carefully examined. The high ultimate strength of PC usually leads to relatively small sections

under high loads resulting in large deflections and the probability of lateral instability. Bearing these in mind in addition to the inherent low stiffnesses and the high ultimate strains of PC, it is evident that the conditions of serviceability might be most critical for design.

In this work ultimate strength design will be discussed in detail for pure flexure and combined flexure and compressive axial loads. The serviceability limiting states are not included. Before establishing such limiting states a thorough revision and assessment of the practical structural performance of PC under service loads and the consequent deformations has to be carried out. With the traditional limits for deformations, crack width and ductility the use of PC structures will be limited to fields of application where there is no need for such stringent serviceability requirements.

8.2. Factors of safety and their significance

One of the most important features of the ultimate strength design is that it allows for the selection of more realistic factors of safety than those considered in the elastic theory. The progressive reduction in these factors of safety as a result of refinement of the structural analyses and better knowledge of the properties of the material, can be considered as an outstanding outcome from the economic point of view. The mutual relationship between performance and cost is essentially related to the chosen magnitudes of the factors of safety.

It should be borne in mind that no matter how far the

structural analysis is refined or how much our material knowledge is increased , factors of safety will have to be applied in the design of reinforced concrete structures. This is mainly because of the inevitable variations in the strength of concrete and steel and the assumpotions usually involved in the analysis. The uncertainity in the magnitude of the loads applied requires the use of load factors.

Variation in strength is primarily due to the heterogeneity of concrete and the way it is mixed, cured and cast. With the highest possible quality control and site supervision, strength of a given concrete grade will still vary from a slab to a beam, from a beam to a column and even within the same member, strength of concrete will change in horizontal and vertical directions depending on the size of the member. The dispersion in strength may further increase with increased number of batches and by casting at different times with slightly different environments. Consistency of the mix constituents over several mixes of the same concrete does not actually exist.

Variation in the live loads is in the nature of these loads, and no one can claim fixed values for them. It is therefore imperative that the range within which these loads can vary should be covered by appropriate load factors based on accumulated experience.

Additional factors of safety should be considered to compensate for any likely approximation or inaccuracy of the assumptions made in the analyses. The stress occurring in concrete is not merely a function of the associated strain. To

assume that concrete and steel have compatible strains at all times and that no bond slip or bond failure is occurring, is another plausible but inaccurate assumption for which as for many others, factors of safety have to be introduced.

For ultimate strength design the American Concrete Institute ACI has issued its provisions for the factors of safety to be considered. These provisions and the corresponding factors of safety can be used for the design of PC reinforced structures after few necessary modifications have been carried out. The ACI code divides these factors into load factors and capacity reduction factors (121). There was no need to modify the load factors specified by the ACI.

The capacity reduction factors as specified by the ACI require modification to suit the particular structural performance of PC. In this respect the only difference between PCC and PC lies in time dependency and in reduced fire and elevated temperature resistances. The performance of PC at elevated temperature is still a controversial point, and is fundamentally related to the type of resin used and its formulation. For instance in Japan and in the U.S.A., certain special resin formulations resulted in PC with stable performances at temperatures up to 240 C.

For the time being, however, and until new versions of high thermal-resistant resins become economically feasible, all structural applications should be restricted to fields where no elevated temperatures or fire attack can take place.

As for the time-dependency of the stress-strain curve, it has

been shown previously that PC suffers severe deterioration in strength resulting from creep and that the short-term performance is appreciably different from the long term one.

Despite the fact that creep strains and the associated strength reduction can be significant, the relative decrease in the ultimate carrying capacity of a reinforced PC member would usually be much less than the relative decrease in the PC strength. This is partly because of the stress redistribution effect and partly because of the restraint effect of the steel on the creep of PC itself. It can be shown that in flexure for instance, any increase in concrete strain by creep would result in such an increase in the compression zone depth (creep of steel is virtually nil) that the overall percentage reduction in the compression force provided by the concrete would be much smaller than the percentage reduction in the ultimate compressive strength f_{cf} of the stress block.

For PCC Hognestad (122) demonstrated that the influence of sustained load on beams has no significance, and that with columns it can reduce the ultimate carrying capacity by up to only 10%. This reduction is well covered by the specified capacity reduction factors. The same trend should apply to PC but based on its higher time-dependency than PCC, the capacity reduction factors for PC are chosen here to be 0.1 less than the corresponding values in the ACI provisions. This value, 0.1, was found from detailed comparative calculations of the ultimate capacity of PC cross-sections under short-term and long-term conditions.

So for pure flexure the capacity reduction factor is chosen to

be 0.8 instead of 0.9 for PCC, while for flexure and axial compression it is 0.6 instead of 0.7. For design purposes, the ultimate load should at least equal the sum of each service load multiplied by its respective load factor, as specified by the ACI Building Requirements (121).

8.3. Assumptions considered in the design

The design approach as will be given later in this chapter, is primarily valid for PC grades having similar properties to the five PC grades investigated in this work. The main two parameters that can describe any PC grade are considered to be the ultimate axial compressive strength and the secant modulus of elasticity measured at one third of it. Any PC grade having its modulus of elasticity and/or ultimate compressive strength within the range investigated, as given in Chapter Three, can be designed using the following design approach after extrapolating the block stress parameters.

The steel used here was a cold-drawn type whose idealized stress-strain curve is shown in Fig.(8.1). No mild steel is considered in this work. Had it been attempted it would have led to extremely high reinforcement ratios which could not have been accommodated in the section; with mild steel the maximum possible reinforcement ratios will not be great enough to allow PC to be utilised efficiently or economically.

For the calculations of the ultimate strength of members or for proportioning their sections, the following assumptions are made:

[1] Plane sections before bending remain plane after bending.

[2] The stress-strain curve for the cold-worked steel is a trilinear function as shown in Fig.(8.1).

[3] The distribution of concrete stress in the compression zone is defined by the three block parameters k1, k2 and k3 and the ultimate compressive strength f_{cy}. The block parameters can be obtained using the following empirical formulae :

$$K1 = 0.9 - 0.38\ [1 - (\varepsilon cu/0.009)^2] \qquad ...(8.1\text{-a})$$

$$K2 = 0.3 + 0.006\ E_c \qquad ...(8.1\text{-b})$$

$$K3 = 0.27 + 0.03775\ E_c \qquad ...(8.1\text{-c})$$

in which E_c the secant modulus of elasticity in KN/mm2 and the concrete ultimate strain εcu can be obtained from the following empirical formula :

$$\varepsilon cu = 0.00926\ (\ 1 - E_c/86.55\ ) \qquad ...(8.1\text{-d})$$

An alternative set of theoretical calculation formulae can be derived using the previously given sine-function of the stress distribution with the value of $\varepsilon cu = 1.333\ \varepsilon oc$ (see Chapter four).

[4] Tensile strength of concrete and tension stiffening are neglected.

[5] the effect of lateral confinement is neglected.

8.4. Design of reinforced PC members in pure flexure

The previously derived equations [Eqs.(5.1, 5.2)] can be used in the design of rectangular sections whether they are singly or doubly reinforced. Substituting in Eq.(5.1) for L=0.0, then

$T_s = T + T'_s$ ...(8.2-a)

where $T'_s/T_s = R'.f'_s/(R.f_s)$ then

$T'_s = T_s [(R'f'_s)/(R\ f_s)]$ ...(8.2-b)

By eliminating T'_s from Eqs.(8.2-a and 8.2-b) then

$T_s = T/[1-(R'/R)(f'_s/f_s)]$ ...(8.2-c)

$T'_s = T/[(R/R')(f_s/f'_s) -1]$ ...(8.2-d)

From Eq.(5.2) and by substituting for T'_s in terms of T, then

$M/(bd^2f_{cy}) = Z$

$Z = T(1-YT)+T(1-d'/d)/[(R/R')(f_s/f'_s) -1]$ ...(8.3-a)

From Eq.(8.2-c) the tensile reinforcement ratio R in terms of T is as follows :

$R = Tf_{cy}/f_s[1/(1 - \{R'/R\}\ \{f'_s/f_s\})]$ ...(8.3-b)

Using Eqs.(8.3-a,b) the values of R and Z can be obtained for a given value of T and R'/R ratio at given values of G, Y and f_{cy}. If these values are those corresponding to the ultimate strength (ultimate concrete strain ε_{cu}), the values of R and Z at ultimate strength can be calculated and the section can be proportioned. The only provision so far required for calculating R and Z, as can be seen from Eqs.(8.3-a,b), is that the ratio d'/d has to be known. In this work d'/d is taken to be 0.1.

It should be borne in mind that for a given T-value, the compression zone depth will be also known as c/d=T/G, and therefore the strains in the tension and compression steel and consequently the stresses in them can be calculated as

follows:

$$f_s = \varepsilon_{cu}\,(G/T - 1)A + B \qquad \ldots(8.4\text{-a})$$

$$f'_s = \varepsilon_{cu}\,[1 - (d'/d)(G/T)]A + B \qquad \ldots(8.4\text{-b})$$

From Eq.(8.3-b) it is clear that increasing R for a given R'/R ratio will lead to an increase In T-value. By referring to Eq.(8.3-a) this increase in T-value will increase the coefficient Z which implies that for a given moment and section width, the required effective depth will be reduced. Conversely by increasing the effective depth (decreasing Z-value) for a given R'/R ratio would lead to a reduction in the required R-value for a given moment.

Thus Eq.(8.3-a) and Eq.(8.3-b) can provide a basis on which an economic choice of the mutual areas required of tension steel and of PC can be decided. Similarly it can be shown by using these two equations that, for a given R the effective depth required for a given moment can be reduced by increasing the R'/R -ratio and from this standpoint the two equations can tell when the use of compression reinforcement is necessary. For example if the effective depth is to be reduced and no further increase in tension steel can be accommodated in the section, or if the tension steel ratio is fixed at a desired value then the required R'/R ratio can be estimated.

To facilitate the use of these two equations, the values of R and Z were calculated for a wide range of different T and R'/R values. The relationships between Z and T on one hand and R and T on the other were plotted as shown in Figs.(8.2-a, b, c, d &e) for the five PC grades with R'/R as a parameter. In these figures Z and R values are plotted using two opposite

ordinates against T-values as an abscissa. These figures are charts that can be used in different ways to satisfy almost all design requirements.

For a section of given dimensions, made of a given PC grade, the value of Z corresponding to a certain ultimate moment can be calculated from Eq.(8.3-a). A horizontal line at this value of Z would intersect with infinite number of T-Z curves. Each of these can be used to find the required R at the desired R'/R (by projecting the intersections down to the T-R curves respectively).

Conversely, for a given R and R' the required effective depth can be obtained by drawing a horizontal line at the given R-value and using its intersection with the T-R curve of the corresponding R'/R value to determine the relevant values of T and Z. These charts give an infinite number of mutual solutions for the cross-section parameters and they consequently have evident potential when translated into practical design charts for reinforced PC structures in pure flexure.

Despite the versatility of Figs.(8.2), it should be noticed that they have theoretical values of T, Z and R that must be limited to lie within practical boundaries. For example, these figures were derived on the bases of Eq.(5.1) and Eq.(5.2) which assume that the neutral axis lies within the section, or from c/d=0.0 to c/d=1.0. This implies that according to these equations values of T can not be less than zero or more than the value of the parameter G of the PC grade. In addition and from the structural performance point of view, c/d must have a

minimum value high enough to control the magnitudes of curvature and the resulting strains in the tension steel , and to make efficient use of the high strength of PC in the compression zone. At the other extreme, c/d should not be higher than a maximum value small enough to reduce the amount of the tension steel required and to produce a reasonably ductile failure.

In this work the maximum and minimum values of c/d are taken to be 0.6 and 0.25 respectively. This means that the corresponding maximum and minimum values of T will be 0.6G and 0.25G respectively. Values of T outside these two limits, which are represented by vertical lines (2) and (1) on the figures, will not therefore be permitted in design.

In addition another limiting boundary is that for any section subjected to pure flexure, the tension reinforcement ratio can not be allowed to exceed the maximum value that can be practically accommodated. For rectangular sections this value of maximum R is taken here to be 5%. A horizontal line drawn at R=5%, will intersect the various R-T curves at the maximum practical t-values corresponding to each R'/R ratio. This horizontal line, line (3), represents a third boundary for the curves to be used in actual design. The intersection of this line with R-T curve whose R'/R=0.0 would give another maximum practical value of T less than that set above at c/d=0.6 for each PC grade. This value can be calculated exactly by using Eq.(8.3-b) and Eq.(8.4-a) and substituting for R'/R=0.0. By drawing a vertical line at this value of maximum practical T, line (4), the range of T-values within which sections can be

practically proportioned is thus defined by line (1) and line (4) rather than line (1) and line (2).

The intersections of line (3) with different T-R curves having different R'/R can be projected up to the corresponding Z-T curves which on being connected together form another boundary of the maximum practical values of Z , curve (5). These values of maximum possible Z can be calculated by using Eq.(8.3-a) and the associating values of T previously derived. In addition the maximum possible value of R'/R can be found by substituting in Eq.(8.3-b) for T=0.25 G and R=5%.

In this way the design chart is completely defined by the figure ABCD shown in Figs.(8.2) and reproduced in Figs.(8.3-a, b, c, d &e) after eliminating the parts of curves outside the previously mentioned limits; these figures represent the design charts for the five PC grades respectively.

In these charts two limiting values of Z , minimum and maximum, exist at the extreme intersections of Z-T curves with line (1) (c/d=0.25). The maximum value lies at the Z-T curve with the maximum possible R'/R within the limits set, whereas the minimum value is at R'/R=0.0. The corresponding values of the effective depth will be termed respectively as the minimum specific depth d_{sn} and the maximum specific depth d_{sm}. In actual design based on these design charts the required effective depth will lie within these two extreme values of d_{sn} and d_{sm}.

In this respect it might appear unreasonable that unlike PCC, a limiting maximum value of the effective depth should be

specified. Nevertheless, by referring to Figs.(8.2) it can be shown that if the effective depth is increased beyond d_{sm}, the value of c/d will be reduced to a value less than 0.25 with the result that strains in tension steel will be more than three times the ultimate concrete strain ε_{cu}. Bearing in mind that ε_{cu}-values are as much as 0.0071-0.0076, it is quite reasonable to limit the tension steel strains to the value $3\varepsilon_{cu}$ by not allowing T-value less than 0.25 G . The maximum effective depth is a consequence of the assumption that T should not be less than a given value.

These design charts will not allow values of effective depth smaller than d_{sn} as the required reinforcement ratios would then exceed the prescribed maximum values of R and R'/R. It is useful to identify the four corners of each of these design charts before proceeding any further. Corners A and B together represent one single point on the R-T and Z-T curves respectively which have the maximum R'/R ratio at c/d=0.25, and they further represent the case of the minimum specific effective depth with doubly reinforced sections. On the other hand corners C and D correspond to one singly reinforced section proportioned to the minimum effective depth with the maximum possible value of R.

For a given moment and a given PC grade, the value of the effective depth can be made to vary from d_{sn} to d_{sm} (from Z=EB' to Z=EB). The tensile reinforcement ratio can also vary from R=EA' to R=EA, while the values of R'/R can be chosen to have any of the values from zero to the maximum ratio of R'/R. The design charts can be used in many different ways to find

the missing data for the section to be designed. In using these charts the relevant factors of safety previously given must be introduced as will be demonstrated in the following examples.

Example [8.1]

A 250 mm wide rectangular cross-section is to carry a service load bending moment of 200.0 KN.m for dead load and 250.0 KN.m for live load. Using the given cold-drawn steel and the five PC grades, design the section to have the maximum effective depth.

Solution

Using load factors 1.4 and 1.7 for dead and live load respectively, then the ultimate moment Mu will be ;

$Mu=1.4(200) + 1.7(250) = 705.0$ KN.m.

For the maximum effective depth T=0.25 G and R'/R=0.0, then from the design charts minimum Z-values can be found. hence the value of the maximum effective depth can be calculated from the following equation in which the capacity reduction factor $F_{cr}=0.8$ is introduced;

$$d=[Mu/(Zbd^2 f_{cy} F_{cr})]^{0.5} \qquad ...(8.5)$$

The tensile reinforcement ratio R at T=0.25 G and R'/R=0.0, corresponds to point A'in the design charts and can be found directly from them. The derived and calculated values of minimum Z, maximum effective depth , R and A_s are given below for the five PC grades.

Grade	A	B	C	D	E

Zmin.	0.158	0.160	0.168	0.172	0.152
d_{max}(mm)	512.0	495.0	529.0	506.0	494.0
R %	2.54	2.76	2.54	2.64	2.78
A_s (mm2)	3250.0	3415.0	3360.0	3340.0	3433.0

Example [8.2]

The same as given in Example[8.1], except that the sections are to be designed to have minimum effective depth.

Solution

The required sections will be those corresponding to points A and B on the design charts at which R'/R is maximum and R=5%. Substituting for the value of Zmax. corresponding to point B in Eq.(8.5), the minimum depth can be calculated . Knowing maximum values for R'/R and R=5%, the areas of the steel required can be calculated. the results for the five sections are as follows;

Grade	A	B	C	D	E
Zmax.	0.315	0.300	0.350	0.330	0.280
d_{min} (mm)	363.0	361.0	366.0	365.0	364.0
R'/R	0.574	0.515	0.600	0.528	0.520
R'max %	2.870	2.570	3.000	2.640	2.600
A_s (mm2)	4538	4512	4575	4818	4550
A'_s(mm2)	2605	2323	2745	2544	2366

Example[8.3]

The same example [8.1] except that the sections are to be designed for an effective depth d=400.0 mm.

Solution

Using Eq.(8.5) the value of Z required for the given value of effective depth, can be calculated. Using the design charts and by drawing a horizontal line at that calculated value of Z, a range of possible R and R'/R values can be obtained that would provide such a predetermined effective depth. It is clear from the charts that as R increases the associated ratio of R'/R required will also increase and vice versa. Therefore, for the calculated Z-value for each PC grade an infinite number of solutions are available ranging from R'/R max. and Rmin. to R'/R min. and Rmax. These limits of the reinforcement ratios can be directly derived from the design charts or found by extrapolation. The results are as given below.

Grade	A	B	C	D	E
Calculated Z	0.259	0.244	0.294	0.275	0.232
Rmax. %	5.0	5.0	5.0	5.0	5.0
R'/R min.	0.02	0.0	0.15	0.0	0.0
A_s max.(mm2)	5000	5000	5000	5000	5000
A'_smin.(mm2)	100	0.0	750	0.0	0.0
Rmin. %	4.0	4.2	4.4	4.2	4.3
R'/R max.	0.45	0.40	0.52	0.41	0.41
A_s min.(mm2)	4000	4200	4400	4300	4300
A'_smax.(mm2)	1800	1680	2290	1722	1763

Example[8.4]

The same as given in example [8.1] except that the sections are to be designed for a given R=4% and R'/R=0.2.

Solution

Using the R-T curves of the design charts , find the value of T corresponding to R=4% and R'/R=0.2, that is the intersection of 4% R-horizontal line with R-T curve whose R'/R=0.2. In such a case, one specific value of T will exist for each PC grade. Using this value of T, the corresponding value of Z can be obtained from the intersection of a vertical line drawn at T with the Z-T curve of R'/R=0.2. The value of Z can then be used for calculating the required depth from Eq.(8.5). The results for the five PC grades are given below.

Grade	A	B	C	D	E
Z	0.228	0.222	0.256	0.246	0.213
d (mm)	426.0	420.0	428.0	392.0	417.0
A_s (mm2)	4260	4200	4280	3920	4170
A'_s(mm2)	852.0	840.0	856.0	784.0	834.0

In all the above examples, the value of T corresponding to any section chosen is known, hence the position of the neutral axis can be calculated where T=Gc/d. Knowing the position of the neutral axis and the ultimate concrete strain ε_{cu}, the strains and the stresses in the steel can be checked using Eqs.(8.4-a &b). These given examples indicate the versatility of the design charts and numerous further examples could have been cited to emphasize this feature. The use of these charts is almost unlimited and therefore it is left to the designer to satisfy his design requirements as desired. Obviously another alternative for design is direct use of the equations used in the construction of these charts.

8.5. Design of reinforced PC members with flexure and axial

compressive load

The equations used previously in the analyses of reinforced PC columns can be used in the design after various factors of safety are considered. As stated, the additional axial load leads to a function in the third order of T the manual solution of which is not easy. It was also emphasized that unlike beams, columns must have compression steel at least in one side of the column if not both. The use of compression steel in columns is absolutely necessary from the economic and performance points of view.

In Chapter Six, it was shown that the relative contribution of either compression or tension steel to the ultimate carrying capacity will vary depending on the eccentricity ratio er=e/d. It was further found that for er-values less than unity, the compression steel ratio R' should be as high as possible and the tension steel ratio R should be calculated accordingly. At the other extreme, for er-values greater than unity, the R-value should be as high as possible with R'being calculated accordingly.

For rectangular sections with flexure and axial compression , Eq.(5.1) can be rewritten in the following form;

$$T_s = T + T'_s - L \qquad \ldots(8.2\text{-a}')$$

Using Eq.(8.2-a') and the previously derived Eq.(8.2-b), T'_s can be eliminated and by similar operations as those carried out with pure flexure, the values of R, R' and Z could be expressed in terms of T as given in the following three equations;

$$R = f_{cy}(T - L)/f_s/[1 - (R'/R)(f'_s/f_s)] \quad ...(8.6\text{-a})$$

$$R' = f_{cy}(T - L)/f'_s/[(R/R')(f_s/f'_s) - 1] \quad ...(8.6\text{-b})$$

$$Z = T(1 - YT) + (T-L)(1-d'/d)/[(R/R')(f_s/f'_s) - 1] \quad ...(8.6\text{-c})$$

$$\text{in which } L = Z.d/e = Z/er. \quad ...(8.6\text{-d})$$

Substituting in Eq.(8.6-c) for L in terms of Z, the value of Z at a given er-value can be obtained for various T-values and R'/R ratios (d'/d=0.1). Then using the value of Z in either of Eqs.(8.6-a or b), the corresponding values of R and R' can be calculated. It is important to note that while Z or R values in pure flexure were dependent only on T and R'/R, they are further dependent on er-value when moment and axial load are combined.

Equations (8.6-a to 8.6-d) are now sufficient to be used in design after the factors of safety are introduced. For a given load at a given eccentricity and for a known depth and width of the section, a wide range of possible R and R'-values exists, depending on the desired compression zone depth or alternatively on the value of T. This wide range of R and R' is reduced to one single value for each if and only if either of R and R' are known on one hand, or R'/R ratio is fixed on the other. As the use of these equations will lead to undesirably lengthy calculations, design charts for columns similar to those developed for beams can be of great use.

Equations (8.6-a and 8.6-c) represented graphically are shown in Figs.(8.4-a, b, c, d &e) for the five PC grades. In these figures, the values of Z and R are plotted using two opposite ordinates against the values of T as a common abscissa. These

figures correspond to one single value of eccentricity level er=2.0. They can be similarly constructed for any other value of er; as an example, Fig.(8.4-a') is constructed with er=1.0 for grade A.

For deriving the column design charts on the bases of these figures, similar provisions to those considered with pure flexure were taken into account. The first of which is that T-value should be within 0.25 G and 0.6 G, whether the column has small or large eccentricity. Accordingly the range of T is defined by the two vertical lines (1) and (2) as shown in Figs.(8.5). The second provision is that R'/R ratio must not be less than 0.2 and neither of R nor R' should exceed 5% for large or small eccentricity columns respectively. This second provision provides a third limiting vertical line, line (5) in Figs.(8.5), drawn at the T-value corresponding to the intersection of the T-R curve whose R'/R=0.2 and line (3). Accordingly the right-sided boundary of the design charts will be either line (2) or line (5) whichever has the smaller T-value.

It should be stressed that for columns with small eccentricities, the design charts are much more easily derived from Z-T-R' curves than Z-T-R curves allowing a limiting value of R'=5% to be introduced. The figures shown, Figs.(8.5), are for large eccentricity and therefore the provision of R=5% is relevant. By drawing a horizontal line at R=5%, line (3), and projecting the limiting T-values on the corresponding Z-T curves, the upper boundary of the design chart, curve (4), is defined. While maximum value of R'/R in beams reached almost 0.6, this ratio can have much higher

values with columns and in this respect an additional provision had to be considered. That is, for large eccentricity columns where er > unity, R'/R must not be more than 1.0 and consequently R'will be always less than or equal to 5%. Conversly, for small eccentricity columns where er < unity, R'/R should not be less than 1.0 with the result that R can have any value up to a maximum of 5%.

Referring to Figs(8.4), in which er=2.0, the maximum value of R'/R is 1.0 and all the Z-T or R-T family curves are constructed accordingly with R'/R ranging from 0.2 to 1.0. Thus the design charts are confined to the boundaries denoted ABCDEF. The design charts are reproduced in Figs.(8.6-a, b, c, d &e) for the five PC grades with eccentricity level er=2.0. In addition, to demonstrate the effect of the eccentricity level Figs.(8.6-a1, a2 & a3) are constructed for three different values of er.

In these charts it can be shown that a maximum specific effective depth d_{sm} occurs at T=0.25 G corresponding to the minimum value of Z at B', while a minimum specific effective depth d_{sn} exists with R=5% and R'=5% at point C which has a maximum value of Z. In between the two extreme values of d_{sm} and d_{sn} corresponding to a certain er-value, an unlimited number of effective depths are available with various mutual values of R and R' as will be shown in later examples.

It should be borne in mind that while the interaction diagram solves for a given section at various er-values, the developed design charts solve for various sections at given er-value. In particular design cases, one approach may be preferred to the

other. However, these design charts can be translated to similar ones, as shown in Fig.(8.5), that can work as interaction diagrams not only for a given section but also for as many sections as desired provided that they have a known R'/R.

This can be done by using Eq.(8.6-a) and Eq.(8.6-c) for finding R and Z values for different T values at a constant optional R'/R ratio with er-value as a parameter. An example of these interaction design charts is given in Fig.(8.7) for grade A, with R'/R=1.0 and er-values changing from 1.0 to 2.5. Obviously a much wider range of er-values can be considered. The interaction design chart shown in Fig.(8.7) is limited with the vertical lines (1) and (2) as defined before, while the lower boundary, line (3), is drawn at R=5% as the R'/R considered is 1.0. Had the ratio R'/R been more than 1.0, line (3) would have been drawn at R=0.05 R/R'. The intersections of line (3) with various R-T curves can be used to plot the upper boundary, curve (4), as shown in Figs.(8.5 & 8.7). It is noteworthy that the intersection of line (3) with line (1) will concide with an R-T curve having the maximum possible er-value at R=5%, while the intersection with line (2) identifies another R-T curve at the minimum er-value for the same R so that T will not exceed the prescribed limits (points A and D respectively). The intersection of curve (4) with lines (1) and (2) would give the corresponding minimum and maximum values of Z respectively. Similar curves to curve (4) can be constructed for any other value of R < 5%. Knowing the maximum er-value and the associated minimum Z-value, the value of the minimum axial load Pmin can thus be obtained for a column of

any dimensions with a given R'/R.

Conversely, using the minimum er-value and the corresponding maximum value of Z, the maximum axial load that can be supported by a given column can be calculated. It is important to note that for a given section there exist two specific ultimate loads occurring at two specific eccentricities that would satisfy the practical limits given.

In the following, some representative examples are cited to demonstrate how the above mentioned design charts and interaction design charts can be used.

Example [8.5]

A 200 mm wide rectangular cross-section is to carry a service axial load of 180 KN from dead load and 270 KN from live load at an eccentricity level er=2.0. For an effective depth d=400 mm, find the required areas of compression and tension steel (cold-drawn type) for columns made of each of the five PC grades given with [a] R'/R=0.2, [b] R'/R=0.6 and [c] R'/R=1.0.

Solution

Considering load factors of the value 1.4 and 1.7 for dead and live load respectively, then the ultimate load Pu is as follows;

Pu= 1.4(180) +1.7(270) =711 KN.

Taking a capacity reduction factor F_{cr}=0.6, then the required value of Z can be calculated from the following equation;

$$Z = Pu.e/[bd^2 f_{cy} F_{cr}] \qquad ...(8.7)$$

Using the design charts a horizontal line drawn at Z equal to the calculted value will intersect with Z-T curves of R'/R equal 0.2, 0.6 and 1.0 at three distinct points, each of which can be used to find the required value of R corresponding to each R'/R (curves R-T). Having done that, the compression and the tension steel areas can be calculated. The results according to the three R'/R ratios are given below.

Grade	A	B	C	D	E
Z	0.35	0.33	0.39	0.37	0.31
[a] R'/R=0.2 :					
R %	4.56	4.20	4.82	4.38	4.08
A_s (mm2)	3648	3360	3856	3504	3264
A'_s(mm2)	730	672	771	700	653
[b] R'/R=0.6 :					
R %	3.60	3.60	3.84	3.64	3.56
A_s (mm2)	2880	2880	3072	2912	2848
A'_s(mm2)	1728	1728	1843	1747	1709
[c] R'/R=1.0 :					
R %	3.20	3.16	3.36	3.30	3.12
A_s (mm2)	2560	2528	2688	2640	2496
A'_s(mm2)	2560	2528	2688	2640	2496

Example [8.6]

As given in the above example, but it is required to design the section for the maximum possible effective depth at which tensile steel strains will not exceed three times the ultimate concrete strain, with [a] R'/R=0.4 and [b] R'/R=0.8.

Solution :

From the design charts, the minimum Z-value at the given R'/R ratio is that corresponding to the intersection of Z-T curve of the same R'/R value with line (1). Having obtained Zmin., the maximum possible effective depth can be calculated from Eq.(8.5) after substituting for e=er.d. The required values of R and R' can then be found from the respective R-T curves. The results are as follows.

Grade	A	B	C	D	E
[a] R'/R=0.4 :					
Zmin.	0.192	0.200	0.204	0.218	0.189
d_{max} (mm)	726	658	775	680	660
R %	1.80	1.84	1.64	1.80	1.86
A_s (mm2)	2613	2420	2542	2448	2455
A'_s	1045	968	1016	980	982
[b] R'/R=0.8 :					
Zmin.	0.252	0.254	0.268	0.280	0.242
d_{max} (mm)	553	518	589	530	515
R %	2.24	2.40	2.16	2.36	2.42
A_s (mm2)	2477	2486	2544	2501	2492
A'_s(mm2)	1980	1990	2035	2001	1994

Example [8.7]

As in the above example but the sections are to be designed for the minimum possible effective depth.

Solution

From the design charts the minimum depth occurs at the maximum value of Z, i.e., lies on curve (4). For each R'/R

given, the corresponding maximum value of Z can be found. The value of R occurring at the same T-value and R'/R can thus be obtained from the relevant R-T curve. The solution can then be carried out as given in Example [8.6]. The results are as follows;

Grade	A	B	C	D	E
[a] R'/R=0.4 :					
Zmax.	0.405	0.390	0.445	0.430	0.375
d_{min} (mm)	344	337	355	344	323
R %	5	5	5	5	5
A_s (mm2)	3440	3370	3550	3440	3230
A'_s(mm2)	1376	1348	1420	1376	1292
[b] R'/R=0.8 :					
Zmax.	0.490	0.450	0.520	0.495	0.420
d_{min} (mm)	284	293	304	299	296
R %	5	5	5	5	5
A_s (mm2)	2840	2926	3040	2992	2960
A'_s(mm2)	2272	2340	2432	2394	2368

Example [8.8]

A 200 mm wide rectangular cross-section is reinforced with R=3% and has R'/R=1.0. Find the range of eccentricity and the ultimate load that can be supported by such a section if it is made of PC grade A with 450 mm effective depth.

Solution

The interaction diagram for sections made of grade A with R'/R=1.0 is shown in Fig.(8.7). A horizontal line drawn at R=3% will intersect with lines (1) and (2) at R-T curves

having er-values of 2.2 and 1.1 respectively. The corresponding values of Z are 0.32 and 0.5 and are found respectively from the intersections of lines (1) and (2) with curve (4) constructed for R=3%. As Z and er values are known, then the corresponding ultimate load Pu can be found from the following equation;

$$Pu=Zbdf_{cy}F_{cr}/er \qquad ...(8.8)$$

If er is substituted for by er=1.1, the resulting value of Pu will be the maximum axial load that can be taken at this minimum eccentricity. Conversely, if er were substituted for with er=2.2, the calculated load Pu will be the minimum and Pu min.=667.6 KN and Pu max.=2086 KN.

For the given column cross-section, the magnitude of the load can increase from 667 KN acting at 990 mm eccentricity up to 2086 KN with 495 mm eccentricity. These are the ranges within which mutual alteration in Pu and e can be carried out.

Example [8.9]

For a 250x500 mm rectangular section made of PC grade A and cold-drawn steel of the given type, find the ultimate load that can be supported at an er-value of [a] 1.5, [b] 2.0 and [c] 2.5 if the section has R=4% and R'/R=1.0. Find also the maximum load capacity.

Solution

From Fig.(8.7) a horizontal line drawn at R=4% will intersect the three desired T-R curves (with the given er-values) at three points which can be used for finding the corresponding Z-values. Knowing Z,the ultimate load Pu can be calculated by

using Eq.(8.8). For the maximum load this column can support, the intersection of the horizontal line with the vertical line, line (2), pinpoints an R-T curve with the minimum er-value. Using this value of minimum er and the associated value of Z, the maximum load Pu max. can also be calculated. The results are as given below.

er	1.5	2.0	2.5
Z	0.48	0.41	0.375
Pu (KN)	2040	1306	956

For Pu max., er=1.3 then Z=0.54 and Pu max=2648 KN.

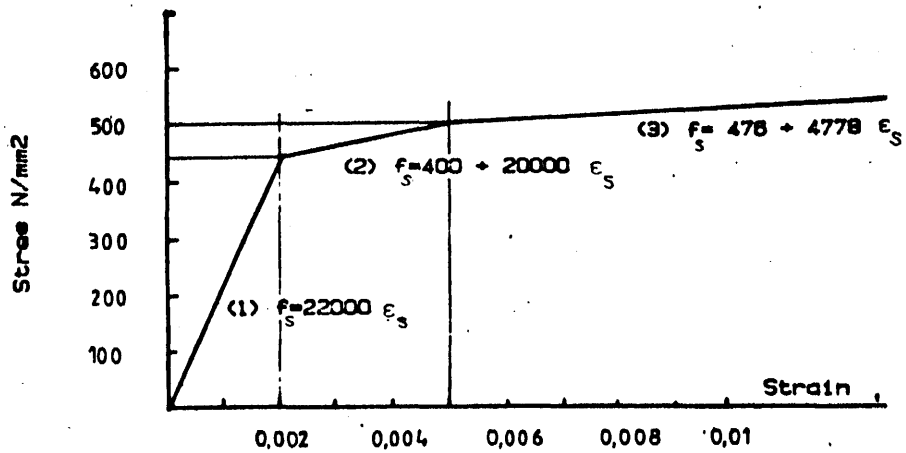

Fig. 8.1 Idealized trilinear stress-strain curve for the steel used.

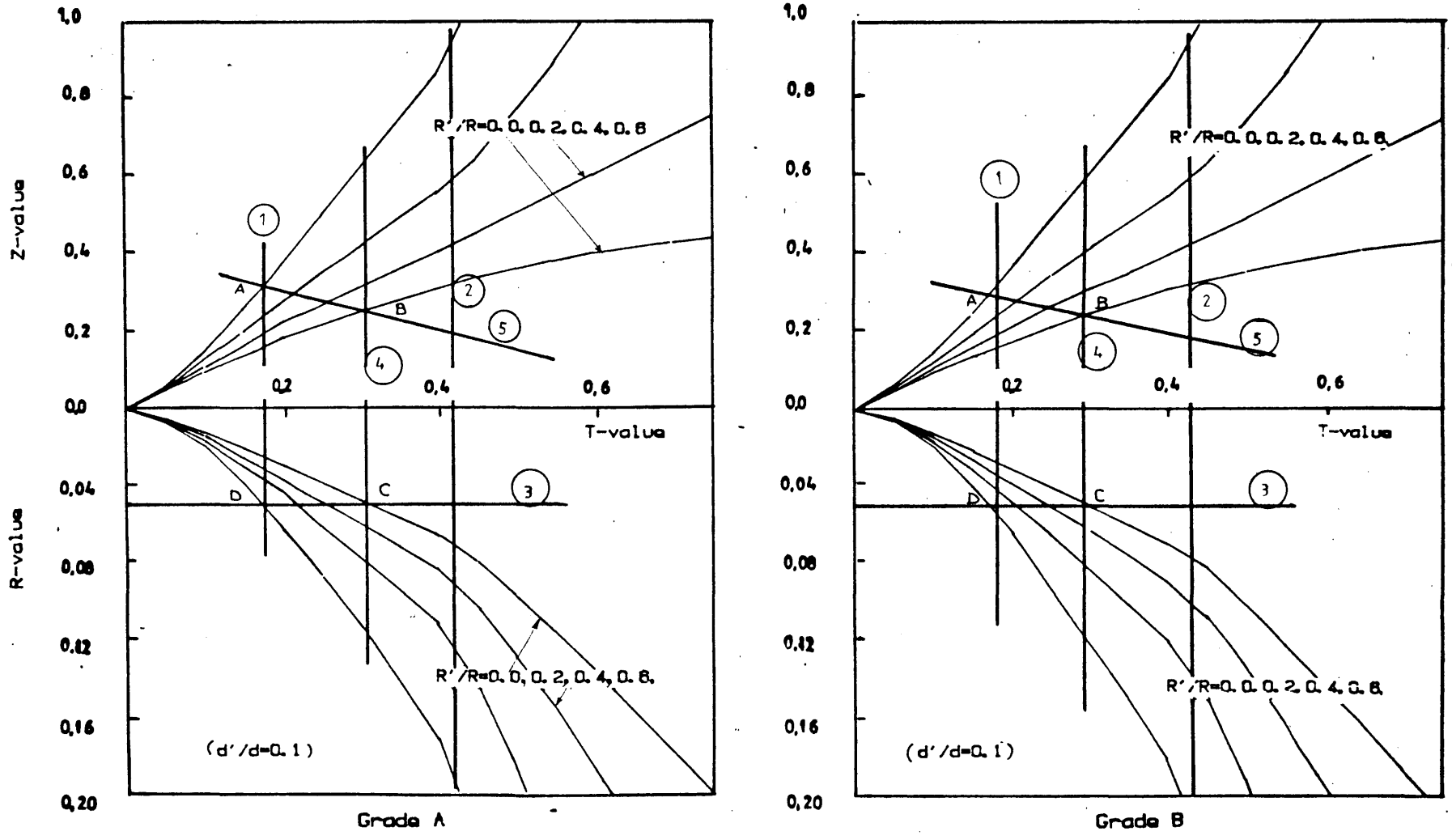

Fig. 8.2 Relationships between compression zone depth, reduced moment and tension reinforcement ratio for various compression reinforcement ratios in pure flexure
(Grade A & B)

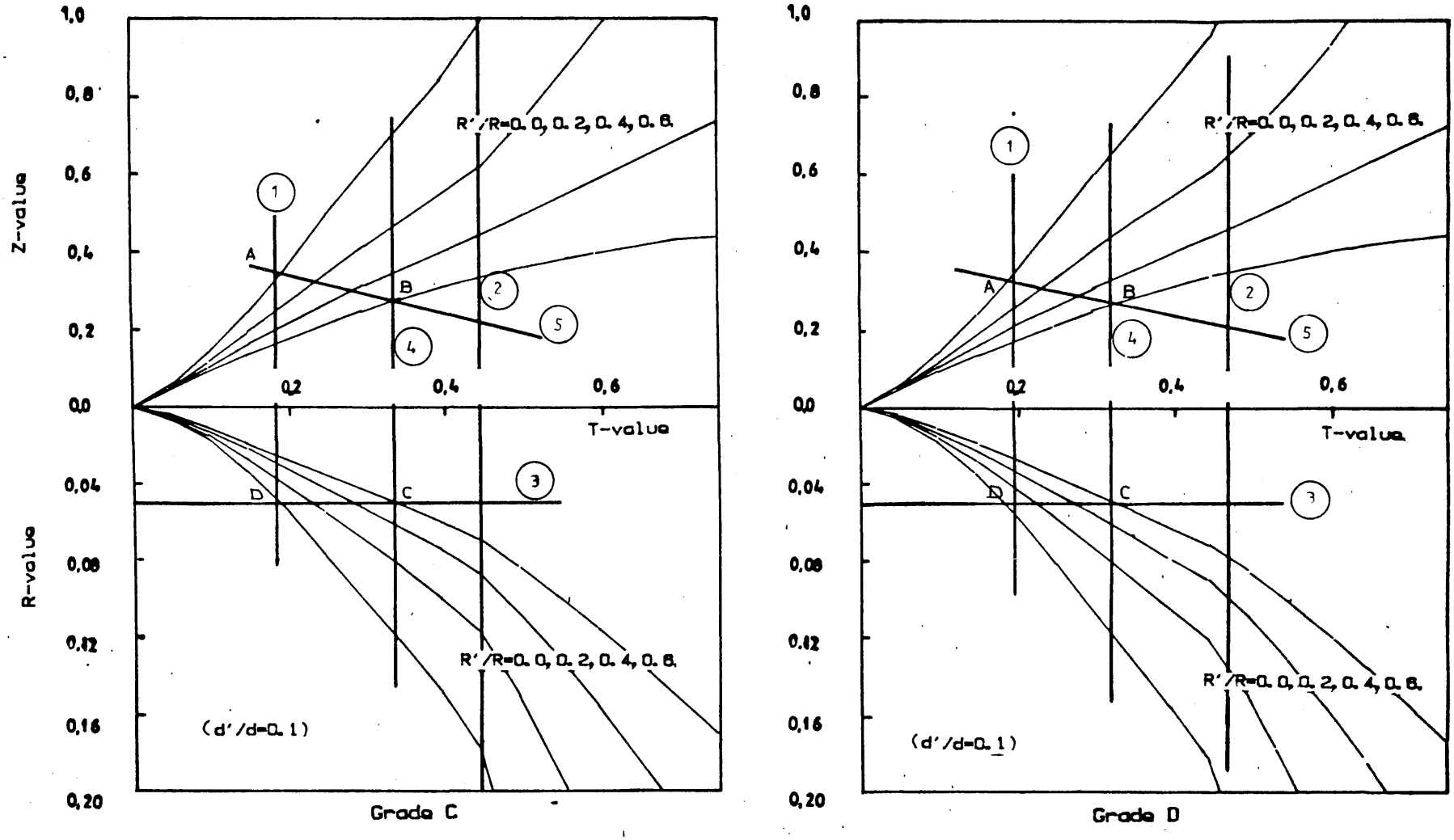

Fig. 8.2 Relationships between compression zone depth, reduced moment and tension reinforcement ratio for various compression reinforcement ratios in pure flexure
(Grade C & D)

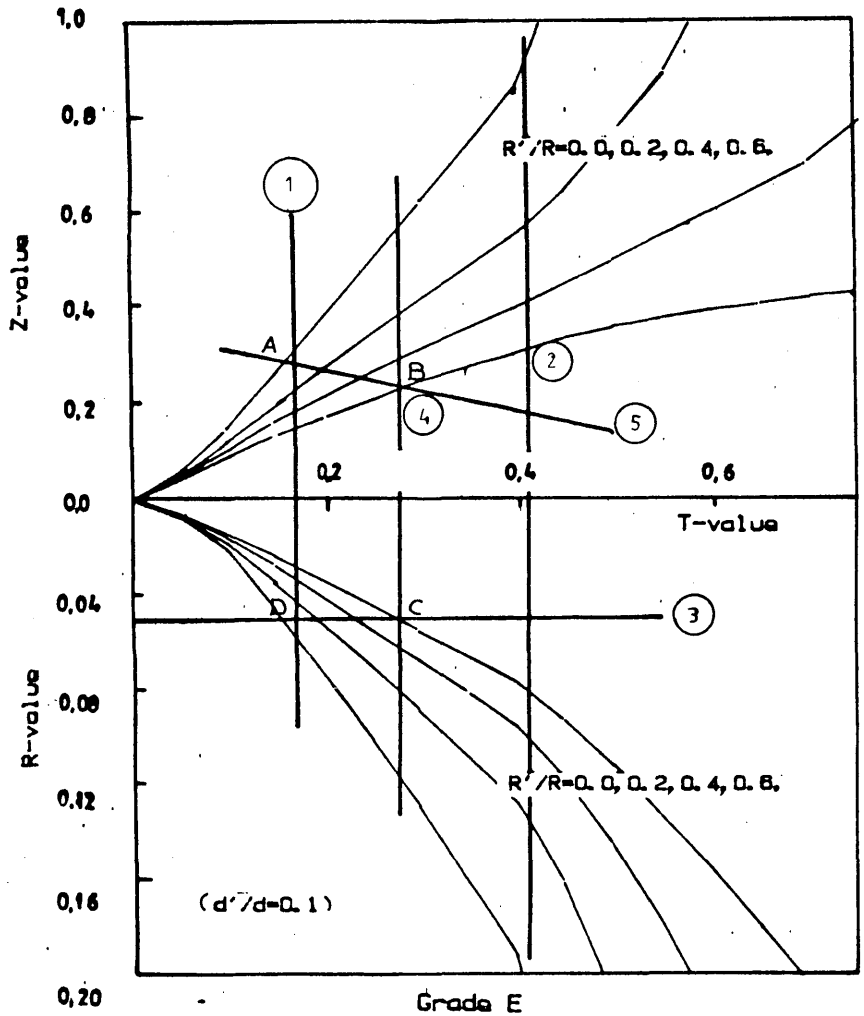

Fig. 8.2 Relationships between compression zone depth, reduced moment and tension reinforcement ratio for various compression reinforcement ratios in pure flexure
(Grade E)

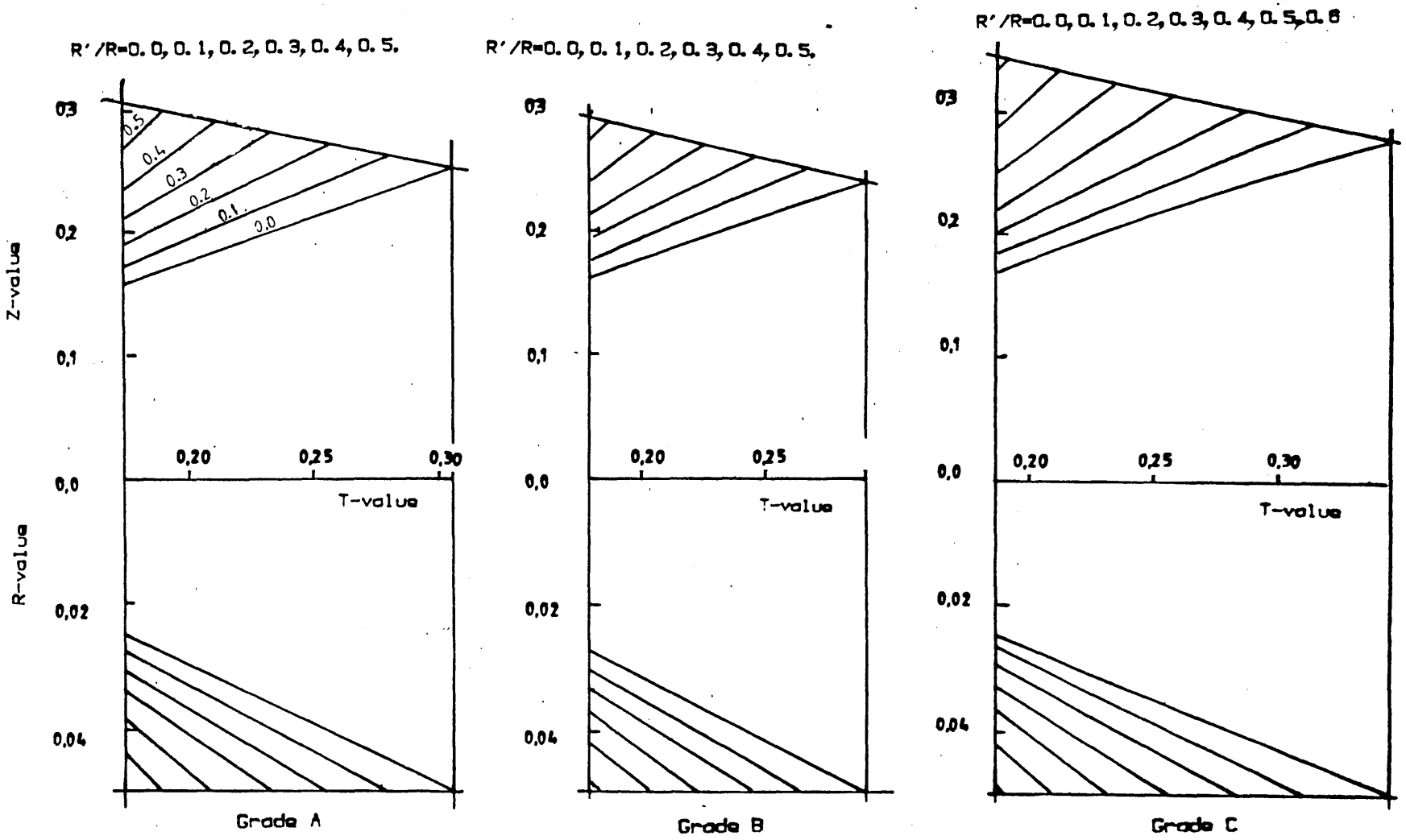

Fig. 8.3 Design charts for reinforced PC members with pure flexure.
(Grade A, B & C)

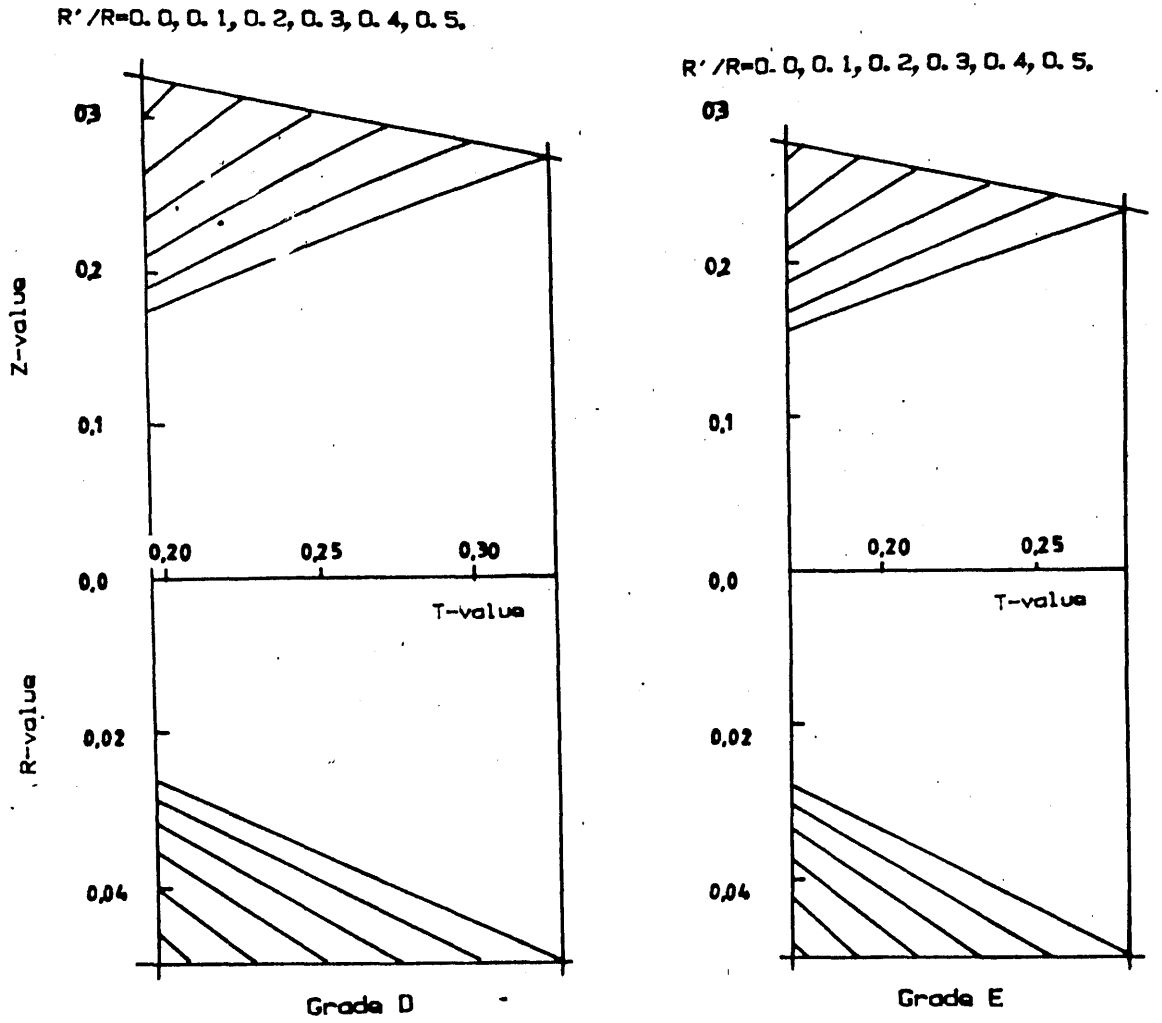

Fig. 8.3 Design charts for reinforced PC members with pure flexure.
(Grade D & E)

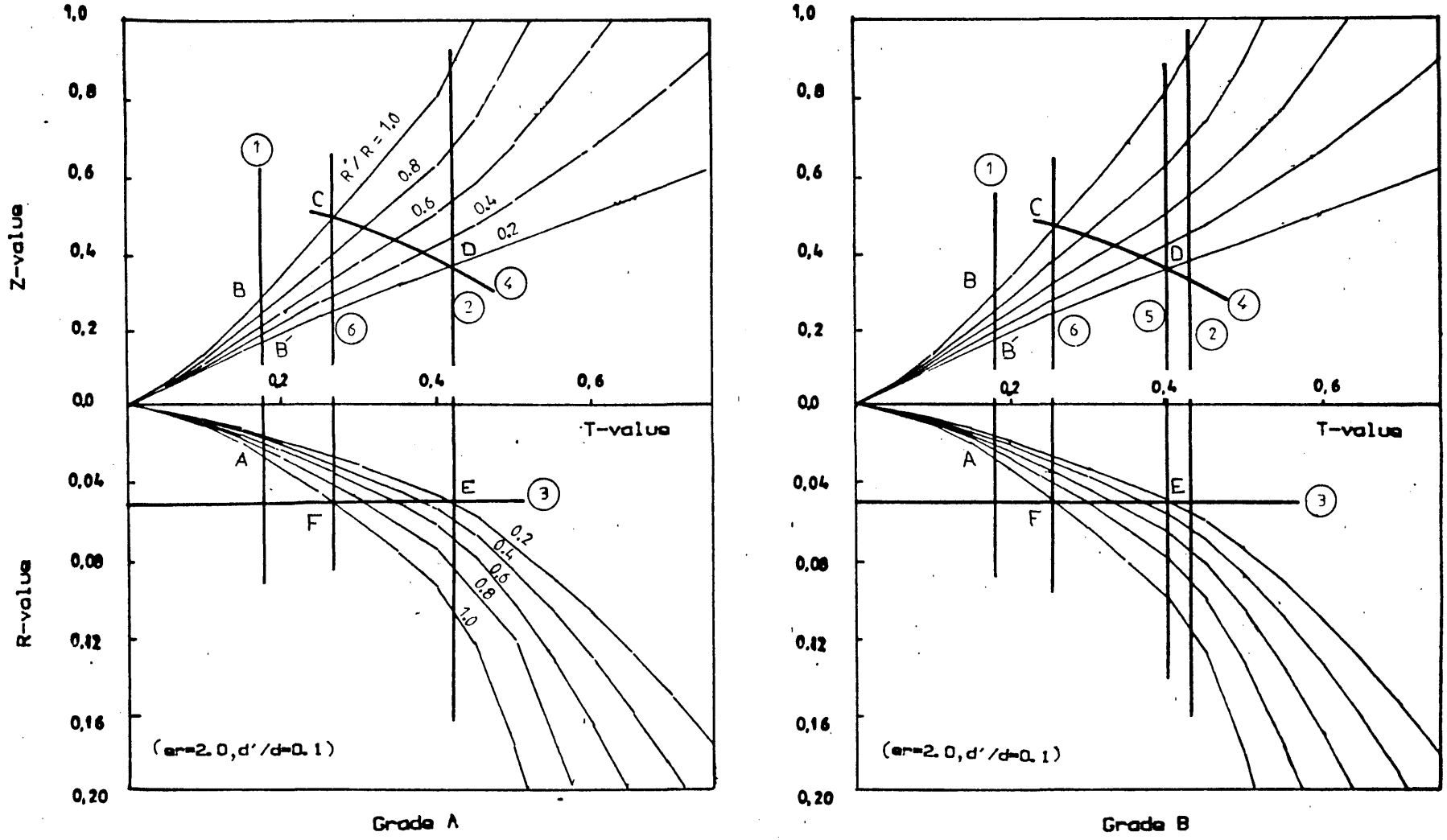

Fig. 8.4 Relationships between compression zone depth, reduced moment and tension reinforcement ratio for various compression reinforcement ratios in pure flexure and axial load.
(Grade A & B)

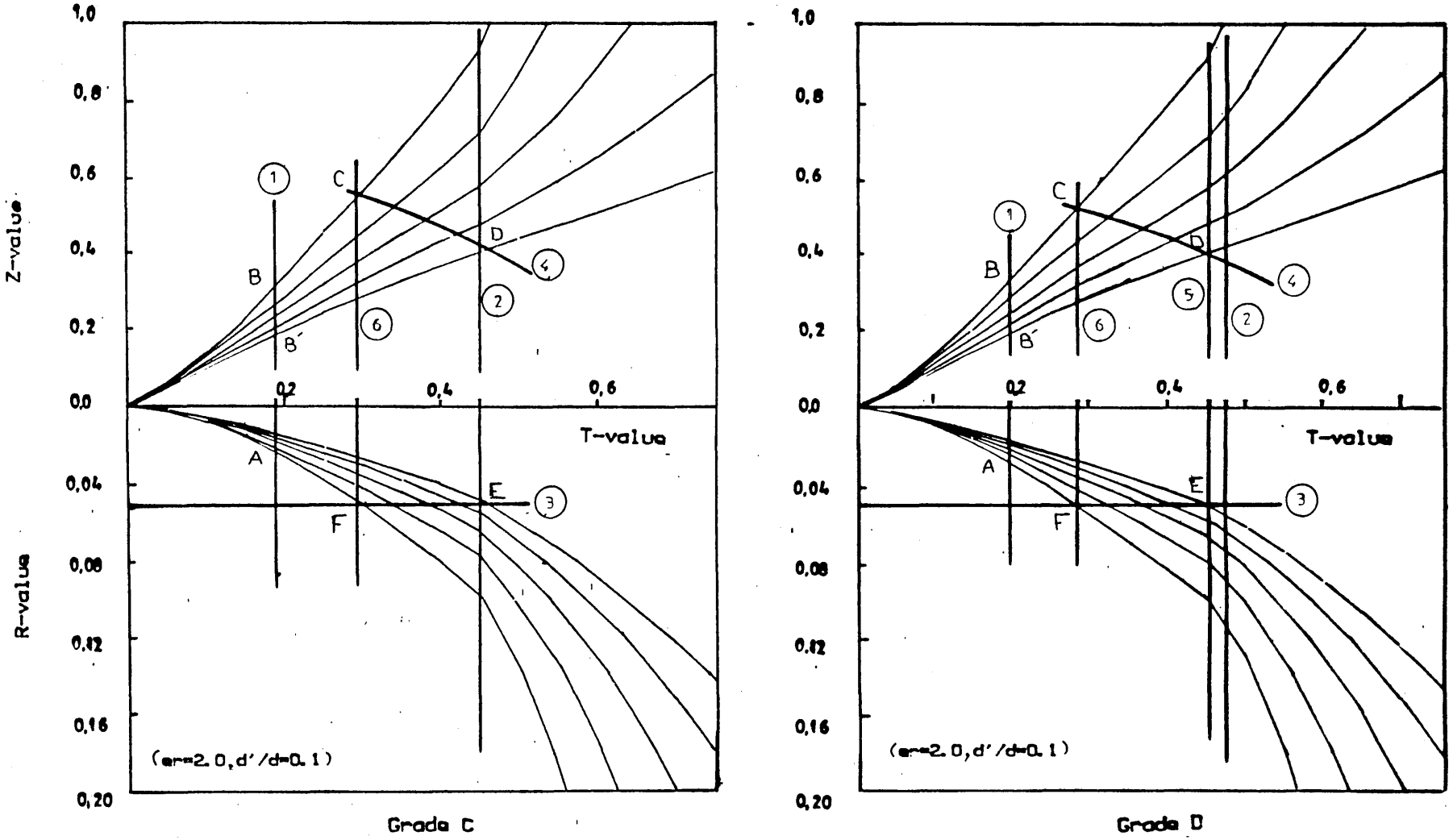

Fig. 8.4 Relationships between compression zone depth, reduced moment and tension reinforcement ratio for various compression reinforcement ratios in pure flexure and axial load.
(Grade C & D)

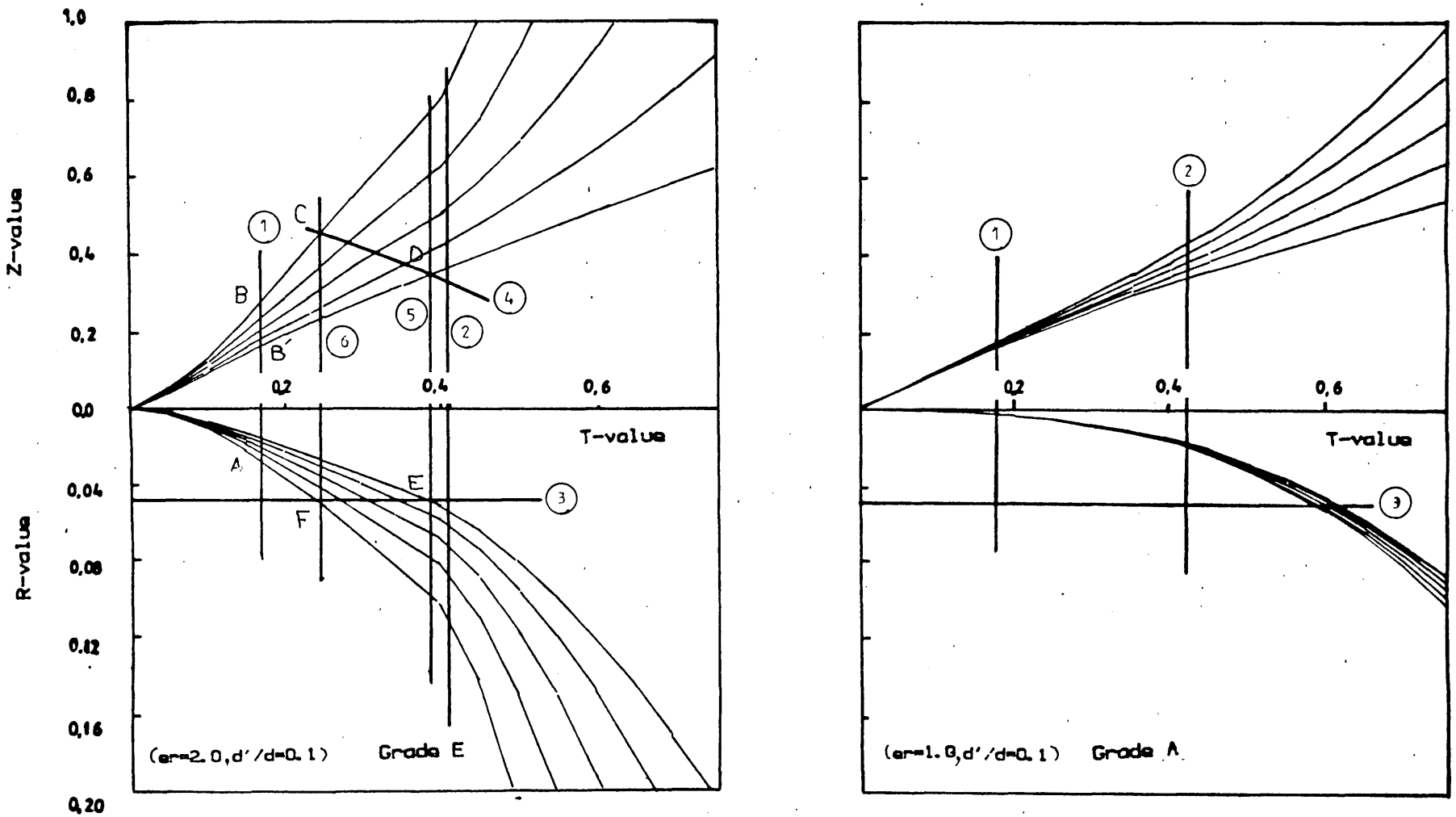

Fig. 8.4 Relationships between compression zone depth, reduced moment and tension reinforcement ratio for various compression reinforcement ratios, in pure flexure and axial load.
(Grade E & A [er=1])

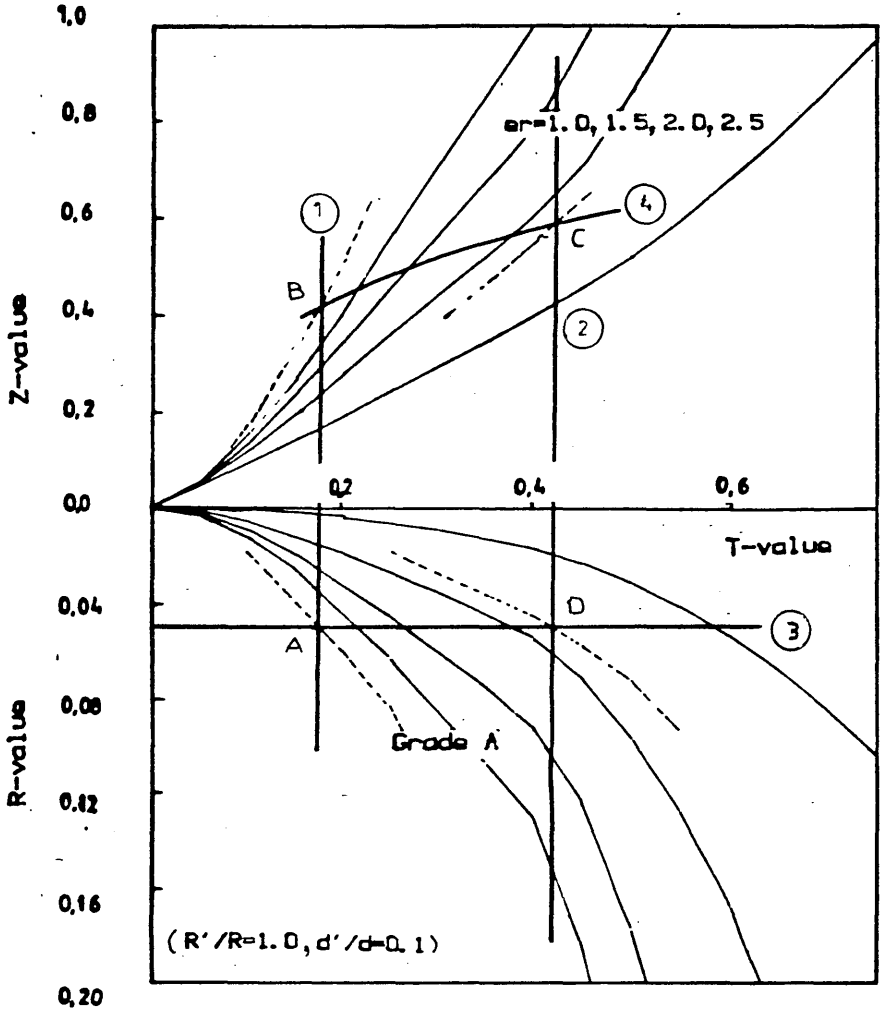

Fig. 8.5 Relationships between compression zone depth, reduced moment and tension reinforcement ratio for various eccentricity levels.

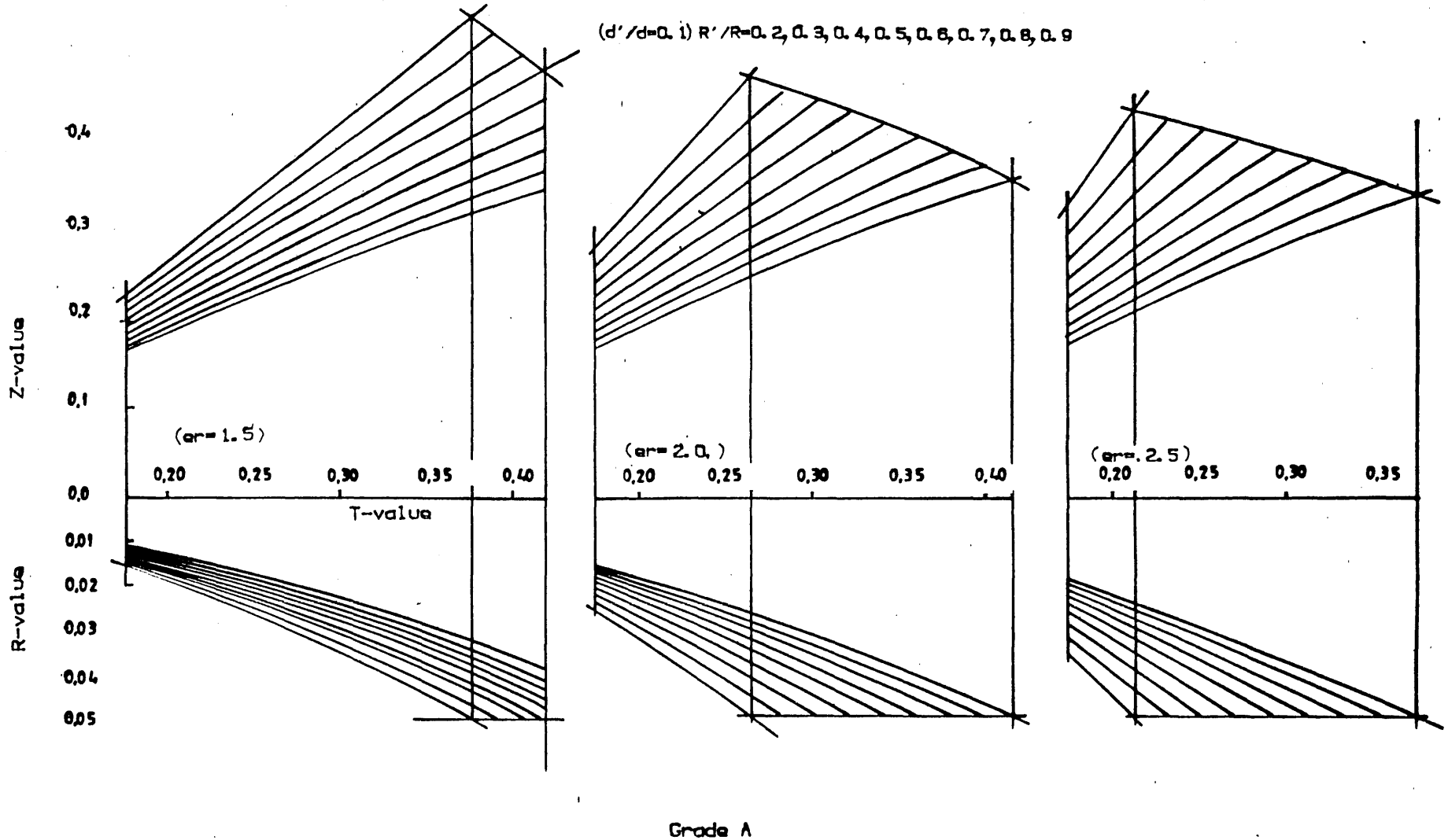

Fig. 8.6 Design charts for reinforced PC members with flexure and axial load (Grade A)

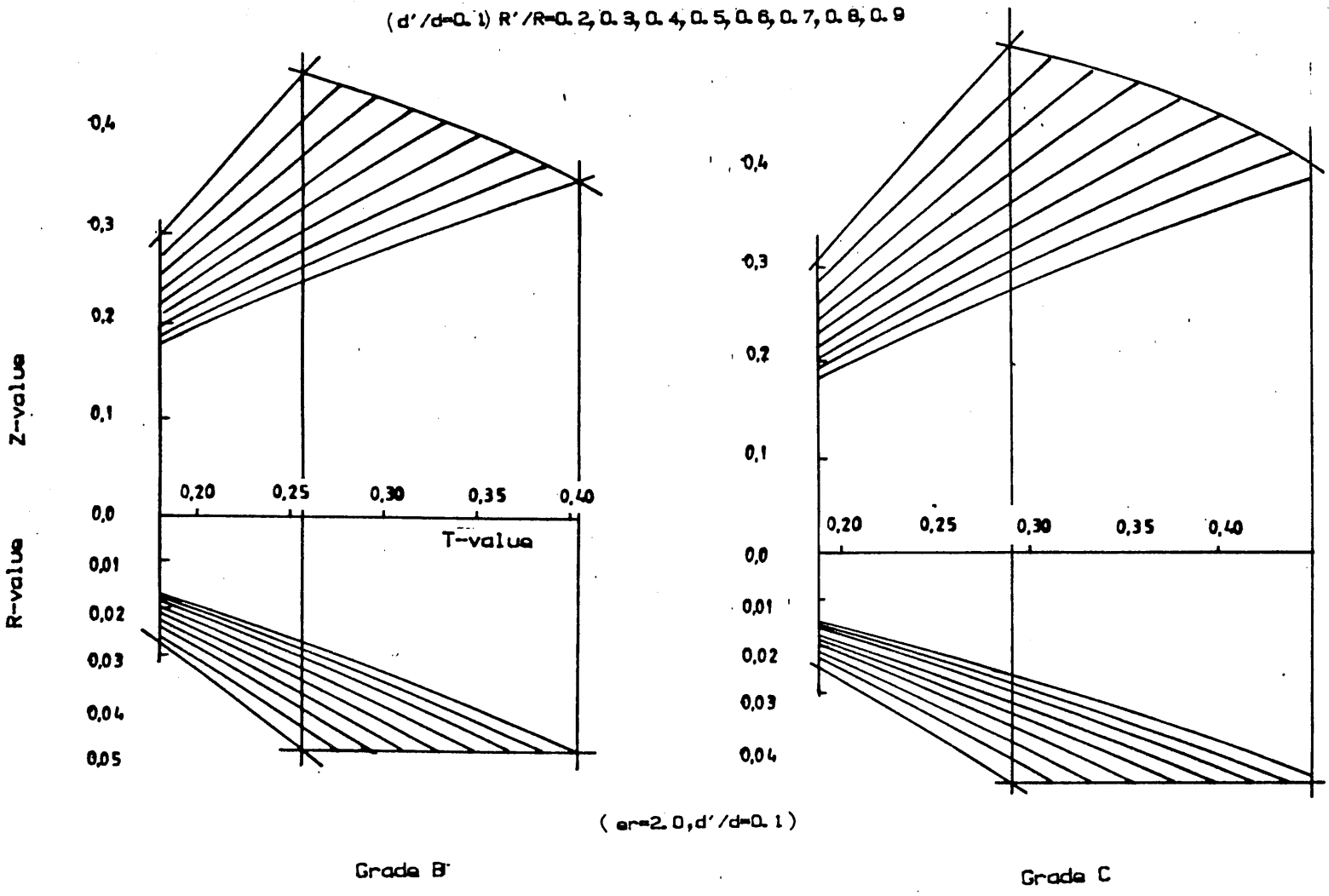

Fig. 8.6 Design charts for reinforced PC members with flexure and axial load (Grade B & C)

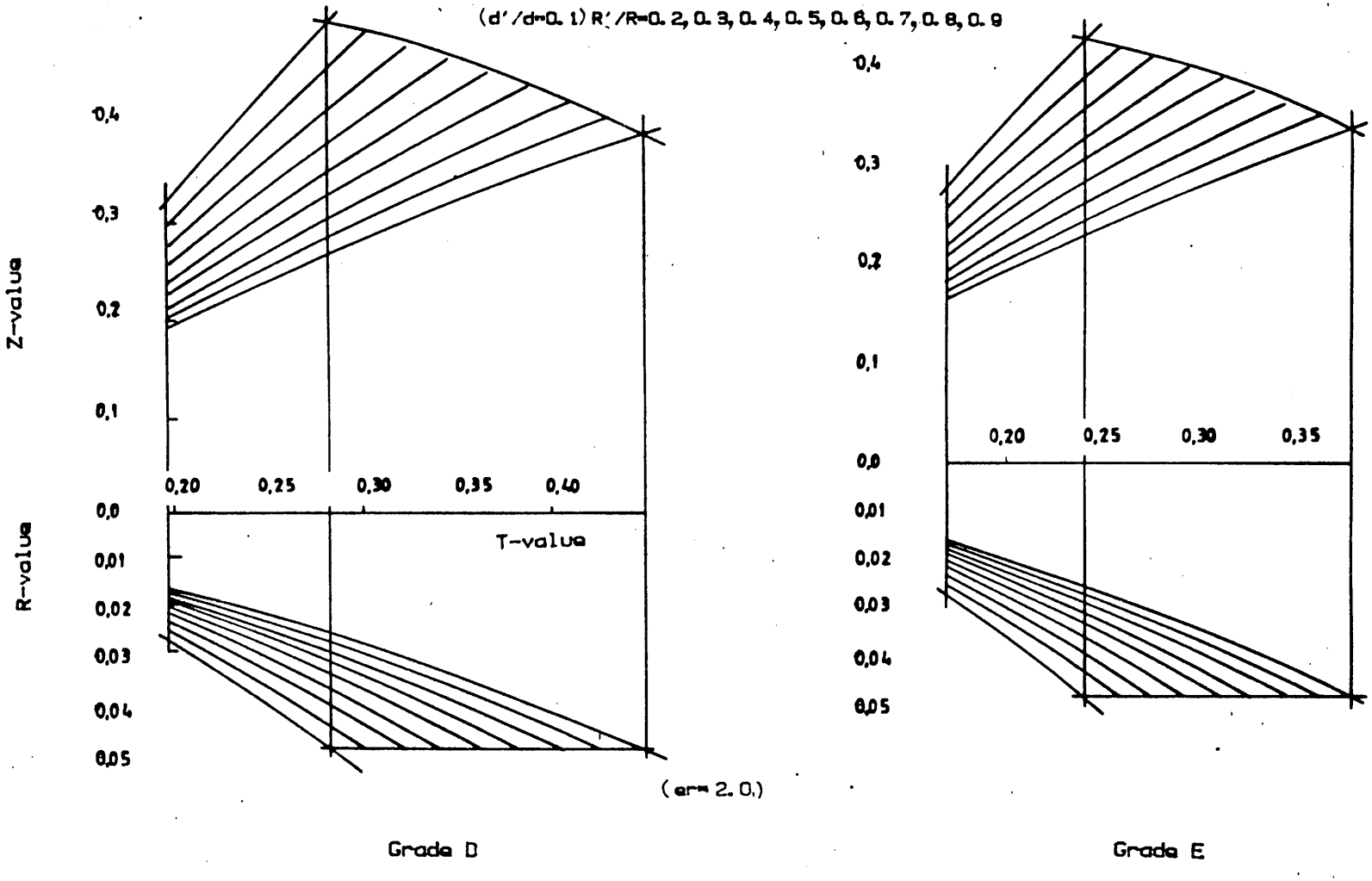

Fig. 8.6 Design charts for reinforced PC members with flexure and axial load (Grade D & E)

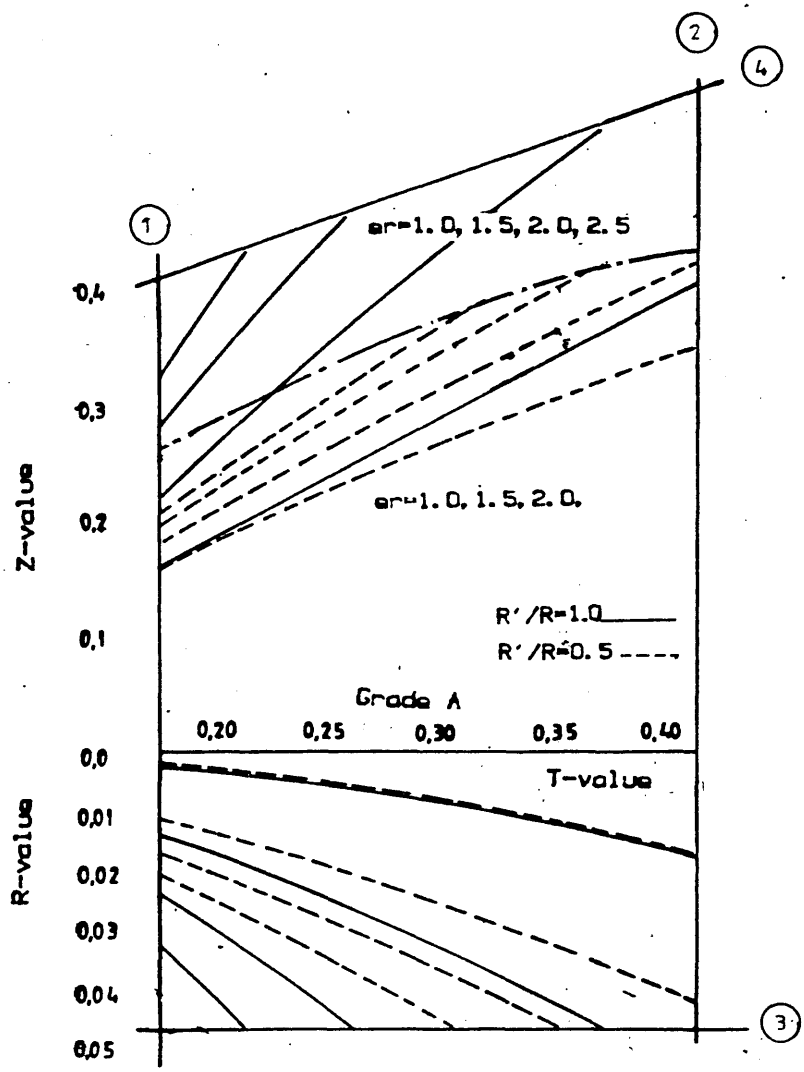

Fig. 8.7 Interaction diagrams for columns made of grade A-PC.

CHAPTER NINE

GENERAL CONCLUSIONS AND RECOMMENDATIONS FOR FUTURE WORK

9.1. General

In this experimental study of PC structural performance, the work was made to cover as wide a range of properties and structural applications as possible. Mix design and its optimization for resin mortars and PC were investigated with the object of producing fairly representative properties reproduceable at the lowest cost. Recognizing the importance of the stress distribution of PC in flexure at ultimate strength, the stress block shape and parameters were derived experimentally and were expressed theoretically. Assessment of short-term mechanical properties was carried out using full-scale structural members made of reinforced PC. On comparing the actual applied loads with the calculated ones the derived properties and parameters of the different PC grades were found to be reasonably accurate.

It was also found that time-dependency can reduce some of the material merits as recorded on a short-term basis. Although the long-term strength and the sustained strength as defined were up to 20% to 30% less than the short-term strength, it was not found necessary to modify the short-term findings and the deterioration in strength by creep was accounted for by chosen magnitudes of factors of safety. A general ultimate strength flexure theory was proposed and representative design charts are provided.

The following represents the general conclusions that can be

drawn from this work.

9.2. Conclusions regarding mix-proportioning

[1] PC mix-proportioning can be controlled at two levels, either by controlling the individual bulk properties of the various igredients or by controlling the synergetic properties existing at the interfacial planes of these ingredients. PC properites are related to the additive and synergetic interactions of the different constituents on the macro and micro-structure levels.

[2] The enhancement of PC properties by controlling the individual bulk properties is the most economic and practical approach. This can be achieved in several ways as follows :

(a) Aggregates and fillers must be carefully selected. It does not make sense to use poor quality aggregates and fillers with highly expensive resins used with the intention of producing high quality concretes. The aggregates must have gradings that provide minimum void ratios, the highest possible degree of compaction, minimum surface areas and as high a maximum aggregate-size as possible. High quality aggregates with good mineralogical properties should be used to be compatible with the high strength that the polymeric base-matrix usually offers.

(b) The fractional volumes of aggregates and fillers in the mix should be as high as workability considerations will allow. These materials in addition to being low cost filling materials , play an essential role in the rheological performance of PC. Fine powders when used with resin provide a

better-performance matrix with a lower coefficient of thermal expansion, less setting microcracking and higher stiffness. Aggregates provide the necessary restraining effect for controlling creep in the sytem matrix.

(c) Moisture content in the aggregates must be limited to prevent the presence of water leading to serious limitations to the high performance of PC; an economic compromise must be made between losses in performance and the costs of having dried aggregates.

(d) The filler type must be the most compatible and its content must be optimized for each specific resin and aggregate; it is necessary to establish these clearly if a proper mix-design is to be reached.

[3] For PC made with fine aggregates or for resin mortars , there exists an optimum surface area of the aggregates used compatible with a given mixing ratio. A mix-design method based on the fineness of the aggregates can be of great help in mix-proportioning and in predicting strength.

[4] Elevated temperatures have a deleterious influence on the performance of PC and only by enhancement of the properties of the polymer matrix can these effects be avoided.

[5] The resin is the dominating constituent in the design of PC mixes. Strength of PC is directly proportional to the resin content yet the structural performance of PC is reduced by increased resin contents. For the structural use of PC, a compromise has to be made between strength and stiffness by controlling the resin content.

[6] Polyester resin type should be chosen to suit particular applications, as cheap general-purpose resins may prove in the long run to be more expensive than high cost specially-formulated resins. Special resins that can provide desired high chemical resistance, high weatherability and toughness are available and are being continually developed by modifying the types and ratios of acids used in the manufacture of polyesters.

[7] Additives to the resin can greatly modify its reactivity and viscosity, and consequently can modify PC workability and consistency. Unless it is absolutely necessary, no additives other than the required catalysts and accelerators should be employed. Before using these two, the optimum curing temperature relevant to them has to be investigated if efficient and economic use is to be made of them.

[8] The gel time, rate of polymerization and optimum amounts of accelerators and catalysts should be found for PC proportioning irrespective of the manufacturer's data on these materials and the recommended amounts of the additives. This is because all the data provided for the resin is altered by the presence of aggregates and becomes very misleading.

[9] Workability of PC is as dependent on the mixing ratio as on the resin viscosity itself. However, Reducing the resin viscosity by using compatible monomers like styrene, will have unfavourable consequences in the form of increased reactivity and rapid mix stiffening. Workability is more efficiently improved by using well graded aggregates and fillers in correct proportions. A ratio of coarse:fine aggregates of 4:5

with 10% filler content by weight appear to be reasonable proportions from which the best performance/workability mix can be reached through trial mixes.

[10] Casting troubles such as segregation and resin bleeding are likely to happen if due attention is not given to mix proportioning. Bleeding can be controlled by adjusting the amount of the fine materials in the mix (fillers and fine sand) and by special casting and vibrating techniques.

[11] Dry mixing of the mix ingredients is useful in producing a uniform mix and in saving time and energy needed for mixing. In addition the use of preaccelerated resins can have considerable potential in mix handling where the possibility of dangerous direct contact between accelerators and catalysts can be avoided.

9.3. Conclusions regarding the structural performance of PC

[1] For given materials the stiffness of PC is inversely related to its compressive strength. Hence for proper presentation of PC at least the compressive strength and the modulus of elasticity have to be quoted.

[2] All strengths pertaining to a given PC grade (shear, tension, bond, etc.) are directly proportional to the compressive strength while properties such as shrinkage, time-dependent strains, micro and macrostrains and ultimate strains are inversely proportional to the stiffness or modulus of elasticity.

[3] Shear and bond strengths in PC are approximately the same

ratios of compressive strength as in PCC. On average, shear and bond strength are 10% and 12% of compressive strength respectively.

[4] The stress-strain curve at all points in the compression zone with a strain gradient , is different from the stress-strain curve recorded under axial compression for the same PC grade. In flexure, ultimate conditions occur at higher values of strain than in axial compression.

[5] The method adopted in deriving the stress block shape and parameters in flexure by using eccentrically loaded plane prisms was effective. The stress block parameters as found experimentally gave good agreement with the actual measurements of strains and loads for reinforced members at all stages of loading up to failure. Those block parameters at ultimate strength could be expressed empirically as functions of the modulus of elasticity of each PC grade.

[6] A general sine function can express the stress-strain curves for different PC grades in flexure. The constants of that function Ko3 and ε_{oc} are dependent only on the secant modulus of elasticicty and can be calculated using the equations given in Chapter Four. Knowing these constants and the ultimate compressive strength f_{cy}, the stress-strain curve can be obtained up to any strain level, and can be of considerable use in checking the serviceability limiting states before ultimate strength is reached.

[7] The assumption of a linear strain profile in flexure was experimentally verified and was observed with all test specimens which had a strain gradient, regardless of the type

of loading, ratio of reinforcement or specimen shape and size.

[8] Neglecting lateral confinement effects, and tension stiffening effects not only simplifies the analysis and design, but also does not lead to any significant inaccuracy in the calculations.

[9] A theoretical value for the ultimate strain of PC can be taken as 4/3 times the macrocracking strain ε_{oc} which can be calculated using the empirical equation derived for it. This expression of ultimate strain was proved to be conservative. It should be noted that ultimate strains in PC are very much higher than those of PCC and can range up to 0.01.

[10] Although PC can be made to set within a few minutes or within a few days, its mechanical properties , unlike PCC, stabilize relatively quickly and rate of strength development becomes zero at relatively short ages. In addition, apart from the thermal, chemical and physical shrinkages that occur during polymerization, PC can be said to be a shrinkage-free material at late ages. This can lead to considerable simplification in the calculation of time-dependent deformations under loading.

[11] Deviation of the stress-strain curve from linearity is dependent on the stress level as much as on the rate of loading itself. Faster rates of loading produce lower microcracking strains at higher stress levels, and higher ultimate strengths at lower macrocracking strains with lower reserve carrying capacity. Slower rates of loading can reduce the modulus of elasticity by as much as 20%.

[12] Long-term strength of PC can be of the order of 0.75 to 0.85 of the short-term strength. The long-term strength of PC can be expressed in a power expression whose constants are only dependent on PC grade itself.

[13] The creep response of PC can be estimated from creep tests lasting for periods as relatively short as 60 days. The effects of age at loading and shrinkage can be neglected for PC tested in creep after complete curing.

[14] Although absolute values of creep strains for PC are much higher than those of PCC at the same stress-level, specific creep for both is comparable. The value of the creep coefficient for PC is almost equal to that of PCC, and it depends primarily on the stress level and on the mix proportions (resin content and aggregate fractional volume and its properties).

[15] Creep of PC can be expressed as a general power function of time irrespective of the stress level as effect of the stress is embodied indirectly in the value of instantaneous strain. The constants of these creep expressions depend only on the grade of PC. The suggested creep expressions are valid for any stress level that is low enough not to initiate time-dependent failure.

[16] Unlike creep, creep recovery of PC tends to stop after 30-50 days of unloading depending on the stiffness of the PC grade and the original stress level. The coefficient of creep recovery k_r or instantaneous creep recovery k_i as defined previously, is significantly smaller than unity. This indicates the serious consequences which creep might have in

PC structures subjected to reversible or frequently recurrent loads.

[17] The sustained strength of PC is smaller than the long-term strength and it is in the range of 60-70% of the short-term strength. Despite the high time-dependency of PC, there was no need to modify the stress block shape and parameters derived from short-term tests. This is mainly because of the fact that stress redistribution due to creep in a reinforced PC member will be such that no significant reduction in the total ultimate capacity can take place. Based on previous experience with PCC it was decided to take the less advantageous creep and shrinkage properties of PC into account only in the choice of the magnitudes of capacity reduction factors. These factors range from 0.6 for flexure with axial compression loads to 0.8 for pure flexure.

[18] The creep coefficient of PC could be expressed as a power function of time and can be satisfactorily used in calculating the effective modulus of elasticity for each PC grade. The importance of having such an effective value is that it can help derive the modular ratio often required in checking the serviceability of PC structures using any of the elastic or transformed section approaches.

[19] Mild steel with low yield strength of the order 250-350 N/mm2 should not be used with PC if efficient and economic use of PC is to be obtained. For cold-drawn steel without a definite yield point, the concept of under, over or balanced reinforcement ratio does not apply and it was necessary to introduce an alternative approach based on specific

reinforcement ratios which would allow prescribed strains at ultimate conditions. Consequently, the mode of failure for reinforced PC structures can be chosen, depending on the reinforcement ratios, to be either ductile, with sufficient warning deflections and cracking, or brittle with small deflections and cracking.

[20] Rectangular PC cross-sections reinforced with high tensile steel and subjected to normal forces, can be categorised into sections with small or large eccentricity. Small eccentricity sections are those having normal force acting at a distance from the centroid of the tension steel less than the effective depth and vice versa.

[21] The suggested design charts for reinforced PC members are versatile, convenient to use and easy to construct. Using the versatility of these charts, economical optimization of the section can be achieved on the bases of the mutual areas of PC and steel required for a given ultimate load.

9.4. Conclusions regarding the economical feasability of reinforced PC structures

The construction cost items of PC can be briefly categorised into the following; (a) material costs., (b) workmanship cost and (c) maintenance cost. PC is a very expensive construction material if the price is expressed on a volume basis. However, the true assessment of costs for construction materials has to be carried out on wider basis which includes the strength produced per unit volume. For example, for an ultimate moment of 600 KN.m, it can be shown that average quality PCC would

require a cross-sectional area twice that required by PC if both sections were made with the same grade of steel and equal reinforcement areas. This ratio can be shown to be more than two, if the member considered is subjected to combined moment and axial load. For columns with small eccentricity that ratio of cross-sectional areas would increase more than for columns with large eccentricity. The reduced area of PC cross-sections would reduce the volume required for supporting given loads.

In pure flexure, for example, with cross-sectional area reduction of 50%, the price of PC on volume/strength basis is reduced by 50%. This is only one aspect that can justify the cost of PC in construction. Another important feature is that with reduced volumes of PC members, a considerable saving in dead load can be gained and the load for which they are to be designed is reduced accordingly. For example, if the above mentioned value of ultimate moment results from 40% dead load, the overall ultimate moment when using PC can be reduced by 20%. This saving in dead load would lead to further reduction in the required cross-sectional area with a ratio less than 50%. Hence the evaluation of costs on a volume/strength basis can partially justify the apparent high costs of the material judged on a volume basis.

The labour costs required in making PC are comparable to those of PCC. No special mixing, casting or vibrating techniques are required for the processing although a few precautions are required on site to ensure industrial safety. All the experience accumulated in the processing of PCC is adaptable to PC production. However as structural members made of PC are

usually lighter and stronger, costs of transportation and errection involved in PC construction may be considerably lower than those of PCC, and can therefore help reduce the overall construction costs especially in precast applications.

The major justification for the use of the relatively expensive PC in construction is by far maintenance costs. In certain applications, the use of PC can have significant potential. For example, PC can replace PCC in those parts of structures where it is necessary to provide better freeze-thaw resistance and better corrosion and abrasion resistances. This can save the whole structure the disasterous situation in which maintenace costs can be more than the construction costs. Similarly PC when used in heavy duty industrial floorings, bridge decks, irrigation structures and the like can prove in the long run that they are not as expensive as first thought.

The above are some of the features which should be considered when assessing the economic potential of PC as a construction material. Other features might arise such as the aesthetic and decorative uses of PC in construction which can save some of the finishing costs. Curing times of ordinary PCC can in some cases be very expensive. PC can be made to cure within a few hours and to support loads in remarkably short times. This can be of great use in precasting operations or in other urgent construction works.

9.5. Recommendations for future work

Despite the great amount of research devoted to the study of PC, quite a few aspects pertaining to the efficient use of PC

in the construction industry remain to be explored. Based on the previous work and on this work, the following aspects may be recommended for future work :

[1] The response of PC to dynamic and/or loads likely to cause fatigue is a feature which is most required for practical use of PC.

[2] The thermo-dependent properties of PC and their possible enhancement by the use of new versions of resins which are being continuously improved. This could dramatically broaden the structural use of PC.

[3] Standardization of different PC processing stages from the preliminary choice of mix ingredients up to casting is a field of research which should be given due attention. No standard techniques are accepted for mixing, vibrating, curing and testing. The measurement of workability is so far a matter of personal opinion.

In addition, shape and size of test specimens are at present optional with the result that experimental observations vary from one country to another, from one researcher to another and the actual physical property of the material is lost in between. For these reasons much of the work that has been done on PC can not easily be related between different researchers.

[4] Study is required of the serviceability limiting states and the possible compromise between them and the high ultimate strength that PC can offer. In this respect, lateral instability and buckling which are likely to occur with limited cross-sectional areas of PC must be studied.

[5] Detailed study should be made of the economical feasibility of PC in construction based on the various features previously mentioned and through which PC may or may not justify its use.

REFERENCES.

(1) Schorn, H., "Theoretical comparison between resin concrete, resin modified concrete and resin impregnated concrete," Proc. of the 4th International Congress on Polymers in Concrete, ITW, Darmstadt W.G., Sep. 1984, pp. 3-11.

(2) Cresson, L., British patent No. 191, 474, Jan. 1923, Ditmar, R., British patent No.214, 224, Mar. 1924; etc.

(3) Itakura, M., "Concrete pipes modified with vinyl emulsion," (in Japanese), Journal of the Japan Society for Testing Materials, Vol. 2, No. 10, pp. 488-489.

(4) Ohama, Y., "Development of concrete-polymer materials in Japan," Proc. of the 2nd International Congress on Polymers in Concrete, College of Engineering, The University of Texas at Austin, U.S.A., Oct. 1978, pp., 121-134.

(5) Teichmann, H., "Polymer dispersions for cement and concrete," Proc. of the 1st International Congress on Polymers in Concrete, The Concrete Society, London, May 1975, pp.112-124.

(6) Harreus, "Synthetic resin dispersions as a mortar and concrete admixture," Proc. of the 1st International Congress on Polymers in Concrete, The Concrete Society, London, May 1975, pp.125-130.

(7) De Vekey, R.C., "The properties of polymer modified cement pastes," Proc. of the 1st International Congress on Polymers in Concrete, The Concrete Society, London, May 1975, pp. 97-

104.

(8) Bell, R.L. and Dingley, R.G., "The mechanical properties of hydrated portland cement pastes modified with an SBR polymer latex," Proc. of the 1st International Congress, The Concrete Society, London, May 1975, pp. 162-167.

(9) Hughes, B.P. and Guest, J.E., "Polymer modified fibre reinforced cement composites," Proc. of the 1st International Congress on Polymers in Concrete, The concrete Society, London, May 1975, pp. 85-92.

(10) Mangat, P.S., Baggot, R. and Evans, D.A., "Creep characteristics of polymer modified concrete under uniaxial compression," Proc. of the 3rd International Congress on Polymers in Concrete, Nihon University, Koriyama, Japan, May 1981, pp.193-208.

(11) Steinberg, M. and Dikeou, J.T., et. al., "Concrete polymer materials - First Topycal Report," Brookhaven National Laboratory and U.S. Bureau of Reclamation, BNL No. 50134 (T-509) and USBR Gen. Report 41, Dec. 1968.

(12) Dikeou, J.T. and Kukacka, L.E., et. al., "Polymerization makes tougher concrete," Journal of the American Concrete Institute, No. 10, Proc. Vol. 66, Oct. 1969, 829 pp.

(13) "Polymers in concrete," Report by the American Concrete Institute, SP-40, Detroit, U.S.A., MI, 1973.

(14) "Polymers in concrete," Report by the American Concrete Institute, SP-58, Detroit, U.S.A., MI, 1978.

(15) "Concrete polymer materials- Fifth Topycal Report," Brookhaven National Laboratory and the U.S. bureau of Reclamation.

(16) Dikeou, J.T., "Polymers in concrete: New construction achievements on the horizon," Proc. of the 2nd International Congress on Polymers in Concrete, College of Engineering, the University of Texas at Austin, Oct. 1978, pp. 1-8.

(17) Bach, L., Hastrup, K. and Radjy, F., "Pore structure, mechanical properties and polymer characteristics of porous materials impregnated with MMA," Proc. of the 1st International Congress on Polymers In Concrete, The Concrete Society, London, May 1975, pp. 43-53.

(18) Ohama, Y., "Molecular weight of polymer formed in polymer-impregnated concrete," Proc. of the 1st International Congress on Polymers In Concrete, The Concrete Society, London, May 1975, pp. 60-63.

(19) Rio, A. and Biagini, S., "Recent progress in the field of P.I.C.," Proc. of the 1st International Congress on Polymers In Concrete, The Concrete Society, London, May 1975, pp.14-21.

(20) Schorn, H., "Limits in the modification of characteristics by the trnsformation of cement concrete into P.I.C.," Proc. of the 1st International Congress on Polymers In Concrete, The Concrete Society, London, May 1975, pp. 31-36.

(21) Manning, P.G. and Hope, B.B., "The role of polymers in polymer impregnated paste and mortar," Proc. of the 1st

International Congress on Polymers In Concrete, The Concrete Society, London, May 1975, pp. 37-42.

(22) Fowler, D.W. and Paul, D.R., "Status of concrete-polymer materials in the U.S.A.," Proc. of the 3rd International Congress on Polymers In Concrete, Nihon University, Koriyama, Japan, May 1981, pp. 20-31.

(23) Valore, R.C. and Naus, D.J., "Resin bound aggregate material systems," Proc. of the 1st International Congress on Polymers In Concrete, The Concrete Society, London, May 1975, pp. 216-222.

(24) Anonymous, "U.S. bridge dangers cited," ASCE News, June 1977, Vol. 2, No. 6.

(25) Fowler, D.W. and Paul, D.R., "Polymer concrete for repair of bridge decks," Proc. of the 2nd International Congress, College of Engineering, The University of Texas at Austin, U.S.A., Oct. 1978, pp.338-350.

(26) Murai, N. and Mizuno, S., "Thermosetting plastics swelled with grainy fillers," Review of the Electrical Communication Laboratory, Vol. 9, No. 9-10, Sep.-Oct. 1961,pp. 581-588.

(27) Okada, K., Sakamura, A., Murai, N. and Sato, Y., "Resin concrete," (in Japanese), Journal of the Society of Materials Science, Japan, Vol.16, No. 167, Aug. 1967, pp.667-675.

(28) Okada, K., Koyanagi, W. and Yonezawa, T., "Thermo-dependent properties of polyester resin concrete," Proc. of the 1st International Congress on Polymers In Concrete, The Concrete Society, London, May 1975, pp. 210-215.

(29) Okada, k. and Ohama, Y., "Status of concrete-polymer composites in Japan," Proc. of the 3rd International Congress on Polymers In Concrete, Nihon University, Koriyama, Japan, May 1981, pp. 3-16.

(30) Staynes, B.W., "Epoxide resin concrete as a structural material," Proc. of the 1st International Congress on Polymers in Concrete, The Concrete Society, London, May 1975, pp. 340-345.

(31) Johnson, R.P., "Glued joints for structural concrete," The Structural Engineer-Oct. 1963, "Creep tests on glued joints," Conference of the Institution of Structural Engineers, 1966.

(32) Staynes, B.W., "Epoxide resin concrete as a structural material with special reference to the limit state design philosophy," Ph.D. thesis, National Council of Academic Awards, U.K., May 1972.

(33) Neville, A.M., Properties of concrete , Pitman publishing ltd, 3rd edition 1981, pp. 33-35.

(34) Nutt, W.O., "The advancing concrete," Proc. of the 3rd International Congress on Polymers In Concrete, Nihon University, Koriyama, Japan, May 1981, pp.35-44.

(35) Fowler, D.W. and Paul, D.R., "Status of concrete-polymer materials in the U.S.," Proc. of the 3rd International Congress on Polymers In Concrete, Nihon University, Koriyama, Japan, May 1981, 30 pp.

(36) Ohama, Y., "Strength of polymer modified mortars using

Super High Early Strength cement," Proc. of the 1st International Congress on Polymers In Concrete, The Concrete Society, London, May 1975, pp. 151-156.

(37) Fukuchi, T. and Ohama, Y., "Process technology and properties of 2500 kg/cm2- strength P.I.C.," Proc. of the 2nd International Congress on Polymers In Concrete, College of Engineering, The university of Texas at Austin, Oct.1978, pp.45-56.

(38) Katawaki, K. and Paul, D.R., "Effect of depth of polymer impregnation and cracking on corrosion of reinforced steel," Proc. of the 3rd International Congress on Polymers In Concrete, Nihon University, Koriyama, Japan, May 1981, pp.904-917.

(39) Paturoev, V.V. and Fantalov, A.M., "Fundamentals of polymer concrete structure formation and factory production technology," Proc. of the 3rd International Congress on Polymers In Concrete, Nihon University, Koriyama, Japan, May 1981, pp. 642-643.

(40) Czarnecki, H.L., "Introduction to material model of polymer concrete," Proc. of the 4th International Congress on Polymers In Concrete, ITW, Darmstadt, W.G., Sep. 1984, p. 63.

(41) Watanabe, A. and Yamasaki, T., "Studies on hardening shrinkage stress of resin concrete," Proc. of the 3rd International Congress on Polymers In Concrete, Nihon University, Koriyama, Japan, May 1981, pp. 437-439.

(42) Kobayashi, K. and Ito, T., "Several physical properties

of resin concrete," Proc. of the 1st International Congress on Polymers In Concrete, The Concrete Society, London, May 1975, pp. 236-240.

(43) Fowler, D.W., Meyer, A.H. and Paul, D.R., "Law temperature curing of polymer concrete," Proc. of the 4th International Congress on Polymers In Concret, ITW, Darmstadt, W.G., Sep. 1984, pp. 421-434.

(44) Depuy, G.W., "Applications of polymers in concrete in the U.S.A.," Proc. of the 4th International Congress on Polymers In Concrete, ITW, Dramstadt, W.G., Sep. 1984, pp. 79-82.

(45) Ohama, Y., "Recent research and development of concrete - polymer composites in Japan," Proc. of the 4th International Congress on Polymers In Concrete, ITW, Darmstadt, W.G., Sep. 1984, pp.21-26.

(46) Nutt, W.O., "Polymer concrete comes of age," Proc. of the 4th International Congress on Polymers In Concrete, ITW, Darmstadt, W.G., Sep. 1984, pp. 37-43.

(47) Shaw, D.N., "Polymer concretes - U.K experience," Proc. of the 4th International Congress on Polymers In Concrete, ITW, Darmstadt, W.G., Sep. 1984, pp.85-87.

(48) Fontana, J.T., "Formulations and properties of PIC with thermal conductivities of 0.08 to 0.12 Btu/hr-ft-F," Proc. of the 4th International Congress on Polymers In Concrete, ITW, Darmstadt, W.G., Sep. 1984, pp. 99-102.

(49) John, B.S. and Kane, F., "New applications of polymer

concrete in bridge and tunnel rehabilitation," Proc. of the 4th International Congress on Polymers In Concrete, ITW, Darmstadt, W.G., Sep.1984, pp.447-450.

(50) Sakamoto, O., "A new continuous spraying system for resin mortar," Proc. of the 4th International Congress on Polymers In Concrete, ITW, Darmstadt, W.G., Sep. 1984, pp.293-298.

(51) Tsuka, T. and Okada, T.,"Quick setting resin mortar for small diameter tunnel lining," Proc. of the 4th International congress on Polymers In Concrete, ITW, Darmstadt, W.G., Sep.1984, pp.195-200.

(52) Neville, A.M., Properties of concrete, Pitman publishing ltd., 3rd edition 1981, pp.203-205.

(53) Ohama, Y., "Properties of polyester resin concrete with various styrene contents," Proc. of the 20th Japan Congress on Material Research, The Society of Materials Science , Koyoto, Japan, 1977, pp.360-363.

(54) Fessenden, R. j. and Fessenden , J. S., The basis of organic chemistry, Allyn and Bacon Inc., 1971, Chapter One.

(55) Bares, R.A., "Causes of polyester resin filler surfacing system failures," Proc. of the 2nd International Congress on Polymers in Concrete, College of Engineering, The University of Texas at Austin, U.S.A, Oct. 1978, pp. 322-328.

(56) Ohama, Y. and Hamatsu, M., "Techniques for strength improvement of polymer concrete made with wet aggregates," Proc. of the JCI 6th Conference, 1984, Japan Concrete Institute , Tokyo

(57) Lubin, G., Handbook of fibre glass and advanced Plastic

composites. Polymer technology series, van Nostrand reinhold company, 1969, Chapter Two.

(58) Shapiro, S.S. and Wilk, M.B., "An analysis of Variance Test for normality," Biometrika, Vol. 52.

(59) B.S. 2846 Part 1: 1975.

(60) Neville, A.M., Properties of concrete , Pitman publishing ltd., 3rd edition 1981, pp.653-665.

(61) Czarnecki, H.L., "Introduction to material model of polymer concrete," Proc. of the 4th International Congress on Polymers In Concrete, ITW, Darmstadt, W.G., Sep. 1984, pp.59-64.

(62) Bares, R., "Some basic features in mechanics of inhomogeneous materials," Proc. of the 1971 International Conference on Mechanical Behaviour of Materials, The Society of Material Science, Japan, 1972, Vol. 5, pp.42-53.

(63) Gamski, K., "Resinous binder concrete," Proc. of the 1st International Congress on Polymers In Concrete, The Concrete Society, London, May 1975, pp.223-229.

(64) Paturoev, V.V. and Fantalov, A.M., "Fundamentals of polymer concrete structure formation and factory production technology," Proc. of the 3rd International Congress on Polymers In Concrete, Nihon University, Koriyama, Japan, May 1981, pp.638-648.

(65) Czranecki, H.L., "Expansive resin concrete : Some fundemental questions," Proc. of the third International

Congress on Polymers In Concrete, Nihon University, Koriyama, Japan, May 1981, pp.744-754.

(66) Manson, J.A., Overview of current research on polymer concrete materials and future needs. Application of PC, ACJ SP-69, 1981, pp. 1-17.

(67) Solomatov, W.J., Approach of general building composite material theory (in Russian), No. 8, 1980, pp.61-70.

(68) Gunasekaran, M. and Perry, E.R., "Polymer concrete for high voltage electrical insulation," Proc. of the 2nd International Congress on Polymers In Concrete, College of Engineering, The University of Texas at Austin, U.S.A., Oct. 1978, pp.187-191.

(69) Ohama, Y., "Effect of coarse aggregate on compressive strength of polyester resin concrete," , The International Journal of Cement Composites, Vol.1, No. 3, 1979, pp.111-115.

(70) Demura, K., Ohama, Y. and Shinizu, A., "Proposed mix proportioning of polyester resin concrete," Proc. of the 4th International Congress on Polymers In Concrete, ITW, Darmstadt, W.G., Sep. 1984, pp.265-269.

(71) Ohama, Y., "Determination methods for working life of polyester resin concrete," Proc. of the 20th Japan Congress on Material Research, Kyoto, Japan, 1977, pp. 173-175.

(72) Megahed, T.N., Polymers in concrete, M.Sc. thesis, Alexandria University, Egypt, 1981, pp.178-186.

(73) Swamy, R.N., "Some engineering implications of design in polymer concrete," Proc. of the 1st International Congress on

Polymers In Concrete, The Concrete Society, London, May 1975, pp. 349-356.

(74) Mindess, S. and Young, J. F., Concrete, Civil Engineering and Mechanics Series, 1981, pp. 453-468.

(75) Neville, A.M., Properties of concrete , Pitman publishing ltd., 3rd edition 1981, p.545.

(76) Aguado de Cea, A., Martinez, A. and Salla, J.M., "Effects of different factors in mixing and placing of polymer concrete," Proc. of the 4th International Congress on Polymers In Concrete, ITW, Darmstadt, W.G., Sep.1984, pp.299-303.

(77) Okada, K., Kobayashi, K. and Tukunaga, H., " Fundamental studies on structural use of resin concrete ," Proc. of the 3rd International Congress on Polymers In Concrete, Nihon University, Koriyama, Japan, May 1981, pp.538-552.

(78) Helal, M.S., Experimental study of mechanical properties and structural applications of polymer concrete, Ph.D thesis , Rice University 1981.

(79) Fowler, D., "Static and cyclic behaviour of polymer concrete beams," Proc. of the 4th International Congress on Polymers in Concrete, ITW, Darmstadt, W.G., Sep. 1984, pp. 159-164.

(80) Hognestad, E., "A study of combined bending and axial load in reinforced concrete members," Bulletin No. 399, University of Illinois Engineering Experiment Station, Urbana, Nov. 1951, 128 pp.

(81) Ramaley, D. and Mc Henry, D., "Stress-strain curves for

concrete strained beyond the ultimate load", Laboratory Report No. SP-12 , U.S. Bureau of Reclamation, Denver, Mar. 1947, pp.23.

(82) Blanks, R.F. and Mc Henry, D., "Plastic flow of concrete relieves high-load stress concentrations," Civil Engineering, Vol. 19, No. 5, May 1949, pp. 320-322.

(83) Gilkey, H.J., Discussion of a paper by V.P.Jensen, "The plasticity ratio of concrete and its effects on the ultimate strength of beams," ACI journal, Nov. 1943, Supplement, Proc. Vol. 39, pp. 584-6 to 584-15.

(84) Hadley, H.M., "When concrete becomes discrete," Civil Engineering, vol. 20, No. 4, April 1950, pp. 249-251.

(85) Hognestad, E., Hanson, N.W. and Mc Henry, D., "Concrete stress distribution in ultimate strength," Journal of the ACI, Dec. 1955, Title No. 52-28.

(86) Baker, A.L.L., "Recent research in reinforced concrete and its application to design," Journal of the Institute of Civil Engineers, London, Vol.35, No.4, Feb. 1941, pp. 262-298.

(87) Herr, L.A. and Vandegrift, L.E., "Studies of compressive stress distribution in simply reinforced concrete near the point of failure," Proc. Highway Research Board, Vol.30, 1950, pp.114-125.

(88) Brice, L.P., "Essaie de mesure des contraintes dans une section flechie d'une poutre en beton arme," Publications, International Association for Bridge and Structural Engineering, Zurich, Vol. 10, Nov. 1950, pp. 19.

(89) Parme, A.L., Discussion of a paper by C.P. Siess, "Review of research on ultimate strength of reinforced concrete members," ACI Journal, June 1952, Proc. Vol. 48, pp. 862-864.

(90) Prentis, J.M., "The distribution of concrete stress in reinforced and prestressed concrete beams when tested to destruction by a pure bending moment," Magazine of Concrete Research, London, No. 5, Jan. 1951, pp. 73-77.

(91) Hamann, H., "Berechnung der Druckspannungs-kurve in stahlbeton - Biegequer Schnitt," Schweizerische Bauzeitung, Zurich, Vol.70, No. 44, Nov. 1, 1952,pp.629-630.

(92) Lee, L.H.N, "Inelastic behaviour of reinforced concrete members subjected to short-time static loads," Proc. ASCE, Vol. 79, separate No. 286, Sep. 1953, 26 pp.

(93) Rusch, H., "Research towards a general flexural theory for structural concrete," Journal of the ACI, July 1960, Title No. 57-1, pp. 9-22.

(94) Imamura, K., Nakano, M. and Tsuji, K., "Reinforced resin concrete research in NTT," Proc. of the 3rd International Congress on Polymers In Concrete, Nihon University, Koriyama, Japan, May 1981, pp. 572-583.

(95) Park, R. and Pauly, T., Reinforced concrete structures, A Wiley-interscience publication, John Wiley and Sons, Inc., pp.479-482.

(96) Neville, A.M., Creep of concrete: Plain, reinforced and

prestressed, North-Holand publishing Company, Amsterdam, 1970, 25 pp.

(97) Neville, A.M.,"Role of cement in the creep of mortar," Journal of the ACI, Proc.55, 1959, pp.963-984.

(98) Freudenthal, A.M. and Roll, F., "Creep and creep recovery of concrete under high compressive stress," Journal of the ACI, Proc.54, 1958, pp.1111-1142.

(99) Neville, A.M., Properties of concrete, Pitman publishing ltd, 3rd edition 1981, pp. 281-284.

(100) Neville, A.M., Creep of concrete: Plain, reinforced and prestressed, North-Holand publishing Company, Amsterdam, 1970, 23 pp.

(101) Neville, A.M., Creep of concrete: Plain, reinforced and prestressed, North-Holand publishing Company, Amsterdam, 1970, pp.258-271.

(102) Hansen, T.C., "Creep and stress relaxation of concrete," Swedish Cement and Concrete Research Institute, Stockholm, Proc.31, 1960, 112 pp.

(103) Lee, F.M. and Lee, C.R., "Shrinkage and creep in concrete," The Society of Cemical Industry, London, Symp. on The Shrinkage and Cracking of Cementive Materials, May 1946, pp. 7-17.

(104) Lynam, C.G., Growth and movement in portland cement concrete, London, Oxford University Press, 1934, 139 pp.

(105) Czarnecki, L., "Expansive resin concrete : Some

Fundamental questios," Proc. of the 3rd International congress on Polymers In Concrete, Nihon University, Koriyama, Japan, May 1981, pp.746-747.

(106) Putlajew, I. and Mychibowa, I., "Reducing shrinkage, shrinkless and expansive Polymer concrete with FA monomer," Beton i Zhelezobeton, No. 9, 1973, pp. 29.

(107) Irtuganowa, S.M., "Polymer concrete mixture," USSR patent 420, 591, 1972.

(108) Czarnecki, L. and Broniewski, T., "Resin concrete and polymer impregnated concrete; A comparative study," Proc. of the 3rd International congress on Polymers In Concrete, Nihon University, Koriyama, Japan, May 1981, pp. 99-109.

(109) Bailey, W.J, "Synthesis of monomers that expand on polymerizatio," Journal of Elastoplastics, Vol.5, No. 3, July 1973, pp. 142-151.

(110) Ohama, Y. and Komiyama, M., "Early strength and length change of polyester resin concrete with shrinkage reducing agent," Proc. of the 22nd Japan Congress on Materials Research, The Society of Materials Science, Kyoto, 1979, pp. 356-359.

(111) Davydov, S.S., Chebanenko, A.I., Fantalov, A.M. and Kluckin, V.I., "Armoured polymeric concrete bearing structures for industrial construction," Proc. of the 3rd International congress on Polymers In Concrete, Nihon University, Koriyama, Japan, May 1981, pp 836-839.

(112) Watanabe, A. and Yamasaki, T., "Studies on hardening

shrinkage stress of resin concrete," Proc. of the 3rd International congress on Polymers In Concrete, Nihon University, Koriyama, Japan, May 1981, pp. 435-446.

(113) Koyanagi, W., Murai, N., Hayashi, F. and Ohno, S., "Stresses in reinforcement and in polyester resin concrete generated by setting shrinkage," Proc. of the 3rd International congress on Polymers In Concrete, Nihon University, Koriyama, Japan, May 1981, pp. 553-566.

(114) Broniewski, T., Jamrozy, Z. and Kapko, J., "Long life strength polymer concrete," Proc. of the 1st International congress on Polymers In Concrete, The Concrete Society, London, May 1975, pp.179-184.

(115) Macleod, A.A., Ind. Eng. Chem., Vol.47, 1319, 1955.

(116) Helal, M.S., Experimental study of mechanical properties and structural applications of polymer concrete, Ph.D thesis, Rice University 1978, pp.45-49.

(117) Neville, A.M., Creep of concrete: Plain, reinforced and prestressed, North-Holand publishing Company, Amsterdam, 1970, pp. 92.

(118) Ohama, Y., "Creep of resin concrete and polymer impregnated concrete," Proc. 17th Japan Congress on Material Research, 1974, pp.140-143.

(119) Ayyar, R.S. and Deshpande, S.N., "Creep studies on polymer mortars," Proc. of the 3rd International congress on Polymers In Concrete, Nihon University, Koriyama, Japan, May 1981, pp.504-522.

(120) CEB, "Recommendations for an International Code of Practice for reinfoerced concrete," Comite Europeen du Beton (CEB), Paris, 1964 [English translation available from Cement and Concrete Ass., London, 156 pp.]

(121) ACI Committee 318, "Building Code Requirements for reinforced concrete (ACI 318-32,33) .

(122) Rusch, H., Research towards a general flexural theory for structural concrete," ACI Journal, Vol.57, No. 1, July 1960, pp.1-28, Discussion in Journal ACI, Vol. 57, No. 9, March 1961, pp. 1147-1164.